U.S. Department of Energy • Office of Fossil Energy
National Energy Technology Laboratory

2005 Office of Fossil Energy Fuel Cell Program Annual Report

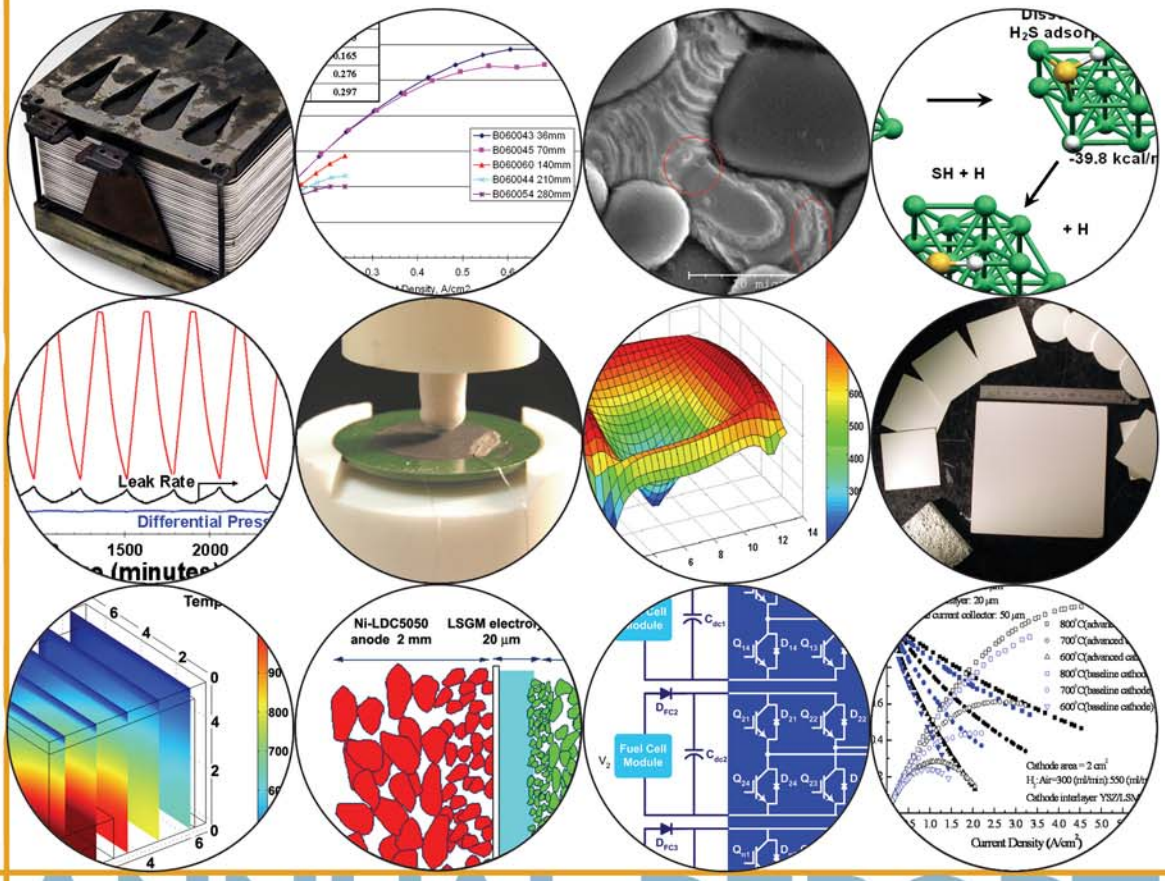

FUEL CELL ANNUAL REPORT

2005 Office of Fossil Energy Fuel Cell Program Annual Report

September 2005

CONTENTS

I Introduction 1

II SECA Industry Teams 11

1 Acumentrics Corporation: Development of a Low-Cost 10-kW Tubular SOFC Power System 13

2 Cummins Power Generation: 10-kW Solid Oxide Fuel Cell Power System Commercialization 18

3 Delphi Automotive Systems LLC: Solid State Energy Conversion Alliance Delphi SOFC 22

4 FuelCell Energy, Inc.: Thermally Integrated High Power Density SOFC Generator 26

5 GE Hybrid Power Generation Systems: Solid State Energy Conversion Alliance (SECA) Solid Oxide Fuel Cell Program 31

6 Siemens Westinghouse Power Corporation: Small-Scale Low-Cost Solid Oxide Fuel Cell Power Systems 37

III SECA Core Technology Program. 41

A Materials 43

1 Argonne National Laboratory: SOFC Research and Development 43

2 Arcomac Surface Engineering, LLC: Oxidation Resistant, Cr Retaining, Electrically Conductive Coatings on Metallic Alloys for SOFC Interconnects 47

3 Ceramatec, Inc.: Metal Interconnect for SOFC Power Systems 51

4 Georgia Institute of Technology: Novel Sulfur-Tolerant Anodes for Solid Oxide Fuel Cells 55

5 Georgia Institute of Technology: Functionally Graded Cathodes for Solid-Oxide Fuel Cells 60

6 Lawrence Berkeley National Laboratory: Development of Inexpensive Metal Alloy Electrodes for Cost-Competitive Solid Oxide Fuel Cells 67

7 National Energy Technology Laboratory: Advanced Fuel Cell Development 72

8 NexTech Materials, Ltd.: Continuous Process for Low-Cost, High-Quality YSZ Powder 77

9 Oak Ridge National Laboratory: Reliability and Durability of Materials and Components for Solid Oxide Fuel Cells 82

10 Pacific Northwest National Laboratory: SOFC Compressive Seal Development at PNNL 90

11 Pacific Northwest National Laboratory: SOFC Anode Materials Development at PNNL 94

12 Pacific Northwest National Laboratory: SOFC Cathode Materials Development at PNNL 97

13 Pacific Northwest National Laboratory: SECA Core Technology Program Activities – PNNL 101

14 Pacific Northwest National Laboratory: SOFC Interconnect Materials Development at PNNL 105

15 Sandia National Laboratory: Reliable Seals for Solid Oxide Fuel Cells 109

16 Tennessee Technological University: Developing Fe-Based Alloys for Intermediate-Temperature SOFC Interconnect Application 113

III SECA Core Technology Program (Continued)

A Materials (Continued)

17 University of Cincinnati: Innovative Seals for Solid Oxide Fuel Cells 117

18 University of Connecticut: Low-Cost Integrated Composite Seal for SOFC: Materials and Design Methodologies....121

19 University of Missouri - Rolla: Resilient and Thermochemically Stable Sealing Materials for Solid Oxide Fuel Cells....125

20 University of Pittsburgh, Materials Science and Engineering Department: Fundamental Studies of the Durability of Materials for Interconnects in Solid Oxide Fuel Cells....129

21 University of Utah: Electrically Conductive, Corrosion-Resistant Coatings through Defect Chemistry for Metallic Interconnects....138

B Fuel Processing....143

1 Argonne National Laboratory: Technology Development in Support of SECA 143

2 ChevronTexaco Corporation: Development of Ni-Based Sulfur-Resistant Catalyst for Diesel Reforming....146

3 Goodrich Turbine Fuel Technologies: Integrated Injection and Mixing Systems for Diesel Fuel Reforming....150

4 Los Alamos National Laboratory: Diesel Reforming for Solid Oxide Fuel Cell Auxiliary Power Units....156

5 National Energy Technology Laboratory: Fundamental Reforming Studies - Role of Catalytic O_2 Supports on Fuel Reforming 162

6 National Energy Technology Laboratory: Hexaaluminate Reforming Catalyst Development 167

7 National Energy Technology Laboratory: Diesel Fuel Reforming Kinetics....171

C Power Electronics 177

1 Oak Ridge National Laboratory: Trade Study for Integrating Numerous SECA SOFC Modules....177

2 Virginia Polytechnic Institute and State University: A Low-Cost Soft-Switched DC/DC Converter for Solid Oxide Fuel Cells 181

D Modeling and Simulation 187

1 Georgia Institute of Technology: An Integrated Approach to Modeling and Mitigating SOFC Failure....187

2 University of Florida: Determination of Electrochemical Performance and Thermo-Mechanical-Chemical Stability of SOFCs from Defect Modeling 194

3 University of Illinois: An Investigation to Resolve the Interaction between Fuel Cell, Power Conditioning System and Application Load 201

4 University of Washington: Advanced Measurement and Modeling Techniques for Improved SOFC Cathodes....209

IV Hybrids....215

1 FuelCell Energy, Inc.: Direct Fuel Cell/Turbine Power Plant 217

2 General Electric: Solid Oxide Fuel Cell Hybrid System for Distributed Power Generation 222

3 National Energy Technology Laboratory: The Hybrid Performance Project (Hyper) 228

V Advanced Research 233

1 California Institute of Technology: Enhanced Power Stability for Proton-Conducting Solid Oxide Fuel Cells 235

2 Pacific Northwest National Laboratory: High Temperature Electrochemistry Center 241

3 University of Florida: Electrocatalytically Active High-Surface-Area Cathodes for Low-Temperature SOFCs 249

4 University of Utah--OSP: Active Cathodes for Super-High Power Density Solid Oxide Fuel Cells through Space Charge Effects 254

VI Small Business Innovation Research (SBIR), Historically Black College and University (HBCU), & University Coal Research (UCR) Projects 259

1 Boston University: Materials System for Intermediate-Temperature SOFC 261

2 Ceramatec, Inc.: Lanthanum Gallate Electrolyte Based Intermediate-Temperature Solid Oxide Fuel Cell Development 266

3 Ceramatec, Inc.: Advanced Net-Shape Insulation for Solid Oxide Fuel Cells 270

4 Duke University: Carbon Ionic Conductors for Use in Novel Carbon-Ion Fuel Cells 275

5 FuelCell Energy: Advanced Control Modules for Hybrid Fuel Cell/Gas Turbine Power Plants 278

6 NexTech Materials, Ltd.: Highly Textured Glass Composite Seals for Intermediate-Temperature SOFCs 282

7 Southern University and A&M College: Dense Membranes for Anode-Supported All-Perovskite IT-SOFC 285

8 TDA Research, Inc: Sorbents for Desulfurization of Natural Gas and LPG 288

9 The Research Foundation of SUNY: Feasibility of a SOFC Stack Integrated Optical Chemical Sensor 293

10 University of Akron: Carbon-based Fuel Cell 297

11 Virginia Tech: Modeling and Design for a Direct Carbon Fuel Cell with Entrained Fuel and Oxidizer 300

VII Novel Generation 305

1 Ramgen Power Systems, Inc.: Development and Testing of a Rotating Supersonic Shock Compressor 307

VIII Acronyms & Abbreviations 311

IX Primary Contact Index 317

I Introduction

I Introduction

The U. S. Department of Energy (DOE) Office of Fossil Energy, through the National Energy Technology Laboratory (NETL), is forging government/industry partnerships to develop a portfolio of fuel cell-based stationary systems for clean, efficient power production.

Fuel cells have long been recognized for their unsurpassed efficiencies and essentially pollution-free and quiet performance. Costs and other technical challenges have prohibited entrance into mainstream power markets. To remove these barriers, NETL has structured unique alliances under the Solid State Energy Conversion Alliance (SECA) to mobilize the nation's scientific community and government and industry resources. Envisioned are cost-competitive fuel cell technologies that, by 2010, can be strategically placed and operated on infrastructure fuels at or near customer sites (distributed generation), and by 2015 integrated into zero-emission coal-based central power systems. These goals equate to removing environmental concerns associated with fossil fuel use while simultaneously establishing a foundation for a hydrogen-based economy and a secure energy future in the United States.

Carl Bauer, Director, National Energy Technology Labroratory

Ralph Carabetta, Principal Deputy, NETL Director, Strategic Center for Coal

The Fossil Energy Fuel Cell Program is managed at the National Energy Technology Laboratory, under the Strategic Center for Coal.

Fuel Cell Research and Development

The Office of Fossil Energy and NETL are pleased to present this FY 2005 Office of Fossil Energy Fuel Cell Program Annual Report, a compilation of abstracts from the fuel cell and distributed generation projects managed through these offices.

Solid State Energy Conversion Alliance. SECA was created to accelerate solid oxide fuel cell (SOFC) development and deployment into the marketplace by making them an affordable option for energy generation. The SECA alliance is comprised of three groups: Industry Teams, Core Technology Program participants, and federal government experts. The Industry Teams design the fuel cells and handle most hardware and market penetration issues. The Core Technology Program, made up of universities, national laboratories, small businesses, and other R&D companies, address fundamental technological issues common to most Industry Teams. Findings under the Core Technology Program are made available to all Industry Teams under unique intellectual property provisions, which serves to accelerate development.

From L to R: Wayne Surdoval (SECA Coordinator), Joseph Strakey (Director, Office of Coal and Power Research and Development), and Mark Williams (Technology Manager, Fuel Cells)

The federal government experts facilitate interaction between Industry Teams and the Core Technology Program, manage the SECA Program, and encourage a national perspective rather than company-specific views in the development effort.

Industry Teams. To achieve cost targets, multiple Industry Teams are engaged in developing 3-10 kW SOFC modules that can be mass produced and aggregated to meet a broad range of applications. This mass customization approach leverages the economies of high-volume mass production and requires reaching a full spectrum of large markets, such as residential-commercial-industrial power, auxiliary power for mobile applications, telecommunications, battery replacement, and similar and specialized applications for the military. Producing a common module for these vast markets will create the opportunity for high-volume production needed to reduce costs.

Team	Design	Manufacturing
Acumentrics	♦ Anode supported-microtubular ♦ 750 °C ♦ Thermally matched materials ♦ Robust & rapid start-up	♦ Extrusion ♦ Dip processing ♦ Spray deposition ♦ Co-sintering
Cummins	♦ Electrolyte supported-planar ♦ 825 °C ♦ Thermally matched materials ♦ Seal-less stack	♦ Tape casting ♦ Screen printing ♦ Co-sintering
Delphi	♦ Anode supported-planar ♦ 750 °C ♦ Ultra compact ♦ Rapid transient capability	♦ Tape casting ♦ Screen printing ♦ 2-stage sintering
FuelCell Energy	♦ Anode supported-planar ♦ < 700 °C ♦ Low cost metals ♦ Thermal integration	♦ Tape casting ♦ Screen printing ♦ Co-sintering ♦ Electrostatic deposition
General Electric	♦ Anode supported-radial ♦ 750 °C ♦ Hybrid compatible ♦ Internal reforming	♦ Tape calendaring ♦ 2-stage sintering
Siemens Westinghouse	♦ Cathode supported-flattened oval ♦ 800 °C ♦ Seal-less stack	♦ Extrusion ♦ Plasma spray

SECA Industrial Team Design and Manufacturing

Core Technology Program. The Core Technology Program provides comprehensive applied research support in six thrust areas. This structure and the provisions in place reduce costs by leveraging resources so that all six teams do not engage in separate fundamental research programs. The approach also ensures that only major issues are addressed. The core technology areas are as follows:

- Materials – Researches kinetics and mechanisms of material failures, and identifies new techniques and materials to overcome challenges and reduce cost;
- Fuel Processing and Reforming – Investigates reforming technologies that remove impurities from fuels and enable efficient operations;

- Manufacturing – Explores new manufacturing techniques that hold promise for achieving the SECA cost targets at realistic production volumes;
- Controls and Diagnostics – Optimizes instrumentation and controls requisite to safe, efficient operation of fuel cells and balance-of-plant systems;
- Power Electronics – Optimizes fuel cell power system efficiency in conversion of fuel cell output to usable DC (direct current) and AC (alternating current) power;
- Modeling and Simulation – Creates precise models to aid developers in predicting behavior and identifying areas of improvement in fuel cells and fuel cell power systems.

Dave Berry in the NETL Fuel Processing Facility, part of the Core Technology Program. NETL is applying extensive experience gained in gasification and synthesis gas-related R&D to reforming diesel and middle distillate transportation fuels for fuel cell-based auxiliary power unit applications. Activities include research into the role of oxygen in catalyst performance and sulfur tolerance, exploring new catalysts with improved thermal stability and resistance to carbon formation, and studying the kinetics of diesel reforming.

Randy Gemmen in front of the DOE Fuel Cell Test Facility. The facility, which was designed to support the SECA program, is configured with both AC- and DC-load banks and can accommodate fuel cells up to 10 kilowatts in size. The facility can be used to provide independent verification of the performance and efficiency of prototype fuel cells developed by SECA Industry Team.

Dave Tucker at the NETL Hybrid Performance Facility (HYPER). The HYPER facility is being used to develop control strategies for the reliable operation of fuel cell turbine hybrids. The facility provides a unique opportunity for researchers to explore issues related to coupling fuel cells and gas turbines. While efficiency benefits of hybrids are well recognized, controlling the flow of power from both the fuel cell and turbine during load changes presents challenges stemming from significantly different operating characteristics and response times.

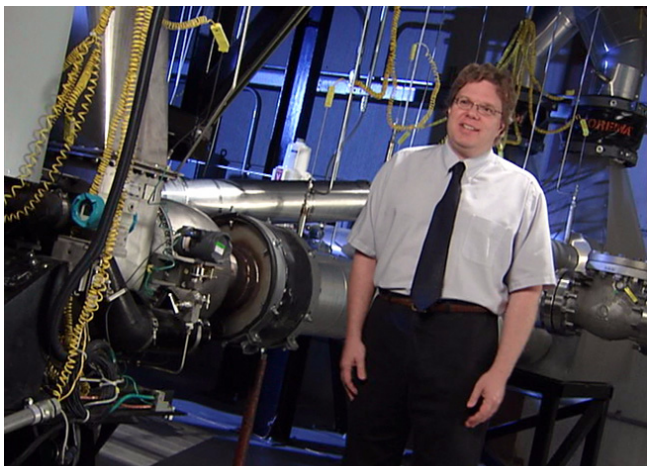

Fuel Cell Turbine Hybrids. The Hybrids Program provides research advances in fuel cell turbine hybrid systems by linking technologies to generate electricity from coal syngas at high efficiencies. Power-producing systems that contain a combination of high-temperature fuel cells and gas turbines have the potential for ultra-high efficiency in converting fossil fuels to electricity. The combined efficiency of a hybrid system can be raised to greater than 70 percent, and NOx, sulfate, and particulate emissions are essentially eliminated while carbon dioxide emissions are reduced significantly.

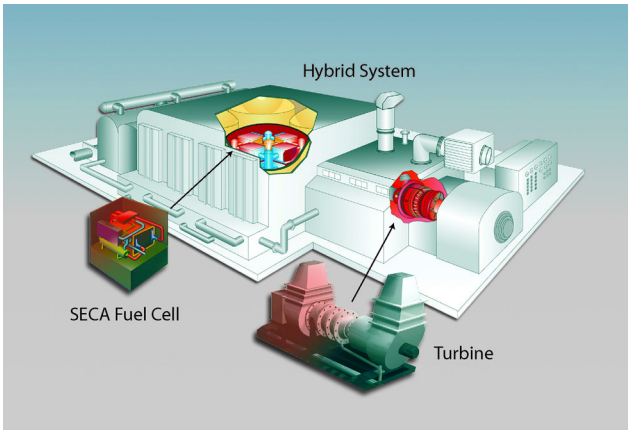

SECA Fuel Cell Turbine Hybrid System

In FY 2005, the Office of Fossil Energy launched an initiative to begin the process of integrating SECA SOFCs showing the most promise for scale-up into the FutureGen-type central power system (greater than 100 MWe, 60 percent efficient higher heating value, 90 percent carbon dioxide capture, and $1000/kW or less capital cost). The objective of the program is to have a SECA SOFC-based power island that costs $400/kW with 50 percent efficiency (HHV). SECA SOFCs are to provide the majority of the power, whether applied in a stand-alone or fuel cell turbine hybrid configuration.

Advanced Research in Electrochemistry. The High Temperature Electrochemistry Center (HiTEC) was formed in 2002 to provide crosscutting, multidisciplinary research that leads to advanced electrochemical technologies to minimize the environmental consequences of using fossil fuels in energy generation. HiTEC supports all areas of the Fuel Cell Program by developing electrochemical energy-conversion technologies, such as energy storage using electrochemical concepts, reversible fuel cells, and membranes. The program objectives are to reduce fuel cell stack costs, shorten development time, and increase fuel flexibility of fuel cells.

FY 2005 Key Program Accomplishments

Virginia Polytechnic Institute and State University Develops a Converter That Can Boost Low DC Voltage to Household and Commercial Applications

Researchers at Virginia Polytechnic Institute and State University developed a highly efficient converter that can boost low DC voltage produced by SOFC stacks to the higher voltage required for conversion to AC for household and commercial applications. The boost is significant because it provides another technological step in increasing the efficiency and reducing the size and cost of fuel cells.

Siemens Westinghouse's Next-Generation High Power Density Cell Demonstrates Significant Improvements

Siemens Westinghouse Power Corporation (SWPC) initiated fabrication and testing of its next-generation high power density (HPD) cell design, Delta9, that shows significantly increased power. This achievement will help SWPC to meet power density and cost targets under the SECA program. SWPC's Delta9 corrugated design has built-in fuel channels that allow for a more compact stack design with a shorter current path and lower cell resistance, resulting in increased power density.

Delphi Successfully Tests their First Fully Independent Stationary Power Unit

Delphi Automotive Systems and Battelle Columbus Laboratories, one of six SECA Industry Teams, has successfully completed the initial test sequence on the first fully independent stationary power unit (SPU). The Delphi SPU, operating independently of the grid, produced a peak net power output of 1.5 kW. The system was able to support parasitic loads and externally applied loads. This new Generation 3 system surpassed several standing milestones, including gross power output, net power output, system run-time, and system efficiency. This system integration achievement constitutes a strong step forward into meeting the SECA Phase I system targets.

FuelCell Energy Successfully Operates Their 3-kW SECA SOFC System for 1,000 Hours

FuelCell Energy and Versa Power Systems, one of six SECA Program Industry Teams, tested the operation of their 3-kW SOFC system and reported successful operation for more than 1,000 hours. The 3-kW system, supplied with city pipeline natural gas fuel, has been successfully operated independently and has produced an average gross DC power of 3.65 kW and an average net power AC output of 2.80 kW. An automated control system manages the entire process, allowing the system to run unattended. The test that is currently being performed is significant because it is facilitating the operation of a SOFC stack under actual system conditions.

Fuel Cell Project Manager is Rookie of the Year!

The Department of Energy's very own Shawna Toth was awarded this year's Gold Award in the Pittsburgh Federal Executive Board's Rookie of the Year category. Shawna is a Project Manager in the Power Systems Projects Division at the National Energy Technology Laboratory. This past year, Shawna rapidly learned about the entire Fuel Cell Technology Area and coordinated project data for over 50 projects and 6 project managers to formulate budget tables and program implementation plans for the $78 million program. In addition to her exemplary project management work, Shawna led an initiative last year to investigate the process time and resource consumption for processing proposal reviews, selections, and contractual award negotiations. The results of Shawna's efforts are widely viewed as highly beneficial, have been adopted by several other project management divisions, and have been shared with DOE personnel working on the President's E-Government Initiative.

Shawna Toth Receives Gold Award

GE Improves Fuel Cell Performance

In the race to speed SOFC technology out of niche markets and into widespread commercial use, GE Hybrid Power Generation Systems has kicked fuel cell performance into high gear. GE researchers have increased power density while maintaining efficiency and reliability with the development of full-size single-cell SOFC modules that consistently achieve a power density of 520 milliwatts per square centimeter at 80 percent fuel utilization and 480 milliwatts per square centimeter at 88 percent fuel utilization. This represents about an 80 percent increase over their 2004 baseline performance. The cells have also demonstrated stable operation at 95 percent fuel utilization—a record for full-size planar SOFCs.

DOE Awards $1.4 Million for Electrochemistry–Fossil Fuel Energy-Conversion Research

The Department of Energy's High Temperature Electrochemistry Center (HiTEC) has awarded $1.4 million to support five research projects that will foster novel electrochemical-based power generation and energy storage technologies for use in large, central coal-fired power plants. Advances in electrochemistry—the interconversion of electrical and chemical energy—will enable the power industry to maximize efficiency while minimizing the environmental effects of using fossil fuels.

Project results are expected to benefit the President's FutureGen and Global Climate Change Initiatives, which seek to reduce and then eliminate power plant emissions, advance hydrogen as a viable source of electric power, and reduce greenhouse gases while strengthening the outlook for U.S. and global economies. Expected benefits include:

- Highly efficient energy technologies and expanded energy choices.
- Power generation and energy storage technologies with near-zero emissions.
- Low-cost electrochemical process materials and systems that are modular and scalable to help meet a growing worldwide demand for energy.

The projects will be managed for the Department of Energy by NETL and are listed below:

- Photo-Activated Low-Temperature Micro Fuel Cell Power Source
- The Techno-Economic Feasibility of Highly Efficient, Cost-Effective, Thermoelectric SOFC Hybrid Power-Generation Systems
- The Use of High-Temperature Electrochemical Cells for the Co-Generation of Chemicals and Electricity
- A High-Temperature Electrochemical Energy-Storage System Based on Sodium Beta-Alumina Solid Electrolyte (BASE)
- The Effect of Coal Contaminants on Solid Oxide Fuel Cell System Performance and Service Life

Coal-Based Fuel Cells: A Giant Leap for Fuel Cell Technology

The Department of Energy awarded the first two projects selected under the new Fuel Cell Coal-Based Systems Program. The projects will be conducted by two research teams: one led by General Electric Hybrid Power Generations Systems and the other by Siemens Westinghouse Power Corporation. They share the same goal: to develop the fuel cell technology required for central power stations to produce affordable, efficient, environmentally friendly electricity from coal.

The two teams will research, develop, and demonstrate fuel cell technologies that can support power generation systems larger than 100 megawatts capacity. Key system requirements to be achieved include:

- At least 50 percent overall efficiency in converting the energy contained in coal to grid electrical power.
- Capture of 90 percent or more of the system's carbon dioxide emissions.
- Cost of $400 per kilowatt, exclusive of the coal gasification unit and carbon dioxide separation subsystems.

Summary

The fuel cell technology being developed by the SECA Program is building a bridge between today's fossil fuel energy economy and tomorrow's hydrogen economy. As these progress reports show, the SECA Program is on track to meeting its goals of producing efficient, affordable, low-emission, and robust fuel cells that are able to operate using the current fuel production and distribution infrastructure. The combination of basic R&D and application of the new technologies developed by the Industry Teams is proving to be highly effective. The fuel cell technology being developed by SECA has application to residential and commercial power, industrial combined heat and power, transportation auxiliary power units, and eventually, mega-watt scale units for advanced power plants using coal with high efficiency and very low emissions. Together with other DOE programs, the Office of Fossil Energy is working towards a future with reduced dependence on petroleum, an improved environment, and expanded economic opportunities. The following reports describe how the projects currently underway will help us to build that future.

II SECA Industry Teams

II SECA Industry Teams

II.1 Development of a Low-Cost 10-kW Tubular SOFC Power System

Norman Bessette
Acumentrics Corporation
20 Southwest Park
Westwood, MA 02090
Phone: (781) 461-8251; Fax: (781) 461-8033; E-mail: nbessette@acumentrics.com

DOE Project Manager: Don Collins
Phone: (304) 285-4156; E-mail: Donald.Collins@netl.doe.gov

Objectives

- Design a common low-cost generator to meet all chosen markets.
- Develop an anode-supported micro-tubular cell capable of twice the power density presently achieved.
- Design, build, and test an inverter with 94% efficiency for conversion from direct current (DC) to alternating current (AC).
- Test prototype of a natural gas fueled unit meeting and exceeding Solid State Energy Conversion Alliance (SECA) goals.

Approach

- Increase the current collection points per tube to increase cell power.
- Improve anode conductivity and stability to allow a greater power per unit length of cell tube.
- Decrease solid oxide fuel cell (SOFC) generator component costs through advanced manufacturing techniques.
- Perform preliminary testing on liquid fuels to determine critical operating parameters.
- Develop the AC/DC high-efficiency conversion end building off our existing 98% efficient DC/DC regulator.

Accomplishments

- *Demonstrated Cell Power Density Increases from 150 to 297 mW/cm^2:*
  Different geometry cells have been manufactured and tested showing the viability of doubling the power per tube. This has been accomplished by adjusting the anode tube chemistry while also changing the number of current collection points on the tube. This accomplishment has the ability to cut the required number of tubes per kilowatt in half and also dramatically reduce the size of the fuel cell generator.
- *Implemented Advanced Generator Manifolds Reducing Cost by over $1000/kW:*
  One of the first advanced manufacturing techniques pursued to decrease overall cost of the SOFC generator was validated. A metal injection molding (MIM) process that was previously only capable of making low-temperature aluminum parts was developed to net shape cast high-temperature metal parts. This process allows for the saving of many labor hours of machining and overall cost reduction of the SOFC generator.

- *Demonstrated Generator Operation on Diesel and Synthetic Diesel Fuel:*
  A 5-kW SOFC generator has been tested and proven to operate successfully on liquid diesel fuel. This unit also operated on synthetic diesel fuel made by renewable domestic sources. The unit was baseline tested on natural gas and found to have nearly identical performance on liquid fuels as on natural gas.
- *Demonstrated an Advanced Heat Exchanger Capable of Meeting SECA Phase I Cost Targets:*
  During the past year, a number of advanced heat exchangers have been tested. A heat exchanger design that integrates the geometries of a shell and tube heat exchanger and a flat plate heat exchanger has achieved high electrical efficiency and low cost.
- *Independent Audit of SECA Phase I Cost and Performance Goals Successfully Completed:*
  In keeping with the Government Performance and Results Act, an independent audit of the Acumentrics program was completed by Spencer Management Associates and Argonne National Laboratory to determine the technical risk of meeting the SECA Phase I cost and performance targets. The program requires achieving <$800/kW and stable operation over 1500 hours to pass the first gate of the program. It was determined that Acumentrics should exceed the cost targets, and the probability of achieving performance goals is high.

Future Directions

- *Complete Full-Scale Testing of Multiple Current Collection Cells:*
  Preliminary testing has been completed on a number of cells showing multiple electrical take-offs. Further work is required to electrically test a number of these cells to demonstrate long-term stability as well as repeatability and thermal cycle toughness. Upon completion of this testing, cells will be validated for production and utilization in the Phase I test unit.
- *Complete 95%-Efficient Inverter Development:*
  With the integration of an inverter capable of over 95% efficiency versus the market standard of 82-90%, overall system efficiencies can rise by nearly 5 percentage points. This improvement in overall efficiency can be equated to fuel savings to reduce the overall cost of electricity. Another option is to operate the fuel cell stack at a lower cell voltage point, thereby increasing the individual cell power and reducing the number of fuel cells and the overall capital cost.
- *Complete SECA Phase I Generator Performance Testing:*
  The SECA Phase I generator design is nearing completion, and key components are going through validation testing at this time. As these tests are completed, the final bill of materials will be generated for the prototype machine. The machine will be built during the next year, and a test plan will be finalized between Acumentrics and the DOE project manager. The unit will then be tested according to this plan.

Introduction

The Acumentrics SECA program has focused on the design and manufacture of micro-tubular SOFC power systems approaching twice the power density now achieved with state-of-the-art anode-supported tubular designs. As a result of DOE funding and a focused research effort, these cells are now very near to achieving this goal. These units will be capable of entry into the telecommunication, remote residential, and military markets. Operation on fuels including natural gas and propane will be developed for the telecommunication and remote residential markets. Operation on liquid fuels, including diesel and JP-8, will be developed for the military markets.

Working with Acumentrics to define market segments and market requirements are a number of key investors that are strategic players in their respective markets. They include:

- Chevron for remote markets and liquid fuels.
- General Dynamics for liquid fuels as well as military operations.
- Northeast Utilities and NiSource for integration in the natural gas and electricity infrastructure.
- Sumitomo Corporation of Japan for product definition and introduction into the Japanese market.

Approach

To achieve the final SECA goal of a manufactured unit cost of less than $400/kW, work can focus on increasing cell power, thereby decreasing the number of cells per kilowatt, or it can focus on decreasing the cost of each component. With such an aggressive goal, work must address both paths. To increase cell power, work is centered on improved materials as well as enhancements in geometry. Cells with increased anode conductivities to decrease electrical bus losses are being investigated. Improved conductivity of cathodes is also being investigated to decrease the potential loss associated with the electrochemical reaction on the airside. Increases in cell tube diameter as well as multiple contact points along the length are also being studied.

For subsystem cost reductions, the machine is divided into four major sub-systems: the SOFC generator, the control system, the power conditioning system, and the fuel and airflow system. In the SOFC generator, advanced materials and manufacturing techniques are being investigated, including metal injection molding (MIM) as well as metal stampings. Vacuum cast insulation to near net shape is also being considered. For the control system, a Controller Area Network bus architecture is being developed, and control of all valves and power electronics is being integrated. For the power electronics sub-system, the focus is on improving the overall DC/AC conversion efficiency to avoid excessive losses which compromise overall system efficiency and require more cells and therefore more cost. In the air and fuel sub-system, removal of redundant components as well as qualification of equivalent components at lower cost is the path chosen.

Results

In an attempt to increase the overall power per cell, work has focused on optimizing the geometry of the fuel cell as well as the performance of the individual layers. Work on the anode tube has comprised changes in the overall composition to improve conductivity as well as introduction of higher-conductivity internal layers. Over the past year, cells with higher-conductivity internal layers

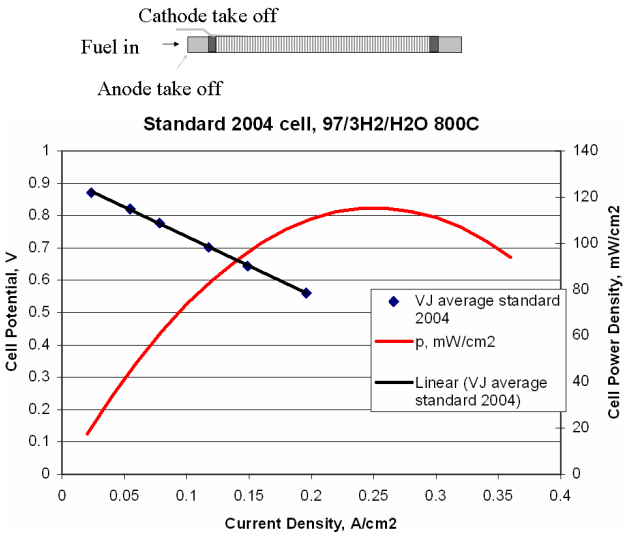

Figure 1. Standard Cell Performance

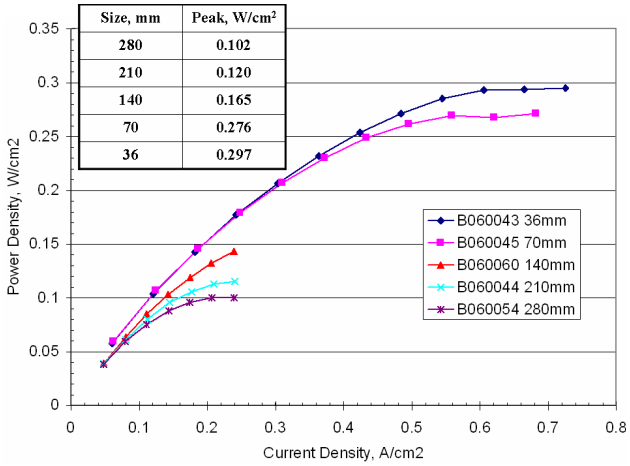

Figure 2. Power Density Advancements (800°C, 75% fuel utilization)

have achieved substantial power gains. Cells have now completed over one year's continuous testing. During that one year of testing, the degradation has been less than 1%/500 hours, which is substantially better than the SECA Phase I requirement of 2%/500 hours.

In addition to improved anode conductivity, work has focused on cell geometry and multiple take-off connections. Since the current Acumentrics design requires power take-off at a single end, the peak power density remains at 115 mW/cm^2, as seen in Figure 1. To determine length effects, multiple cells of increasing length were tested. As seen in Figure 2, the peak power density approaches 300

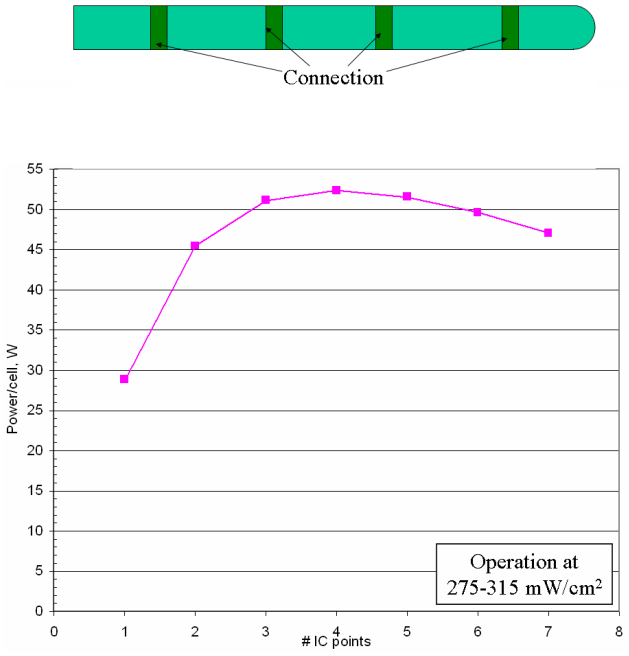

Figure 3. Multiple Take-off Cell

Figure 4. MIM Manifold & Cap Samples

mW/cm^2 as the overall length decreases from 280 mm to 36 mm. To take advantage of this phenomenon, a tube must be designed with multiple take-offs, allowing for longer-length tubes achieving the power density of shorter-length tubes. Figure 3 shows such a tube design which analytically has been shown to achieve greater than 50 W, or nearly 300 mW/cm^2. This cell design is presently being fabricated and undergoing initial high-temperature testing. If fabrication is successful, the existing SOFC generators will be able to achieve the same power level with 50-65% fewer fuel cells, resulting in significant cost and size savings.

On the topic of advanced manufacturing for generator components, a number of significant accomplishments can be reported. Metal injection molded manifolds have been fully validated for performance at high temperatures. The MIM process allows for intricate shapes, such as the fuel manifolds for SOFCs, to be made in a process similar to that of injection molded plastics. To date, this process has been limited to simple aluminum components, but through research with a number of vendors, application of the process has been expanded to include parts made of high-temperature alloys. Figure 4 shows not only the manifold but also the braze cap made from the MIM process. This advancement reduces the cost of the total SOFC generator by nearly $2000/kW and provides a process capable of meeting the SECA cost targets.

Another advancement in generator components has been in the thermal recovery area. Tests have been performed on both ceramic and metallic heat exchangers with reasonable success. Metallic recuperators have been designed by combining the positive features of both shell and tube as well as flat plate heat exchangers. This new design allows for high thermal effectiveness, which aids overall system electrical efficiency, resulting in low overall cost. The unit also results in low pressure drop, allowing it to be easily integrated into the existing natural gas fuel infrastructure located in the United States without the need for costly and inefficient boost compressors. At the same time, ceramic heat exchangers have been designed and tested which would provide a further cost reduction beneficial to the later stages of the SECA program. These units to date have performed reasonably well on thermal cycle testing but have not achieved the overall thermal effectiveness needed for the design. Further work will concentrate on improving that thermal effectiveness through changes in the airflow geometry.

To boost the overall system efficiency, a DC/AC inverter was further advanced which has an overall conversion efficiency of over 94%. This unit, when fully developed, has the ability to replace an existing inverter package that is 86-87% efficient. This would then result in a boost in overall generator system efficiency of over 3 points. Another advantage of this design is the usage of many components being developed for the 48V automotive conversion which is occurring at this time. This will allow for leveraging of the volume cost reductions seen in the automotive industry into the fuel cell industry.

Conclusions

Continual advancements have been made toward the SECA cost and performance targets in the Acumentrics SOFC program. Cell power advancements outlined before the program have been achieved. Cost reductions in certain key fuel cell stack components have been validated and implemented in demonstration units. Further work on all of these tasks will be performed to achieve the ultimate goal of $400/kW.

FY 2005 Publications/Presentations

1. "Status of the Acumentrics SOFC Program", N.F. Bessette, Presented at the Annual SECA conference, Pacific Grove, CA., April 18, 2005.

II.2 10-kW Solid Oxide Fuel Cell Power System Commercialization

Daniel Norrick
Cummins Power Generation
1400 73rd Avenue NE
Minneapolis, MN 55432
Phone: (763) 574-5301; Fax: (763) 528-7229; E-mail: Daniel.a.norrick@cummins.com

DOE Project Manager: Don Collins
Phone: (304) 285-4156; E-mail: Donald.Collins@netl.doe.gov

Subcontractors:
SOFCo-EFS Holdings LLC, Alliance, Ohio

Objectives

- The objective of the Cummins Power Generation (CPG) and SOFCo-EFS Holdings LLC (SOFCo) Solid State Energy Conversion Alliance (SECA) development program is to demonstrate the SECA Phase 1 solid oxide fuel cell (SOFC) objectives through technical progress in the following areas:
- SOFC stacks that achieve target performance, stability, and cost.
- Waterless catalytic partial oxidation (CPOX) reforming process that efficiently and cost-effectively converts natural gas or propane into a hydrogen-rich synthesis gas for mobile applications.
- SOFC hot box (an insulated enclosure containing SOFC stacks, manifolds, heat exchangers, start-up burner, and reformer) design that is compact and can be mass-produced at a cost meeting the SECA Phase 1 cost target.
- SOFC system balance of plant, including air and fuel supply systems, that meets the cost and reliability targets.
- A control system to manage the SOFC power system, including regulation of fuel and air flows, management of electrical power generation, and load sharing. The control system must operate in conjunction with an energy storage system through start-up, steady-state and transient loads, and shut-down, including emergency shut-down, without damage to the SOFC stack.
- An efficient electrical power conditioning system to convert DC voltages and invert to produce useable AC output.

Approach

The CPG-SOFCo approach coordinates development in the following major areas:

- Planar solid oxide fuel cell, ceramic interconnect, and stacks
- Planar SOFC manufacturing and scale-up for economic manufacturing
- Dry CPOX fuel reforming
- Fuel cell balance of plant (BOP)
- Fuel cell and power electronics system controls
- Power conditioning

Specifically, the CPG-SOFCo team is conducting the following work:

- Develop and evaluate advanced solid oxide fuel cells that provide the required performance and are compatible with the SOFCo ceramic interconnect.

- Conduct a progressive sequence of SOFC stack tests to validate development of materials and assembly methods for useable stacks that can achieve high fuel utilization (good sealing) and low degradation rates.
- Develop a CPOX reforming process and scale-up to system-sized units.
- Design and develop a hot box subsystem which can be delivered to CPG for integration into complete SOFC power systems.
- Develop control hardware and software required to regulate system operation.
- Integrate the BOP components, hot box subsystem, and controls into a working deliverable prototype. Initiate prototype operation with stack simulators for system shakedown, followed by installation of SOFC stacks and operation of the full prototype through the SECA Phase 1 test sequence.

Accomplishments

- Advanced scandia-stabilized zirconia (ScSZ) electrolyte-supported cells demonstrated improved cell performance.
- Degradation of short stacks was reduced to approximately 3% per 500 hours.
- Fuel utilization in excess of 80% with natural gas reformate was demonstrated, confirming the viability of SOFCo's stack assembly method and the materials used for seals and electrical contacts between the cells and interconnects.
- Dry (waterless) CPOX reforming for natural gas and propane was successfully demonstrated. The bench-scale CPOX reactor was scaled up for use in a 5-kilowatt-scale prototype system, demonstrated and characterized for carbon-free operation in the design operating range.
- Control hardware and software have been developed to provide steady-state and transient control of a SOFC system.
- A kilowatt-scale prototype (C1) operated for over 600 hours on natural gas reformate during characterization for system control design. Testing on the C1 prototype validated system models and control algorithms, and provided valuable information on system transient response.
- A 5-kilowatt, thermally integrated, four-stack hot box assembly comprising stacks, manifolds, recuperator, CPOX reformer, start-up burner, insulation, and structural housing has been designed and constructed for the C2 deliverable prototype.
- The C2 deliverable prototype balance of plant, including air and fuel supply systems, is nearing completion and scheduled to begin testing in August.
- Progress has been made with cost-effective BOP utilizing high-volume, low-cost, mass-production components from industrial and automotive sources.

Future Directions

- Refine the composition and microstructure of the electrodes for the advanced electrolyte-supported cell as required to achieve the Phase 1 target performance.
- Use instrumented short stacks and continued optimization of materials and stack design to assemble stacks that further reduce the non-cell contributions to resistance and power degradation rates.
- Complete the compilation of design information to support final cost estimating.
- Complete the final tailoring and development of the DC boosts for the fuel cell and battery system.
- Complete the development of the control system and integration with the fuel cell, balance of plant, and power electronics.
- Conduct the SECA Phase 1 evaluation test, including steady-state and transient evaluations, and report results to the National Energy Technology Laboratory (NETL) before shipping the unit to NETL for evaluation.

Introduction

Solid oxide fuel cell power systems offer the potential to generate electrical power from hydrogen or hydrocarbon fuels cleanly and efficiently. The objective of the CPG-SOFCo project is to design and develop a 3-10 kW SOFC-based power system that can be competitive with existing small diesel generating systems in terms of cost and package size, but offer significant benefits in efficiency, emissions, lower noise and vibration. Achieving these objectives requires advancement in five major areas:

- Cell, interconnect, and SOFC stack performance and robustness
- Optimizing manufacturing processes for production of cells, interconnects, and stack assemblies
- System design, thermal integration, and packaging of the hot components and sub-systems, including stacks, fuel reformer, and heat exchangers, and insulation system
- Control system for regulating air and fuel flows to the stacks in proportion to electrical load and operating temperatures, and for managing electrical load distribution between the fuel cell and batteries during steady-state and transient loading
- Electrical power conditioning, including DC voltage boosts (converters) and DC to AC power (inverter)

The team has made significant progress in all five areas during 2005 and is on schedule to meet the objectives of Phase 1 of the SECA program.

Results

Development work has continued to improve cell performance, primarily through the development of scandia-stabilized zirconia electrolytes to improve ionic conductivity and reduce cell area-specific resistance (ASR). Through this work, ASRs have been reduced and are approaching the Phase 1 target value (Figure 1).

In addition to improvements in cell and stack ASR, stacks have been developed to provide improved degradation performance. The linkage between cell improvement and stack improvement is

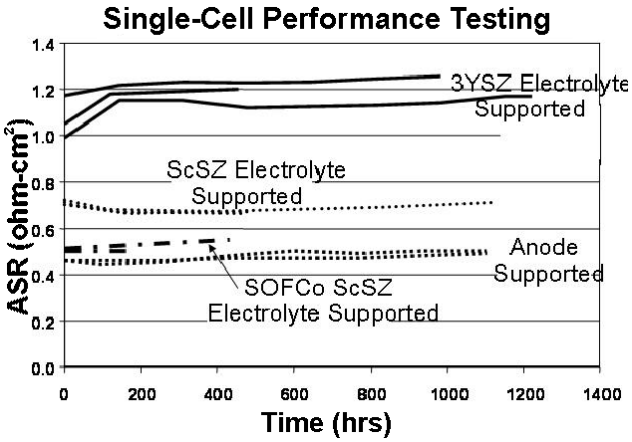

Figure 1. Progressive ASR Reduction

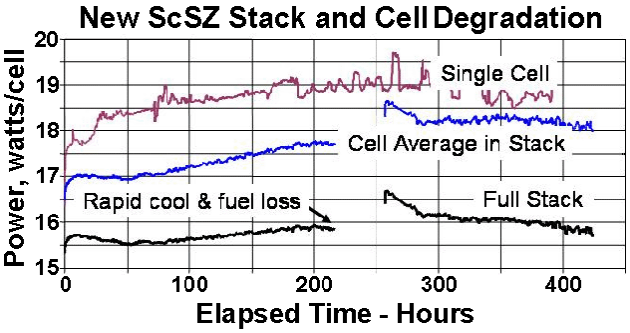

Figure 2. Cell Improvement in Stacks

illustrated in Figure 2. Typical stack power degradation at constant voltage has been improved to 3% per 500 hours (Figure 3), nearing the Phase 1 target of 2% per 500 hours.

Carbon-free dry (waterless) CPOX reforming for natural gas was successfully demonstrated. A kilowatt-scale CPOX reactor was scaled up for use in the 5-kilowatt deliverable system. Long-term testing with natural gas showed carbon-free stable operation, and stacks operated on the reformate demonstrated no problems through extended testing.

A progression of stack tests have validated the stack assembly process and the integrity of the stack sealing system. Stacks of up to 70 cells have been constructed and tested. A typical 70-cell stack installation in a stack test fixture is shown in Figure 4. Target fuel utilization of 80% has been demonstrated on stacks of all sizes.

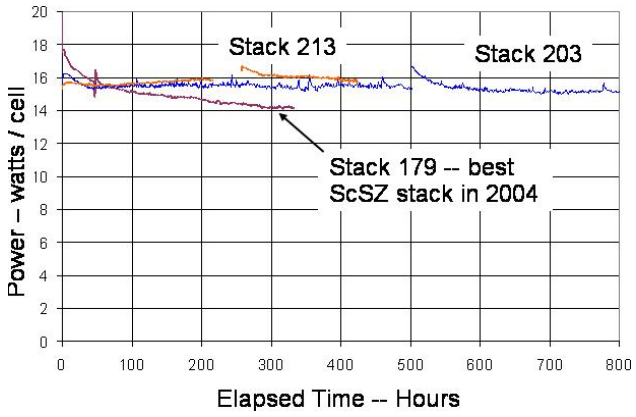

Figure 3. Improved Stack Degradation

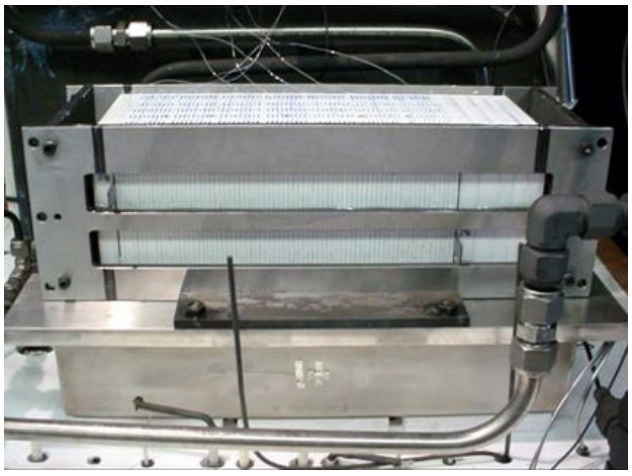

Figure 4. 70-Cell Stack in Stack Test Fixture

Design and manufacturing work to scale-up the ceramic interconnect from approximately 10 by 10 cm to 15 by 15 cm has demonstrated the ability to produce high-quality parts meeting design requirements at lower specific manufacturing costs.

Testing of a kW-scale demonstrator unit at CPG in Minneapolis has provided valuable information validating system modeling and control strategy. During testing, CPG-developed controls exhibited excellent steady-state and transient stability and response.

CPG demonstrated a high-efficiency inductor-based DC-DC boost system which will be used to control current flow and voltage supply to the inverter section from the fuel cell stacks and from the batteries. A second transformer-based DC-DC bi-directional boost is developed to provide and regulate a mix of energy flows from the fuel cell and the system's battery pack.

Conclusions

- Electrolyte-supported cells with ScSZ electrolytes provide improved SOFC performance.
- Planar SOFC stacks in the range of 70 repeat units can be constructed and successfully operated at high fuel utilizations.
- A dry (waterless) catalytic partial oxidation reformer system can provide a suitable fuel stream from commercial natural gas without sulfur removal and without forming carbon.
- A compact kilowatt-scale SOFC power system can be started and operated within design parameters in both steady-state and transient operating modes.

FY 2005 Publications/Presentations

1. "Planar SOFC Stack with Low-Cost Multi-Layer Ceramic Interconnect", Z. Liu, E. Barringer, R. Goettler, Ninth International Symposium on Solid Oxide Fuel Cells (SOFC IX) in Quebec City, Canada, May 17, 2005 (available at www.sofco-efs.com).
2. K. Kneidel et al, "Development of SOFC Power Systems Using Multi-Layer Ceramic Interconnects", 2004 Fuel Cell Seminar Abstracts, pp.109-112., November 2004.
3. D. Norrick, "10kWe SOFC Power System Commercialization Program Progress", SECA Annual Workshop, April 20, 2005, Monterey, CA (available at www.cummins.com).

II.3 Solid State Energy Conversion Alliance Delphi SOFC

Steven Shaffer (Primary Contact), Mike Faville, Sean Kelly, Karl Haltiner, Subhasish Mukerjee, David Schumann, Gail Geiger, Larry Chick, John Absmeier, John MacBain
Delphi Automotive Systems LLC
5725 Delphi Drive
Troy, Michigan 48098
Phone: (585) 359-6615; Fax: (585) 359-6061; E-mail: steven.shaffer@delphi.com

DOE Project Manager: *Magda Rivera*
Phone: (304) 285-1359; E-mail: Magda.Rivera@netl.doe.gov

Subcontractors:
Battelle/Pacific Northwest National Laboratory, Richland, WA
Electricore, Inc., Valencia, CA

Objectives

- Develop a 5-kW solid oxide fuel cell (SOFC) power system for a range of fuels and applications.
- Develop and demonstrate technology transfer efforts on a 3-10 kW stationary distributed power generation system that incorporates endothermic reforming of methane, and then natural gas.
- Initiate development of a 5-kW system for future mass-market automotive auxiliary power unit applications, incorporating endothermic reforming of gasoline.

Approach

- Develop and test major subsystems and individual components as building blocks for applications in targeted markets.
- Integrate major subsystems and individual components into a "close-coupled" architecture for integrated bench testing.
- Integrate major subsystems and individual components into a stationary power unit (SPU) for the stationary market.
- Integrate major subsystems and individual components into an auxiliary power unit (APU) for the transportation market.

Accomplishments

- Gen 3 cassettes (repeating units for stack) were successfully fabricated and tested. The Gen 3 cassettes have a 50% reduction in thickness and weight compared to Gen 2 cassettes. The cassettes are fabricated using high-volume manufacturing processes like stamping, brazing and laser welding.
- Over twenty Gen 2 stack subsystems were built and tested. Power density of 420 mW/cm^2 at 0.7 V/cell at 750°C was achieved in the stack laboratory with simulated recycle reformate. Thermal cycling tests in a furnace with 60 minutes heat-up from room temperature to 750°C demonstrated five thermal cycles with minimal degradation.
- Demonstrated 1617 W gross power in a Gen 2 APU. Solid model design geometry, computational fluid dynamics (CFD), finite element analysis (FEA), and thermal analysis were completed for the Gen 3 APU. Particular attention was placed on system pressure drop and thermal management concerns.
- Thirty-cell Gen 3 stacks were fabricated and tested (see Figure 1). Power density of greater than 500 mW/cm^2 at 0.7 V/cell at 750°C was achieved with simulated reformate.

- Extensive CFD analysis was completed on the integrated component manifold (ICM), process air module (PAM), and cathode air heat exchanger (CHEX) to reduce pressure drops within specified allocations and improve the temperature gradients in the SOFC plant.
- A new commercial combustible gas sensor has been sourced, and prototype samples have been ordered for possible implementation as part of system safety and diagnostics.
- The catalytic partial oxidation (CPOX) reformer has been further developed. Both gasoline and methane CPOX reformers are under test. We are currently developing the endothermic methane/natural gas and gasoline reformer technology. This technology will be utilized in the SPU demonstration system.
- A cart-based endothermic reformer/stack system was successfully tested for over 300 hours with reformate quality well within specified requirements.
- Designed a full-scale development system.
- Prepared initial detailed system cost estimate.

Figure 1. Gen 3 Solid Oxide Fuel Cell 30-Cell Stack

Future Directions

- Design, build and test a full-scale SPU demonstration system during Q2-Q4, 2005.
- Finalize detailed system cost estimate during Q3-Q4, 2005.
- Test the Delphi Demonstration System A SPU and operation of the system at the DOE National Energy Technology Laboratory site in Q4, 2005.

Introduction

The objective of this project is to develop a 5-kW solid oxide fuel cell power system for a range of fuels and applications. Delphi is developing a 3-10 kW system for stationary distributed power generation applications that incorporates endothermic reforming of natural gas. Delphi is also initiating development of a 5-kW system for later use in a mass-market automotive auxiliary power unit. The automotive unit will incorporate endothermic reforming of gasoline.

These two complementary fuel cell systems will be introduced to their respective markets: the distributed power generation market for electric power and the transportation systems market for advanced automotive power trains. Developing both industrial and transportation applications based on similar components increases the potential production volumes of the components and therefore reduces the potential cost.

Approach

Delphi's approach is to evaluate components and subsystems at increasingly integrated levels. The system integration levels are Level 0, Level I, and Level II. Level 0 integration represents the individual testing and development of the major subsystems and components. Level I integration represents the close coupling of the major system modules such that all major system functions are represented and functional during the test. Level II integration represents the final product package, integration, and function for the SOFC power plant, or APU as shown in Figure 2. In the laboratory, a stand is employed to hold the product and facilitate fuel, air, electrical, and exhaust connections, but the intended construction and function of the system should be representative of product intent at this integration level.

Figure 2. SOFC APU System Modules

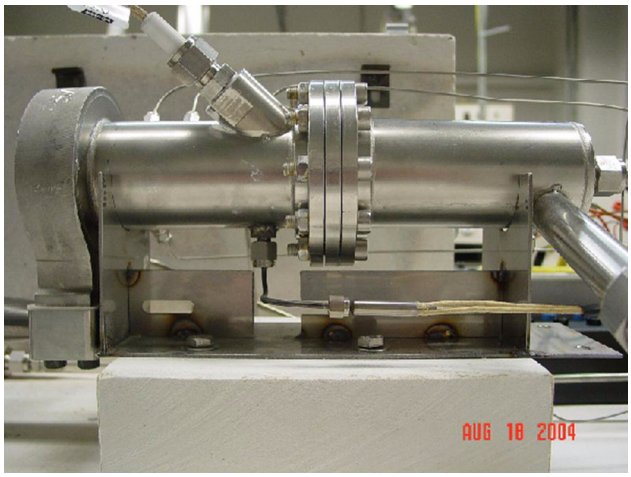

Figure 3. Tubular CPOX Reformer Assembly

Results

The Generation 3 (Gen 3) auxiliary power unit (APU) was adapted for use as a stationary power unit (SPU 1) by replacing the Gen 3.0T gasoline catalytic partial oxidation (CPOX) fuel reformer with the new Gen 4.1T CPOX (see Figure 3) natural gas fuel reformer. This design was the target for first system integration and test of a methane-fueled SPU.

The electrical and electronics system has advanced in several areas. A variety of studies have resulted in electrical architecture designs for development and potential future product applications. Innovation in the power and signal distribution subsystem enables simplified system integration, commonality across applications, and reduced debug efforts. The electrical and electronics system has advanced towards a more production intent implementation.

Cathode development efforts have been focused on improving the long-term durability of $(La,Sr)(Co,Fe)O_3$ (LSCF) cathodes for use in Cr-free operation. Interconnect development focused on improving cathode and anode contact as well as minimizing Cr interaction with the cathode. Stack results have demonstrated power densities of greater than 500 mW/cm^2 at 0.7 V at 750°C operating temperature. Stacks have demonstrated greater than 2000 hours continuous durability with less than 10% degradation (less than 1% in the last 1000 hours). Thermal cycling tests have shown greater than 5 thermal cycles with no degradation in power.

Process air module (PAM) components have been built and tested on dynamometer and airflow stands. Since the PAM is a major contributor to parasitic power loss, particular attention is being given to identifying the sources of the PAM losses. Test data is used to refine the CFD analysis model so that alternative manifold design features can be studied to reduce the PAM power losses. Thermal testing of an instrumented motor and controller was completed at worst case ambient temperature conditions so that the minimum airflow limit of the air-cooled PAM could be established. Durability testing of the motor and controller is ongoing.

Prototype part fabrication of a third-generation integrated component manifold was completed. This design incorporated a new gas phase combustor (GPC). Results from system tests indicated improved gas distribution, improved gas mixing, and reduced pressure drop in the manifold. Improved GPC light-off and sustained ignition was also achieved with this GPC design.

Reformer catalyst durability was demonstrated to over 2000 hours for steady-state partial oxidation of gasoline fuel while meeting acceptable reformate quality. Modifications were made to the durability test to permit similar studies with natural gas or diesel fuels. The durability test was modified to match differing APU power requirements by cycling through five different sets of operating conditions. Catalyst formulations were identified for partial oxidation of low-sulfur diesel fuel, and appropriate processing regimes and catalysts were identified for

processing of diesel fuel containing up to 50 ppmw sulfur.

Conclusions

- Reformer changes (from gasoline to natural gas) permit the stack and balance of plant to be applied as an auxiliary power unit (mobile) or as a stationary power unit.
- Hardware durability increases are achieved by managing Cr in the balance of plant and by refining catalysts in the reformer.
- Continued development of balance of plant and reformer, in addition to basic stack work, is essential to delivering a product that can operate on real-world liquid and gaseous fuels, including those with minimal typical sulfur content.

Special Recognitions & Awards/Patents Issued

1. Patent issued: The U.S. Patent Office Grant Numbers: 6759155, 6773845, 6786254, 6821667, 6830844, 6893768

FY 2005 Publications/Presentations

1. November 2004: 2004 Fuel Cell Seminar, San Antonio, TX: Presentation only
   SOFC APU Development Update
   Steven Shaffer
   Delphi Corporation
2. January 2005: SECA Core Technology Workshop, Tampa, FL: Presentation only
   Material Interconnect Development
   Dr. Diane England
   Delphi Corporation
3. April 2005: SECA Annual Workshop, Pacific Grove, CA: Presentation only
   Development Update on Delphi's Solid Oxide Fuel Cell System
   Steven Shaffer
   Delphi Corporation
4. May 2005: SOFC IX - Industrial Workshop, Quebec, Canada: Presentation only
   Development Update on Delphi’s Solid Oxide Fuel Cell System
   Steven Shaffer
   Delphi Corporation
5. May 2005: SOFC IX - Industrial Workshop, Quebec, Canada: Presentation only
   Development Update on Delphi’s Solid Oxide Fuel Cell Stack
   Subhasish Mukerjee
   Delphi Corporation

II.4 Thermally Integrated High Power Density SOFC Generator

Pinakin Patel
FuelCell Energy, Inc.
3 Great Pasture Road
Danbury, CT 06813
Phone: (203) 825-6072; Fax: (203) 825-6273; E-mail: ppatel@fce.com

DOE Project Manager: Magda Rivera
Phone: (304) 285-1359; E-mail: Magda.Rivera@netl.doe.gov

Subcontractors:
Versa Power Systems, Golden, Colorado (VPS Calgary, GTI, MSRI, University of Utah, Dana)

Contributors:
Brian Borglum, Peng Huang, Randy Petri, Robert Remick, Tad Armstrong, Anil Virkar

Objectives

Research and development in Phase 1 shall focus on the research, design and manufacture of a planar solid oxide fuel cell (SOFC) power generator for stationary applications (3-10 kW) using natural gas as the standard fuel. Goals of the Phase 1 project include the following:

- Design a thermally integrated, internal reforming fuel cell stack and compact balance-of-plant (BOP) package and system.
- Develop optimal cell structure having the target power density and endurance at lower operating temperatures (≤800°C).
- Develop fuel processing system for operation on U.S. natural gas as the baseline fuel and initiate development of fuel processing systems for broadly available fuels such as diesel.
- Test prototype 3-kW system on natural gas fuel.

Approach

The development efforts to achieve the above goals are organized in the following tasks:

- *System Design & Analysis*
  In this task, work shall focus on prototype design, system -level modeling and analysis. Work will also concentrate on fuel processor subsystem development and thermally integrated power system (TIPS) development.
- *Cell Design, Development and Optimization*
  In this task, work shall focus on improvements in cell performance through material changes and refinements. Composition and morphology of the anode, electrolyte, and cathode will be addressed to increase cell performance. Thermo-mechanical modeling of cells will be performed.
- *Stack Design and Development*
  In this task, work shall focus on the development of 3-10 kW stack design to resolve manifold design and stack thermal issues and improve stack performance. Focus of work will be on the internal reforming stack design.
- *Product Development and Packaging*
  Work shall concentrate on the integration of SOFC subsystems (electrical BOP and mechanical BOP) with the SOFC stack to maximize electrical efficiency and to reduce heat losses, overall system weight, and cost.

- *Process Development for Cost Reduction*
  Work shall focus on SOFC cost reduction by manufacturing process improvements and adaptation of mass production techniques.
- *Prototype Test and Evaluation*
  Work shall focus on the test and evaluation of the prototype system against the minimum Solid State Energy Conversion Alliance (SECA) technical requirements.

Accomplishments

- A single cell [100 cm^2 size, stainless steel interconnects (lower cost)] was operated for 26,000 hours.
- At 600°C, a power density of 500 mW/cm^2 was achieved using the advanced cathodes.
- An 80-cell stack tower produced 3.5 kW DC power and met the design targets. Twenty-cell stacks (building block) have been operated for up to 8,000 hours with good stability.
- Designed, built and operated a complete 2-kW system assembled with a single tower with the new, lower-cost stacks (84 cells) on natural gas fuel. The system was operated in a grid-parallel mode for 3,000 hours with a peak net AC electrical efficiency of 36% (LHV) [46% gross DC electrical efficiency (LHV)].
- Initial test results for the 3-kW prototype system operating on pipeline natural gas fuel showed peak net AC electrical efficiency of 39% (LHV) [51% gross DC electrical efficiency (LHV)].

Future Directions

- Continue testing of the 3-kW system on natural gas fuel and identify further improvement options. Initiate 10-kW advanced system design and subsystem development.
- Optimize electrodes for lower-temperature operation and redox tolerance.
- Validate alternate fabrication processes to improve cell performance and reduce cost.
- Develop high power density stack design incorporating modeling results, advanced gaskets and internal reforming cell design to extend the stack life and to reduce the system cost.

Introduction

The FuelCell Energy, Inc. (FCE) team includes Versa Power Systems (VPS), VPS Calgary, Gas Technology Institute (GTI), Materials and Systems Research, Inc. (MSRI), University of Utah (UU) and Dana. The efforts in this period focused on the critical technology development areas to meet the SECA program goals for the 3-10 kW SOFC generator. The FCE team has made significant progress in cell, stack and system technology areas and has met all the planned milestones.

Approach

The FCE team is focusing to develop a 3-10 kW SOFC system operating at 700°C, with a power density of >0.5 W/cm^2 at 0.7 V/cell by Phase 3. The Phase 1 efforts will focus on development of cell and stack design, leading to a prototype 3-kW system operating on natural gas fuel, with lower heating value (LHV) efficiency target of >35% and a degradation rate of <2%/500 hours.

The cell technology approach is based on the record-setting performance achieved by MSRI and VPS Calgary. The baseline cell materials will be Ni/YSZ cermet for anode, yttria-stabilized zirconia (YSZ) as electrolyte and lanthanum strontium manganese oxide or other ceramic for cathode. In the stack design, internal and external manifold designs will be evaluated and innovative seal designs will be adopted. For high power density (300-500 mW/cm^2) operation, efficient cooling of the SOFC is required to assure robust long-term operation of the system. Triple mode cooling—internal reforming combined with radiative and sensible cooling modes—is being developed. A 3-kW baseline system in Phase 1 and an advanced 10-kW system in Phases 2 and 3 will be developed to meet the SECA technical targets.

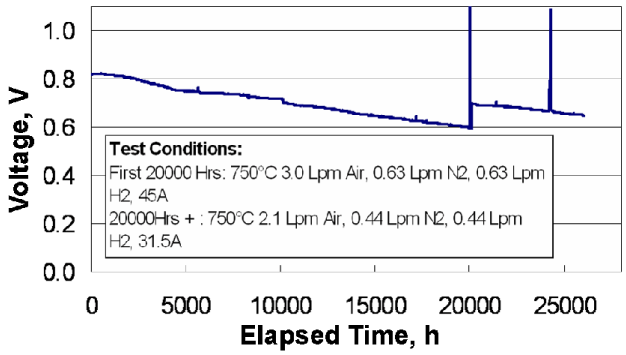

Figure 1. Bench-mark Cell Testing: The 100-cm^2 cell assembled with stainless steel interconnects was operated for 26,000 hours.

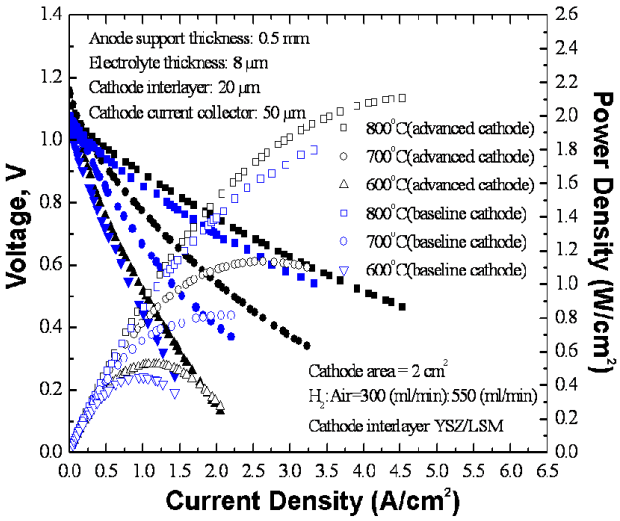

Figure 2. Reduction in Cell Operating Temperature: At 600°C, a power density of 500 mW/cm^2 at 0.7 V was achieved in a button cell.

Results

Cell Technology Development

Validation of the low-cost, single-fire process (TSC: tape casting – screen printing – co-firing) developed by VPS Calgary continued in single cells as well as stacks. The TSC process incorporates mass production techniques for low cost while yielding high-quality SOFC trilayers. A 100-cm^2 single cell assembled with stainless steel interconnects accumulated over 26,000 hours of operation under simulated system conditions at 750°C (Figure 1). This cell validated the readiness of the basic cell materials and design to meet the SECA technical targets. Sulfur- and redox-tolerant anodes are desirable to reduce the overall system cost. Cell tests with 1 to 10 ppm H_2S in hydrogen fuels are being conducted to establish maximum allowable limits for steady-state and transient operations. Initial test results show that the sulfur effect is significant at 10 ppm H_2S and increases as the temperature is lowered from 800°C to 700°C (up to 30% loss in cell voltage). However, this effect is mostly recoverable. Endurance tests are planned to obtain the long-term test data. An advanced cathode for lower temperature has been developed. Button cells built with the advanced cathode demonstrated 500 mW/cm^2 at 600°C, as shown in Figure 2.

A large-area (400 cm^2) cell assembled with the low-cost sheet-metal hardware derived from FCE's Direct Fuel Cell (DFC) technology was operated on methane fuel for over 5,000 hours. A series of formulations were developed for the cathode-side contacts to decrease the cathode-side ohmic area specific resistance (ASR) and to improve the thermal cycling capability. Short-stack test results show that a 50% reduction in the cell ASR is feasible.

Stack Technology Development

The major accomplishment during the reporting period was a transition from the current baseline stack design to the advanced lower-cost stack design. The newer stacks eliminate expensive brazed interconnects and simplify fabrication and assembly processes. The internal reforming capability in the stacks has been increased from <25% to 50%. The newer stacks have internal manifolds and external compression system. An 80-cell stack tower shown in Figure 3 produced 3.5 kW power output. The stack performance stability was validated through 20-cell stack tests for up to 8,000 hours (Figure 4).

Internal reforming of methane helps remove the heat generated in the stack. Particularly at higher power densities (>300 mW/cm^2), this type of cooling is beneficial. Stacks (5-21 cells) were assembled with direct internal reforming (DIR) hardware. These stacks were operated on methane-containing fuel, demonstrating 25 to 70% internal reforming. While the test results are quite encouraging, opportunities for further improvements in the DIR stack have been identified.

Figure 3. KW-class SOFC Stack Tower: The internally manifolded 80-cell stack tower produced 3.5 kW.

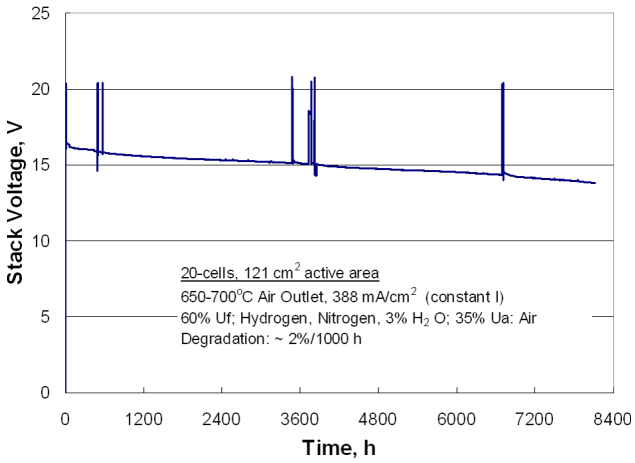

Figure 4. Stack Endurance Testing: Achieved over 8,000 hours of operation with good stability.

System Technology

A second 2-kW Aurora system was assembled with the new, low-cost stack (84 cells), and operation on natural gas fuel began. The system accumulated 3,000 hours of operation with a peak net AC electrical efficiency of 36% at 2-kW rated power. The system instrumentation was modified to thermally map both the stack tower and radiative air heat exchanger during different radiative cooling loads in a full thermally integrated system. As expected, the test results showed that the radiative heat transfer is quite effective in the stack cooling and air preheating. It also reduces the heat exchanger and insulation costs, while minimizing the parasitic power requirements in the air blower.

The 2-kW Aurora system hardware has been scaled up to 3-kW level. The initial performance of the 3-kW system is meeting the design goals. On pipeline natural gas fuel and in grid-parallel mode, the 3-kW system achieved a peak net AC electrical efficiency of 39% (LHV) [51% gross DC electrical efficiency (LHV)]. In parallel, preliminary design of the advanced 10-kW system was initiated. This system is expected to include additional design features such as water self-sufficiency using anode recycle, elimination of anode purge gas, improved desulphurization, enhanced system performance, simplified system design, and scaled-up stack power output. The 10-kW system planned for Phase 2 is expected to perform at approximately 45% net AC electrical efficiency and achieve lower costs than the 2- and 3-kW systems.

Conclusions

The basic cell technology and low-cost materials have been validated through a 26,000-hour cell test, indicating the readiness to meet SECA Phase 1 targets. The technology development of the planar SOFC cell, stack and system indicates that higher power density (300-500 mW/cm^2) operation in a sustained mode is facilitated by internal reforming and radiative cooling. The modular stack design, leading to a stack tower concept using 4 stack modules, offers a low-cost near-term option to build 3-10 kW size SOFC systems. System net AC electrical efficiencies up to 39% have been demonstrated on pipeline natural gas fuel.

The achievements to date provide an excellent foundation towards SECA Phases 2 & 3.

FY 2005 Publications

1. P. Patel, Thermally Integrated High Power Density SOFC Generator, SECA Annual Conference, Asilomar, CA, April 18-21, 2005.
2. B. Borglum, The Status of SOFC Development at Versa Power Systems, Solid Oxide Fuel Cell – IX, S.C. Singhal and J. Mizusaki, Editors, PV 2005-07, p. 89-97, The Electrochemical Society, Pennington, NJ (2005).

II.5 Solid State Energy Conversion Alliance (SECA) Solid Oxide Fuel Cell Program

Nguyen Minh (Primary Contact), Tony Campbell, Tom Logan
GE Hybrid Power Generation Systems
19310 Pacific Gateway Drive
Torrance, CA 90502-1031
Phone: (310) 538-7250; Fax: (310) 538-7250; E-mail: nguyen.minh@ge.com

DOE Project Manager: Travis Shultz
Phone: (304) 285-1370; E-mail: Travis.Shultz@netl.doe.gov

Objectives

- Develop a fuel-flexible and modular system (3 to 10 kW) that can serve as the basis for configuring and creating low-cost, highly efficient, and environmentally benign power plants tailored to specific markets.
- Demonstrate a prototype system of the baseline design with desired cost projections and required operating characteristics (Phase I); assemble and test a packaged system for a selected specified application (Phase II); field test a packaged system for extended periods (Phase III).

Approach

(Phase I)

- Establish a baseline system concept and analyze its performance characteristics.
- Perform a study to estimate system costs.
- Develop a robust, reliable, high-performance solid oxide fuel cell (SOFC) stack technology amenable to low-cost manufacturing.
- Develop a fuel processor as a pre-reformer for processing a variety of fuels.
- Evaluate system thermal management to establish a suitable recuperation scheme for the system.
- Develop and implement a flexible control structure incorporating required sensors.
- Identify a flexible, low-cost power management subsystem.
- Evaluate component integration.
- Design, assemble and test a prototype system to demonstrate performance meeting the program requirements.

Accomplishments

Key accomplishments in FY 2005 are summarized below.

- System Design and Analysis
  - The prototype system design, including analysis of its performance, was completed. The analysis indicated that the efficiency target of 35% could be reached or exceeded by this design.
- Cost Estimate
  - Projected cost estimates were updated and a cost report submitted and audited. High-volume manufacturing costs for the prototype system were estimated based upon actual prototype system performance and hardware cost estimates. From these data, a total system cost of $724/kW (5.4 kW basis) was calculated. This estimate is below the projected cost requirement of $800/kW for Phase I of the project.

- Stack Technology
  - High power densities of 0.36 W/cm^2 (0.52 A/cm^2 at 0.7 V) and 0.34 W/cm^2 (0.48 A/cm^2 at 0.7 V) have been achieved at 80% and 88% fuel utilizations (FU), respectively, with simulated autothermal reforming (ATR) gas (32.2% H_2, 6.8% CH_4, 8.4% CO, 5.8% CO_2, 29.8% N_2, 17% H_2O) for single-cell modules.
  - Multi-cell stacks up to 40 cells have been assembled and tested and have demonstrated highly efficient performance on both dilute hydrogen and ATR surrogate. For example, a 40-cell SOFC stack with 16-cm diameter cells achieved 1.40 kW at 0.428 A/cm^2 with 80% fuel utilization and an average cell voltage of 0.673 V (44.7% stack efficiency) using simulated ATR reformate.
  - A number of 20-cell stacks were built and tested to improve both cell-to-cell and stack-to-stack reproducibility. At all operating conditions, the power of each stack was within 5% of the mean power.
- Fuel Processing
  - An ATR pre-reformer integrated with a 3-cell SOFC stack has been operated at 0.400 A/cm^2, 73% fuel utilization and has performed stably for approximately 2400 hours.
- Control
  - A control system was designed and implemented for the SECA prototype system. The control strategy is composed of a top-level supervisory control structure and lower-level active controls. The supervisory controls provide load management, operating mode management, and built-in test for online diagnostics and error handling. The lower-level active control loops provide setpoint tracking for flows and temperatures throughout the system.
- Balance of Plant (BOP)
  - Bill of materials was developed and completed for BOP components. Several components were designed and custom made for the prototype (e.g., cathode air blower, power electronics, heat exchangers), and others were off-the-shelf components selected and validated for suitability for the prototype system.
- Prototype Assembly
  - A prototype system design was completed, including system schematic, package drawing, bill of materials, and heat and material balances.
  - A prototype was built and has been tested according to the test plan.
  - The system has achieved a peak efficiency of 40.9% (exceeding the SECA target of 35%) and peak DC net power of 5.43 kW.

Future Directions

- Prototype testing will continue and will be completed at GE Hybrid Power Generation Systems (GE HPGS) according to the test plan.

Introduction

This project focuses on developing a low-cost, high-performance solid oxide fuel cell (SOFC) system suitable for a broad spectrum of power generation applications. The overall objective of the project is to demonstrate a fuel-flexible, modular 3-to-10-kW system that can be configured to create highly efficient, cost-competitive, and reliable power plants tailored to specific markets. The key features of the SOFC system include a fuel-flexible pre-reformer; a low-cost, high-power-density SOFC stack; integrated thermal management; and suitable control and power management subsystems. When fully developed, the system is expected to meet the projected cost of $400/kW.

Approach

The SOFC system is a stationary power module (3 to 10 kW) capable of operating on different fuels. The system consists of all the required components for a self-contained unit, including fuel cell stack, fuel processing subsystem, fuel and oxidant delivery subsystem, thermal management subsystem, and various control and regulating devices.

- The SOFC is a compact of anode-supported cells (fabricated by the GE HPGS tape-calendering process) and metallic interconnects. The stack design is based on an advanced concept that maximizes cell active area and minimizes sealing. The fuel cell can operate directly on light hydrocarbon fuels and incorporates materials for high performance at reduced temperatures (<800°C). These characteristics provide a low-cost, fuel-flexible fuel cell suitable for operating under various conditions. The tape calendering process for manufacturing thin-electrolyte, anode-supported cells is a potentially low-cost, mass-customization technique suitable for high-volume production and automation using available commercial equipment.
- The fuel processor is a catalytic reactor that functions as a pre-reformer. The system employs an integrated thermal management approach to utilize byproduct heat, reduce heat losses, and, consequently, increase the overall system efficiency. The system also has a flexible control structure that can be modified or optimized for different applications.

The project consists of three phases. Phase I of the project focuses on developing system components having the required operating characteristics, resolving critical technological issues, and demonstrating a prototype system. The Phase I work concentrates on system design and analysis, the cost study, stack technology development, fuel processing development, controls and sensors, power electronics, and system prototype assembly and testing. Phase II will demonstrate a packaged system selected for a specified application and further improve technology and assess system cost. Phase III will extend the Phase II effort to field test a packaged system for extended periods to verify the required performance, cost, reliability, and lifetime for commercial uses.

Results

System Design and Analysis

A conceptual design was developed for a natural gas-fueled, 3-10 kW SOFC system for stationary applications. The design included an autothermal reforming (ATR) fuel processor and a SOFC stack that can process light hydrocarbons internally (internal reforming). This system conceptual design served as the foundation for the detailed design of a prototype system that was subjected to various performance analyses. The effects of a number of critical performance factors such as SOFC stack performance, system heat loss, auxiliary power, and pressure drop were determined for the prototype system. From these analyses, it was determined that the efficiency target of 35% could be reached or exceeded by this design (Figure 1).

Cost Estimate

The system cost estimate study was completed, and the cost estimate report was submitted and audited. The cost estimate involved projecting the costs of the SOFC stack; fuel processor; fuel, air, and water delivery subsystems; thermal management; electrical system; packaging; and assembly. The system power rating was based on the demonstrated peak power of the prototype system. The total system cost projected in this study is $3910 assuming volume production of 50,000 units per year. Based on 5.4 kW peak power demonstrated in the prototype system testing, the total system cost estimate is $724/kW.

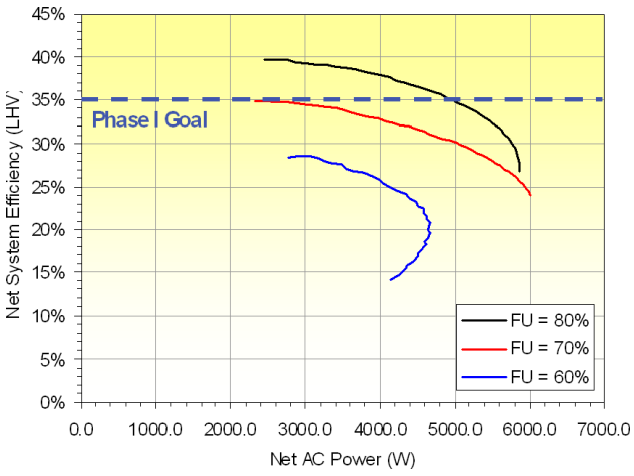

Figure 1. Prototype System Efficiency Projections

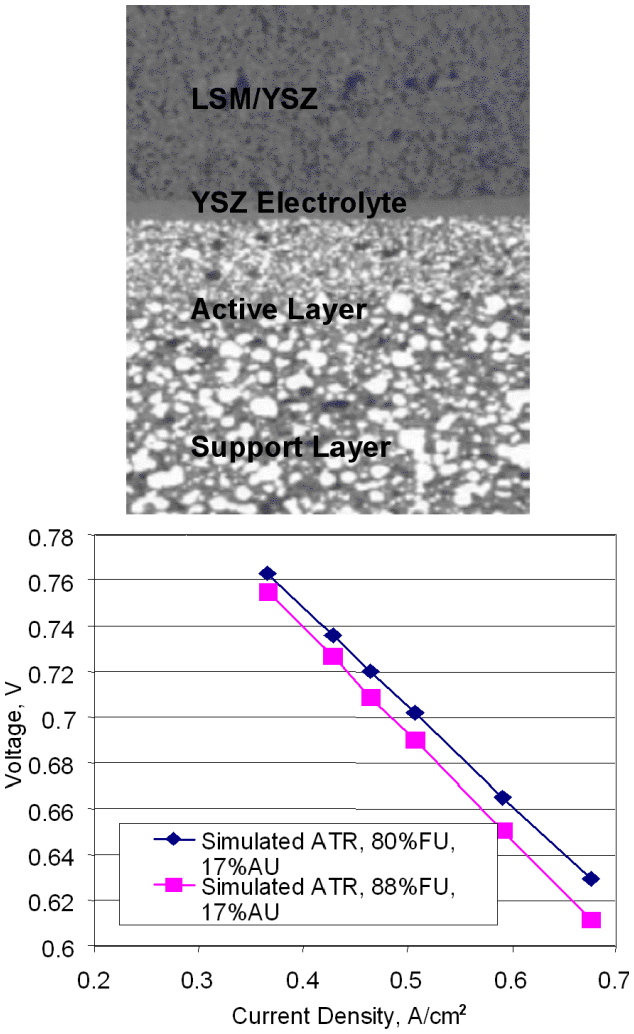

Figure 2. Typical Microstructure of Anode-Supported Cell and Cell Performance at 800°C with Simulated ATR Fuel (80% and 88% Fuel Utilization)

Stack Technology Development

Anode-supported cells up to 30 cm in diameter have been tested, and excellent performance has been demonstrated at fuel utilization levels suitable for practical applications. As an example, Figure 2 shows the microstructure of a 16-cm (6.3") diameter anode-supported cell and the typical performance of such a cell (tested as a single-cell module, i.e., a single-cell stack or a cell with anode and cathode interconnect flow fields). As can be seen from Figure 2, high power densities of 0.36 W/cm^2 (0.52 A/cm^2 at 0.7 V) and 0.34 W/cm^2 (0.48 A/cm^2 at 0.7 V) have been achieved at 80% and 88% fuel utilizations (FU), respectively, with simulated ATR

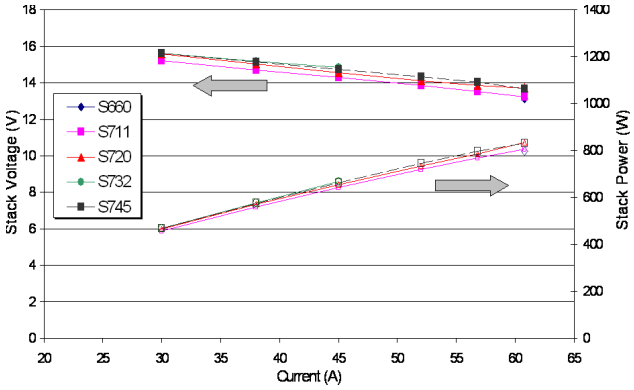

Figure 3. Performance of 20-Cell Stacks (Simulated ATR Fuel, 80% Fuel Utilization)

gas (32.2% H_2, 6.8% CH_4, 8.4% CO, 5.8% CO_2, 29.8% N_2, 17% H_2O). This cell architecture has demonstrated extraordinarily high fuel utilization for anode-supported cells. Fuel utilization up to 95% and stack efficiency greater than 55.5% have been realized using dilute hydrogen as fuel (800°C and ambient pressure stack operation).

Multi-cell stacks up to 40 cells have been assembled and tested and have demonstrated highly efficient performance on both dilute hydrogen and ATR surrogate. For example, a 40-cell SOFC stack with 16-cm diameter cells achieved 1.40 kW at 0.428 A/cm^2 with 80% fuel utilization and an average cell voltage of 0.673 V (44.7% stack efficiency) using simulated ATR reformate. In addition, a number of 20-cell stacks were built and tested to improve both cell-to-cell and stack-to-stack reproducibility. At all operating conditions, the power of each stack was within 5% of the mean power (Figure 3). At the design point of 0.428 A/cm^2 and 80% fuel utilization in simulated ATR fuel, the average cell power density reached 0.288 W/cm^2. This performance is sufficient to exceed the performance requirements of Phase I.

Fuel Processing

An ATR processor was designed and developed for the SECA system. Several prototypes were built based on the design, and their operation was evaluated. The fuel processor was tested extensively (as a stand-alone component and as an integrated SOFC stack/fuel processor subsystem) prior to incorporation into the system and was found to demonstrate the ability to meet the necessary system

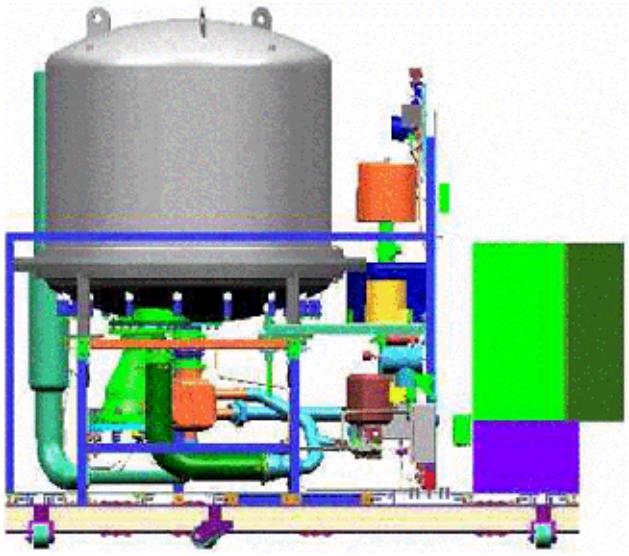

Figure 4. Prototype System

requirements (steam-to-carbon ratio, oxygen-to-carbon ratio, outlet reformate temperature, methane slip, pressure drop). A long-term test of a 3-cell SOFC stack integrated with an ATR has been conducted. The SOFC/fuel processor subsystem was operated at 0.400 A/cm^2 and 73% fuel utilization and has performed stably for approximately 2400 hours.

Control

A control system was designed and implemented for the prototype system. The control strategy is composed of a top-level supervisory control structure and lower-level active controls. The supervisory controls provide load management, operating mode management, and built-in test for online diagnostics and error handling. The lower level active control loops provide setpoint tracking for flows and temperatures throughout the system.

Prototype System

Figure 4 shows a conceptual packaging layout of the hardware for the prototype system. The system consists of the SOFC stacks and other components required for efficient operation on natural gas, including an ATR fuel processor used as a pre-reformer. The system was designed to allow component access so that it could be easily modified and improved during the various stages of integration that led up to the final system test. Many of the key system operating features (component/subsystem integration, thermal management including self-sustaining operation, and control subsystem including startup and shutdown) were verified using sub-scale SOFC stacks prior to the assembly and testing of the final prototype configuration. The final prototype system testing is currently underway. The system has achieved a peak efficiency of 40.9% and peak DC net power of 5.43 kW. The system is operating at the normal condition for the first steady-state hold period. At the completion of 1000 hours, the unit will undergo ten power cycles before operating for an additional 500 hours at the normal operating condition. At the conclusion of this period, a peak efficiency and peak power points will be repeated.

Conclusions

- A design of the SECA prototype system was developed. Analysis of the design showed performance exceeding the efficiency target of 35%.
- The results of the cost estimate study indicated a total projected system cost of $724/kW (5.4 kW basis). The estimate is below the projected cost requirement of $800/kW for Phase I of the project.
- SOFC single-cell modules and multi-cell stacks were built and operated and showed significant performance improvements. Multi-cell stacks showed performance sufficient to exceed the performance requirements of Phase I.
- A SOFC stack integrated with an ATR fuel processor has operated stably for approximately 2400 hours.
- A multi-level design for the control subsystem was developed and implemented in software for the prototype system.
- A bill of materials was developed and completed for the BOP components. Several components were designed and custom made for the prototype, and others were off-the-shelf components selected and validated for suitability for the prototype system.
- A prototype system was built and has been tested with hydrogen and methane. The key operating features of the prototype system were verified. The system has achieved a peak efficiency of

40.9%, exceeding the target of 35%, and peak DC net power of 5.43 kW.

FY 2005 Publications/Presentations

1. N. Minh, "Solid Oxide Fuel Cell Technology Development Status", 2004 Fuel Cell Seminar Extended Abstracts, Courtesy Associates, Washington, DC, 2004.
2. N. Q. Minh, "SECA Solid Oxide Fuel Cell Program", presented at the SECA 6th Annual Workshop in Pacific Grove, CA, April 18-21, 2005.
3. N. Q. Minh, "Solid Oxide Fuel Cell Systems for Stationary Power Generation Applications," in SOFC IX, Electrochemical Society, Pennington, NJ, 2005, p. 76.

II.6 Small-Scale Low-Cost Solid Oxide Fuel Cell Power Systems

Shailesh D. Vora
Siemens Power Generation
1310 Beulah Road
Pittsburgh, PA 15235
Phone: (412) 256-1682; Fax: (412) 256-1233; E-mail: Shailesh.vora@siemens.com

DOE Project Manager: Don Collins
Phone: (304) 285-4156; E-mail: Donald.Collins@netl.doe.gov

Subcontractors:
Blasch Precision Ceramics, Albany, NY

Objective

- To develop a commercially viable 5-10 kWe solid oxide fuel cell power generation system that achieves a factory cost goal of $400 per kWe.

Approach

- Improve cell performance through new cell design and new materials.
- Lower operating temperature from 1000°C to 800°C.
- Eliminate internal fuel reformers through on-cell reformation.
- Develop low-cost, high-volume manufacturing processes.
- Use low-cost module materials due to lower operating temperature.
- Simplify balance of plant (BOP) design by elimination of parts.

Accomplishments

- Demonstrated 75% higher power density for high power density (HPD) cells compared to tubular cells. A new cell design that combines the seal-less feature and a flattened cathode with integral ribs has been chosen for this project. The ribs reduce the current path length by acting as bridges for current flow. This cell design, due to shorter current path, has lower cell resistance and hence higher power output than tubular cells. During FY 2005, HPD cells produced 75% higher power than tubular cells at 0.65 V, 900ºC operating temperature and 80% fuel utilization.
- Demonstrated over 3000 hours voltage stability for HPD cells at 1000°C and 80% fuel utilization**.** There was no noticeable voltage degradation for a HPD cell when tested at conditions described above. This exceeds SECA program goals for voltage stability.
- Fabricated multiple six-cell bundles with HPD cells. Each cell has an active area of approximately 900 cm^2, and the estimated bundle power is approximately 1.2 kWe. Six such bundles (36 cells) will be utilized in a proof-of-concept system described below.
- Completed assembly of a proof-of-concept system with HPD cells. The primary objective of this system is to demonstrate operation of HPD cells in a generator environment. The system comprises 36 HPD cells and will run on natural gas fuel. Fuel reformation will be internal to the cell stack.

Future Directions

- Optimize HPD cell design in terms of number of channels and dimensions.

- Develop cell materials for operation at 800°C.
- Improve cell performance through optimized cell design and new materials.
- Test proof-of-concept system.

Introduction

The objective of this project is to develop a standard high-performance, low-cost solid oxide fuel cell (SOFC) system that can be manufactured in high volume for application in a number of different end uses, including residential applications and as auxiliary power units (APUs) in commercial and military transportation applications. The proposed project is a ten-year, three-phase project with prototype SOFC systems being tested at the end of every phase. Performance and cost improvements made during each phase will be incorporated in each prototype, and products based on each prototype will be made ready for market entry, as they become available.

Approach

We have identified key technical issues that must be resolved to achieve low-cost commercial SOFC systems. We will focus on cost reductions and performance improvements to transform today's SOFC technology into one suitable for low-cost mass production of small systems for multi-market applications. The key advances identified are as follows:

- Improved cell performance through design and materials innovations to more than double the power and thus reduce cost per kWe
- On-cell reformation of natural gas fuel to eliminate high-cost internal reformer components
- Sulfur-tolerant anodes to eliminate the fuel desulfurization system
- Use of low-cost insulation and containment vessels by lowering the system operating temperature
- High-efficiency (95%) power conditioning systems to improve overall system electrical efficiency
- Cost-effective fuel processing systems for operation of the standard SOFC module on alternate fuels

In addition to the key advances noted above, adoption of more automated mass production techniques for cell, module and BOP manufacturing will ensure overall SOFC system cost effectiveness.

Results

Prior to the start of the project, it was recognized that Siemens Westinghouse's seal-less tubular cell design would not be able to meet the cost and performance targets of the program. A need to develop a cell with higher power density and compact design was identified. A new design that combined the seal-less feature and a flattened cathode with integral ribs was chosen. This new design, referred to as high power density (HPD) cell, has closed end similar to the tubular design. The ribs reduce the current path length by acting as bridges for current flow. The ribs also form air channels that eliminate the need for air feed tubes. This cell design, due to shorter current path, has lower cell resistance and hence higher power output than tubular cells.

Analytical modeling was initiated to optimize the number of ribs (channels) for maximum power and mechanical stability from thermal stresses during operation. Based on initial results, HPD cell designs with five channels (HPD5) and 10 channels (HPD10) were selected for cell preparation to develop manufacturing processes and electrical performance testing.

Several HPD5 and HPD10 cells were fabricated and tested for electrical performance. Figure 1 shows cylindrical and HPD cells. The HPD5 cell showed over 50% higher power density and HPD10 showed over 75% higher power density compared to cylindrical cells, with the target being 100% more power density for the 10-year project. Figure 2 shows voltage versus current density comparison of the cylindrical and the two HPD cells. Figure 3 shows voltage stability of the HPD5 cell over more than 3000 hours of operation.

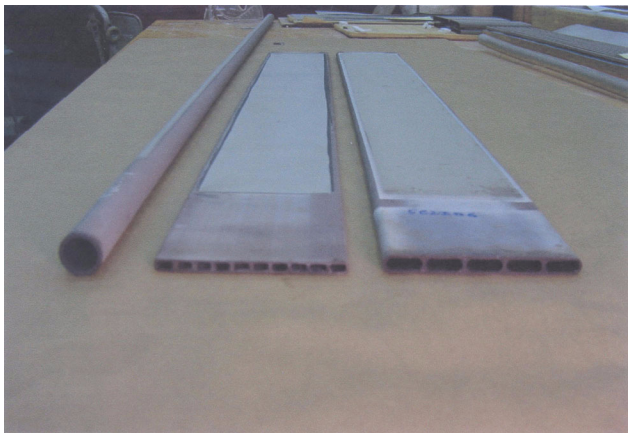

Figure 1. Cylindrical and HPD Cells

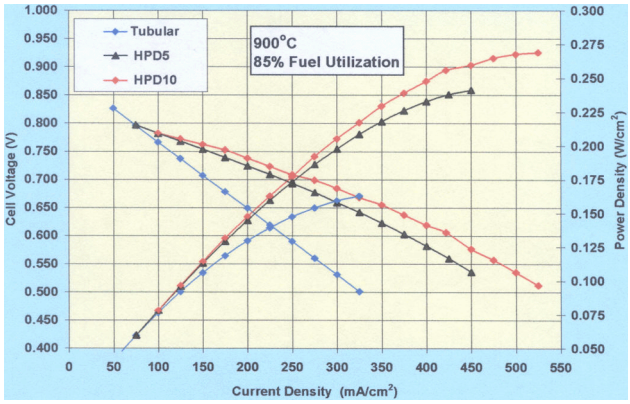

Figure 2. Voltage versus Current Density Comparison of Cylindrical and HPD Cells

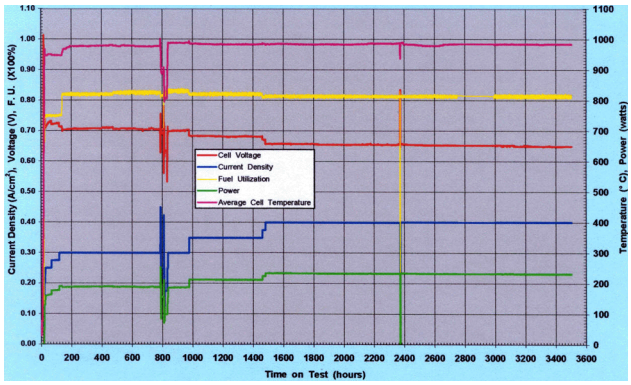

Figure 3. Voltage versus Time Plot for HPD5 Cell

Efforts were also directed towards the development of cell-to-cell connections to bundle cells. Several bundles with HPD5 cells were fabricated.

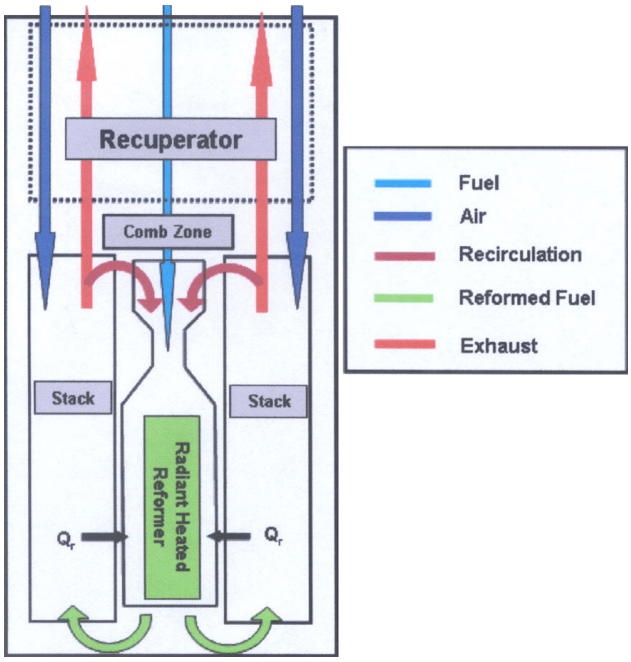

Figure 4. Flow Schematics of Proof-of-Concept Stack

Assembly of a proof-of-concept system for residential applications was completed. This generator consists of 36 HPD cells. The stack is divided into two sub-stacks of 18 cells with a central internal reformer for natural gas fuel. Figure 4 shows the flow schematics of the proof-of concept stack.

Conclusions

Fabrication processes for HPD cells were established, and electrical testing showed significant improvement in power density over cylindrical cells. A proof-of concept system with 36 HPD cells was constructed.

FY 2005 Publications/Presentations

1. S. D. Vora, "Cell Power Enhancement in Seal-less SOFCs", Presented at the 2004 Fuel Cell Seminar, November 1-5, 2004, San Antonio, TX.
2. S. D. Vora, "SECA Program at Siemens Westinghouse", Presented at the SECA Annual Workshop and Peer Review Meeting, April 18-21, 2005, Pacific Grove, CA.
3. K. Huang, "Electrochemical Characterization on Cathode and its Interface with Electrolyte of SWPC's Cathode Supported SOFCs", Presented at the SOFC-IX Symposium, May 15-20, 2005, Quebec City, Canada.

4. G. DiGiuseppe, “High Power Density Cell Development at Siemens Westinghouse”, Presented at the SOFC-IX Symposium, May 15-20, 2005, Quebec City, Canada.
5. R. Draper and G. DiGiuseppe, “High Power Density Solid Oxide Fuel Cells for Auxiliary Power Unit Applications”, Presented at ASME Fuel Cell 2005, Fuel Cell Science, Engineering and Technology Conference, May 23-25, 2005, Ypsilant, MI.
6. S. D. Vora, “Advances in Solid Oxide Fuel Cell Technology at Siemens Westinghouse”, Presented at the Risoe International Energy Conference 2005, May 23-25, 2005, Risoe National Laboratory, Denmark.

III SECA Core Technology Program

III.A Materials

III.A.1 SOFC Research and Development

Michael Krumpelt (Primary Contact), Terry A. Cruse
Argonne National Laboratory
Argonne, IL 60439
Phone: (630) 252-8520; Fax: (630) 252-4176; E-mail: krumpelt@cmt.anl.gov

DOE Project Manager: Lane Wilson
Phone: (304) 285-1336; E-mail: Lane.Wilson@netl.doe.gov

Objectives

- Explore the effects and mechanisms of chromium migration in solid oxide fuel cells (SOFCs).

Approach

- Operate cells with different cathodes and bipolar plate materials.
- Identify chromium deposits in cathodes.
- Determine weight loss of chrome compounds in simulated cathode gas.

Accomplishments

- It was shown that the amount of chromium in the cathodes correlates with the oxide ion conductivity of the cathodes.
- The conclusion was reached that chromium migrates from the bipolar plate surface as a volatile oxyhydroxide species and is electrochemically reduced in the cathode at the active sites.
- For manganite cathodes, the reduction occurs at the triple phase boundaries, but in ferrites, chromium deposits throughout the cathode.

Future Directions

- The extent of performance degradation caused by chromium will be quantified based on typical stack designs and materials selection.
- Methods for diminishing the chromium migration will be explored.

Introduction

Chromium contamination of SOFC cathodes has been observed by several groups of researchers developing cells with metallic bipolar plates. Hilpert et al. have attributed the chromium transport to the formation of volatile oxyhydroxide species that form when chromium-containing steels are exposed to oxygen and water at elevated temperatures [1, 2]. The volatile oxyhydroxide, $CrO_2(OH)_2$, can form either by reaction of the surface oxide with oxygen and water, or by direct reaction of metallic chromium [3]. It has also been shown that $CrO_2(OH)_2$ is the dominant species in the gas phase when water is present [4], and that the cathode acts as a nucleation site for the deposition of chromium [5]. Quadakkers et al. provide an overview of this and other issues related to metallic-based interconnects [6]. There is also work that indicates that both the cathode and electrolyte compositions can play a role in chromium poisoning [7]. In an earlier report, we presented cell degradation data for two types of steel [8]. In this report, we present results with Crofer 22. We also

measured the vapor loss of chromium oxyhydroxide from chromium oxide and two ternary compounds.

As discussed by Hilpert and others [9,10], the chromium oxyhydroxide is presumed to be reduced to chromium trioxide at the triple phase boundaries in the cathode as shown:

$$2CrO_2(OH)_2 + 6e^- + 3V^{\cdot\cdot} = Cr_2O_3 + 2H_2O + 3O^{2-} \quad [1]$$

It is further presumed that the oxide deposits block the access of oxygen to the electrochemically active sites and cause the performance decay of the cell. However, one might ask whether the chromium oxide interacts with the cathode and forms lanthanum chromite or perhaps the mixed perovskite $(La_{0.8}Sr_{0.2})\ Mn_xCr_{1-x}O_3$. The latter would be expected to have diminished oxide ion conductivity, and perhaps that is the reason for the performance decline of the cells. To test this hypothesis, we deliberately added chromium to cathodes and determined cell performance.

Approach

SOFCs of 2.5 cm x 2.5 cm with bipolar plates of Crofer 22 APU were operated at a constant voltage of 0.7 V for 50-200 hours. To enhance the chromium poisoning effect, we placed particles of the metal interconnect on top of the cathode. Next, a Pt current collector was placed on top of the cathode and particles. A plate of interconnect, with slits cut in it, was then placed on top of the Pt current collector. Separate cells with lanthanum ferrite (LSF), lanthanum manganite (LSM), or an A-site-deficient LSF cathode were operated at 700°C and 800°C. The air contained 2% humidity. The cells were operated until only 50% of the initial current was supported at 0.7 V. Post-operation analysis was done by scanning electron microscopy (SEM), and Cr distribution was determined by energy dispersive x-ray spectroscopy (EDS).

Weight loss from ~100-mg fine powder samples of Cr_2O_3, $LaCrO_3$, and $MnCr_2O_4$ was determined using a ThermoCahn thermogravimetric analyzer. The powders were prepared by a solid state synthesis reaction. Alumina powder was used as a standard. Runs were carried out using various combinations of temperature, 700°C and 800°C, and between 0 mol% and 25 mol% H_2O in a carrier gas of 20.1% O_2 in Ar. A flow rate of 50 sccm was used. The materials were allowed to reach temperature and given 1 hour to equilibrate.

Results

Full Cell Tests

Figure 1 provides SEM cross-section images of three different cathodes, all placed in contact with a Crofer 22 APU interconnect. Figure 1a shows an LSM cathode after 200 hours of operation; Figures 1b and 1c show a similar analysis of two different LSF cathodes after 50 hours. The length of time the cells were run was determined by how long it took to lose half their initial current at 0.7 V. The data indicate that the LSM cathode contained the least amount of chromium in the bulk of the cathode but a significant accumulation at the electrolyte interface. The LSF cathodes contained a higher chromium content that had accumulated more rapidly.

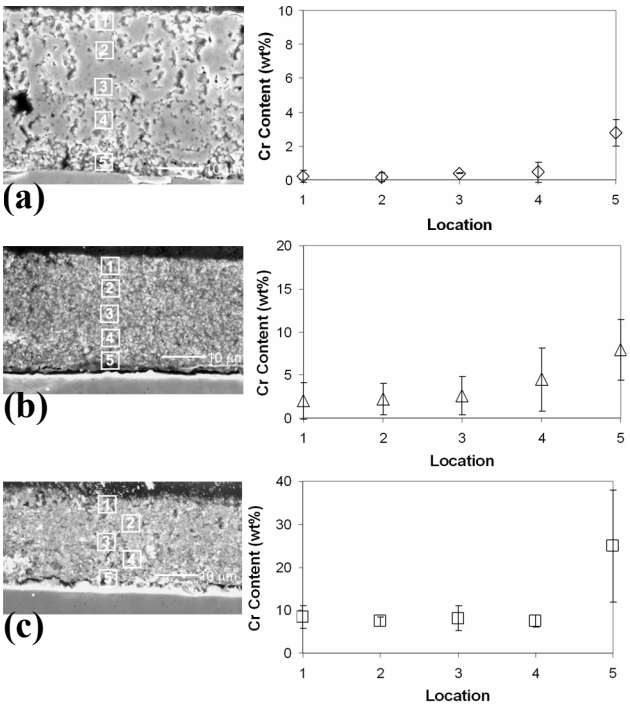

Figure 1. SEM of (a) LSM cathode, (b) LSF cathode, and (c) A-site-deficient LSF operated at 800°C with a Crofer 22 APU interconnect. The charts to the right correspond to the chromium content determined by EDS for points 1 through 5 for each cathode.

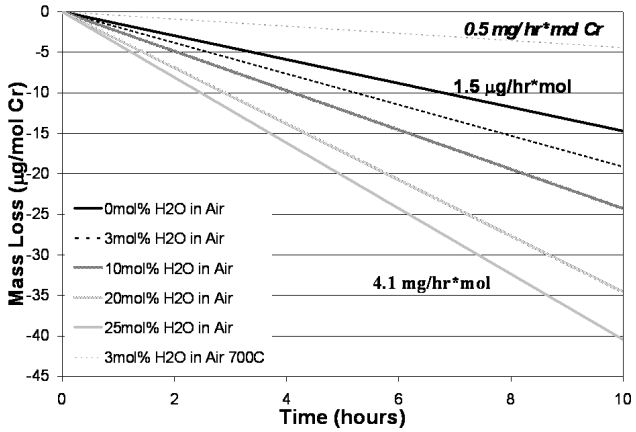

Figure 2. Mass Loss for Cr_2O_3 at 800°C with Various Levels of Water Content

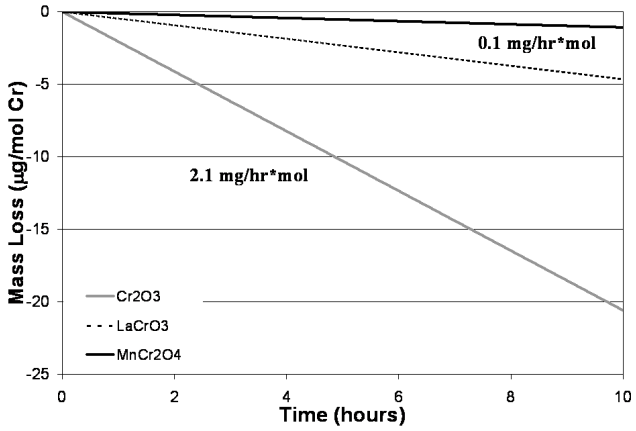

Figure 3. Mass Loss at 800°C, Air with 3 mol% Water, Normalized Relative to Moles of Chromium in the Compound

Thermogravimetric Analysis

Shown in Figure 2 are the mass losses of chromium oxide powder measured by thermogravimetric analysis in flowing air at 800°C with 0, 3, 10, 20, and 25 mol% water in air. Chromia reacts with oxygen and water to form a volatile species, and the weight loss is clearly related to the water content in the air, as one would expect for the formation of $CrO_2(OH)_2$.

Unlike most steels, Crofer 22 APU does not form a chromium oxide coating on the surface, but instead the manganese chromium spinel, $MnCr_2O_4$. Figure 3 shows the weight loss from the spinel along with chromia and the lanthanum chromium perovskite. From thermodynamic data, one would have

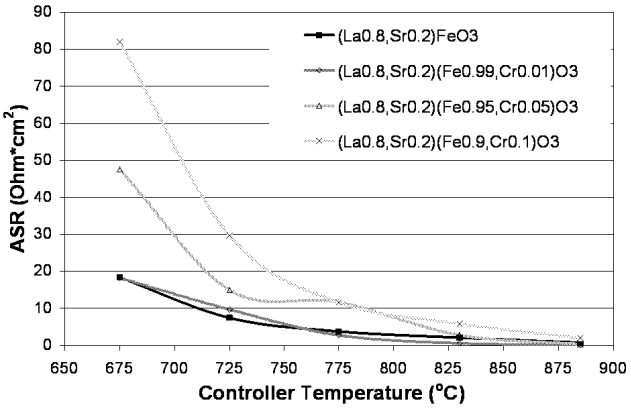

Figure 4. Effects of Chromium Doping on LSF for Various Concentrations and Temperatures

anticipated a difference in mass loss due to the volatility of the oxyhydroxide of about two orders of magnitude; however, only one order was observed.

Electrochemical Properties of Cr-Doped LSF

The effects of deliberately doping chromium into a cathode are seen in Figure 4. The area-specific resistances are plotted versus temperature for lanthanum ferrite doped with 0, 1, 5, and 10% chromium on the B site. One percent doping does not seem to have an effect, but 5 and 10% do.

Discussion

The electrochemical reduction of chromium oxyhydroxide, as shown in Equation 1, requires oxide ion vacancies in addition to electrons. In a comparison of the chromium concentrations and profiles in the three different cathode materials in Figure 1, it is readily apparent that the material with the lowest oxide ion conductivity (LSM) has also the lowest chromium content, which is largely concentrated at the electrolyte interface. Conversely, the substoichiometric LSF, which has the largest number of oxide ion vacancies, has the highest chromium content. Further, chromium is distributed across the entire cathode because the oxide ion formed by the reduction of the oxyhydroxide can be readily transported though the LSF to the electrolyte. These results show that the deposition of chromium is an electrochemical process.

It is tempting to correlate the volatility from the thermogravimetric measurements with the deposits

in the cathodes. Using the surface area of the oxide in the thermogravimetric experiment and the surface area of the Crofer in the electrochemical cells, we project the total chromium volatization in the cells to be very roughly 5,000 µg. We estimate the chromium contents in the cathodes to be approximately 150 µg in LSM, 800 µg in stoichiometric LSF, and 1,200 µg in substoichiometric LSF. This suggests that only a small fraction of the available chromium is actually reduced on the less active cathodes.

As mentioned, all the cathodes discussed here had lost approximately half their current density at a fixed potential of 0.7 V, when the cells were shut down, but the LSF cathodes contained obviously more chromium than the LSM cathode. Therefore, the LSF cathodes appear to be more tolerant to chromium contamination. Since the LSF cathodes have more active sites for oxygen reduction, it is conceivable that the loss of activity is caused by blockage of active sites. Alternatively, it is also possible that the number of oxide ion vacancies in the cathodes is decreased by chromium ions entering the cathode lattice and going into a plus four oxidation state. Figure 4 is consistent with such a mechanism. More work will have to be done to clarify the issue.

References

1. Hilpert, K., D. Das, M. Miller, D. H. Peck and R. Wei, *J. Electrochem. Soc*., 143, 3642 (1996).
2. Gindorf, C., L. Singheiser, and K. Hilpert, *Steel Research*, 72, 528 (2001).
3. Fryburg, G., F. Kohl, and C. Stearns, *J. Electrochem. Soc.,* 121, 952 (1974).
4. Ebbinghaus, B. B., *Combustion and Flame*, 93, 119 (1993).
5. Jiang, S. P., et al., *J. European Ceramic Society*, 22, 361 (2002).
6. Quadakkers, W. J., J. Piron-Abellan, V. Shemet, and L. Singheiser, *Materials at High Temperatures*, 20, 115 (2003).
7. Matsuzaki, Y. and I. Yasuda, *J. Electrochem. Soc*., 148, A126 (2001).
8. Kaun, T. D., T. A. Cruse, and M. Krumpelt, *Ceramic Engineering and Science Proceedings*, 25, (2004).
9. Jiang, S. P., *J. Power Sources,* 124, 390 (2003).
10. Matsuzaki, Y. and I. Yasuda, *J. Electroch. Soc.,* 148, A126 (2001).

Publications/Presentations

1. T. A. Cruse, M. Hash, T. Kaun, and M. Krumpelt, Interaction of Interconnect Materials with SOFC Cathodes, Fuel Cell Seminar, November 1-5, 2004, San Antonio, Texas.

III.A.2 Oxidation Resistant, Cr Retaining, Electrically Conductive Coatings on Metallic Alloys for SOFC Interconnects

Vladimir Gorokhovsky
Arcomac Surface Engineering, LLC
151 Evergreen, Suite D
Bozeman, MT 59715
Phone: (406) 522-7620; Fax: (406) 522-7617; E-mail: vigase@aol.com

DOE Project Manager: Travis Shultz
Phone: (304) 285-1370; E-mail: Travis.Shultz@netl.doe.gov

Objectives

- Enable the use of inexpensive metallic alloys as planar solid oxide fuel cell (SOFC) interconnects via protective coatings.
- Develop and demonstrate novel, cost-effective deposition processes to establish dense and uniform protective and functional coatings on metallic substrates.
- Evaluate protective coatings during exposures relevant to SOFC interconnects.
- Optimize deposition process parameters to maximize SOFC metallic interconnect performance and ultimately reduce cost.

Approach

- Design coating deposition process formulations based upon thermodynamic modeling and prior art.
- Deposit a matrix of candidate coatings on metallic substrates of interest for SOFC interconnects.
- Evaluate coated samples during exposure to SOFC interconnect conditions.
- Analyze sample performance and optimize coating deposition processes.
- Develop coating deposition system to meet Solid State Energy Conversion Alliance (SECA) SOFC interconnect cost and performance requirements.

Accomplishments

- Reduced metallic alloy oxidation rate by an order of magnitude. Rutherford backscattering spectroscopy (RBS) results indicate stainless steel samples with un-optimized, nanolayered CrN/AlN coatings exhibit an order of magnitude increase in oxidation resistance compared to uncoated counterparts.
- Developed and tested new, hybrid coating process combining electron beam physical vapor deposition (EBPVD), thermal evaporation and filtered arc deposition (FAD) to deposit dense $(Co,Mn)_3O_4$ coatings in an economically favorable process.
- Significantly reduced Cr volatility. Un-optimized coated samples of Crofer 22 APU [1] exhibited a fifteen-fold decrease in Cr volatility compared with their uncoated counterparts. Effectively complete blocking of Cr volatility is hopeful.
- Demonstrated 2,400+ hours of low and stable area specific resistance (ASR) values. Coated stainless steel samples demonstrated low and stable ASR values in air at 800°C for over 2,400 hours in contact with Ag paste.

Future Directions

- Evaluate coated stainless steels in more prototypical SOFC interconnect operating conditions. In collaboration with SOFC developers, samples of coated stainless steel will be subjected to SOFC small stack and other relevant testing to determine in-situ performance of coated stainless steel samples.
- Analyze the SOFC interconnect related performance of coated stainless steel samples to determine best coating system(s). Subsequent to SOFC stack testing, coated stainless steel samples will undergo a myriad of surface analyses to understand protection and performance improvement mechanisms.
- Conduct combined process performance and economic evaluations to elucidate the efficacy of novel coating approaches to enable use of inexpensive metallic alloys as interconnects in planar SOFC systems.

Introduction

The Arcomac Surface Engineering, LLC (ASE) SECA project has focused on the development of protective and functional coatings to enable the use of inexpensive metallic alloys as interconnects in planar SOFC systems. Currently, the interconnect component of planar SOFC systems accounts for a dominant portion of the overall SOFC stack cost. Inexpensive metallic alloys are under consideration for this component; however, when exposed to SOFC interconnect operation, metallic alloys form blanketing oxide scales, which dramatically degrade SOFC performance and limit device lifetime. To date, deleterious issues with Cr volatility, electrical resistance, and thermal-mechanical and chemical incompatibilities have restricted the use of metallic alloys as interconnects in planar SOFC systems. ASE has developed advanced coating deposition technologies that show promise for resolving these issues in an economically viable manner.

Approach

To achieve the cost and performance goals of SECA, the use of inexpensive metallic alloys as interconnect components is under investigation. Commercially available alloys exhibit unacceptable performance during SOFC interconnect operation. ASE is developing advanced, hybrid deposition technologies to establish protective coatings on commercially available alloys of interest to the SOFC interconnect application. Desired coating compositions and architectures are determined through thermodynamic and transport modeling in addition to prior art. Appropriate deposition materials are acquired, and deposition processes are designed and executed using ASE equipment. Coated samples are tested in conditions simulating SOFC interconnect operation, and performance of the sample coupons is analyzed. Results are employed to assist in developing new coating deposition process formulations. Promising coating systems from preliminary testing are then subjected to more prototypical SOFC interconnect conditions for further technical evaluations. Concurrently, economic evaluations of the coating process and interconnect component fabrication are ongoing.

Results

Figure 1 schematically illustrates the ASE-developed Filtered Arc Plasma Source Ion Deposition (FAPSID) surface engineering system [2]. The FAPSID system is an advanced, hybrid coating deposition chamber consisting of two dual large area filtered arc sources in conjunction with two unbalanced magnetron sputtering devices, two electron beam evaporators and a thermal resistance evaporation source in one universal vacuum chamber layout. This system has demonstrated the capability to deposit nanocomposite, nanolayered coatings with a wide variety of compositions and architectures.

The present ASE two-segment hybrid coating approach is shown schematically in Figure 2. Filtered arc deposited, nanolayered coatings of CrN/AlN, as shown in the tunneling electron microscopy (TEM) image in Figure 3a, have been investigated to comprise a lower, oxidation-resistant, bond segment coating. Additional elements such as Co, Ti, Mn, Y, and O have also been investigated for use in the lower, bond segment coating. This layer is designed to function as an effective barrier, blocking both inward and outward diffusion of oxidizing species, while acting as an adhesion system to the upper coating segment. A matrix of these lower segment coatings has been successfully deposited with

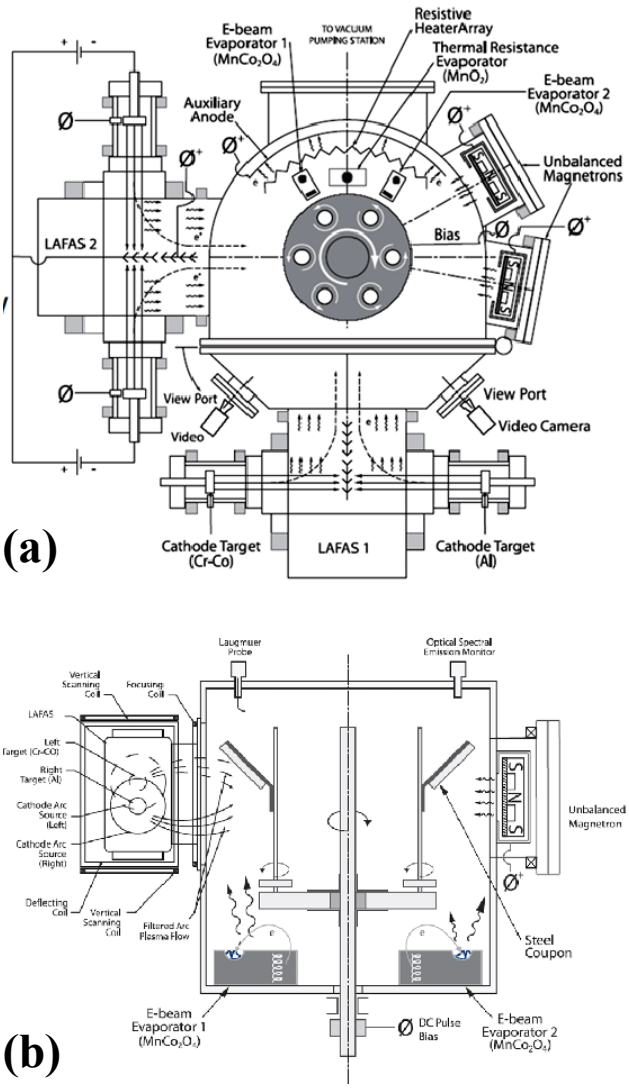

Figure 1. Schematic Illustration of the FAPSID Surface Engineering System, Showing (a) Top View and (b) Side View

excellent adhesion to metallic substrates under consideration for SOFC interconnects. Filtered arc-assisted EBPVD $(Co,Mn)_3O_4$ coatings after 800°C oxidation in air, as shown in the surface scanning electron microscopy (SEM) image in Figure 3b, comprise an electrically conductive, Cr-retentive and SOFC cathode-compatible upper coating segment. Other hybrid deposition methods employing filtered arc-assisted thermal resistance evaporation are also being explored to deposit the upper segment coating. A matrix of upper segment coatings has been successfully deposited in combination with and apart from the matrix of lower segment coating compositions.

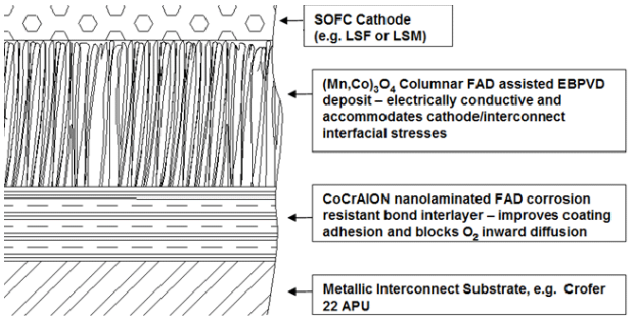

Figure 2. ASE's Two-Segment, Hybrid Coating Concept

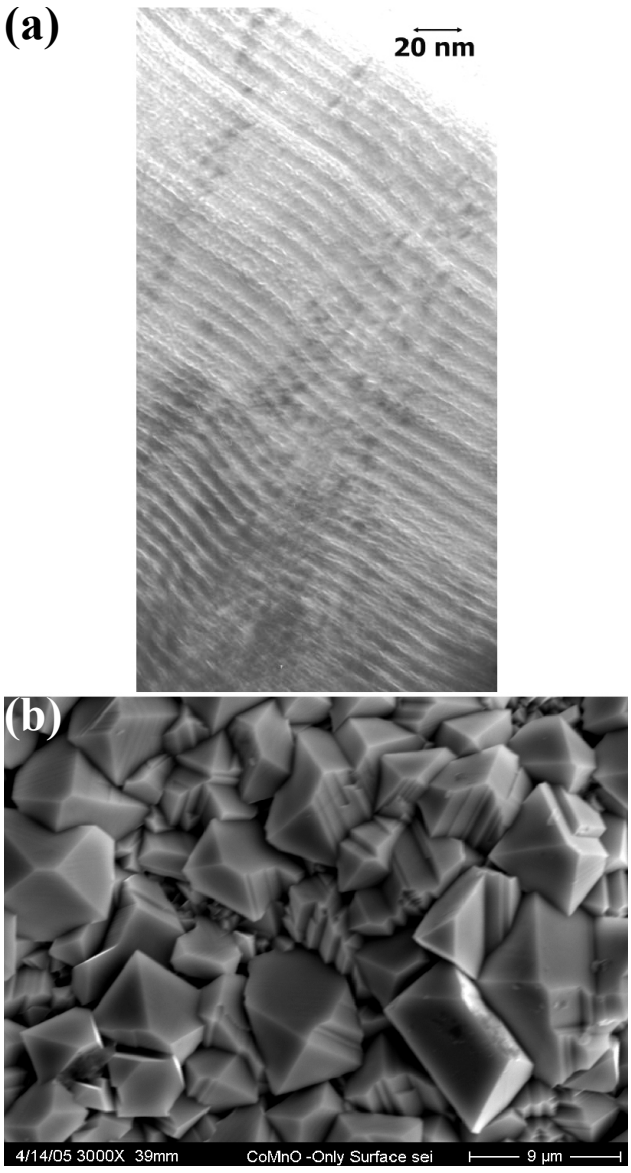

Figure 3. (a) Cross-Sectional TEM Image of FAD CrN/AlN Nanolayered Lower Segment Coating on Stainless Steel; and (b) Surface SEM Image of Filtered Arc-Assisted EBPVD $(Co,Mn)_3O_4$ Upper Segment Coating after 800°C Oxidation in Air

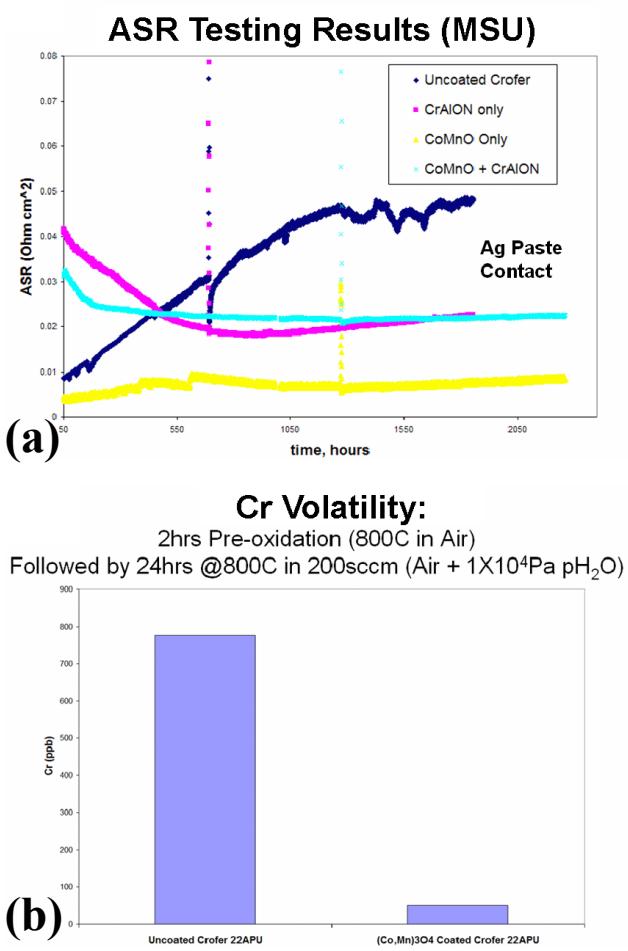

Figure 4. Summary of Preliminary ASR and Cr Volatility Results from Coated and Uncoated Crofer 22 APU

SOFC interconnect-related behavior of coated and uncoated samples—i.e., high-temperature oxidation, ASR, and Cr volatility—has been investigated in collaboration with researchers at Montana State University (MSU), Pacific Northwest National Laboratory, Lawrence Berkeley National Laboratory, and NASA-Glenn Research Center. Figure 4 displays a summary of the ASR and Cr volatility results. Low ASR values, excellent adhesion, oxidation stability and promising Cr volatility data suggest the efficacy of the ASE two-segment coating approach.

Conclusions

ASE has developed advanced coating deposition processes that may enable the use of inexpensive metallic alloys as interconnect components in planar SOFC systems. A wide variety of coating compositions and architectures is being investigated to meet SECA SOFC interconnect performance and cost requirements. A large-scale deposition system, offering favorable economics through high throughput and advanced hybrid design, is currently under development.

FY 2005 Publications/Presentations

1. "High temperature oxidation, Cr volatility and surface electrical conductivity of ferritic steel with and without filtered arc Cr-Al-O-N and/or filtered arc-assisted e-beam Co-Mn-O coatings," V.I. Gorokhovsky, Presented at the International Conference on Metallurgical Coatings and Thin Films (ICMCTF 05) in San Diego, CA, May 5, 2005
2. "Multilayer nanostructured cermet coatings for SOFC metallic interconnects," V.I. Gorokhovsky, Presented at the Sixth Annual SECA Workshop in Pacific Groove, CA, April 21, 2005
3. "Oxidation resistant, Cr retaining, conductive coatings on metallic alloys for SOFC interconnects," V.I. Gorokhovsky, Presented at the SECA Core Technology Peer Review Workshop in Tampa, FL, January 27, 2005

References

1. Crofer 22 APU "High Temperature Alloy" MSDS No. 8005 June, 2004 ThyssenKrupp VDM
2. V. Gorokhovsky, US Patent Application No.US2004/0168637 A1.

III.A.3 Metal Interconnect for SOFC Power Systems

S. (Elango) Elangovan
Ceramatec, Inc.
2425 South 900 West
Salt Lake City, UT 84119-1517
Phone: (801) 978-2162; Fax: (801) 972-1925; E-mail: Elango@ceramatec.com

DOE Project Manager: Lane Wilson
Phone: (304) 285-1336; E-mail: Lane.Wilson@netl.doe.gov

Objectives

- Select a surface treatment process for commercial ferritic stainless steel to reduce oxide scale growth rate.
- Optimize treatment process conditions to provide a stable, conductive scale.
- Measure the scale properties in conditions relevant to solid oxide fuel cells (SOFCs).
- Evaluate treated metal interconnects under SOFC stack conditions.

Approach

- Select a heat treatment process to achieve a thin, dense scale of a conductive oxide composition.
- Measure scale conductivity in air at target operating temperature.
- Measure air-side scale conductivity when the opposite side is exposed to fuel conditions (dual atmosphere test condition).
- Evaluate scale morphology under fuel cell operating conditions.
- Evaluate the effect of surface treatment on chromium volatility.
- Measure interconnect repeat unit resistance under stack operating conditions.

Accomplishments

- The surface treatment was found to reduce the scale growth rate as determined by thermogravimetry at 750°C. The treated metal coupons showed a parabolic rate constant of 5×10^{-9} $gm^2/cm^4/hr$ compared to 7×10^{-8} $gm^2/cm^4/hr$ of uncoated coupons. The low oxidation rate of treated interconnects will enable achieving the target fuel cell operating life of 40,000 hours.
- Scale resistance was 10 $milliohm.cm^2$ in air at 750°C and less than one $milliohm.cm^2$ in humidified hydrogen.
- Scale morphology was characterized as a function of treatment process and test conditions relevant to fuel cell operation.
- Stable, low resistance was demonstrated under dual atmosphere test conditions.
- Significant reduction in chromium evaporation was observed with treated metal coupons.
- No detectable reactivity of treated metal and potential cell joining perovskite compositions was observed.

Future Directions

- Measurement of interconnect resistance in repeat unit test.
- Verification of performance improvement in fuel cell stack tests.

Introduction

Interconnects perform essential functions in a fuel cell stack, namely, electrical connection between adjacent cells and separation of air and fuel. In many cases, they also provide structural support for the stack. The use of a commercial alloy offers the potential for low-cost interconnect components that help to achieve the DOE target of low-cost, modular fuel cell stacks.

The SOFC interconnect must simultaneously satisfy several functional requirements. These functions require materials with high electronic conductivity for the series connection of individual single cells, gas impermeability to separate fuel and oxidant gases, chemical stability and conductivity over a large oxygen concentration range in order to maintain integrity in both the fuel and air atmospheres. Thermal expansion match with the rest of the cell elements is desired. Metal interconnects are very desirable from the viewpoint of manufacturing cost in addition to other functional requirements, provided that the high conductivity can be maintained at the operating conditions. Metal also lends itself to ease of fabrication of gas channels; greater control over dimensions to help improve the conformity; and uniform reactant distribution to ensure uniform current density, high fuel utilization and high fuel efficiency. The use of thin metallic sheets will reduce overall weight in the fuel cell system. High thermal conductivity of metal interconnects will help distribute the heat generated during the operation of the cell, thereby reducing the cooling air requirement as well as eliminating thermal stress failure of ceramic components caused by sharp thermal gradients.

The principal requirements of metal interconnects can be summarized as follows: 1) thermal expansion match with other cell components, 2) oxidation resistance in air and fuel at the operating temperature, 3) conductive interface (scale) in air and fuel atmospheres, 4) prevention of reactivity with electrode materials to form insulating compounds, 5) low volatility of major or minor constituents that poison electrode activity, 6) compatibility with anode and cathode environments, 7) uniformity in contact with the cells, 8) thermal cycle capability, and 9) cost. The present work focuses on the development and evaluation of conductive oxide scale on commercial ferritic stainless alloys.

Approach

A commercial stainless steel alloy was selected. The surface oxide scale was modified using an appropriate coating and heat treatment process to provide a dense conductive oxide scale. The growth rate, resistivity, and morphology of the scale were determined as a function of time for the various surface treatment conditions. The evaluations were made both in single atmosphere (air or fuel) and dual atmosphere (air and fuel on the opposite sides) conditions. Comparison of chromium evaporation characteristics of treated and untreated metal coupons was made using MgO powder as the chromium-getter.

Results

Thermogravimetry of a 400-series commercial stainless steel was performed. Both untreated and treated coupons were evaluated. Two types of treatments were done. The first one was to heat treat the coupon to grow a controlled, dense oxide scale layer (treatment 50C940). In a second variation, an additional treatment was performed to provide a stable chromium oxide composition as the outer layer (treatment MI2). The comparison of the oxide scale growth, via weight gain, is shown in Figure 1. The pre-grown oxide layer was found to reduce the scale growth significantly, while the second treatment provided an additional reduction in scale growth rate.

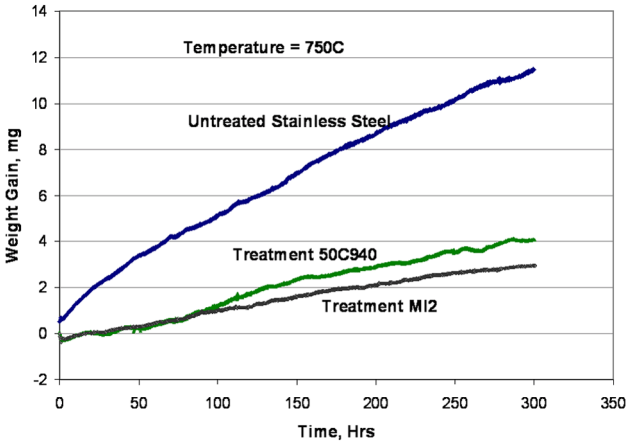

Figure 1. Thermogravimetry of Ferritic Stainless Steel Coupons

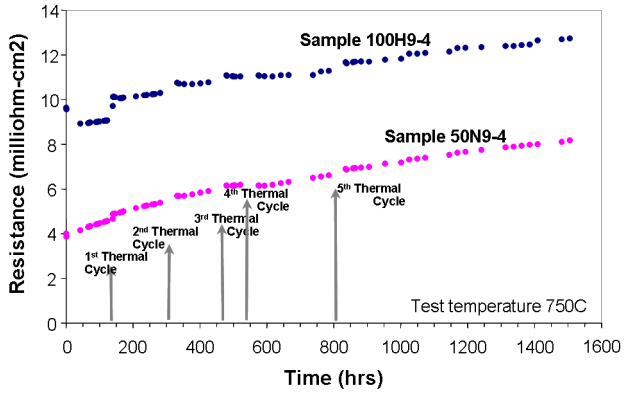

Figure 2. Resistance of Coupon Couples in Air at 750°C

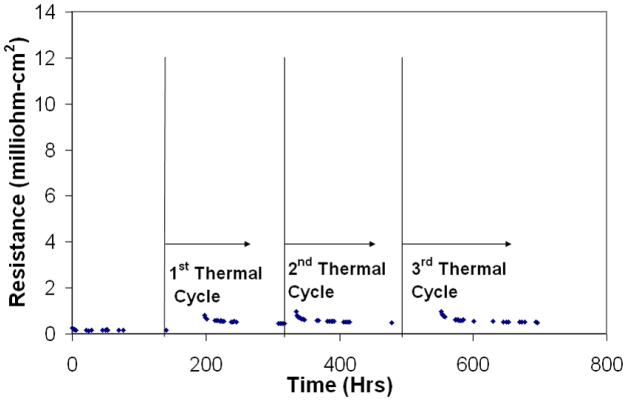

Figure 3. Resistance of Coupon Couples in Humidified Hydrogen at 750°C

The resistances of the coupons were measured after they were surface treated. Two coupons were sandwiched using a conductive perovskite (e.g., cobaltite) as the contact paste. The change in measured resistance values of the coupon couples at 750°C in air is shown in Figure 2. The coupons were subjected to several thermal cycles. Similar measurements were also made in humidified hydrogen using nickel paste as the contact layer, shown in Figure 3. In both atmospheres, the resistance values were below 10 milliohm.cm^2, meeting the target interconnect resistance.

Earlier work showed that the oxide scale on the air side is disrupted when the opposite side is exposed to hydrogen at the target cell operating temperature. In order to evaluate the effect of dual atmosphere exposure, resistance of coupon couples was measured when one coupon was exposed to dual atmosphere. The test arrangement and the results of a test using the graded scale composition are shown

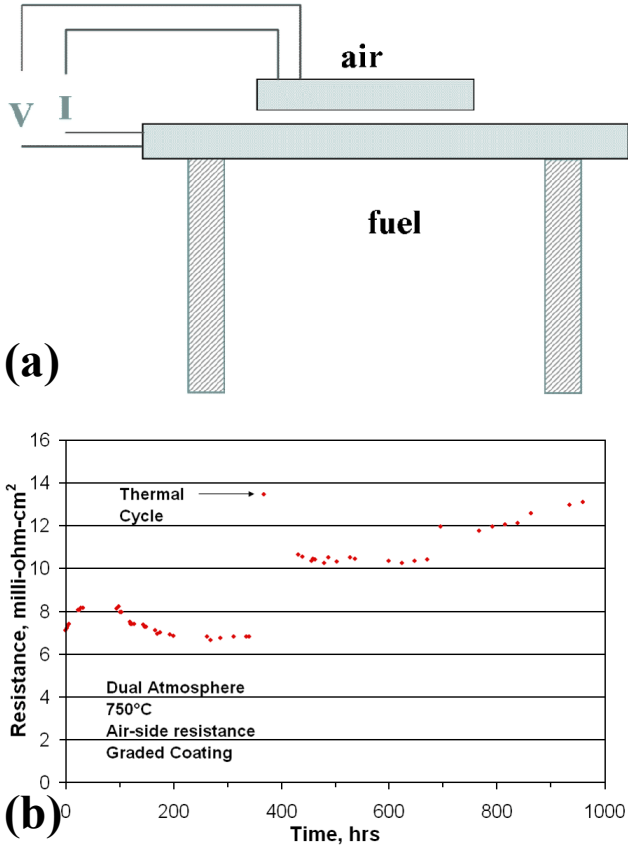

Figure 4. Test Configuration and Resistance of Coupon Couples in Dual Atmosphere

in Figure 4. The low resistance measured under realistic exposure conditions is encouraging, although additional work is needed in characterizing possible changes in scale morphology under such conditions.

Chromium evaporation characteristics of the untreated and treated metal coupons were evaluated using an MgO-getter. A schematic of the test arrangement is shown in Figure 5. Various coupons were exposed to the getter material at 750°C for 300 hours. A significant reduction in chromium content was noted for the treated coupons, as shown in Table 1.

Table 1. ICP Analysis of Al_2O_3 Powder (ppm by weight)

	Baseline powder	Powder exposed to untreated coupon	Powder exposed to treated coupon	Powder exposed to treated and LSCo thermal sprayed coupon
Cr	< 0.5	250	140	4.1

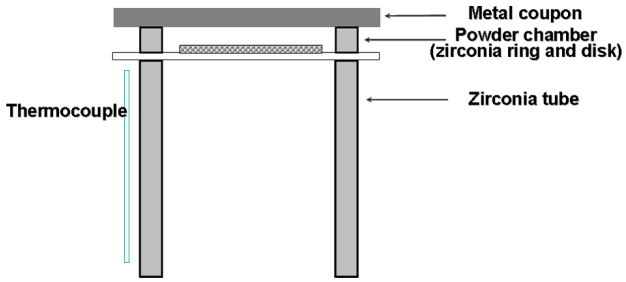

Figure 5. Test Configuration for Chromium Evaporation Assessment

Mixtures of treated and untreated stainless steel powder and perovkite powder were heat treated to evaluate the reactivity. The treated metal powder did not show any evidence of new phases based on X-ray diffraction analysis.

Conclusions

- Surface treatment to commercial ferritic stainless steel is shown to reduce the oxidation rate in air at SOFC operating temperature.
- The resistance values of the stainless interconnect meet the target.
- The surface treatment provides improved stability to the scale under dual atmosphere exposure conditions.
- A significant reduction in chromium evaporation rate was demonstrated.
- The treatment also suppresses reactivity of metal with cell joining perovskite materials.

FY 2005 Publications/Presentations

1. "Selection and Surface Treatment of Alloys in Solid Oxide Fuel Cell Systems," S. Elangovan, S. Balagopal, J. Hartvigsen, I. Bay, D. Larsen, M. Timper, and J. Pendleton, submitted to the Journal of Materials Engineering and Performance, 2005.
2. SECA Annual Workshop and Core Technology Program Peer Review Workshop, Pacific Grove, CA, April 2005.

III.A.4 Novel Sulfur-Tolerant Anodes for Solid Oxide Fuel Cells

Meilin Liu (Primary Contact), Shaowu Zha, Zhe Cheng, Jian Dong, Yongman Choi
School of Materials Science and Engineering, Georgia Institute of Technology
771 Ferst Drive
Atlanta, GA 30332-0245
Phone: (404) 894-6114; Fax:(404) 894-9140; E-mail: meilin.liu@mse.gatech.edu

DOE Project Manager: Lane Wilson
Phone: (304) 285-1336; E-mail: Lane.Wilson@netl.doe.gov

Objectives

- Understand the effect of sulfur poisoning on fuel cell performance and the recovery process under various operating conditions.
- Investigate the detailed mechanisms for sulfur poisoning of nickel-based anodes.
- Establish scientific principles for rational design of better sulfur-tolerant anodes that show high performance.
- Explore new sulfur-tolerant materials to meet Solid State Energy Conversion Alliance (SECA) program objectives.

Approach

- Characterize sulfur poisoning and regeneration processes using a DC polarization technique and impedance spectroscopy.
- Analyze and predict the thermodynamic stability of nickel in fuel environment containing 50 ppm H_2S.
- Examine nickel-sulfur interactions on the anode surface using x-ray diffraction (XRD) and Raman microspectroscopy.
- Compute and model sulfur adsorption on Ni and Cu surfaces using quantum chemistry calculations.
- Synthesize and test vanadium- and molybdenum-based materials as potential sulfur-tolerant anodes.

Accomplishments

- A DC polarization technique and electrochemical impedance spectroscopy have been used to evaluate *in-situ* the poisoning effect of hydrogen sulfide on nickel-based anodes. The adsorbed sulfur bonds to nickel very fast, leading to a rapid decrease in cell performance. The recovery process of the poisoned anode can be realized by continuous flowing of a clean fuel gas. The degree of sulfur poisoning decreases and the recovery rate increases with increasing operating temperature. Also, the regeneration rate increases with the current passing through the cell.
- For Ni-YSZ anodes exposed to hydrogen containing 100 ppm H_2S at 727°C, thermodynamic calculations indicate that Ni-YSZ would be stable, and XRD analysis was unable to detect any changes. However, the vibration modes of Ni_3S_2 were detected using Raman spectroscopy, suggesting that Raman spectroscopy could be a powerful tool for *in-situ* study of sulfur poisoning of solid oxide fuel cell (SOFC) anodes.
- Interactions between sulfur and Ni- or Cu-based anodes for SOFCs have been examined by ab initio periodic density functional theory (DFT) calculations to predict the sulfur tolerance and vibrational frequencies for adsorbed sulfur species. Sulfur prefers being located at the high-coordination adsorption sites on both Ni (111) and Cu (111) surfaces.
- Some new perovskite- and pyrochlore-phase based complex oxides have been developed for highly sulfur-tolerant anode materials. Vanadium-based compounds ($SrVO_3$ and $La_{0.7}Sr_{0.3}VO_3$) and $Gd_2Ti_{1.4}Mo_{0.6}O_7$

demonstrate good sulfur tolerance and high catalytic activity in H_2S-containing fuels and thus are possible candidates for modifying the surface of the Ni-YSZ anode.

Future Directions

- Elucidate the mechanisms for H_2S adsorption, decomposition, and interaction with nickel and oxide materials using *in-situ* characterization techniques in order to facilitate the design of new anode materials with sulfur tolerance.
- Model the anode-sulfur interactions using quantum chemistry principles. Conduct more detailed studies of transition-metal oxide/sulfide/oxysulfide surfaces to assist the search for H_2S-tolerant materials both theoretically and experimentally.
- Investigate new classes of sulfur-tolerant materials. Modify the Ni-YSZ with an additive/Ni surface decorative/protective layer that has suitable redox chemistry, where H_2S is selectively adsorbed/captured by the additive and subsequently oxidized to elemental sulfur or SO_2.

Introduction

One of the unique advantages of SOFCs over other types of fuel cells is the possibility of direct internal reforming of commercial hydrocarbon fuels, thereby eliminating the need for a separate fuel processing subsystem. However, all fossil fuels contain some sulfur; in reforming, the sulfur is converted to gaseous hydrogen sulfide (H_2S). Current SOFC anodes have very limited tolerance to H_2S. As a result, the H_2S concentration in the feed fuel must be reduced to no more than a few ppmv for optimum performance [1-3]. Although considerable efforts have been devoted to the development of sulfur-tolerant anode materials [4,5], a detailed understanding of the sulfur poisoning mechanism is still lacking.

This project focuses on the exploration of new sulfur-tolerant anode materials having high electronic conductivity, good chemical and thermal stability in sulfur-containing atmospheres, and high catalytic activity for preferential oxidation of H_2S to SO_2. Also, unique anode/catalyst architecture(s) will be designed to achieve high performance and long-term stability. A broad, in-depth study will be performed to provide a theoretical basis for understanding sulfur degradation processes and conceptualizing strategies for sulfur tolerance. The study will include a wide range of measurements to (i) characterize intermediate species and reaction products, (ii) correlate catalytic properties with anode composition and microstructure as well as fuel cell performance, (iii) follow sulfur-hydrogen-oxygen interactions on anode surfaces, and (iv) model and predict the electrochemical reactions and transport processes within the anode. Various characterization techniques will be used to probe surface reactions involving sulfur or sulfur-containing compounds, *in-situ*, in an SOFC under practical operating conditions perturbed by various electrical and chemical stimuli, and the gas phase chemistry, electrochemistry, and electrical responses will be simultaneously monitored.

Approach

We used a DC polarization technique and electrochemical impedance spectroscopy to evaluate *in-situ* the poisoning effect of hydrogen sulfide on nickel-based anodes. Both symmetrical cells and functional solid oxide fuel cells were prepared and tested in various atmospheres. An EG&G potentiostat/galvanostat operating in potentiostatic mode was used to continuously monitor the current passing through the cell at a constant voltage. Impedance responses of the cell under open-circuit conditions were also measured in the clean fuel mixture after it was exposed to 50 ppm H_2S and after it was regenerated.

For the spectroscopic studies, porous Ni-YSZ samples were exposed to H_2S-containing fuel at 727°C for 5 days. The nickel-sulfur interactions on the anode surface were examined using Raman microspectroscopy and XRD after the samples were cooled down to room temperature.

Solid-state reaction method was used to prepare perovskite $SrVO_3$, $La_{0.7}Sr_{0.3}VO_3$ (LSV) and

pyrochlore $Gd_2Ti_{1.4}Mo_{0.6}O_7$ (GTMO) anode materials. Electrical conductivity and chemical stability were examined in reducing atmosphere with and without H_2S. Functional solid oxide fuel cells based on these new anode materials were fabricated and tested to evaluate their sulfur tolerance.

Results

Both thermodynamic calculations and H_2S exposure experiments have been done to examine the reactions between sulfur and nickel-based anodes. At high H_2S concentrations, nickel will react with sulfur to form bulk Ni-S reactants. Nickel still exists in the metallic state at P_{H_2S}/P_{H_2} values below 10^{-2} – 10^{-3}. However, sulfur will bond to Ni very strongly to form a surface nickel sulfide and, hence, block the active Ni sites which are essential for H_2 dissociation and surface diffusion. We have successfully identified the formation of surface Ni_3S_2 using Raman spectroscopy (as shown in Figure 1),

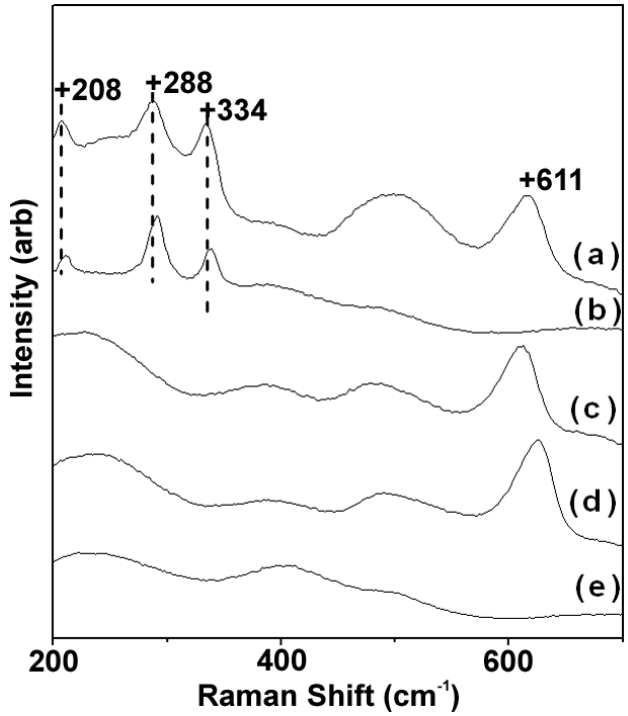

Figure 1. Raman spectra of different samples: (a) Ni-YSZ cermet after exposure to H_2 containing 100 ppm H_2S at 727°C for 120 hours, (b) Raman spectra of reference Ni_3S_2 sample (containing small amount of Ni_7S_6) for comparison, (c) Ni-YSZ cermet before exposure to H_2 containing 100 ppm H_2S, (d) YSZ pellet, (e) Ni foil.

although such surface nickel sulfide cannot be detected by XRD measurement.

The fuel cell, with a configuration of Ni-YSZ/ YSZ/LSM, was tested by exposing the Ni-YSZ anode to a clean fuel mixture (50% H_2 / 1.5% H_2O / 48.5% N_2) and a fuel mixture containing 50 ppm H_2S (50 ppm H_2S / 50% H_2 / 1.5% H_2O / 48.5% N_2) in turn. Shown in Figure 2 are plots of the current density as a function of time. The adsorbed sulfur bonds to Ni very fast, forming surface nickel sulfide and thus causing a quick degradation in performance due to the blocking of active Ni sites for hydrogen oxidation. The performance can be recovered by switching back to the clean fuel mixture without

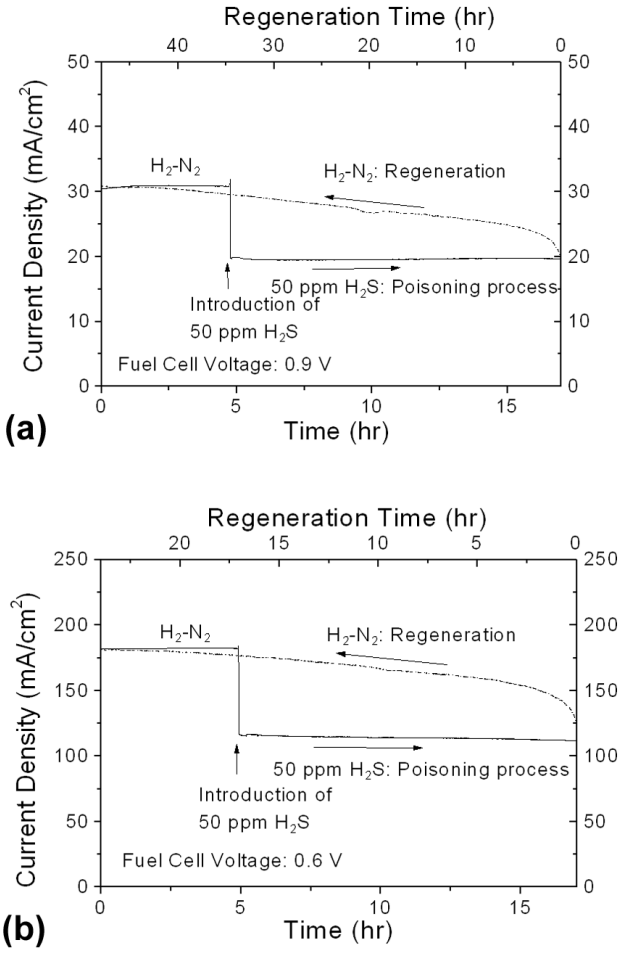

Figure 2. Plots of cell current densities as a function of time for an SOFC at different cell voltages at 800°C, showing the effect of sulfur poisoning and regeneration processes. The Ni-YSZ anode was fed by a clean gas mixture, a gas mixture containing 50 ppm H_2S, and a clean gas mixture in turn.

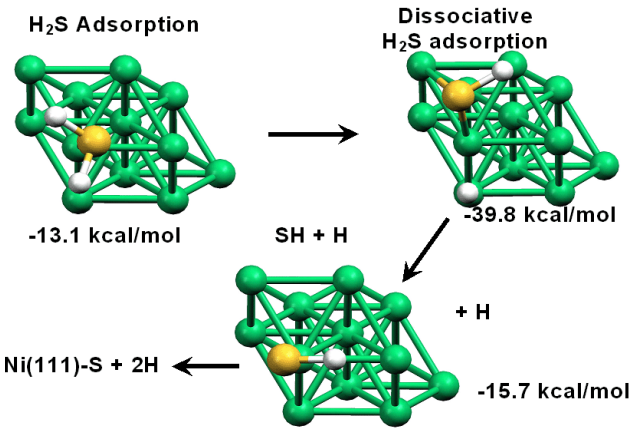

Figure 3. H_2S decomposition on Ni (111) surface. Note: Energies are relative to the energy for Ni (111) + H_2S.

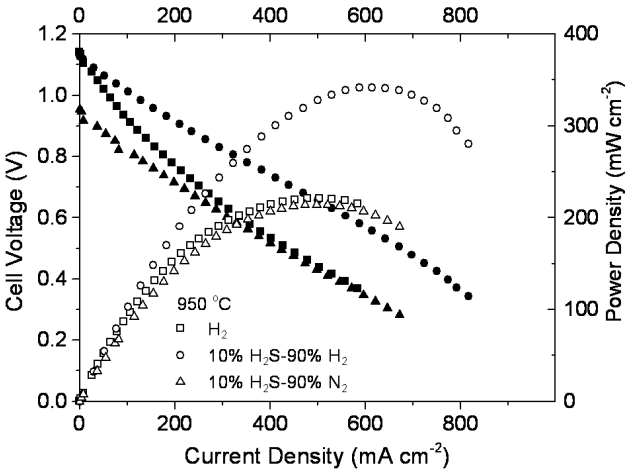

Figure 4. Typical performances at 950°C of a fuel cell with $Gd_2Ti_{1.4}Mo_{0.6}O_7$ anode operating in different humidified fuels: H_2, 10% H_2S in H_2, and 10% H_2S in N_2.

H_2S. Both the poisoning effect and the regeneration process are strongly influenced by the operating temperature. Higher temperature can alleviate the H_2S poisoning effect and accelerate the recovery process. A higher fuel cell operation current is also favorable for the recovery process.

Quantum chemistry calculation has been used to estimate the adsorption energy of sulfur species on different surface sites of both Ni and Cu. Figure 3 shows the hypothetical H_2S decomposition processes on the Ni surface. It is demonstrated that the adsorption of sulfur on the Ni surface is extremely quick (in 110×10^{-15} s) under SOFC operating conditions at 700°C. This theoretical prediction well supported our experimental results. The possible step-by-step adsorption processes proposed are consistent with our investigations using DC polarization measurements and Raman spectroscopy.

Several material families such as perovskite $La_{1-x}Sr_xVO_3$ (LSV) and pyrochlore $Gd_2Ti_{2-x}Mo_xO_7$ are investigated as sulfur-tolerant anodes. Shown in Figure 4 are the current-voltage characteristics and the corresponding power densities for a fuel cell using $Gd_2Ti_{1.4}Mo_{0.6}O_7$ as the anode. A moderate performance was obtained when the anode was fed on pure H_2. In comparison, the cell performance increased significantly when a high concentration of H_2S was introduced into the feed. The GTMO anode based SOFC was further tested using only H_2S as the fuel. The open circuit voltage was 0.2 V lower than that for H_2 containing 10% H_2S, due to lower concentration of fuel. A peak power density of 214 mW cm^{-2} was obtained at 950°C. These performance data were collected at a flow rate of 12 mL min^{-1}, implying a fuel utilization of about 60% at higher current densities. These results demonstrate that the GTMO represents a promising sulfur-tolerant anode material for SOFCs. Vanadium-based compounds also demonstrated excellent sulfur tolerance and high catalytic activity in high H_2S-containing fuels and thus are possible candidates for modifying the surface of the Ni-YSZ anode.

Conclusions

Thermodynamic calculations demonstrated that the Ni-S system shows many phase transitions at high temperatures and over a wide range of H_2S concentrations. At P_{H_2S}/P_{H_2} values below $10^{-2} - 10^{-3}$, nickel still exists in the metallic state at 600 – 1000°C. The formation of surface Ni_3S_2 can be determined using Raman spectroscopy, although this surface nickel sulfide cannot be detected by XRD measurement. Quantum chemical calculations suggested that surface sulfides are significantly more stable than bulk nickel sulfides. The adsorbed sulfur bonds to Ni very fast, forming surface nickel sulfide and leading to degradation in performance due possibly to the blocking of active Ni sites for hydrogen oxidation.

For both symmetrical cell and functional fuel cells, the degradation in performance can be recovered, at least in part, by switching from the H_2S-containing fuel to a clean fuel. Both the degree and rate of H_2S poisoning and the rate of the regeneration process are strongly influenced by the operating temperatures. High temperature can alleviate the H_2S poisoning and enhance the recovery process. Fuel cell operation current is also favorable for the recovery process.

The adsorption of sulfur on nickel is chemical in nature. Thus, it is still critical to develop new anode materials or to modify the conventional Ni anode surface to achieve sulfur tolerance. Both perovskite-based vanadium compounds and pyrochlore-based $Gd_2Ti_{1.4}Mo_{0.6}O_7$ demonstrated remarkable tolerance to sulfur and high catalytic activity in high H_2S-containing fuels and thus are possible candidates for modifying the surface of the Ni-YSZ anode.

FY 2005 Publications/Presentations

1. S. Zha, P. Tsang, Z. Cheng, and M. Liu, "Electrical Properties and Sulfur Tolerance of $La_{0.75}Sr_{0.25}Cr_{1-x}Mn_xO_3$ under Anodic Conditions", *Journal of Solid State Chemistry*, 178, 1844-1850, 2005.
2. S. Zha, Z. Cheng, and M. Liu, "A Sulfur-Tolerant Anode for SOFCs", *Electrochemical and Solid State Letters,* in press.
3. Z. Cheng, S. Zha, L. Aguilar, and M. Liu, "Properties of $La_{1-x}Sr_xVO_3$ as Candidate Sulfur Resistant Anode Materials for SOFC", *Solid State Ionics*, in press.
4. J. Dong, Z. Cheng, S. Zha, and M. Liu, "Identification of Nickel Sulfides on Ni-YSZ Cermet Exposed to H_2 Fuel Containing H_2S Using Raman Spectroscopy", *Journal of Power Sources*, accepted.
5. Z. Cheng, L. Aguilar, S. Zha, J. Dong, D. Wang, and M. Liu, "A Solid Oxide Fuel Cell Running on Sour Natural Gas", *Electrochemical and Solid State Letters*, submitted.
6. S. Zha, Z. Cheng, and M. Liu, "Sulfur Poisoning and Regeneration of Ni-based Anodes", *Journal of Catalysis*, submitted.
7. Y. M. Choi, C. Compson, M. C. Lin, and M. Liu, "Sulfur Tolerance of Ni and Cu Anodes for Solid Oxide Fuel Cells Predicted by Periodic *Ab Initio* Density Functional Theory", *Chemical Communications*, submitted.
8. J. Dong, S. Zha, and M. Liu, "Study of Sulfur-Ni Interactions Using Raman Spectroscopy", Poster, 207th ECS Meeting, Canada, 2005.
9. S. Zha, Z. Cheng, Y. Choi, and M. Liu, "Sulfur-Tolerant Anodes for SOFCs", Presented to the Annual SECA meeting, Monterey, CA, April 18-21, 2005.

References

1. Y. Matasuzaki, I. Yasua, Solid State Ionics 132 (2000) 261.
2. D.W. Dees, et al, in Proceedings of the First International Symposium on SOFCs, PV 89-11, p. 317, The Electrochemical Society Proceedings Series, Pennington, NJ (1989).
3. J. Geyer, et al, in Proceedings of the 5th International Symposium on SOFCs (SOFC-V), PV 97-40, p. 585, The Electrochemical Society Proceedings Series, Pennington, NJ (1997).
4. R. Mukundan, E.L. Brosha, F.H. Garzon, Electrochem. Solid-State Lett. 7 (2004) A5.
5. L. Aguilar, S. Zha, S. Li, M. Liu, J. Winnick, Electrochem. Solid-State Lett. 7 (2004) A324.

III.A.5 Functionally Graded Cathodes for Solid-Oxide Fuel Cells

Meilin Liu (Primary Contact), Harry Abernathy, Y. M. Choi, Rupak Das, Jian Dong, Erik Koep, Ying Liu, David Mebane, Robert Williams Jr., and Yuelan Zhang
School of Materials Science and Engineering, Georgia Institute of Technology
771 Ferst Drive
Atlanta, GA 30332-0245
Phone: (404) 894-6114; Fax: (404) 894-9140; E-mail: meilin.liu@mse.gatech.edu

DOE Project Manager: Lane Wilson
Phone: (304) 285-1336; E-mail: Lane.Wilson@netl.doe.gov

Objectives

- Elucidate oxygen reduction mechanism on perovskite cathode materials.
- Investigate bulk- versus surface-mediated electrochemical processes using patterned cathodes.
- Provide a model for prediction of potential and current distributions in a patterned mixed-conducting electrode.
- Complete preliminary mathematical modeling of cathodic processes such as adsorption, dissociation, charge transfer, and surface transport.
- Identify active reaction sites for different mixed ionic/electronic conducting (MIEC) cathode materials.

Approach

- Carry out *in-situ* surface Raman and Fourier transform infrared (FTIR) measurements to detect adsorbed oxygen species and interpret the spectroscopic data by means of quantum-chemical calculations.
- Fabricate patterned electrodes using photolithography and pulsed-laser deposition (PLD) and analyze the electrodes using electrochemical impedance spectroscopy (EIS).
- Develop a methodology for analyzing the effect of sheet resistance on patterned electrode performance using a finite element technique.
- Model measured impedance spectra on metal and MIEC cathodes as a function of temperature, partial pressure of oxygen, and overpotential to elucidate gas-surface interactions.
- Determine significant active sites for triple-phase boundary (TPB), mixed-conductor surface, and electrolyte surface with patterned electrodes using tip-enhanced Raman scattering (TERS) and surface-enhanced Raman spectroscopy (SERS), and interpret the surface spectroscopic results using quantum-chemical calculations.

Accomplishments

- *In-situ Surface Raman Scattering and FTIR Studies of MIEC Electrodes:*
  SERS was successfully applied to examine Ag-$Sm_{0.5}Sr_{0.5}CoO_3$ (SSC) cathode material prepared by a combustion chemical vapor deposition (CCVD) method. In addition, gadolinia-doped ceria (GDC) and undoped CeO_2 were used to identify adsorbed oxygen species using *in-situ* surface Raman spectroscopy and quantum-chemical calculations, confirming that the band at 831 cm^{-1} is attributed to peroxide-like oxygen species. To calculate oxygen reduction kinetic parameters on an SSC pellet, rapid scan time-resolved spectroscopy (TRS) was utilized by changing the atmosphere from 100% O_2 to 1% O_2.
- *Patterned Electrodes Fabricated by Photolithography and PLD:*
  The characteristic thickness at 700°C for dense lanthanum strontium manganese oxide (LSM) was found to be 0.36 μm. Above 0.36 μm, ionic diffusion is sufficiently difficult such that oxygen ion transport

through the LSM electrode is essentially negligible. Beyond this point, the surface of the LSM electrode cannot be effectively used, and the behavior of the electrode is determined largely by the TPB of the electrode.

- *Modeling of Sheet Resistance for Patterned Electrodes:*
  A thickness of 0.06 μm is the lower cathode thickness limit for LSM, as the sheet resistance becomes unreasonably high below this point. For a particular geometry, similar studies as this one can be performed, and the percent utilization can be calculated for all the geometries.
- *Theoretical Faradiac Impedance Calculations:*
  Elementary reaction pathways on platinum cathode material were updated to apply to both platinum and MIEC cathode materials, analyzing experimental impedance spectra.

Future Directions

- Conduct TERS and SERS measurements to determine oxygen reduction sites on lanthanum strontium manganese oxide (LSM), lanthanum strontium cobalt oxide (LSC), lanthanum strontium iron oxide (LSF), and strontium samarium cobalt oxide (SSC) and to examine potential-dependent effects.
- Propose more reliable oxygen reduction mechanisms on cathode materials using quantum-chemical calculations and mathematical modeling.
- Develop a 3-D model for patterned electrodes, including surface diffusion and gas-phase diffusion, and analyze the model with respect to varying the model parameters, including electrochemical constants and electrode geometry.

Introduction

Solid oxide fuel cell (SOFC) research at Georgia Institute of Technology (GT) has focused on both experimental and theoretical understanding of oxygen reduction mechanism on cathode materials in SOFCs. Elucidation of the detailed mechanism – in particular, the rate-limiting processes – is a critical step in developing low-temperature SOFCs (400ºC to 700ºC), leading to cost reduction due to the ability to use less expensive materials. Cell performance at the desired lower temperatures is limited by interfacial polarization resistances, specifically by those associated with the cathode. The cathode interfacial polarization resistance can be reduced by dramatically accelerating the oxygen reduction rate based on understanding of various elementary processes at the interface: the transport of oxygen gas through the porous cathode, the adsorption of oxygen onto the cathode surface, the reduction and dissociation of the oxygen molecule (O_2) into the oxygen ion (O^{2-}), and the incorporation of the oxygen ion into the electrolyte for it to be transported across to the anode.

To systematically carry out the Solid State Energy Conversion Alliance (SECA) project, five research approaches have been included:

- Experimental determination of the rate-limiting step in the oxygen reduction mechanism at the cathode using *in-situ* FTIR and Raman spectroscopy.
- Fabrication and testing of micro-patterned cathodes to compare the relative activity of the TPB to that of the rest of the cathode surface.
- Construction of a mathematical model to predict cathode performance based on different geometries and microstructures.
- Fabrication of cathodes that are graded in composition and microstructure to generate large amounts of active surface area near the cathode/ electrolyte interface.
- Application of advanced quantum-chemical calculations to interpret measured spectroscopic information, as well as to guide design of highly efficient cathode materials.

Approach

Advanced experimental and theoretical methods have been applied to the design of functionally graded cathode materials in SOFCs in terms of lowering the operating temperature below 700°C.

To elucidate oxygen reduction on MIEC electrodes using *in-situ* Raman scattering, it has become necessary to increase the signal-to-noise ratio of the peaks associated with surface species. Otherwise, the Raman signal from the surface is not strong enough to be detected above the background noise. The enhanced Raman signal is being created by either (1) depositing silver nanoparticles on the cathode surface (surface-enhanced Raman spectroscopy, or SERS) or (2) placing a metallic atomic force microscope tip within a few nanometers of the cathode surface (tip-enhanced Raman scattering, or TERS). To generate a SERS effect, a CCVD method was used to co-deposit the cathode material with the silver particles. Other deposition methods, including sputtering and colloidal silver precursors, have also been used. Along with the spectroscopic measurements, quantum-chemical calculations were carried out to interpret the experimental data at the molecular level.

For fabrication of patterned electrodes, dense $La_{0.8}Sr_{0.2}MnO_3$ (LSM) electrodes of precisely controlled geometries were patterned by photolithography and fabricated via PLD on yttria-stabilized zirconia (YSZ) electrolytes. All electrode arrays contained constant surface area and TPB length while varying only in thickness. Impedance analysis of cells with patterned electrodes of different thicknesses was performed to study the effect of the interfacial resistance as a function of electrode thickness.

To model the patterned electrodes, we utilized the commercial finite element code Femlab, as well as the commercial computational fluid dynamics code Fluent. The sheet resistance of patterned electrodes was estimated as a function of the geometry and feature size. The effect of sheet resistance on the utilization of the electrodes was examined as well. The geometrical parameters were varied in order to show the dependence of interfacial conductance and TPB length utilization on the sheet resistance at different electrode thicknesses.

To directly model the impedance spectroscopic data, various oxygen reduction mechanisms were proposed for perovskite MIEC materials, since the mechanism on platinum metal surface didn't reproduce experimental impedance measurements due to different surface properties. For a new model, we have simulated the Faradiac impedance, $Z_F(\omega)$, in the equivalent circuit to represent the theoretical response. We have also simulated the total impedance, $Z(\omega)$, to more closely match with our experimental techniques.

Results

SERS has been used to examine the bulk cathode material and atomic and molecular species adsorbed on the cathode surface. Shown in Figure 1(a) are enhanced Raman spectra under various atmospheres

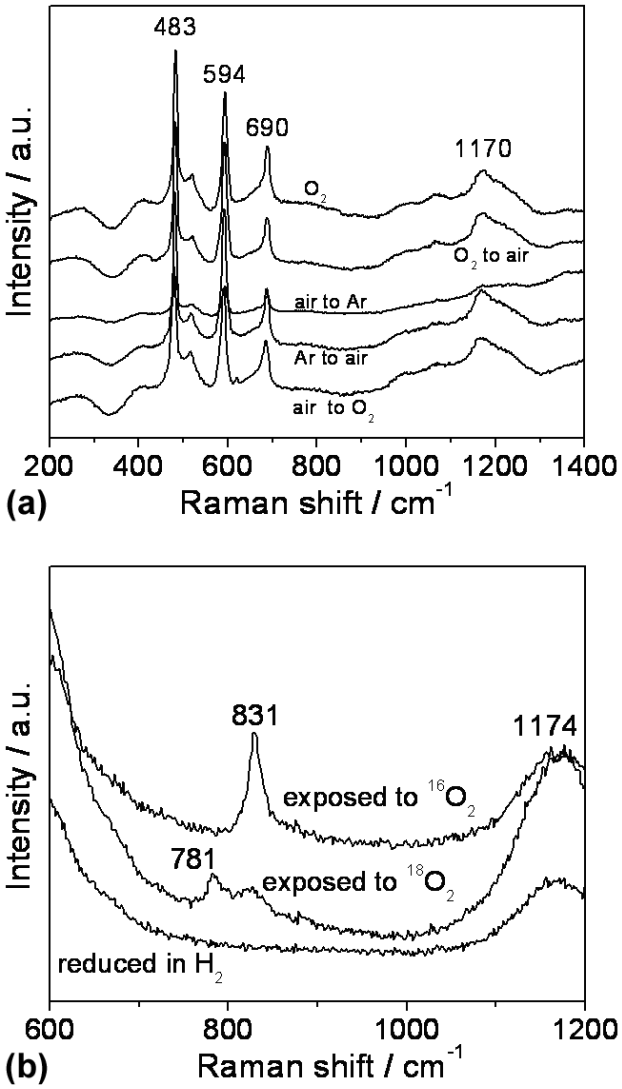

Figure 1. (a) Enhanced Raman spectra for composite cathode material Ag-SSC at 25°C. (b) Raman spectra of CeO_2 nanopowder pellet that had been reduced under 5% H_2 and then exposed to $^{16}O_2$- and $^{18}O_2$-containing atmospheres.

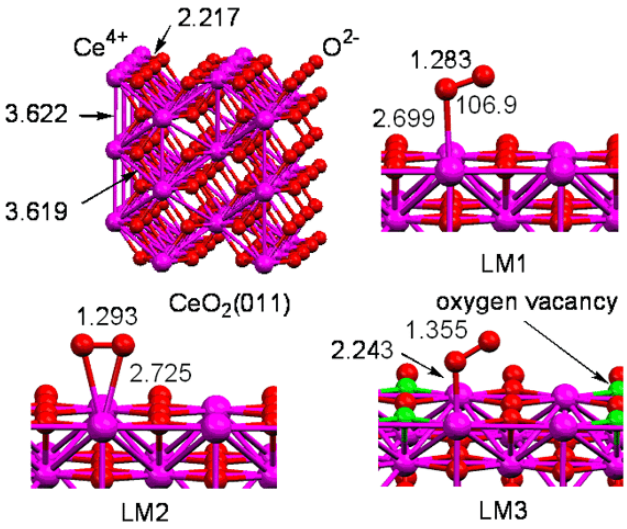

Figure 2. Optimized geometries of adsorbed intermediates for oxygen reduction on CeO_2(011) surface. The bond lengths and angles are in Å and degrees, respectively. Cerium atoms, oxygen atoms, and oxygen vacancies are in purple, red, and green, respectively.

for composite cathode material Ag-SSC (SSC 50 wt. % and Ag 50 wt. %) prepared by CCVD. The SERS study gave two new vibration modes at 594 and 1170 cm^{-1}. To test the validity of the computational methods being used for interpreting the experimental data, especially for adsorbed oxygen species, a simpler material system was chosen. Cerium oxide (CeO_2) was chosen because (1) its AO_2 fluorite structure is a simpler lattice than the defective ABO_3 perovskite structures of typical SOFC cathode materials and (2) it has a well-studied Raman spectra, electronic structure, and defect chemistry. Figure 1(b) compares the Raman spectrum of a nanocrystalline ceria pellet before and after exposure to oxygen after being reduced in 5% hydrogen. After exposure to $^{16}O_2$, a new peak appeared at 831 cm^{-1}. To confirm that this peak was indeed an oxygen-containing species, another Raman spectrum was recorded after exposing the pellet to 10% $^{18}O_2$ (balance argon) for 15 minutes (also shown in Figure 1(b)). The peak shifted from 831 cm^{-1} to 781 cm^{-1}. The ratio between the two peak positions is 1.06, which is the ratio expected for a change from ^{16}O to ^{18}O (i.e., $\sqrt{18/16} = 1.06$), confirming that the band at 831 cm^{-1} is attributed to an adsorbed oxygen species.

To assign the observed bands for adsorbed oxygen on the CeO_2 surface, we preliminarily estimated the vibration frequencies with the optimized geometries in Figure 2 using the Vienna ab-initio simulation package (VASP). The estimated vibrations of LM1 and LM2 optimized on perfect fluorite CeO_2 are 1212 and 1298 cm^{-1}, respectively, while that of LM3 on defect CeO_2 is 1098 cm^{-1}. Based on the quantum-chemical calculations, the observed band at 831 cm^{-1} may be attributed to LM3 optimized on the defect fluorite CeO_2 surface within the uncertainty of the theory used. More detailed interpretations for MIEC cathode materials are planned with the same aforementioned approach.

The use of rapid scan time-resolved spectroscopy (TRS) in conjunction with our FTIR emission spectroscopic studies has allowed us to refine the time-dependent FTIR data being used to determine experimentally oxygen reduction kinetic parameters. By taking emission spectra on a smaller time scale, we have been able to isolate changes in the cathode's emissivity that are due to small changes in sample temperature from those that are due to structural changes in the material. By subtracting out the thermal effects, we can now more confidently calculate the surface reaction rate and bulk diffusivity of the cathode using FTIR emission spectroscopy.

To quantify the effect of electrode thickness on the performance of dense LSM electrodes, we fabricated patterned electrodes. The electrode array consisted of 60 patterned rectangular electrodes 40 µm in width separated by 60 µm gaps. A platinum current collector was lithographically patterned and deposited on top of the working electrode. The current collector consisted of 12 identical 50-µm wide platinum strips separated by exactly 490 µm. All 12 platinum strips were connected to a platinum pad in order to facilitate wire attach (see Figure 3(a)). Figure 3(b) displays the dependence of the interfacial impedance on the electrode strip thickness at 700 and 750°C. Several unique traits are observed in each temperature range. In particular, note the peak conductance, located between 0.18 µm and 0.22 µm, followed by a rapid decay with increasing thickness. It should also be noted that the decay behavior appears to asymptotically approach a non-zero value. This value, believed to be about 0.012 Ω^{-1}, has been attributed to standardized factors within the cell. Among these are the TPB and surface transport contributions of the LSM array as well as the

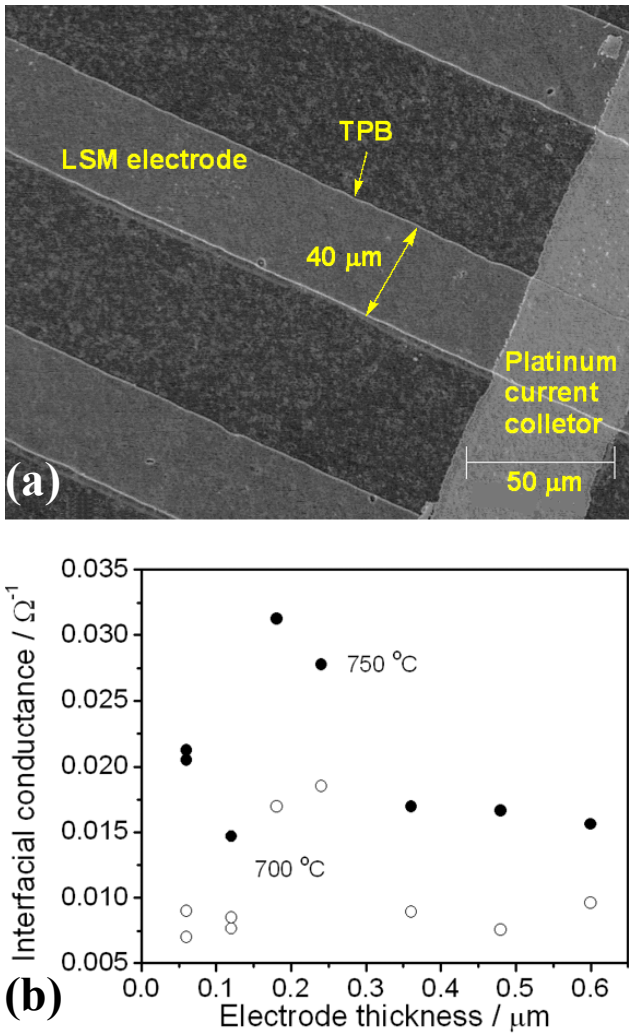

Figure 3. (a) SEM image of LSM patterned electrodes (with constant TPB length and surface area) on a YSZ substrate. The width of the LSM strip is 40 μm, and the gap between two adjacent strips is 60 μm. Platinum current collector strips run perpendicular to the LSM strips. (b) Plot of the inverse of interfacial resistance vs. electrode thickness. The horizontal axis has been compressed in some regions to accommodate the scope of all the tested electrodes.

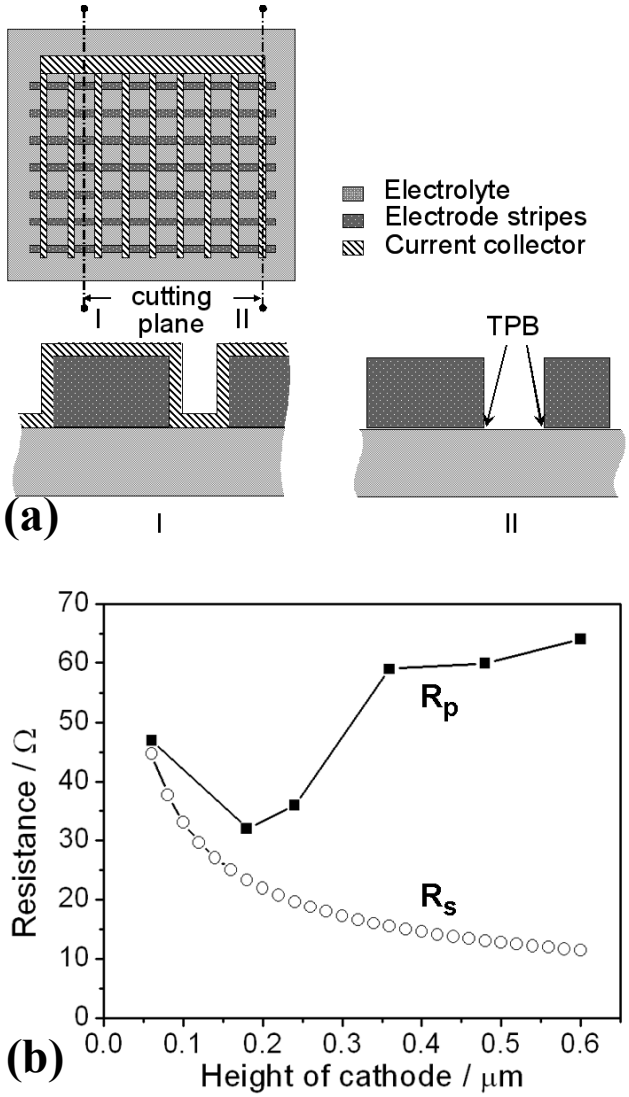

Figure 4. (a) Top and cross-sectional views as seen through the cutting plane. (b) Comparative plot of sheet (R_s) and interfacial (R_p) resistances as a function of electrode thickness.

catalytic contributions of the platinum current collector. Since these factors have been systematically controlled through the design and fabrication stages, their contributions should be constant over the entire range of electrode thickness. Consequently, the background noise value can be subtracted from the overall conductance to yield the contribution merely from a pathway depending upon bulk transport through the dense MIEC.

Shown in Figure 4(a) is the configuration of the full-scale electrode system used for the modeling study of the patterned electrodes. The current collector is placed as the topmost layer and has 11 stripes. The stripes are connected at one end. The gap between each pair of successive stripes is 490 μm. The electrode bars are in 60 parallel rows below this layer. The bottom-most layer is the electrolyte (substrate). As illustrated in Figure 4(b), the sheet resistance shoots up at small feature sizes (i.e., below 0.18 μm), whereas the interfacial resistance trend reverses. Electrode thicknesses below 0.18 μm show tremendous ohmic losses as the sheet resistance (i.e.,

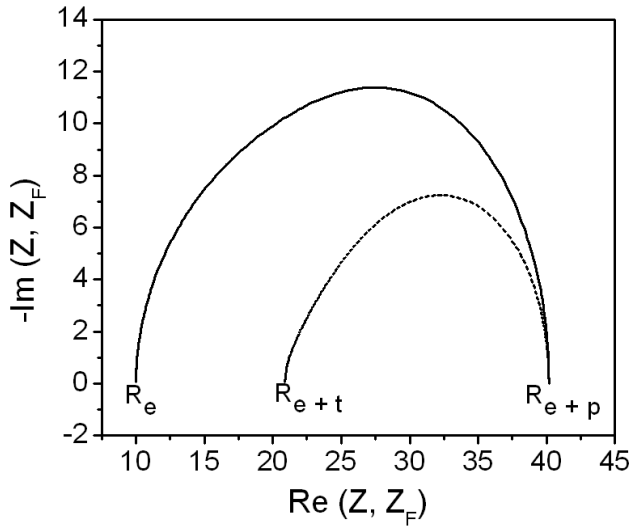

Figure 5. Impedance spectra showing typical calculated total impedance, Z (solid line), and the calculated Faradaic impedance, Z_F (dashed line), responses for a proposed mechanism at T = 700°C, P = 1 atm, R_e = 10 Ω, $C_{dl} = 2\times10^{-6}$ F. R_e, R_t, and R_p correspond to electrolyte resistance, charge transfer resistance, and polarization resistance, respectively.

via the electronic conductivity) dominates the performance, and the entire electrode may no longer be assumed utilized at 100%. The outcome of the sheet resistance calculations may in turn be used to make necessary corrections and help remake the design of the patterned electrodes. In addition, this work clears up some confusing behavior previously observed on thin film LSM electrodes, wherein polarization resistance initially decreases with thickness for very thin films but then increases again as thicknesses grow beyond a threshold value. The need for systematic guidance towards fabricating patterned electrodes of optimum geometry motivated this research. While patterned LSM electrodes were used for this model study, our proposed computational approach is applicable to any patterned electrode.

Reaction mechanisms have been developed to describe the oxygen reduction process occurring at the MIEC cathode materials. Experimental impedance measurements typically include a double layer capacitance, C_{dl}, and a resistive element attributed to the electrolyte, R_e. These additional elements obscure the Faradaic impedance of the system, Z_F. To be able to more directly compare experimental data and theoretical calculations, a method was used to determine the total impedance from knowledge of the Faradaic impedance. From knowledge of the electrolyte resistance and the double layer capacitance, values for the total electrode impedance were computed. Illustrated in Figure 5 are the results comparing total impedance to Faradaic impedance, in which the total impedance can quickly show the electrolyte resistance and the polarization resistance, but hides the charge transfer resistance, R_t.

Conclusions

In the past year, the SOFC research at GT made significant progress in terms of elucidation of oxygen reduction mechanism, both experimentally and theoretically. *In-situ* vibrational spectroscopy, such as surface Raman scattering and FTIR, has provided the spectroscopic information for the gas-surface interactions, which was interpreted by quantum-chemical calculations at the molecular level. Furthermore, micro-patterned LSM electrodes analyzed by a standard SOFC electrochemical impedance spectroscopic method have been successfully modeled with a finite element technique. The combination of our experimental approach and the phenomenological and quantum-chemical modeling is a valuable tool to design more efficient cathode materials.

FY 2005 Presentations

1. H. Abernathy and M. Liu, "Measurement of Oxygen Diffusivity of SOFC Cathode Materials Using FTIR Emission Spectroscopy", ECS Meeting, Honolulu, HI, October 2004.
2. E. Koep, C. Compson, and M. Liu, "LSM Patterned Electrodes for Solid Oxide Fuel Cells", ECS Meeting, Honolulu, HI, October 2004.
3. Y. M. Choi, H. Abernathy, R. Williams Jr., and M. Liu, "Computational Approach to Solid-Gas Interactions in SOFCs", ECS Meeting, Quebec City, Canada, May 2005.

FY 2005 Publications

1. Y. Liu, S. Zha, and M. Liu, "Novel Nanostructured Electrodes Fabricated by Combustion CVD", *Advanced Materials*, **16** (3) 256-260, 2004.
2. Y. Liu, S. Zha, and M. Liu, "Nano-composite Electrodes Fabricated by a Particle-Solution Spraying Process for Low-Temperature SOFCs", *Chemistry of Materials*, **16**, 3502-3506, 2004.

3. S. Zha, A. Moore, H. Abernathy, and M. Liu, "GDC-Based Low Temperature SOFCs Powered by Hydrocarbon Fuels", *Journal of the Electrochemical Society*, **151**, A1128-1133, 2004.
4. Y. Liu, W. Rauch, S. Zha, and M. Liu, "Fabrication of Nanostructured Electrodes for Solid Oxide Fuel Cells Using Combustion CVD", *Solid State Ionics*, **166,** 261-268, 2004.
5. Y. Liu, C. Compson, and M. Liu, "Nanostructured and Functionally Graded Cathodes for Intermediate Temperature Solid Oxide Fuel Cells", *Journal of Power Sources*, **138,** 194-198, 2004.
6. Y. Liu and M. Liu, "Porous Electrodes for Low-temperature Solid Oxide Fuel Cells Fabricated by a Combustion Spray Process", *Journal of the American Ceramic Society*, **87** (11), 2139-2142, 2004.
7. Q. H. Wu, A. Thissen, W. Jaegermann, and M. Liu, "Photoelectron Spectroscopy Study of Oxygen Vacancy on Vanadium Oxides Surface", *Applied Surface Science*, **236** (1-5), 473-478, 2004.
8. E. Koep, C. Compson, M. Liu, and Z. Zhou, "A Photolithographic Process for Investigation of Electrode Reaction Sites in Solid Oxide Fuel Cells", *Solid State Ionics*, **176** (1-2), 1-8, 2005.
9. S. Zha, Y. Zhang, and M. Liu, "Functionally Graded Cathodes for SOFCs Fabricated by Sol-gel/Slurry Coating", *Solid State Ionics*, **176**, 25-31, 2005.
10. Q. H. Wu, M. Liu, and W. Jaegermann, "X-ray Photoelectron Spectroscopy of $La_{0.5}Sr_{0.5}MnO_3$", *Materials Letters*, **59** (12), 1480-1483, 2005.
11. R. Das, D. Mebane, E. Koep, and M. Liu, "Modeling of Patterned Mixed-Conducting Electrodes and the Importance of Sheet Resistance at Small Feature Sizes", *Solid State Ionics*, submitted.
13. E. Koep, D. Mebane, R. Das, C. Compson, and M. Liu, "The Characteristic Thickness for a Dense LSM Electrode", *Electrochemical and Solid State Letters*, accepted.

III.A.6 Development of Inexpensive Metal Alloy Electrodes for Cost-Competitive Solid Oxide Fuel Cells

Steven J. Visco (Primary Contact), Craig Jacobson, and Lutgard C. De Jonghe
Lawrence Berkeley National Laboratory
Materials Science Division
Berkeley, CA 94720
Phone: (510) 486-5821; Fax: (510) 486-4881; E-mail: sjvisco@lbl.gov

DOE Project Manager: Lane Wilson
Phone: (304) 285-1336; E-mail: Lane.Wilson@netl.doe.gov

Objectives

- Improve low temperature performance (650 – 700°C) of air electrode using catalyst infiltration technology.
- Demonstrate long-term stability of catalyst-infiltrated air electrodes.
- Engineer performance of interconnect alloys through control of oxide scale growth and conductivity.
- Minimize Cr vaporization from stainless steel alloys.
- Assist Solid State Energy Conversion Alliance (SECA) vertical team members by tackling relevant solid oxide fuel cell (SOFC) technical hurdles and transferring technology to industry teams.

Approach

- Develop low-cost metal salt infiltration technology to boost the performance of the air electrode, particularly at temperatures below 700°C.
- Measure the baseline performance and long-term stability of commercially produced air electrodes with and without infiltrated catalyst.
- Determine oxidation rates and Cr vaporization rates of commercial and specialty alloys under consideration for interconnect plates.
- Synthesize $MnCo_2O_4$ spinel and related powders for coating interconnect alloys.
- Analyze Cr vaporization coated alloys to determine quality of coating for minimization of Cr loss.
- Analyze Cr vaporization data to understand fundamental limits of coatings.

Accomplishments

- *Increased Fuel Cell Power by 80%*
  Through the use of catalyst infiltration, the maximum power for anode-supported cells was improved dramatically at temperatures below 700°C. The Lawrence Berkeley National Laboratory (LBNL) group infiltrated LSM-YSZ (LSM: lanthanum strontium manganese oxide; YSZ: yttria-stabilized zirconia) cathodes with a precursor for the catalyst $Sm_{0.6}Sr_{0.4}CoO_{3-}$ (SSC); Ni-YSZ supported cells with YSZ electrolyte were tested with and without infiltrated SSC. The improvement in cathode performance was largest at low temperature.
- *Demonstrated Single-Step Infiltration of LSM and LSF Electrodes*
  Through the use of a unique proprietary process, the LBNL group has demonstrated capability to infiltrate the entire perovskite electrode [LSM and lanthanum strontium ferrite (LSF) so far] into a porous electrolyte matrix. The resulting composite electrode has sufficient electrical continuity and catalytic activity to achieve excellent electrochemical performance at 650°C.

- *Successfully Determined the Cr Vaporization Rates for a Number of Coated and Uncoated Stainless Steel Alloys in Humidified Air*
  The LBNL team set up and calibrated a transpiration apparatus for the determination of Cr volatility from chromia-containing samples; the data are in good agreement with the literature and thermodynamic calculations.
- *Decreased Chromium Vaporization by a Factor of 20 to 40 through the Use of Low-Cost Coatings*
  The LBNL group measured Cr vaporization rates for coated and uncoated 430 stainless steel and Crofer alloy; both the uncoated 430 and Crofer alloys exhibit unacceptably high Cr volatility. However, the coated alloy samples showed a marked decrease in Cr vaporization; notably, the low-tech, low-cost coatings developed at LBNL did a better job at reducing Cr loss than did the coatings produced by physical vapor deposition.

Future Directions

- *Determine Long-term Stability of Infiltrated Electrodes*
  InDec/H.C. Starck has agreed to supply LBNL with symmetrical LSM/YSZ/LSM and LSCF-CeO_2/YSZ/CeO_2-LSCF (LSCF: lanthanum strontium cobalt ferrite) cells to assess baseline performance of commercial air electrodes with and without infiltrated catalyst. The LBNL group will determine the performance and degradation rate of the cells in air at 650°C for 1000-hour tests, after which the electrodes will be infiltrated with appropriate catalysts and the test will be repeated. In this way, the long-term stability of infiltrated electrodes can be separated from the long-term stability of the standard electrodes. The LBNL team will run tests on both electrode types and with multiple infiltration species, and will do post-mortem studies on the electrode morphology.
- *Optimize Infiltration Technology*
  The data collected from the long-term stability studies will be used to adjust and optimize the composition and amount of infiltrated catalyst.
- *Optimize Protective Alloy Coatings*
  We have developed low-cost coatings for stainless steel interconnects that reduce Cr vaporization by a factor of 20-40. We will continue to optimize these coatings for high electrical conductivity, adherence, thermal expansion match, and minimization of Cr volatility.
- *Technology Transfer*
  The LBNL group will assist in the transfer of technology to any industrial team requiring our assistance.

Introduction

Among the most challenging hurdles to the commercialization of solid oxide fuel cell technology is the need to manage cost such that SOFCs are competitive with entrenched power generation technologies. The LBNL group has long maintained that the key to a cost-effective SOFC solution is to develop systems operating in the 650 to 700°C range. It now appears that many of the SECA industrial teams are pursuing that goal as well. The use of metal alloy interconnects allows for inexpensive SOFC stack designs. However, in order to achieve the 40,000-hour life needed for distributed generation, it is clear that stainless steel interconnects will have to be maintained at temperatures below 800°C. Since electrode kinetics (and electrolyte conductivity) are thermally activated, the clear implication is that careful attention must be paid to SOFC performance as the temperature is lowered. The LBNL group has developed an infiltration technique whereby standard LSM electrodes can be modified to perform well at temperatures as low as 650°C. Electrode modification can be as simple as infiltrating a metal nitrate such as $Co(NO_3)_2$ or can involve a mixture of precursors to form a known electrocatalyst such as $Sm_{0.6}Sr_{0.4}CoO_{3-}$ (SSC). Assuming that SOFC electrode performance and stability at 650 to 700°C is adequate for commercialization, there are still issues with the use of metal interconnects that must be addressed. Although the oxidation of stainless steel at

temperatures between 650°C and 750°C is sufficiently low to meet SECA goals, the loss of chromium in the air electrode environment is a problem both in terms of cathode poisoning and regulatory limits for Cr exposure. Accordingly, many groups involved in SOFC development have undertaken development of coatings to minimize both steel oxidation and Cr vaporization. Research at LBNL is quite encouraging in that relatively simple and low-cost coatings lead to significant reduction in Cr volatility.

Approach

In order to achieve SECA commercialization targets, a number of SOFC developers are targeting reduced operating temperatures as a means of controlling cost. The LBNL effort is aligned with that goal through the use of electrode infiltration technology to boost the performance of the air electrode. Two techniques are currently used: 1) infiltration of an air electrode with cobalt nitrate or a mixture of metal nitrates to form a specific perovskite that decorates the air electrode with nanoparticulate catalyst; 2) complete synthesis of the entire perovskite electrode in a single step through introduction of a highly concentrated perovskite precursor into a porous electrolyte matrix. Electrochemical characterization of both types of electrodes shows good performance at reduced temperature and stable performance in 100-hour tests. In order to minimize the effect of air electrode variability on the assessment of infiltrated electrode stability, the LBNL group will initiate testing of commercial air electrodes from InDec/H.C. Starck infiltrated in our laboratory. The LBNL team has also fabricated and calibrated a transpiration apparatus (Figure 1) to accurately measure the vaporization of Cr from chromium-containing samples. In this apparatus, samples are held in a heated quartz tube that is exposed to flowing humidified air, and exhausted Cr is collected in a cold trap, dissolved in nitric acid, and sent to an analytical lab for quantitative analysis using inductively coupled plasma mass spectrometry. The setup was calibrated by exposing a Cr_2O_3 sample to humidified air and comparing the analytical data to that predicted by theory and reported in the literature. Then, pre-oxidized stainless steel samples were exposed in the same manner and Cr vaporization rates determined; coated samples were similarly tested.

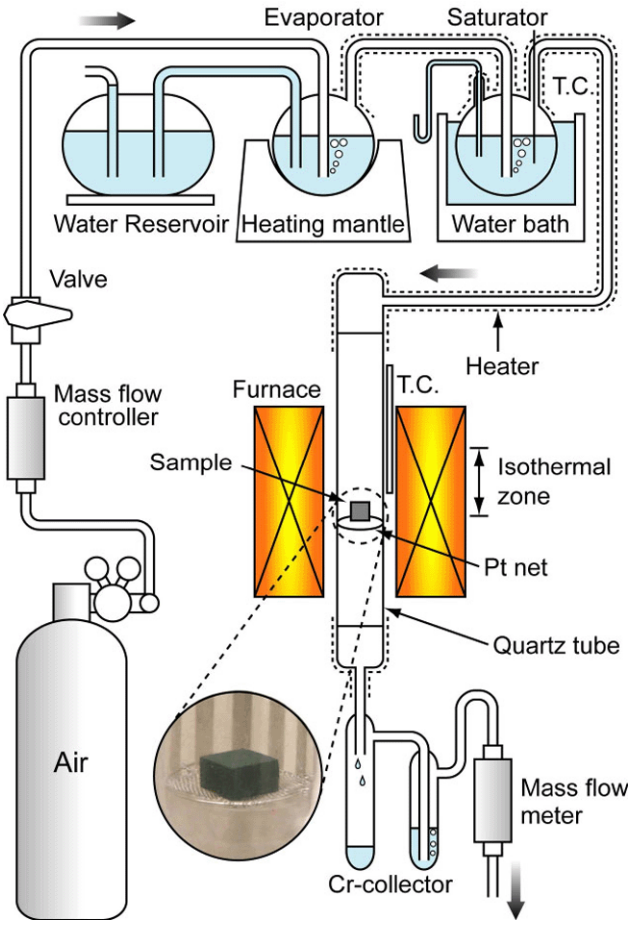

Figure 1. Chromium Transpiration Apparatus

Results

The use of catalyst infiltration as developed at the Lawrence Berkeley National Laboratory provides a simple, cost-effective means of boosting fuel cell performance at reduced operating temperatures. In the case of LSM-YSZ cathodes infiltrated with SSC, the improvement in performance can be as high as 80% at temperatures below 700°C (Figure 2). Assuming the LBNL group can demonstrate long-term stability (projected to 40,000 hours) for such cathodes, this technology will be a clear candidate for technology transfer. The LBNL team has also developed a process whereby a porous electrolyte matrix can be infiltrated in a single processing step to form the entire air electrode structure (Figure 3); this unique result offers tremendous flexibility in electrode design. The performance of the single-step

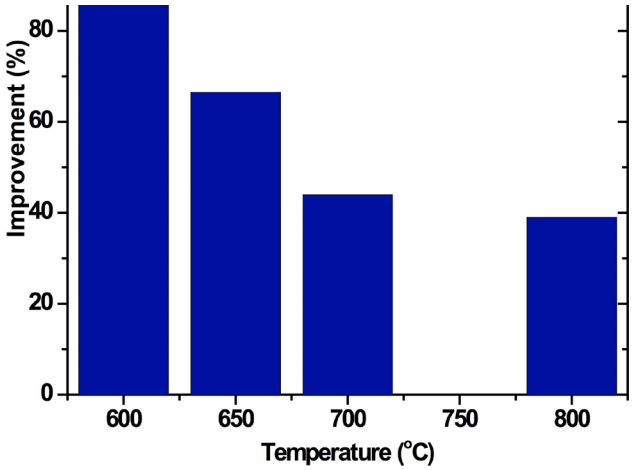

Figure 2. Performance of Infiltrated LSM-YSZ as a Function of Temperature

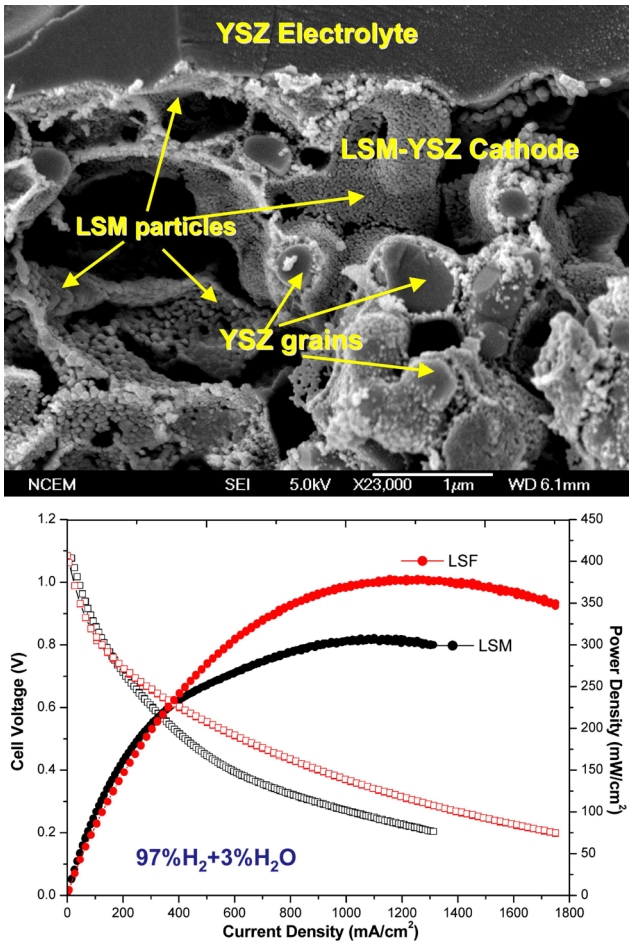

Figure 3. Single-Step Infiltrated Cathode Structure and Performance

infiltrated electrodes is quite good, as shown in Figure 3. The availability of air electrodes with low

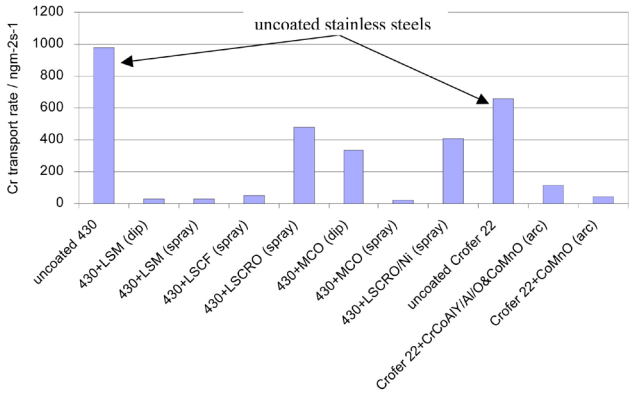

Figure 4. Chromium Vaporization for Coated and Uncoated Stainless Steels

overpotential at reduced temperatures supports the trend toward lowering the operating temperature of the SOFC stack, with the key benefit of greatly reduced stack cost enabled through the use of inexpensive metal components. However, the potential for cathode poisoning due to Cr vaporization remains a major concern for the adoption of metal stack technology. The recent construction of a transpiration apparatus at LBNL through SECA funding has provided much insight regarding the magnitude and pathway to alleviation of this problem. LBNL successfully measured Cr vaporization from coated and uncoated stainless steel alloys; as can be seen in Figure 4, the rate of Cr loss in uncoated alloys is rather high, even for the Crofer alloys developed at Juelich. The good news is that by application of a coating, even one of intermediate quality, the Cr vaporization rate is markedly suppressed. Importantly, the simple low-cost aerosol application of powder coatings such as $La_{0.65}Sr_{0.3}MnO_{3-\gamma}$, $La_{0.6}Sr_{0.3}Co_{0.8}Fe_{0.2}O_3$, and $MnCo_2O_4$ reduced Cr vaporization by a factor of 21-40, while the more costly e-beam coatings only reduced Cr vaporization by a factor of 6-15.

Conclusions

The use of inexpensive catalyst infiltration improves significantly the performance of conventional SOFC air electrodes at temperatures below 700°C. Alternatively, air electrodes fabricated by single-step infiltration of a porous electrolyte matrix also demonstrate excellent low-temperature performance. The LBNL group has found that low-cost ceramic coatings can decrease chromium

vaporization from iron chromium alloys by a factor of 20 to 40 times, the critical factor being the formation of a dense layer of the ceramic coating.

FY 2005 Publications/Presentations

1. Yamahara K, Jacobson CP, Visco SJ, De Jonghe LC, *"Catalyst-infiltrated supporting cathode for thin-film SOFCs,"* Solid State Ionics, vol. 176, no. 5-6, 14 February 2005, pp. 451-6. Publisher: Elsevier, Netherlands
2. Matus YB, De Jonghe LC, Jacobson CP, Visco SJ, *"Metal-supported solid oxide fuel cell membranes for rapid thermal cycling,"* Solid State Ionics, vol. 176, no. 5-6, 14 February 2005, pp. 443-9. Publisher: Elsevier, Netherlands.
3. Chen X, Hou PY, Jacobson CP, Visco SJ, De Jonghe LC, *"Protective coating on stainless steel interconnect for SOFCs: oxidation kinetics and electrical properties,"* Solid State Ionics, vol. 176, no. 5-6, 14 February 2005, pp. 425-33. Publisher: Elsevier, Netherlands.
4. Yamahara K, Jacobson CP, Visco SJ, Zhang X-F, De Jonghe LC, *"Thin film SOFCs with cobalt-infiltrated cathodes,"* Solid State Ionics, vol. 176, no. 3-4, 31 January 2005, pp. 275-9. Publisher: Elsevier, Netherlands.
5. Steven J. Visco, Craig Jacobson, Hideto Kurokawa, Tal Sholklapper, Chun Lu, Xuan Chen, Peggy Hou, and Lutgard C. De Jonghe, "Development of Novel Electrode Structures and Stabilization of Metal Components for Cost Competitive SOFCs," presentation at the Solid State Energy Conversion Alliance 6th Annual Workshop, Asilomar, Pacific Grove, California, April 18-21, 2005.
6. Steven J. Visco, Craig Jacobson, Hideto Kurokawa, Tal Sholklapper, Chun Lu, and Lutgard De Jonghe, "Improvement of SOFC Electrodes through Catalyst Infiltration & Control of Cr Volatilization from FeCr Components," presentation at Solid State Energy Conversion Alliance Core Technology Review, Tampa, Florida, January 27-28, 2005.

Special Recognitions & Awards/Patents Issued

1. U.S. Patent No. 6,846,511; Steven J Visco; Craig Jacobson; Lutgard C. DeJonghe, *"Method of making a layered composite electrode/electrolyte"* issued January 25, 2005.
2. U.S. Patent No. 6,887,361; Steven J Visco; Craig Jacobson; Lutgard C. DeJonghe, *"Method for making thin-film ceramic membrane on non-shrinking continuous or porous substrates by electrophoretic deposition"* issued May 3, 2005.

III.A.7 Advanced Fuel Cell Development

Randall Gemmen (Primary Contact), Chris Johnson, Richard Pineault
National Energy Technology Laboratory
3610 Collins Ferry Rd.
Morgantown, WV 26507
Phone: (304) 285-4536; E-mail: Randall.Gemmen@netl.doe.gov

Subcontractors:
Fluent, Inc., Morgantown, WV
Drexel University, Philadelphia, PA
University of Utah, Salt Lake City, UT
University of West Virginia, WV

Objectives

- Evaluate DOE-sponsored solid oxide fuel cell (SOFC) systems.
- Analyze performance of SOFCs under dynamic loading.
- Assess high-temperature sensors for SOFC application.
- Test and evaluate coatings for fuel cell interconnects.

Approach

- Develop new fuel cell systems test facility.
- Experimentally (button cells) and numerically investigate dynamics of SOFC operation.
- Apply existing indium-tin-oxide (ITO) strain sensors to SOFC substrates and cells to determine signal response.
- Apply coatings to Crofer interconnect material substrates and investigate role of silica on surface resistance.

Accomplishments

- A new DOE test facility has been developed for testing SOFC systems.
- The effects of reverse current conditions within a cell/stack predicted by model investigations of fuel cell dynamics were evaluated experimentally to determine possible performance limitations.
- ITO strain sensors have been demonstrated to show viable signal levels at the high temperature conditions of solid oxide fuel cells.
- Doped $LaCrO_3$ coatings were applied to Crofer having varying degrees of silicon content, and results for the 800°C annealed coatings show a linear increase in area-specific resistance with silicon content.

Future Directions

- Apply new DOE test facility to DOE program evaluations of sponsored SOFC systems.
- Experimentally investigate reverse current conditions over times and ranges of current reversal identified by models.
- Identify a protocol for application of high-temperature strain gages to SOFC substrates (calibration to signal analysis).
- Investigate new low-cost MnCo and chromite coating methods for interconnects.

Introduction

Because a fully functional hydrogen economy will take many years to create, the U.S. DOE is supporting the development of solid oxide fuel cells through the Solid State Energy Conversion Alliance (SECA) program as a way to efficiently use existing fossil fuel resources. The goal of this program is to provide low-cost fuel cell systems for mass markets. To achieve this goal will require new and innovative SOFC design and analysis tools, materials, and test and evaluation capability. The work performed here accomplishes all these objectives by developing test capability for the evaluation of SOFC systems, applying advanced analysis tools for the purpose of better understanding solid oxide fuel cell operation, assessing the application of existing high-temperature sensors for SOFC application, and evaluating interconnect material options for SOFC design engineers.

Approach

Systems Test and Evaluation Capability

The U.S. Department of Energy's National Energy Technology Laboratory has recently completed construction of a fuel cell test facility that will be used for evaluating the performance of prototype fuel cell systems developed by government-sponsored fuel cell developers (Figure 1). The recently constructed (Phase I) portion of the facility is configured to handle fuel cell systems running on natural gas or methane with a nominal power rating of 3 to 10 kW.

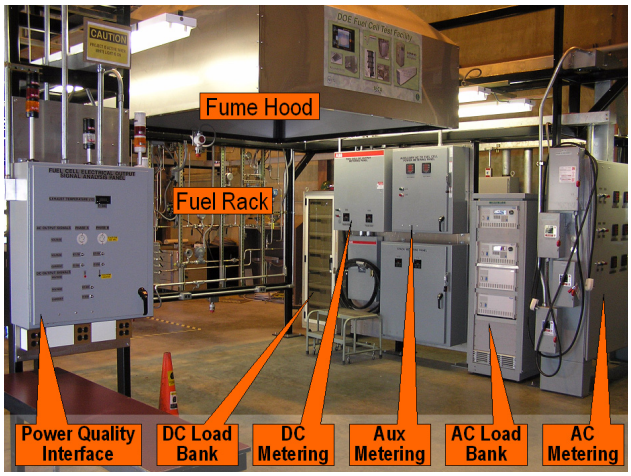

Figure 1. Photograph of DOE Fuel Cell Test Facility Used for Systems Test and Evaluation

Dynamic Load Studies

Both model and experimental studies are used to investigate the performance of fuel cells under dynamic loads. It has already been shown that certain fuel cell transients may likely induce conditions within the cell that result in current reversal [Gemmen and Johnson, (2005)]. This project experimentally studied reverse current conditions over a wide range of current reversal to provide a full understanding of the effects such conditions may produce, and also to perform accelerated testing of potential degradation mechanisms to determine if more extensive and detailed studies are necessary.

Strain Gage Evaluation

Existing high-temperature strain gages developed for the gas turbine industry are applied to SOFC-based substrates [yttria-stabilized zirconia (YSZ) wafers and complete cells]. The specimens are placed in a dedicated test rig, where known mechanical stress is placed on the cell. The response of the sensor is measured to determine if sufficient signal exists at conditions representative of SOFC operation.

Perovskite Interconnect Coatings

In previous work, it was determined that impurities in the high-temperature alloy, specifically silicon, can contribute significantly to lower than desired performance of the alloys in real tests due to the formation of silica particles and, in some cases, continuous silica layers that decrease the area-specific resistance (ASR) of the interconnect material. The effect of silicon content on the ASR was further investigated by applying lanthanum chromite coatings ($La_{0.9}Sr_{0.1}Cr_{0.9}Co_{0.1}CrO_3$) on Crofer substrates via DC-magnetron sputtering. The substrates were annealed at 800°C, and their ASR values were measured.

Results

Systems Test and Evaluation Capability

The new DOE Fuel Cell Test Facility (DFC) is presently being readied for shakedown using both an Acumentrics, Inc., SOFC unit, and a Fuel Cell Technology, Ltd., unit. The shakedown activity will

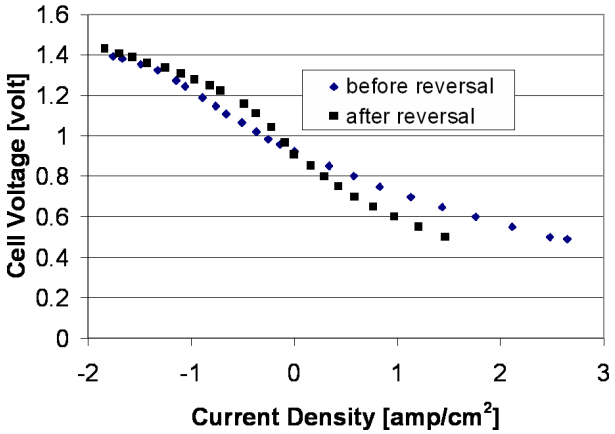

Figure 2. V-I Curve for Standard SOFC Cell Using 35% H_2O at the Anode. The data denoted 'after reversal' is the data taken after operating the cell voltage under reverse current for 1.5 hours.

provide a detailed evaluation of the measurement and safety hardware design of the Phase I facility. In addition, this activity will allow the development of data analysis methods and test protocols. DOE's Solid State Energy Conversion Alliance program will be the first program to use this facility for assessing industrial team progress in reaching the goal of achieving highly efficient 3-10 kW solid oxide fuel cell systems at a cost of less than $400/kW.

Dynamic Load Studies

Experimental results of current reversal showed that failure of a button SOFC fuel cell (Ni+YSZ/YSZ/LSM) can result from the operation of current reversal. A V-I curve of a cell is shown in Figure 2. The data was taken by initially conditioning the cell for approximately 3 hours at a constant voltage of 0.7 V, over which time the cell current increased to 1.2 A/cm^2. A V-I curve was then taken by increasing the cell voltage up to 1.42 volts. The cell was put under a "stress load" of -0.9 A/cm^2 for only a short time (1.5 hours) to provide an accelerated durability study under reverse operation. After the stress loading, another V-I curve was obtained over the same cell voltage range. As can be seen, the cell degraded slightly in performance in both its fuel cell and electrolysis modes.

Additional cells of the same design were also tested under reverse current conditions and had similar degradation over time. As a first step in trying to identify the cause of the degradation,

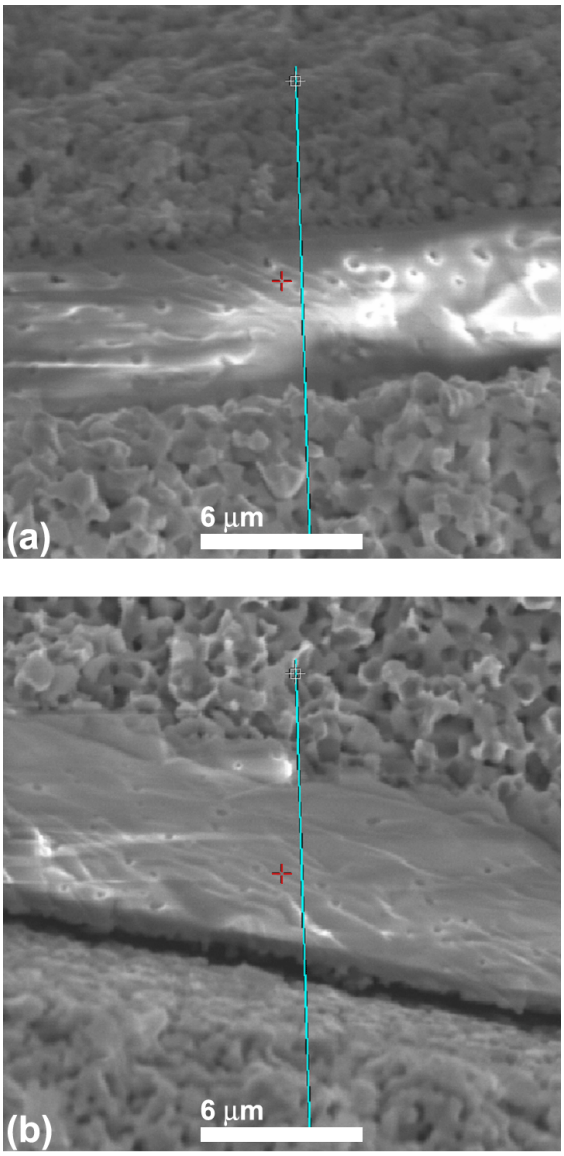

Figure 3. SEM of Standard Cell Operated in Positive Current Mode (left), and Another in Reverse Current Mode (right) for 5 Hours. Both cell specimen micrographs shown where unpolished. Lower portion of the left image shows a separated cathode with a less porous interlayer.

fractured cross sections of a cell run under reverse current conditions and a cell run only in normal fuel cell mode were examined using scanning electron microscopy (SEM). Figure 3 compares the SEM image of a cell that had experienced reverse (negative) current operation for a period of about 5 hours to one that was run in normal mode (positive current). As can be seen from the SEM, the cathode of the cell that experienced reverse current has

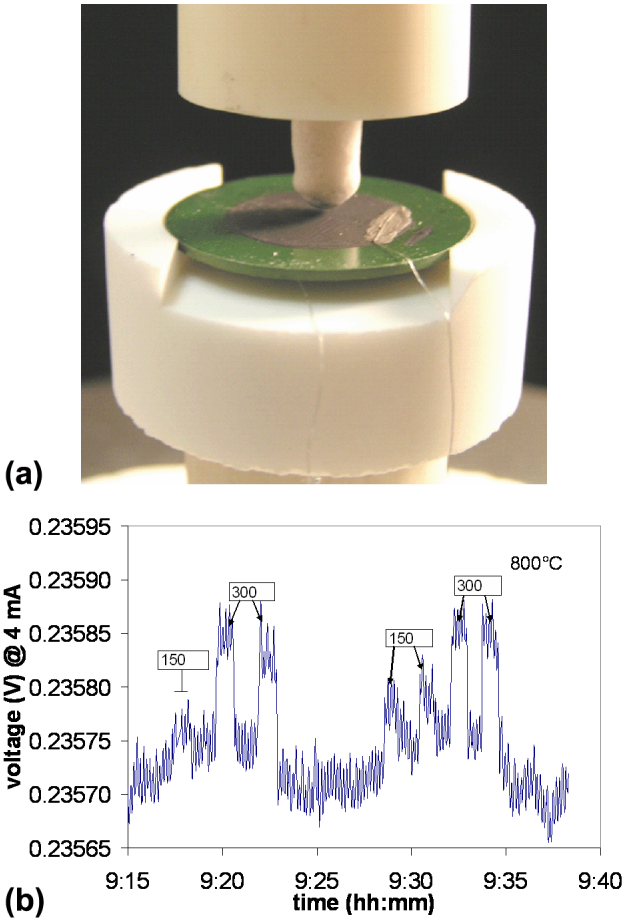

Figure 4. Response of an ITO Strain Sensor Due to Known Mechanical Displacement of the YSZ Substrate (displacement, in microns, is shown next to the signal response)

separated from the electrolyte over a significant length. This could be simply due to the process of fracturing the cell for SEM analysis; however, we have not seen such results for numerous other cells run only in normal fuel cell mode.

Strain Gage Evaluation

Figure 4 shows a response of a strain gage applied to an YSZ substrate and operated at 800°C. As can be seen, even at these extreme temperatures, a viable signal-to-noise ratio exists for these sensors. It can also be seen that these sensors have a strong thermal response (the background oscillations are due to slight temperature changes). Hence, temperature-compensated sensors will be needed for future engineering application. These latter sensors are the subject of on-going study.

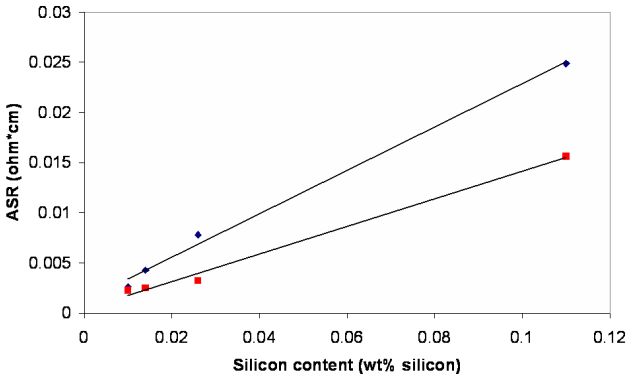

Figure 5. ASR vs. Silicon Content in CROFER APU 22 Sample with a $La_{0.9}Sr_{0.1}Cr_{0.9}Co_{0.2}O_3$ Sputtered Coating. Heated only during the ASR measurement.

Perovskite Interconnect Coatings

Figure 5 shows the ASR values measured for the $La_{0.9}Sr_{0.1}Cr_{0.9}Co_{0.1}CrO_3$-coated CROFER APU 22 samples containing varying levels of silicon, plotted as a function of silicon content. The lower curve shows the initial measurement of the ASR, and the upper curve shows the second measurement, done immediately after the first. ASR is clearly a strong function of silicon content. The lower the silicon content, the lower the ASR value. Also note that the second measurement in all samples is higher in ASR value. This is due to the fact that changes in the film composition and structure are still rapidly taking place, and the more continuous silica layer shown in prior long-term tests has not yet been formed. Further long-term testing of each of these specimens will be performed to identify their long-term relative behavior.

Conclusions

A new systems test and evaluation facility is now ready for use by DOE programs to assess progress in meeting their stated development goals. The first SOFC systems testing is planned to begin in the first part of FY 2006. Insight continues to be made in the area of dynamic solid oxide fuel cell response. New fuel cell models that include the capability to calculate current reversal show that certain load transients can induce current circulation within the cell. Such conditions should be considered by fuel cell engineers during the design of these systems, especially in light of the experimental work showing possible failure modes due to such operation. New

high-temperature strain gage sensors have been shown to be viable for SOFC application. Further work to demonstrate the proper protocol needed to obtain quantifiable information is underway. Finally, insight into the effect of alloy silicon content on the ASR performance of coated metal interconnects is being obtained. From this work, limits to the amount of silicon in SOFC interconnects will be identified.

FY 2005 Publications/Presentations

1. Gemmen, R.S. and C. Johnson (2005), "Effect of load transients on SOFC operation—current reversal on loss of load," In Press, J. Power Sources, 2005.
2. Gemmen, R.S. (2005), "High temperature strain gages for SOFC application," presented at the 2005 SECA Core Technology Review, Tampa, FL.
3. Gemmen, R.S. (2005), "DOE Fuel Cell Test Facility," presented at the 2005 Fuel Cell Projects Merit Review, Morgantown, WV.
4. Johnson, C. and R.S. Gemmen (2005), "The effect of inverter ripple on solid oxide fuel cell performance," presented at the 29th International Cocoa Beach Conference and Exposition on Advanced Ceramics and Composites, January 23-28, 2005, DoubleTree Oceanfront Hotel, Hilton Oceanfront Hotel, Cocoa Beach, FL.
5. Orlovskaya, N., A. Coratolo, C. Johnson, and R. Gemmen (2005), "Structural characterization of $LaCrO_3$ perovskite coating deposited by magnetron sputtering on an iron based chromium containing alloy as a promising interconnect material for SOFCs," accepted for publication in the Journal of the American Ceramic Society.

References

1. Gemmen, R.S. and C. Johnson (2005), "Effect of load transients on SOFC operation—current reversal on loss of load," In Press, J. Power Sources, 2005.
2. Johnson, C. and R.S. Gemmen (2005), "The effect of inverter ripple on solid oxide fuel cell performance," presented at the 29th International Cocoa Beach Conference and Exposition on Advanced Ceramics and Composites, January 23-28, 2005, DoubleTree Oceanfront Hotel, Hilton Oceanfront Hotel, Cocoa Beach, FL.

III.A.8 Continuous Process for Low-Cost, High-Quality YSZ Powder

Scott L. Swartz, Ph.D. (Primary Contact), Michael Beachy, and Matthew Seabaugh
NexTech Materials, Ltd.
404 Enterprise Drive
Lewis Center, OH 43035
Phone: (614) 842-6606; Fax: (614) 842-6607; E-mail: swartz@nextechmaterials.com

DOE Technology Development Manager: Shawna Toth
Phone: (304) 285-1316; E-mail: Shawna.Toth@netl.doe.gov

Objectives

- Develop a robust process for producing yttrium-stabilized zirconia (YSZ) powder that can be tailored to meet the Solid State Energy Conversion Alliance (SECA) industry team needs.
- Produce YSZ powder in 5-10 kg batches, and demonstrate reproducibility of the process.
- Demonstrate the advantages of tailoring YSZ powder characteristics to specific requirements of fabrication processes used in solid oxide fuel cell (SOFC) manufacture.
- Demonstrate that the process provides YSZ powder at low manufacturing cost.

Approach

- Use chemical precipitation methods to produce hydroxide precursors that can be converted into crystalline YSZ via thermal treatments.
- Use ball milling and attrition milling methods to reduce particle size of YSZ powders to below one micron.
- Use uniaxial and isostatic pressing methods followed by sintering to fabricate ceramic samples for density and ionic conductivity measurements.

Accomplishments

- Established a homogeneous precipitation process for preparing an yttrium-zirconium hydrous oxide precursor, which can be converted to crystalline YSZ via calcination.
- Established calcination and milling methods to prepare YSZ powders with controlled surface area and particle size distribution.
- Demonstrated that YSZ powder produced by the process can be sintered to densities greater than 98 percent theoretical at temperatures less than 1400ºC.
- Demonstrated sintered YSZ ceramics with high ionic conductivity (>0.04 S/cm at 800ºC), equivalent to the best values reported in the literature.
- Demonstrated a high surface area and fine particle size grade of YSZ powder that can be sintered at ultra-low temperatures (1200 to 1250°C).
- Demonstrated that the manufactured cost of YSZ powder produced using the process will be less than $25 per kilogram at large production volumes.

Future Directions

- Continued process refinements aimed at increasing performance and reducing manufacturing costs.
- Demonstration of advantages of using tailored YSZ powders in fabrication processes used for the manufacture of SOFCs. Planar and tubular SOFC components will be fabricated using tailored YSZ powder, and these components will be characterized and tested.

- Production of evaluation samples of YSZ electrolyte powder, NiO/YSZ anode powder, and/or SOFC components produced from these powders, for evaluation by SECA's industry teams.
- Continual updates to the manufacturing cost analyses, incorporating process refinements that are implemented.

Introduction

One of the current barriers to reducing the manufacturing cost of SOFCs is the high cost of some of the critical raw materials. The availability of a low-cost, highly reliable and reproducible supply of engineered raw materials is needed to assure successful commercialization of SOFC technology. The yttrium-stabilized zirconia (YSZ) electrolyte material is a primary ingredient for two of the three layers comprising an SOFC element: the dense electrolyte layer and the porous nickel-based cermet (Ni/YSZ) anode layer. In addition, YSZ often is used as a performance-enhancing additive to lanthanum strontium manganite (LSM) based cathode layers. In practice, the same YSZ raw material is used for each of the component layers, even though different fabrication processes are used for each layer. Significant opportunities for performance optimization and cost reduction would be possible if the YSZ raw material were tailored for each component layer. The project focuses on the development of synthesis technology for YSZ powder that is "tailored" to the process-specific needs of different SOFC designs being developed under DOE's SECA program.

Approach

NexTech's approach to developing a low-cost YSZ electrolyte powder production process is based on the following principles: (1) the process must be scaleable to high volume (500 tons per year) at a cost of less than $25/kilogram; (2) the process must be sufficiently versatile so that powder characteristics can be tailored to a specific customer's requirements; (3) the process must be reliable, providing consistent batch-to-batch quality; and (4) the process must provide a relatively pure YSZ powder that meets performance criteria relative to particle size, surface area, sintering activity, and ionic conductivity. The process being developed in this project is based on homogeneous precipitation (see Figure 1). With homogeneous precipitation, the pH and solids content remain constant throughout the process, which is the key to achieving uniformity and reproducibility of the finished product. Another attribute of the homogeneous precipitation process is that it can be made continuous with constant replenishment of the feed solutions. This provides considerable cost and reliability advantages relative to current chemical synthesis processes.

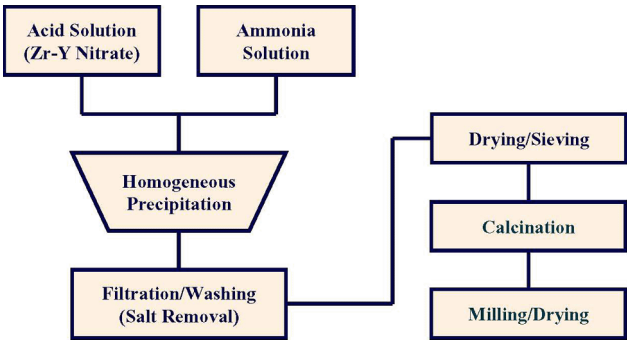

Figure 1. Homogenous Precipitation Process for YSZ Powder

In the project, synthesis studies are being conducted to identify optimum precipitation conditions for producing hydrous oxide precursors. These precursors then are processed into YSZ powders by washing and drying of the precipitates, calcination of the dried precursor to form a crystalline YSZ powder with targeted surface area (~10 m^2/gram), and milling of the calcined YSZ powder to sub-micron particle size. The YSZ powders are subjected to a comprehensive characterization protocol, involving x-ray diffraction, chemical analyses, particle size distribution, surface area measurements, and sintering studies. Performance of sintered YSZ ceramics is being assessed by density measurements, ionic conductivity measurements, mechanical property measurements, and scanning electron microscopy.

Results to Date

In this project, NexTech has demonstrated a laboratory-scale continuous (homogeneous) precipitation process for YSZ electrolyte powder

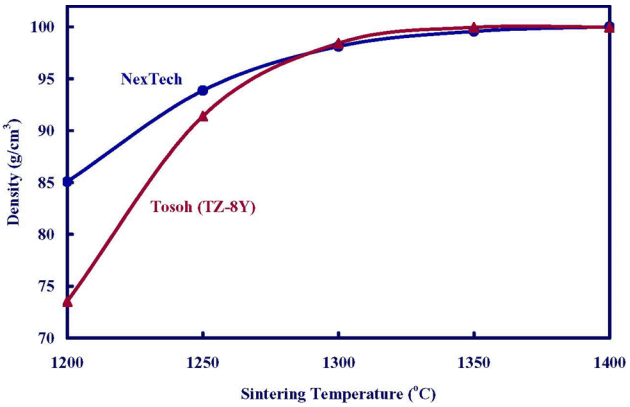

Figure 2. Sintering Performance of NexTech's YSZ Powder (baseline process), Compared to Commercially Available YSZ Powder (Tosoh, TZ-8Y)

with equivalent, and in some ways superior, performance to YSZ powder that is commercially available from non-domestic suppliers. Key results to date are discussed below:

- The initial precipitation conditions were shown to have a profound effect on the performance of fully processed (calcined and milled) YSZ powders. After optimization of precipitation conditions, YSZ powders produced by NexTech's baseline process sinter to high densities (>98 percent theoretical) at temperatures of 1300ºC and higher. The NexTech powder also exhibits improved low-temperature sinterability compared to commercial powder (Tosoh, TZ-8Y) with similar surface area (see Figure 2).
- NexTech demonstrated reproducibility of its synthesis process by producing three separate batches of YSZ powder and characterizing these powders through all stages of processing. Particle size distribution measurements (see Figure 3) indicated average particle sizes of 0.30, 0.27 and 0.31 microns, and surface areas of the three powders ranged from 13.9 to 14.5 m^2/gram. Sintering performance and ionic conductivity were identical for the three batches (within experimental error of the measurements).
- NexTech demonstrated improved densification through doping with alumina (Al_2O_3), nickel oxide (NiO), manganese oxide (Mn_2O_3) and cobalt oxide (CoO) dopants, especially at low sintering temperatures (less than 1300ºC).

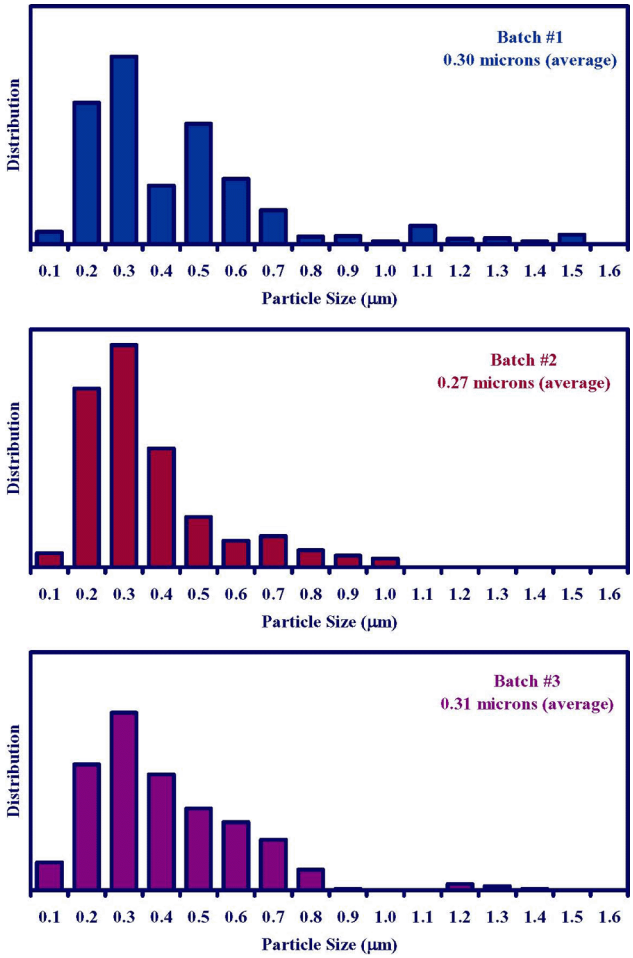

Figure 3. Particle Size Distributions of YSZ Powder from Three Separate Batches

NiO and Mn_2O_3 dopants resulted in significant depression of ionic conductivity, whereas this effect was less pronounced with Al_2O_3 and CoO dopants (depending on the dopant amount and method of incorporation). Results obtained with CoO dopants are presented in Figures 4 and 5. With a 0.1 wt% addition of CoO, the sintering temperature was reduced by about 50°C, with little change in ionic conductivity at 800°C. With increased cobalt doping (1 wt%), the sintering performance is further improved, but with a significant loss of ionic conductivity.

- NexTech's synthesis process also was demonstrated for scandium-stabilized zirconia (ScSZ) electrolyte compositions, both partially stabilized ScSZ-6 and fully stabilized ScSZ-10 compositions. The increased conductivity of ScSZ electrolytes was confirmed (see Figure 6).

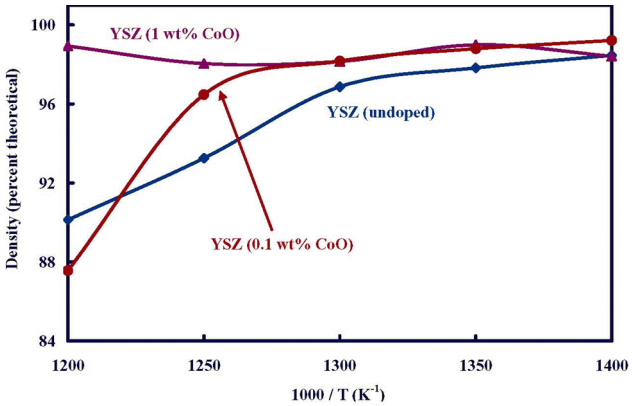

Figure 4. Effect of Cobalt Doping on Sintering Performance of YSZ Powder

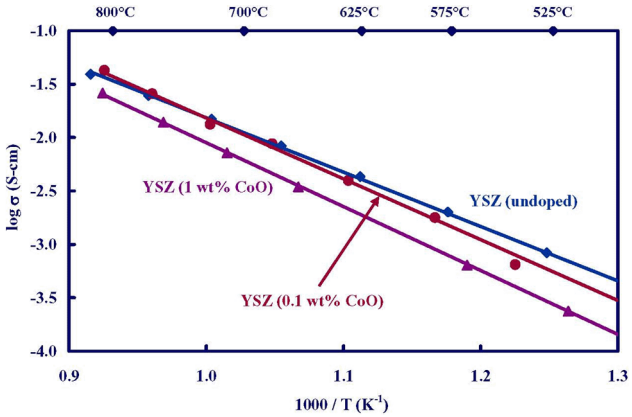

Figure 5. Effect of Cobalt Doping on Ionic Conductivity of Sintered YSZ Ceramics

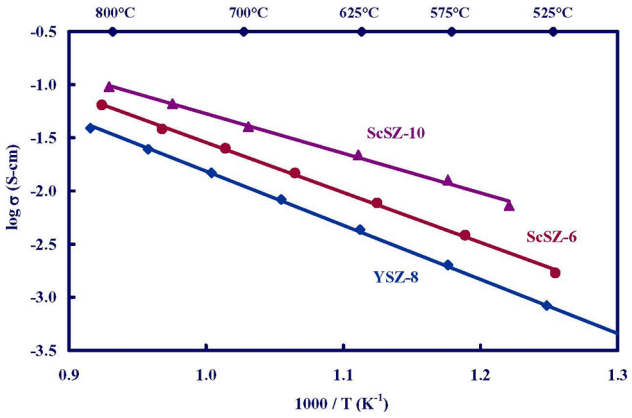

Figure 6. Ionic Conductivity of Yttrium-Stabilized and Scandium-Stabilized Zirconia Ceramics

- A manufacturing cost analysis confirmed that YSZ powder prepared by NexTech's homogeneous precipitation process could be manufactured at a cost of less than $25 per kilogram (see Figure 7). This analysis was based on a production volume of 500 metric tons per year, which is a fraction of the volume necessary when SOFCs are in full-scale production.

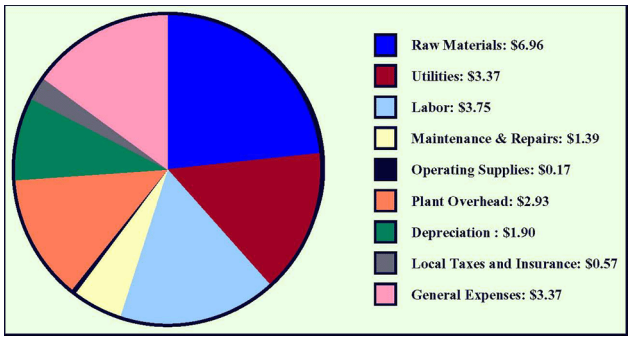

Figure 7. Results of Manufacturing Cost Analysis

Conclusions

- Homogeneous precipitation is a promising route for the continuous synthesis of hydrous oxide precursors to high-quality YSZ powders. The initial precipitation conditions have a profound effect on downstream milling performance (after calcination) and on subsequent sintering and electrical performance. Important synthesis variables include concentrations of the precipitant solutions, feed rates during precipitation, and the pH during precipitation.
- The processing of the precipitated hydroxide slurries prior to drying was critically important to achieving high-performance YSZ powders. For aqueous processing, surfactants were required to allow hydroxide precipitates to be dried directly from aqueous suspensions. An alternative approach, based on solvent exchange of the precipitated hydroxides into isopropyl alcohol prior to drying, also was demonstrated.
- Several oxide dopant strategies were identified that led to significant improvements in sintering performance of YSZ ceramics. Dopants such as aluminum oxide, nickel oxide, cobalt oxide, and manganese oxide all were found to increase ceramic densities, especially with low sintering temperatures (~1200 to 1300ºC). Aluminum and cobalt oxide dopants were the most effective for reducing sintering temperature without adversely affecting ionic conductivity.

- Based on a manufacturing cost analysis, YSZ powders prepared by the homogeneous precipitation process can be manufactured at a cost of less than $25 per kilogram at high production volumes. This analysis identified specific unit operations where cost can be reduced upon further optimization.

FY 2005 Publications/Presentations

1. S.L. Swartz, et al., *Continuous Process for Low-Cost, High-Quality YSZ Powder*, SECA Core Technology Workshop (Tampa, Florida, January 27, 2005).

III.A.9 Reliability and Durability of Materials and Components for Solid Oxide Fuel Cells

Edgar Lara-Curzio (Primary Contact), *M. Radovic, R. M. Trejo, K. An, C. R. Luttrell, T. R. Watkins, H. Wang, K. L. More, C. Cofer, B. Armstrong, and C. Walls*
Oak Ridge National Laboratory
1 Bethel Valley Rd.
Oak Ridge, TN 37831-6969
Phone: (865) 574-1749; Fax: (865) 574-6098; E-mail: laracurzioe@ornl.gov

DOE Project Manager: *Travis Shultz*
Phone: (304) 285-1370; E-mail: Travis.Shultz@netl.doe.gov

Objectives

- To determine the thermal properties of Ni/YSZ and yttria-stabilized zirconia (YSZ).
- To study the effect of thermal cycling and aging on the properties of solid oxide fuel cell (SOFC) materials.
- To assess the creep resistance of Ni/YSZ.
- To determine the slow-crack growth (SCG) parameters for Ni/YSZ and YSZ as a function of temperature.
- To support the Solid State Energy Conversion Alliance (SECA) industrial teams in the development of reliable SOFCs.

Approach

- Standardized test methods were employed to determine the thermal properties of Ni/YSZ and YSZ.
- A test facility was assembled for subjecting Ni-YSZ and Ni-YSZ/YSZ to thermal cycling and thermal aging. The effect of thermal cycling and thermal aging on the physical and mechanical properties of these materials was determined as a function of the number of thermal cycles and aging time.
- The resistance of Ni-YSZ to creep deformation was determined through stress-relaxation.
- The fracture toughness and SCG behavior of Ni-YSZ and YSZ were determined as a function of temperature using the double-torsion (DT) test method.
- The probability of failure of test specimens subjected to temperature gradients was determined experimentally and compared to that predicted by ceramic analysis and reliability evaluation of structures (CARES).

Accomplishments

- Determined the thermal properties of Ni-YSZ as a function of temperature and porosity.
- Developed methodologies and experimental facilities to assess the resistance of SOFC materials to thermal cycling, thermal aging and thermal shock.
- Found that H_2 reduction, thermal cycling and thermal aging modify the magnitude of residual stresses in NiO-YSZ/YSZ.
- Found that Ni-YSZ is prone to creep deformation at 800°C.
- Verified that CARES can be used to predict the reliability of SOFC materials when subjected to an arbitrary stress distribution.

Future Directions

- Continue investigating the role of microstructure on the reliability and durability of SOFC materials, the role of microstructure on their resistance to SCG, and how microstructure evolves after thermal cycling, thermal aging and creep.
- Implement models to predict the reliability of SOFC multilayers that account for residual stresses when multilayers are subjected to arbitrary loading conditions.
- Continue supporting the SECA industrial teams in the development of reliable SOFCs.

Introduction

The durability and reliability of SOFCs depend on the ability of their components to withstand mechanical stresses that arise during processing and service. Specifically, the reliability and durability of a SOFC are determined by the spectrum of stresses acting on SOFC components and their stochastic distribution of strengths. The stress distribution in SOFCs, which is a complex function of geometry, residual stresses, temperature gradients and external mechanical loads, can be determined through the use of computational tools and knowledge of the physical and mechanical properties of the SOFC materials. The stochastic distribution of strengths of SOFC materials is primarily determined by the type and distribution of strength-limiting flaws which are intrinsic to the material or that are introduced during processing and/or manufacturing. Because flaws can grow in size with time, the distribution of strengths, and hence the reliability of SOFCs, will also evolve with time.

Approach

Table 1 lists the materials that were used in this project (Figure 1). The Ni-based materials were prepared from a powder mixture of 75 mol% NiO and 8 mol% Y_2O_3-stabilized ZrO_2 (YSZ). Different amounts of organic pore former (0, 15 or 30 vol%) were added to the powder mixture to obtain test specimens with different porosity. Green test specimens were prepared by tape casting four 250-μm thick layers, which were subsequently laminated. A 15-μm thick layer of YSZ was screen-printed over some of the NiO-YSZ test specimens to obtain bilayers. Mono- and bilayer discs were sintered at 1400°C in air for 2 hours and subsequently reduced in 4% H_2 + 96% Ar at 1000°C. Different experimental techniques were used to determine the physical and mechanical properties of, and residual stresses in, the materials used in this project. Analyses of thermal stresses in SOFCs were carried out using the computer program ANSYS. The computer program CARES was used [2] to perform reliability calculations.

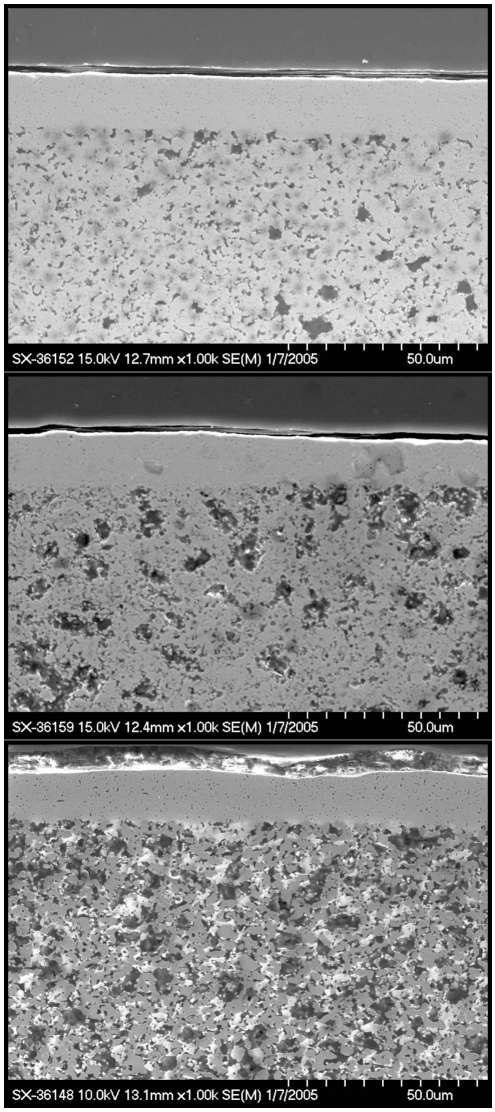

Figure 1. Scanning electron micrographs of (a) 26-bilayer, (b) 34-bilayer, (c) 40-bilayer. Note porosity difference among these materials.

Table 1. Materials Used in This Investigation

Nomen-clature	Initial concentration of pore former (vol%)	Average porosity after sintering and NiO reduction (vol%)[1]	
26-bilayer	0	26	Ni-YSZ 26% porosity + YSZ
34-bilayer	15	34	Ni-YSZ 34% porosity + YSZ
40-bilayer	30	40	Ni-YSZ 40% porosity + YSZ
26-mono-layer	0	26	Ni-YSZ 26% porosity
34-mono-layer	15	34	Ni-YSZ 34% porosity
40-mono-layer	30	40	Ni-YSZ 40% porosity

1. Porosity varied between 0.5 and 1.7%

Results

Thermal Properties

The heat capacity, thermal diffusivity, thermal conductivity and thermal expansion of SOFC materials were determined as a function of temperature. The heat capacity, c_p, was determined by differential scanning calorimetry. It was found that for the range of porosities examined, porosity didn't have an effect on the magnitude of the heat capacity of Ni-YSZ. The peak in heat capacity, which was observed both on heating and cooling near 300°C (Curie Temperature), corresponds to the ferromagnetic to paramagnetic transition in nickel. Thermal diffusivity was measured by the Laser Flash method. It was found that while the thermal diffusivity of Ni-YSZ increased with increasing porosity, it decreased with temperature. The thermal conductivity was determined according to the following relationship: $k = \rho\, c_p\, \alpha$, where k, ρ, c_p, and α are thermal conductivity, density, heat capacity and thermal diffusivity, respectively. Figure

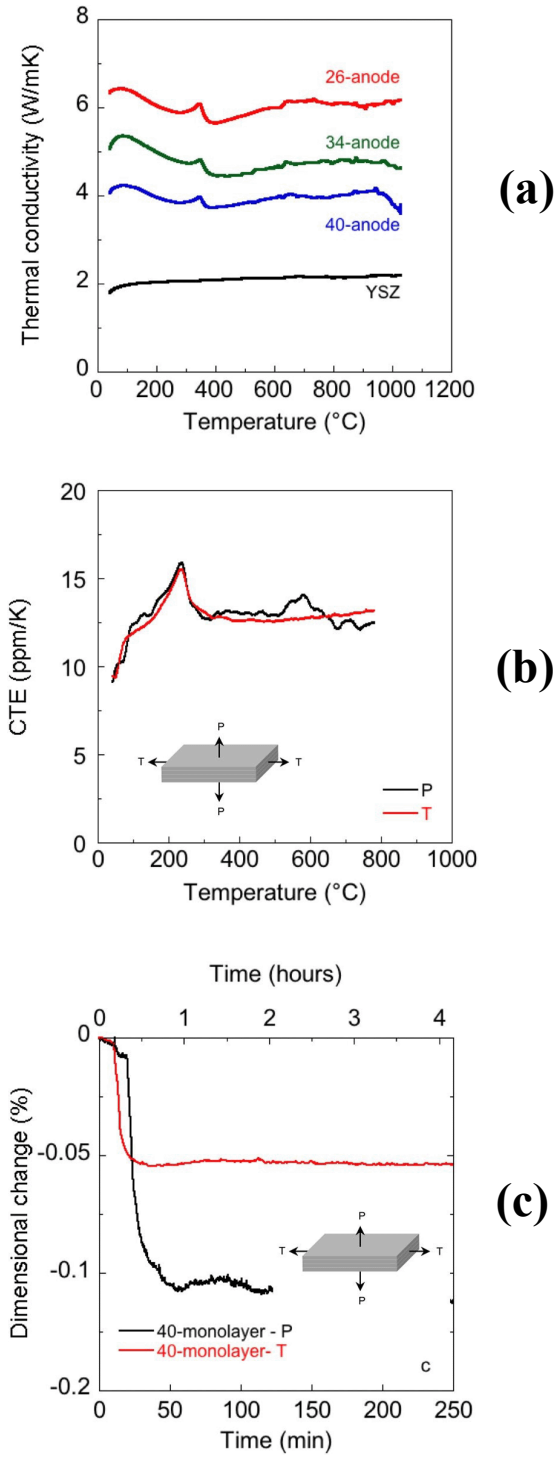

Figure 2. Thermal properties of SOFC materials: (a) thermal conductivity vs. temperature; (b) coefficient of thermal expansion for 40% porous Ni-YSZ cermet as a function of temperature; (c) dimension changes (shrinkage) of NiO-YSZ during H_2 reduction. Inset shows measurement directions.

2a shows plots of thermal conductivity versus temperature for YSZ and Ni-YSZ. It was found that while the thermal conductivity of Ni-YSZ doesn't change with temperature up to 1000°C, it does decrease with increasing porosity.

The thermal expansion and dimensional changes that NiO-YSZ undergoes during H_2 reduction were determined using a thermo-mechanical analyzer. Measurements were obtained in the direction of the tape thickness and in the direction of tape casting. Test specimens were heated to 800°C in air at a rate of 3°C/min, followed by isothermal reduction at 800°C in 4% H_2 + 96% Ar for 24 hours, cooling to 20°C, heating to 800°C and cooling again to 20°C at the a rate of 3°C/min in a gas mixture of 4% H_2 + 96% Ar. The coefficient of thermal expansion (CTE) of a 34-monolayer, which is plotted in Figure 2b as a function of temperature, exhibited a peak at the Curie temperature in both measuring directions. The coefficient of thermal expansion of Ni-YSZ changed between 10 ppm/K at 100°C and 15 ppm/K at 800°C independently of porosity or measurement direction. Figure 2c illustrates the dimensional changes experienced by a 40-monolayer during H_2 reduction. It was found that NiO-YSZ shrinks as a result of the reduction of NiO into Ni by as much as 0.11% and that the amount of shrinkage increases with the amount of initial porosity. It was also found that shrinkage is anisotropic and that it is more pronounced in the stacking direction. These results are important because they revealed the anisotropic nature of reduction-induced shrinkage and because reduction-induced dimensional changes will affect the magnitude of residual stresses in SOFCs.

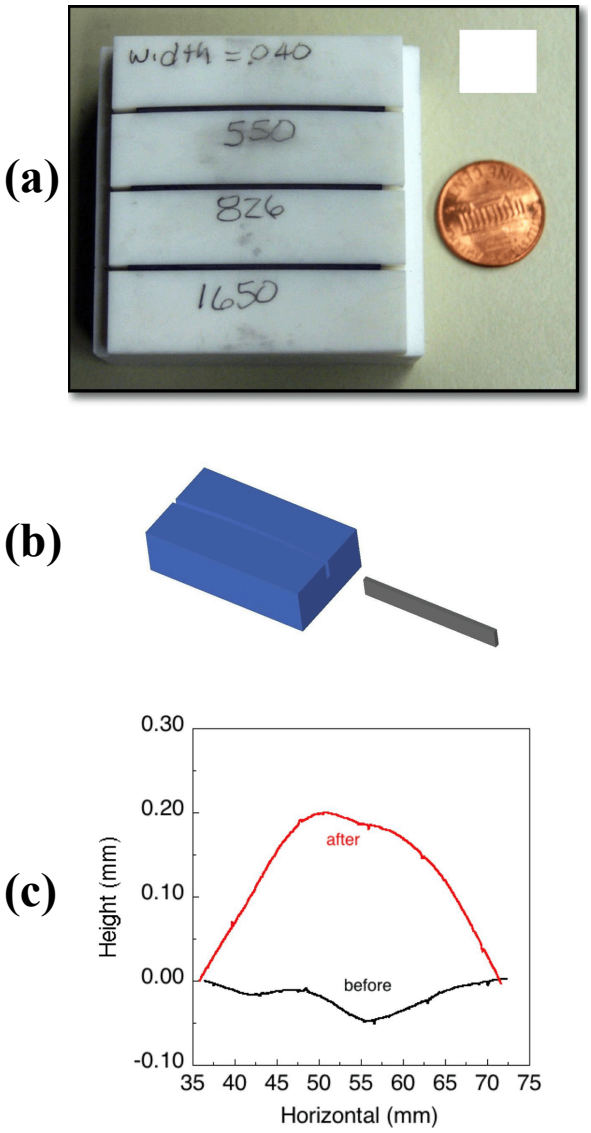

Figure 3. Creep behavior of Ni-YSZ. (a) Macor® fixture with machined slots and test specimens for stress-relaxation testing. The numbers written on the fixture correspond to the radius of curvature of the slots in millimeters. (b) Schematic of fixture for stress-relaxation testing. (c) Curvature recorded before and after 50-hr stress relaxation test at 800°C at an initial elastic stress of 45 MPa for a 40-monolayer test specimen.

Creep behavior of Ni-YSZ

Creep deformation is one of the mechanisms responsible for changes in residual stresses in Ni-YSZ/YSZ bilayers at high temperature, particularly during thermal cycling and thermal aging (this topic is discussed below). To assess the propensity of Ni-YSZ for creep deformation, 40-monolayers were subjected to stress-relaxation testing. Test specimens were subjected to pure bending using a Macor® fixture in which three grooves with different radii of curvature had been machined (Figures 3a and 3b). The radius of curvature of the grooves was selected so that the maximum elastic tensile stresses in the beams were 15 MPa, 30 MPa and 45 MPa. The fixture with the test specimens was placed in a furnace and held at 800°C for 50 hours in a gas mixture of 4% H_2 + 96% Ar. The curvature of the test specimens was determined using a profilometer before and after the test. It was found that the test

specimens retained the curvature imposed by the fixture, which demonstrates the propensity of Ni-YSZ for creep deformation at 800°C. Figure 3c compares the curvature of a 40-monolayer test specimen before and after stress relaxation testing under an initial elastic stress of 45 MPa. These results will help understand how residual stresses evolve in SOFCs as a function of time.

Fracture behavior of Ni-YSZ

The effects of porosity, temperature and environment on the fracture toughness and SCG behavior of Ni-YSZ materials were investigated using the DT test method. Test specimens were pre-cracked at ambient conditions, and the fracture toughness was determined from the maximum load, P_f, at which pre-cracked test specimens failed during fast loading. Fracture toughness results for Ni-YSZ specimens with different porosity are shown in Figure 4a as a function of temperature. It was found that the fracture toughness of Ni-YSZ decreased both with temperature and porosity.

The SCG behavior of Ni-YSZ was determined using the load relaxation mode of the DT test configuration. Pre-cracked test specimens were loaded at a constant displacement rate up to 95% of the fracture load. Then, the crosshead of the mechanical testing machine was arrested, and the load relaxation due to stable crack propagation was recorded as a function of time. The crack growth rate, *da/dt*, was calculated directly from the rate of load relaxation, *dP/dt*. Examples of SCG curves are shown in Figure 4b. It was found that the v-K curves shift towards lower stress intensity, indicating higher crack growth rates, as the porosity increases. Preliminary results from the microstructural characterization of test specimens indicated that, as expected, the microstructure of these materials does play a significant role on their SCG behavior (Figure 4c).

Residual Stresses

The magnitude of residual stresses in the YSZ layer of bilayer test specimens was determined by X-ray diffraction between 20°C and 900°C, before and after H_2 reduction. It was found that the residual stress in the YSZ layer was highly compressive at

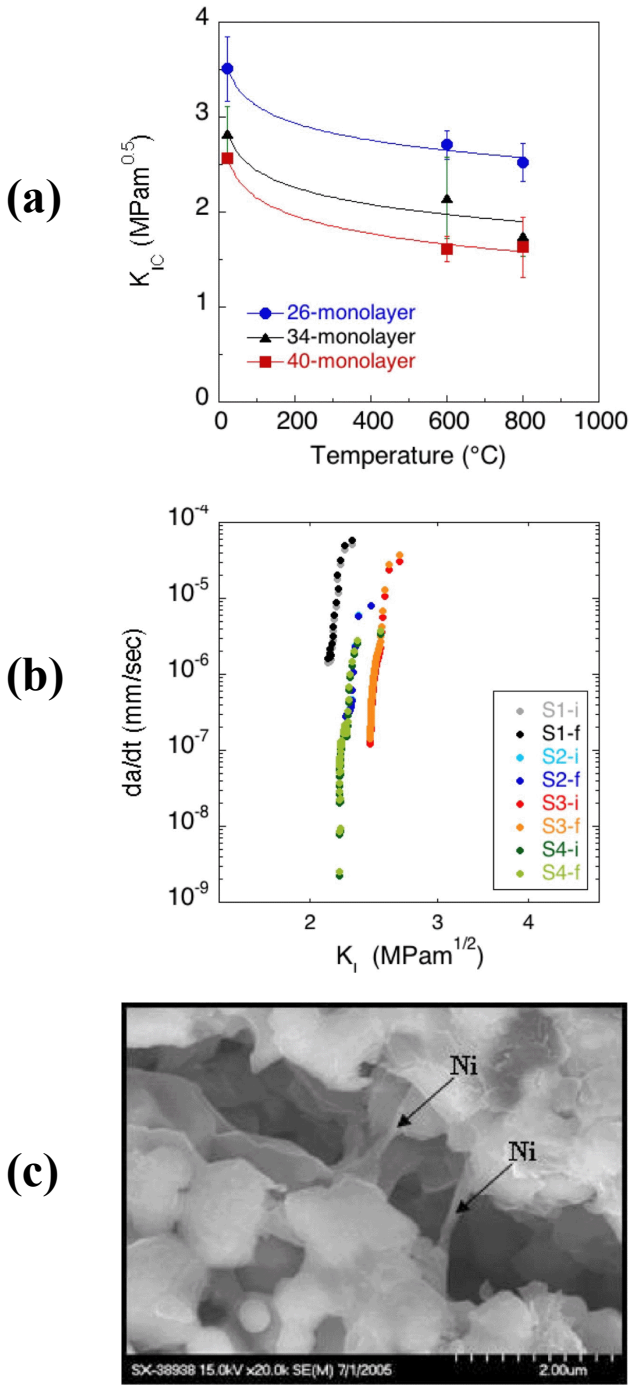

Figure 4. Fracture toughness and SCG behavior of SOFC materials. (a) Fracture toughness of Ni-YSZ as a function of temperature and porosity. (b) Plots of crack velocity versus stress intensity factor for 40-monolayer Ni-YSZ test specimens. (c) Scanning electron micrographs illustrating the interaction between crack propagation and microstructure in Ni-YSZ during SCG testing at 600°C.

20°C and that its magnitude decreased linearly with increasing temperature. The zero-stress reference temperature for NiO-YSZ was found to be 1030°C, which is much lower than the sintering temperature. This discrepancy can be explained if NiO-YSZ and YSZ undergo stress relaxation through creep and/or plastic deformation at temperatures between the sintering and the zero-stress temperatures. After reduction, the residual stress in the YSZ layer was also found to be compressive, but its magnitude was smaller than that for the unreduced state. As dictated by equilibrium, the NiO-YSZ and Ni-YSZ layers are under residual tension. The changes in residual stresses before and after reduction and the decrease in the zero-stress temperature are the result of increases in porosity when NiO reduces into Ni and of Ni plastic deformation.

Effect of Thermal Cycling and Thermal Aging on Residual Stresses

To quantify the effect of thermal cycling on the properties of SOFC materials, Ni-YSZ and YSZ/Ni-YSZ test specimens were subjected to 1, 25, 250 or 1250 thermal cycles between 100°C and 800°C in 4% H_2 + 96% Ar. Figure 5a shows the thermal cycling schedule used for those tests. To differentiate between the effect of thermal exposure at 800°C and thermal cycling, thermal aging tests were carried out at 800°C for up to 625 hours, which is the cumulative time that test specimens experienced at 800°C after 1250 cycles. Porosity, elastic moduli, biaxial strength and residual stresses were determined as a function of the number of thermal cycles and aging time. In all cases, except for 26-bilayers for which porosity changed by as much as 10%, the porosity and stiffness didn't change significantly as a result of thermal aging or thermal cycling. Figure 5b shows a plot of the residual stresses at 20°C in the YSZ layer of bilayer test specimens as a function of time/number of thermal cycles. It was found that the YSZ layer was invariably under residual compression and that the magnitude of the compressive stress decreased with increasing porosity in the Ni-YSZ layer. However, the magnitude of the compressive residual stress in the YSZ layer was found to decrease with the number of thermal cycles, and to become more compressive after thermal aging. While the increase in the magnitude of the compressive residual stress in the

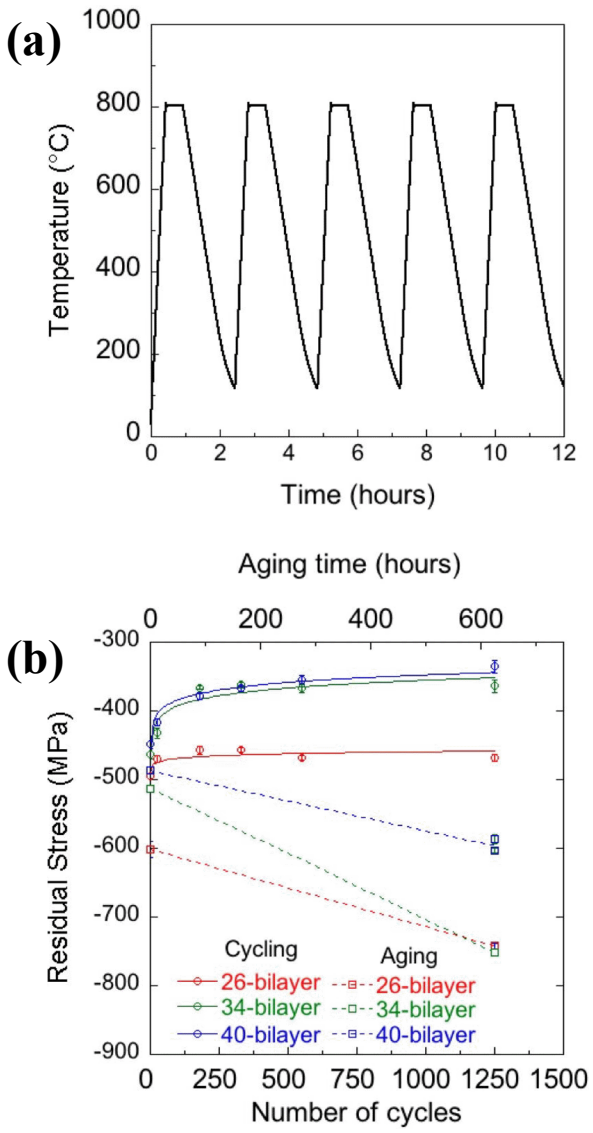

Figure 5. Results of thermal cycling and aging experiments. (a) Thermal schedule used for thermal cycling. (b) Residual stresses in YSZ layer as a function of thermal cycles and aging time.

YSZ layer after thermal aging can be explained if, for example, Ni experiences sintering, this argument by itself cannot explain the opposite trend observed after thermal cycling. In this case, the decrease in the magnitude of residual stresses with thermal cycling could be explained if Ni-YSZ experienced cracking or if porosity increased as a result of thermal cycling. However, the changes observed in porosity and elastic constants of these materials after thermal cycling were too small to support this argument. To

better understand these trends, the microstructure of test specimens was characterized before and after thermal cycling and thermal aging by electron microscopy. Preliminary quantitative image analysis of these micrographs revealed that there was a slight coarsening of small grains as a result of thermal cycling, but additional work is in progress to further understand these results.

The equibiaxial flexural strength of a total of 12 test specimens was determined using the ring-on-ring testing for each cycling/aging condition, and the results were analyzed using Weibull statistics. The characteristic strength of 34-bilayers and 40-bilayers was found to decrease with the number of thermal cycles or aging time by as much as 20%. However, the biaxial strength of 26-bilayers followed an opposite trend and increased by as much as 5% with the number of thermal cycles. These results are important because they demonstrate that thermal cycling and thermal aging degrade the strength of Ni-YSZ.

Reliability of SOFCs

The strength of the ceramic materials used in SOFCs is stochastic, and it can be described by a statistical distribution (e.g., Weibull distribution). During operation, SOFC materials will be subjected to complex states of stress that include residual stresses, stresses from external loads (e.g., during fuel cell assembly) and thermally induced stresses (e.g., from temperature gradients). From a mechanics perspective, the reliability of SOFCs will be determined by the intersection of the distribution of strengths and the spectrum of stresses.

One of the objectives of this project is to develop a methodology to predict the reliability and durability of SOFCs, and the proposed approach uses the computer program CARES. To demonstrate the applicability of CARES, experiments were carried out by subjecting NiO-YSZ disc-shaped test specimens to arbitrary temperature gradients using an infrared spot heater. The surface temperature distribution was recorded using an infrared camera and then used as input to compute the corresponding stress distribution in the test specimen using the finite-element stress analysis program ANSYS. With the stress distribution and the isothermal strength distributions of the material, the computer program CARES was used to predict the reliability of the test specimens, which was then compared with the experimentally determined failure rate.
To distinguish failures induced by the temperature gradient from those that would result from thermal shock, a series of tests was carried out to find the critical heating rate associated with thermal shock failures, and it was determined that for the heating rates examined, the properties of test specimens were not affected by the heating rate. Experiments were carried out for two different magnitudes of temperature gradient, $\Delta T_{max} = 300°C$ and $\Delta T_{max} = 400°C$, which were obtained by adjusting the focal point of the spot heater. Seventeen test specimens were evaluated for each condition.
Table 2 lists a comparison of the actual and predicted failure rates for the NiO-YSZ test specimens.
The good agreement between the predicted and experimentally determined failure rates provides confidence on the applicability of CARES to predict the reliability and durability of materials for SOFCs. Ongoing work is focused on applying the methodology to Ni-YSZ/YSZ bilayers so that residual stresses can be included in the analysis. Also, a testing configuration with localized cooling is being used, in addition to localized heating, to probe strength-limiting flaws both in the interior and perimeter of the test specimens.

Table 2. Comparison of Actual and Predicted Failure Rates for NiO-YSZ Test Specimen

Temperature gradient	Predicted failure rate (CARES)	Actual failure rate
440°C	84 %	15/17 (88%)
300°C	54 %	7/17 (45%)

Summary

The thermal conductivity, heat capacity, thermal diffusivity and thermal expansion of Ni-YSZ were determined between 20 and 1000°C. It was found that the thermal conductivity of Ni-YSZ had a slight dependence on temperature and that it decreased with increasing porosity. Also, it was found that these materials shrank by as much as 0.12% during H_2 reduction at 800°C and that shrinkage was

anisotropic and largest in the direction of tape casting.

The fracture toughness and SCG behavior of Ni-YSZ were determined as a function of temperature. It was found that fracture toughness decreased both with temperature and porosity from 4.5 $MPam^{0.5}$ for 26-monolayer at 20°C to 1.6 $MPam^{0.5}$ for 40-monolayer at 800°C.

It was also found that the state of residual stress in Ni-YSZ/YSZ bilayers was modified by thermal cycling and thermal aging and that the characteristic strength decreased after thermal cycling and thermal aging. Work is in progress to establish correlations between these results and changes in the microstructure of these materials. The viability of the computer program CARES to predict the reliability of SOFC materials when subjected to an arbitrary stress distribution was demonstrated. Stress relaxation tests revealed that Ni-YSZ is prone to creep deformation at 800°C.

FY 2005 Publications/Presentations

1. M. Radovic and E. Lara-Curzio, "Mechanical Properties of Tape Cast Nickel-based Anode Materials for Solid Oxide Fuel Cells before and after Reduction in Hydrogen," *Acta Materialia,* 52 (2004) 5747–5756
2. M. Radovic and E. Lara-Curzio, "Elastic Properties of Nickel-Based Anodes for Solid Oxide Fuel Cells as a Function of the Fraction of Reduced NiO," *J. Am. Ceram. Soc.,* 87 [12] 2242–2246 (2004)
3. E. Lara-Curzio and M. Radovic, "The Effect of Friction on the Magnitude of the Equibiaxial Strength Determined by the Ring-on-Ring Test," Presented at 28th Annual Cocoa Beach Conference & Exposition on Advanced Ceramics & Composites, Cocoa Beach, Florida, January 24-28, 2005
4. M. Radovic, E. Lara-Curzio, R. M. Trejo, T. Watkins, and C. A. Walls, "Effect of Thermal Cycling on the Properties of Ni-YSZ Anodes and Ni-YSZ/YSZ Bilayers," Presented at 28th Annual Cocoa Beach Conference & Exposition on Advanced Ceramics & Composites, Cocoa Beach, Florida, January 24-28, 2005

References

1. M. Radovic and E. Lara-Curzio, "Mechanical Properties of Tape Cast Nickel-based Anode Materials for Solid Oxide Fuel Cells before and after Reduction in Hydrogen," *Acta Materialia* 52 (2004) 5747–5756
2. N. N. Nemeth, J. M. Manderscheid and J. P. Gyekenyesi, "Ceramic Analysis and Reliability Evaluation of Structures (CARES)," NASA TP-2916, August (1990)

III.A.10 SOFC Compressive Seal Development at PNNL

Yeong-Shyung "Matt" Chou (Primary Contact), Jeff Stevenson
Pacific Northwest National Laboratory
P.O. Box 999, MS K2-44
Richland, WA 99352
Phone: (509) 375-2527; Fax: (509) 375-2186; E-mail: Yeong-Shyung.Chou@pnl.gov

DOE Project Manager: Lane Wilson
Phone: (304) 285-1336; Fax: (304) 285-4638; E-mail: Lane.Wilson@netl.doe.gov

Objectives

- Develop cost-effective seals for solid oxide fuel cell (SOFC) stacks that offer low leak rates and desired reliability during long-term operation and thermal cycling.
- Improve understanding of degradation mechanisms affecting seal performance, including intrinsic materials degradation in SOFC environment and interactions with other SOFC components.

Approach

- Perform preliminary evaluation of seal concepts.
- Synthesize, fabricate and test seal materials and designs under SOFC-relevant conditions (atmosphere and temperature).
- Evaluate tested seal components to improve understanding of degradation processes during seal operation.

Accomplishments

- Developed a low-cost "hybrid" compressive seal based on mica paper with glass-ceramic or metallic interlayers.
- Demonstrated low leak rate and stability of hybrid seals during long-term testing with extensive thermal cycling.

Future Directions

- Develop durable, low-cost glass (glass-ceramic) seals with minimal materials/interfacial interaction/ degradation and engineered interface for optimal shear strength at various sealing temperatures.
- Study interfacial reaction/degradation at various stages of operation, temperatures, and environments.

Introduction

Planar SOFC stacks require adequate seals between the interconnect and the cells in order to prevent mixing of the oxidant and fuel gases, and to prevent leaking of gases from the stack. In addition, these seals must also allow the stack to be thermally cycled repeatedly (between ambient conditions and the operating temperature). Several different approaches to sealing SOFC stacks are available, including rigid, bonded seals (e.g., glass-ceramics), compliant seals (e.g., viscous glass), and compressive seals (e.g., mica-based composites). Rigid seals typically soften and flow slightly during stack fabrication (at a temperature above the operating temperature) but then become rigid (to avoid excessive flow or creep) when cooled to the operating temperature. The thermal expansion of rigid seals must be closely matched to the other stack components in order to avoid damaging the stack during thermal cycling. Compliant seals attempt to simultaneously perform the sealing function and prevent thermal stress generation between adjacent components. Compressive seals typically utilize

materials such as sheet-structure silicates that do not bond adjacent SOFC components; instead, the sealing material acts as a gasket, and gas-tightness is achieved by applying a compressive force to the stack. Both compliant and compressive seals potentially improve the ability of the stack to tolerate thermal expansion mismatch between the various stack components.

Recent Core Technology Program seal development work at Pacific Northwest National Laboratory (PNNL) has focused on a novel "hybrid" mica-based compressive seal concept. Initial development efforts focused on hybrid seals based on naturally cleaved Muscovite mica sheets, which offered leak rates several orders of magnitude lower than those measured with "plain" mica compressive seals. The seals, however, did not exhibit the desired thermal cycle stability, as the leak rates tended to increase with increasing thermal cycles. Microstructural characterization of cycled seals revealed undesirable degradation of the Muscovite mica due to coefficient of thermal expansion (CTE) mismatch with the mating materials. Improvements in thermal cycle stability have been obtained with seals based on Phlogopite mica paper, which has a higher "x-y (parallel to basal plane)" CTE (~11 ppm/^{o}C) than Muscovite mica (~7 ppm/^{o}C). Recent seal work has focused on optimizing Phlogopite paper-based hybrid seals to maintain low leak rates during long-term operation and thermal cycling.

Approach

Candidate seals were evaluated by studying seal quality (i.e., leak rate or open circuit voltage) as a function of temperature, gas pressure and composition, and applied compressive load. For leak rate measurements, the seals were tested with simulated stack components using a test fixture which applied the desired compressive load and then measured changes in gas pressure due to leakage. Stability and resistance to chemical interaction with other SOFC components were evaluated through thermogravimetric analysis, x-ray diffraction, electron microscopy, and optical microscopy. The hybrid seals consisted of commercially available Phlogopite mica paper sandwiched between thin layers of glass or metal. The seals were typically fabricated by inserting the mica paper between polymer tapes (prepared by conventional tape casting techniques) which contained the glass powder, or between metal foils. Sealing was accomplished by placing the tri-layer structure between the stack component materials to be sealed.

Results

Due to space constraints, only results for hybrid Phlogopite mica seals with Ag interlayers are reported. Long-term (4000 hours) ageing and short-term cycling tests were performed. Seals were tested between an Inconel600 (2"x2") fixture and an yttria-stabilized zirconia (YSZ) electrolyte plate under a compressive stress of 12 psi. A reducing gas of ~2.7% H_2/balance Ar with ~3% H_2O was passed over the sample to simulate the SOFC anode environment. The seal was subjected to alternating periods of isothermal testing at 800°C and repeated short-term thermal cycling from ~100°C to 800°C, with dwells at 800°C for 2 hours for leak testing. The leak rates over the entire period of isothermal ageing, the 1st stage of thermal cycling, and the 2nd stage of thermal cycling are shown in Figures 1, 2, and 3, respectively. It is evident that the hybrid mica seal with Ag interlayers showed good thermal stability over the entire (4000 hours) period of isothermal ageing. In addition, the leak rates remained fairly stable during the two stages of short-term thermal cycling, with leak rates in the range of ~0.02 to ~0.04 sccm/cm of seal perimeter. It is interesting to note that the leak rates increased slightly to ~0.04 sccm/cm after the 1st stage of

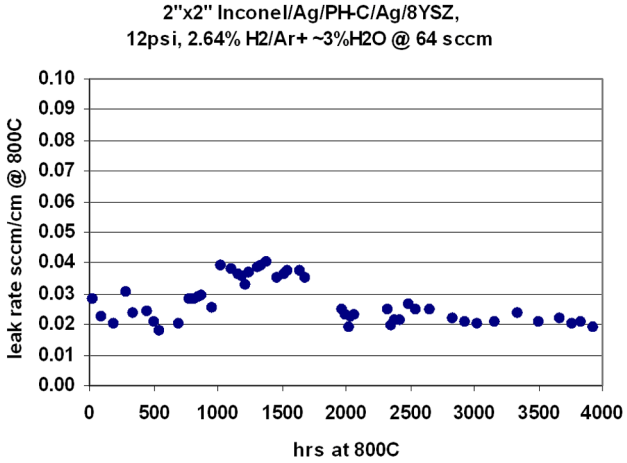

Figure 1. Leak Rate of Hybrid Phlogopite Mica Seal with Ag Interlayer: Complete Data for Ageing Tests at 800°C

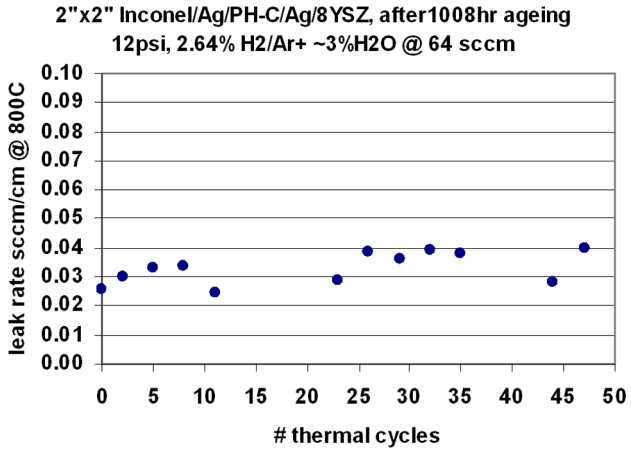

Figure 2. Leak Rate of Hybrid Phlogopite Mica Seal with Ag Interlayer: Thermal Cycling Data after Isothermal Ageing for 1008 hrs

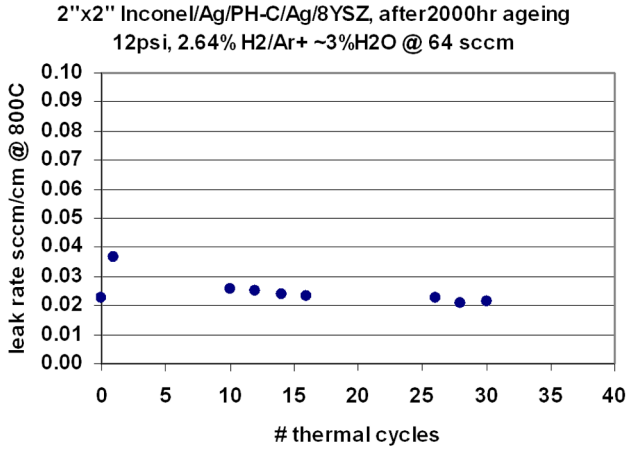

Figure 3. Leak Rate of Hybrid Phlogopite Mica Seal with Ag Interlayer: Thermal Cycling Data after Isothermal Ageing for 2000 hrs

ageing, but gradually decreased to ~0.02 sccm/cm after about 3000 hours. The current results are quite promising since the duration of this test represents ~1/10 of the desired life time (40,000 hours) for stationary SOFC applications. A leak rate of 0.02 sccm/cm would likely represent less than 1% of the total fuel flow in an actual SOFC stack.

Conclusions

Low-cost, easily fabricated "hybrid" seals based on Phlogopite mica were found to offer stable, low leak rates under relatively low applied compressive stress during isothermal and thermal cyclic exposure conditions.

FY 2005 Presentations

1. "Compressive Seal Development for Solid Oxide Fuel Cells," Y.-S. Chou, J.W. Stevenson, and P. Singh, 6th Annual SECA Alliance Workshop, Pacific Grove, CA, April 17-22, 2005.
2. "Compressive Seal Development for Solid Oxide Fuel Cells," Y.-S. Chou, J.W. Stevenson, and P. Singh, SECA Core Technology Program Review Meeting, Tampa, FL, January 27-28, 2005.
3. "Combined Aging and Thermal Cycling of Compressive Mica Seals for Solid Oxide Fuel Cells," Y.-S. Chou and J.W. Stevenson, 2nd International Symposium on Solid Oxide Fuel Cell (SOFC) Materials and Technology, 29th International Conference on Advanced Ceramics and Composites (American Ceramic Society), Cocoa Beach, FL, January 23-28, 2005.
4. "Glass-Mica Composite Seals for Solid Oxide Fuel Cells," Y.-S. Chou and J.W. Stevenson, 2nd International Symposium on Solid Oxide Fuel Cell (SOFC) Materials and Technology, 29th International Conference on Advanced Ceramics and Composites (American Ceramic Society), Cocoa Beach, FL, January 23-28, 2005.
5. "Glass-Mica Composite Seals for Solid Oxide Fuel Cells," Y.-S. Chou and J.W. Stevenson, 2nd International Symposium on Solid Oxide Fuel Cell (SOFC) Materials and Technology, 29th International Conference on Advanced Ceramics and Composites (American Ceramic Society), Cocoa Beach, FL, January 23-28, 2005.
6. "Status of Compressive Mica Seals at PNNL: Effect of Long-term Thermal Cycling and Temperature Gradients," Y.-S. Chou and J.W. Stevenson, 2004 Fuel Cell Seminar, San Antonio, TX, November 1-5, 2004.
7. "Compressive Mica Seals for Solid Oxide Fuel Cells," Y.-S. Chou and J.W. Stevenson, ASM Materials Solutions Conference, Columbus, OH, October 18-20, 2004.

FY 2005 Publications

1. Y.-S. Chou and J.W. Stevenson, "Long-term Thermal Cycling of Phlogopite Mica-based Compressive Seals for Solid Oxide Fuel Cells," Journal of Power Sources, 140, 340 (2005).
2. Y.-S. Chou and J.W. Stevenson, "Novel Infiltrated Phlogopite Mica Compressive Seals for Solid Oxide Fuel Cells," J. Power Sources, 135, 72 (2004).

3. Y.-S. Chou and J.W. Stevenson, "Long-term Thermal Cycling of Phlogopite Mica Based Compressive Seals for Solid Oxide Fuel Cells," in Developments in Fuel Cells and Lithium Ion Batteries (Ceramic Transactions Volume 161), edited by Arumugan and Manthiram, p. 69, American Ceramic Society, Westerville, OH (2004).

4. Y.-S. Chou and J.W. Stevenson, "Infiltrated Phlogopite Micas with Superior Thermal Cycle Stability as Compressive Seals for Solid Oxide Fuel Cells," in Developments in Fuel Cells and Lithium Ion Batteries (Ceramic Transactions Volume 161), edited by Arumugan and Manthiram, p. 89, American Ceramic Society, Westerville, OH (2004).

III.A.11 SOFC Anode Materials Development at PNNL

Olga Marina (Primary Contact), Larry Pederson, Jeff Stevenson
Pacific Northwest National Laboratory
P.O. Box 999, MS K2-44
Richland, WA 99352
Phone: (509) 375-2337; Fax: (509) 375-2186; E-mail: Olga.Marina@pnl.gov

DOE Project Manager: Lane Wilson
Phone: (304) 285-1336; E-mail: Lane.Wilson@netl.doe.gov

Objectives

- Develop solid oxide fuel cell (SOFC) anode compositions which will satisfy advanced anode requirements including redox tolerance, sulfur tolerance, and carbon tolerance while offering low polarization losses and long-term stability.
- Improve understanding of mechanisms affecting anode performance, including both intrinsic factors (e.g., composition, microstructure) and extrinsic factors (e.g., S poisoning).

Approach

- Synthesize, process, and characterize candidate SOFC anode compositions.
- Assess anode performance using half-cell and full-cell testing.
- Evaluate effects of redox cycling and exposure to sulfur compounds and hydrocarbon fuels on anode performance.

Accomplishments

- Quantified sulfur and hydrocarbon tolerance of Pacific Northwest National Laboratory's (PNNL's) ceramic composite anode relative to traditional nickel/yttria-stabilized zirconia (Ni/YSZ) SOFC anodes.
- Improved understanding of S degradation mechanisms for Ni-based and ceramic composite anodes.

Future Directions

- Optimize ceramic anode composition and microstructure.
- Develop current collection and contact materials for anode/interconnect interfaces.

Introduction

The current state-of-the-art anode material is a Ni/YSZ cermet (a composite of Ni metal and YSZ ceramic). Overall, this material offers many good properties, including high electrical and thermal conductivity, reasonable thermal expansion, and chemical and dimensional stability in the fuel gas environment. While Ni/YSZ is satisfactory for cells operating on clean, reformed fuel, advanced SOFC designs are likely to place additional constraints on the anode, such as tolerance of highly oxidizing environments and/or the capability of tolerating significant quantities of sulfur and/or hydrocarbon species in the fuel stream. Ni/YSZ anodes are not stable in oxidizing environments at high temperature. To simplify SOFC system requirements, it is desirable that the anode material be stable not only while exposed to the fuel environment during operation, but also when exposed to more oxidizing conditions (i.e., air) during system startup and shutdown.

Previous work at PNNL has resulted in the development of a promising 2-phase ceramic anode based on a mixture of doped strontium titanate and

doped ceria. Optimized compositions in this system offer excellent dimensional and chemical stability during redox cycling, appropriate coefficient of thermal expansion, and good electrocatalytic activity towards hydrogen reduction. Stable performance with fuels containing H_2S and methane has also been demonstrated.

Approach

Composite ceramic anode powders in the Sr-La-Ti-Ce-O system were prepared (both by single-step co-synthesis and by mixing separately prepared powders) by glycine/nitrate combustion synthesis. The powders were calcined and then attrition milled to reduce the average particle size to less than 0.5 μm. The resulting powders were characterized by dilatometry, x-ray diffraction, energy dispersive x-ray, scanning electron microscopy, and transmission electron microscopy. Electrode inks were prepared by mixing the powder with a commercial binder in a 3-roll mill, and then screen-printed in a circular pattern onto YSZ pellets or membranes. The screen-printed electrodes were sintered in air at 900-1000°C.

The cells were mounted between two vertical alumina tubes and isolated from the environment by sealing with gold rings when heated to 900°C in air. After that, fuel was introduced into the anode compartment to reduce the anode. The opposite side of the cell was supplied with air. Experiments were performed at atmospheric pressure in the temperature range 550-900°C. Electrochemical measurements were carried out using a Solartron 1280 frequency response analyzer in combination with a Solartron 1286 potentiostat or an Arbin BT4 potentiostat.

Results

To improve the understanding of effects of sulfur impurities on the performance of ceramic and Ni-YSZ anodes, testing was carried out on half-cells (*vs.* Pt/air) with either Ni-YSZ or $Sr_{0.65}La_{0.35}TiO_3$-$Ce_{0.7}La_{0.3}O_{1.85-\delta}$ (70/30 mole%) anodes under identical experimental conditions: T=850°C, H_2/H_2O=97/3 kPa, and a flow rate of 200 cm^3/min. H_2S concentration in the fuel varied from 0 to 1,000 ppm. The dependence of current density on overpotential was obtained, and exchange current densities were determined from Tafel plots by extrapolating measured currents from the linear high field region to obtain y-intercept values (corresponding to zero voltage) for both ceramic and Ni-YSZ anodes. The exchange current densities are plotted as a function of H_2S concentration in Figure 1. The exchange current density of the Ni-YSZ anode decreased by an order of magnitude on addition of 10 ppm of H_2S, indicating that 90% of the initially active sites were no longer active. In the case of the doped titanate/ceria composite anode, the reduction in active sites occurred more slowly with increasing H_2S concentration; a similar decrease in activity happened only in the presence of 750-1,000 ppm of H_2S. These results indicate that the interaction between S and titanate/ceria is much weaker than between S and Ni. This fact may explain the observed fast recovery of the titanate/ceria anode upon removal of H_2S from the fuel gas. On the contrary, the Ni-YSZ anode recovered very slowly, presumably due to the slow desorption of sulfur from the surface.

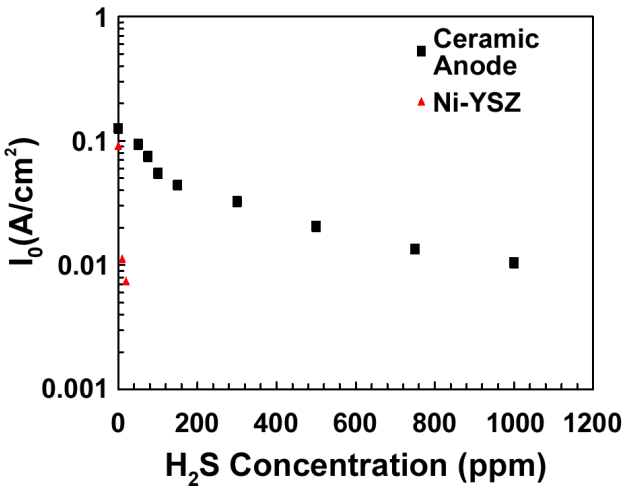

Figure 1. Exchange Current Densities Obtained from the Tafel Plots of Ceramic and Ni-YSZ Anodes as Functions of H_2S Concentration at 850°C

The sulfur coverage of the active sites was estimated, and the results were fitted using the Langmuir-type adsorption/reaction inhibition model. As shown in Figure 2, the sulfur adsorption on the titanate/ceria anode followed a single-site occupation model; that is, $\frac{\theta}{1-\theta}$ was proportional to kP. This indicates that when an H_2S molecule adsorbs on the surface, it eliminates one active site. For the Ni-YSZ

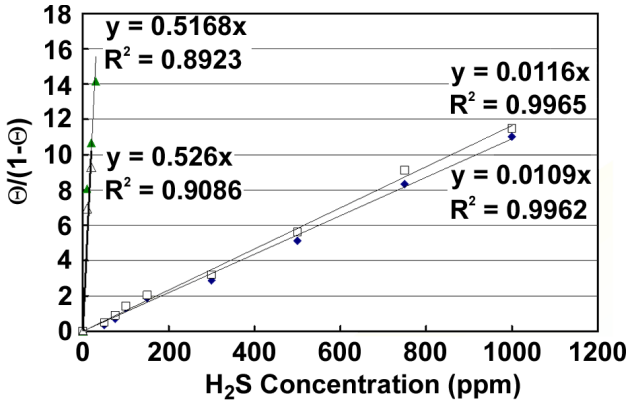

Figure 2. Langmuir Isotherm Fitting of Ni-YSZ (triangles) and Titanate/Ceria (diamonds and squares) Anode Performance as a Function of H_2S Concentration: Single-Site Adsorption Assumed

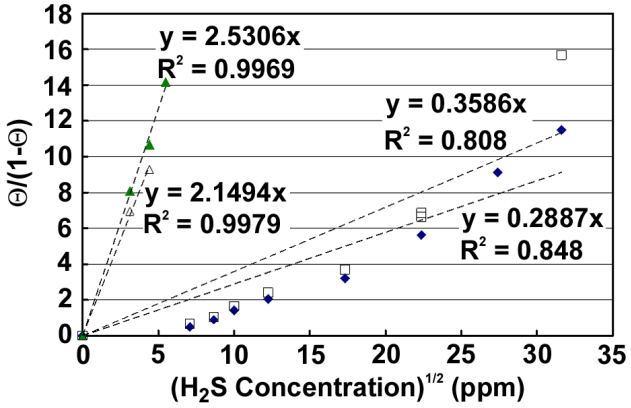

Figure 3. Langmuir Isotherm Fitting of Ni-YSZ (triangles) and Titanate/Ceria (diamonds and squares) Anode Performance as a Function of H_2S Concentration: Multiple-Site Adsorption Assumed

anode, the trend was different, and $\frac{\theta}{1-\theta}$ was more closely proportional to $\sqrt{kP}$ (see Figure 3). This indicates multiple-site occupation by the H_2S molecule, possibly due to a dissociative adsorption. However, due to the strong Ni-S interaction, the results for Ni-YSZ are less conclusive than for the ceramic anode.

Conclusions

Composite ceramic anodes show better tolerance of H_2S in the fuel stream than Ni/YSZ anodes. Single-site occupation appears to occur for H_2S adsorption on the ceramic anode, while multiple-site occupation may dominate in nickel-based anodes.

FY 2005 Presentations

1. "SECA Core Technology Program – PNNL: Cell Materials Development," J.W. Stevenson, S.P. Simner, M. Anderson, O.A. Marina, and A. Mueller, 6th Annual SECA Alliance Workshop, Pacific Grove, CA, April 17-22, 2005.
2. "Operation of Ceramic Solid Oxide Fuel Cell Anodes in Hydrocarbon Fuels," O.A. Marina, L.R. Pederson, and J.W. Stevenson, 2nd International Symposium on Solid Oxide Fuel Cell (SOFC) Materials and Technology, 29th International Conference on Advanced Ceramics and Composites (American Ceramic Society), Cocoa Beach, FL, January 23-28, 2005.
3. "Effect of Sulfur and Hydrocarbon Fuels on Titanate/Ceria SOFC Anode," O.A. Marina and J.W. Stevenson, SECA Core Technology Program Review Meeting, Tampa, FL, January 27-28, 2005.
4. "Sulfur-Tolerant Ceramic Anodes for Solid Oxide Fuel Cells," O.A. Marina, J.W. Stevenson, and L.R. Pederson, 2004 Fuel Cell Seminar, San Antonio, TX, November 1-5, 2004.

III.A.12 SOFC Cathode Materials Development at PNNL

Steve Simner (Primary Contact), Mike Anderson, Jeff Stevenson
Pacific Northwest National Laboratory
P.O. Box 999, MS K2-44
Richland, WA 99352
Phone: (509) 375-4577; Fax: (509) 375-2186; E-mail: steven.simner@pnl.gov

DOE Project Manager: Lane Wilson
Phone: (304) 285-1336; E-mail: Lane.Wilson@netl.doe.gov

Objectives

- Develop solid oxide fuel cell (SOFC) cathode materials and microstructures offering low polarization losses and long-term stability at intermediate SOFC operating temperatures (650-800ºC).
- Improve understanding of mechanisms affecting cathode performance, including both intrinsic factors (e.g., composition, microstructure) and extrinsic factors (e.g., Cr poisoning).

Approach

- Synthesize, process, and characterize candidate SOFC cathode compositions.
- Quantify performance of SOFC cathode materials on anode-supported cells.
- Evaluate effects of various interconnect alloys and Cr sources on cathode performance.

Accomplishments

- Evaluated effects of various current collectors on Sr-doped lanthanum ferrite (LSF) cathode performance.
- Obtained 2000 hours stable performance for Sr-doped lanthanum manganite (LSM)/samarium-doped ceria (SDC) composite cathode.

Future Directions

- Complete joint study (with Argonne National Lab and General Electric) on Cr poisoning of LSM cathodes.
- Investigate effects of various current collectors on cathode performance.
- Investigate degradation mechanisms of lanthanum cobalt-ferrite based cathodes.
- Optimize performance and stability of LSM-based cathodes.

Introduction

Minimization of cathodic polarization losses represents one of the greatest challenges to be overcome in obtaining high, stable power densities from SOFCs. Cathodic polarization exhibits a high activation energy relative to other internal power losses, so the need to improve cathode performance becomes increasingly important as the targeted SOFC operating temperature is reduced. The severe environmental conditions experienced by the cathode during operation limit the number of likely candidate materials. In particular, the cathode material must be stable at the SOFC operating temperature in air, and it must have high electronic conductivity, high catalytic activity for the oxygen reduction reaction, and a thermal expansion compatible with the SOFC electrolyte. Chemical interactions with the electrolyte and interconnect materials must be minimal. In addition, the cathode material must have a stable, porous microstructure so that gaseous oxygen can readily diffuse through the cathode to the cathode/electrolyte interface.

For high-temperature SOFCs operating at around 1000ºC, the preferred cathode material is A- and B-

site doped lanthanum manganite, which offers adequate electrical conductivity and electrocatalytic activity, reasonable thermal expansion, and stability in the SOFC cathode operating environment. For SOFCs operating at substantially lower temperatures, such as 650-800ºC, alternative cathode materials may be required. Alternative perovskite compositions – typically containing La on the A site and transition metals such as Co, Fe, and/or Ni on the B site – have received attention. In general, they offer higher oxygen ion diffusion rates and exhibit faster oxygen reduction kinetics at the electrode/electrolyte interface than lanthanum manganite, but are subject to degradation of performance over time.

Approach

Cathode powders were synthesized using the glycine-nitrate combustion technique. The powders were processed to obtain the desired particle size distribution, and then sintered onto anode-supported yttria-stabilized zirconia (YSZ) membranes with an SDC interlayer. After attachment of current collectors, the resulting cells were placed into test fixtures, and their current-voltage data was evaluated. After cell tests were completed, the cells were analyzed by scanning electron microscopy (SEM)/energy dispersive spectroscopy (EDS).

Results

One area of focus was the investigation of the effects of various current collector/contact materials on performance of LSF cathodes. Figure 1 compares power density data at 0.7 V/750ºC (over a 500-hour period) for several different cathode current collectors (Pt, Ag, Au and Crofer22 APU coated with a spinel protection layer) utilized in conjunction with nominally identical anode-supported cells with LSF cathodes.

LSF Cathode with Pt Current Collector

For the LSF-20 based cell utilizing a Pt cathode current collector, rapid degradation was observed [~22% increase in area-specific resistance (ASR)] over the initial 20-30 hours of operation, followed by equally rapid cell conditioning and eventual performance stability after ~200 hours. These performance characteristics are actually typical for LSF cells utilizing Pt current collectors, though

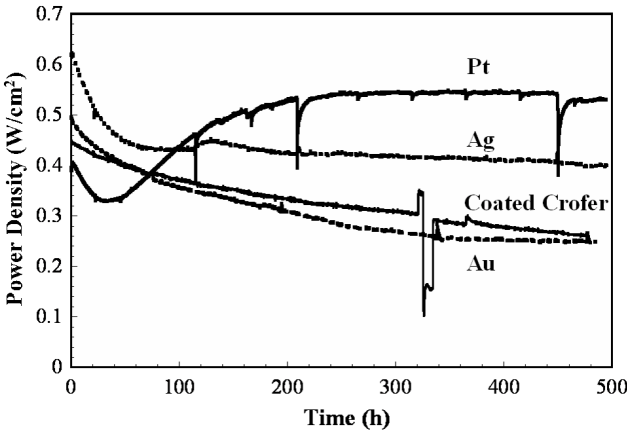

Figure 1. Long-Term Performance for LSF-Based Cells Utilizing Platinum, Silver, Gold and Spinel-Coated Crofer22 APU Cathode Current Collectors

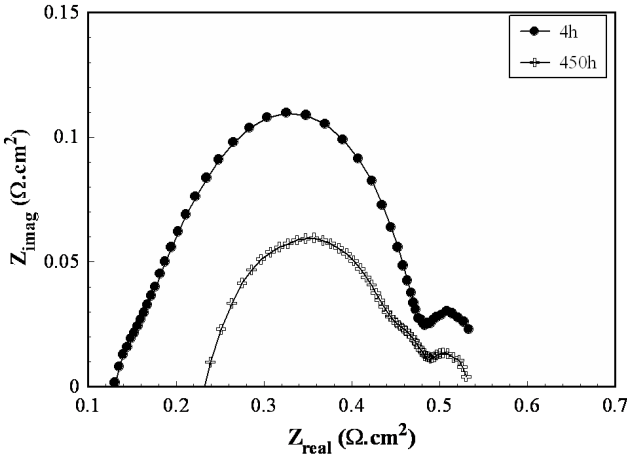

Figure 2. Impedance Data for Anode-Supported SOFC with LSF-20 Cathode and Pt Cathode Current Collector

mechanisms responsible for the initial degradation have not been established. Impedance data for this cell are shown in Figure 2. The ohmic resistance of the cell (high frequency intercept) increased in magnitude over time. SEM analysis of the tested cell revealed Pt deposition at the LSF-SDC interface; this is likely the result of $PtO_2(g)$ evaporation from the Pt surface and subsequent reduction at the LSF-SDC interface. The improvement in cathode performance over time may have been due to a catalytic effect of the deposited Pt on the oxygen reduction kinetics. The increasing ohmic resistance during the duration of the cell test may also be related to Pt volatility. Volatilization of Pt may have resulted in reduced

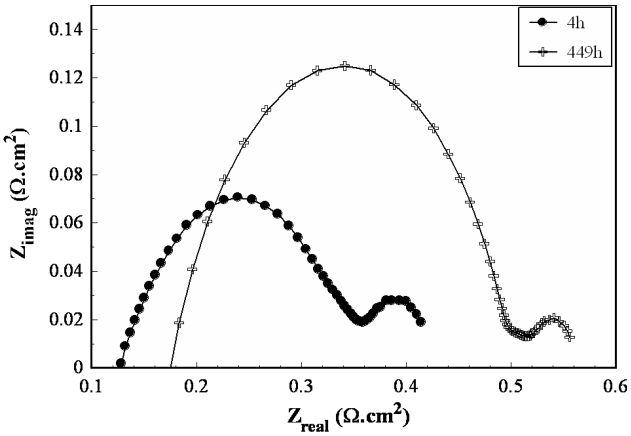

Figure 3. Impedance Data for Anode-Supported SOFC with LSF-20 Cathode and Ag Cathode Current Collector

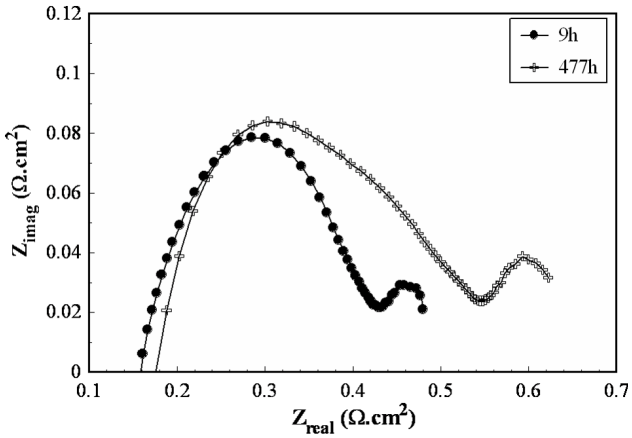

Figure 4. Impedance Data for Anode-Supported SOFC with LSF-20 Cathode and Au Cathode Current Collector

contact area between the LSF cathode and the Pt current collector, and hence increased contact resistance.

LSF Cathode with Ag Current Collector

For the cell with a Ag current collector, the initial ASR was substantially lower than that of the LSF-Pt cell; however, similar to the LSF-Pt sample, the LSF-Ag cell subsequently exhibited rapid initial degradation. Impedance data for this cell are shown in Figure 3. As for the LSF-Pt cell, the ohmic resistance increased over time. Significant Ag migration to the LSF-SDC interface was observed in the tested cell, and it would seem likely that movement of Ag from the Ag current collector to the LSF-SDC increased the contact resistance at the current collector/cathode interface.

The deposition characteristics of the LSF-Ag cell appeared to be somewhat different compared to the LSF-Pt sample in that the Ag appeared to migrate deeply into the pores in the SDC layer, while Pt deposited primarily at the active LSF-SDC interface. In fact, there were regions of the SDC interlayer that were completely infiltrated with the Ag metal.

LSF Cathode with Au Current Collector

The cell with an LSF cathode and Au current collector exhibited continuous degradation which was most rapid over the first 100 hours. Impedance data for this cell are shown in Figure 4. Unlike the LSF-Pt and LSF-Ag cells, the LSF-Au cell showed little change in ohmic resistance during the 500-hour test period. This may be related to the lack of Au volatilization from the Au-cathode interface; SEM analysis of the tested cell found no evidence of migration of Au to the cathode-electrolyte interface. The degradation of the LSF-Au cell is somewhat difficult to explain. Rigorous SEM/EDS analysis was conducted on the pre- and post-tested cells utilizing each of the noble metal current collectors, but no prominent differences were observed in either microstructure or composition to account for the continuous degradation of the LSF-Au or LSF-Crofer22 APU cells. It is possible that LSF (or the combination of an LSF cathode with an SDC interlayer on an anode-supported YSZ membrane) is subject to some form of intrinsic degradation that is suppressed when sufficient noble metal is deposited at the cathode-electrolyte interface. The fact that cell tests with a spinel-coated Crofer22 APU current collector and LSF contact paste showed similar degradation to cell tests with a Au current collector is consistent with the explanation that, in the absence of Pt or Ag, LSF is subject to an intrinsic degradation of performance.

Conclusions

Based on the results of this study, Au appears to be the most stable current collector choice for the measurement of intrinsic properties of LSF cathodes, as both Ag and Pt appear to affect the cathode performance by accumulating at the LSF-SDC interface.

FY 2005 Presentations

1. "SECA Core Technology Program – PNNL: Cell Materials Development," J.W. Stevenson, S.P. Simner, M. Anderson, O.A. Marina, and A. Mueller, 6th Annual SECA Alliance Workshop, Pacific Grove, CA, April 17-22, 2005.
2. "Cathode-Metallic Interconnect Compatibility," S.P. Simner, M. Anderson, G. Xia, Z. Yang, and J.W. Stevenson, 2nd International Symposium on Solid Oxide Fuel Cell (SOFC) Materials and Technology, 29th International Conference on Advanced Ceramics and Composites, Cocoa Beach, FL, January 23-28, 2005.
3. "Cathode Development at PNNL," S.P. Simner, M. Anderson, Z. Yang, G. Xia, and J.W. Stevenson, SECA Core Technology Program Review Meeting, Tampa, FL, January 27-28, 2005.
4. "SOFC Cathode Interaction with Volatile Chromia Sources," S. Simner, M. Anderson, J.-Y. Kim, K. Meinhardt, Vince Sprenkle, and J.W. Stevenson, 2004 Fuel Cell Seminar, San Antonio, TX, November 1-5, 2004.

FY 2005 Publications

1. S.P. Simner, M.D. Anderson, G.-G. Xia, Z. Yang, L.R. Pederson, and J.W. Stevenson, "SOFC Performance with Fe-Cr-Mn Alloy Interconnect," J. Electrochem.Soc., 152, A740 (2005).
2. S.P. Simner, M.D. Anderson, and J.W. Stevenson, "La(Sr)FeO_3 SOFC Cathodes with Marginal Copper Doping," J. Am. Ceram. Soc., 87, 1471 (2004).

III.A.13 SECA Core Technology Program Activities – PNNL

Prabhakar Singh
Pacific Northwest National Laboratory
P.O. Box 999, MS K2-44
Richland, WA 99354
Phone: (509) 375-5945; Fax: (509) 375-2186; E-mail: Prabhakar.Singh@pnl.gov

DOE Project Manager: Don Collins
Phone: (304) 285- 4156; E-mail: Donald.Collins@netl.doe.gov

Objectives

- Identify and prioritize technology development needs
- Disseminate technical information to Solid State Energy Conversion Alliance (SECA) industrial teams
- Coordinate SECA Core Technology Program (CTP) activities
- Participate in and organize technical and topical meetings and workshops
- Publish and present technical papers and reports

Approach

- Hold SECA CTP meetings to present technical findings
- Organize topical area workshops to identify and prioritize tasks
- Provide quarterly, annual and topical reports
- Meet with industrial clients on a regular basis
- Lead and organize technical society meetings

Accomplishments

- Held SECA CTP workshops
- Provided quarterly progress reports and topical reports to SECA participants
- Held workshops at Argonne National Laboratory (ANL) and Pacific Northwest National Laboratory (PNNL) on solid oxide fuel cell (SOFC) interconnection and Cr evaporation
- Developed an alloy development and corrosion mechanism evaluation plan with University of Pittsburgh, Albany Research Center and Allegheny Technology, Inc.
- Published technology update on silica transport
- Presented invited lectures at technical societies, universities and industries
- Organized American Society for Metals (ASM), American Ceramic Society (AcerSoc) meetings on SOFC technology

Future Directions

- Hold SECA CTP meetings and topical workshops
- Provide topical and CTP progress reports to SECA participants
- Develop technology roadmap in consultation with industries
- Provide technical solutions to SECA participants
- Organize technical society meetings to exchange technical information

- Publish technical findings in national and international journals
- Prioritize technology development needs in conjunction with industry teams

Introduction

The purpose of the Solid State Energy Conversion Alliance Core Technology Program (SECA-CTP) at PNNL is to focus universities, national laboratories, and other research agencies toward finding solutions to the crosscutting technical barriers in the development of low-cost, high-power-density solid oxide fuel cells (SOFCs) for a broad range of applications meeting SECA's cost and performance targets. This project will emphasize the development of materials and cost-effective fabrication techniques for the various components in the SOFC stack (electrolyte membrane, cathode, anode, interconnect, and seals). Computer modeling will be advanced and used to simulate and optimize the SOFC stack and system design and to verify the dependence of thermal, mechanical, and electrochemical properties on materials selection and geometry. The results will be disseminated/ transferred to all SECA industry teams and to appropriate CTP participants. The project will develop technology roadmaps as well as identify and prioritize technologies to be made available for use by all of the industry integration teams within SECA. A modular approach to system design will be emphasized. The ability to manufacture modular SOFC units at low cost allows the SOFC technology to penetrate a number of power generation markets, e.g., stationary distributed power units, portable military power units, and auxiliary power units for vehicles. High efficiency coupled with multi-fuel capability makes the system ideal for hydrocarbon- and coal-based fuel utilization with the potential for CO_2 sequestration.

The management of SECA's Core Technology Program will continue to involve interactions with universities, national laboratories and industrial team members on a frequent basis to disseminate technical information gained through workshops and meetings. The management activity will involve holding workshops and topical area meetings with Industry Integration Team (Core Technology Program and government sponsored) representatives. These workshops will ensure that research is adequately progressing and is addressing the current R&D as well as technology needs of the industry teams. The topical workshops will also be a forum to identify and prioritize other technical issues (that had not been addressed) and to promote technology transfer. Technical roadmaps will be updated and used to focus research activities. Additionally, PNNL and the National Energy Technology Laboratory (NETL) will provide oversight and the necessary review of projects that are part of the CTP. These activities will require travel and coordination with the Core Technology Program participants. PNNL will work with the NETL Project Management Team and provide recommendations from the CTP participants about technology issues/gaps that should be addressed.

The national Core Technology Program management will facilitate the exchange and dissemination of technical information, generated by the SECA-CTP participants, in a timely manner to all SECA industrial team members. The information exchange and dissemination will be achieved through meetings, workshops, written topical reports, and documents. During FY 2005 and beyond, the program management takes the added responsibility of providing technical discussions and progress reports to industrial teams on a pre-scheduled basis to expedite the development of SOFC power generation systems that meet the goals and objectives of the SECA initiative. The Core Technology Program will also interact with other government agencies to gather and disseminate technical information related to SOFCs. Program management will work with the thrust area leaders and CTP participants to define tasks, technical milestones, schedules, and deliverables. Both short-term and long-term progress and accomplishments will be reviewed internally. Technical experts in the areas of interest will be consulted from time to time to provide technical support and guidance.

Approach

To meet the overall cost and performance targets of the Solid State Energy Conversion Alliance, the

SOFC component development

- Cell anode and cathode
  - Intermediate temperature cathode materials
  - Sulfur, carbon, redox tolerant anode materials
- Alloy Interconnects
  - Bulk alloy evaluation and protective surface modifications
- Seals
  - Mica-based compressive seals, brazes, compliant seals

SOFC modeling

- Modeling of cells and stacks – transient and steady state
- System modeling

SOFC fuel processing

- On anode reformation and carbon formation prevention

Experimental support of modeling

- Model verification experiments, materials properties measurements

Program Management, coordination and integration

Figure 1. SECA CTP Activities at PNNL

SECA CTP will focus on coordinating technology development activities at universities, national laboratories and industries. Technical findings will be disseminated through topical reports. Technology gaps will be identified, and workshops will be held to develop roadmaps. Approaches for FY 2005 include the following:

- Hold frequent meetings with industrial teams to discuss technical progress. Provide a written report to each team member summarizing the status.
- Provide quarterly progress reports describing the technical status and issues, if any.
- Provide topical/annual reports after completion of the task.
- Hold workshops to present the technology status. Also, use the workshop as the forum to develop consensus and prioritization of technical activities.

- Utilize technical expertise of attendees to address interconnect challenges
- Achieve consensus regarding the technical status, issues and on going activities
- Identify and prioritize potential approaches for solving remaining challenges
- Develop a technology "Road Map" for future R&D activities

Figure 2. Workshop Objectives and Goals

- Organize and participate in the Annual SECA Program Review Meeting.
- Participate in national/international meetings to present status/findings.
- Coordinate with technical societies.
- Coordinate with NETL on all aspects of the SECA CTP.
- Responsibilities related to SOFC modeling include university interactions, training and workshops including the development of a master modeling plan and organizing and providing a training course for all SECA industry teams.

In FY 2005, a workshop on SOFC interconnects and Cr transport was held to review the technology status and disseminate the technical findings to SECA industry teams. A technology roadmap was developed. A training session was conducted to present the recent advances in the modeling software to SECA members. In FY 2006 and beyond, this exercise will be repeated and new findings presented. Ways to expedite early validation of on-going cell component materials development work will be examined in consultation with the CTP coordination team. Figures 1 and 2 show PNNL technical activities and workshop objectives.

Results

SECA CTP workshops were held in Tampa, Florida, and Pacific Grove, California, to review technical progress made in core thrust areas related to materials, modeling, fuel processing, power electronics and manufacturing. Two additional topical workshops were held at ANL and PNNL to understand and develop roadmaps for SOFC current

collectors/gas separators and Cr evaporation in oxidant gas atmosphere. Input from industry teams and materials manufacturers was extensively utilized for the development of advanced concepts. A review of high-temperature silica transport in SOFC environment was presented at the American Ceramic Society. Several invited lectures were given at technical society (ASM, AcerSoc, TMS, AVS, ECS, etc.) meetings. SOFC technology and technology status were also presented at universities (University of Connecticut, University of Pittsburgh, Georgia Institute of Technology, etc.) to help familiarize and train students and teaching staff. Technical society meetings were organized to bring forward experts working in the field and disseminate information to industrial participants and academia with the on-going research activities.

Conclusions

The SECA Core Technology Program at PNNL emphasizes the development of advanced component materials, modeling and design tools, and fuel processing techniques as well as coordinates technology development activities at universities, national laboratories and industries. Core Technology facilitates the exchange and dissemination of technical information, generated by the SECA-CTP participants, in a timely manner to all SECA industrial team members. The information exchange and dissemination is achieved through meetings, workshops, written topical reports, and documents.

FY 2005 Publications/Presentations

1. P. Singh and L. Pederson. "Coatings and Deposition Processes for Solid Oxide Fuel Cells: A Review" *International Conference on Metallurgical Coatings and Thin Films, American Vacuum Society, 2005.*
2. P. Singh. "Corrosion Processes in Bi-Polar Dual Atmosphere Conditions" *Gordon Research Conference, Colby Sawyer College, NH, 2005.*
3. P. Singh. "SOFC Power Generation Systems: Technology Status and R&D Needs" *Connecticut Global Fuel Cell Center, University of Connecticut.*

References

1. P. Singh et al. "Vapor phase silica transport during SOFC operation at 1000C", *29th International Conference on Advanced Ceramics and Composites, American Ceramic Society, January 2005*

III.A.14 SOFC Interconnect Materials Development at PNNL

Zhenguo "Gary" Yang (Primary Contact), Guanguang Xia, Prabhakar Singh, and Jeff Stevenson
Pacific Northwest National Laboratory
P.O. Box 999, MS K2-44
Richland, WA 99352
Phone: (509) 375-3756; Fax: (509) 375-2186; E-mail: zgary.yang@pnl.gov

DOE Project Manager: Lane Wilson
Phone: (304) 285-1336; E-mail: Lane.Wilson@netl.doe.gov

Objectives

- Develop cost-effective, optimized materials for intermediate-temperature solid oxide fuel cell (SOFC) interconnect and interconnect/electrode interface applications.
- Identify and understand degradation processes in interconnects and interconnect/electrode interfaces.

Approach

- Perform comprehensive properties evaluation of conventional and experimental alloys (oxidation, corrosion, electrical and mechanical).
- Investigate the degradation mechanism of alloy interconnect materials and their interfaces under SOFC operating conditions.
- Develop improved interconnect materials (via surface or bulk modification) and cathode/interconnect contact materials.

Accomplishments

- Completed evaluation of properties of Ni-based alloys with increased Mn content.
- Evaluated long-term performance of Mn-Co spinel protection layers.

Future Directions

- Evaluate dual atmosphere oxidation of alloys in air/simulated reformate environments.
- Continue development of optimized protective oxide layers to minimize electrical resistance and Cr volatility at surfaces of alloy-based interconnects.
- Develop electrical contacts at electrode/interconnect interfaces.

Introduction

With the reduction in SOFC operating temperatures, low-cost high-temperature oxidation alloys have become promising candidates to replace lanthanum chromite, a ceramic that can withstand operating temperatures in the 1000°C range. To improve the understanding of the advantages and limitations of alloy interconnects, Pacific Northwest National Laboratory (PNNL) has been engaged in systematic evaluation and development of candidate materials. Challenges to be overcome include chromia scale evaporation, scale electrical resistivity, oxidation/corrosion under interconnect dual exposure conditions, and scale adherence and compatibility with adjacent components, such as seals, electrodes and/or electrical contact materials.

Approach

Oxidation behavior of candidate alloys is being investigated under dual atmosphere conditions typical of SOFC interconnect operation conditions. Studies are being performed in air/hydrogen and air/

simulated reformate environments. Modifications to candidate alloys, including increased Mn content in Ni-based alloys, are being investigated. Spinel protection layers for SOFC interconnects are under development; spinel layer compositions, microstructures, and fabrication techniques are being optimized.

Results

Due to space limitations, only work related to spinel protection layers is discussed. Protection layers are intended to serve several functions. First, they protect metallic interconnects from further environmental attack and improve the metallic interconnect surface stability. Second, they serve as a barrier to Cr migration from the chromia-forming alloy interconnect. Third, protection layers help minimize the interfacial contact resistance. $(Mn,Co)_3O_4$ spinels were thermally grown as protection layers on ferritic stainless steels including Crofer22 APU and AISI430 via a slurry coating approach. Systematic evaluations indicated that the spinel protection layers not only significantly decreased the contact resistance between a perovskite cathode material and the stainless steel interconnect material, but also inhibited the sub-scale growth on the stainless steel.

To examine its long-term performance and thermomechanical stability, Crofer22 APU with the thermally grown spinel protection layer was evaluated via a long-term thermal cycling test that lasted for a period of six months and included a total of 125 thermal cycles (plus three occurrences of unscheduled power failure). During the test (see Figure 1), the contact area-specific resistance (ASR) between the Sr-doped lanthanum ferrite (LSF) cathode and the metallic interconnect at 800ºC decreased from the starting value of 15.0 mOhm.cm^2 to 14.3 mOhm.cm^2, demonstrating excellent stability. Scanning electron microscopy (SEM) analysis on the cross-section of the tested sample at the edge areas, where there was no contact paste applied, as shown in 2(a), indicated good thermomechanical stability of the thermally-grown protection layers. No spallation or chipping was observed, and the sub-scale only grew to a thickness of 2.5~3.0 μm. In contrast, as shown in Figure 2(b), spallation or chipping was observed on the Crofer22 APU without

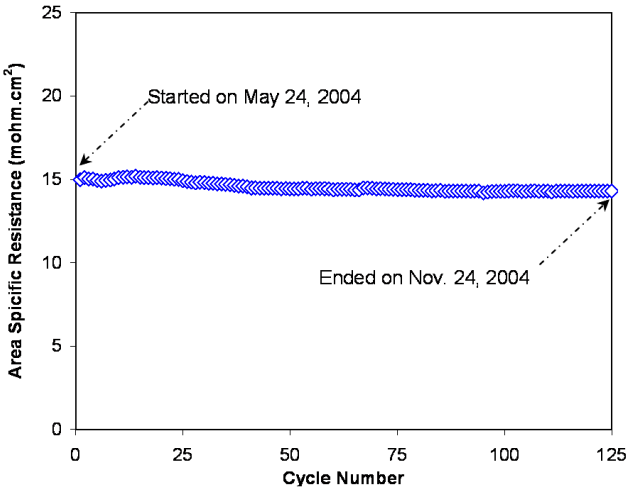

Figure 1. Contact ASR of $La_{0.8}Sr_{0.2}FeO_3$||$La_{0.8}Sr_{0.2}Co_{0.5}Mn_{0.5}O_3$||Crofer 22 APU (with spinel protection layer) as a Function of Thermal Cycles

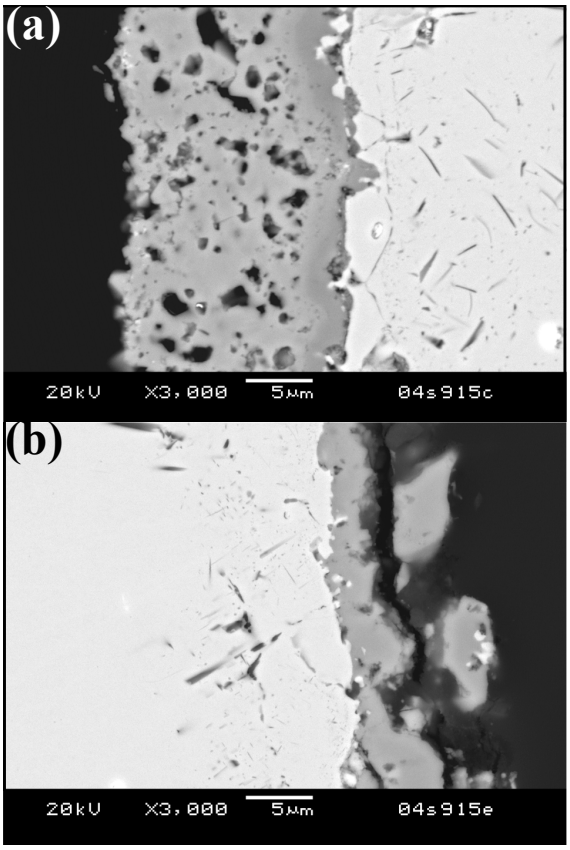

Figure 2. SEM Images of the Cross-Section of Crofer22 APU after Testing for 6 Months, Including over 125 Thermal Cycles: (a) at the side with a thermally grown $Mn_{1.5}Co_{1.5}O_4$ spinel protection layer, and (b) at the side without protection

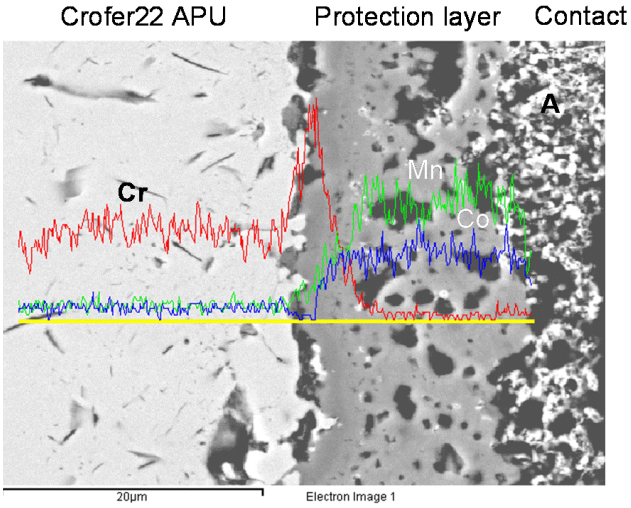

Figure 3. Microstructural and Compositional Analyses on the Spinel Protection Layer Subjected to a Contact ASR Measurement for a Period of Six Months, Including Thermal Cycling

the protection layer, and the scale grew to a thickness of over 10 µm, which is consistent with previous work. The spalled fragments were identified by energy dispersive spectroscopy (EDS) point analysis to be primarily $(Mn,Cr)_3O_4$ spinel. Thus, the spinel protection layer on Crofer22 APU not only drastically reduced the interfacial ASR, but also inhibited the scale growth on the ferritic stainless steel by limiting oxygen ion diffusion inward through the spinel layer. The excellent thermomechanical stability and stable electrical performance were attributed to reduced sub-scale growth, an improved strain tolerance of the porous (closed porosity) microstructure, and a good thermal expansion match between the spinel and the metal substrate.

Also, the spinel protection layer acted as an effective mass transport barrier in stopping chromium migration from the metal. EDS analysis (see Figure 3) revealed a sharp Cr profile across the interface between the sub-scale and the spinel protection layer, with no chromium detectable in the spinel protection layer and at its surface after the six-month thermal cycling test. No Cr was found in the Sr- and Co-doped lanthanum manganite (LSCM) contact material or the LSF cathode material. For example, the EDS analysis of the contact layer at point "A" in Figure 3 gave 17.7% Mn, 6.0% Co, 17.0% La, 7.0% Sr, 52% O, and no Cr.

Conclusions

Thermally grown spinel protection layers significantly decreased cathode/interconnect contact resistance and also inhibited the sub-scale growth on the stainless steel. The layers exhibited excellent structural and thermomechanical stability, as verified by a long-term thermal cycling test. Finally, the spinel protection layers can act effectively as a barrier to outward diffusion of chromium cations, preventing subsequent chromium migration into the cathode and contact materials.

FY 2005 Presentations

1. "Advanced Interconnect Development," Z.G. Yang, G. Maupin, S. Simner, P. Singh, J. Stevenson, and G. Xia, 6th Annual SECA Alliance Workshop, Pacific Grove, CA, April 17-22, 2005.
2. "Anomalous Oxidation of Ferritic Stainless Steels in Air/Hydrogen Fuel Dual Environment," Z.G. Yang, D.M. Paxton, P. Singh, J.W. Stevenson, M.S. Walker, and G. Xia, 2005 TMS Annual Meeting, San Francisco, CA, February 13-17, 2005.
3. "Development of Spinel Protection Layers on Metallic SOFC Interconnects," Z.G. Yang, G. Xia, and J.W. Stevenson, 2nd International Symposium on Solid Oxide Fuel Cell (SOFC) Materials and Technology, 29th International Conference on Advanced Ceramics and Composites (American Ceramic Society), Cocoa Beach, FL, January 23-28, 2005.
4. "Study of Interactions and Contact Resistance at Cathode/Interconnect Interfaces in SOFCs," Z.G. Yang, G. Xia, S.P. Simner, and J.W. Stevenson, 2nd International Symposium on Solid Oxide Fuel Cell (SOFC) Materials and Technology, 29th International Conference on Advanced Ceramics and Composites (American Ceramic Society), Cocoa Beach, FL, January 23-28, 2005.
5. "Advanced Interconnect Development," Z.G. Yang, G.D. Maupin, S.P. Simner, P. Singh, J.W. Stevenson, and G. Xia, SECA Core Technology Program Review Meeting, Tampa, FL, January 27-28, 2005.
6. "Investigation of High Temperature Oxidation Resistant Alloy Interconnect Materials for Use in Planar SOFC Stacks," Z.G. Yang, G. Xia, P. Singh, and J.W. Stevenson, 2004 Fuel Cell Seminar, San Antonio, TX, November 1-5, 2004.
7. "Evaluation of Ni-Based Alloys for Potential SOFC Interconnect Applications," Z.G. Yang, G. Xia, P. Singh, and J.W. Stevenson, ASM Materials Solutions Conference, Columbus, OH, October 18-20, 2004.

9. "Corrosion of Ferritic Stainless Steels during High Temperature Simultaneous Exposures to Moist Air and Reforming Gases," Z.G. Yang, G. Xia, P. Singh, and J.W. Stevenson, ASM Materials Solutions Conference, Columbus, OH, October 18-20, 2004.
10. "Investigation of Interfacial Interactions and Electrical Resistance between Conductive Oxide Cathodes and Alloy Interconnects in SOFCs," G. Xia, Z.G. Yang, S. Simner, and J.W. Stevenson, ASM Materials Solutions Conference, Columbus, OH, October 18-20, 2004.

FY 2005 Publications

1. Z.G. Yang, G.G. Xia, P. Singh, and J.W. Stevenson, "Electrical Contacts between Cathodes and Metallic Interconnects in Solid Oxide Fuel Cells," J. Power Sources, in press (2005).
2. Z.G. Yang, G.G. Xia, P. Singh, and J.W. Stevenson, "Effects of Water Vapor on Oxidation Behavior of Ferritic Stainless Steels under Solid Oxide Fuel Cell Interconnect Exposure Conditions," Solid State Ionics, in press (2005).
3. Z.G. Yang, G.G. Xia, and J.W. Stevenson, "$Mn_{1.5}Co_{1.5}O_4$ Spinel Protection Layers on Ferritic Stainless Steels for SOFC Interconnect Applications," Electrochemical and Solid-State Letters, 8, A168 (2005).
4. Z.G. Yang, J.S. Hardy, M.S. Walker, G.G. Xia, S.P. Simner, and J.W. Stevenson, "Structure and Conductivity of Thermally Grown Scales on Ferritic Fe-Cr-Mn Steel for SOFC Interconnect Applications," J. Electrochem. Soc., 151, A1825 (2004).
5. Z.G. Yang, M.S. Walker, P. Singh, J.W. Stevenson, and T. Norby, "Oxidation Behavior of Ferritic Stainless Steels under SOFC Operating Conditions," J. Electrochem. Soc., 151, B669 (2004).
6. Z.G. Yang, G.G. Xia, K.D. Meinhardt, K.S. Weil, and J.W. Stevenson, "Glass Sealing in Planar SOFC Stacks and Chemical Stability of Seal Interfaces," in Surfaces, Interfaces, and the Science of Ceramic Joining (Ceramic Transactions Volume 158), edited by K. S. Weil, I. E. Reimanis, and C. A. Lewinsohn, p. 135, American Ceramic Society, Westerville, OH (2004).

III.A.15 Reliable Seals for Solid Oxide Fuel Cells

Ronald E. Loehman (Primary Contact), Mathieu Brochu, Bryan Gauntt, Melissa Malone
Sandia National Laboratories, MS 1349
Albuquerque, NM 87185-1349
Phone: (505) 272-7601; Fax: (505) 272-7304; E-mail: loehman@sandia.gov

DOE Project Manager: Travis Shultz
Phone: (304) 285-1370; E-mail: Travis.Shultz@netl.doe.gov

Objectives

- Develop reliable, cost-effective sealing techniques for solid oxide fuel cells (SOFCs).
- Determine performance-limiting features of sealing methods.
- Optimize seal properties.
- Determine seal degradation mechanisms and predict useful seal lifetimes.

Approach

- We are making glass matrix composite seals with a wide range of chemical and mechanical properties.
- The composite approach allows glass and filler properties to be optimized independently.
- Seal thermal and mechanical strains are reduced by selecting glass compositions with glass transition temperatures (T_gs) below the SOFC operating temperature.
- Viscosity, coefficient of thermal expansion (CTE), and other seal characteristics can be tailored by adding unreactive powder.
- The volume fraction of the glass phase can be reduced to a minimum for the seal, which reduces reactivity with fuel cell materials.

Accomplishments

- We modified our glass compositions to provide better control over flow and thermal expansion properties.
- Glass sealants exhibit little or no reactivity with SOFC anode materials at 750-800°C. Glass seal compositions show little or no reactivity with stainless steel interconnect materials at 750°C.
- Preoxidizing interconnect materials enhances glass wetting and adhesion required for sealing.

Future Directions

- Develop screening test for adhesion of different seal compositions and processes.
- Conduct further tests of effects of environmental exposure on seal properties.
- Refine reaction studies of sealants with SOFC components.
- Perform more fundamental mechanical tests on composite seal materials at operating temperatures; e.g., flexural strength and fracture toughness.
- Investigate shaping and forming methods for composite seals such as tape casting and screen printing

---

Introduction

Developing reliable methods for sealing solid oxide fuel cell stacks presents the most challenging set of performance criteria in the entire field of ceramic joining. For SOFC applications, the requirements on the sealing method include:

- adhesion of the sealing material to fuel cell components from room temperature to as high as 1000°C

- ability to provide a leak-tight seal at the SOFC operating temperature
- ability to maintain a seal while accommodating strains from SOFC components with different coefficients of thermal expansion (CTEs)
- lack of adverse reaction between the sealing material(s) and the fuel cell components
- chemical and physical stability of the sealant at temperatures up to 1000°C in oxidizing and reducing atmospheres
- thermal shock tolerance
- electrically insulating for some SOFC designs

All of the above properties must be maintained for SOFC operating lifetimes of up to 40,000 hours. The list is written in approximate order of decreasing stringency. That is, no matter what the SOFC design, the seal must be adherent and leak-tight. On the other hand, some stack designs may require joining only similar materials and, thus, a matched CTE seal may be sufficient. Note also that the requirements may be contradictory. For example, being leak-tight and adherent at high temperatures suggests a refractory, stiff sealant, which may work against the requirement for thermal strain accommodation. Such situations are common, and seal developers know that seal design is specific to a particular component geometry and usually requires compromises among competing requirements.

Approach

Under DOE sponsorship, this project is developing an approach to sealing SOFCs that can be tailored to the specific requirements of the vertical teams in the DOE/SECA (Solid State Energy Conversion Alliance) program. The technique combines extensive capabilities in ceramic joining and composites that have been developed at Sandia over the past 20 years. In our judgment, relief of thermal expansion mismatch stresses will require SOFC seals to incorporate either a ductile metal or a high-viscosity glass that can relieve stresses through viscous creep. Other design and operational constraints on SOFCs, which as discussed above frequently are in opposition, severely restrict the options for seal materials. Based on our prior experience in ceramic joining and on results obtained so far on this project, we believe we have greatest design flexibility using ceramic-filled glasses and metal-filled glass composites. We have demonstrated that we can control properties such as glass transition temperature and thermal expansion coefficient by varying the compositions, amounts, and microstructures of the different phases. The choices are guided by thermochemical and composite microstructural models that allow us to target specific seal properties for a given design. Several seal systems are showing promise in functional tests.

Results

We have shown that our SOFC sealing technique can be tailored to fit a wide range of SOFC specifications. The essence of the method is to engineer ceramic-filled glass composites, metal-filled glass composites, and/or ceramic-filled metal composites that can meet SOFC requirements. This approach combines extensive capabilities in composites and ceramic joining that have been developed by Sandia National Laboratory staff over the past 15 - 20 years.

The composite seals require a glass matrix that is slightly fluid at the SOFC operating temperature to reduce thermal strains. In technical terms, this requires a glass transition temperature that is below the cell operating temperature. Our compositional modifications vary the glass T_gs and expansion coefficients and thus give us a wider choice of matrix materials for our composite seals. The flow properties are reflected as differences in the rate of spreading of a molten glass drop on the substrate of interest. For example, a more fluid glass at a given temperature will spread faster and assume a lower contact angle than one that is less fluid. In a recent series of tests at 750°C, ten glass compositions exhibited a range in contact angles after 5 minutes on 410 stainless steel (a typical SOFC alloy) from 80° (low flow, poorer wetting) to 20° (faster flow, good wetting). No one glass is necessarily better than another for all use conditions. Rather, the results demonstrate that our glasses span a wide range of physical properties, which allows us a lot of options in engineering optimized SOFC seals (Figure 1).

Constructing SOFC stacks may require seals to Ni – YSZ (yttria-stabilized zirconia) anodes. Thus, we tested different glasses for reactivity using a

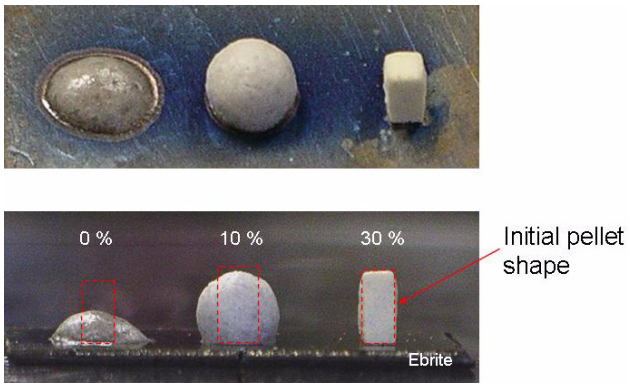

Figure 1. Top and side views of sealants heated on Ebrite stainless steel for 10 min at 850°C. Sealants are Glass 14a with indicated volume fraction of YSZ powder. The seal wetting and flow properties are controlled by the glass-powder ratio.

sessile drop test geometry in which small glass specimens were heated on anode material for different times at fixed temperature. During heating, we monitored the change in glass contact angle with time. After cooling, we sectioned the interface and analyzed it for evidence of reaction using electron microscopy and energy dispersive spectroscopy (EDS). The results typically show well-bonded interfaces with no evidence of Ni dissolution (the expected reaction mechanism) in the glass within the resolution of the measurement. In other experiments, we mixed up to 30 vol% Ni powder into different glasses and heated the specimens for up to 50 hours at 800°C as an extreme test of glass-Ni reactivity. Our most stable glasses showed no change in coefficient of thermal expansion after heating and no microscopic evidence for Ni dissolution.

Reactivity of glasses with interconnect materials was evaluated using the sessile drop method described above. Microscopic examination of interfaces showed no evidence of Cr dissolution (the most reactive constituent of stainless steel) or reaction products with the glass within the resolution of the technique. As an extreme test, we heated mixtures of glass and pure Cr powder at 750°C for increasing times. Similar to the case with stainless steels, no reaction products were observed at the interface, as shown in Figure 2. Since increasing temperature accelerates chemical reactions, we heated glass–Cr mixtures at 850°C. The results, as

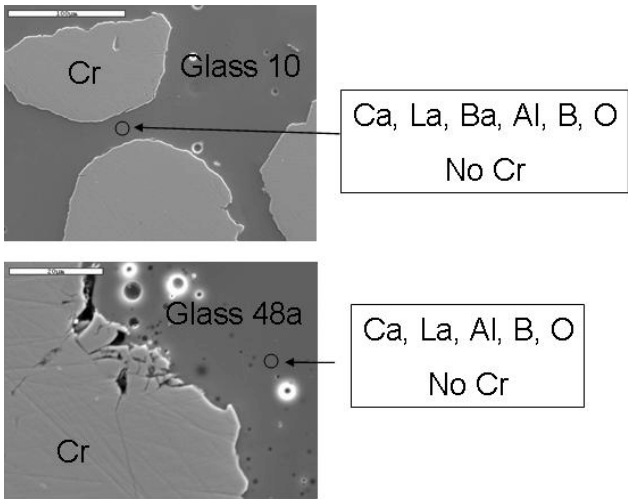

Figure 2. Glass-Cr Powder Composites Heated for 3 hr at 750°C Show No Evidence of Cr Dissolution in the Glass

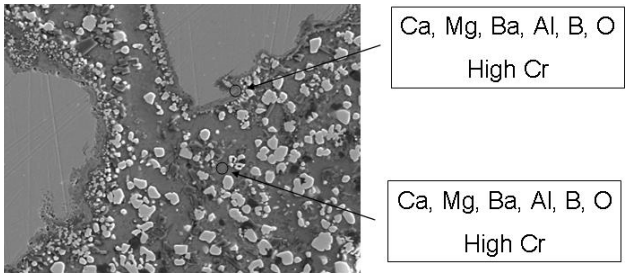

Figure 3. Glass-Cr Composites Heated at 850°C Show Cr_2O_3 Layer on Cr Particles and Cr Dissolution in the Glass

presented in Figure 3, showed that under those more extreme conditions, Cr reacts and dissolves in the glass. More work will be required to extrapolate the results for pure Cr and 850°C testing to realistic SOFC operating conditions and materials.

Preoxidizing 304 stainless steel housings used for electrical connectors has been shown to promote wetting and bonding with glass insulators. We extended those results by demonstrating that preoxidizing E-brite and 410 stainless steels is similarly beneficial for SOFC sealing (Figure 4). Heating the alloy at 1000°C for 5-30 minutes in Ar/1000 ppm O_2 produces a surface oxide layer 1-3 mm thick that is primarily Cr_2O_3 with a little SiO_2. Glass melted on the preoxidized alloy wets and adheres to the alloy in as little as 2 minutes, whereas reaching a steady-state contact angle on the bare

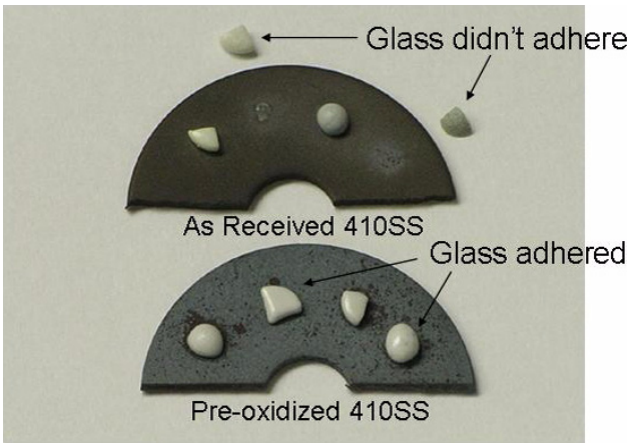

Figure 4. Glass Sealed at 850°C in Air Adhered Better to Preoxidized 410 Stainless Steel Than to the As-Received Form

alloy requires heating for 5 minutes or more. Minimizing time at the sealing temperature reduces the extent of undesirable interface reactions, so preoxidation of the interconnect may offer significant benefits in manufacturing SOFC stacks.

Conclusions

- Glass seal compositions provide excellent control over flow and thermal expansion properties.
- Seal compositions are stable in contact with anodes at 750-800°C and with stainless steel interconnect materials at 750°C.
- Preoxidizing interconnect materials offers advantages in SOFC seal processing.

FY 2005 Publications/Presentations

1. R.E. Loehman, et al., "Development of glass-ceramic composites for sealing solid oxide fuel cells", keynote talk, 29th Cocoa Beach conference, January 26, 2005
2. M. Brochu, B.D. Gauntt, D. Zschiesche, R. Shah and R.E. Loehman, "Development of glass/nano-ceramic composites for sealing solid oxide fuel cells", Ceramic Engineering and Science Proceedings, 2005
3. R.E. Loehman, "Materials challenges in the development of solid oxide fuel cells", invited seminar, Rice University, November 2004

III.A.16 Developing Fe-Based Alloys for Intermediate-Temperature SOFC Interconnect Application

J.H. Zhu
Department of Mechanical Engineering
Tennessee Technological University
115 W. 10th St., Box 5014
Cookeville, TN 38505
Phone: (931) 372-3186; Fax: (931) 372-6340; E-mail: jzhu@tntech.edu

DOE Project Manager: Lane Wilson
Phone: (304) 285-1336; E-mail: Lane.Wilson@netl.doe.gov

Subcontractors:
Oak Ridge National Laboratory, Oak Ridge, TN
University of Missouri, Rolla, MO

Objectives

- Develop new Fe-Ni based alloys without Cr or with low Cr for intermediate-temperature solid oxide fuel cell (SOFC) interconnect application.
- Demonstrate suitable oxidation resistance, oxide scale area-specific resistance (ASR), and coefficient of thermal expansion (CTE) for these new alloys.
- Determine the effect of stoichiometry and doping addition on the electrical conductivity of the $(Ni,Fe)_3O_4$ spinel.

Approach

- Utilize physical metallurgy principles to identify the potential alloying elements for the new Fe-Ni alloys.
- Use thermal oxidation to form a dual-layer oxide structure with an outer layer of Cr-free $(Ni,Fe)_3O_4$ spinel and an inner layer of protective oxide on the alloy substrates.
- Increase the electrical conductivity of $(Ni,Fe)_3O_4$ via doping with other elements.
- Characterize the CTE, oxidation resistance, and oxide scale ASR of the new Fe-Ni alloys as well as their compatibility with cathode materials.

Accomplishments

- The composition of the spinel phase formed on a Fe-Ni alloy coupon exposed in air at 800°C for 500 h was found to be close to $Ni_{0.9}Fe_{2.1}O_4$. This spinel possessed very high electrical conductivity; as a result, the ASR of the oxide scale formed on a number of $(Fe,Ni)_3O_4$-forming Fe-Ni alloys after oxidation for 500 h in air at 800°C was relatively low and comparable to that of Ebrite, Crofer, and Haynes 230 after similar exposure.
- Several $NiFe_2O_4$-based spinel pellets were synthesized, and it was found by X-ray diffraction (XRD) that all the pellets with $x \geq 0.2$ in $Ni_{1-x}Fe_{2+x}O_4$ showed the presence of some second phase, in addition to the primary spinel phase. For $x < 0.2$, the electrical conductivity of the spinel phase increased as x in $Ni_{1-x}Fe_{2+x}O_4$ increased. Reactive element doping (e.g., Y and La) was found to increase the electrical conductivity of the $(Fe,Ni)_3O_4$ spinel.
- Thermogravimetric analysis of the Fe-Ni alloys with different Ni contents indicated that the oxidation rate of these alloys decreased as the Ni content in the alloys increased, while all the Fe-Ni alloys with 40-60%

Ni exhibited thermal expansion behavior compatible with other cell components. The Fe-Ni alloys with about 60% Ni deserve special attention in light of oxidation resistance considerations.

- Over 100 alloys were made by arc melting and drop casting, with various alloying additions employed in order to narrow down some promising compositional ranges for further alloy development. Several strategies have been identified to improve the oxidation resistance of the Fe-Ni alloys.

Future Directions

- *Systematic evaluation of the Fe-(45-60)Ni alloys with various alloying additions*
  A series of alloys based on Fe-(45-60)Ni with additions of transition metals, reactive elements, etc. will be thermo-mechanically processed and then evaluated with regard to CTE, oxidation resistance and oxide scale ASR. The compatibility of the new alloys with the SOFC cathode will also be experimentally evaluated.
- *Identification and demonstration of best protective inner-layer oxide*
  The best protective inner-layer oxide (NiO, Cr_2O_3, or mixed oxides) will be identified. Thermal oxidation will be utilized to facilitate its formation. Particularly, cyclic oxidation tests (25 cycles with 20-hour holding time per cycle, with a total of 500 hours exposure time) at 800°C will be conducted to assess the oxide scale spallation resistance during thermal cycling.
- *Optimization of the composition range of the new Fe-Ni base alloys*
  The composition range of the new Fe-Ni base alloys with superior properties for interconnect applications will be optimized, and the performance of these alloys will be compared to Crofer, Ebrite, H230, and other interconnect alloys reported in the literature.

Introduction

Currently, almost all of the metallic interconnect candidates for SOFCs are Cr_2O_3-forming alloys because Cr_2O_3 not only has good oxidation resistance, but also possesses adequate electrical conductivity. However, the volatile Cr species from Cr_2O_3 evaporation (especially in the presence of water vapor) may migrate to and poison the cathode, leading to decreased electrochemical activity of the cathode and degradation in SOFC system performance over long-term operation. This Solid State Energy Conversion Alliance (SECA) project has focused on the design and characterization of new Fe-Ni alloys with low Cr or without Cr for SOFC interconnect application, which is expected to completely resolve the Cr poisoning issue for SOFC stacks.

Approach

To resolve the Cr poisoning issue resulting from the interconnect alloys in a SOFC stack, two approaches can be pursued: (1) surface coating and (2) new alloy development. Surface coatings with less Cr volatility might reduce the severity of the Cr evaporation problem, but it would be difficult to completely mitigate this issue by surface coatings alone. Our work has focused on alloy design of new Cr-free or low-Cr Fe-Ni alloys using physical metallurgy principles. The Fe-Ni alloys with about 40-60 wt.% Ni are expected to have suitable CTE match with other cell components. These alloys are expected to form a double-layer surface oxide structure with a Cr-free, electrically conductive $(Fe,Ni)_3O_4$ spinel outer layer to provide a surface seal for the alloys and an oxidation-resistant, electrically conductive oxide inner layer to provide adequate oxidation resistance. This project is being carried out as an interdisciplinary and collaborative endeavor with the involvement of two universities and one national laboratory.

So far, we have demonstrated the feasibility to form the double-layer oxide structure via thermal oxidation for the Fe-Ni alloys, the suitability of the electrical conductivity of the $(Fe,Ni)_3O_4$ spinel, and the promises offered by the Fe-Ni alloy system.

Results

The initial oxidation behavior of a Fe-50Ni-0.05Y alloy and several Fe-Ni alloys with different Ni content was studied using a thermo-balance. The

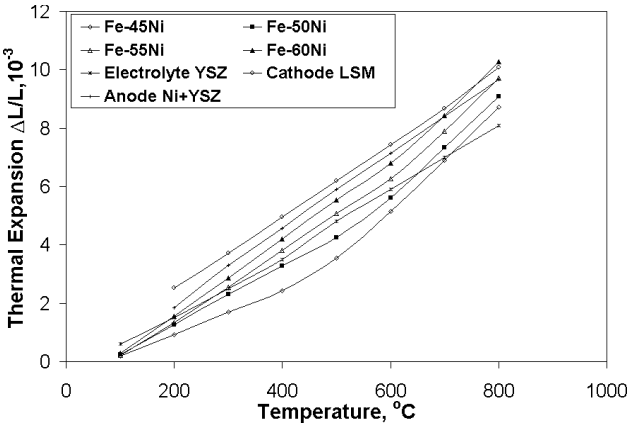

Figure 1. Thermal Expansion vs. Temperature for the Fe-Ni Alloys (wt.%), as Compared to Other Cell Components

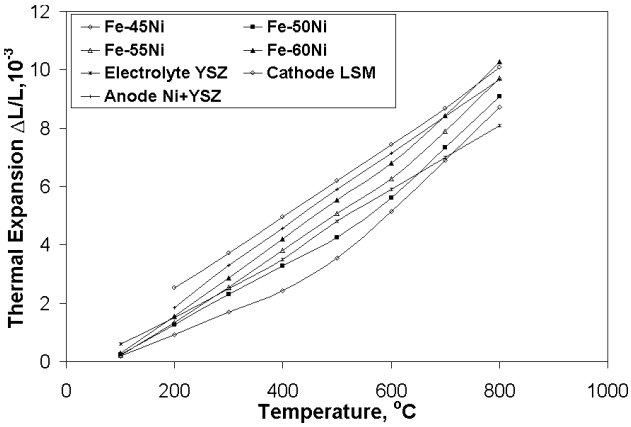

Figure 2. Mass Gains of the Fe-Ni Alloys (wt.%) after Oxidation for 500 Hours at 800ºC in Air

mass gain in air (cathode environment) of the alloys increased with the increase in oxidation temperature, while no weight change was observed in Ar+4% H_2 saturated with H_2O (simulated anode environment). As the Ni content increased from 45 to 60 wt.%, the oxidation rate of the Fe-Ni alloys at 800°C in air decreased. As shown in Figure 1, with the increase in Ni content in the binary Fe-Ni alloys, the thermal expansion increased correspondingly. However, the thermal expansion behaviors of the Fe-Ni alloys are all relatively close to those of the other cell components up to 800°C.

Our initial alloy development efforts focused on the optimization of Ni content in the Fe-Ni alloys. Based on the short-term oxidation kinetics study, it is clear that a higher Ni content should be favored in consideration of alloy oxidation resistance. To further demonstrate the effect of Ni content on the oxidation resistance, long-term oxidation behavior of the Fe-Ni alloys with different Ni contents was studied in air at 800°C. Figure 2 presents the mass gain of the Fe-Ni alloys with different Ni contents after isothermal oxidation for 500 hours in air at 800°C. The weight gain of the alloys decreased with the increase in Ni content in the alloys. This can be explained by the cross-sectional observations with scanning electron microscopy (SEM), as shown in Figure 3. The oxide scale became thinner with the increase of Ni content in the alloys. The thickness of the Fe_2O_3 top layer also decreased with the increase of Ni content in the alloys. While no NiO sub-layer was formed underneath the $(Fe,Ni)_3O_4$ spinel layer

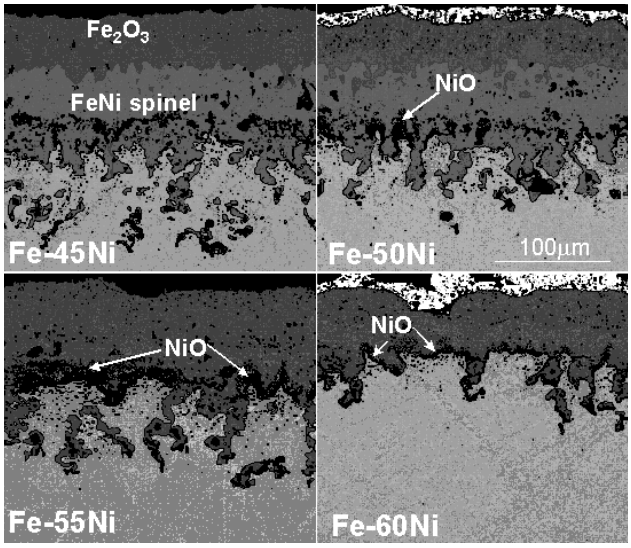

Figure 3. SEM Cross-Sectional Images of the Fe-Ni Alloys (wt.%) after Oxidation for 500 Hours at 800ºC in Air

for Fe-45Ni, NiO was observed between the spinel and substrate on Fe-50Ni, Fe-55Ni, and Fe-60Ni. The continuity of the NiO layer improved with the increase of Ni content in the alloys, as shown in Figure 3. Therefore, the enhancement of oxidation resistance of the higher-Ni-content alloys is most likely due to the formation of the NiO layer between the spinel and substrate.

As shown in Figure 4, the ASRs of the oxide scales grown on the binary Fe-Ni alloys after oxidation for 500 hours in air at 800°C decreased also with the increase in Ni content. Furthermore, the ASRs of the oxide scales on these alloys were

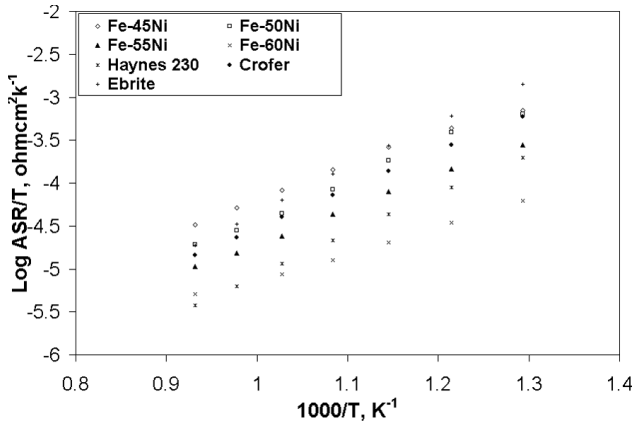

Figure 4. Comparison of the Scale ASRs for the Fe-Ni Alloys with Several Other Interconnect Alloys

comparable to those of current interconnect alloys such as Ebrite, Crofer and Haynes 230. Bearing in mind that the Fe-Ni alloys formed much thicker oxide scales than the current Cr-forming interconnect alloys, these results implied superior electrical conductivity of $(Fe,Ni)_3O_4$. Indeed, based on the measurements of bulk $(Fe,Ni)_3O_4$ samples, the electrical conductivity of $(Fe,Ni)_3O_4$ was several orders of magnitude higher than that of Cr_2O_3, and reactive element doping further increased the electrical conductivity of the spinel.

While the formation of a top $(Fe,Ni)_3O_4$ layer is relatively straight-forward, as demonstrated in our initial study, the best protective inner-layer oxides (NiO, Cr_2O_3, or mixed oxides) and their formation mechanisms via thermal oxidation are still to be determined. We have identified several alloy compositions which exhibited relatively slow oxidation rate and stable ASRs (up to 1500 hours) in air at 800°C.

Conclusions

The formation of an electrically conductive, Cr-free spinel outer layer over a protective, electrically conductive oxide inner layer on the Fe-Ni based alloys is highly desirable to mitigate the Cr poisoning problem in the SOFC stack. Our preliminary results indicate that it is feasible to develop Cr-free or low-Cr Fe-Ni alloys with balanced properties for SOFC interconnect application. While these new alloys possess promising CTE and oxide scale ASR, their oxidation resistance needs further improvement. A number of innovative approaches have been identified to further enhance the oxidation resistance of these alloys, which will be the focus of our future research.

FY 2005 Publications/Presentations

1. "Tailoring Fe-Ni Alloys for Intermediate Temperature SOFC Interconnect Application", J.H. Zhu, S.J. Geng, Z.G. Lu, M.P. Brady, I.G. Wright, X.D. Zhou, and H. Anderson, Presented at the SECA Core Technology Peer Review Workshop, Tampa, FL, January 27-28, 2005.

III.A.17 Innovative Seals for Solid Oxide Fuel Cells

Professor Raj N. Singh
University of Cincinnati
Department of Chemical and Materials Engineering
Cincinnati, OH 45221-0012
Phone: (513) 556-5172; Fax: (513) 556-3773; E-mail: Raj.Singh@uc.edu

DOE Project Manager: Travis Shultz
Phone: (304) 285-1370; E-mail: Travis.Shultz@netl.doe.gov

Objectives

- Select self-healing glasses to function as seals for solid oxide fuel cells (SOFCs)
- Demonstrate functionality of the self-healing seals by leak tests
- Measure stability of the self-healing glass in SOFC environments
- Develop approaches to toughening self-healing glasses as seals for SOFCs
- Survey commercial glasses suitable for making seals for SOFCs

Approach

- Select glasses suitable for self-healing and expansion matching, measure thermophysical properties, prepare seals with SOFC components, and test seals over a range of temperatures including thermal cycles
- Determine thermal stability of the glasses in SOFC environments, measure thermal properties after annealing, and fabricate seals for leak testing at cell operating conditions
- Develop approaches for toughening sealing glasses through reinforcing phase, select a reinforcing fiber, fabricate reinforced glasses, and incorporate toughened glasses into seals and seal tests
- Perform literature search on glasses suitable for seals in SOFCs

Accomplishments

- Demonstrated ability of a self-healing glass in sealing SOFC components through leak tests over a range of temperatures between 25 and 800°C
- Achieved over 80 thermal cycles between 25 and 800°C without leak of a self-healing glass and accumulated over 230 hours of hermetic cell performance at 800°C
- These results provide great promise towards meeting Solid State Energy Conversion Alliance (SECA) goals for seals for SOFCs

Future Directions

- *Self-Healing Glass Development*
  Self-healing glasses identified above will be further refined, selected properties measured, thermal stability of the glasses determined, and glasses used in making seals. Seal test results will be obtained to assess suitability of the glasses for making seals.
- *Toughening of Glass*
  Glasses identified in the above tasks will be toughened to enhance their fracture toughness, which is expected to enhance durability. This will involve identification of a suitable fiber, fabrication of the fiber-reinforced glass, property measurements of glasses, and applications of toughened glasses in making seals and seal testing.

- *Survey of Commercial Glasses*
  Commercial glasses will be surveyed for their suitability for seals in a SOFC.

Introduction

A functioning SOFC requires seals that prevent electrode leakage and internal gas manifold leakage if internal gas manifolds are utilized. The seals must prevent the mixing of fuel and oxidant streams as well as prevent reactant escape to the surrounding environment. The seal material must be electrically isolating and be mechanically and chemically stable in contact with interfacing cell components in humid dual reducing and oxidizing conditions. Particularly important is the ability to seal between metallic and ceramic components with differing coefficients of thermal expansion (CTE), and do so while exposed to temperature transients over a range from room temperature up to SOFC operating temperature (800ºC). This project is developing innovative sealing concepts for both short- and long-term functionality of SOFCs, addressing the aforementioned issues.

Approach

A novel concept of *in situ* crack healing by glasses is pursued in this project. The fundamental idea underlying this concept is based on the fact that a glass with suitable low viscosity can heal cracks created by thermal expansion mismatch between materials that are being joined by a glass seal in a SOFC. The functionality of this innovative sealing approach based on *in situ* crack healing by a glass is demonstrated and quantified. Toughening and strengthening of the glass by fibers/whiskers is pursued to minimize or eliminate bulk cracking of the seals. These concepts are pursued further in Phase I to address sealing capabilities and durability issues related to a functioning seal for a SOFC.

Results

Self-healing glasses were selected, fabricated, and used for making seals. A test fixture was constructed for leak testing, and leak tests under appropriate SOFC test conditions were performed. The assembled system was successful in meeting the project goals of testing seals at both room and high temperatures. The results demonstrated self-healing behavior of seals with a significant capability for thermal cycles between 25 and 800°C. These results are very promising for meeting some of the goals of the SECA program for SOFCs. The details on these activities are given below.

Developing seals suitable for joining electrolyte (yttria stabilized zirconia – YSZ) to a metal using a glass that can show self-healing behavior requires selection of glasses with appropriate thermophysical properties and expansion match with YSZ and metals. A number of glasses were considered and obtained from various sources. Samples of glass powders were used for x-ray diffraction studies to ensure that the starting materials are indeed amorphous in crystal structure. The glass and YSZ powders were processed to fabricate samples for measurements of properties and testing. Expansion behaviors of all the samples, glasses, metals, and YSZ were measured between 25 and 1000°C in a high-temperature dilatometer. Figure 1 shows the expansion behavior of a glass used in a self-healing study along with the expansion data for YSZ and Crofer metal.

The diffusion processes at high temperatures can heal cracks in ceramics and glasses. Crystalline ceramics require higher temperatures for healing than some of the glasses because of the thermally activated nature of the diffusion process responsible for healing. The self-healing behavior was studied

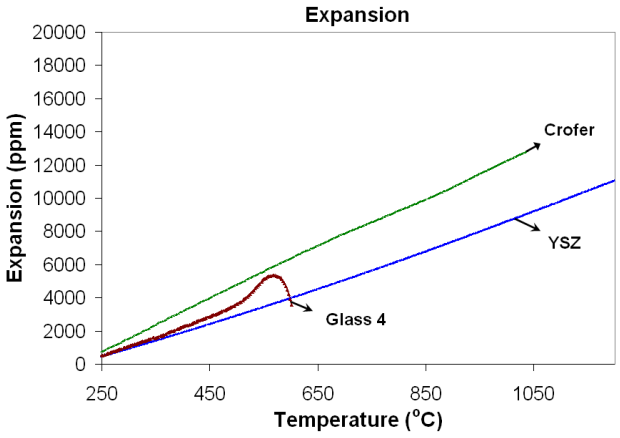

Figure 1. Thermal expansion behavior of materials used for making self-healing seals for SOFCs.

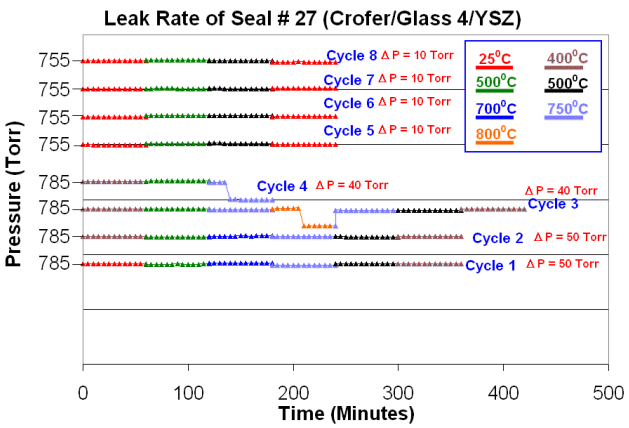

Figure 2. Pressure-time plots of the leak tests of a Crofer-Glass-YSZ seal. This seal developed leaks in the 3rd and 4th cycles and then healed to create a hermetic seal. The data shows hermetic seals after healing to 8th cycle.

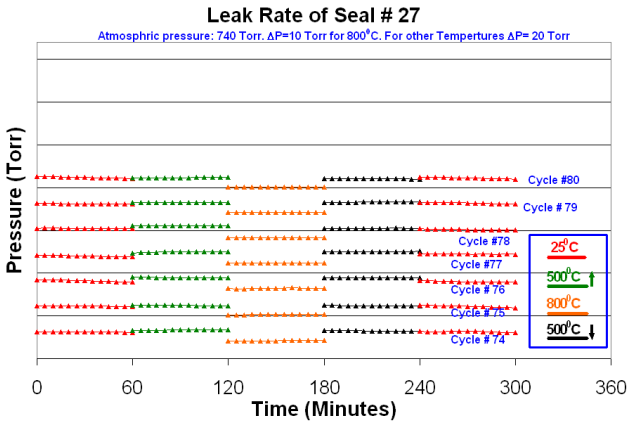

Figure 3. Pressure-time plots between 74-80 thermal cycles of the leak tests of the seal made using Crofer-Glass-YSZ. This seal continues to show hermetic behavior even after 80 thermal cycles between 25 and 800°C.

by heating the glass to desired temperatures between 25 and 1000°C and observing the surface of the glass sample with cracks with a video camera (in a unique facility). The temperature-time history of the self-healing process was recorded, including the detected beginning and end of the self-healing process. These data were used for selecting the processing temperatures for making the seals and appropriate conditions required for demonstration of the self-healing behavior.

The leak test fixture developed was used for leak tests at room temperature and high temperatures. A seal was made using Crofer metal, Glass 4, and YSZ. The YSZ was sealed to Crofer by this glass, and then the Crofer metal was welded to 304 SS housing. The inside of the SS 304 housing was connected to the high-pressure side of the seal, and the outside of the SS 304 housing was maintained at atmospheric pressure. During the test, the seal assembly was heated to the desired temperature inside a furnace, and the seal was pressurized from inside for leak testing while the pressure was monitored as a function of time. Figure 2 shows the results of leak testing up to 8 thermal cycles. The leak tests were performed at room temperature and at various temperatures during heating as well as during cooling. The data show that the seal developed a leak in the 3rd and 4th cycles, but after each cycle, the seal was heated to 800°C for healing and became hermetic. The same seal has been tested further for its durability against thermal cycles, and the results in Figure 3 show that the seal remains hermetic even after 80 thermal cycles and 236 hours of seal testing at 800°C. Further testing of this seal continues to accumulate more data.

These results on thermal-cycle-ability of SOFC seals are quite promising for developing seals that meet the SECA goals for SOFCs.

Conclusions

- Glasses were selected for demonstration of self-healing behavior and potential for making seals that display self-healing response. The thermal properties, densification behavior, and wetting behavior of glasses with YSZ electrolyte, Crofer, SS 430, and nickel metals were determined to assess suitability for making seals.
- A new methodology based on video imaging of cracks was applied to characterize self-healing behavior of all the selected glasses and glass-ceramics as a function of temperature and time. Generally, glass-ceramics showed slower self-healing kinetics than the glassy state, but the exact kinetics was dependent on the specific glass or glass-ceramics.

- A seal test system was designed and built for testing seals both at room and elevated temperatures up to 1200°C. This facility was extensively used in developing hermetic seals that display self-healing behavior.
- Seals incorporating some of the more promising glasses were fabricated. The effects of up to 80 thermal cycles between 25 and 800°C and 236 hours at 800°C on hermeticity of the seals were demonstrated. Self-healing behaviors of the leaking seals were also demonstrated. These results are important for achieving the SECA goals for SOFC sealing systems.

FY 2005 Publications/Presentations

1. Program Monthly Reports between October (2004) and May (2005).
2. Interim Decision Point Program Report (March, 2005).
3. R.N. Singh, "High Temperature Seals for Solid Oxide Fuel Cells," Ceram. Eng. Sci. Proc. (2004).
4. R.N. Singh and S. Parihar, "Layered Composite Seals for Solid Oxide Fuel Cells," Ceram. Eng. Sci. Proc. (2004).
5. R.N. Singh, "High Temperature Seals for Solid Oxide Fuel Cells (SOFC)," ASM Conf. Proceedings (2004).
6. S. Parihar and R.N. Singh, "Self-Healing Glass Seals for Solid Oxide Fuel Cells," Proc. of Am. Ceram Soc. Annual Meeting (2005).

III.A.18 Low-Cost Integrated Composite Seal for SOFC: Materials and Design Methodologies

Xinyu Huang (Primary Contact)
University of Connecticut
44 Weaver Rd, Unit 5233
Storrs, CT 06269-5233
Phone: (860) 486-5284; Fax: (860) 486-8378; E-mail: xinyu@engr.uconn.edu

DOE Project Manager: Travis Shultz
Phone: (304) 285-1370; E-mail: Travis.Shultz@netl.doe.gov

Subcontractors:
Inframat Corp., Farmington, CT
Physical Acoustics, Princeton Junction, NJ

Objectives

- Prove a novel layered composite seal concept (materials and structures) for solid oxide fuel cells (SOFCs).
- Characterize the sealing and the mechanical performance of the layered composite seal and demonstrate a design methodology.

Approach

- Down-select a set of constituent materials and fabricate small-scale composite seal samples (button samples) for material characterization and seal testing.
- Test button samples for seal performance, mechanical strength, long-term material stability and compatibility.
- Analyze failed samples and determine failure modes and mechanisms; model stress and strain in the seal structure.

Accomplishments

- Completed design, assembly, and qualification of an automated SOFC seal leak testing stand.
- Developed a robust alumina-zirconia composite coating on Fe-Cr based metallic substrates using low-cost ceramic powders; fabricated sub-scale composite seal button samples infiltrated with various glass-based fillers.
- Demonstrated thermo-cycle resistance from 800ºC to 150ºC with a heating and cooling rate of 5ºC/min. After 40 cycles, leak rates of less than 0.017 sccm/cm were found, and after 80 cycles, leak rates of less than 3.1 sccm/cm were found. (Leak rate was measured with helium at 2 psid at 800ºC.)
- Observed healing behavior of the composite seal when using a low-softening point filler glass. The leak rate of the sample with cracked filler glass was restored to the level before cracking by heating the composite seal above the softening temperature of the filler glass.

Future Directions

- Continue with leakage testing to determine leak rates as a function of thermo-cycling and aging time; perform root cause analysis by analyzing failed seal samples.
- Evaluate additional filler materials in composite seal configuration.

- Perform long-term material compatibility studies and characterize failed samples for morphological change and chemical interactions.
- Perform mechanical testing and complete modeling efforts.

Introduction

Maintaining stable hermetic sealing is critical for SOFC stacks to achieve high efficiency and longevity. Sealing SOFC stacks is a challenging task for many reasons. The adherents to be sealed often have very different thermo-elastic properties; the temperature field in SOFC stacks is typically non-uniform, particularly in transient conditions, such as during start-up and shut-down. As a result, large thermal stresses can be induced in the seals and the adjacent components if rigidly bonded. Commonly used glass seals and the materials in a SOFC cell assembly to be jointed or sealed are brittle. Existing glass and glass ceramic seals have shown poor resistance to mechanical failure during thermo-cycling, among other operating conditions. In the long term, sealing glass reacts with Fe-Cr based interconnect material, resulting in a weakened interface [1]. Compressive mica and mica composite seals [2] have been shown to have excellent thermo-cycling stability. However, they require expansive high-temperature load-frame to maintain a high compressive force.

SOFC sealing material is subjected to a complex set of requirements, including good wetability to adherends, good chemical compatibility, good match of thermal expansion coefficients, high electrical resistivity, etc. In addition, the aggregated material and fabrication cost of seals has to be low to ensure commercial viability. It is unlikely that such a large set of suitable mechanical/physical/chemical properties occur in one material. Attempting to break the current technical barriers related to SOFC seals, the authors are investigating a novel integrated composite seal concept (materials and structures) and its associated thermal mechanical design methodologies.

Approach

The approach being pursued is to engineer composites of multiple constituent materials or ingredients. The authors are investigating a multi-layered composite seal structure (Figure 1) that consists of thin layers of oxidation-resistant metals, porous ceramics, and fillers/glasses. The seal structure will be directly fabricated onto the surfaces of mating adherends using low-cost manufacturing methods such as atmospheric plasma spray (APS). During stack assembly, sealing can be achieved through a simple heat/pressure-assisted curing process. As such, stack cost can potentially be lowered by reducing the total number of parts and by simplifying the assembly process. Properly designed multi-layered composite structure enables a gradual transition of thermo-elastic properties from the substrate to the glass fillers, alleviating stress concentrations. Plasma-sprayed ceramic layers can form strong bonds with properly prepared metal substrate. The ceramic layer is electrically insulating and has shown very good thermal shock resistance. Filling in the pores and gaps between the ceramic layers, a thin layer of glass joins the adherends together and forms a hermetic seal. Because of the excellent refractory properties of the coating, the requirements (wetting, dielectric, chemical properties, etc.) on the filler materials can be relaxed; hence, many types of filler materials can be utilized in the composite seal structure. Eliminating direct contact between the glass and the alloy, the composite seal will also have improved long-term stability.

Small-scale sealed specimens will be subjected to thermo-cycles and sustained loading similar to fuel cell operating conditions in air. Post-mortem

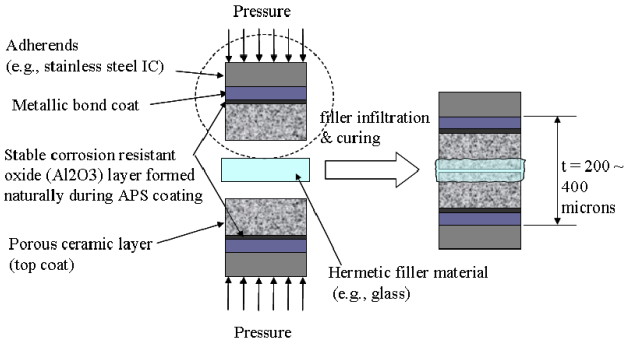

Figure 1. Concept of an Integrated Composite Seal for SOFC Stacks Being Developed at the University of Connecticut

analysis will be conducted to investigate interfacial failure modes and failure mechanisms. These activities will be iterated for different combinations of material compositions in order to achieve high interfacial bond strength and good sealing performance. To demonstrate the above composite seal concept, the authors are following an iterative process including material selection, fabrication, screening, seal performance evaluation, and mechanical performance evaluation.

Results

As part of the layered composite seal, a porous alumina-YSZ (yttria-stabilized zirconia) ceramic coating on Fe-Cr based interconnect material has been developed. The coating was made from low-cost commercially available powders and deposited by atmospheric plasma spray method. The coating composition was optimized for high mechanical strength/toughness, low electric conductivity, and good refractory properties. The coating has demonstrated superior high-temperature stability, high electrical resistivity and superior thermal shock resistance (survived repeated water quench from 850ºC). The projected cost for material and fabrication of the coating is less than $1 per square inch coated area. The microstructure of the coating was characterized by optical and scanning electron microcopy. The bulk of the coating consists of flattened "splats" with inter- and intra- splat micro-cracks. The porosity of the coating was revealed to be greater than 15%, as determined by mercury intrusion porosimetry.

To facilitate sealing performance measurements, an automated SOFC seal leak test stand was developed and qualified. The test stand consists of a pneumatic loading module for maintaining a constant compressive load, a heating and temperature control module, and a leak rate testing module to measure the flow rate of test media. SOFC seal samples up to 5 inches in diameter can be placed in the heated chamber and maintained at temperature anywhere from room temperature to 1100ºC. The temperature can also be cycled repeatedly with controlled heating and cooling rates. The leak rate in the range from 0.1 to 125 sccm can be continuously monitored.

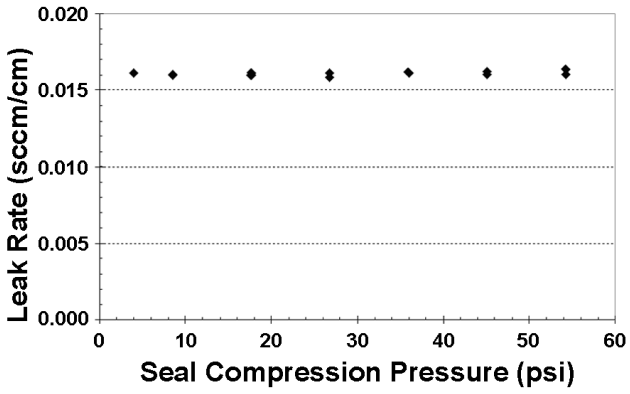

Figure 2. Measured composite seal leak rate as a function of the applied compressive pressure on the substrates. The composite seal leak rates are shown to be independent of the compression force.

Composite seal samples have been made using commercial glasses as well as glasses provided by several Solid State Energy Conversion Alliance (SECA) peers (Richard Brow, University of Missouri-Rolla; Raj Singh, University of Cincinnati; Ron Loehman, Sandia National Laboratories). The filler glass was infiltrated into the porous ceramic coating, and interconnect-to-interconnect and interconnect-to-electrolyte seal samples have been made and tested. At steady state, a typical leak rate of 0.016 sccm/cm (helium at 2 psid) was found. As shown in Figure 2, it was discovered that the leak rate of the composite seal is independent of the compressive force exerted on the sealed substrate. It was found that the leak rate is proportional to the differential pressure of the test media. The measured leak rate of a sample as a function of differential pressure is shown in Figure 3. Such behavior allows us to reliably predict leak rate at lower differential pressure using leak rate measured at higher differential pressure.

Thermo-cycle testing has been conducted with a 1.5" diameter interconnect-to-interconnect seal sample. The temperature was programmed to cycle between 800ºC and 150ºC using a ramp rate of approximately 5ºC/min. The sealed chamber was filled with pure helium gas and maintained at about 2 psig. After more than 40 cycles, leak rates of less than 0.017 sccm/cm were found; after 80 cycles, leak rates of less than 3.1 sccm/cm were found. Figure 4 shows the data recorded near the end of an 80-cycle

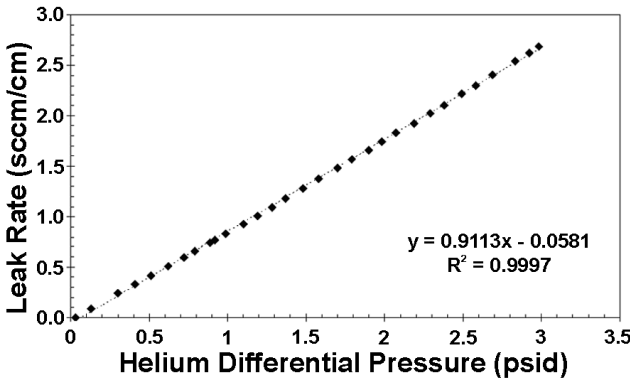

Figure 3. Measured leak rate as a function of differential pressure of helium gas that was used as the test media. The leak rate is shown to be proportional to applied differential pressure.

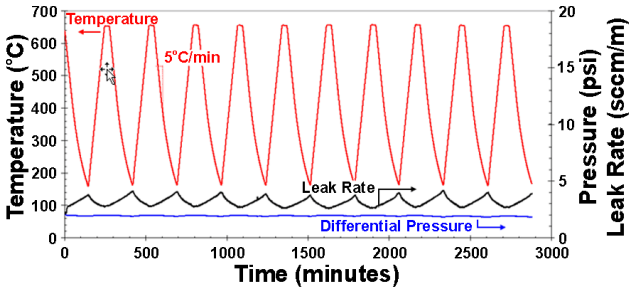

Figure 4. Thermal Cycling Performance of a Composite Seal near the End of an 80-Cycle Test

test. It was also observed that a "failed" composite seal with cracked filler glasses with a low softening point can be "healed" multiple times. The "healing" involves heating the seal to about the softening point of the filler (typically 800ºC) and dwelling for one hour.

Conclusions

In the first year of the program, the University of Connecticut team has made significant progress on proving the novel composite seal concept. A streamlined procedure has been established, from material selection and seal sample fabrication, to material characterization and seal performance testing under relevant conditions. The layered composite seal has shown good steady-state sealing performance and reasonable thermo-cycle resistance. Future work will focus on proving the durability of the composite seal, further improving the thermal cycle resistance, and establishing the mechanical testing, modeling and design approaches.

FY 2005 Publications/Presentations

1. "Low-Cost Integrated Composite Seal for SOFC: Materials and Design Methodologies," X. Huang, K. Ridgeway, S. Narasimhan, Y. Du, K. Reifsnider, C. Ma, F. Shu, Presented at the Sixth Annual SECA Workshop, Asilomar, CA, April 18-21, 2005.

References

1. Z. Yang, J.W. Stevenson, K.D. Meinhardt, "Chemical interactions of barium-calcium-aluminosilicate-based sealing glasses with oxidation resistant alloys," Solid State Ionics, 160 (2003), 213~225.
2. S.P. Simner, J.W. Stevenson, "Compressive mica seals for SOFC applications," J. of Power Sources 102 (2001), 310~316.

III.A.19 Resilient and Thermochemically Stable Sealing Materials for Solid Oxide Fuel Cells

Richard K. Brow
University of Missouri-Rolla
Materials Science & Engineering Department
222 McNutt Hall
Rolla, MO 65409-0330
Phone: (573) 341-6812; Fax: (573) 341-6934; E-mail: brow@umr.edu

DOE Project Manager: Travis Shultz
Phone: (304) 285-1370; E-mail: Travis.Shultz@netl.doe.gov

Objectives

- Develop, characterize, fabricate, and test a hermetic solid oxide fuel cell (SOFC) seal based on a thermochemically stable glass-ceramic system.
- Fabricate seals between SOFC component materials at temperatures below 900°C and characterize stability in oxidizing and reducing environments at temperatures up to 800°C.

Approach

- Optimize glass compositions with the requisite thermal and chemical properties for SOFC seals.
- Develop techniques to produce composite seals using glasses and filler materials (ceramic and metallic) chosen to improve seal resiliency during thermal cycling.
- Characterize the hermeticity of seals after thermal cycling between use temperatures (up to 800°C) and room temperatures.

Accomplishments

- *Promising sealing glasses developed.*
  Several 'baseline' glass compositions have been developed that appear to possess requisite thermal and chemical properties as 'host materials' for resilient composite seals. The glasses have thermal expansion coefficients in the range 10-12x10^{-6}/°C, have low volatility rates in wet forming gas at 750°C, and form well-adhered bonds to stainless steel interconnect materials and to Y-stabilized zirconia (YSZ).
- *Glass-crystallization kinetics studied.*
  We have developed a new thermal analytical technique that provides a quantitative measure of the degree of crystallization of a glass-ceramic material and have used this technique to characterize new SOFC materials.

Future Directions

- *Develop resilient 'composite' sealing materials.*
  We will prepare and characterize composites between baseline glasses and ceramic and metallic fillers to modify the thermal expansion/contraction characteristics of the sealing materials to better survive thermal cycling.
- *Prepare and characterize hermetic seals.*
  We will prepare hermetic seals between YSZ and Cr-steel interconnect alloys using optimized sealing materials and characterize hermeticity using a helium manifold currently under development. Hermeticity will be tested after subjecting the seals to a series of thermal cycles between 750°C and room temperature.

- *Test SOFC cells.*
  The sealing materials will be used to fabricate prototype, operational SOFC cells, and the cells will be thermally cycled between 750°C and room temperature at least ten times to characterize the effects of the seals on cell performance.

Introduction

Planar SOFC configurations are relatively simple to manufacture and have higher power densities and efficiencies than other configurations, but require hermetic seals to prevent mixing of the fuel and oxidant streams within the cell stack and to seal the stack to the system manifold. Within the SOFC stack, an effective seal must have a thermal expansion match to the fuel cell components, must be electrically insulating and must be thermochemically stable under the operational conditions of the stack. The seal should exhibit no deleterious interfacial reactions with other cell components, should be stable under both the high-temperature oxidizing and reducing operational conditions, should be created at a low enough temperature to avoid damaging cell components (under 850°C for some materials), and should not migrate or flow from the designated sealing region during sealing or cell operation. In addition, the sealing system should be able to withstand thermal cycling between the operational temperature and room temperature. That is, thermal stresses that develop because of mismatches in the thermal contraction characteristics of the different SOFC materials must either be reduced to well below the failure strengths of the materials or must be relieved in some fashion.

Approach

The objective of this project, which started in October 2004, is to develop novel glass compositions for resilient glass-ceramic hermetic seals for solid oxide fuel cells. The glasses are based on novel alkaline earth silicate compositions that possess invert molecular structures and so possess the viscosity characteristics to seal at relatively low temperatures, but crystallize to form a thermally stable sealing material. (Invert glasses do not possess the continuous cross-linked silicate structures of more typical silicate glasses.) The 'resiliency' will be obtained by engineering the characteristics of the ceramic and residual glassy phases of the glass-ceramic seal. A ceramic phase will be selected to induce microcracks in the seal upon cooling. The residual glassy phase will be designed to flow and heal those microcracks when the seal is reheated. The controlled release of stress through microcracking and subsequent viscous 'resealing' will allow the seals to survive the stringent thermal cycling requirements for SOFCs.

Crystallized glasses with desirable thermal and chemical properties will be prepared and evaluated at the University of Missouri-Rolla. The glasses will be sealed (as thin films) to SOFC component materials, including YSZ electrolytes and ferritic stainless steel interconnect materials. Long-term stability experiments will be performed, as will thermal cycling experiments. The electrical characteristics of the thin-film seals will be evaluated, and *in situ* impedance measurements under simulated SOFC use conditions will be made to provide information about the long-term thermochemical stability of seal couples.

Results

We have developed and characterized several glass compositions that appear to possess the chemical and thermal properties desirable for a host matrix for resilient composite sealing materials. The glasses are based on the alkaline earth-zinc-silicate system, with other oxides added to control crystallization behavior and to tailor thermal properties. Certain compositions possess good thermal expansion matches to YSZ, before and after crystallization. For example, Figure 1 shows the expansion difference between a crystallized glass (designated 'glass #27') and YSZ, after heat-treatment at 750°C for up to 28 days. The expansion characteristics of the glass-ceramic do not change significantly below about 600°C. Above 600°C, the expansion coefficient of the glass-ceramic increases relative to the YSZ. We believe this is related to the expansion characteristics of the residual glass. X-ray diffraction analyses of the crystallized glasses indicate that pyrosilicate and orthosilicate (e.g., $Ca_2ZnSi_2O_7$, $CaSrAl_2Si_2O_7$, Sr_2SiO_4, etc.)

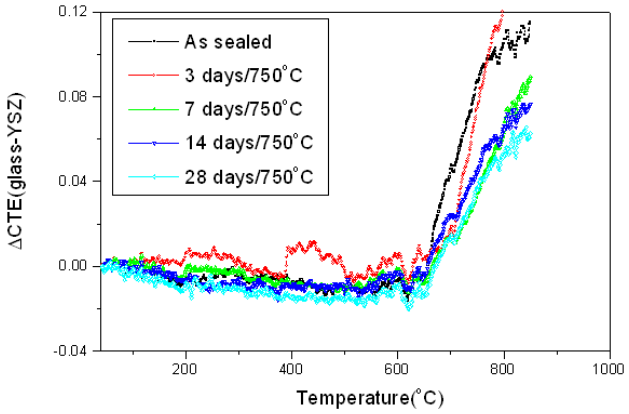

Figure 1. Thermal Expansion Characteristics of Sealing Glass #27 after Being Held at 750°C for up to 28 Days

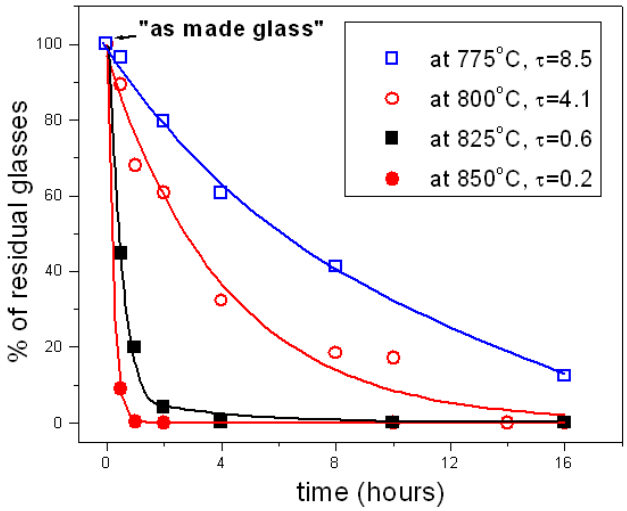

Figure 2. The Amount of Residual Glass in Glass #27 after Thermal Treatments in Air for Different Times and Temperatures, as Determined by Differential Thermal Analysis

phases dominate. Weight loss measurements from glasses held in wet forming gas at 750°C for up to 28 days indicate that the glass-ceramics are thermochemically stable.

We have studied the crystallization kinetics of the sealing glasses using a new quantitative differential thermal analytical (DTA) technique developed at the University of Missouri-Rolla [1]. Glasses are held at different temperatures for various times and a DTA scan is collected. The area under the crystallization peak is then used as a relative measure of the amount of residual glass in the heat-treated sample. A larger crystallization peak means more residual glass after heat treatment, whereas no DTA crystallization peak means no residual glass in the sample. Figure 2 shows a summary of the DTA analyses of glass #27. Similar studies are presently underway to evaluate other compositions and to characterize how the addition of 'filler materials' affects the crystallization kinetics of the base glasses.

The glasses adhere well to YSZ and to Cr-steel interconnect alloys. Figure 3 shows a scanning electron micrograph image of the interface of a glass #27/E-brite seal after four days at 750°C. (Image provided by Ron Loehman, Sandia National Labs.) No evidence for the formation of deleterious interfacial reaction products is evident, in contrast to reports on BaO-containing glasses [2]. Adhesion tests indicate bond strengths of 40 MPa, with failure in the glass, not at the interface.

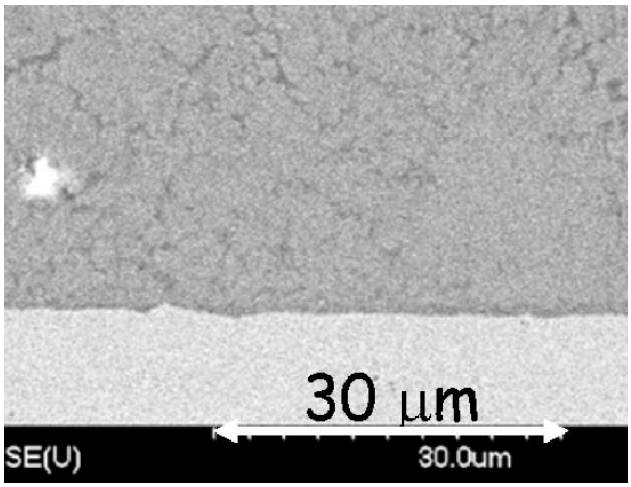

Figure 3. Scanning Electron Micrograph of a Glass #27 (top)-E-brite (bottom) Interface, after Four Days at 750°C (From Ron Loehman, Sandia National Labs)

Conclusions

- We have developed glasses that, when crystallized, possess thermal properties that make them candidates for SOFC seals.
- We have bonded these glasses to YSZ and to Cr-steel interconnect alloys, including E-brite, Crofer APU 22 and 430SS.
- Protocols for preparing glass/filler composite sealing materials are presently being developed.

FY 2005 Publications/Presentations

1. S. T. Reis, R. K. Brow, "Designing Sealing Glasses for Solid Oxide Fuel Cells," Proceedings of the ASM Materials Solution Conference, Fuel Cells: Materials, Processing and Manufacturing Technologies, Columbus, OH, October 18-20, 2004.
2. R. K. Brow and S. T. Reis, "Designing Sealing Glasses for Solid Oxide Fuel Cells," ASM Materials Solution Conference, Fuel Cells: Materials, Processing and Manufacturing Technologies, Columbus, OH, October 18-20, 2004 (INVITED).
3. S. T. Reis*, R. K. Brow, and P. Jasinski, "Developing Glass Seals for Solid Oxide Fuel Cells," 2nd International Symposium on Solid Oxide Fuel Cells: Materials and Technology, 29th International Cocoa Beach Conference and Exposition on Advanced Ceramics and Composites, Cocoa Beach, FL, January 23-28, 2005.
4. R. K. Brow*, T. Zhang, and S. T. Reis, "Thermochemically Stable Sealing Materials for Solid Oxide Fuel Cells," SECA Core Technology Workshop, Tampa, FL, January 27, 2005.
5. R. K. Brow*, "Glass Seals for Solid Oxide Fuel Cells," Iowa State Materials Science & Engineering Seminar, Ames, IA, March 3, 2005 (INVITED).
6. T. Zhang*, S. T. Reis, and R. K. Brow, "Glass Seals for Solid Oxide Fuel Cells," 107th Annual Meeting of the American Ceramic Society, Baltimore, MD, April 10-13, 2005.
7. R. K. Brow, "Thermochemically Stable Sealing Materials for Solid Oxide Fuel Cells," Solid State Energy Conversion Alliance 6th Annual Workshop, Pacific Grove, CA, April 18-21, 2005 (INVITED).
8. R. K. Brow, "Sealing Glasses for Solid Oxide Fuel Cells," 17th University Conference on Glass Science and 1st International Materials Institute Workshop on "New Functionality in Glasses", Penn Stater Conference Center Hotel, State College, PA, June 26-30, 2005 (INVITED).

References

1. C. S. Ray, S. T. Reis, R. K. Brow, W. Höland, W. Rheinberger, "A New DTA Method for Measuring Critical Cooling Rate for Glass Formation," *Journal of Non-Crystalline Solids*, **351** 1350-58 (2005).
2. N. Lahl, D. Bahadur, *et al*. (2002) *J. Electrochem. Soc*. 149[5] A607-A614.

III.A.20 Fundamental Studies of the Durability of Materials for Interconnects in Solid Oxide Fuel Cells

Gerald H. Meier (Primary Contact), *Frederick S. Pettit*
Department of Materials Science and Engineering
848 Benedum Hall
University of Pittsburgh
Pittsburgh, PA 15261
Phone: (412) 624-9720; Fax: (412) 624-8069; E-mail: ghmeier@engr.pitt.edu, pettit@engr.pitt.edu

DOE Project Manager: Lane Wilson
Phone: (304) 285-1336; E-mail: Lane.Wilson@netl.doe.gov

Subcontractors:
Jack L. Beuth, Carnegie Mellon University (CMU), Pittsburgh, PA
James R. Rakowski, ATI Allegheny Ludlum, Brackenridge, PA
Bruce Kang, West Virginia University (WVU), Morgantown, WV

Objectives

- To develop mechanism-based evaluation procedures for the stability of solid oxide fuel cell (SOFC) interconnect materials and to use these procedures to study and modify a group of alloys which have already been identified as candidate interconnect materials, i.e., ferritic stainless steels.
- To study fundamental aspects underlying the thermomechanical behavior of interconnect materials and develop accelerated testing protocols. (CMU Subcontract)
- To investigate the potential for the use of "new" metals as interconnect materials.
- Development of a durable, conductive ceramic/metal (cermet) material suitable for long-term use as a contacting material in the cathode chamber of a SOFC. (WVU Subcontract)

Approach

- Characterize exposed fuel cell interfaces.
- Study and attempt to control growth rates of chromia scales on Cr and ferritic alloys.
- Study the adhesion of chromia scales subjected to cyclic oxidation conditions in simulated fuel cell atmospheres.
- Investigate evaporation of Cr-oxide species both theoretically and experimentally.
- Measure stresses in oxide scales on ferritic alloys using x-ray diffraction (XRD).
- Perform indentation testing to evaluate interface adhesion of thermally grown oxide scales and deposited coatings.
- Develop a mechanism-based, accelerated testing protocol for evaluating the thermomechanical stability of oxides and coatings on metallic interconnects.
- Evaluate the possibility of reducing the oxidation rate of pure Ni.
- Evaluate the use of Fe-Ni alloys (Invar) with low coefficient of thermal expansion (CTE) as interconnects.
- Evaluate the use of coatings to limit oxide evaporation from chromia-forming interconnect alloys.
- Evaluate the properties of Ag as contact material in the SOFC cathode chamber.

Accomplishments

- Characterized the oxidation behavior of a variety of ferritic stainless steels in simulated fuel cell atmospheres over the temperature range 700-900°C.
- Discovered that exposure under some fuel cell operating conditions can promote sigma phase formation in some ferritic stainless steels.
- Discovered that it is possible to modify a ferritic stainless steel to form an overlayer of TiO_2, which should suppress the evaporation from the underlying chromia scale.
- Determined that the growth rate of chromia on ferritic alloys can be greatly suppressed by surface doping with CeO_2.
- Adapted an indentation technique for measuring interfacial fracture toughness to oxides formed on interconnects and to coatings applied to interconnects.
- Established qualitative links between observed spallation behavior in indentation tests and trends in specific weight measurements for specimens exposed in simulated anode gas and simulated cathode gas environments.
- Used interfacial toughnesses measured in specimens subjected to short exposure times to estimate times for spontaneous spallation (failure) of chromia scales.
- Ascertained that it may be possible to modify nickel by alloying and surface doping to allow its use as an intermediate-temperature interconnect material.
- Identified a promising candidate material (CuO) for use with silver in the development of contacting material for the cathode chamber of solid oxide fuel cells.
- Initial testing indicates that the contact material in development is suitable in terms of ductility and electrical conductivity for use in the solid oxide fuel cell.
- Initial evaporation testing in high-air-flow, high-temperature environments indicates that the candidate contact material may be well suited for long-term use as a contacting material in the cathode chamber, based on limited loss of silver in exposed samples.

Future Directions

- Evaluate the oxidation behavior of ferritic stainless steels under dual atmosphere conditions, with one side of the specimen exposed to a simulated fuel cell cathode gas and the other side exposed to a simulated anode gas.
- Continue the development of indentation as an accelerated testing technique for chromia scales and deposited coatings.
- Develop a conceptual understanding of the interplay between interconnect failure mechanisms of chromia scale growth, scale spallation and scale evaporation.
- Continue the study of coatings to reduce oxide evaporation from chromia-forming alloys.
- Perform extensive studies on Ti-doped ferritic stainless steels to evaluate their ability to suppress evaporation of Cr-containing species and meet the other requirements for an interconnect material.
- Continue to investigate Cr-free alloys as possible interconnect materials.
- Evaluate samples of contact materials made with different starting parameters such as particle size and sintering time.
  - Microstructure
  - Ductility
  - Conductivity

- Evaluate CTE for candidate contact materials in order to reduce or eliminate thermal expansion mismatch issues.
- Further evaluate contact material composition to determine if current fabrication procedure is practical for real-world usage.
  - Ball-milling, dry-pressing, and sintering
  - Ag-precipitation onto ceramic particles
- More precisely measure conductivity of candidate contact materials.
- Develop relation for mass loss over time for candidate contact material operating in a realistic fuel cell cathode environment.

Introduction

One of the most important technical challenges for solid oxide fuel cells operating in the temperature range 700-900°C is the design of interconnects (current collectors). These components, in addition to electrically connecting individual cells in a stack, must separate the anode compartment of one cell from the cathode compartment of the adjacent cell. This means that one side of an interconnect is exposed to the fuel, typically hydrogen or hydrocarbons in which the oxygen partial pressure is low, and the other side is exposed to the oxidant, which is typically air with some amount of water vapor.

Interconnect material requirements include a variety of physical, chemical, and electrical properties. The optimal interconnect material would have the following properties:

- Low electrical resistivity.
- Impermeability to anode and cathode gases.
- Stability in both anode and cathode gases under thermal cycling conditions.
- Chemical compatibility with other cell components.
- Close match in coefficient of thermal expansion with other components.
- Good mechanical properties.
- High thermal conductivity.
- Ease of fabrication.
- Low cost.

Ceramic interconnects usually have favorable values of properties 2, 3, 4, and 5. However, they are usually deficient in the other desired properties.

Metallic interconnects are attractive in that they have favorable values of properties 2, 6, 7, 8, and 9. With respect to property 1, although metallic materials have low electrical resistivity, they react with SOFC gases to form oxide layers, which generally have high electrical resistivity. Oxidation-resistant alloys are designed to form one of three protective oxides: alumina, silica, or chromia. Of these, the electrical resistivities of alumina and silica are much too high for interconnect applications. For metallic interconnects, interconnect system resistance can be greatly increased by oxide layer thickening and spallation. For chromia-formers, evaporation of the chromia scale can severely degrade cathode performance. Thus, chromia scale growth, scale spallation and scale evaporation are the three principal "failure mechanisms" for interconnects forming chromia scales on their surfaces. Because the mechanisms are coupled, alloy changes to address one failure mechanism can affect one or more of the other failure mechanisms, making alloy design a complex task.

The research being performed at WVU is concerned with the contact areas between the interconnect and the cathode in the SOFC. Figure 1 illustrates a fuel cell stack consisting of two cells.

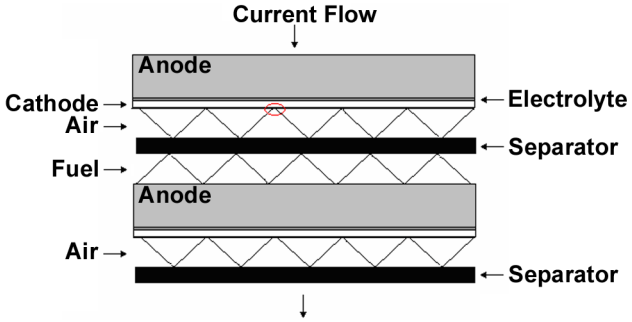

Figure 1. Schematic of a Fuel Cell Stack

The main area of concern is circled in red in the figure. Potential problems could involve the loss of conduction path due to the formation of non-conducting scales in the oxidizing environment of the cathode chamber, or loss of the contact between the components due to thermal stresses caused by mismatches in CTE of the materials. Therefore, any candidate materials will need to resist oxidation while possessing high conductivity and ductility, making silver a possible candidate material.

Silver has not been a good candidate in the past due to high volatility at SOFC operating temperatures. However, with the operating temperatures lowered to around 800°C, silver could be a viable option for SOFC material development.

Approach

The project consists of four major tasks aligned with its four objectives.

Task 1: Mechanism-based Evaluation Procedures

A variety of chromia-forming interconnect alloys are being subjected to thermal cycling in air, in simulated anode gas (Ar-H_2-H_2O) and with simultaneous exposure to air on one side and simulated anode gas on the other. Combined exposures have been shown at Pacific Northwest National Laboratory (PNNL) to often yield different behavior than exposures with the same gas on both sides of the specimen. Exposure temperatures range from 700°C to 900°C. Oxidation kinetics are being tracked by mass change measurements, and corresponding changes in oxide scale resistances are being measured. Exposed specimens are being examined in cross-section by scanning electron microscopy (SEM) to document changes in structure with exposure.

Methods are being studied to slow the growth of chromia scales on Cr and ferritic alloys with exposure in order to decrease the contribution of the scale to interconnect resistance. The effect of alloying additions (e.g., Mn, Ti) to ferritic steels to form a sealing outer layer over the chromia scale to reduce harmful CrO_3 and $CrO_2(OH)_2$ evaporation is being evaluated. The ability of chromite coatings to reduce evaporation from chromia-forming interconnect alloys is also being investigated.

Task 2: Fundamental Aspects of Thermomechanical Behavior (CMU)

Understanding the resistance of growing chromia scales to spallation requires a fundamental understanding of the mechanics of chromia adhesion. From a fracture mechanics standpoint, the adherence of protective oxide scales to alloy substrates is governed by 1) the stored elastic energy in the scale, which drives delamination, and 2) the fracture toughness of the alloy/oxide interface, which quantifies the resistance to fracture.

The stored elastic energy in the scale is increased by increases in the scale thickness (which can be measured by cross-section SEM) and increases in the residual stress in the scale. In this task, x-ray diffraction (XRD) is being used to measure stresses in chromia films formed on pure chromium and chromia-forming alloys after the exposures described for Task 1.

An indentation test is also being used to measure the fracture toughness of chromia/alloy interfaces for the same exposures. In the test, the chromia scale is penetrated by the indenter and the plastic deformation of the underlying substrate induces compressive radial strains in the substrate. These strains are transferred to the coating, and the associated coating stress drives the extension of a roughly axisymmetric interface crack. The interfacial toughness can be determined from the results of a mechanics analysis of the indentation problem and a measurement of the delamination radius.

SOFCs must be able to operate for very long periods of time (e.g., 40,000 h with hundreds of thermal cycles). Clearly, testing interconnect alloy modifications over this time period is not feasible, and accelerated testing protocols are needed. In addition to subjecting specimens to exposures at higher temperatures and increasing thermal cycle frequency, XRD and indentation are being used as accelerated testing techniques, yielding insight into scale durability after short exposure times.

Task 3: Alternative Material Choices

Metallic materials other than chromia-formers are being considered for use as low-temperature

SOFC interconnects. Experiments similar to those described for Task 1 are being performed on pure Ni. Its only oxide, NiO, has no vapor species with high partial pressures, and it has a higher electrical conductivity than chromia. NiO should not even form in the anode gas. In addition, low-CTE, dispersion-strengthened Ni is being considered. The alternatives being considered are dispersing Y_2O_3 or Li_2O in Ni. The latter would also provide a potential source of Li^{+1} cations to dope the NiO scale.

Low-CTE Fe-Ni alloys (Invar) are also being considered. Because the CTE of Invar is substantially lower than that of typical ceramic SOFC components, increasing Ni content may allow the interconnect CTE to be matched to that of SOFC ceramic components. Neither component of these alloys will form oxide in the anode gas.

Task 4: Development of Durable Contacting Material (WVU)

At present, candidate cermets have been developed by ball-milling of various oxide powders with silver or silver-oxide powders, followed by dry-pressing and sintering in a high-temperature furnace. The cermets are evaluated by SEM to determine the compatibility of silver with the candidate oxide materials, as well as the dispersion of silver throughout the cermet. The cermets are also tested for hardness/ductility using Vickers hardness testing. Conductivity is evaluated using a simple multimeter test. A thermomechanical analyzer is also used to evaluate the CTE of the materials to verify compatibility with other SOFC components. Lastly, cermets are placed in a high-temperature furnace to be exposed to the SOFC operating temperature (~800°C) while a high-volume air flow is introduced to simulate the cathode environment of the SOFC.

All measurements—conductivity, hardness, and mass—are taken before and after exposure to the simulated cathode environment in order to make a determination of the effects on the cermet material.

Results

Task 1: Mechanism-based Evaluation Procedures

The cyclic oxidation of a group of ferritic stainless steels has been evaluated under conditions pertinent to fuel cell operation. The alloys are (compositions in wt%):

- 22 Cr Ferritic (Fe-22 Cr-1 Mo-1 Si-2 Mn)
- E-BRITE (Fe-26 Cr-1 Mo)
- AL 453 (Fe-22 Cr-0.6 Al-0.3 Mn + 0.1 Ce/La)
- Crofer (Fe-22 Cr-0.5 Mn-0.08 Ti-0.016 P-0.06 La)
- ZMG 232 (Fe-22 Cr-0.5 Mn-0.4 Si-0.2 Al-0.22 Zr-0.04 La)

Cycle times of 1 hour were used, with exposure temperatures of 700°C and 900°C. The exposure environments included

- Dry air (simulated cathode gas)
- Air + 0.1 atm H_2O
- $Ar/H_2/H_2O$ (simulated anode gas) ($P_{O2} = 10^{-17}$ atm at 900°C and 10^{-20} atm at 700°C)

Exposure in air plus water vapor at 700°C and 900°C resulted in accelerated growth of chromia scales and accelerated oxide spallation from alloys that did not contain a reactive element (e.g., 22 Cr Ferritic). External layers of $MnCr_2O_4$ were observed to form on Crofer at 900°C. These may result in reduced oxide evaporation. Oxide growth rates were substantially lower at 700°C than at 900°C. Sigma phase was observed to form at 700°C in the alloys with higher chromium, Mo, and Si concentrations, e.g., 22 Cr Ferritic and E-BRITE. The sigma phase formation was more extensive in atmospheres containing water vapor. This phase must be avoided because it is very brittle and tends to crack.

It was found that even small amounts of Al or Si (less than 0.5 wt%) result in the formation of continuous alumina or silica films, which greatly increase the area-specific resistance (ASR). Therefore, future alloy development should hold these elements to the minimum values possible.

A major problem with chromia-forming alloys is oxide volatility as CrO_3, particularly in the cathode gas, since the CrO_3 partial pressure increases with oxygen partial pressure. The volatile species are reduced at electrochemically active sites on the cathode during SOFC operation, which inhibits the required oxygen reduction. Analysis of the Cr vapor species indicates that water contents above about

0.1% in air result in partial pressures of $CrO_2(OH)_2$ which exceed the partial pressure of CrO_3 and result in cathode poisoning. There are three potential solutions to this problem:

- Develop cathode materials that are not affected by Cr contamination.
- Suppress the evaporation of Cr species from ferritic alloys.
- Develop Cr-free materials with suitable interconnect properties.

The latter two approaches are being pursued in this research. Approach 3 is the basis for Task 3, described below.

Evaporation suppression can be accomplished by a dense coating of a material with greatly reduced Cr_2O_3 activity, e.g., $LaCrO_3$. In the past, samples coated with 5 m $La_{0.8}Sr_{0.2}CrO_3$ have either become porous after exposure or exhibited mudflat cracks during a pretreatment to improve the coating density. Both of these situations are undesirable because they can allow volatile gas species to form and escape. Some experiments have been done to gain a better understanding of the cracking phenomenon.

It has been proposed that there is a thickness relationship to the cracking in the coatings. Samples with coatings of 0.2, 0.8, 5.5, and 10 m were pretreated for 2 hours at 800°C in Ar-4% H_2 to validate this proposal. The two thicker coatings did indeed show profuse cracking during observation using scanning electron microscopy. While the 0.2 m and the 0.8 m thick coatings did not show vertical cracking, the chromia layers formed underneath them were significantly thicker. The 0.8 m coating also displayed large-scale delaminations of the outer coating layer (the coating was applied in two steps). Filling the cracks with La_2O_3 is being attempted.

Another way to reduce evaporation of Cr-containing species is to add an alloying element which will form a sealing layer over the chromia scale. Crofer 22 APU is known to form a $MnCr_2O_4$ layer on top of a protective Cr_2O_3 layer, which also hinders vaporization. The kinetics of development of this layer are being studied.

An ideal approach to suppressing Cr volatility would be to develop an alloy which forms a Cr-free oxide overlayer. Experiments on Ni-based superalloys indicated that Ti additions might provide such a layer. Four heats of novel Fe-Cr-Ti alloys and one Ti-free control heat were produced in a vacuum induction melting furnace in the form of fifty-pound ingots at ATI Allegheny Ludlum. The chemical composition of each ingot was determined at ATI Allegheny Ludlum's Analytical Services Laboratory (results reported in weight percent in Table 1).

Table 1. Chemical Compositions of Ingots of Four Novel Fe-Cr-Ti Alloys and One Ti-free Control Alloy (Wt%)

	Heat Identification Code				
Element	**RV 2103**	**RV 2104**	**RV 2095**	**RV 2096**	**RV 2097**
Cr	21.8	21.8	22.1	22.2	22.2
Ti	0.004	0.84	1.65	2.72	3.98
Mn	0.033	0.030	0.031	0.024	0.023
C	0.010	0.013	0.010	0.016	0.017
N	0.018	0.018	0.011	0.008	0.008
Ce	0.004	0.027	0.031	0.027	0.027
La	0.001	0.009	0.012	0.012	0.010
Al	0.005	0.005	0.008	0.030	0.049
Si	0.043	0.042	0.036	0.020	0.020

Extensive manufacturing trials were carried out to evaluate the processing characteristics of the high-Ti stainless steels. The ingots were successfully hot-rolled to 10 mm, surface-conditioned, and then cold-rolled to 1 and 2 mm thick for oxidation testing and mechanical/physical property determination.

Preliminary oxidation experiments indicate that these alloys can indeed form a continuous TiO_2 overlayer. A patent disclosure has been filed, and this approach will be vigorously pursued.

In attempts to reduce the growth rate of chromia and, therefore, the electrical resistance, E-BRITE samples have been doped with CeO_2 using pulsed laser deposition. Oxidation experiments for 100 hours at 800°C in air show that the doping drastically reduced the thickness of the chromia scale. Alternative deposition techniques for the dopant are also being considered. There are several tests that

will be done to determine the strength and lifetime of the effect.

Work is in progress to standardize the ASR measurement technique. Testing using the Pt paint method has shown agreement with measurements done at the National Energy Technology Laboratory on the same Crofer 22 APU sample exposed for 100 hours at 800°C in air. A sample exposed for 200 hours was also tested using this method and displayed a reasonable increase in ASR, but the Pt electrode area is in question. Testing is also being done using a lanthanum strontium cobalt oxide (LSCo) contact paste.

Task 2: Fundamental Aspects of Thermomechanical Behavior (CMU)

Indentation testing to determine the fracture toughness of chromia scale/alloy interfaces has been performed on 22 Cr Ferritic specimens exposed in wet air and simulated anode gas environments at 900°C. Specimens exposed in wet air for 100 hours and longer showed indentation-induced flaking of the chromia scale, indicative of a thin chromia scale and a non-uniform interfacial toughness. The size of the region experiencing debonding did not change with exposure. This behavior is consistent with weight gain measurements and observations via optical microscopy of spontaneous flaking of chromia scales in these specimens.

Specimens exposed in simulated anode gas showed peeling of a comparatively thick, intact chromia scale with an increase in debond size with exposure. This behavior is also consistent with weight gain measurements and observations of a thickening chromia scale remaining attached to the alloy. Fracture mechanics analysis of the indent problem, coupled with residual stresses measured by XRD and oxide thicknesses measured by cross-section SEM, yielded interfacial fracture toughness values for these specimens. Toughness values for a specimen exposed for 364 hours in simulated anode gas and oxide growth data have been used to predict that spontaneous spallation will occur at approximately 800 hours. This prediction is consistent with observations of specimens exposed for 800 hours and more.

Task 3: Alternative Material Choices

Experiments are being carried out on pure Ni as a possible alternative interconnect material, since the oxygen partial pressure in the anode gas is too low to oxidize Ni. The primary challenge in making Ni perform satisfactorily as an interconnect is to reduce the electrical resistance of the thermally grown oxide that forms on the cathode side during fuel cell operation.

Efforts to decrease the electrical resistance of the interconnect oxide are three-fold. First, we are trying to reduce the scale thickness by the use of surface dopants. Pulsed laser deposition is used to deposit thin films of SrO and CeO_2 onto the surface of nickel. Our tests have shown that these coatings decrease the thickness of NiO grown on Ni by over a factor of 2. ASR is proportional to scale thickness, and we expect the resistance to decrease accordingly.

Secondly, we are trying to reduce the resistivity of the NiO by alloying, using a Ni-5 wt% Cu alloy. Under the test conditions, NiO grows, but an appreciable amount of Cu is found in the scale. If the copper is ionized to the Cu^{+1} state, these ions dissolved in the scale should increase the conductivity of the scale.

Finally, the resistance introduced by the thermally grown oxide is being by-passed by the use of high-conductivity pathways. Silver is not considered as a possible interconnect material due to the high permeability of hydrogen and oxygen in silver, which causes water nucleation and mechanical instability. However, silver may be able to provide a high-conductivity pathway through another material. Systems in which silver wires are passed through nickel and silver powder is melted into holes drilled in nickel are being examined.

In addition to these tests, the mechanical stability of nickel under dual atmosphere conditions has been verified. In tests of up to 600 hours, the air/moist hydrogen conditions to which an interconnect is simultaneously exposed in a fuel cell did not affect the oxidation behavior of the Ni interconnects.

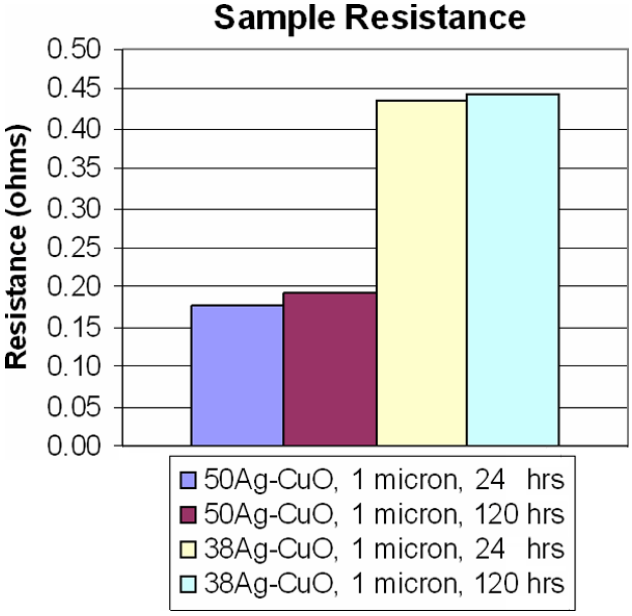

Figure 2. Resistance Comparison of Samples with Different Compositions

Task 4: Development of Durable Contacting Material (WVU)

The process of ball-milling powders and sintering in a high-temperature furnace has produced Ag-cermet samples exhibiting characteristics, specifically ductility and conductivity, that could be acceptable for use in the SOFC operating environment.

It has been observed that modification of the amount of silver used in the sample results in changes in the properties of the sample. When the amount of silver is increased, a decrease in the resistance of the cermet is observed, which is to be expected. The bar chart in Figure 2 illustrates the differences in resistance of samples made with different volume percents of silver and sintered for different durations. It is clear that the samples containing a higher volume percent of silver are much less resistive than those with lower levels of silver. It also appears that resistance of the samples is not a function of sintering time.

Initial experiments have shown little effect at the surface of the samples exposed to high-temperature and high-volume air flow. An example of the SEM analysis of an exposed sample is shown in Figure 3. Although these experiments were conducted under

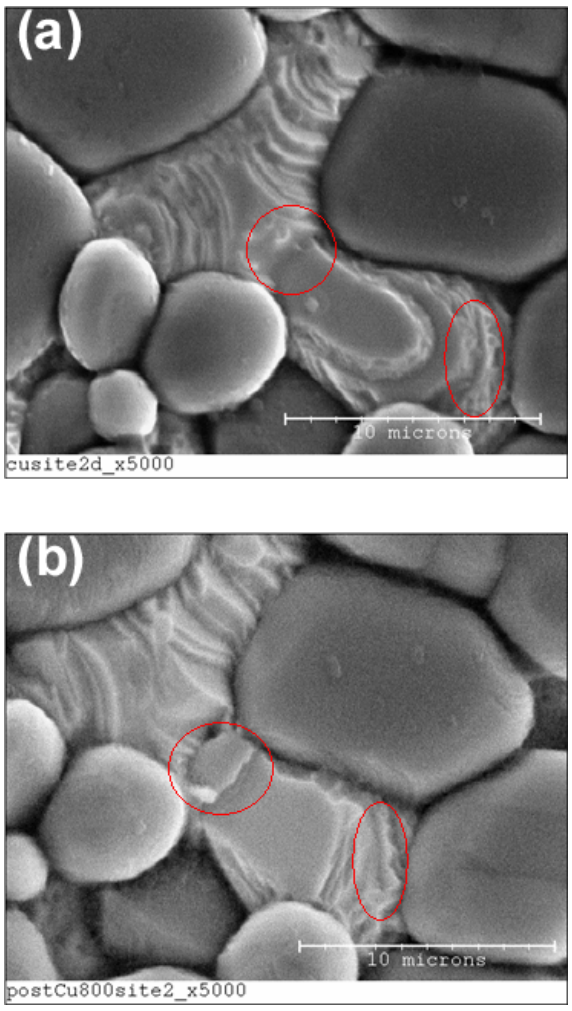

Figure 3. Comparison of Sample Before and After Exposure to a Simulated Cathode Environment

exaggerated air-flow conditions, the duration of the samples' exposure was very low (90 hours) relative to the target operating time of a conventional SOFC; therefore, further testing is needed.

To improve the properties of the material, evaluation of the effects of modifying parameters such as volume percent of silver, initial particle size, sintering time and sintering temperature are ongoing.

Conclusions

The aim of this project is to evaluate the chemical and thermomechanical stability of interconnect alloys in simulated fuel cell environments and to develop new contact materials. The oxidation of a group of ferritic stainless steels

has been characterized at both a typical operating temperature (700°C) and, to obtain more rapid results, at an elevated temperature (900°C). The development of ferritic stainless steels that form oxide overlayers to suppress chromia evaporation has yielded very positive results. X-ray diffraction and indentation fracture testing have been used to characterize the mechanical durability of chromia scales grown on interconnect alloys. In addition to providing insights into mechanisms causing chromia spallation, these test techniques offer an alternative means of accelerating oxidation testing. The understanding gained from these tests will be used to suggest ways to optimize the properties of ferritic alloys. A parallel study is being carried out to evaluate the potential use of alternate interconnect alloys, particularly those based on Ni.

Considerable progress is being made in the development of a suitable contacting material for the cathode chamber of the SOFC. Thus far, promising materials and processes have been developed to fabricate an appropriate sample material in terms of ductility and conductivity. The current processes are practical and inexpensive, making them a realistic option for use in future industry. Further testing is ongoing to verify that the materials in development will be appropriate for long-term use in industry.

FY 2005 Publications/Presentations

1. G. H. Meier, "Overview of Conductive Scale Growth", SECA Fuel Cell Workshop, Argonne National Lab., Argonne, IL, July, 2004.
2. G. H. Meier, "Oxidation of Ferritic Alloys for Interconnects in Solid Oxide Fuel Cells", ASM International, "Materials Solutions", Columbus, OH, October 2004.
3. J. L. Beuth, "Interfacial Fracture Testing to Investigate the Mechanics of SOFC Interconnect Alloy Durability," ASM Materials Solutions Conference, Columbus, OH, October, 2004.
4. S. J. Laney, F. S. Pettit, and G. H. Meier, "Reactive Evaporation of Cr_2O_3", Topical Report on SECA Award No. DE-FC26-02NT41578, Univ. of Pittsburgh, 2004.
5. G. H. Meier, "Fundamental Studies of the Durability of Materials for Interconnects in Solid Oxide Fuel Cells", SECA Workshop on Solid Oxide Fuel Cells, Tampa, FL, January 2005.
6. G. H. Meier, "Oxidation Problems in Solid Oxide Fuel Cells", presented at the 2005 ASM/TMS Spring Symposium; "Materials for Extreme Environments", presented at the GE Global Research Center in Niskayuna, NY, May 2005.
7. N. Dhanaraj, J. L. Beuth, G. H. Meier, F. S. Pettit, J. Hammer and S. Laney, "Interfacial Fracture Testing to Evaluate the Durability of SOFC Interconnect Alloys", paper accepted for the ASM Materials Science and Technology Conference and Exhibition, Pittsburgh, PA, September 2005.

III.A.21 Electrically Conductive, Corrosion-Resistant Coatings through Defect Chemistry for Metallic Interconnects

Anil V. Virkar
University of Utah
Department of Materials Science & Engineering
122 S. Central Campus Drive
Salt Lake City, UT 84112
Phone: (801) 581-5396; Fax: (801) 581-4816; E-mail: anil.virkar@m.cc.utah.edu

DOE Project Manager: Lane Wilson
Phone: (304) 285-1336; E-mail: Lane.Wilson@netl.doe.gov

Objectives

- To synthesize and characterize electronically conductive coating materials with ultra-low oxygen diffusion coefficient, using site-specific doping and through fundamental understanding of defect chemistry, for application on metallic interconnects in intermediate temperature (800°C) solid oxide fuel cells (SOFCs).
- To apply the coatings on low thermal expansion, relatively inexpensive stainless steels and other alloys, and investigate oxidation kinetics in air and fuel atmospheres.
- To conduct preliminary short stack (4-cell) test using 5 cm x 5 cm active area cells to validate ex-situ results.
- To initiate work on the development of low-cost processes for the deposition of the coatings on metallic interconnects.
- To offer coated interconnect foils to the Solid State Energy Conversion Alliance (SECA) vertical teams under suitable confidentiality agreements.

Approach

- Conduct literature search to identify suitable perovskite and non-perovskite materials exhibiting high electronic conductivity but very low oxygen ion conductivity. Non-perovskite materials of interest include spinels and bronzes.
- Synthesize perovskite oxides with transition element on the B-site, with site-specific doping to suppress oxygen vacancy concentration.
- Fabricate sintered bars and discs of the materials. Sintered bars will be used for the measurement of total conductivity as a function of temperature. Discs will be used for measuring ionic conductivity using electron-blocking electrodes.
- Deposit thin coatings of the materials on stainless steels and nickel-based alloy foils, and investigate oxidation kinetics.
- Conduct theoretical analysis of oxidation kinetics of coated and pristine alloys.
- Develop a method for the measurement of area-specific resistance (ASR), and apply it to the foils oxidized under various conditions.

Accomplishments

- Identified a number of materials with low oxygen ion conductivity (possibly lower than 10^{-7} S/cm at 800°C) by taking into account ionic size effect.
- Fabricated $LaMnO_3$-based materials with dopant level as high as 20% on the B-site to suppress oxygen ion conductivity.

- Measured total conductivity over a temperature range from room temperature to 800°C, and measured oxygen ion conductivity at 800°C.
- Sputter-deposited 1- and 3-micron coatings of various materials on Haynes 230, Inconel 718, and SS 430.
- Conducted preliminary oxidation studies in air up to 28 days at 800°C.
- Examined oxide scale formed and measured its thickness on coated and pristine materials for oxidation times up to 28 days.
- Measured total ASR of the coated and pristine samples after oxidation. It was observed that the pristine samples exhibited significant oxidation. However, even samples with as small as 1 micron coating were highly resistant to oxidation.

Future Directions

- Deposit coatings of thicknesses up to 5 microns on both sides of the foils, and evaluate performance in air, fuel, and dual atmospheres.
- Measure ASR on coated and pristine foils subjected to various oxidative treatments.
- Develop theoretical models for oxidation kinetics and verify the models experimentally.
- Conduct a short stack test with the best coating material, as determined by ex-situ oxidation studies.

Introduction

Planar SOFC stacks are preferred over their tubular counterpart due to compact design, higher power and energy density, and projected lower cost. However, planar SOFC stacks require interconnects or bipolar plates to keep fuel and oxidants separate and to electrically connect adjacent cells. From the standpoint of cost and ruggedness, metallic interconnects are preferred. However, metallic interconnects of choice are stainless steels or nickel-chromium-based alloys, which are prone to oxidation. The oxide scale formed increases the ASR, which adversely affects the SOFC performance and efficiency and thus, in balance, also adversely affects the cost. The potential remedy is the development of either baseline alloys that are oxidation-resistant, or suitable coating materials which can suppress oxidation kinetics. From the standpoint of cost and practicality, the preferred approach is the development of suitable coating materials.

To date, several coating materials have been tried, with varying degrees of success. The approach, however, has not been systematic, and it has relied on trial and error. As a result, most of the coatings used to date were very thick (several or several tens of microns). This increases the potential for spalling, which is undesirable. The approach selected in this work is based on fundamental chemistry of materials and has the potential to develop coatings that are adherent and very thin (typically less than 5 microns, and maybe as thin as 1 micron), and yet can suppress oxidation kinetics to greater than 40,000 hours of operating life.

Approach

Possible coating materials are perovskites with a transition metal, capable of exhibiting multiple valence states. An example is $LaMnO_3$. The approach involves doping a material such as $LaMnO_3$ (LM) with suitable elements, which tends to suppress oxygen vacancy concentration, without significantly reducing electronic defect concentration. Powders of various coating materials, doped appropriately, are made. Samples of the materials are made by sintering. Two types of electrical tests are performed: (a) measurement of total electrical conductivity and (b) measurement of oxygen ion conductivity using blocking electrodes. Thin coatings (1 to 5 microns) are then deposited on foils of various alloys. For the initial investigation, Haynes 230, Inconel 718, and SS 430 were the alloys selected. The coated and uncoated foils are subjected to air and fuel for various periods of time and over a range of temperatures, up to ~800°C. Samples are oxidized for various periods of time, up to a maximum of six months. The oxide scale thickness is measured using scanning electron microscopy (SEM). The observed kinetics of oxidation is compared with the theoretical models developed. The ASR of the samples is also measured as a

function of time of oxidation, with measurements conducted over a range of temperatures. Finally, a short stack will be tested using coated interconnects exhibiting the best properties.

Results

Identified a number of possible perovskite and non-perovskite materials with potential for good electronic conductivity and low oxygen ion conductivity. This was achieved using crystal chemistry considerations. Criteria based on ionic size were used to identify materials with low oxygen vacancy mobility. Criteria based on defect chemistry were used to identify materials with low oxygen vacancy concentration.

Samples of perovskite and non-perovskite structures were fabricated in the form of discs and bars. Total electrical conductivity, which is mainly electronic, was measured over a range of temperatures using a four-probe DC method. Figure 1 shows the total conductivity measured as a function of temperature (Arrhenius plot) on several prospective coating materials. The lowest measured value was ~4 S/cm, which shows that the ASR is expected to be low.

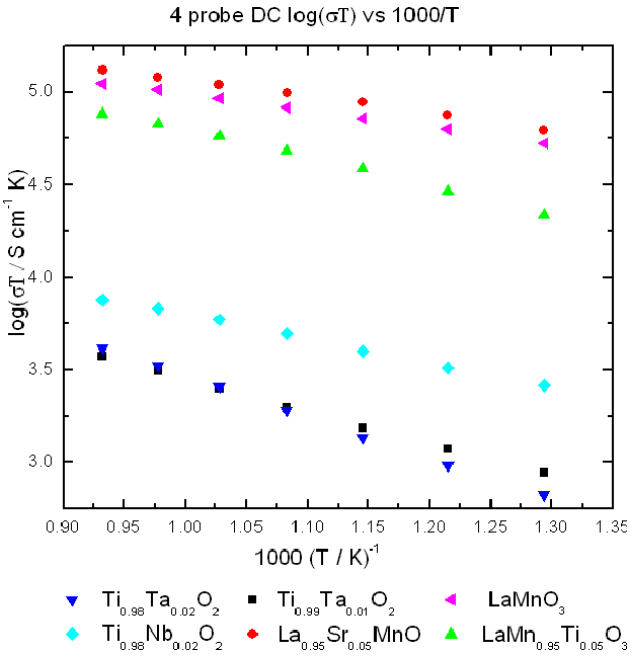

Figure 1. Arrhenius plots of conductivity of a number of coating materials. The total conductivity is predominantly electronic, with oxygen ion conductivity orders of magnitude lower.

Tri-layer, sandwich samples comprising a disc of the material of interest sandwiched between two YSZ discs were fabricated. The YSZ discs serve as electron-blocking electrodes. It is important that the interfaces are well-formed, free of defects such as cracks. Figure 2 shows an SEM image of one of the

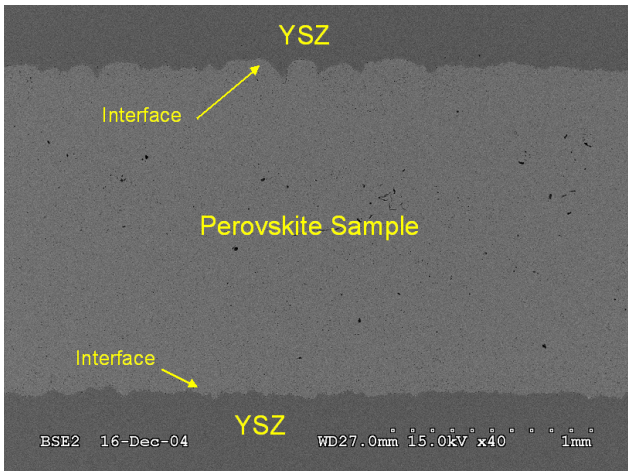

Figure 2. An SEM image of the tri-layer structure comprising a perovskite sample sandwiched between two YSZ discs, the latter serving as electron-blocking electrodes. Note the well-bonded interfaces.

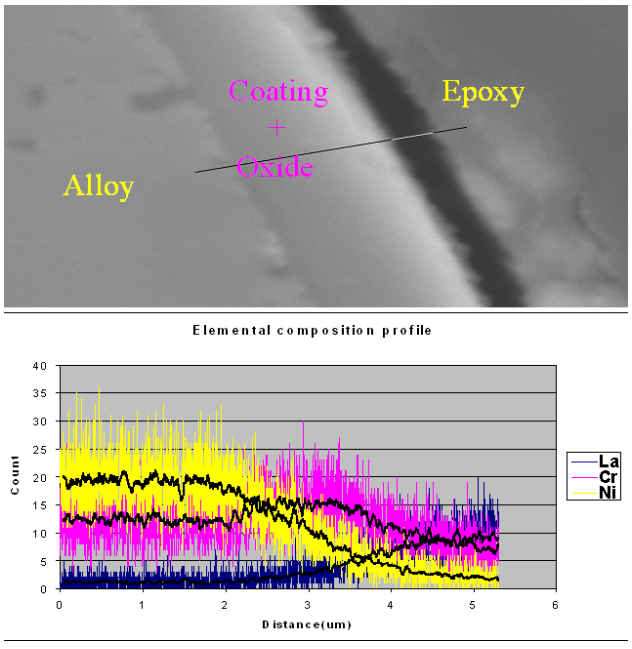

Figure 3. Composition profiles of elements La, Cr, Ni across metal-oxide layer-coating interface. Metal on left side, coating on right side, and oxide layer in the center.

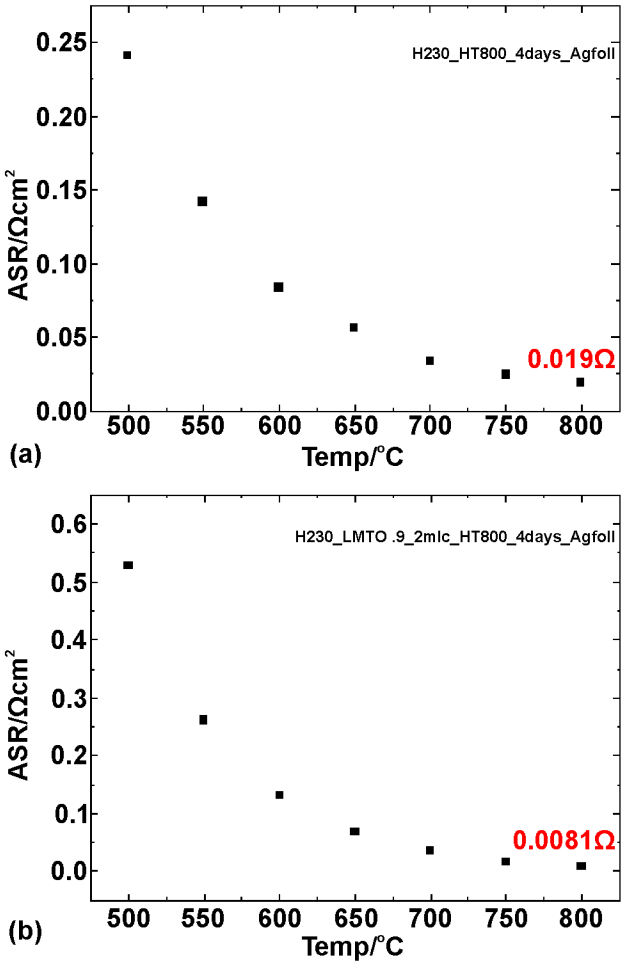

Figure 4. Plots of ASR vs. temperature for (a) Uncoated H230 alloy foil, (b) LMT0.9 coated H230 alloy foil oxidized at 800°C for 4 days. The ASR values at 800°C are highlighted in red. Note that the ASR of the coated alloy foil is less than half that of the uncoated foil at 800°C.

tri-layer samples. Using the blocking electrode method, preliminary measurements of oxygen ion conductivity have been made. The lowest value measured at 800°C is ~10^{-7} S/cm, which is satisfactory. Experiments on other coating materials are underway to identify materials with even lower oxygen ion conductivity.

Successfully deposited a number of coating materials on foils of several alloys. The thickness of the coatings was varied between 1 and 3 microns.

Coated and pristine samples were subjected to oxidation studies. It was observed that coated foils exhibited very low oxidation kinetics. The oxide scale was typically about a micron in thickness even after three weeks at temperature. The oxide scale formed under the coating. The coating was strongly adherent, especially on the nickel-based alloy foils. Figure 3 shows an SEM image of a foil of H230 with a protective coating, and an oxide scale formed under the coating. Also shown in the figure is the chemical analysis conducted using energy dispersive x-ray.

ASR was measured over a range of temperatures on as-received foils and coated foils after oxidative treatments. Figure 4 shows the results of ASR measurements on uncoated and coated H230 foils after oxidation in air at 800°C for 4 days. It is seen that the coated foil exhibits ASR at 800°C less than half that of the uncoated foil.

Conclusions

Defect chemistry plays a major role in oxygen ion transport through oxides, and thus determines the suitability of a given material as a coating. Coating materials based on $LaMnO_3$ (perovskite) and TiO_2 (non-perovskite) were successfully made.

Electronic and ionic conductivities of coating materials are in accord with defect chemistry, and that defect chemistry provides a scientific basis for the design of oxidation-resistant coatings.

High-quality, strongly adherent coatings can be sputter deposited. The resulting foils exhibit improved oxidation resistance over the baseline foils. Even after several days at 800°C, the coating continues to remain well-bonded.

Coated foils also exhibit much lower ASR as compared to pristine foils.

III.B Fuel Processing

III.B.1 Technology Development in Support of SECA

Michael Krumpelt (Primary Contact), Di-Jia Liu
Argonne National Laboratory
Argonne, Illinois 60439
Phone: (630) 252-8520; Fax: (630) 252-4176; E-mail: krumpelt@cmt.anl.gov

DOE Project Manager: Magda Rivera
Phone: (304) 285-1359; E-mail: Magda.Rivera@netl.doe.gov

Objectives

- Improve the thermal stability of reforming catalysts for diesel fuel.
- Improve the sulfur tolerance of the catalysts.
- Determine long-term stability.

Approach

- Synthesize and characterize perovskites that are stable in hydrogen and oxygen and have redox chemistry on the "B" site.
- Explore the effects of different dopants on the A and B sites.
- Verify that the doped catalysts are chemically and thermally stable and relatively unaffected by sulfur-containing fuel.

Accomplishments

- The new perovskite catalysts were shown to remain single phase in both reducing and oxidizing conditions, proving that the catalysis is occurring by redox chemistry on the B site and not on small metallic particles supported on an oxide matrix.
- The effect of 50 ppm of dibenzothiophene in dodecane was shown to be minimal.

Future Directions

- Optimize the composition of the catalysts in terms of cost, sulfur tolerance, and activity for aromatics, aliphatics and other diesel components.
- Determine the long-term stability.
- Work with a private-sector organization on scaling up the process.

Introduction

Auxiliary power units (APUs) for heavy-duty vehicles could reduce emissions and conserve fuel on the North American continent, where engines are kept running while drivers rest. An APU must have enough power to keep the cabin air-conditioned or heated in hot or cold climatic conditions, respectively, and may have to also supply electricity for refrigeration of loads. The amount of fuel needed will be significant, and drivers may resist having to refuel the APU with anything other than the diesel fuel used for the engine.

Converting diesel fuel into a hydrogen-rich gas that is suitable for solid oxide fuel cells is more challenging than converting gasoline because of the multi-cyclic aromatics and the aromatic sulfur

compounds in diesel fuel. To break down these compounds, the operating temperature of the reformer needs to be raised, and the reforming catalyst needs to have a significant tolerance for sulfur. In making these statements, it is assumed that an autothermal reactor (ATR) [1] is used and that the diesel fuel is not desulfurized at the refinery.

When the operating temperature of the ATR exceeds about 800°C, catalyst stability becomes an issue. Noble metal catalysts such as rhodium, palladium or platinum on alumina or ceria not only lose some activity due to adsorption of hydrogen sulfide on the metal surface, but are further affected by evaporation and consolidation of the metal.

Approach

In earlier work, we noticed that noble metals interact with supports containing oxide ion vacancies to form noble metal ions, which facilitate the oxidation of the hydrocarbon molecules. In this project, we extended the concept to perovskite matrices. The latter are ternary oxides of the general composition ABO_3, where the "A" cation is either a rare or an alkaline earth element and the "B" cation is a three- or four-valent transition element. The bipolar plate material $LaCrO_3$ and the cathode material $LaMnO_3$ in solid oxide fuel cells are typical examples of perovskites. Since the catalyst has to be stable in oxidizing as well as reducing conditions, we chose $LaCrO_3$ and $LaAlO_3$ as host lattices. By substituting a small amount of an element that can undergo redox chemistry on the "B" site, we were hoping to facilitate the autothermal reforming reactions. Such catalysts would be expected to be more thermally stable than finely dispersed noble metals on alumina.

As reported last year, ruthenium doped into either the chromite or aluminite matrix proved successful. To verify that the ruthenium was in fact substituted for the chromium on the B site and not present as ruthenium oxide or metal on the surface of the perovskite, we used synchrotron x-ray spectroscopy, as shown in Figure 1.

The effect of sulfur species on the activity of the catalyst was determined by adding 50 ppm of dibenzothiophene to the fuel.

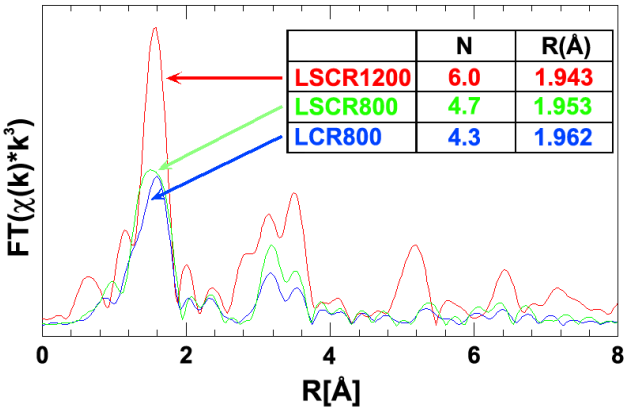

Figure 1. Radial Distribution Functions Obtained from k^3 Weighed Fourier Transformation of Extended X-ray Absorption Fine Structure Spectra for $La_{0.8}Sr_{0.2}Cr_{0.95}Ru_{0.05}O_3$ Calcined at 1200°C (LSCR1200), $La_{0.8}Sr_{0.2}Cr_{0.95}Ru_{0.05}O_3$ Calcined at 800°C (LSCR800) and $LaCr_{0.95}Ru_{0.05}O_3$ Calcined at 800°C (LCR800), Respectively

Results

Figure 1 shows the radial distributions around the ruthenium ions for two different samples of $La_{0.8}Sr_{0.2}Cr_{0.95}Ru_{0.05}O_3$, one sintered at 800°C and the other at 1200°C. A third sample does not contain strontium on the A site but still contains 5% Ru on the B site. The first coordination shell is at a radius of 1.943 to 1.962 in Angstrom units and consists of oxygen ions. The sample sintered at 1200°C has a coordination number of 6, as one would expect for a perovskite lattice. The samples sintered at 800°C have coordination numbers of 4.3 and 4.7, an indication that the structure is not fully developed at the lower sintering temperature.

A secondary coordination shell is at a radius of about 2.6 Å. It corresponds to the lanthanum ions occupying the A site of the perovskite.

These results are significant in proving that the catalytic activity is associated with individual ruthenium ions rather than ruthenium oxide or ruthenium metal grains decorating the surface of the perovskite. Such single-atom catalysis is novel. To illustrate how the catalysis works, we refer to Figure 2a, showing the perovskite crystal structure, and Figure 2b, illustrating the reforming mechanism. The surface oxygen that is adjacent to the ruthenium

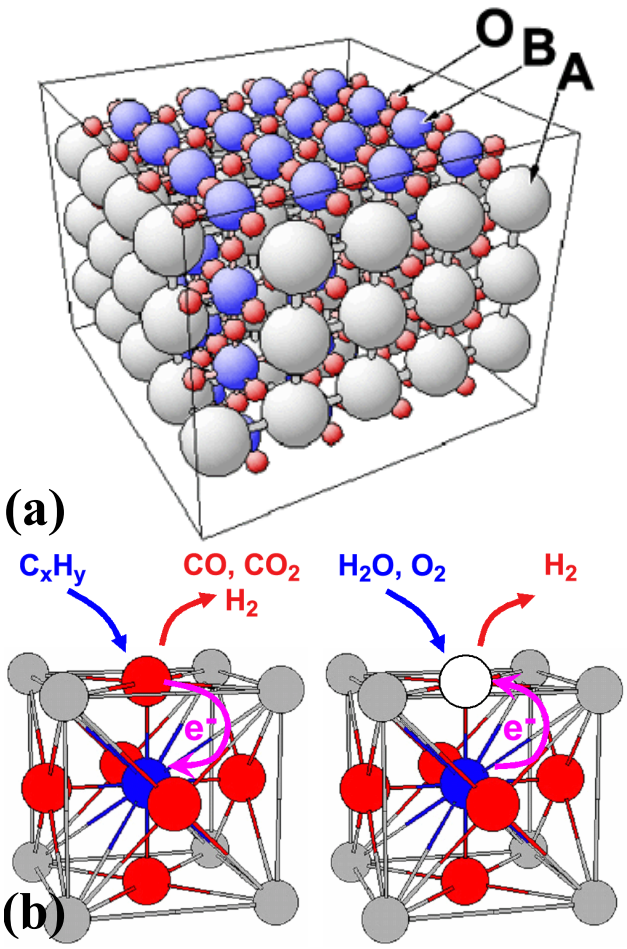

Figure 2. (a) Perovskite Lattice Structure.
(b) Mechanism of Hydrocarbon Reforming

ion in the center of the cube is more weakly bonded than the oxygen next to chromium (not shown). These oxygen ions react nucleophilicly with the hydrocarbon molecules in the gas phase, leaving an oxide ion vacancy and a ruthenium atom in a zero oxidation state.

The vacancy is then filled with an oxygen from the gas phase, and ruthenium is re-oxidized, restoring the catalyst to its original state.

To investigate sulfur tolerance, we conducted a 100-hour aging test using a dodecane/dibenzo-thiophene fuel mixture containing 50 ppm of dibenzothiophene. The experiment was carried out at 800°C at a gas hourly space velocity of 50,000 hr^{-1}. Shown in Figure 3 are the plots of reforming efficiency and COx selectivity obtained during the study. No appreciable decrease was observed.

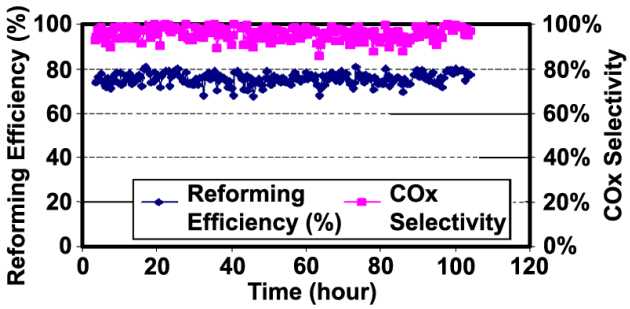

Figure 3. Reforming Efficiency and COx Selectivity Obtained during 100-hour Aging Test of $LaCr_{0.95}Ru_{0.05}O_3$ at $H_2O/C = 1.5$, $O_2/C = 0.5$ and GHSV = 50,000 hr-1

Conclusions

The ruthenium-doped chromites and aluminites have been shown to be excellent catalysts for the autothermal reforming of hydrocarbons. Unlike conventional catalysts, the active site is imbedded into a stable matrix. No metal surfaces are exposed to the gas stream, and adsorption of sulfur species is minimal, as hoped. Long-term stability still needs to be established.

References

1. D-J. Liu, M. Krumpelt, H.-T. Chien, and S.-H. Sheen, Proceedings of ASM Materials Solutions Conferences, Columbus, OH, October 18-21, 2004, ASM International.

FY 2005 Publications/Presentations

1. D.-J. Liu, M. Krumpelt, H.-T. Chien, and S.-H. Sheen, Proceedings of ASM Materials Solutions Conferences, Columbus, OH, October 18-21, 2004, ASM International.
2. "Diesel Reforming for Solid Oxide Fuel Cell Application", D.-J. Liu, S.-H. Sheen, and M. Krumpelt, Presented at the SECA Core Technology Peer Review Workshop, Tampa, FL, January 27-28, 2005.

III.B.2 Development of Ni-Based Sulfur-Resistant Catalyst for Diesel Reforming

Gunther Dieckmann
Chevron Energy Research and Technology Company
100 Chevron Way
Richmond, CA 94802
Phone: (519) 242-2218; Fax: (510) 242-2823; E-mail: ghdi@chevrontexaco.com

DOE Project Manager: Magda Rivera
Phone: (304) 285-1359; E-mail: Magda.Rivera@netl.doe.gov

Objectives

- Reform real sulfur-containing diesel fuels under minimum recycle conditions to produce hydrogen and carbon monoxide for use in solid oxide fuel cells.
- Test utility of radio frequency coke suppression in preventing catalyst aging when reforming diesel fuel containing 50 ppm sulfur.
- Determine the maximum sulfur concentration that the catalyst can handle.
- Develop a commercially viable low-cost sulfur-resistant reforming catalyst.
- Demonstrate that the catalyst can reform a real diesel fuel in long-term aging tests for greater than 3000 hours (in Phase II if approved).

Approach

- Reform a low-sulfur diesel fuel using Chevron's sulfur-resistant reforming catalyst under a minimum recycle gas rate of only 20%. Determine if the catalyst activity is acceptable.
- Increase the sulfur content of the fuel until the catalyst's reforming activity is "strained". In other words, develop a rapid aging test.
- Apply radio frequency coke suppression to improve activity or catalyst life, and then determine the optimum frequency and field strength.
- Optimize the catalyst formulation (in Phase II if approved).
- Perform long-term aging tests in Phase II.

Accomplishments

- Determined that Chevron's low-cost Ni-based reformer catalyst can readily reform a low-sulfur diesel fuel of the type that will be on the market in the United States in 2006.
- Established that 50 ppm S diesel fuel reduces the activity of the catalyst and decreases catalyst life. Coking appears to be leading to catalyst deactivation.
- Demonstrated that Chevron's Ni-based reformer catalyst can adsorb greater than 95% of the sulfur in the feed for the first 1 to 2 hours following regeneration. A two-bed system could be installed to desulfurize/ reform low sulfur containing feeds so that the current sulfur-sensitive anode catalyst system can still be used.
- Radio frequency coke suppression appears to improve catalyst activity.

Future Directions

- Continue radio frequency coke suppression experiments.
- Select the most advantageous sulfur-resistant reforming catalyst formulation. If possible, prepare the catalyst in a monolith form.
- Conduct long-term, 3000 hr, aging tests using the optimized catalyst formulation with a real diesel fuel.

Introduction

For diesel, jet or gasoline fuel to be used in a fuel cell, the liquid hydrocarbon fuel must first be reformed into hydrogen and carbon monoxide. Typically, the hydrocarbon fuel is first mixed with a limited amount of air and, in some systems, a small amount of off-gases from the anode of the fuel cell stack to supply steam. The resulting mixture is then passed over a nickel or platinum group metal catalyst to produce hydrogen and carbon monoxide, which are then sent to the fuel cell stack to produce electricity. Reformer catalysts based on low-cost nickel are preferred because they are cheaper to manufacture and more durable than platinum group metal catalysts. Unfortunately, even sub part per million levels of sulfur in the fuel can poison most reformer catalysts, resulting in a product stream with a high concentration of partially reformed hydrocarbons that will coke or foul most anode catalysts used in fuel cell stacks.

Thus, Chevron, Argonne National Laboratory, and the National Energy Technology Laboratory at Morgantown are developing Ni-based (low-cost) reforming catalysts that can tolerate the levels of sulfur found in reformulated gasoline or in low-sulfur 2006 diesel fuel. Developing a sulfur-resistant reforming catalyst is a far better approach than trying to adsorb the complex sulfur compounds found in the various fuels in a separate system prior to reforming, since most sulfur compounds found in severely hydrotreated diesel are not easily adsorbed, and many of the proposed adsorbents are pyrophoric. The Chevron catalyst has the ability to reform heavy hydrocarbons (including aromatics) found in diesel fuel while also adsorbing sulfur. After reforming, the feed sulfur is transformed into hydrogen sulfide, which can be easily adsorbed. This type of dual functional catalyst is currently needed, since the anode catalysts in solid oxide fuel cells and molten carbonate fuel cells are also based on nickel and are poisoned by sulfur. In the future, if sulfur-resistant anode catalysts are successfully developed, the requirement for sulfur adsorption can be dropped; however, the reforming catalyst will still need to resist sulfur poisoning.

Approach

We have found that the most serious problem with development of a sulfur-resistant reforming catalyst is coking, and that Ni-based catalysts tend to coke more than platinum group metal-based catalysts. However, Ni-based catalysts are preferred not only because they are significantly cheaper, but also because they are more durable. Both of these issues are critical in ultimately developing a viable auxiliary power unit with a cost of less than $400/kW. Not only does coke block catalytic sites, leading to the production of undesirable heavy hydrocarbons that will coke or foul anode catalysts, it also leads to aging of the catalyst due to metal stripping. To minimize coke production on the catalyst, we first focused on optimizing the pilot plant design, introduced the use of detergents in the fuel to prevent fuel pulsing in the orifice [1], and applied a radio frequency electromagnetic field to the reformer catalyst bed to suppress metal-catalyzed coking [2]. Most of Phase I of this project is aimed at understanding the frequency and electric field strength effects on reforming catalyst activity and life. Phase II of this project (if approved) will be directed towards optimizing the catalyst formulation (there are a number of competing formulas), developing a monolith version of the catalyst, and performing a long-term (3000+ hours) aging test.

Results

Our first achievement was to demonstrate that a real 7 ppm sulfur containing diesel fuel purchased at a filling station was easily reformed over Chevron's Ni-based reformer catalyst at an oxygen-to-carbon ratio of 1.0 using a minimum simulated 20% recycle

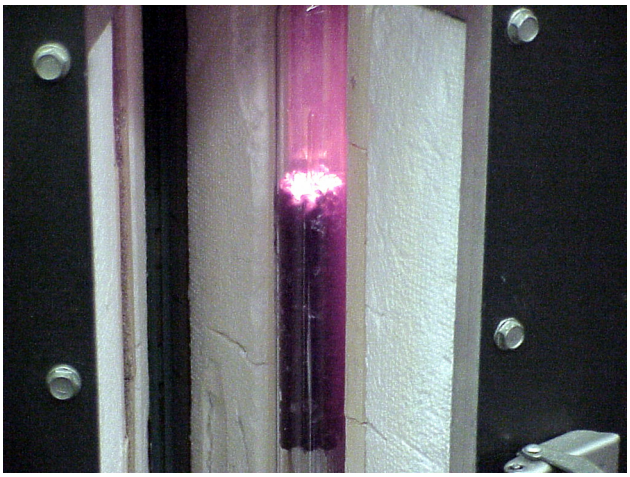

Figure 1. Low-Sulfur Diesel Is Reformed over Chevron's Catalyst

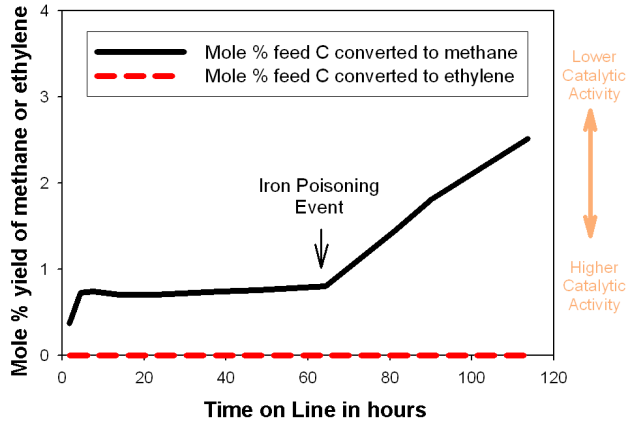

Figure 2. Catalytic Activity of Chevron's Catalyst Reforming a 7 ppm S Diesel Fuel

stream consisting of steam in nitrogen gas (H_2O-to-C ratio of 0.2). This fuel is representative of a low-sulfur diesel fuel that will be available in the U.S. market in 2006. Figure 1 shows the flame front of the reformer catalyst bed. In order to maximize performance, it is absolutely critical that this flame front remain steady and even with time. Figure 2 shows the yield of methane and higher hydrocarbons as a function of time on line. Chevron's sulfur-resistant catalyst easily reformed the fuel, producing only a tiny amount of methane. No higher hydrocarbon species such as ethylene, propylene or higher were produced that could potentially foul an anode catalyst in a fuel cell stack. The reformer catalyst appeared very stable for at least the first 60 hours. It is important to understand that the catalyst was regenerated every 8 to 10 hours by stopping the

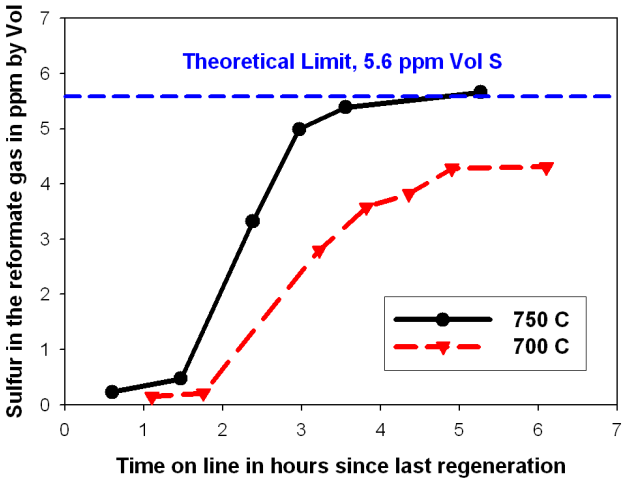

Figure 3. Concentration of Sulfur in the Reformate Gas Stream from Reforming a 50 ppm S Diesel Fuel at Two Different Temperatures

feed and allowing the air to burn off any deposited coke, as well as strip away the adsorbed sulfur as SOx. Chevron's catalyst was then rapidly activated (i.e., the Ni was reduced) in a matter of seconds once the fuel was started again. There was a one-time incident at around 60 hours on line, where iron was accidentally deposited onto the front part of the catalyst bed (360 ppm Fe). This resulted in deactivation of the catalyst due to metal-catalyzed coking. Apparently, under these low steam conditions, iron makes coke (at least on this particular catalyst). It is not clear at this point in time if the other alternative sulfur-resistant reforming catalysts will be as sensitive to iron poisoning. As a consequence, the pilot plant was rebuilt to remove any potential source of iron. In real commercial reformers, great care will need to be taken in selecting metallurgy [3] and in process design to avoid upstream metal-catalyzed coking incidents that may deposit iron on the reformer catalyst if this turns out to be a general problem.

Given the early success of reforming a real low-sulfur diesel fuel, the project objectives were modified to focus on reforming a higher 50 ppm S diesel fuel with and without radio frequency coke suppression.

Figure 3 shows the concentration of sulfur (as hydrogen sulfide) in the reformate gas produced at 750°C or 700°C by reforming a 50 ppm S diesel fuel over slightly aged (50 hours) Chevron catalyst. This

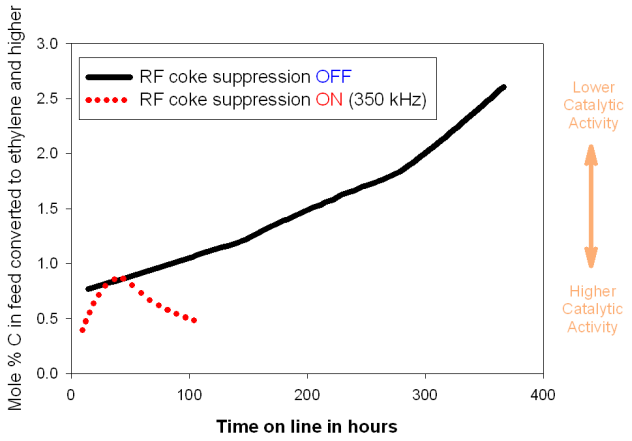

Figure 4. Catalytic Activity and Aging of Chevron's Catalyst Reforming a 50 ppm S Diesel Fuel with and without Radio Frequency (RF) Coke Suppression

graph shows that for the first 1 to 2 hours, greater than 95% of the sulfur is adsorbed by the catalyst. Past this point in time, the adsorptive capacity is reached. Since the breakthrough curve should be a function of the sulfur content of the fuel, a real 2006 diesel fuel with less than 15 ppm S should show sulfur breakthrough after more than 6 hours on line. It is interesting to note that the Chevron catalyst continues to reform the diesel fuel long after sulfur has broken through the bed, indicating that the two functions are separate.

Figure 4 shows that reforming a 50 ppm sulfur containing feed in contrast to 7 ppm S fuel (see Figure 2) produces non-methane hydrocarbons (such as ethylene, propylene, and higher) that have the potential of fouling Ni-based anode catalysts in solid oxide fuel cells, and that the concentration of these compounds increases as a function of time as the catalyst ages. However, if the catalyst bed is exposed to a radio frequency field of 350 kHz, the amount of coke produced on the catalyst is dramatically reduced, and for the short period of time that we have run the current experiment, it appears to be yielding beneficial results. We will need to run the experiment for the full 300 to 400 hours to be really certain if radio frequency coke suppression is working.

Conclusions

Chevron's current sulfur-resistant reformer catalyst is capable of reforming low-sulfur reformulated gasoline and low-sulfur diesel fuels that are available or will soon be available in the United States and Europe. When fresh, Chevron's catalyst can be used to adsorb the sulfur from the feed to produce very low sulfur (<0.20 ppm vol) reformate gas that can be fed directly to a solid oxide fuel cell with a Ni-based anode catalyst.

FY 2005 Publications/Presentations

1. "Development of Ni-Based Sulfur Resistant Catalyst for Diesel Reforming", G. H. Dieckmann, Presented at the SECA Core Technology Peer Review Workshop, Tampa, Florida, January 27, 2005

References

1. U.S. Patent 6,660,050
2. U.S. Patent 6,790,547
3. U.S. Patent 6,803,029

III.B.3 Integrated Injection and Mixing Systems for Diesel Fuel Reforming

Chien-Pei Mao
Goodrich Turbine Fuel Technologies
811 4th Street
West Des Moines, Iowa 50265
Phone: (515) 271-7291; Fax: (515) 271-7296; E-mail: Chien-Pei.Mao@goodrich.com

DOE Project Manager: Don Collins
Phone: (304) 285-4156; E-mail: Donald.Collins@netl.doe.gov

Subcontractors:
NASA Glenn Research Center, Cleveland, Ohio

Objectives

- Develop reliable, cost-effective diesel fuel injection and mixing concepts for auto-thermal reformer (ATR) and catalytic partial oxidation reformer (CPOX) for use with solid oxide fuel cell (SOFC) auxiliary and distributed power generation systems
- Determine operating/performance limitations of various injection and mixing concepts for diesel fuel reforming
- Establish coke-tolerant fuel injection and mixing systems at minimal inlet pressures
- Perform design optimization for cost reduction and swiftly transition the injection technology to the Solid State Energy Conversion Alliance (SECA) industry teams

Approach

- Design and fabricate four promising injector concepts for performance evaluation
- Investigate various mixing devices and chamber configurations for the most uniform distribution of mixture temperature, velocity and concentration
- Characterize key flow field parameters using thermocouples and advanced laser diagnostic techniques, including statistical laser extinction tomography, Raman spectrometry and phase Doppler interferometry
- Utilize computational fluid dynamics (CFD) and finite element analysis (FEA) tools to analyze injector/mixer flow field structure and temperature distribution to help mitigate problems of auto-ignition, injector coking and carbon formation

Accomplishments

- Constructed a steam/hot air test rig for injector/mixer performance development and flow field characterization
- Completed the design and fabrication of two multipoint impingement injectors
- Completed the design and fabrication of two single-point gas-assisted injectors
- Completed the design and fabrication of two high-energy piezoelectric injectors
- Conducted CFD and FEA analyses for the above three injector/mixer concepts
- Developed an effective piezoelectric driver for investigation of both continuous and pulsed fuel injection applications
- Tested and refined mixing chamber configurations for each injector concept to achieve uniform feed stream distributions for optimal reformer performance

Future Directions

- Finish design and fabrication of a pre-heating simplex injector for performance evaluation
- Complete high temperature rig tests and laser diagnostics for the remaining injector/mixer concepts
- Compare performance data for all four injection concepts and down select the most promising design for various diesel fuel reforming applications
- Utilize statistical design-of-experiment techniques to establish correlation equations for the most promising injector concept
- Investigate effect of spray pulsation on mixture pattern, circumferential uniformity and temperature distribution
- Incorporate carbon-tolerant design features to enhance injector/mixer service life

---

Introduction

Fuel processors are a very important component of SOFC systems, enabling them to compete with other auxiliary power units (APU) in remote stationary and mobile power generation markets. Current state-of-the-art fuel processors are limited to using gaseous fuels, such as natural gas, hydrogen and liquefied petroleum gas (LPG). In the near term, however, liquid hydrocarbon fuels are the preferred choice for SOFC power systems because of their availability and existing distribution networks.

Currently, the liquid fuel reforming technology is not yet viable for commercial applications. One of the major technical barriers for liquid fuel processing is reactor durability. The performance of the reforming catalysts quickly deteriorates as a result of carbon deposition, sulfur poisoning and loss of precious metals due to sintering or evaporation at high temperatures. To mitigate these problems, numerous studies are being conducted to optimize catalyst materials and reactor design/operation.

One of the engineering approaches that could immediately offer some benefits towards alleviating problems associated with liquid fuel reforming is to improve feed stream preparation. Poor feed stream preparation such as inadequate atomization, wall impingement, and non-uniform mixing could easily lead to local conditions which favor carbon deposition and formation of hot spots in the reactor. Because liquid fuels are difficult to reform, a proper selection of injection and mixing systems for feed stream preparation plays an essential role in the development of reliable and durable liquid fuel processors.

Approach

In a typical ATR and CPOX reactor, liquid fuel is injected into preheated steam and/or air streams near the top of a mixing chamber. The liquid fuel must evaporate and be thoroughly mixed with the surrounding steam and air within a short distance prior to entering the catalytic reactor. During operation, the injection and mixing system must be able to accommodate varying power demands in a relatively short response time. In most mobile APU applications, there are very limited inlet pressures available for liquid atomization and feed stream mixing, making it especially challenging for the design and development of fuel injection/mixing systems.

This program focuses on developing several integrated injector/mixing chamber systems suitable for diesel fuel reforming in SECA applications. Four different injection concepts are being evaluated for their performance and limitations, including a multipoint impingement injector, a gas-assisted simplex injector, a high-energy piezoelectric injector and a preheating simplex injector. Analytical tools and advanced experimental instruments are utilized to help characterize the flow field structure and refine the injector and mixing chamber design.

CFD analysis is conducted to predict injector flow rates, pressure drops and upstream flow uniformity to reduce development iterations. It is also used to assess the overall flow field structure and mixing capability at high temperatures. In addition, finite element thermal analysis is performed to determine the distribution of metal temperature for the assessment of internal coking, steam

condensation, material growth and excessive stresses.

A steam/hot air test rig has been constructed to facilitate the injector and mixing chamber development. Injector flow rates can be accurately calibrated to meet reformer requirements at high temperatures. During development, the test rig is also useful for conducting flow visualization and for preliminary screening of various injector concepts and design modifications. More detailed measurements are conducted at ambient and high temperatures using advanced laser diagnostic techniques including phase/Doppler interferometry, Raman spectrometry and laser extinction tomography. These measurements provide flow field parameters such as droplet size, droplet velocity, flow pattern, uniformity index, mixture concentration and temperature, which are all critical for injector/ mixing chamber evaluation.

In addition to developing injector/mixing chamber concepts, this project also plans to investigate the effect of pulsed excitation on fuel flows for evaluation of reduced power consumption and to incorporate carbon-resistant design features for extended service life.

Results

To date, three injection concepts have been designed and fabricated for performance evaluation. Experimental tests were conducted at both ambient and high temperature conditions that are representative of the fuel reformer operation. These tests were designed to examine the effects of injector designs, mixing chamber configurations, fuel properties and feed stream operating conditions on mixture characteristics and flow field structure. The results were used to help refine the injector/mixer performance. Figure 1 shows the mixture characteristics of an excellent feed stream preparation produced by a multipoint impingement injector/mixer system near the mixing chamber exit.

A porcupine thermocouple device was mounted near the exit of the injector/mixing chamber to determine the temperature distribution across the flow field at nine different radial locations. Flow field uniformity was evaluated using a uniformity index defined by the following formula:

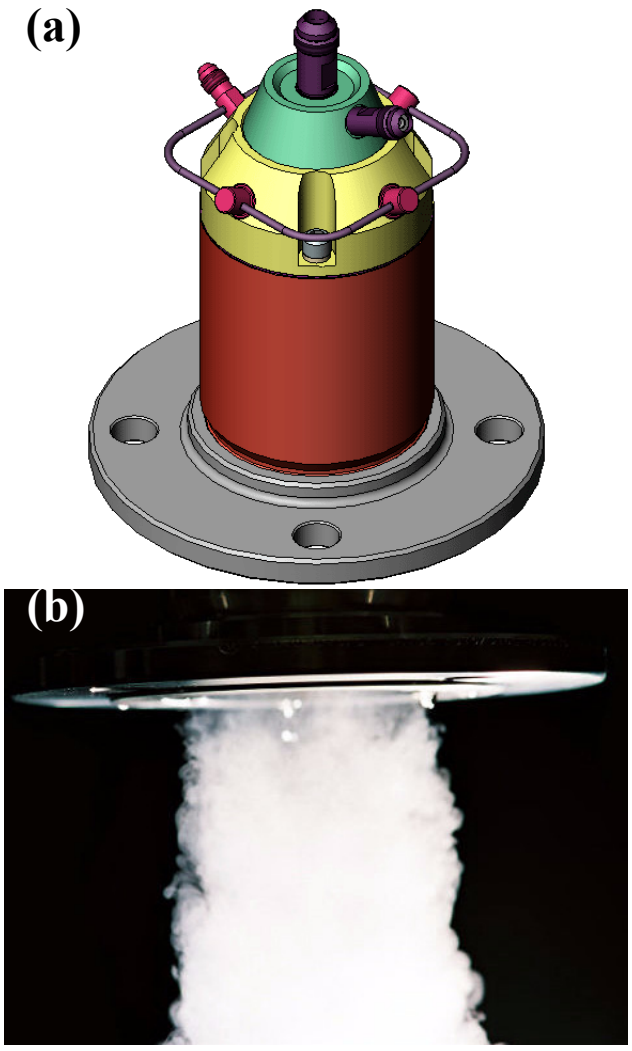

Figure 1. Fuel Mixture Characteristics Produced by a Multipoint Impingement Injector/Mixer System

Uniformity Index = (max. temperature – min. temperature) / average temperature

Table 1 lists the temperature results for a multipoint impingement injector/mixer system at 1 inch downstream from the chamber exit. For a multipoint impingement injector, the temperature field appears to be quite uniform for all test points because the uniformity index is less than 5%.

To examine wall impingement and droplet evaporation, spray characterization was conducted in an ambient environment and measurements were obtained for droplet sizes, droplet velocities, angles, trajectories and volume fluxes. This information not only helps us understand flow field structure, but also establishes minimum acceptance criteria for injector

Table 1. Temperature Results for a Multipoint Impingement Injector/Mixer System

	Section A (1 inch Downstream)		
Test Point	**Average Temperature (°F)**	**(Max.-Min.) Temperature (°F)**	**Uniformity Index UI (%)**
Pt. 1 – Fuel 5 pph, Air 25 pph/ 930°F, Steam 10 pph/550°F	525	10	1.91
Pt. 2 – Fuel 1.5 pph, Air 7.5 pph/ 930°F, Steam 3 pph/ 550°F	551	23	4.17
Pt. 3 – Fuel 2 pph, Air 12 pph/ 930°F, Steam 5 pph/ 550°F	553	20	3.62

sprays. Figure 2 shows a comparison of droplet mean diameters between the impingement injector and gas-assist injector concepts. Although the two injector sprays exhibit different size distributions, both injector concepts meet the droplet size requirement of less than 30 µm at the simulated maximum flow condition for a typical 10-kW ATR reformer.

To investigate mixture uniformity, ten different mixing chamber configurations were constructed for flow field evaluation using the laser extinction tomography technique. Each mixing chamber configuration contained different mixing devices, such as a mixing swirler and multiple layers of mesh screens. Figure 3 illustrates the measured mixture pattern for an integrated gas-assist injector/mixing chamber that contains a double-swirler mixer. This mixture pattern exhibits excellent uniformity in the circumferential distribution. Test results indicated that mixing devices had a significant impact on mixture pattern. Each injector concept must be properly integrated with an optimized mixing chamber configuration and mixing devices in order to achieve the best mixture pattern for the reactor.

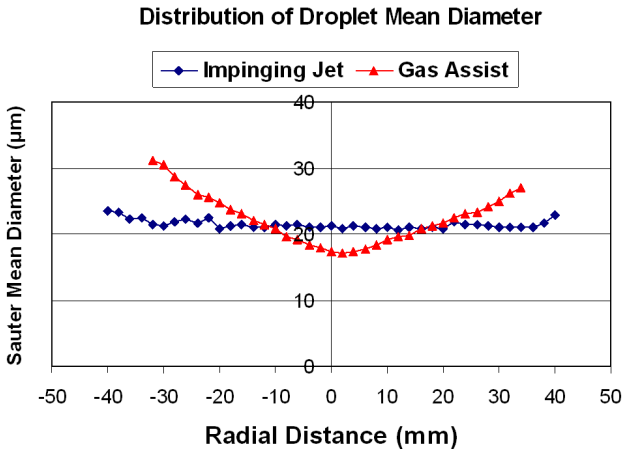

Figure 2. Comparison of Droplet Mean Diameters Between an Impingement Injector and a Gas-Assist Injector

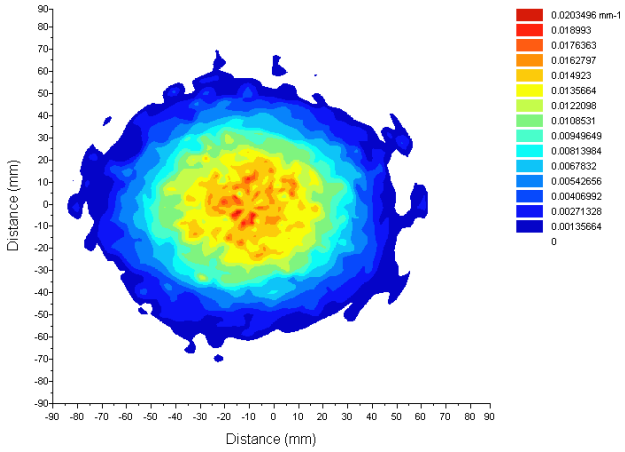

Figure 3. Uniform Mixture Pattern Produced by an Integrated Gas-Assist Injector/Mixing Chamber

For the injector/mixer system evaluation, the most valuable data was obtained in a high temperature environment from the Raman spectrometry instrument shown in Figure 4. During measurements, an intense laser beam was projected into the flow field to induce Raman radiation. The scattered Raman signals were collected by the spectrometer and a photo detector unit to determine the wavelength and signal intensity. The wavelength and light intensity can be used to identify the concentration of the gas species. This data allowed us to understand the effects of feed stream operating parameters on mixture distribution. Distributions of fuel, steam and nitrogen were plotted against the radial distances across the flow field to reveal the

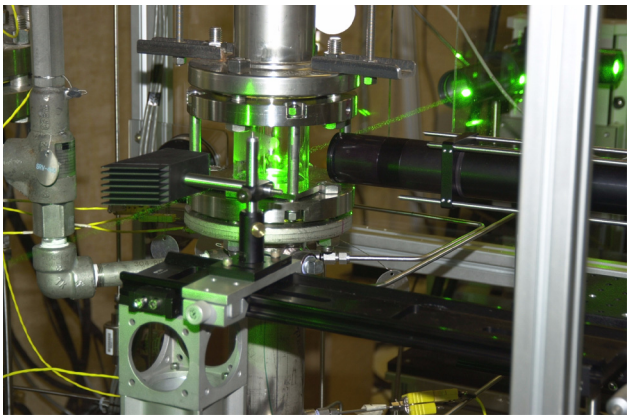

Figure 4. Raman Spectrometry Instrument Used for Measurements of Species Distribution

influence of fuel property, inlet pressure, inlet temperature, mixing chamber and mixing device on mixture uniformity for the selected injector/mixer designs.

Raman data indicated that the impingement injector provided relatively uniform species distribution. The signal quality, however, varied with feed stream operating conditions due to varying extent of carbon deposits on the quartz window. Since steam flow was utilized to atomize the diesel fuel, it had a major impact on fuel distribution. As the steam flow rate increased, fuel concentration was mostly distributed in the center field, with less severe carbon deposits on the wall. It was also observed that higher steam temperature appears to provide stronger Raman signals and more uniform species distribution across the flow field.

The investigation also revealed that fuel properties have a significant effect on the mixture distribution. A series of tests was conducted using the same injector/mixer for a back-to-back comparison between diesel and Jet-A fuels. Results indicated that the Raman signal strength for Jet-A fuel was much stronger than that of the diesel fuel. The distribution of Jet-A fuel appeared to be more uniform and more repeatable, signifying a more complete evaporation and mixing process.

Depending on the injector concepts, it was found that mixing devices could provide additional improvements to flow stability and mixture uniformity. For instance, the mixture uniformity was significantly improved by adding a central swirler inside the mixing chamber for the gas-assist injection concept. For the impingement injector concept, however, adding mixing devices did not seem to provide any noticeable benefits.

Conclusions

The present investigation has generated a large database on the design and development of various injection and mixing systems. It contains information concerning the influence of the critical injector design/operation parameters on fuel mixture preparation. This engineering knowledge could immediately be applied to help alleviate problems associated with diesel fuel reforming, thereby improving reformer durability. Not only will this database help engineers understand the limitations of injection and mixing systems for diesel fuel processing, but it will also be used in further analyses of injector/mixer design optimization, manufacturing cost reduction and injector/reactor performance correlation. The following is a list of the major observations for the present study:

- The multipoint impingement injector produces fine droplets and uniform mixture pattern when a minimum of 2 psig inlet pressure is available from either the steam or airflow feed lines.
- The gas-assist injector is a simple and robust design that can also produce fine droplets and uniform mixture distribution with sufficient inlet air or steam pressures. Due to high droplet inertia, it requires a mixing chamber equipped with a central swirler to help stabilize the mixture flow.
- The high-energy piezoelectric injector is the best performer in fuel atomization for reformers with very limited steam or air inlet pressures. It has the potential to provide good atomization and mixing over a wide range of flow rates. However, the driver electronics need to be optimized to meet the requirement of low parasitic power consumption.
- It will be difficult to meet the stringent requirements of liquid fuel reforming using a single injection concept. The idea of a hybrid injection system or a pulsed modulated injection system may need to be explored in order to achieve low power consumption, adequate atomization and mixing. For example, a hybrid

piezoelectric/gas-assist injector may allow fuel reformers to operate for many hours and over a wide range of flow rates. Using this hybrid system, the piezoelectric injector would only be operated at low flow rate conditions to minimize power consumption, and the gas-assist injector would be utilized for high flow rate conditions.

Special Recognitions & Awards/Patents Issued

1. "An Integrated Fuel Injection and Mixing System for Fuel Cell Reformers", U.S. Patent application was filed on April 15, 2005.

FY 2005 Publications/Presentations

1. "Innovative Injection and Mixing Systems for Diesel Fuel Reforming", Presented at the Sixth Annual SECA Workshop, Pacific Grove, California, April 18-21, 2005.

III.B.4 Diesel Reforming for Solid Oxide Fuel Cell Auxiliary Power Units

Rodney L. Borup (Primary Contact), W. Jerry Parkinson, Michael A. Inbody, Dennis Guidry, and Eric L. Brosha
Los Alamos National Laboratory
P.O. Box 1663
Los Alamos, NM 87545
Phone: (505) 667-2823; Fax: (505) 665-9507; E-mail: borup@lanl.gov

DOE Project Manager: Magda Rivera
Phone: (304) 285-1359; E-mail: Magda.Rivera@netl.doe.gov

Objectives

- Research and develop technologies for cost-effective and durable onboard diesel reformers for solid oxide fuel cell (SOFC) auxiliary power unit (APU) applications
- Examine fundamentals of the diesel reforming process
  - Characterize the key parameters of the diesel reforming process
    - Fuel vaporization, mixing and reactor feed conditions
    - SOFC anode exhaust recycle for water availability
  - Determine the factors that limit durability
    - Catalyst sintering and deactivation
    - Carbon formation during operation and startup
  - Develop and test processes to extend durability
- Develop models to provide a design and operation basis for diesel reforming
  - Modeling of carbon formation
  - Modeling of SOFC anode exhaust recycle system
  - Kinetic modeling to describe details of diesel reforming process

Approach

- Examine catalytic partial oxidation and steam reforming
  - Experimental measurements
    - Isothermal reforming measurements for detailed kinetic measurements
    - Adiabatic reformer operation for development of SOFC anode recycle simulation and appropriate fuel feed conditions
  - Modeling
    - Carbon formation equilibrium
    - Reformer operation with anode recycle

Accomplishments

- Conducted experimental measurements of diesel reforming
  - Simulated real-world diesel reforming operation
  - Evaluated the effect of SOFC anode exhaust recycle on reactor operation
  - Defined the effect of sulfur containing hydrocarbons on carbon formation

  - Defined the effect of aromaticity levels on carbon formation
  - Examined catalyst sintering
  - Examined reforming activity and carbon formation tendency of nano-particle nickel catalysts
- Conducted modeling of carbon formation and diesel reforming with recycle operation
  - Modeled reformer efficiency and parasitic losses due to the effects of anode exhaust recycle
  - Defined different thermodynamic states of carbon

Future Directions

- Examine reformer durability
  - Catalyst sintering and deactivation
    - Stabilize active catalyst particles
  - Reformer operational profiles for reducing catalyst sintering
    - Examine multipoint air injection to reduce oxidation temperature
- Study carbon formation
  - Examine additives (such as dimethyl ether and oxygenates) for tendency to prevent carbon formation
  - Investigate stand-alone startup and processes
- Determine reformer durability and hydrocarbon breakthrough effect on SOFC
  - Incorporate SOFC 'button' cell operating on reformate
- Complete carbon formation model and distribute
  - Develop 'user-friendly' interface and user manual

Introduction

The use of a solid oxide fuel cell (SOFC) to provide auxiliary power for diesel trucks can increase fuel efficiency and reduce emissions by reducing diesel engine idling time. The potential high-volume market for SOFC auxiliary power units (APUs) could provide the driver for high-volume manufacturing to reduce the cost of SOFC modules, a key goal of the Solid State Energy Conversion Alliance (SECA) program. The logical fuel of choice for a diesel truck SOFC APU is diesel fuel. SOFCs are being researched that directly oxidize hydrocarbon fuels, but the power densities are lower than those of SOFCs that use the products of reforming diesel fuel – H_2, CO, CO_2, H_2O, N_2, and hydrocarbons such as methane. Since the SOFC is the most costly component of the system, increasing the power density provides benefits in reducing volume, mass, and cost that can offset the cost and complexity of adding a diesel reformer to the system. The objective of this project is to research and develop the technology to enable that diesel reformer to be cost-effective and durable.

Diesel fuel can be reformed into a H_2/CO-rich fuel feed stream for an SOFC by autothermal reforming (ATR), a combination of partial oxidation (POx),

$$C_nH_m + \frac{n-x}{2}O_2 \rightarrow (n-x)CO + C_xH_y + \frac{m-y}{2}H_2 \quad (1)$$

and steam reforming.

$$C_nH_m + nH_2O \rightarrow nCO + \frac{2n+m}{2}H_2 \quad (2)$$

The typical autothermal reformer is an adiabatic, heterogeneous catalytic reactor, and the challenges in its design and operation, particularly durable operation, on diesel fuel are manifold. These challenges begin with the vaporization and mixing of diesel fuel with air and steam where pyrolysis can occur and improper mixing leads to hot spots and incomplete conversion. Carbon formation during operation and startup can lead to catalyst deactivation and fouling of downstream components, reducing durability. The exotherm of the POx reaction can generate temperatures in excess of 800°C [1], where catalysts rapidly sinter, reducing their lifetime.

Water addition helps to reduce carbon formation, so a key issue becomes the source of the water onboard the vehicle. Our research begins to address these issues through an experimental and modeling examination of the fundamentals of these processes. The intent is to provide a design and operation basis for a durable diesel reformer for an SOFC APU.

Approach

Our approach employs experimental measurements in diesel reformer reactors and microscale reactors along with development and application of chemical models to interpret and codify experimental results. Experimental measurements of diesel reforming are made in an adiabatic heterogeneous catalytic reactor to simulate real-world diesel reformer operation and to identify commercial design issues. Experiments conducted in the adiabatic reactor were complemented by experiments conducted in a well-controlled and well-defined isothermal microscale reactor, which can be used for measurements of kinetics of diesel reforming.

The equilibrium conditions for carbon formation have been modeled as a function of operating conditions, fuel composition, and thermodynamics of deposited carbon species. Modeling of the reformer system and SOFC anode recycle was conducted to examine the relative parasitic losses due to recycling the SOFC anode.

Modeling Results

The equilibrium composition in a chemically reacting system is a function of the final temperature, pressure and the feed composition. The conditions for forming solid carbon were determined from the equilibrium compositions of reactions at various temperatures, pressures and feed compositions. Modeling of the equilibrium conditions for the formation of solid carbon has led to the conclusion that the thermodynamics of the actual carbon are poorly understood. As a result, we have modeled the thermodynamics of carbon formation.

Two forms of amorphous carbon come from the two following reactions:

$$CH_4 \rightarrow C_1^* + 2H_2 \qquad (3)$$

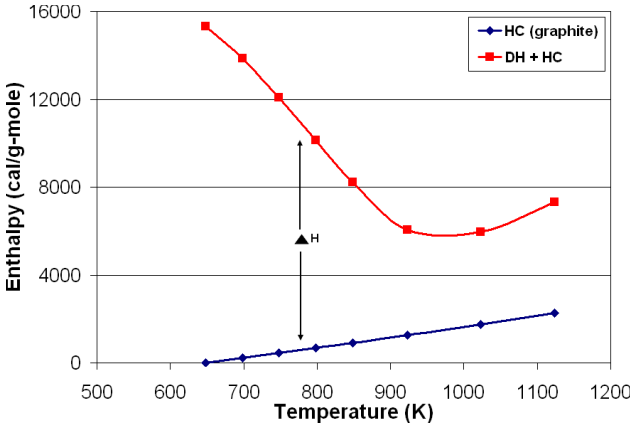

Figure 1. Enthalpy for C_2^* Carbon, Referenced to Graphite, with 0 Enthalpy at 648 K

$$2CO \rightarrow CO_2 + C_2^* \qquad (4)$$

A heat capacity for graphite carbon [2] is:

$$Cp = 4.03 + 0.00114T - 204000/T^2 \qquad (5)$$

For a constant temperature reaction,

$$G = H - TS \qquad (6)$$

For the reaction

$$C\ (\text{graphite}) \rightarrow C^*\ (\text{amorphous}), \qquad (7)$$

graphite converting to any amorphous carbon, G becomes G_f, the Gibb's free energy of formation for the amorphous carbon. Since

$$dH = CpdT, \text{ then } H = H_{ref} + \int CpdT, \qquad (8)$$

we can then integrate from reference 298 K to some desired temperature T. Figure 1 is a plot showing computed H for graphite and amorphous carbon. H was computed by means of adding the change in Gibb's Function with respect to T to the graphite numbers in each case to give the upper curves.

The important conclusion from Figure 1 is that the upper curves show a negative heat capacity for the amorphous carbons in general. Since $H_1 - H_2 = Cp\ (\text{average})(T_1 - T_2)$, the upper curves in all the figures, for at least the lower temperature range, show that Cp (average) has to be negative. These calculations verify that our data do predict negative heat capacities (impossible) over at least some temperature ranges. We should also note that

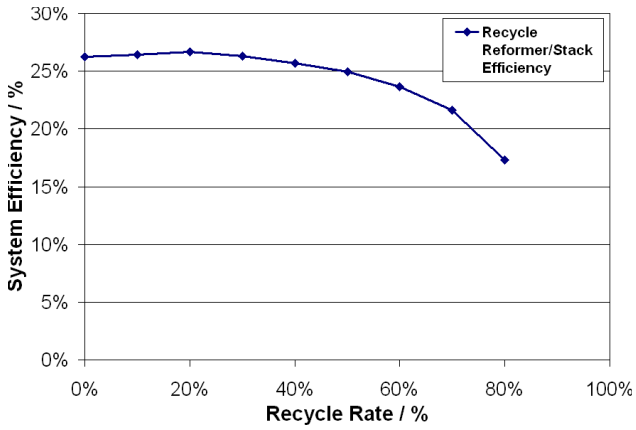

Figure 2. Effect of Anode Recycle on System Efficiency from Compression Energy Penalty

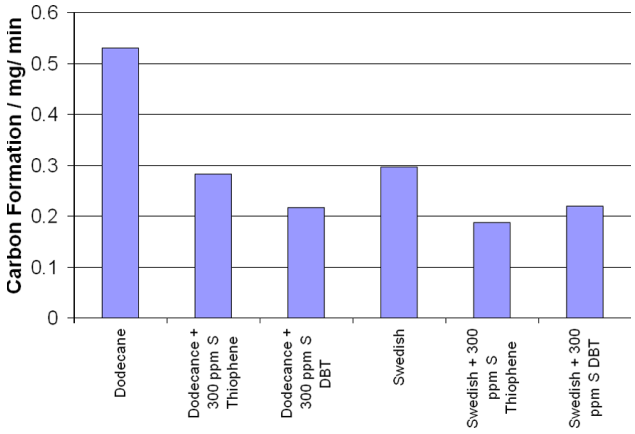

Figure 3. Sulfur-Containing Hydrocarbon Compound Effect on Carbon Formation; Addition of Thiophene and Dibenzothiophene to Dodecane and Low-Sulfur Swedish Diesel Fuel at 300 ppm S

some of the data, at higher temperatures, do predict positive heat capacities. These carbon enthalpies show that carbon thermodynamics are not consistent over a range of temperatures. Apparently, carbon species with different thermodynamics are formed; something like a phase change or a change in carbon composition is happening to these amorphous carbons over the range of temperatures.

To supply water for the reforming reaction, the anode gas of the SOFC can be recycled to the reformer. This requires compression and, thus, a parasitic loss to the system. To compare relative performance measures as a function of recycle ratio, this was modeled. To accomplish the efficiency modeling, a number of assumptions were used, including constant SOFC fuel utilization of 0.5, constant SOFC operating voltage of 0.7 V and good thermal integration of the SOFC anode gas recycle with the diesel reformer. A minimum outlet reformer temperature of ~800°C was used. The results of this modeling are summarized in Figure 2.

At the lowest recycle ratios, there is not enough water available to conduct the reforming reaction; therefore, the efficiency is lower as high oxygen/ carbon ratios must be used to convert the hydrocarbons to H_2 and CO. As the recycle ratio increases, the parasitic power consumption increases; however, the oxygen requirement decreases due to recycled water. It appears that the maximum efficiency is obtained at approximately 20% recycle ratio.

Experimental Results

The design and operation of the diesel reformer with recycle operation has been previously reported [3], as has the carbon formation for a number of operating conditions [4]. In prior experiments, commercial diesel fuel showed a higher propensity for carbon formation than did low-sulfur Swedish diesel fuel, and one hypothesis was that this was due to the sulfur content. Carbon formation with the commercial diesel fuel was on average three times higher than that for the low-S Swedish diesel fuel.

Experiments were conducted using an isothermal microscale reactor to clarify the effects of sulfur and the aromatic content of the hydrocarbons. Figure 3 shows carbon formation for low-sulfur Swedish diesel fuel and dodecane ($C_{12}H_{24}$) with and without 300 ppm sulfur added as thiophene and dibenzothiophene (DBT) for autothermal reforming (ATR) (O/C = 1.0, S/C = 0.34). The ATR conditions simulate similar adiabatic measurements for an SOFC anode recycle of 35%. The addition of sulfur compounds (thiophene and DBT) does not increase carbon formation, although higher carbon formation was observed from pure dodecane than from Swedish diesel. There was also no detectable sulfur (by x-ray fluorescence) in carbon samples regardless of sulfur content in fuel (dodecane and low-S Swedish diesel fuel). The carbon formation mechanism does not

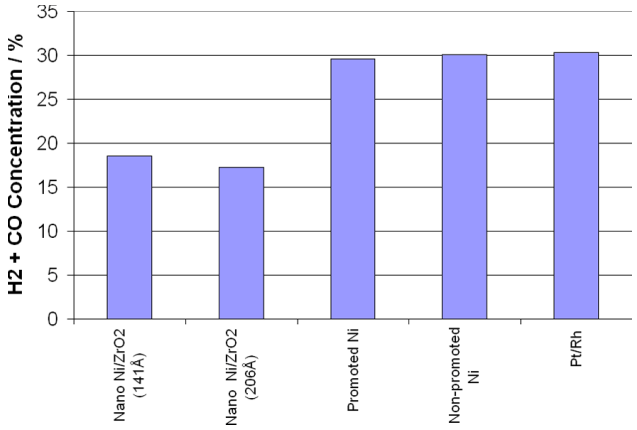

Figure 4. Hydrogen plus CO Concentrations for Nano-Particle Nickel Supported on Zirconia, Nano-Particle Nickel, Promoted Nickel, Non-Promoted Nickel and Pt/Rh

seem be affected by the presence of sulfur or these sulfur compounds.

Carbon formation measurements were also made with the addition of various aromatic and cyclic components, specifically, xylene, decalin, tetralin, naphthalene, anthracene and phenanthrene. When these compounds were added to low-sulfur Swedish diesel fuel, the carbon formation (during ATR at constant O/C = 0.95) was increased nearly uniformly by a factor of 2x. When these components were added to dodecane, increased carbon formation was observed with the 2- and 3-ringed aromatic components (naphthalene, anthracene and phenanthrene).

Carbon formation shows different tendencies with different catalysts and tends to be worse over nickel catalysts. However, results have shown that nano particle nickel catalysts can show higher stability than traditional nickel catalysts during the steam reforming of CH_4. Thus, these catalysts were examined for their capability for reforming of diesel fuel. Figure 4 shows the outlet concentrations of hydrogen plus carbon monoxide during diesel reforming over various nickel catalysts and a standard Pt/Rh reforming catalyst. Good activity for the nanocomposite nickel catalysts was not observed, as the diesel fuel conversion was not complete; in addition, a higher propensity for carbon formation was observed with nanocomposite nickel catalysts. Potentially, these nanoparticle nickel catalysts have a better application as SOFC anodes for CH_4 conversion.

Conclusions

- Diesel fuel reforming has been conducted under isothermal and adiabatic conditions.
- Diesel reforming under adiabatic operation was performed with simulated SOFC anode recycle.
- Modeling suggests that the optimum efficiency point for diesel reforming occurs with SOFC anode recycle of ~20% due to required O/C, reformer temperature and parasitic compression losses.
- Carbon formation mechanism does not seem to be affected by the presence of sulfur or the presence of sulfur compounds (thiophene and dibenzothiophene).
- Addition of cyclic and multi-ringed aromatic components increases carbon formation.
- Modeling shows that carbon thermodynamics are not constant with temperature.
- Different thermodynamic carbon species appear to be formed.
- Nanoparticle nickel catalysts do not appear suitable for diesel reforming.

FY 2005 Publications/Presentations

1. DIESEL REFORMING FOR SOFC AUXILIARY POWER UNITS, Rodney L. Borup, Michael A. Inbody, José I. Tafoya, Dennis R. Guidry and W.J. Parkinson, Fuel Cell Seminar, San Antonio, Texas, November 1-5, 2004.
2. EFFECT OF SOFC ANODE EXHAUST RECYCLE ON DIESEL REFORMING, Rodney L. Borup, Michael A. Inbody, W.J. Parkinson, Dennis R. Guidry and Eric L. Brosha, 5th Annual Logistic Fuel Processing Conference, Panama City, Florida, January 25-26, 2005.
3. EFFECT OF SOFC ANODE EXHAUST RECYCLE ON DIESEL REFORMING, Rodney L. Borup, Michael A. Inbody, W.J. Parkinson, Dennis R. Guidry and Eric L. Brosha, 2nd International Symposium on Solid Oxide Fuel Cells, Cocoa Beach, Florida, January 23-28, 2005.
5. DIESEL REFORMING FOR AUXILIARY POWER UNITS, Rodney L. Borup, Michael A. Inbody, W.J. Parkinson, Dennis R. Guidry and Eric L. Brosha,

DOE SECA CTP (Solid State Energy Conversion Alliance Core Technology Program), Tampa Bay, Florida, January 27, 2005.

6. DIESEL REFORMING WITH SOFC ANODE RECYCLE, Rodney L. Borup, Michael A. Inbody, W.J. Parkinson, and Dennis R. Guidry, ECS - Electrochemical Society, Las Vegas, NV, June 12-17, 2005.
7. DIESEL REFORMING WITH SOFC ANODE EXHAUST RECYCLE, Rodney L. Borup, Michael A. Inbody, W.J. Parkinson, Dennis R. Guidry and Eric L. Brosha, Fuel Cell Seminar, Palm Springs, CA, To be presented November 14-18, 2005.

References

1. Ahmed, S., Presentation to Department of Energy, Washington DC, May 01, 2003.
2. Stull, D.R. and Prophet, H., eds. JANAF Thermochemical Tables, 2nd. Ed., U.S. Dept of Comm., U.S. Gov. Prtg Off. Washington, D.C. 1971.
3. Borup, R.L., Parkinson, W.J., Inbody, M.A., Tafoya, J.I. and Vigil, W.J., *"Diesel Reforming for SOFC APU*", DOE SECA Program, FY 2003 Progress Report (2003).
4. Borup, R.L., Parkinson, W.J., Inbody, M.A., Tafoya, J.I. and Guidry, D.R., "*Diesel Reforming for Solid-Oxide Fuel Cell Auxiliary Power Units*", DOE SECA Program, FY 2004 Progress Report (2004).

III.B.5 Fundamental Reforming Studies - Role of Catalytic O_2 Supports on Fuel Reforming

David A. Berry (Primary Contact) and Maria Salazar-Villalpando (Parsons)
U. S. Department of Energy
National Energy Technology Laboratory
P. O. Box 880
3610 Collins Ferry Road
Morgantown, WV 26507-0880
Phone: (304) 285-4430; Fax: (304) 285-4469; E-mail: David.Berry@netl.doe.gov

Subcontractor:
Parsons, Morgantown, WV

Objectives

- Investigate the role of oxygen-conducting supports in hydrocarbon reforming and their role in decreasing carbon formation and/or increasing sulfur tolerance.
- Develop a fundamental knowledge base for developing more long-duration reforming catalysts for auxiliary power units.

Approach

- Carbon formation, catalytic activity, H_2 selectivity, and catalyst stability are the main catalytic parameters studied during the partial oxidation reaction of CH_4 and higher hydrocarbons.
- Several sample matrices of ceria-based catalysts are studied to elucidate the effect of the following catalyst variables in the partial oxidation of methane and higher hydrocarbons:
  - metal type (Pt, Ni, Rh)
  - support type (CeO_2 and Al_2O_3)
  - catalyst ionic conductivity
  - dopant type (La, Gd, Zr)
  - dopant concentration (GDC10 & GDC30)
  - oxygen storage capacity
- Catalyst characterization includes ionic conductivity, surface area, crystal phase and catalyst reduction temperature.
- Experimental variables include temperature, space velocity, oxygen/carbon ratio and time on stream.
- Mechanistic studies include
  - Labeling doped ceria catalysts with $^{18}O_2$,
  - Conducting the partial oxidation of methane (POM) reaction over $^{18}O_2$ labeled catalysts, and
  - Performing prior and post reaction experiments by Nuclear Reaction Analysis (NRA) to complement the isotopic studies and obtain ^{18}O concentration profiles and total oxygen concentration in the catalysts.
- Studies related to sulfur tolerance are planned for the following stage of this project.
- Partial oxidation of higher hydrocarbons than CH_4 is planned for the following stage of this project.

Accomplishments

- Catalyst characterization has been completed, which included ionic conductivity, surface area, crystal phase and catalyst reduction temperature.
- Several sample matrices of ceria-based catalysts which include materials with different metal type, support type, dopant type and dopant concentration have been tested during the partial oxidation of methane, having as experimental variables temperature, space velocity, oxygen/carbon ratio, and time on stream.
- This work has revealed that catalysts with higher ionic conductivity show a trend towards less carbon formation than in materials with lower ionic conductivity.
- Doped Pt-based catalysts showed higher stability in CH_4 conversion than doped Rh (although similar) and Ni based catalysts.
- Pt/CeO_2 showed higher and more stable CH_4 conversion than Pt/Al_2O_3, mainly due to the higher oxygen storage capacity of the former catalyst.
- Mechanistic studies have been initiated by labeling doped ceria catalysts with $^{18}O_2$.
- A review paper was published.
- A Solid State Energy Conversion Alliance (SECA) merit review was conducted.
- An oral presentation has been accepted to be presented at the American Institute of Chemical Engineers (AIChE) Fall Meeting, 2005.

Future Directions

- Conduct the POM reaction over $^{18}O_2$ labeled catalysts.
- Collaborate with Pacific Northwest National Laboratory to determine ^{18}O concentration profiles and total oxygen concentration in the catalysts by NRA analysis prior and post reaction experiments.
- Determine/correlate NRA results with amount of carbon generated during catalytic studies.
- Determine lattice oxygen contribution in products generation during partial oxidation reactions.
- Determine catalytic activity of doped ceria catalysts in the absence of gaseous oxygen to correlate results with oxygen storage capacity.
- Studies related to sulfur tolerance will be conducted.
- Partial oxidation of higher hydrocarbons will be conducted.

Introduction

The U.S. Department of Energy is sponsoring development of high-temperature fuel cell power systems based on solid oxide technology through its Solid State Energy Conversion Alliance (SECA) program. The program is geared toward mass manufacturing of fuel cells for high-volume markets and multiple applications. One of those markets/ applications is a diesel-fueled auxiliary power unit (APU) for long-haul truck transportation. The fuel processor is a critical component of this system and must be able to provide a clean, tailored synthesis gas to the fuel cell stack for long-term operation. Key characteristics desired for the processor (and the system) include low cost, high efficiency, maximum thermal integration, low maintenance intervals, and acceptable startup and transient response. There are also several barrier issues that must be overcome to achieve these characteristics. Carbon formation, particularly upon startup, must be minimized to avoid coking of the catalysts in the reformer and downstream fuel cell. Fuels containing sulfur can poison both the reforming catalysts and the fuel cell anode.

Ceria-based catalysts are being investigated in this work in order to fundamentally understand the role of oxygen-conducting supports in reforming of diesel fuel compounds and their role in decreasing carbon deposition. Ceria-based catalysts have shown ability to decrease carbon formation during partial

oxidation of hydrocarbons [1,2]. It has been speculated that this property is due to the high oxygen ion mobility of the catalysts. In this project, this assumption is investigated, and an attempt is made to obtain a reaction mechanistic scheme to get a better understanding of carbon formation and mitigation.

Approach

Carbon formation, catalytic activity, H_2 selectivity, catalyst reducibility and stability were studied during the partial oxidation of methane (POM). Catalyst variables included metal type (Pt, Ni, Rh), support type (Al_2O_3 and CeO_2), catalyst ionic conductivity, dopant type (La, Gd, Zr), dopant concentration (GDC10 & GDC30) and oxygen storage capacity. More than a hundred experiments were carried out to study the influence of the following variables: temperature, oxygen/carbon ratio, time on stream and space velocity. Characterization of ceria-based catalysts included catalyst phases, ionic conductivity, temperature-programmed reduction profiles and surface areas. A tubular reactor was used to conduct the experimental tests during the POM reaction. A ceramic furnace heated the reactor, and a thermocouple was centered within the catalyst bed to measure and control the reaction temperature. Typically, a 250-mg sample was placed in the middle of the reactor, using sand as the packing material. The reaction was conducted at 700ºC. In general, mixtures of 10% CH_4, 5% O_2 (oxygen/carbon ratio O/C=1), balance N_2 at a total flow rate of 324 cm^3/min (standard temperature and pressure) were delivered to the reactor. The reacting gases were all certified with helium (99.999%), used without any further purification. A mass spectrometer connected on line analyzed the feed and product gas streams. A cold trap at the outlet of the reactor was used to condense out any water from the product gas stream. Preliminary studies to screen the catalytic activity of pure CeO_2 and sand at 700°C were conducted prior to the catalyst testing. Low conversions of methane on sand and pure ceria were detected: 15% and 20%, respectively. Carbon monoxide and H_2 were not detected; CO_2 was the only product.

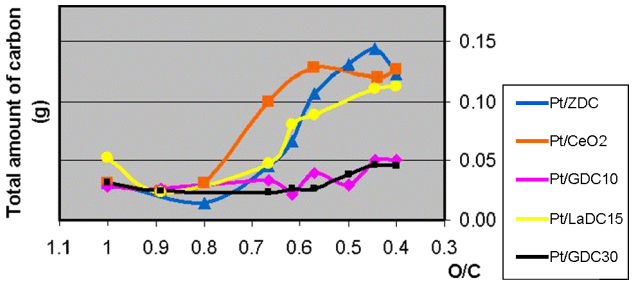

Figure 1. Carbon Formation vs. O/C on Pt Catalysts during the POM Reaction at 700°C

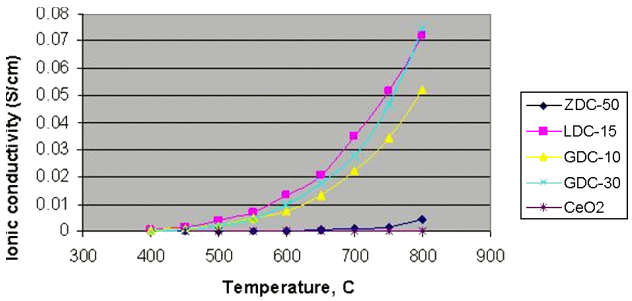

Figure 2. Ionic Conductivity of Doped Ceria Supports

Results

During the second year of the project, significant progress was demonstrated on all main tasks. Only the main results are presented here. In order to study the influence of ionic conductivity on carbon formation, carbon formation was observed during partial oxidation of methane (POM) using ceria-doped catalysts. Results showed a correlation between the ionic conductivity of the catalysts and the amount of carbon generated. Catalysts with higher ionic conductivity showed a trend towards less carbon formation than in the materials with lower conductivity (Figure 1). A lower amount of carbon was obtained by Pt/GDC10 and Pt/GDC30. The ability of these catalysts to mitigate carbon formation may be due to the high oxygen ion mobility (ionic conductivity) of the doped ceria supports that speeds the surface carbon oxidation and avoids the catalyst deactivation. The higher ionic conductivity shown by GDC15, GDC30 and GDC10 compared to ZDC and the un-doped CeO_2 (Figure 2) may be correlated to the close ionic radii of Gd^{3+} and La^{3+} cations compared to that of the Ce^{4+} cation. When there is a mismatch between the dopant and the host radii, a minimum in the binding energy between ion vacancies and dopant cations is

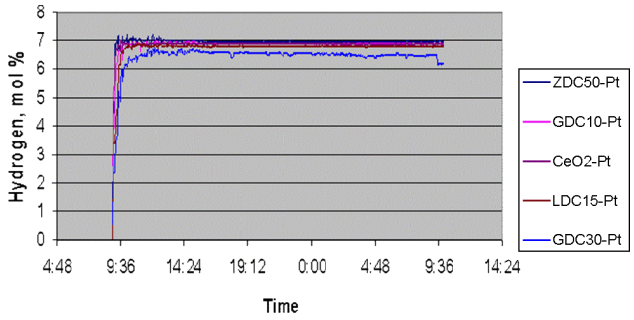

Figure 3. Stability of Pt Catalysts during the POM Reaction at O/C=0.4 and 700°C

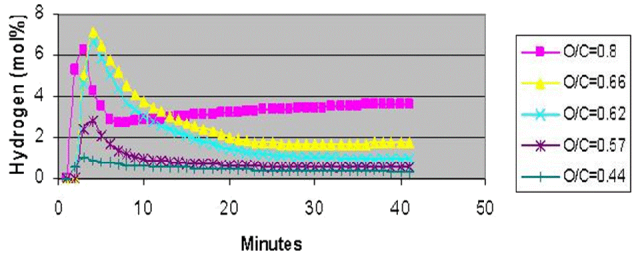

Figure 4. H_2 Generation vs. O/C Ratio during the POM Reaction on Pt/Alumina at 700°C

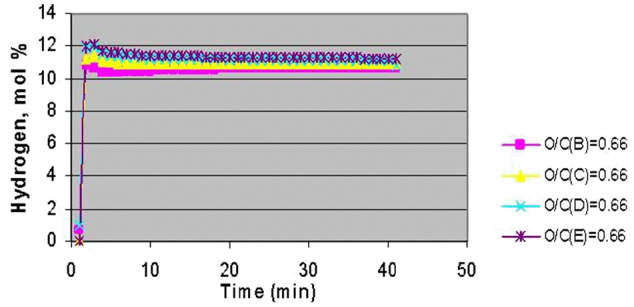

Figure 5. Regeneration of Catalytic Activity of Pt/GDC10 during POM Reaction at 700°C

predicted, resulting in high values of ionic conductivity [3]. Pt-ceria doped catalysts were highly active and selective for the POM reaction and showed stable performance for at least 20 h. This reaction was carried out at lower oxygen concentration (oxygen/carbon ratio=0.4) than the stoichiometric required to accelerate deactivation due to carbon formation. Results showed that all catalysts maintained stable conversion through the whole testing period (Figure 3). The POM reaction was also carried out on Pt/Al_2O_3 in the oxygen/carbon ratio range of 0.8 to 0.4 (Figure 4). Results showed deactivation and loss of catalytic activity in a short period of time, which may be due to the lower oxygen storage capacity this material has compared with Pt-ceria based catalysts. After conducting the POM reaction on Pt-ceria based catalysts, the generated carbon was oxidized with air and the reaction was immediately re-run on the same catalysts without any further catalyst pretreatment. Results showed that catalysts were fully regenerated after carbon build-up, and initial conversions and selectivity were recovered (Figure 5).

Conclusions

- We found a general correlation between the ionic conductivity of doped ceria catalysts and the amount of carbon generated. Catalysts with higher ionic conductivity showed a trend towards less carbon formation than in the materials with lower conductivity. The decreasing order trend in carbon formation is: Pt/CeO_2 > Pt/ZDC > Pt/LDC15>Pt/GDC10 > Pt/GDC30. All catalysts followed this trend but Pt/LDC15.
- Doping CeO_2 with La, Gd and Zr caused an ionic conductivity enhancement. A comparison of results showed the following trend: LDC15 > GDC10 > GDC30 > ZDC50 > CeO_2, where LDC15 showed the highest ionic conductivity.
- Pt-based catalysts were more stable than the Ni and Rh catalysts during the partial oxidation of methane.
- Pt/CeO_2 allowed higher and more stable CH_4 conversion than Pt/Al_2O_3, which may be due to the higher oxygen storage capacity of the former catalyst.
- Pt-based catalysts were fully regenerated after carbon build-up; initial conversions and selectivity were recovered.

Presentations

1. Salazar-Villalpando, Maria D.; Berry, David A.; Gardner, Todd H.; Shekhawat, Dushyant; Floyd, Donald. "Catalytic partial oxidation of methane on Rh-ceria based catalysts: Effect of reducibility", *accepted for presentation* at AIChE Fall Meeting, 2005.
2. Salazar-Villalpando, Maria D.; Berry, David A.; Gardner, Todd H.; Shekhawat, Dushyant. "Synthesis gas by partial oxidation and the role of oxygen-conducting supports: A review". Presented at the Second International Conference on Fuel Cell Science, Engineering and Technology, June 16, 2004.

FY 2005 Publications

1. Salazar-Villalpando, Maria D.; Berry, David A.; Gardner, Todd H.; Shekhawat, Dushyant; Celik, Ismail. Synthesis gas by partial oxidation and the role of oxygen-conducting supports: A review. Fuel Cell Science, Engineering and Technology, 2004, Rochester, New York, USA. Fuel Cell, 2004, p. 681-690.

References

1. Applied Catalysis A: General 225(2002) 63-75.
2. Applied Catalysis B: Environmental 19 (1998) 267.
3. Catalysis by Ceria and Related Materials edited by A. Trovarelli. Catalytic Science Series. Vol. 2 Imperial College Press, 2002.

III.B.6 Hexaaluminate Reforming Catalyst Development

Todd H. Gardner (Primary Contact), Dushyant Shekhawat and David A. Berry
U. S. Department of Energy
National Energy Technology Laboratory
3610 Collins Ferry Road
P.O. Box 880
Morgantown, WV 26507-0880
Phone: (304) 285-4226; Fax: (304) 285-0943; E-mail: Todd.Gardner@netl.doe.gov

Objectives

- Develop a durable, low-cost middle distillate reforming catalyst.
- Evaluate the activity and selectivity of transition metal doped hexaaluminate-type catalysts
  - Using n-tetradecane as a model diesel fuel compound.
  - Using dibenzothiophene (DBT) as a model sulfur compound.

Approach

- Synthesize and characterize transition metal doped hexaaluminate-type catalysts.
- Characterize catalysts by x-ray diffraction (XRD), BET (Bruner, Emmett and Teller surface area measurement) and temperature-programmed reduction (TPR).
- Evaluate catalyst activity and selectivity with model fuel compounds.
- Evaluate catalyst stability toward deactivation.

Accomplishments

- Synthesized 20 different hexaaluminate ($M_I(M_{II})_yAl_{12-y}O_{19-\alpha}$) catalyst formulations containing M_I = Ba, Sr, La and M_{II} = Co, Fe and Ni.
- Characterized catalysts by XRD, TPR and BET.
- Evaluated the activity and stability of synthesized hexaaluminate samples using n-tetradecane as a model compound.
- Evaluated the stability of $BaNi_{0.4}Al_{11.6}O_{19-\alpha}$ over 100 continuous hours of n-tetradecane partial oxidation.
- Evaluated the stability of 1 wt% $Rh/SrNi_{0.4}Al_{11.6}O_{19-\alpha}$ over 100 hours of n-tetradecane partial oxidation in the presence of 50 ppm w/w sulfur as DBT.

Future Directions

- Improved catalyst activity:
  - Evaluate activity and selectivity of platinum group metal (PGM) doped hexaaluminate catalysts.
- Improved carbon formation resistance:
  - Evaluate the effect of O_2-ion conducting films.
- Improved sulfur resistance:
  - Evaluate the effects of high-temperature operation on sulfur resistance.
  - Evaluate bi-metallic dopant combinations for sulfur resistance.

Introduction

Reforming of middle distillate fuels is a very attractive source of H_2 and CO for distributed fuel cell power. However, these fuels contain heavy hydrocarbons that are prone to coking and contain organosulfur compounds which are not easily removed. The simplest reforming technology is passive, where a catalyst is employed to reform the middle distillate into H_2 and CO and to convert the organosulfur compounds into more easily removed H_2S. This approach necessitates the development of a catalyst which does not deactivate under the reforming conditions.

For this application, the National Energy Technology Laboratory (NETL) is developing a new class of catalysts based on transition metal doped hexaalumina. The use of hexaalumina is of growing importance in catalysis due to its refractory nature [1, 2]. The thermal stability of hexaalumina is attributed to its structure, which has proven useful in retaining the large surface area necessary for catalytic reaction [2]. In this project, catalytically active metals are doped directly into the hexaalumina lattice, resulting in an atomically dispersed catalyst system that has been shown to possess high activity [3, 4].

Approach

The formation of carbon on the surface of a reforming catalyst is favored under conditions where the relative rate of hydrocarbon adsorption is faster than that of the surface reaction [5]. The rate as well as the strength of hydrocarbon adsorption is linked to the dispersion and ensemble of active sites. Elemental carbon has been shown to preferentially adsorb onto fivefold-coordinated Ni sites [6]. The effect of site coordination has also been shown to influence the adsorption of sulfur compounds. Besten and Selwood [7] have reported that a critical ensemble of 4 Ni atoms was required for H_2S dissociation and bulk nickel sulfide formation.

The aim of the present study has been to reduce the formation of large ensembles of active sites that are responsible for forming carbon and strongly adsorbing sulfur compounds through the atomic dispersion of catalytically active metals within the lattice of hexaalumina. A series of catalysts based on transition metal doped hexaalumina, with the general formula $M_I(M_{II})_yAl_{12-y}O_{19-\alpha}$, were prepared by co-precipitation from nitrate salt precursors. Catalyst activity and selectivity were investigated as a function of M_I-site (La, Sr and Ba) and M_{II}-site (Co, Fe and Ni) dopant type. Select samples were treated with a 0.1 wt% rhodium promoter to enhance activity and selectivity.

n-Tetradecane was used as a model diesel fuel compound to screen catalysts for activity and selectivity during partial oxidation. The sulfur tolerance of hexaaluminate catalysts was assessed by partial oxidation of n-tetradecane containing 50 ppm w/w sulfur as DBT. Experiments were conducted at an O/C = 1.2, a gas hourly space velocity (GHSV) = 50,000 $cm^3h^{-1}g^{-1}$, a temperature of 850°C and a pressure of 2 atm. Catalyst activity and selectivity were reported as H_2 yield and CO selectivity for the different hexaaluminate-type catalyst samples. The stability of two select catalysts was assessed over 100 hours of continuous operation.

Results

H_2 yield and CO selectivity may be calculated based on the definitions provided in equations (1) and (2). Table 1 is a compilation of H_2 yields and CO selectivities for n-tetradecane partial oxidation over various hexaaluminate-type catalysts. For Ni-hexaaluminate samples, M_I = Ba and Sr produced the

Table 1. Partial Oxidation Performance of n-Tetradecane over Hexaaluminate Catalysts[+].

Catalyst	Promoter	H_2 Yield (mol H_2/mol fuel)	CO Selectivity (%)
$SrNi_{0.4}Al_{11.6}O_{19-\alpha}$	0.1 wt% Rh	11.76	76.2
$SrNi_{0.4}Al_{11.6}O_{19-\alpha}$	--	11.25	75.9
$BaNi_{0.4}Al_{11.6}O_{19-\alpha}$	--	10.74	72.9
$LaNi_{0.4}Al_{11.6}O_{19-\alpha}$	--	9.33	58.4
$LaCo_{0.4}Al_{11.6}O_{19-\alpha}$	--	9.04	56.5
$LaCo_{0.4}Al_{11.6}O_{19-\alpha}$	0.1 wt% Rh	11.33	77.6

[+] GHSV=50,000 cm^3/g/h, Temp=850°C, P=2 atm, O/C=1.2.

greatest H_2 yields and CO selectivities. Ni- and Co-containing hexaaluminate samples promoted with 1 wt% Rh produced the highest H_2 yields and CO selectivities. Table 2 is a compilation of H_2 yields and CO selectivities for n-tetradecane partial oxidation over various hexaaluminate-type catalysts where the fuel contained 50 ppm w/w sulfur as DBT. Similar to n-tetradecane partial oxidation, the sample containing M_I = Sr produced higher H_2 yields and CO selectivities than the M_I = La catalyst. The presence of the 1 wt% Rh promoter did enhance CO selectivity of the $SrNi_{0.4}Al_{11.6}O_{19-\alpha}$ catalyst in the presence of DBT.

$$H_2\ \text{Yield} = \frac{\text{mol } H_2}{\text{mol Fuel}} = \frac{[H_2]\cdot F_{T,o}}{[C_{14}H_{30}]\cdot F_{T,i}} \quad (1)$$

$$\text{CO Selectivity (\%)} = \frac{\text{mol CO}}{\text{mol C}}\cdot 100 = \frac{[CO]\cdot F_{T,o}}{14[C_{14}H_{30}]\cdot F_{T,i}}\cdot 100 \quad (2)$$

Table 2. Partial Oxidation of n-Tetradecane/DBT (50 ppm w/w S) over Hexaaluminate Catalysts[+].

Catalyst	Promoter	H_2 Yield (mol H_2/mol fuel)	CO Selectivity (%)
$LaNi_{0.4}Al_{11.6}O_{19-\alpha}$	--	2.29	40.2
$SrNi_{0.4}Al_{11.6}O_{19-\alpha}$	--	10.02	60.9
$SrNi_{0.4}Al_{11.6}O_{19-\alpha}$	0.1 wt% Rh	10.67	70.1

[+] GHSV=50,000 cm^3/g/h, Temp=850°C, P=2 atm, O/C=1.2.

X-ray diffraction patterns for cobalt-, iron- and nickel-doped lanthanum hexaalumina are shown in Figure 1. All three catalysts show similar hexaaluminate-type structure. The presence of corresponding cobalt, iron or nickel oxides was not observed. In the $LaFeAl_{11}O_{19-\alpha}$ sample, a minor lanthanum aluminate phase was detected.

Figure 2 is a 100-hour stability test for the partial oxidation of n-tetradecane over $BaNi_{0.4}Al_{11.6}O_{19-\alpha}$ catalyst. The catalyst showed excellent stability and carbon formation resistance over this time period.

Figure 3 is a 100-hour test conducted on a mixture of n-tetradecane and dibenzothiophene (50 ppm w/w sulfur) over 1 wt% $Rh/SrNi_{0.4}Al_{11.6}O_{19-\alpha}$ catalyst. In order to observe the difference between sulfur-free operation and operation on n-tetradecane

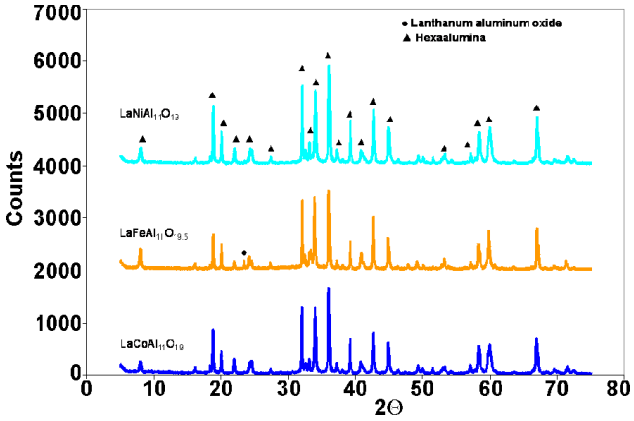

Figure 1. X-ray Diffraction Patterns of $LaCoAl_{11}O_{19-\alpha}$, $LaFeAl_{11}O_{19-\alpha}$, and $LaNiAl_{11}O_{19-\alpha}$ Hexaaluminate-type Catalysts. All catalysts exhibit hexaaluminate-type structure.

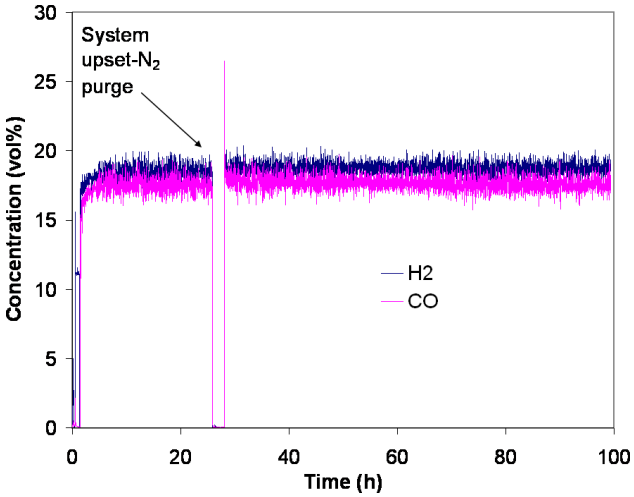

Figure 2. Partial Oxidation of n-Tetradecane over $BaNi_{0.4}Al_{11.6}O_{19-\alpha}$ for 100 Hours; GHSV=50,000 cm^3/g/h, Temp=850°C, P=2 atm, O/C=1.2.

containing sulfur, the first 5 hours of reaction were performed without DBT. n-Tetradecane with 50 ppm w/w DBT was then introduced as a step function. H_2 and CO concentrations both dropped upon the introduction of DBT, indicating the preferential adsorption of DBT over n-tetradecane. H_2 and CO selectivities remained unchanged before and after the introduction of sulfur. Over the 100-hour test, the hexaaluminate catalyst exhibited good stability in the presence of 50 ppm w/w sulfur as DBT and n-tetradecane.

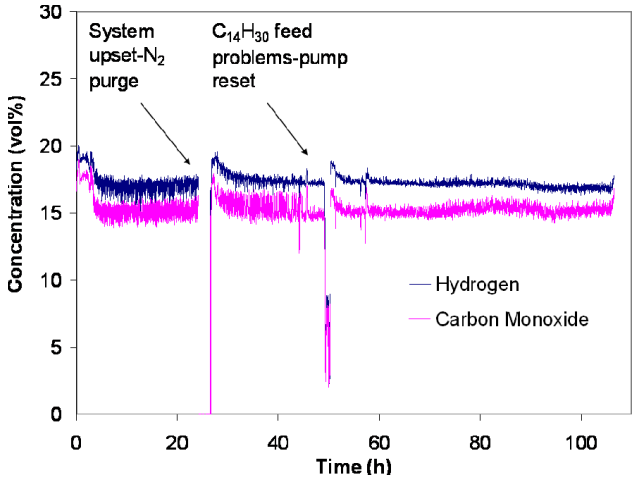

Figure 3. Partial Oxidation of n-Tetradecane with DBT (50 ppm w/w sulfur) over 1 wt% $Rh/SrNi_{0.4}Al_{11.6}O_{19-\alpha}$ for 100 Hours; GHSV=50,000 $cm^3/g/h$, Temp=850°C, P=2 atm, O/C=1.2.

Conclusions

NETL synthesized catalysts exhibiting similar hexaaluminate-type structure. Several hexaaluminate-type catalysts for n-tetradecane partial oxidation showed variation between samples with similar Ni content. Samples promoted with 1 wt% Rh produced the greatest H_2 yields and CO selectivity. $BaNi_{0.4}Al_{11.6}O_{19-\alpha}$ showed excellent partial oxidation stability over 100 hours of operation. A 100-hour test in the presence of 50 ppm w/w sulfur as DBT on 1 wt% $Rh/SrNi_{0.4}Al_{11.6}O_{19-\alpha}$ showed good sulfur resistance and stability.

FY 2005 Publications/Presentations

1. 2005 Annual SECA Core Program Review
2. "Partial Oxidation of n-Tetradecane over Lanthanum Nickel Hexaaluminate," AIChE Fall Meeting, Austin, TX, 2004, Gardner, T. H., Shekhawat, D., Berry, D. A.
3. "Hexaaluminate-type Catalysts for the Reforming of Hydrocarbon Fuels to Hydrogen and Carbon Monoxide," Patent filed, Gardner, T. H., Shekhawat, D., Berry, D. A.

References

1. Machida, M., Shiomitsu, T. and Eguchi, K., *J. Solid State Chem.* 95 (1991) 220-223.
2. Machida, M., Eguchi, K. and Arai, H., *J. Catal.* 103 (1987) 385-393.
3. Xu, Z., Zhen, M., Bi, Y. and Zhen, K., *Catal. Lett.* 64 (2000) 157-161.
4. Gardner, T. H., Shekhawat, D., Berry, D. A., AIChE Fall Meeting, Austin, TX (2004).
5. Rostrup-Nielsen, J. R., Catal. Sci. & Tech., Ed. J. R. Anderson and M. Boudart, Vol. 5, pp. 90-91, Springer-Verlag, NY, 1984.
6. Bengaard, H. S., Norskov, J. K., Sehested, J., Clausen, B. S., Nielsen, L. P., Molenbroek, A. M. and Rostrup-Nielsen, J. R., *J. Catal.*, pp. 365-384, Vol. 209 (2002).
7. Besten, I. E. and Selwood, P. E., *J. Catal.*, Vol. 1, pp. 93-102 (1962).

III.B.7 Diesel Fuel Reforming Kinetics

Dushyant Shekhawat (Primary Contact), David A. Berry, and Todd H. Gardner
U. S. Department of Energy
National Energy Technology Laboratory
P. O. Box 880
3610 Collins Ferry Road
Morgantown, WV 26507-0880
Phone: (304) 285-4430; Fax: (304) 285-4403; E-mail: Dushyant.Shekhawat@netl.doe.gov

Objectives

- Develop the kinetic reaction rate and general methodology for the kinetic rate determination for diesel fuel reforming to support the development of auxiliary power units (APUs) in commercial diesel truck transportation and other related applications as being sponsored by the National Energy Technology Laboratory's (NETL's) Solid State Energy Conversion Alliance (SECA) Fuel Cell Program

Approach

- Conduct ternary fuel compound studies
- Develop surface response maps for ternary fuel mixtures
- Evaluate the reforming properties of additional model compounds that are structurally different than the original model compounds to examine if similar behavior exists
- Propose initial kinetic network for individual model compounds

Accomplishments

- Conducted ternary fuel compound studies
- Developed surface response maps for steam reforming (SR), partial oxidation (POX) and autothermal reforming (ATR) over Pt catalysts for three component fuels
- Investigated how the number of rings or the type of substituents in aromatics and naphthenes can affect the reforming characteristics of the fuel
- Studied the effect of branching in alkanes as well as in the side chain of aromatics and naphthenes on the reforming properties

Future Directions

- Develop an intrinsic kinetic expression for a surrogate middle distillate fuel
- Characterize the carbon formation
- Initiate studies to define a generic kinetic methodology for any catalyst scheme or fuel components
- Obtain experimental reactor performance data to validate reaction models and provide for fuel reactant mixing modeling capability suitable for computational fluid dynamics (CFD) modeling codes
- Develop a detailed kinetic model that incorporates CFD

Introduction

The U.S. Department of Energy is sponsoring development of high-temperature fuel cell power systems based on solid oxide technology through its Solid State Energy Conversion Alliance (SECA) program. The program is geared at mass manufacturing of fuel cells for high-volume markets and multiple applications. One of those markets/ applications is a diesel-fueled auxiliary power unit

(APU) for long-haul truck transportation. The fuel processor is a critical component of this system and must be able to provide a clean, tailored synthesis gas to the fuel cell stack for long-term operation. Key characteristics desired for the processor (and the system) include low cost, high efficiency, maximum thermal integration, low maintenance intervals, and acceptable startup and transient response. There are also several barrier issues that must be overcome to achieve these characteristics. Carbon formation, particularly upon startup, must be minimized to avoid coking of the catalysts in the reformer and downstream fuel cell. Fuels containing sulfur can poison both the reforming catalysts and the fuel cell anode. High thermal mass components (some of which may have heat-ramp restrictions) can limit startup times and transient response. And finally, cost targets must be achieved to ensure commercial success. Depending on the system approach taken, technology is needed to resolve these barriers.

Better knowledge of the reforming kinetics as a function of fuel composition, catalyst formulation, oxygen-to-carbon ratio, steam-to-carbon ratio, and temperature is required to ensure dynamic operation of fuel reformer during transients and during the long-term operations. It also helps in understanding how the structure of the liquid fuel components affects the overall reforming reaction rate, the rate of carbon formation, and the propensity of sulfur poisoning. It can assist in formulating an optimal catalyst as well as fuel, if desired, for the fuel reforming process. An intrinsic kinetic expression can be used for further high-level overall modeling of fuel cell systems. For example, the set of kinetic rate expressions derived from this work can be included in a detailed three-dimensional CFD model of diesel reformers. Superior models would assist in designing the reactors and reaction parameters without conducting a series of unnecessary experiments. Furthermore, better models can be helpful in control, scale-up, and on-board diagnostics of the fuel reformer.

Determination of a detailed kinetic rate expression for liquid hydrocarbon reforming is very complicated because liquid hydrocarbons are complex mixtures of hundreds of components, and each one undergoes several different reactions. For example, in addition to the reactions associated with reforming, other reactions may take place: water-gas shift, carbon formation, methanation, hydrocracking, dehydrocyclization, dehydrogenation, hydrogenation, ring opening, etc. Also, the activity of the catalyst changes rapidly during the reaction. Computation of the rate parameters can be very challenging since the reaction kinetics involves a large number of species and reactions at various reaction conditions where corresponding differential equations can be very stiff.

For such complex reactions, the experimental rate data are fit into power law or even first-order rate expressions for simplification. Unfortunately, these tend to be limited to a specific catalyst, fuel composition, and operating condition. It would be desirable to develop predictive models to account for variations in these parameters, but meager information is available on the kinetics of liquid hydrocarbon reforming to produce syngas. Literature is limited mostly to kinetic studies of steam reforming of single paraffinic components.

For the autothermal reforming of diesel with steam and oxygen, a complex reaction network is expected. Elucidation of this network and the development of a generalized complex network model for platinum catalysts will be the initial focus of this body of work. The overall kinetic approach employed will balance the level of detail that can accurately be accommodated by CFD code with the ability to easily update kinetic parameters for a new catalyst system.

Approach

Understanding the reaction mechanisms and pathways for the chemical system is necessary to develop appropriate reaction kinetics. We used the surface response mapping technique to map characteristic responses (e.g. yield, conversion, etc.) to input variables [temperature, gas hourly space velocity (GHSV), etc.] over a defined region. This technique identifies the significance of parameters and their interactions. Also, different hypothetical reaction pathways of the reforming reaction are established based on the response surface methodology studies. The feasibility of each of the proposed hypothetical kinetic schemes can be evaluated with respect to the experimental results

using a regressive technique. As the most important mechanisms and reaction pathways are defined, appropriate kinetic parameters will be determined for the corresponding kinetic scheme. This will initially be done for individual reaction systems over a platinum catalyst. Later, it will be extended to more complex fuel mixtures as well as to other catalyst systems as needed to complete the model. Therefore, a generic methodology for the kinetic rate determination for diesel fuel reforming will be developed. Catalyst deactivation (carbon formation and sulfur poisoning) kinetics will also be incorporated in the kinetic model.

A fixed bed reactor system was used to conduct the experiments. The reactor was operated continuously at steady state. γ-Alumina-supported platinum (0.611 wt%) catalyst (surface area 103 m^2/g) was used in this study as a base catalyst. A summary of reaction conditions is given in Table 1.

Table 1. Experimental Conditions

	ATR	SR	POX
O_2/C	0.3	0.0	0.5
H_2O/C	1.5	3.0	0.0
T (^oC)	750 - 850	750 - 850	750 - 850
GHSV (h^{-1})	25,000 - 150,000	25,000 - 150,000	25,000 - 150,000

A mixture of three model compounds from three main hydrocarbon classes present in diesel fuel—paraffins, aromatics, and naphthenes—will be used to understand the ternary effects of feed components. Tetradecane (TD), decalin (DL), and 1-methylnaphthalene (MN) are identified as model compounds to represent paraffins, naphthenes, and aromatics, respectively, found in diesel. A rotatable-central-composite design will be used for process optimization. Also, additional model compounds that are structurally different than the original model compounds were evaluated for their reforming properties. Compounds studied are cetane, isocetane, 1-cetene, tetralin, n-butylcyclohexane, t-butylcyclohexane, n-butylbenzene, isobutylbenzene, t-butylbenzene, and p-cymene. Each model compound will undergo autothermal, partial oxidation, and steam reforming at the temperature and space velocity (SV) range given in Table 1.

Gas chromatography technique was used to identify and separate the reaction products. The gases (N_2, O_2, CO, CO_2, and CH_4) were analyzed using a Thermo Onix mass spectrometer, and the gaseous hydrocarbons were analyzed using a flame ionization detector. Gas chromatography (Perkin Elmer's AutoSystem XL) coupled with mass spectrometry (Perkin Elmer's TurboMass Gold) was used to quantify and identify the complex liquid hydrocarbon product mixture that formed at various hydrocarbon conversions. Yield of product A (H_2, CO, and CO_2) can be defined as

$$\text{Yield of A}(\%) = \frac{\text{Moles of A produced}}{\text{N} \times \text{moles of hydrocarbon fed to the reactor}} * 100$$

where N is the number of moles of hydrogen per mole of hydrocarbon for H_2 yields and is the number of carbons in hydrocarbon fuel for yields of other products. In some cases, H_2 yields may be higher than 100% since steam reforming and water-gas shift reaction also contribute to H_2 production apart from hydrocarbons.

Results

The yields (z) of individual species from hydrocarbon reforming, which depend on the space velocity (x) and reaction temperature (y), can be described by the equation

$$z = b_0 + b_1x + b_2y + b_{11}x^2 + b_{22}y^2 + b_{12}xy \qquad (1)$$

where z = the yield of individual species after completion of the reaction, x = temperature (K), y = gas hourly space velocity (h^{-1}), and $b_0 \ldots b_{22}$ are the coefficients of the model. The coefficients of Equation 1 were estimated by making use of the responses of experiment for the standardized values of x and y, which varied in the range given in Table 1. The relationships between yields (z) and two quantitative variables x (space velocity) and y (reaction temperature) are represented by response surface curves, as shown in Figures 1-2. Coefficients of quadratic Equation 1 are summarized in Table 2 for H_2 and CO yields from autothermal reforming of a benchmark diesel fuel consisting of 40 wt% TD, 40 wt% DL, and 20 wt% MN. Quadratic fit of data from response surface mapping was excellent (>90%).

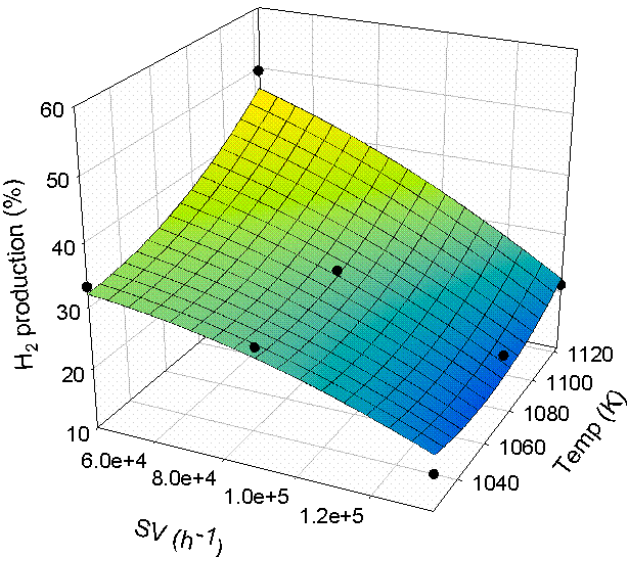

Figure 1. Yield of H_2 from ATR of the Benchmark Diesel Fuel (O_2/C = 0.3 and S/C = 1.5)

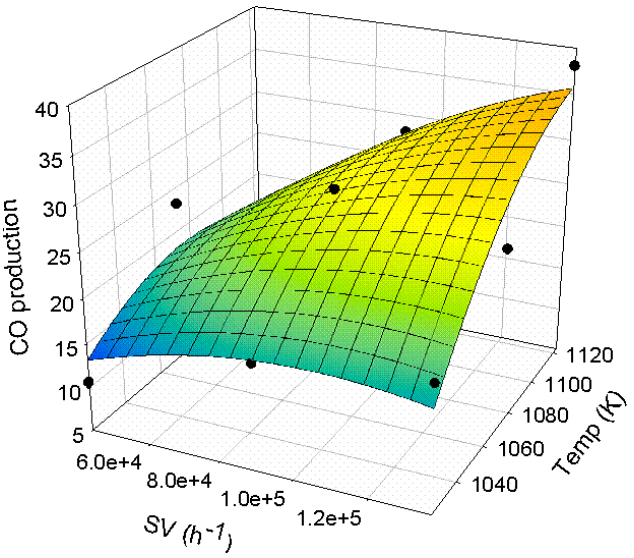

Figure 2. Yield of CO from ATR of the Benchmark Diesel Fuel (O_2/C = 0.3 and S/C = 1.5)

Different hypothetical reaction schemes of the process are established based on the response surface methodology studies. Each of the proposed kinetic schemes is being evaluated with respect to the experimental results using an iterative predictor-corrector method based on the Himmelblau-Jones-Bischoff technique [2, 3]. The following criteria are being utilized to assess the validity of the model: calculated rate constants (positive values and follow Arrhenius Law), minimized value of objective function, and calculated profile of species concentration variations.

Table 2. Coefficients of Quadratic Equations for Autothermal Reforming of Benchmark Diesel Fuel

	Coefficients						R^2
	b_0	b_1	b_2	b_{11}	b_{22}	b_{12}	
H_2	1319.4	-2.58	$1.3e^{-3}$	$1.3e^{-4}$	$-9.8e^{-10}$	$-1.2e^{-6}$	91.9
CO	-1771.6	3.37	$-1.7e^{-3}$	$-1.6e^{-3}$	$-1.2e^{-9}$	$1.9e^{-6}$	92.8
CO_2	1530.4	-2.61	$-2.4e^{-3}$	$1.1e^{-3}$	$-1.8e^{-10}$	$2.3e^{-6}$	92.3

Earlier in this project, individual model compounds representing each hydrocarbon class present in diesel fuel were evaluated to understand their reforming properties over Pt catalysts [1]. It was noted that each model compound kinetically behaved differently upon reforming under similar conditions. Hydrocarbon product distributions depended greatly on the model compound, the type of reforming performed, and the process parameters (space velocity and reaction temperature).

In a ternary benchmark diesel fuel, overall H_2 yields are not simply the additive total of the yields from the individual fuel components. The relative reactivity of one fuel component considerably affects the conversion pattern of the other components as well as the overall product distribution. For example, aromatics are relatively less reactive than paraffins; hence, highly reactive paraffins would consume the available O_2 in POX and ATR reactions. Therefore, the conversion of highly reactive fuel components proceeds toward completion and produces combustion products. Oxygen is not available for the less reactive components; consequently, the less reactive components predominantly undergo pyrolysis reactions.

POX was affected significantly by the difference in the reactivity of fuel components, while SR was not affected much from the difference in reactivity of fuel components because water was present in abundance in SR. ATR was somewhere in the middle.

Higher H_2 and CO selectivities were observed from ATR and POX of HD compared to TD. Higher

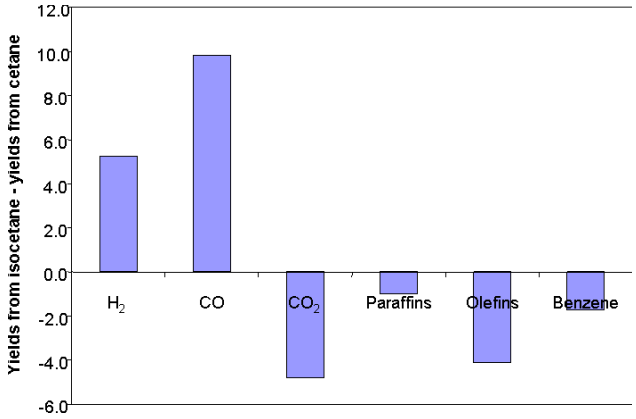

Figure 3. Difference in Yields of H_2, CO, and Other Byproducts from POX of Isocetane and Cetane at 825°C and 50,000 h^{-1}

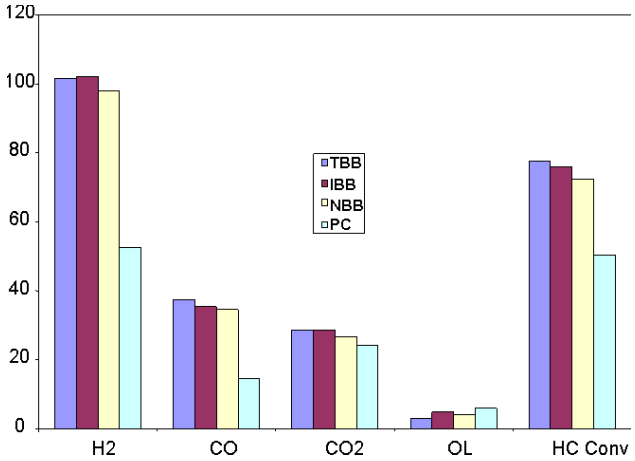

Figure 4. Yields and Conversion from ATR of tert-Butylbenzene (TBB), Isobutylbenzene (IBB), n-Butylbenzene (NBB), and p-Cymene (PC) at 825°C and 50,000 h^{-1}

olefin production and higher carbon formation were observed during the reforming of TD than during the reforming of HD. However, more experiments are needed with lower hydrocarbons such as n-dodecane or n-decane to relate the syngas production to the carbon chain length in n-paraffins.

Reforming of isocetane and cetane was conducted to study how a branched alkane (isoparaffin) may kinetically behave differently than a n-alkane. Figure 3 shows the difference in yields of H_2, CO, and other byproducts from POX of isocetane and cetane. Clearly, POX of isocetane produced higher yields of H_2 and CO compared to n-cetane, while producing less coke precursors such as olefins and aromatics. Different olefin product distribution was observed; more isobutylene was formed from isocetane reforming, while n-cetane formed more ethylene and propylene. Higher activity of isooctane can be devoted to the tertiary C-H bonds present in the isocetane molecule because hydrogen atom abstraction rates are highest for the tertiary C-H bonds and, subsequently, isoparaffins should be attacked quickly; therefore, isoparaffins are more reactive than n-paraffins [4].

The type of substituent in aromatics and naphthenes also significantly affects the overall hydrocarbon conversion, syngas selectivities, and carbon formation. Reforming of four butylbenzene isomers was conducted to study the effect of branching in alkyl substituents on the benzene ring. The reactivity of substituted benzenes increased with increasing order of C-H bonds in alkyl substituents. Product distributions from ATR of tert-butylbenzene, isobutylbenzene, n-butylbenzene, and p-cymene (p-isopropyltoluene) are shown in Figure 4. Carbon formation as well as olefin (OL) production (coke precursors) also depended on the degree of branching in alkyl substituents; tert-butylbenzene produced the least carbon while maintaining the highest conversion and syngas yields compared to n-butylbenzene. Higher benzene formation (dealkylation of substituted benzenes) was observed from all butylbenzene isomers studied. Higher syngas yields, lesser carbon formation, and higher hydrocarbon (HC) conversion were observed from reforming of tert-butylcyclohexane compared to n-butylcyclohexane.

Reforming of decahydronaphthalene, tetrahydronaphthalene, and 1-methylnaphthalene was conducted to investigate the effect of degree of saturation on their reforming properties. There was not significant difference found between the reforming properties of decalin and tetralin; modest higher activity was observed from reforming of decalin compared to tetralin. However, the reactivity of MN was significantly lower compared to tetralin; yields of H_2 were more than double with TL compared to MN. Therefore, the number of aromatics rings in a hydrocarbon greatly affects its activity, and the presence of such compounds in a fuel mixture considerably reduces the syngas yields.

Conclusions

- For the reforming of a fuel mixture, overall yields are not additive of yields from individual fuel components.
- Relative reactivity of one fuel component considerably affects the conversion pattern of others.
- Relative reactivities of alkanes depend on the relative ease with which the different classes of hydrogen atoms are abstracted, and that is as follows: tertiary > secondary > primary > methane.
- Molecules containing higher number of tertiary C-H bonds are relatively more reactive.
- The structure of substituents in aromatics and naphthenes greatly affects the reforming properties of these compounds.

FY 2005 Publications/Presentations

1. D.A. Berry, D. Shekhawat, T.H. Gardner, "NETL On-Site Fuel Processing Activities", 2005 SECA Core Technology Review, January 2005.
2. D.A. Berry, D. Shekhawat, T.H. Gardner, "Development of Reaction Kinetics for Diesel-Based Fuel Cell Reformers", AIChE Annual Meeting 2004, Austin, TX, November 7-12, 2004.

References

1. D.A. Berry, D. Shekhawat, T.H. Gardner, 2003 Annual Merit Review Meeting of Hydrogen, Fuel Cells & Infrastructure Technologies Program, Department of Energy Office of Energy Efficiency, Berkeley, CA, May 18 – 22, 2003.
2. J. Font, A. Fabregat, Computers Chem. Eng., 21(7) (1997) 719-731.
3. D.M. Himmelblau, C.R. Jones, K.B. Bischoff, Ind. & Eng. Chem. Fundamentals, 6(4) (1967) 539-543.
4. R. Subramanian, G.J. Panuccio, J.J. Krummenacher, I.C. Lee, L.D. Schmidt, Chem. Eng. Sci., 59 (2004) 5501-5507.

III.C Power Electronics

III.C.1 Trade Study for Integrating Numerous SECA SOFC Modules

Burak Ozpineci (Primary Contact), Donald J. Adams, Leon M. Tolbert
Oak Ridge National Laboratory, National Transportation Research Center
2360 Cherahala Blvd.
Knoxville, TN 37932
Phone: (865) 946-1329, Fax: (865) 946-1262, E-mail: ozpinecib@ornl.gov

DOE Project Manager: Don Collins
Phone: (304) 285-4156, E-mail: Donald.Collins@netl.doe.gov

Subcontractors:
MESTA Electronics, N. Huntingdon, PA

Objectives

- Identify power topologies that can be used to integrate numerous solid oxide fuel cell modules to supply much higher power than a single module can supply.
- Evaluate the pros and cons of each topology.
- Compare different topologies with respect to each other.

Approach

- Identify the requirements of a power converter for a fuel cell interface.
- Study the electrical supply characteristics of fuel cells.
- Identify power converter topologies with multiple inputs.
- Analyze the possible effects of using several fuel cell modules using multi-input power converters.
- Evaluate the possibility of modifying controls to suit the load by varying voltage output of the fuel cells for better fuel cell utilization.

Accomplishments

- Identified five different families of power converter topologies that can be used to integrate numerous SOFC modules.
- Listed the pros and cons for each power converter topology.
- Developed a level reduction technique applied to multilevel converters integrating several fuel cell modules to increase the fuel cell utilization.
- Built a comparison matrix to compare all these power converter topologies with respect to cost, fault tolerance, reliability, etc.
- Completed the final report.

Future Directions

- Follow the literature for a possible addition to the five power topologies included in this project.
- Examine the possibility of repeating the study for fuel cell hybrid systems.
- Consider conducting a study comparing DC distribution and AC distribution for fuel cell power generation.

Introduction

The U.S. Department of Energy's Solid State Energy Conversion Alliance (SECA) program is targeting solid oxide fuel cell (SOFC) modules in the 3–10 kW range to be made available for residential applications. In addition to residential use, these modules can also be used in apartment buildings, hospitals, etc., where a higher power rating would be required. For example, a hospital might require a 250-kW power supply. To provide this power using the SOFC modules, 25 of the 10-kW modules would be required. These modules can be integrated in different configurations to yield the necessary power. This report will show five different approaches for integrating numerous SOFC modules and will evaluate and compare each one with respect to cost, control complexity, ease of modularity, and fault tolerance.

Approach

The static and dynamic characteristics of SOFCs have been studied to identify the power converter requirements. With these in mind, several multi-input power converter systems have been studied to make sure they will be suitable for integration of numerous SOFCs. Using these converter topologies, the possible effects of integrating several fuel cell modules have been analyzed. Finally, these topologies have been compared with respect to cost, control complexity, reliability, availability (at power system and device levels), fault tolerance, modularity (ability to isolate portions of the system for service or add power generation capacity while other portions of the complete system are still functioning), energy conversion efficiency, and ease of mass customization to enable mass production to drive down costs.

While studying the power converter topologies, it was found that there is a possibility of modifying controls to suit the load by varying voltage output of the fuel cells for better fuel cell utilization. To achieve this, a control technique was developed and analyzed using simulation and some experimentation using batteries instead of fuel cells.

Results

The five power converter topologies selected for integrating numerous fuel cells are series configuration, DC link configuration, high-frequency AC link distribution, cascaded multilevel configuration, and multilevel configuration. A matrix given below compares these configurations with respect to each other.

	A	B	C	D	E
a	1	3	3	3	5
b	1	4	4	4	5
c	4	2	2	2	3
d	1	1	1	1	5
e	5	1	1	1	1
f	5	1	2	2	2
g	1	3	3	2	4
h	1	2	2	2	2

A. Series configuration

B. Cascaded multilevel configuration

C. Multilevel configuration

D. DC link configuration

E. High-frequency AC (hfac) link configuration

a. Cost (capital and operating) (1-Less expensive, 5-More expensive)

b. Control complexity (1-Less complex, 5-More complex)

c. Reliability (1-More reliable, 5-Less reliable)

d. Availability (at power system and device levels) (1-Better availability, 5-Worse availability)

e. Fault tolerance (1-More fault tolerant, 5-Less fault tolerant)

f. Modularity (ability to isolate portions of system for service or add power generation capacity while other portions of the complete system are still functioning) (1-More modular, 5-Less modular)

g. Energy conversion efficiency (1-More efficient, 5-Less efficient)

h. Ease of mass customization to enable mass production to drive down costs (1-Easier, 5-More difficult

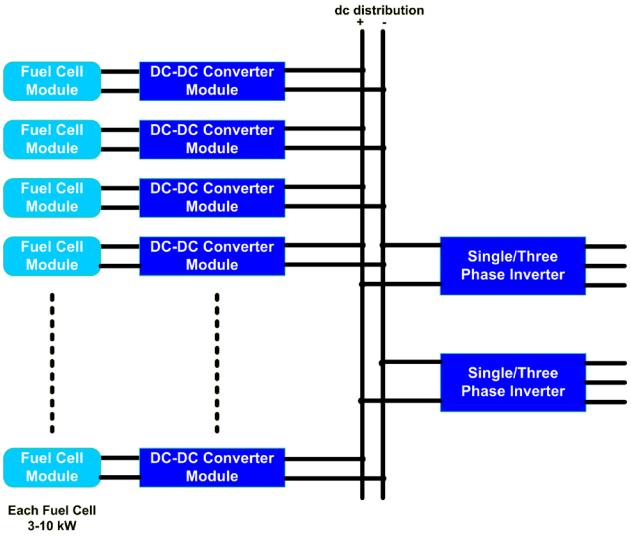

Figure 1. Block Diagram of the DC Distribution Configuration

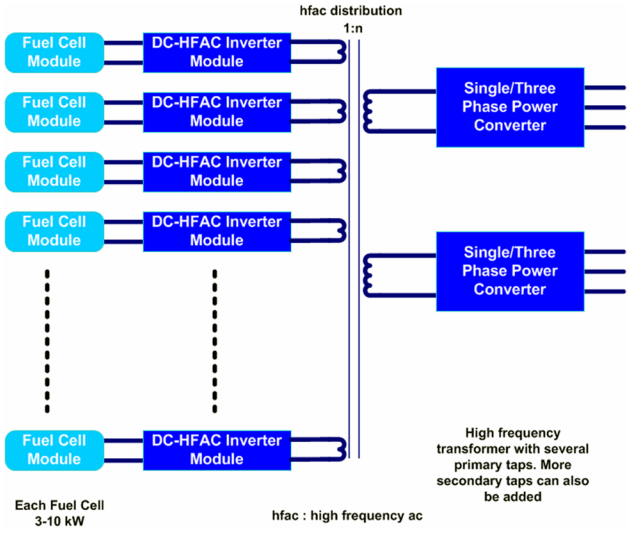

Figure 2. Block Diagram of the hfac Distribution Configuration

Figures 1 and 2 show the block diagrams of the DC link configuration and the hfac link distribution configuration, respectively.

The output voltages of fuel cells vary with load current. The power converter does not always operate at full load at rated fuel cell voltage. As the load current decreases, the fuel cell output voltage increases. This causes challenges in the converter design, since the converter switches have to be derated to accommodate the higher voltages. When numerous fuel cell modules are integrated, as the

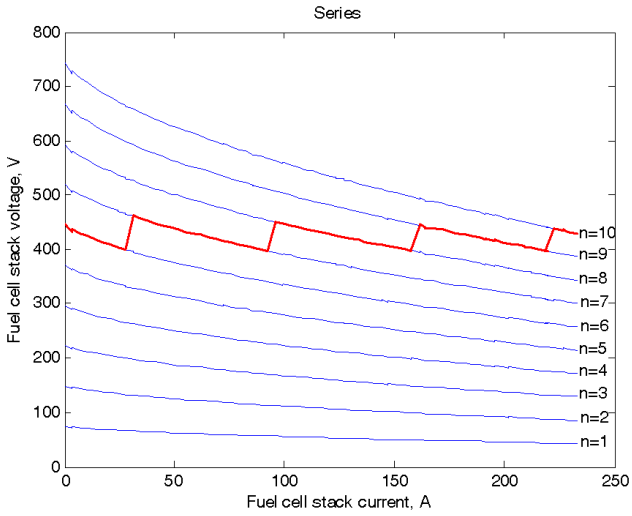

Figure 3. Static Characteristics for up to 10 Fuel Cells in Series and Level Reduction Technique

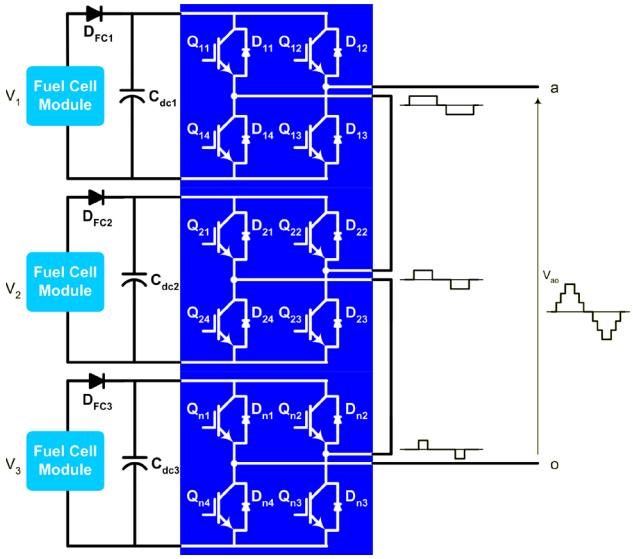

Figure 4. One Phase of a Cascaded Three-Level Inverter

load current decreases, some number of fuel cells can be taken off-line so that the remaining fuel cells can still provide the same power but at a voltage close to the rated value. This is called the level reduction control technique. A cascaded multilevel DC-DC converter is the best choice for this operation. Figure 3 shows the static characteristics of 1 to 10 fuel cells in series and how the level reduction works as the current decreases. As seen in this figure, even though fewer fuel cells are used, they can still supply the required power. Since level reduction technique keeps the fuel cell output voltage lower, lower voltage rated devices can be used in the converters.

Figure 4 shows a cascaded multilevel inverter, which can also be controlled with the level reduction technique. In this case, the inverter switches are turned on and off by a fundamental frequency sine-triangle comparison technique developed for this converter which reduces the inverter levels (or takes fuel cells off-line) automatically, when needed.

Conclusions

Novel multiple-input converter topologies for fuel cells have been reviewed and compared with each other.

With level reduction control technique exploiting the V-I characteristics of fuel cells, the need for derating power semiconductors in fuel cell systems is eliminated. By inhibiting some of the fuel cells and using the inhibited fuel cells in other applications, like charging batteries, the system efficiency and the fuel cell utilization increase. If these fuel cells are left idling, then the life expectancy of the system increases. In addition to these benefits, using a multilevel converter also brings the advantages of modularity and increased reliability.

For the multilevel inverter, a fundamental switching sine-triangle comparison method is introduced. This method decreases the complexity of the level reduction control for the multilevel inverters by eliminating the need for storing separate switching angle look-up tables for each number of DC sources.

The level reduction technique is also applicable to other fuel cell-fed multilevel inverters.

FY 2005 Publications/Presentations

1. B. Ozpineci, D. J. Adams, and L. M. Tolbert, Trade study on aggregation of multiple 10-kw solid oxide fuel cell power modules, Report ORNL/TM-2004/28, November 2004.

III.C.2 A Low-Cost Soft-Switched DC/DC Converter for Solid Oxide Fuel Cells

Jason Lai (Primary Contact), Changrong Liu, Seungryul Moon, Sung Yeul Park, Ken Stanton
Virginia Polytechnic Institute and State University
614 Whittemore Hall
Blacksburg, VA 24060
Phone: (540) 231-4741; Fax: (540) 231-3362; E-mail: laijs@vt.edu

DOE Project Manager: Don Collins
Phone: (304) 285-4156; E-mail: Donald.Collins@netl.doe.gov

Subcontractor:
EPRI Solutions, Knoxville, Tennessee

Objectives

- Develop a low-cost DC-DC converter for low- to high-voltage power conversion as the standard interface between the solid oxide fuel cell (SOFC) source and the load-side DC-AC inverter.
- Achieve 97% DC/DC conversion efficiency for the Solid State Energy Conversion Alliance (SECA) 5-kW solid oxide fuel cells.
- Advance high-power DC-AC converter technology with high-efficiency soft switching and high-performance digital controlled techniques.

Approach

- Develop an interleaved multiphase isolated DC-DC converter (V6 converter) that reduces the high-frequency ripple going back to the fuel cell and the electromagnetic interference (EMI) that appears at the output.
- Develop a current loop control method to eliminate low-frequency ripple going back to fuel cell while maintaining stable voltage control at the converter output.
- Develop a phase-shift modulated soft-switching technique to eliminate switching losses of the DC-DC converter.
- Design an intelligent digital controller for high-performance SOFC power conversions.
- Test the converter with a calorimeter to characterize the converter efficiency.
- Test the converter with fuel cell simulator and SOFC to demonstrate the performance improvement over conventional power electronics designs.

Accomplishments

- *Demonstrated 97% Efficiency with the V6 Converter Prototype*
  The multiphase isolated V6 DC/DC converter has been developed for low-voltage input and high-voltage output, especially for SECA SOFC applications. The prototype 5-kW V6 converter has been tested with a calorimeter to demonstrate 97% efficiency over a wide load range.
- *Demonstrated Low-Frequency Ripple Reduction from 33% to 2%*
  A novel current loop control technique has been developed for fuel cell current ripple reduction. Standard converter design with voltage loop shows 33% peak-to-peak ripple. With the newly developed control, the peak-to-peak ripple is reduced to 2%. This implies that the fuel cell capacity is increased by more than 15%.

- *Developed Precision Digital Control for Multiphase Converter*
  A precision digital control method has been developed for multiphase converter timing control that can meet the requirements of any angle between phases. The V6 DC-DC converter requires 120° between phases. Conventional analog control has difficulty getting precise angles, resulting in unbalanced transformer input and flux saturation.
- *Packaged the V6 Converter and a DC-AC Inverter for Field Testing*
  The beta version V6 converter and an in-house DC-AC inverter are packaged together to fit a standard 5.25" x 19" rack-mount cabinet. The unit has been tested with in-house power supply and is being prepared for field testing.

Future Directions

- *Test the V6 Converter with the Fuel Cell Simulator and SOFC*
  The integrated V6 DC-DC converter and DC-AC inverter will be tested with an in-house fuel cell simulator and with a SECA SOFC at Siemens-Westinghouse in Pittsburgh, Pennsylvania, to demonstrate efficiency improvement over the existing power conditioning system.
- *Develop a Soft-Switching Inverter Achieving 99% Efficiency*
  A new soft-switching inverter is proposed to achieve a DC-AC inverter efficiency of 99%. The technique has been proven with an existing Virginia Tech high-power inverter for motor drive applications. For relatively low-voltage SOFC power conditioning systems, a new design is being conceived for >99% efficiency inverter development.
- *Achieve 96% Efficiency for the Entire Power Conditioning System*
  The integrated V6 DC-DC converter and soft-switching will be able to achieve 96% efficiency, which is at least 6% higher than off-the-shelf power conditioning systems. With ripple reduction, the overall SOFC capacity gain with the entire power conditioning system will be more than 20%.
- *Develop Utility Grid Interconnect Control*
  The existing inverter was designed for standalone mode operation. The proposed work is to design utility grid interconnect control with synchronization and power quality compliance. The utility grid interconnect will be tested at the distributed generation lab of Southern California Edison in Los Angeles, California.
- *Test DC-DC Converter EMI Performance*
  With interleaved DC-DC converter control, the high-frequency ripple is significantly reduced. Its EMI performance will be tested at EPRI Solutions in Knoxville, Tennessee.

Introduction

The Virginia Tech SECA project is to focus on high-efficiency and low-cost DC-DC converter design and prototype development. The Phase I effort was to demonstrate the feasibility and design approach with a bench model. A multiphase interleaved soft-switching V6 DC-DC converter was successfully developed and demonstrated 97% efficiency. The focus this past year was to reiterate the design and to build a field demonstration prototype. The efficiency profile was verified with extensive tests using a homemade calorimeter for accurate loss measurement.

The prototype DC-DC converter and an in-house DC-AC inverter were incorporated for fuel cell interaction testing. It was found that a significant current ripple with twice the AC output frequency was drawn by the fuel cell. The tested fuel cell tripped prematurely with such a current ripple because its balance-of-plant controller sensed the continuous over-current condition. Thus, a novel control technique was then conceived and developed for the ripple current reduction. The proposed control successfully suppresses the fuel cell ripple current content and effectively increases fuel cell capability. The significance to the SECA program and SOFC design of ripple reduction and power converter efficiency is the savings on the fuel cell stack size and the reduction of fuel consumption.

Approach

The major loss components are power semiconductor devices, but the major cost items are typically transformers and passive components. Thus, the proposed V6 DC-DC converter is to eliminate the high-frequency switching ripple through interleaved multiphase converters so that the input capacitor and output filter inductor size and cost can be reduced. With the three-phase 6-leg converter design, the passive component cost and size reduction is 6 times; the associated losses are also reduced at least 6 times. The converter within each phase is modulated with phase shift to achieve zero-voltage switching, thereby eliminating the switching losses to further enhance the efficiency.

While continuing the improvement of the converter design through extensive testing, we found significant current ripple drawn by the fuel cell when a DC-AC inverter is added to the output stage as an active load. The ripple with standard design is 33% peak-to-peak, which significantly limits the output capability of the fuel cell. Such a current ripple can be reduced by adding energy storage capacitors, but the cost and size penalty of these bulky capacitors is not acceptable for our cost target. Thus, we proposed an intelligent control technique that adds a current loop to regulate the converter output average current so that ripple is no longer fed back to the fuel cell, and the resulting ripple with the same energy storage component is reduced to 2% peak-to-peak.

With successful development of ripple reduction and the efficiency target being met, we reiterated the V6 converter design with a new package for field testing and demonstration. Our research collaborator for the SOFC test is Siemens-Westinghouse in Pittsburgh, Pennsylvania, and our collaborator for the EMI test is ERPI Solutions in Knoxville, Tennessee. A Knoxville-based startup company – PEMDA – already licensed the V6 converter for renewable energy applications. The entire Phase II SECA project schedule is shown in Table 1.

Table 1. SECA Phase II Schedule

	Jan-04 Mar-04	Apr-04 Jun-04	Jul-04 Sep-04	Oct-04 Dec-04	Jan-05 Mar-05	Apr-05 Jun-05	Jul-05 Sep-05	Oct-05 Dec-05
1 Define SOFC specification								
2. Define SOFC and DC/DC interface								
3. Define physical package								
4. Design calorimeter								
5. Iterate phase I design 5.1 optimize power circuit 5.2 optimize transformer 5.3 optimize thermal management 5.4 optimize auxiliary power supply 5.5 sensor conditioning 5.6 DSP controller interface 5.7 complete design engineering documentation								
6. Component sourcing								
7 Fabricate beta version DC/DC								
8. Test the beta version DC/DC with power supply								
9. Test beta version DC/DC with SOFC								
10. Tech transfer								

Results

Figure 1(a) shows the proposed V6 DC-DC converter circuit diagram. Rather than the passive load tested in Phase I, the output of this Phase II converter is a DC-AC inverter. Figure 1(b) shows the photograph of the combined 5-kW DC-DC converter and DC-AC inverter prototype. The component sources were all identified, and the V6 DC-DC converter component parts count and costs

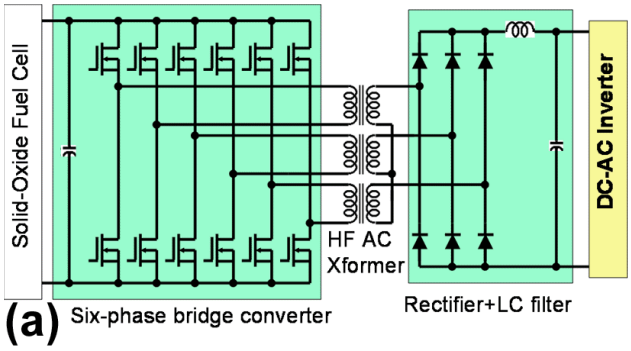

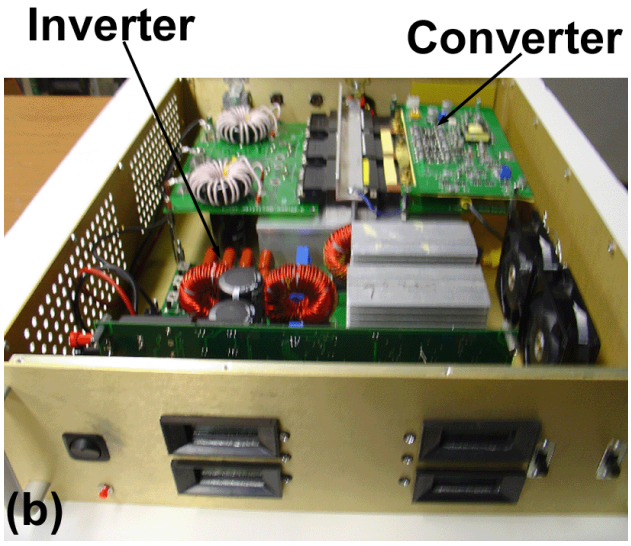

Figure 1. Circuit Diagram and Photograph of the V6 DC/DC Converter: (a) Schematic Circuit Diagram; (b) Photograph of the 5-kW DC-DC Converter and DC-AC Inverter Prototype

Table 2. V6 Converter Prototype Cost Estimate

Key Materials	Parts Count	Qty 1	Qty 10000
Power Circuit	22	$571.00	$154.40
Devices	8	$201.00	$38.40
Capacitors	6	$84.00	$30.00
Transformers	3	$180.00	$45.00
Inductors	2	$24.00	$8.00
Sensors	2	$32.00	$8.00
Contactor	1	$50.00	$25.00
Control Circuit	325	$113.70	$33.22
Resistors	164	$18.59	$2.71
Capacitors	110	46.61	$17.41
Discretes	27	$8.00	$2.42
IC's	24	$40.50	$10.68
Miscellaneous	55	$174.80	$52.44
Total	**402**	**$840.50**	**$227.05**

are shown in Table 2. At quantity of 1, the component cost is about $840, and at quantity of10,000, the component cost is reduced to $227. With a further increase in production quantity, the cost target of $40/kW can be achieved.

For the 3-phase 6-leg DC/DC converter, every two phase-leg pair forms a single-phase full-bridge converter that can be operated at zero-voltage switching condition with phase-shift-modulation control. Three full-bridge converters are phase-shifted 120° with transformer currents interleaving each other to cancel the high-frequency ripple at both input and output; thus, the size of the input filter capacitor and output filter inductor can be largely reduced. The size and cost of these passive components are 6 times lower compared to the single phase-leg converter, and their associated losses are also reduced at least 6 times.

Figure 2 shows the efficiency measurement for the prototype V6 DC-DC converter. Figure 2(a) is the calorimeter setup for accurate loss measurement. Figure 2(b) is the measured V6 converter efficiency profile over a wide load range. The 97% converter efficiency is verified through extensive calorimeter tests.

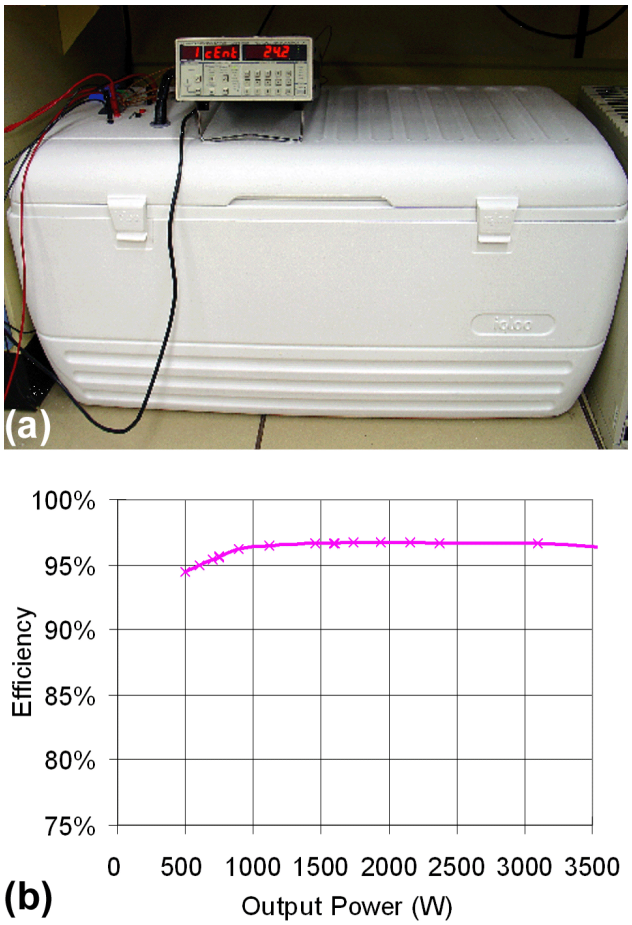

Figure 2. Efficiency Measurement: (a) Calorimeter Setup for Accurate Loss Measurement; (b) Measured V6 Converter Efficiency Curve

When both DC-DC converter and DC-AC inverter are combined, the complete prototype can be tested with the standalone AC load. It was found that the AC load current propagates back to the fuel cell with twice the output frequency and 33% peak-to-peak ripple, which significantly limits the output capability of the fuel cell. Thus, we proposed an intelligent control technique that adds a current loop to regulate the converter output average current. Figure 3 shows the block diagram of the proposed current loop control system. A simple proportional-integral (PI) controller is added as the inner current loop, while a similar PI controller remains as the outer voltage loop. By properly adjusting the loop gain and loop control bandwidth, the DC-DC output current is regulated to be DC, and the ripple is contained at the output capacitor.

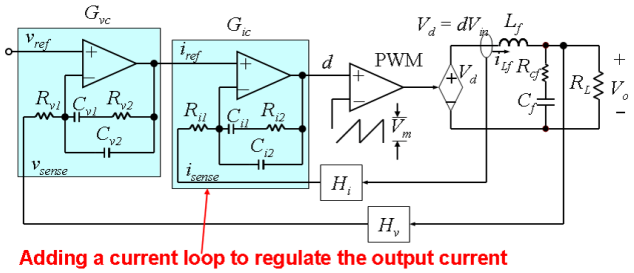

Figure 3. Block Diagram of the Proposed Current Loop Control System

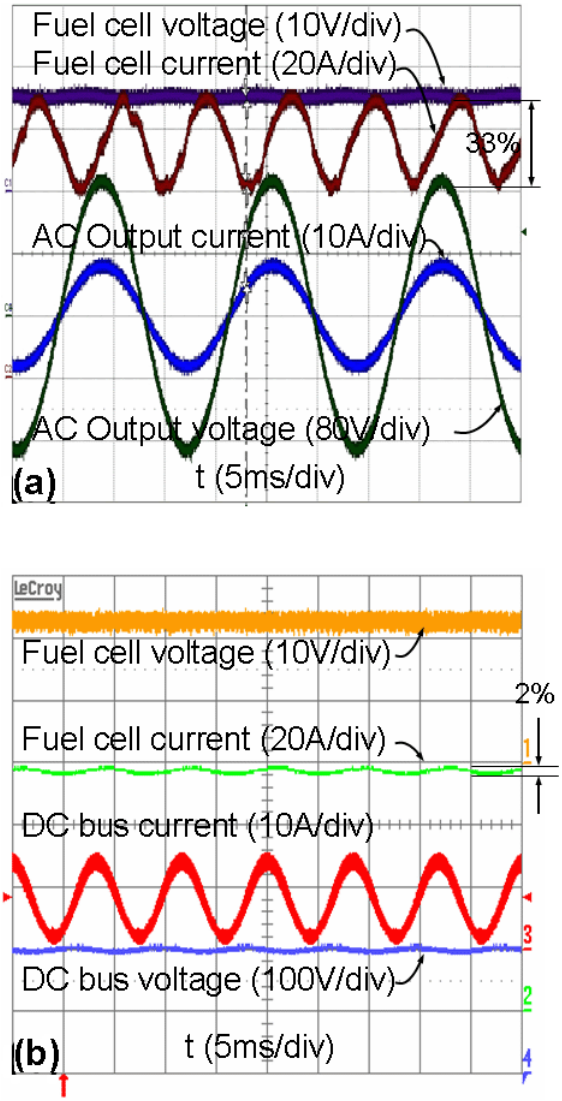

Figure 4. Measured Fuel Cell Current Ripple Reduction Results: (a) With Conventional Voltage Loop Control Only; (b) With the Added Current Loop Control

Figure 4 shows the fuel cell ripple reduction results with the proposed active current ripple elimination control technique. Figure 4(a) shows the results with the conventional voltage-loop controller only. It can be seen that the output AC voltage and current are in phase with 60 Hz frequency. The fuel cell voltage presents a small ripple, but the fuel cell output current contains a 33% peak-to-peak ripple. Figure 4(b) shows the measured results with the proposed active current ripple elimination technique. The fuel cell current ripple is reduced to 2% peak-to-peak, and the fuel cell voltage is purely flat. The converter output current indicates that the 120-Hz ripple content is contained at the output capacitor and is no longer propagating back to the fuel cell.

Conclusions

The proposed V6 DC/DC converter not only achieves the SECA efficiency goal of 97% in a wide power range, but also significantly reduces the passive component size and cost to achieve the $40/kW cost target for power electronics. A novel active fuel cell current ripple elimination control technique was developed to effectively increase the fuel cell capability under AC load conditions. The combination of efficiency gain and ripple reduction allows more than 20% fuel cell size and cost reduction. Major achievements can be summarized as follows.

- Successfully developed the highly efficient V6 DC-DC converter. The technology has been licensed out for renewable energy applications.
- Successfully developed an active current ripple elimination technique without cost penalty. A patent disclosure has been filed.
- Successfully developed the field demonstration V6 converter prototype for low-cost production. The cost spreadsheet indicates the converter can achieve $40/kW in quantity production.

Future work will be the field demonstration with the SOFC and EMI testing.

Special Recognitions & Awards/Patents Issued

1. Ken Stanton, a Ph.D. student funded under the SECA project, received 2004 Fuel Cell Seminar scholarship award to present poster papers.
2. A patent disclosure on Active Fuel Cell Current Ripple Elimination has been filed through Virginia Tech Intellectual Property Office.

FY 2005 Publications/Presentations

1. Changrong Liu, Amy Johnson, and Jih-Sheng Lai, "A Novel Phase-shifting Circuit Using Digital First-In-First-Out (FIFO) for Multiphase Power Converter Interleaved Control," in Proc. of IEEE Workshop on Computers in Power Electronics (COMPEL), Champaign, IL, August 2005, pp. 80–85.
2. Changrong Liu, Amy Johnson, and Jih-Sheng Lai, "A High-Efficiency Multi-Phase DC/DC Converter for Fuel Cell Applications," Poster presentation at 2004 Fuel Cell Seminar, San Antonio, TX, November 2004.
3. Ken Stanton, Michael Schenck, and Jih-Sheng Lai, "Thermally Dependent Electrical Model of a PEM Fuel Cell," Poster presentation at 2004 Fuel Cell Seminar, San Antonio, TX, November 2004.
4. Michael Schenck, Ken Stanton, and Jih-Sheng Lai, "Fuel Cell Converter/Inverter Interaction," Poster presentation at 2004 Fuel Cell Seminar, San Antonio, TX, November 2004.
5. Jih-Sheng Lai, "Fuel Cell Current Ripple Reduction with Active Control Technique," Presentation at SECA Core Technology Program Review Meeting, Tampa, FL, January 27–28, 2005.
6. Michael Schenck, Jih-Sheng Lai, and Ken Stanton, "Fuel Cell and Power Conditioning System Interaction," in Proc. of IEEE Applied Power Electronics Conference, Anaheim, CA, February 2004, pp. 114 – 120.
7. Jih-Sheng Lai, "Power Electronic Technologies for Fuel Cell Power Systems," Presentation at SECA 6th Annual Workshop, Pacific Grove, CA, April 19, 2005.
8. Changrong Liu and Jih-Sheng Lai, "Low Frequency Current Ripple Reduction Technique with Active Control in a Fuel Cell Power System with Inverter Load," in Proc. of IEEE Power Electronics Specialists Conference, Recife, Brazil, June 2004, pp. 2905 – 2911.

III.D Modeling and Simulation

III.D.1 An Integrated Approach to Modeling and Mitigating SOFC Failure

Jianmin Qu (Primary Contact), Andrei Fedorov, and Comas Haynes
Georgia Institute of Technology
801 Ferst Dr.
Atlanta, GA 30332-0405
Phone: (404) 894-5687; Fax: (404) 894-0186; E-mail: jianmin.qu@me.gatech.edu

DOE Project Manager: Travis Shultz
Phone: (304) 285-1370; E-mail: Travis.Shultz@netl.dov.gov

Objectives

- To develop and demonstrate the feasibility of an integrated predictive computer-based tool for fuel cell design and reliability/durability analysis;
- To generate new scientific and engineering knowledge to better enable Solid State Energy Conversion Alliance (SECA) Industry Teams to develop reliable, low-cost solid oxide fuel cell (SOFC) power generation systems;
- To create technology breakthroughs to address technical risks and barriers that currently limit achievement of the SECA performance and cost goals for solid oxide fuel cell systems; and
- To transfer new science and technology developed in the project to the SECA Industry Teams.

Approach

- The Georgia Tech team is using a multi-physics modeling approach to collectively characterize the interdependency between structural issues and electrochemical/thermal transport phenomena in order to create high-fidelity thermo-mechanical failure analysis models.
- Experimental data from national labs (NETL, PNNL and ORNL) will be utilized for model validation. Exploratory studies using these modeling tools will be performed to optimize cell and stack level designs.

Accomplishments

- Developed first-order design criteria for the maximum allowable crack size against delamination and fracture for cracks along the electrolyte/electrode interfaces, on the electrode surfaces, and within the electrolyte, respectively.
- Developed a statistical approach to predict thermal shock induced failure of anode materials and implemented this approach into MARC.
- Developed a computational algorithm for optimal design of heating rate and air flow velocity based on the second-order analytical model of the SOFC heating/cooling during start-up.
- Developed the Fracture Mechanics Analyzer software for analyzing fracture failure in SOFCs and integrated this software into the MARC environment. This software can be used to conduct failure analysis of SOFCs with various pre-existing flaws under various operating conditions.
- Developed two reduced-order, analytical thermal models for convective-conductive cell heating during the start-up and shut-down, which were numerically validated using detailed computational fluid dynamics calculations.

- Developed design maps and accompanying set of guidelines for thermal design of the cell and operating conditions for optimal design of the cell start-up process.
- Provided the detailed guidelines for accounting for radiative heat transfer in various SOFC components from PEN structure (cathode-electrolyte-anode, where the cathode is the positive electrode and the anode is the negative electrode) to thermal insulation to the stack level.
- Simulated the latter-stage thermal ramp of a SOFC stack, inclusive of electrochemical light-off.
- Simulated the progressive resolution of the functionality of electrochemical light-off upon electrochemical operating conditions such as dynamic electrical conditions (voltage-current), reactants number-of-stoichs, etc.

Future Directions

- Develop and implement a computationally efficient transient thermal model.
- Develop a comprehensive model for transient heating/cooling of the cell during the start-up and shut-down by accounting for local thermal non-equilibrium between the cell layers (i.e., electrodes, electrolyte, flow channels, and current collectors) as well as radiative heat exchange between different components.

Introduction

In this work, the Georgia Tech team will take a multi-physics modeling approach to collectively characterize the interdependency between structural issues and electrochemical/thermal transport phenomena in order to create greater fidelity within thermo-mechanical failure analysis models. Once such models and computational algorithms are developed, they can be implemented into various commercial software codes for analysis and simulation. Software such as FLUENT, Star-CD, MARC, ANSYS, and ABAQUS will be used, as needed, for the purpose of validating the convergence and accuracy of the solutions. In this report, the software developed will be integrated into commercial finite element software MARC, which is the platform for SECA's SOFC design, optimization and failure analysis code.

The Phase I project and the early work of the Phase II project have demonstrated the feasibility of simulating thermo-mechanical failure in SOFCs using an integrated approach that takes into account the interdependency between structural issues and electrochemical/thermal transport phenomena. Building upon the success of Phase I and early work of the Phase II project, Georgia Tech further developed and matured the multi-physics modeling approach to a level that can be utilized directly by the SECA Industry Teams.

Realizing the complexity and magnitude of technical challenges associated with modeling and simulating SOFC stack failure, the Georgia Tech team will focus on the specific critical tasks listed below. Computational algorithms and related computer codes for the models developed will be transferred to the SECA Industry Teams directly, as well as to Pacific Northwest National Laboratory (PNNL), the National Energy Technology Laboratory (NETL), and Oak Ridge National Laboratory (ORNL), for integration into the Life Prediction and Structural Modeling Tools under development at these national labs.

Approaches

A Statistical Approach to Predict Thermal Shock Induced Failure of Anode Materials

The Ni/YSZ anode is a mixture of Ni and yttria-stabilized zirconia (YSZ), or a cermet. Due to NiO reduction, the Ni/YSZ anode also contains a large number of voids, making it a porous cermet. In this complicated microstructure, the “strength” measures, such as the failure strength and fracture toughness, will be random variables with certain distributions, such as normal distribution, Weibull distribution, etc. Therefore, the statistical nature of the stresses and strength should be considered in developing the failure criteria in order to gain insight of the reliability of SOFCs. In our study, the probability of failure is formulated with respect to the strength

distribution. Based on the weakest link theory and the principle of independent action for multi-axial stress states, for all $\sigma_1 \geq \sigma_2 \geq \sigma_3 > 0$, the probability of failure is

$$P_f = 1 - \exp[-\int_V (N_V(\sigma_1) + N_V(\sigma_2) + N_V(\sigma_3))dV]$$

For the Weibull two-parameter distribution, the function, $N_V(\sigma)$, is defined as,

$$N_V(\sigma) = \left(\frac{\sigma}{\sigma_{oV}}\right)^{m_V}$$

where the scale parameter σ_{oV} corresponds to the stress level where 63.2 percent of the specimens with unit volume would fail, and m_V is the shape parameter called the Weibull modulus, a dimensionless parameter that measures the degree of strength variability. For the normal distribution, the function $N_V(\sigma)$ is expressed as.

$$N_V(\sigma) = \frac{1}{s_f\sqrt{2\pi}}\int_0^{\sigma} \exp\left[-\frac{1}{2}\left(\frac{x-\bar{\sigma}_f}{s_f}\right)^2\right]dx$$

First-order Thermo-mechanical Failure Criteria

The purpose of developing the first-order failure criteria is to aid the initial design, material selection and optimization of SOFCs. In this study, the global failure criteria are established based on local fracture failure in terms of the warpage of the tri-layer PEN structure (a cell) after processing because such failure tends to be catastrophic. Here, it is assumed that the warpage of each cell is measured before stack assembly. Then, using the global failure criteria, the user can predict whether a cell can survive the stacking assembly process. Clearly, such global failure criteria can also be used for designing the sintering processes in order to avoid excess warpage of the cells. The first-order estimates of the maximum allowable warpage without fracture and maximum allowable curvature during the stack assembly process are, respectively,

$$\frac{W_c}{L} = Y\sqrt{\frac{G_c}{h_2 E_2}}\left(\frac{L}{h_2}\right), \quad \rho_c = \bar{Y}\sqrt{\frac{G_c}{h_2 E_2}}$$

where W is the maximum allowable warpage, L is the cell size, E_2 is the Young's modulus of the electrolyte, h_2 is the thickness of the electrolyte, and

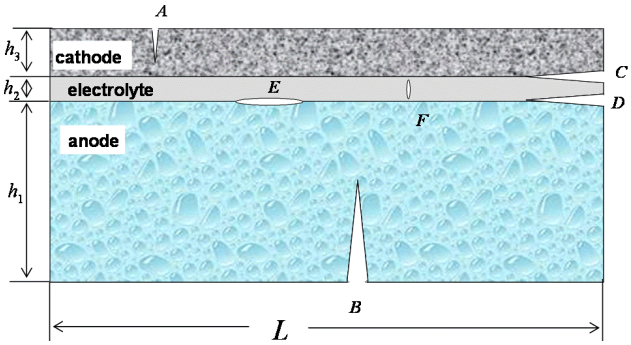

Figure 1. Cracks in a PEN Structure

G_c is the fracture toughness of the material in which the crack is located. Y is a dimensionless constant that depends on the cell geometry, material constants, and crack size and location; see Figure 1.

Fracture Mechanical Analyzer (FMA) Software

Although several commercial finite element software packages offer the capabilities of computing the crack-tip energy release rate, none is capable of computing stress intensity factors (SIFs) for three-dimensional (3-D) cracks subjected to combined mechanical and non-uniform temperature loading conditions, which is a situation typical to SOFC applications. To meet this need, a computer program called Fracture Mechanical Analyzer (FMA) was developed to calculate the SIFs of 3-D cracks, including interfacial cracks in the PEN structure subjected to combined mechanical and thermal loadings. The algorithm is based on the path-independent domain integral formulation in conjunction with the interaction integral method. The FMA program written in MatLab language is essentially an "add-on" to any commercial finite element software. It computes the energy release rate and the individual SIFs based on the crack-tip displacement fields computed from any commercial finite element software. So, in conjunction with commercial finite element software, the FMA program provides a simulation tool for conducting a fracture mechanics analysis. In this project, the FMA program has been integrated into the commercial finite element software MARC, which is the platform for SECA's SOFC design, optimization and failure analysis code. The flow chart of the FMA is shown in Figure 2.

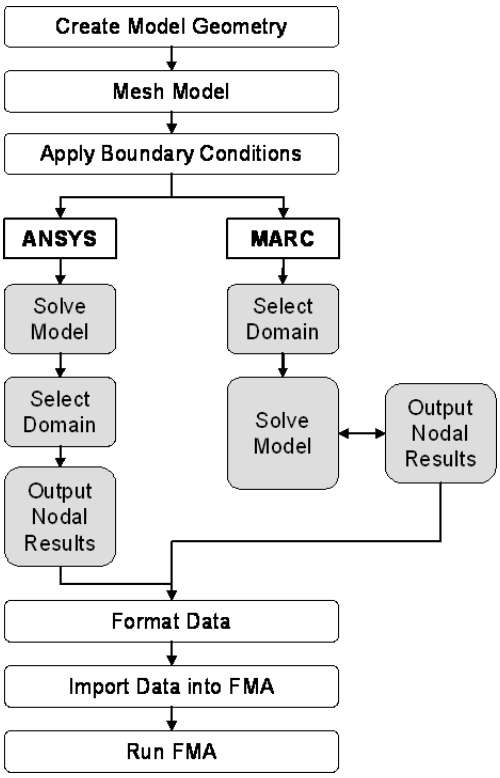

Figure 2. Flow Chart of the Fracture Mechanics Analyzer Software

Optimal Design of Start-Up and Shut-Down to Avoid Thermal Shock Induced Failure

The transient process of heating an SOFC from room temperature to operating temperature (600-800°C) during start-up, or cooling down to ambient during shut-down, may create thermal shock that will lead to fracture failure of the cell. Two major parameters, namely, rate of heating (cooling) and the inlet air flow temperature, are particularly important in shortening the start-up (shut-down) time while minimizing the thermal shock induced failure. One of the objectives of this project is to develop a systematic approach for selecting optimal values for these parameters.

To this end, we considered a SOFC unit cell which is heated by hot air supplied into the oxidizer channel at a specified, time-dependent inlet temperature. A closed-form analytical solution has been obtained for convective-conductive heating, under the assumption of local thermal equilibrium in the direction normal to flow. Given thresholds of maximum allowable temperature gradients and time derivatives, the optimal design is the one that minimizes the total time required to reach a prescribed steady-state operating temperature.

Results

A Statistical Approach to Predict Thermal Shock Induced Failure of Anode Materials

To understand the statistical nature of the failure criteria, the thermal shock tests conducted at ORNL were numerically analyzed by the finite element method. The temperature-dependent Young's modulus of the sample material is considered here. The temperature dependency of the Poisson's ratio and the coefficient of thermal expansion (CTE) are neglected. Their values are taken as 0.25 and 11.8×10^{-6}, respectively. In the thermal shock test, two batches of samples were used. Each batch had 17 samples. The temperature distributions during the test were recorded for each sample just before the sample failed. The corresponding parameters obtained by ORNL for strength distribution are included in Tables 1 and 2 for Weibull and Normal distribution, respectively.

Table 1. Parameters of Strength Distribution in Weibull Distribution

	Charact. strength (MPa)	Weibull Modulus
At 22°C	55.42	4.49
At 600°C	78.95	5.61

Table 2. Parameters of Strength Distribution in Normal Distribution

	Average Strength (MPa)	Standard Deviation
At 22°C	50.73	12.00
At 600°C	72.92	15.02

Shown in Table 3 is the comparison between the predicted failure rate and the actual test data. It can be seen that the Mises stress criterion predicts much higher failure rate than that predicted by the principal stress criterion. In comparison with the experimental data, the failure rates predicted by the principle stress criterion are much closer to the actual tested data. Therefore, we recommend that the principal stress

criterion should be used for the YSZ/Ni cermets under thermal shock conditions. Furthermore, it appears that normal distribution is a better fit of the actual test data than the Weibull distribution, as least for the second batch of samples (Exp. 2).

Table 3. Comparison between the Predicted Failure Rate and the Actual Test Data

	Exp.	Prediction			
		Principal Stresses		Von Mises Stress	
		Weibull	Normal	Weibull	Normal
Batch 1	80%	82%	77%	96%	96%
Batch 2	41%	63%	43%	65%	50%

First-order Thermo-mechanical Failure Criteria

Although various techniques have been developed for sintering the cells, certain warpage of the cell remains after sintering. During the stacking process, cells are flattened in order to be fitted into the cell stack. Flattening exerts additional stresses to the warped cells. Such stress may fracture the cell during the flattening process, if the warpage is excess. For most anode-supported, YSZ-based SOFCs, the crack types *A*, *B*, *C* and *D*, as shown in Figure 1, are particularly vulnerable to the flattening process. The failure criterion developed here provides the first-order estimate of the maximum allowable warpage without fracture.

As an example, consider a cell with the geometry and material parameters listed in Table 4. For this example, the normal stresses are tensile in the cathode and compressive in the electrolyte and anode. Therefore, crack types *A*, *C* and *D* may propagate as the cell is flattened. The values of *Y* corresponding to these cracks are listed in Table 5. For $L = 10$ cm, the maximum allowable warpage W is plotted in Figure 3 against the fracture toughness G_c for these cracks.

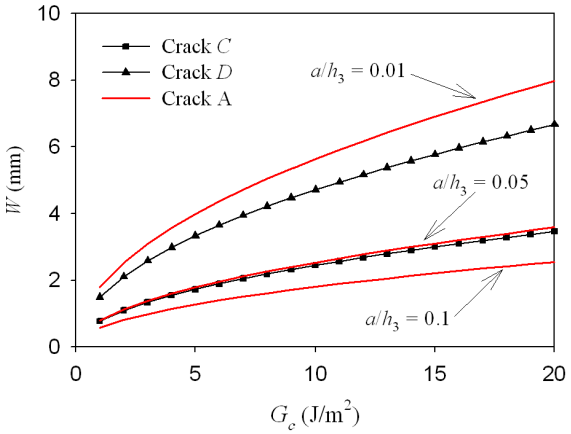

Figure 3. Maximum Allowable Warpage of a PEN Structure vs. Interfacial Fracture Toughness

Table 4. Material Properties and Geometric Parameters of a Cell

	E (GPa)	*v*	CTE(10^{-6}/°C)	h (μm)
Cathode	90	0.3	11.7	75
Electrolyte	200	0.3	10.8	15
Anode	96	0.3	11.2	500

Table 5. Values of the Factor *Y*

	Crack *A*				Crack *C*	Crack *D*
	a = 0.01 h_3	*a* = 0.05 h_3	*a* = 0.1 h_3	*a* = 0.2 h_3		
Y	4.63 e-3	2.08 e-3	1.48 e-3	1.06 e-3	3.87 e-3	2.01 e-3

From Figure 3, if the critical energy release rate, G_c, is fixed, the corresponding critical warpage, W, can be determined. If the warpage of the cell is larger than the value obtained here, delamination may occur.

Fracture Mechanical Analyzer (FMA) Software

To illustrate the capabilities and accuracy of the FMA software, a number of examples of cracks in SOFCs have been examined. Shown in Table 6 are the calculated stress intensity factors for a penny-shaped crack on the electrolyte/anode interface under tensile loading (for which analytical solution exists). The mesh for the computation is shown in Figure 4. It is seen the FMA gives accurate results even for a fairly coarse mesh.

Table 6. Stress Intensity Factors for a Penny-shaped Interface Crack

Normalized Values	Real (KI)	Imaginary (KII)	Ψ (°)
Numerical	0.992	0.074	3.0
Analytical	0.986	0.077	3.1
% Error	-.629	3.390	3.7

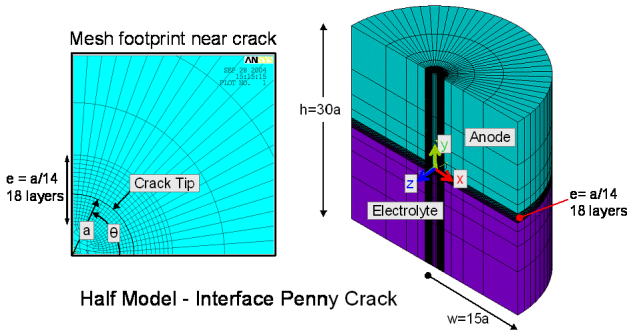

Figure 4. Finite Element Mesh for a Penny-shaped Interface Crack

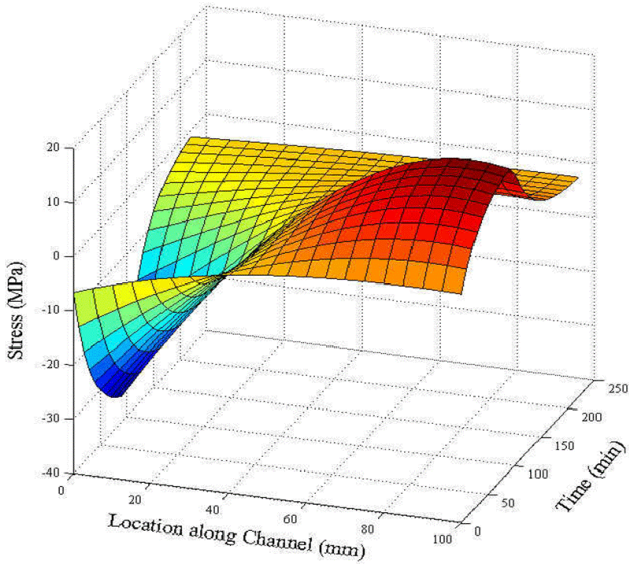

Figure 5. Distribution of Stress: Air Flow Velocity 1 m/s, Heating Rate 0.1°C/s

Optimal Design of Start-Up and Shut-Down to Avoid Thermal Shock Induced Failure

To illustrate how the transient stress evolves during start-up, consider a numerical example based on the material properties listed in Table 7. Figures 5 and 6 show the distributions of the stress for air flow velocity 1 m/s with heating rate 0.1°C/s and air flow velocity 10 m/s with heating rate 1.0°C/s, respectively. The maximum tensile stress vs. air flow velocity is illustrated in Figure 7 for various heating rates. Figure 8 shows the maximum tensile stress vs. heating rate at various air flow velocities.

Table 7. Material Properties

Young's Modulus (GPa)	Poisson's ratio	CTE (10^{-6}/°C)
96	0.3	11.2

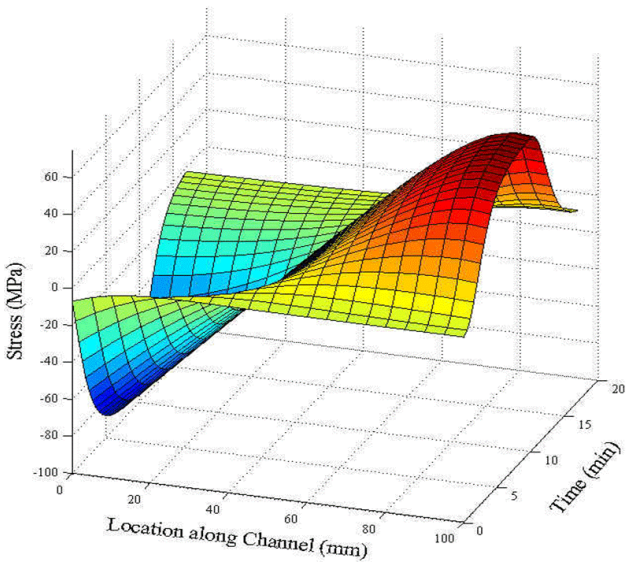

Figure 6. Distribution of Stress: Air Flow Velocity 10 m/s, Heating Rate 1.0°C/s

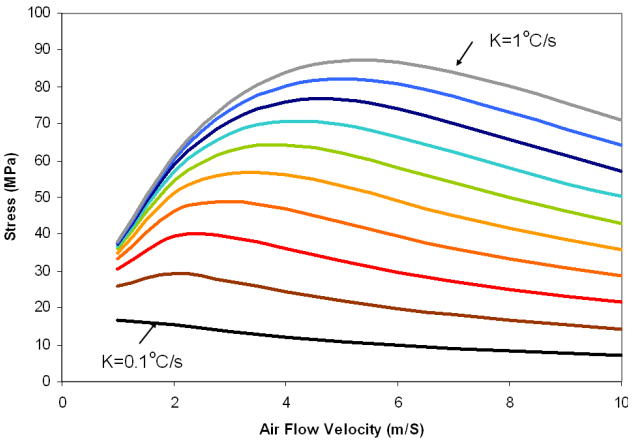

Figure 7. Maximum Tensile Stress vs. Air Flow Velocity at Various Heating Rates

From Figures 5 and 6, it can be seen that the maximum stress appears at the middle of the start-up process. During the start-up, the maximum tensile stress in the cell increases when temperature gradient increases as the heated air flows through the channel, and the maximum tensile stress reaches the largest value when temperature gradient reaches its peak; then, the maximum tensile stress starts to decrease when the temperature field is approaching steady-state and the temperature gradient disappears.

It is seen that increasing the heating rate will always increase the maximum tensile stress in the cell. However, the dependency on the flow velocity is not monotonic. It appears from Figure 7 that for

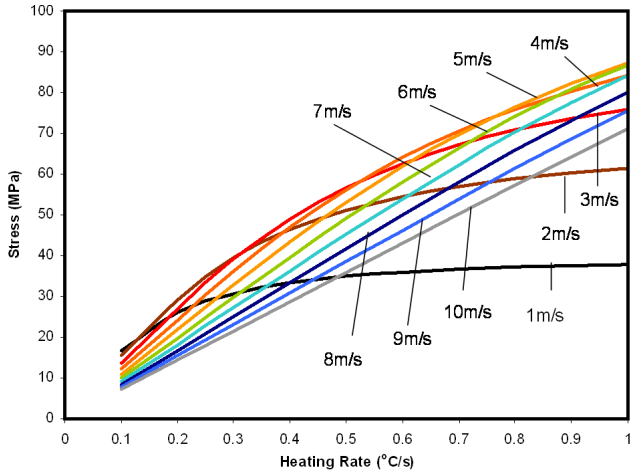

Figure 8. Maximum Tensile Stress vs. Heating Rate at Various Air Flow Velocities

each heating rate, there is a particular flow velocity at which the stress is the highest. Away from this flow velocity, the maximum tensile stress actually is lower. This points out a need to optimize the heating rate and flow velocity in order to shorten the start-up time without damaging the cell.

Conclusions

To develop and demonstrate the feasibility of an integrated predictive computer-based tool for fuel cell design and reliability/durability analysis, we have conducted a systematic study of the thermal-fluid flow, heat transfer and mechanical stresses due to both steady-state and transient temperature fields. Experimental data from national labs (NETL, PNNL and ORNL) have been used in our study for obtaining material data and model validation.

In the past year, we have accomplished several milestones towards the project goals. Particularly, we have developed some first-order design criteria for the maximum allowable crack size against delamination and fracture for cracks along the electrolyte/electrode interfaces, on the electrode surfaces, and within the electrolyte, respectively. We have also developed a statistical approach to predict thermal shock induced failure of anode materials and implemented this approach into MARC. It was found that the maximum normal stress is a good failure criterion to use. Our transient model also indicated that the maximum stress induced by the thermal shock during start-up (shut-down) has a complicated dependency on heating rate and air flow velocity. However, it is possible to select an optimal set of parameters that can reduce start-up time while minimizing thermal shock induced failure.

Our Fracture Mechanics Analyzer software developed in the project provides a software tool for fracture analysis that currently no other commercial code is capable of doing.

FY 2005 Publications/Presentations

1. Damm, D. and Fedorov, A., "Spectral Radiative Heat Transfer Analysis of the Planar SOFC", *ASME International Mechanical Engineering Congress and Exposition*, ASME, Anaheim, CA, November 13-19, 2004.
2. Damm, D. and Fedorov, A., "Radiation Heat Transfer in SOFC Materials and Components", *ASM Symposium on Fuel Cells Materials, Processing, and Manufacturing Technologies*, ASM International, Columbus, Ohio, 2004.
3. Damm, D.L., Fedorov, A.G., "Radiation Heat Transfer in SOFC Materials and Components", *Journal of Power Sources*, 143, pp. 158-165, 2004.
4. Liu, W.N. and Qu, J.M., "Creep Deformation of Ni/YSZ Cermet in SOFCs", *29th International Conference on Advanced Ceramics and Composites*, ACerS, Cocoa Beach, FL, January 23-28, 2005.
5. Johanson, J. and Qu, J.M., "Numerical Simulation of Thermomechanical Failure of Solid Oxide Fuel Cells", *29th International Conference on Advanced Ceramics and Composites*, ACerS, Cocoa Beach, FL, January 23-28, 2005.
6. Damm, D. and Fedorov, A., "Simplified Thermal Analysis of the SOFC Transients during Startup/ Shutdown", final draft accepted by *ASME's Summer Heat Transfer Conference, HT2005,* San Francisco, CA, July 17-22, 2005.
7. Damm, D. and Fedorov, A., "Spectral Radiative Heat Transfer Analysis of the Planar SOFC", accepted for publication by *ASME Journal of Fuel Cell Science and Technology*.

III.D.2 Determination of Electrochemical Performance and Thermo-Mechanical-Chemical Stability of SOFCs from Defect Modeling

Eric D. Wachsman (Primary Contact), Keith L. Duncan, Fereshteh Ebrahimi
Department of Materials Science and Engineering, University of Florida
Gainesville, Florida 32611
Phone: (352) 846-2991; Fax: (352) 846-0326; E-mail: ewach@mse.ufl.edu

DOE Project Manager: Travis Shultz
Phone: (304) 285-1370; E-mail: Travis.Shultz@netl.doe.gov

Objectives

- Advance the fundamental understanding of the continuum-level electrochemistry of oxide mixed ionic-electronic conductors (MIECs) in relation to their performance in solid oxide fuel cells (SOFCs).
- Obtain fundamental constants required for implementing the continuum-level electrochemical model from experiment.
- Extend the models to multilayer structures and incorporate microstructural effects.
- Verify the models through experiment.
- Develop a transient version of the continuum-level electrochemical model.
- Obtain time constants for various transport processes from electrical impedance spectroscopy to examine the effects of transients on SOFC performance.
- Develop and deliver software modules for incorporation of the continuum-level electrochemical model into SOFC failure analysis software used by the National Energy Technology Laboratory (NETL), Pacific Northwest National Laboratory (PNNL), Oak Ridge National Laboratory (ORNL) and the Solid State Energy Conversion Alliance (SECA) industrial teams.

Approach

- Develop a continuum-level electrochemical model for the generation, distribution and transport of defects in oxide MIECs.
- Extend model to include the thermo-mechanical properties, thermo-chemical stability and transient behavior of oxide MIECs.
- Extend model to include multilayer (anode-electrolyte-cathode) SOFCs.
- Incorporate microstructural effects into the continuum-level electrochemical model.
- Design and conduct experiments to obtain thermo-mechanical, thermo-chemical and transient behavior of oxide MIECs for incorporation into model.
- Validate experimentally the continuum-level electrochemical model.

Accomplishments

- Completed a continuum-level electrochemical model for *steady-state* conditions, using potential dependent boundary conditions and non-linear Galvani potential.
- Completed a continuum-level electrochemical model for *transient* conditions, using potential dependent boundary conditions and a linear Galvani potential.
- Compiled software modules for vacancy concentration and electron concentration in *n*-type and *p*-type MIECs.

- Extended the continuum-level electrochemical model to thermo-mechanical and thermo-chemical properties of MIECs.
- Extended the continuum-level electrochemical model to YSZ/LSM (yttria-stabilized zirconia/lanthanum strontium manganite) and YSZ/LSCF (yttria-stabilized zirconia/lanthanum strontium cobalt ferrite) bilayers.
- Measured the thermal expansion of CeO_2, samaria-doped ceria (SDC) and gadolinia-doped ceria (GDC) in air and reducing atmospheres. Results concur with model predictions.
- Obtained time constant for equilibration of material after a change in P_{O2} during chemical expansion.
- Measured the elastic moduli of CeO_2, GDC and YSZ in reducing (H_2) and oxidizing (air) atmospheres using nondestructive and (nanoscale) destructive techniques; both showed that reducing conditions cause a ~30% decrease in the elastic modulus relative to air. Results concur with model predictions.
- Measured the fracture toughness of CeO_2 and GDC in reducing (H_2) and oxidizing (air) atmospheres; results show that reducing conditions cause a ~37% increase in the fracture toughness relative to air.
- Deconvoluted transport processes for optimally sintered LSM and LSCF, with time constants ranging from 10^{-10} (charge transfer) to 10^5 seconds (gas diffusion).

Future Directions

- Complete the extension of the continuum-level electrochemical model to multilayer SOFC architecture.
- Incorporate microstructural effects into the continuum-level electrochemical model.
- Obtain data for the thermo-mechanical properties of polycrystalline YSZ as a function of P_{O2} between air and H_2/H_2O.
- Obtain thermal expansion data for Ni-YSZ, LSM, YSZ and other MIECS in various (reducing or oxidizing) atmospheres.
- Experimentally determine the effect of microstructure on transient behavior of SOFCs.

Introduction

For extensive deployment of SOFCs into industrial and consumer markets to become a reality, some key hurdles need to be cleared. Three of these hurdles are the (i) thermo-mechanical, (ii) thermo-chemical and (iii) transient stability of SOFCs. In our research, we are tackling these hurdles by developing models to relate point defect (atomic-scale anomalies) population distribution and microstructure (the fine structure of a material) to the electrochemical and mechanical properties of SOFC components, which are the actual determinants of the thermo-mechanical, thermo-chemical and transient stability of SOFCs. These fundamental-level models can then be incorporated into system-level models to predict and analyze SOFC performance and response (transient and steady-state) to various inputs.

Approach

An objective of this project is to develop models relating point defect population distribution and microstructure to the electrochemical and mechanical properties of SOFC components. First, we modeled the generation of point defects in oxide mixed ionic-electronic conductors (MIECs) as a function of atmosphere (P_{O2}) and temperature. Since SOFCs operate in a P_{O2} gradient, we then modeled the transport and distribution of defects in an MIEC in a P_{O2} gradient by solving the Nernst-Planck, mass conservation and charge conservation equations for Laplacian and non-Laplacian potential distributions. These two steps produced a continuum-level electrochemical model that relates point defect concentration to operating conditions (such as temperature, P_{O2} gradient and load voltage) and material properties (such as the mass action constant for oxygen exchange between the oxide and the ambient and ionic and electronic diffusivity). Hence, by modeling or applying relationships between point defects and indices for thermo-mechanical, thermo-chemical and transient stability, secondary relationships between these indices and the SOFC operating conditions and material properties can be derived.

An essential complement to the models developed in our research is experimental verification. To this end, experiments are being conducted to confirm the predictions of the models as well as to give more insight into the factors and mechanisms that play a role in the performance of the SOFC components and the overall stability of the SOFC.

Results

Continuum-Level Electrochemical Model — Defect Thermodynamics.

To obtain defect concentration dependence on P_{O2} requires the solution of a system of equations consisting of mass action equations from the defect equilibria and charge, mass and site balance equations. However, depending on the defect species involved, the system of equations can result in high-order polynomials with no analytical solution. The traditional way of simplifying such equation systems divides the equilibria into separate Brouwer regimes where two species dominate [1]. This method generates defect concentration dependence on P_{O2} that is discontinuous across the Brouwer regimes. This is a problem for SOFC materials in a P_{O2} gradient where the defect equilibria span more than one regime. By considering three defects instead of two, we derived equations that are continuous across at least two regimes. Examples of these are

$$c_V(P_{O_2}) = \left[\frac{3}{4}K_r^{\frac{1}{2}}P_{O_2}^{-\frac{1}{4}} + \left(\frac{1}{2}c_A\right)^{\frac{3}{2}}\right]^{\frac{2}{3}}$$

and

$$c_e(P_{O_2}) = K_r^{\frac{1}{2}}P_{O_2}^{-\frac{1}{4}}\left[\frac{3}{4}K_r^{\frac{1}{2}}P_{O_2}^{-\frac{1}{4}} + \left(\frac{1}{2}c_A\right)^{\frac{3}{2}}\right]^{-\frac{1}{3}} \qquad (1)$$

where c_V, c_e and c_A are the concentrations of vacancies, electrons and a trivalent acceptor dopant, respectively. K_r is the equilibrium constant for the oxygen exchange between the oxide and gaseous O_2. The full derivation may be found in our earlier work [2]. Equation (1) is a *low* P_{O2} simplification of more general equations we developed for fluorites and perovskites [2]. Finally, as shown in Figure 1, excellent results were obtained when these equations were fitted to experimental data [3] with K_r as the sole fitting parameter.

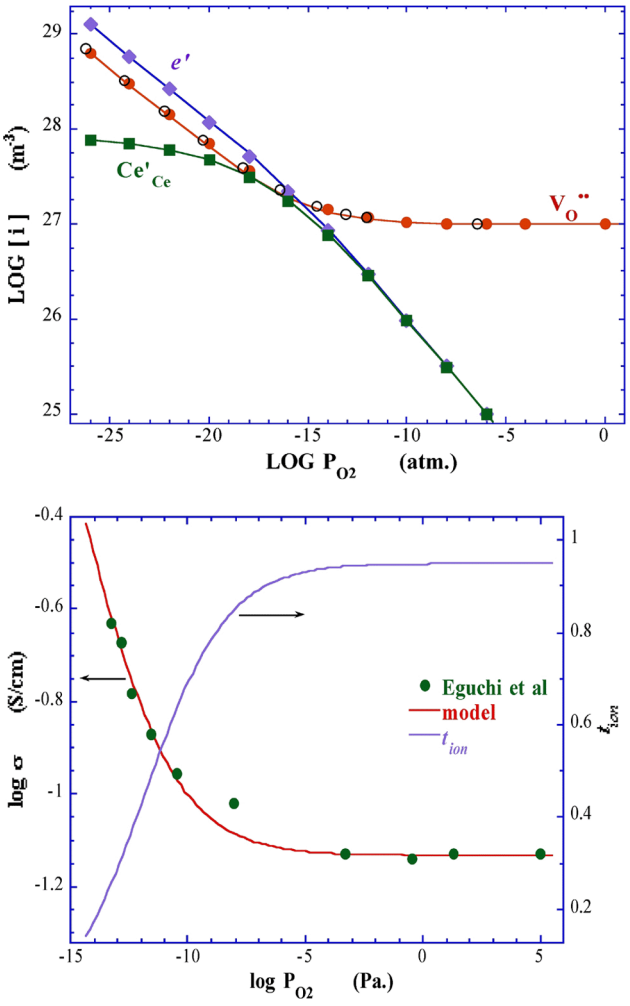

Figure 1. (a) Comparison of SDC Defect Equilibrium Diagrams Obtained Numerically (solid symbols), from the Model (lines), and from Porat and Tuller [11] (open symbols); $c_A = 2 \times 10^{27}$ m^{-3}, $c_M = 8 \times 10^{28}$ m^{-3} (b) Model Fitted to Conductivity Data from Eguchi *et al.* [3] for SDC

Continuum-Level Electrochemical Model — Defect Transport.

To model defect transport in MIECs, we solved the Nernst-Planck, material balance, and current density equations [4]. To simplify the equations and make the derivations more tractable, previous researchers have assumed a linear, i.e., Laplacian, potential distribution. We have been able to relax that assumption and solve for the more general Poisson potential distribution where the Galvani potential is not forced to vary linearly with position inside the MIEC.

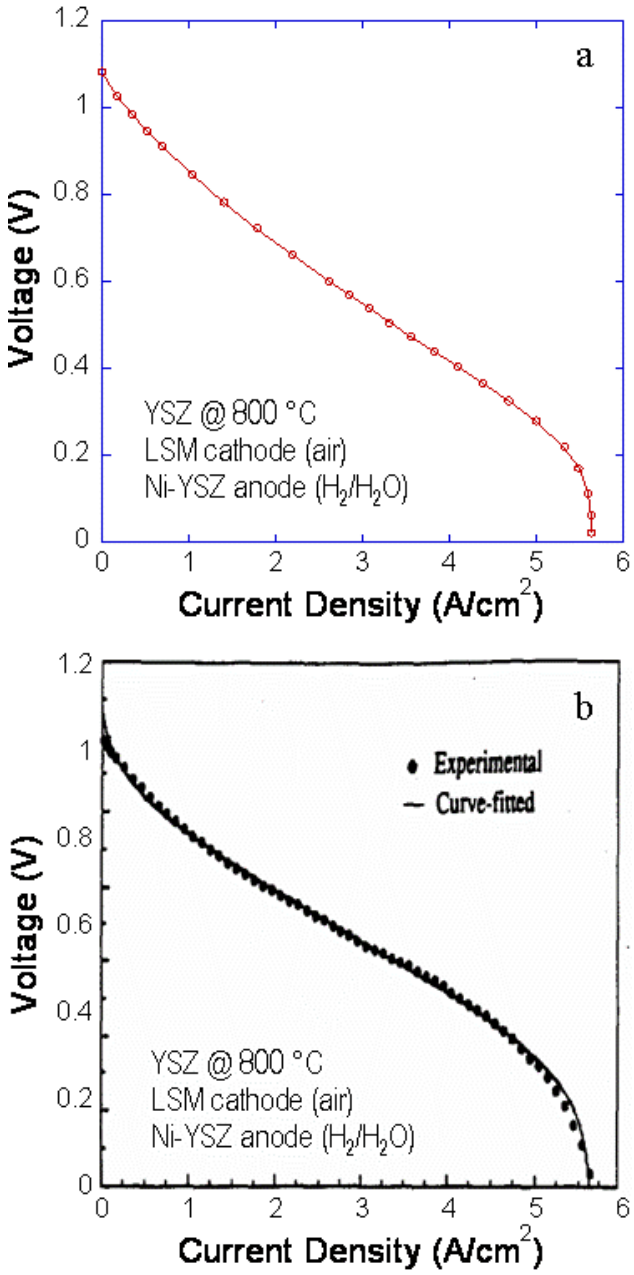

Figure 2. Comparison of Theoretical Models Fit to Experimental Data (a) Present Work (b) Kim *et al* [12]

Previous researchers [6-8] used *fixed* boundary values for the defect concentrations and linear potential distributions. *Fixed* boundary values are independent of the load voltage, Φ_{ext}. This implies that Φ_{ext} only affects the spatial distribution of defects inside the MIEC, which is unrealistic since the activities of *all* the reacting chemical species cannot be held constant while changing the potential at the interface [4, 9]. *Potential-dependent* boundary conditions were obtained by including the effect of the load voltage on the boundary values of the defect concentrations [5]. Our results allow for the prediction of SOFC performance and show that using fixed boundary conditions and assuming a linear potential leads to an overestimation of cell performance. This demonstrates the importance of using the best available electrochemical models in the computation of overall SOFC performance.

Figure 2 shows a comparison of our results with those of Kim *et al* [12] for modeling the I-V characteristics of a Ni-YSZ/YSZ/LSM cell. We were able to model the cell with similar accuracy to Kim *et al* [12]. However, fewer fitting parameters (3 vs. 10) were used in our model to obtain the same fit. Moreover, because the continuum electrochemical model does not assume a uniform vacancy concentration, it is amenable for modeling cells with mixed conducting electrolytes, e.g., GDC.

Continuum-Level Electrochemical Model — Thermo-chemical Expansion.

To extend the model developed above to the thermo-chemical expansion of MIECs, a relationship for the thermo-chemical expansion was derived based on the linear relationship between defect population and the lattice constant, a_0 [10], as given below for acceptor-doped ceria,

$$\frac{\Delta l}{l_0} = \alpha\Delta T + \frac{\beta}{a_0}c_V = \alpha\Delta T + \frac{\beta}{a_0}\left[\tfrac{3}{4}K_r^{\frac{1}{2}}P_{O_2}^{-\frac{1}{4}} + \left(\tfrac{1}{2}A\right)^{\frac{3}{2}}\right]^{\frac{2}{3}} \quad (2)$$

where T is temperature, $\Delta l/l_0$ is expansion, and β is a material constant related to lattice structure. Figure 3a shows that there is significant chemical expansion, which correlates to the onset of mixed conduction [3] (Figure 1). Moreover, we obtained an excellent fit of our model to the data with a single fitting parameter, β.

Continuum-Level Electrochemical Model — Thermo-Mechanical Properties.

The relationship between defect population and elastic modulus was derived from the fundamental relationship

$$Y(P_{O_2}) \approx Y^*\left(\theta c_V(P_{O_2})+1\right)^{-(m+3)} \quad (3)$$

where Y is elastic modulus, m and θ are empirically determined constants (typically $m = 1$ for ionic solids), and the superscript "*" refers to stoichiometric conditions. Similar expressions have also been derived for fracture toughness.

We measured the elastic modulus of individual grains of CeO_2, GDC and YSZ samples annealed in a range of P_{O2}'s between air and H_2 using a nanoindenter. The results are plotted in Figure 3b, showing good fits of the model to the data. Clearly, the continuum-level electrochemical model can facilitate the prediction of the thermo-mechanical properties of SOFCs.

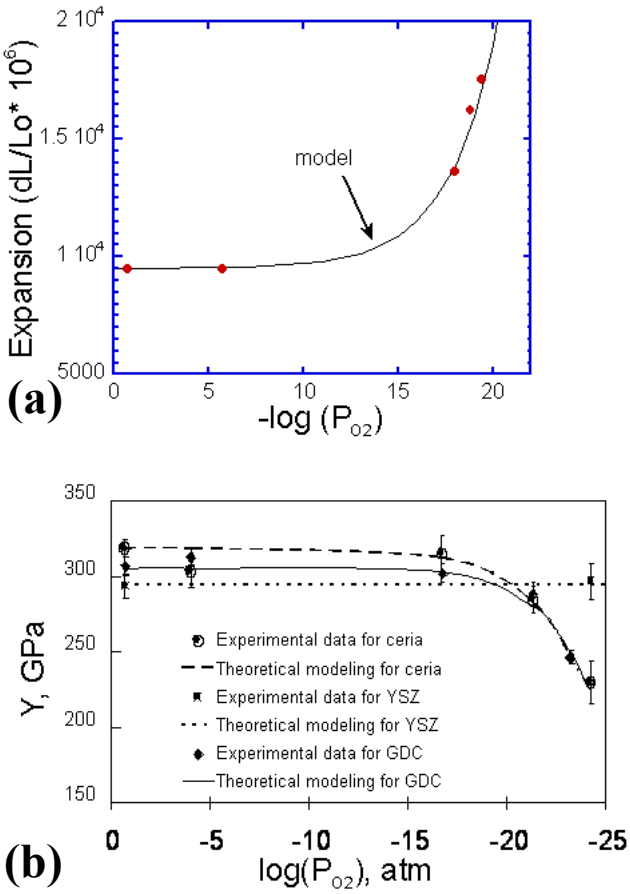

Figure 3. (a) Thermo-chemical Expansion Data and Model Fit for (10 mol%) GDC at 1073 K (b) Theoretical and Experimental Elastic Moduli for Pure Ceria, GDC and YSZ as a Function of P_{O2}

Chemical Stability

The continuum-level electrochemical model was also applied to the chemical stability of YSZ/LSM and YSZ/LSCF interfaces. Our results showed that the thickness ratio dependence of performance was negligible for YSZ/LSM, since LSM does not conduct oxygen vacancies. Conversely, the dependence was more pronounced for YSZ/LSCF, since LSCF is a good oxygen vacancy conductor. For relevant insight into the stability of electrolyte-electrode interfaces, we will need to incorporate the microstructure of the electrode. We are in the process of doing just that.

Transient Response

The continuum-level electrochemical model has been extended to transient conditions. To obtain solutions, we assumed a linear potential distribution. This assumption is best applied to predominantly ionic conductors, e.g., YSZ, or predominantly electronic conductors, e.g., LSM.

Figure 4 shows the evolution of the electron concentration profiles in YSZ. The results show that while the boundary concentrations are established *instantly*, the concentration in the bulk lags behind, ostensibly limited by electron diffusivity and electrolyte thickness.

Figure 4b is a surface plot showing the spatial and temporal distribution of electron concentration, $c_e(x, t)$. In Figure 4b, a load is again introduced to the SOFC, but this time it carries a 60-Hz sinusoidal *ripple* with it. The effect and presence of the *ripple* is evident in the plot, which shows an initial response similar to that in Figure 4a. However, after about 6 s, the lag is no longer evident even though the *ripple* persists. This is a result of the amplitude and frequency of the *ripple*. The amplitude is small enough not to cause great changes in the concentration gradient. The time constant of the electrolyte (~4.5 s) is ~270 times the period of the *ripple*. Hence, the electrolyte does not have enough time to respond to the *ripple* in the bulk, and the *ripple's* effect is seen only at the boundaries.

For transient defect transport, the total thickness, L, is a component of the time constant for the process such that the transient response of the MIEC depends

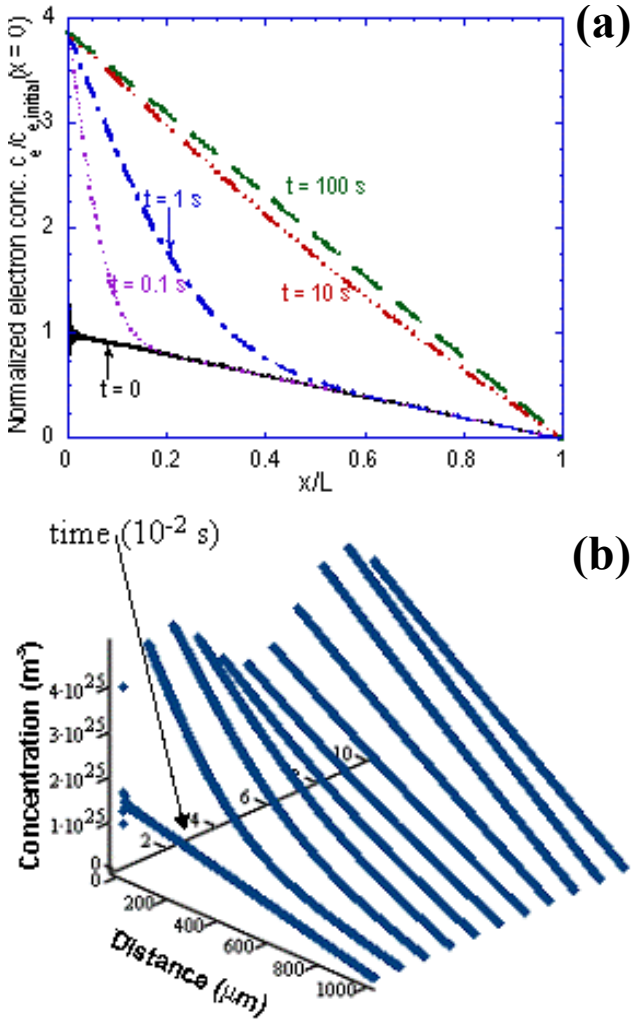

Figure 4. Time-dependent Evolution of Electron Concentration Profiles in a 1 mm Thick YSZ Electrolyte at 800°C: (a) Load Voltage, Φ_{ext}, Goes from *Open-Circuit* Value to $\Phi_{th}/4$ (b) Φ_{ext} Has a 60-Hz Sinusoidal *Ripple*; Anode is at $x = 0$ ($P_{O2} = 10^{-22}$ atm), Cathode at $x = L$ ($P_{O2} = 0.21$ atm)

exponentially on the electrolyte thickness. As the thickness of the electrolyte is reduced to 10 μm, the time scale decreases to ~0.05 s (approaching 60 Hz). This provides important criteria (impact of improved performance with thinner electrolytes versus susceptibility to higher transient voltages or fuel composition variations) if the SOFC is going to be used under transient conditions.

In addition, we are deconvoluting the significant transport mechanisms for electrical impedance spectra. Analysis of our impedance spectroscopy data continues; we have identified a number of temperature-dependent electrochemical processes and their related time constants. Currently, we are trying to correctly identify the physical process responsible for each one.

Software Development

The development of software modules for the continuum-level electrochemical model is in progress. We also intend to offer them to the teams at ORNL, NETL and PNNL for pre-testing to determine the compatibility of the modules with existing failure analysis software and make them available to the SECA industrial teams shortly thereafter. At this point, the program for the *steady-state* continuum-level electrochemical model for defect generation and transport has been completed. Two languages were used: C++ because it is the industry standard, and PHP because of its web-oriented features.

Conclusions

- A continuum-level electrochemical model has been developed that improves on preceding efforts by including a non-linear potential distribution and by including potential-dependent boundary conditions.
- The continuum-level electrochemical model has been extended to describe thermo-mechanical, thermo-chemical and transient stability in MIECs.
- Experimental results concur with the predictions of the continuum-level electrochemical model for electrical conductivity.
- Nanoindentation tests on CeO_2, GDC and YSZ with P_{O2}'s revealed that the elastic modulus of CeO_2 and GDC decreases drastically as the oxygen lattice vacancy concentration increases, and the elastic modulus of YSZ within the studied P_{O2} range was insignificantly changed due to the small number of lattice vacancies produced. GDC and CeO_2 showed very similar trends.
- The continuum-level electrochemical model has been validated through experiment for thermo-mechanical properties (elastic modulus and thermo-chemical expansion).

- The *steady-state* version of the continuum-level electrochemical model has been written in C++ and PHP.

FY 2005 Publications/Presentations

1. "Fabrication of Anode Supported Thick Film Ceria Electrolytes for IT-SOFCs," A. Jaiswal and E.D. Wachsman, Ionics, accepted.
2. "The Search for a Low Temperature SOFC; How Low Can We Go?" MIT Department of Materials Science Seminar, February 18, 2005, Boston, MA.
3. "Modeling the Electrochemical Performance and Thermo-Mechanical-Chemical Stability of Mixed Ionic-Electronic Conductors for Applications in SOFCs," SECA Core Technology Review, January 27-28, 2005, Tampa, FL.
4. "The Impact of Microstructural & Compositional Changes at the LSM/YSZ Interface," American Ceramic Society, 29th International Conference on Advanced Ceramics and Composites, January 24-28, 2005, Cocoa Beach, FL.
5. "Evaluation of Time Constants Governing the Cathodic Reaction in SOFCs," 208th Meeting ECS, Solid State Ionic Devices IV, October 2005, Los Angeles CA.
6. "The Effect of Lattice Vacancies on Mechanical Properties of Cerium Oxide," MRS poster 2004, MRS fall meeting, November 2004, Boston, MA.
7. "The Effect of Lattice Vacancies on Mechanical Properties of Fluorite-structured Oxides- Elastic Modulus," American Ceramic Society, 29th International Conference on Advanced Ceramics and Composites, January 24-28, 2005, Cocoa Beach, FL.
8. "The Effect of Lattice Vacancy Concentration on Mechanical Properties of Fluorite-structured Oxides Fracture Toughness," 208th ECS Meeting; Solid State Ionic Devices IV; Los Angeles, CA; October 2005.
9. "Thermo-chemical expansion of SOFC materials" 208th ECS Meeting, Solid State Ionic Devices IV, October 2005, Los Angeles, CA.
10. "Effect of Potential-Dependent Boundary Conditions and Non-Linear Potentials on Defect Distribution and Transport in *n*-Type Oxide Mixed Ionic-Electronic Conductors," 206th ECS Meeting, October 2004, Honolulu, HI.

References

1. H. L. Tuller, Nonstoichiometric Oxides, ed. O. Sorensen (Academic, N. Y., 1981) ch. 6.
2. K. Duncan, *Ph. D. Thesis*, University of Florida (2001).
3. K. Eguchi, T. Setoguchi, T. Inoue and H. Arai, *Solid State Ionics* 52 (1992) 265.
4. J. Newman, Electrochemical Systems (Prentice-Hall, 1991).
5. E. Wachsman and K. Duncan, Stable High Conductivity Bilayered Electrolytes for Low Temperature SOFCs, DOE Final Report, Contract No. DE-AC26-99FT40712, 2002.
6. I. Riess, *J. Electrochem. Soc.* 128 (1981) 2077.
7. M. Liu, *J. Electrochem. Soc.* 144 1813 (1997).
8. S. Yuan and U. Pal, *J. Electrochem. Soc.* 143 3214 (1996).
9. P. J. Gellings, H. J. A. Koopmans and A. J. Burggraaf, *App. Catalysis* 39 (1988) 1.
10. D-J. Kim, *J. Amer. Ceram. Soc.* 72 (1989) 1415.
11. O. Porat and H. L. Tuller, *J. Electroceramics* 1 (1997) 42.
12. J.-W. Kim, A. Virkar, K.-Z. Fung, K. Mehta and S. Singhal, *J. Electrochem. Soc.* 146 (1999) 69-78.

III.D.3 An Investigation to Resolve the Interaction between Fuel Cell, Power Conditioning System and Application Load

Sudip K. Mazumder (Primary Contact) and Sanjaya Pradhan
University of Illinois at Chicago (UIC)
851 South Morgan Street, Science and Engineering Offices, M/C 15
Chicago, IL 60607
Phone: (312) 355-1315; Fax: (312) 996-6465; E-mail: mazumder@ece.uic.edu

Subcontractors:
Joseph Hartvigsen, S. Elangovan, and Hollist Michelle, Ceramatec Inc.
Michael von Spakovsky, Douglas Nelson and Diego Rancruel, Virginia Tech
Comas Haynes, Georgia Tech

Project Collaborators:
Miladin Radovic and Edgar Lara-Curzio, Oak Ridge National Laboratory (ORNL)
Mohammed Khaleel, Pacific Northwest National Laboratory (PNNL)

DOE Project Manager: Magda Rivera
Phone: (304) 285-1359; E-mail: Magda.Rivera@netl.doe.gov

Objectives

- Conduct comprehensive transient spatio-temporal system modeling of a planar solid oxide fuel cell (PSOFC) based power conditioning system (PCS) on a low-cost Simulink and gPROMS platform, comprising the following subsystems: PSOFC, balance-of-plant (BOPS), power electronics (PES), and application loads (ALs), leading to reduced-order and computationally efficient PCS model.
- Resolve the interactions among PSOFC, BOPS, PES and ALs.
- Analyze the impact of electrical-feedback effects (e.g., load transients, load power factor, high- and low-frequency ripples) on the performance and durability of PSOFC.
- Optimize power-management control system for mitigation of electrical-feedback effects on PSOFC to enhance its life and performance.
- Conduct BOPS parametric optimization for optimal startup, steady-state, and transient performances.

Approach

- Developed the rigorous numerical model of the PSOFC PCS using
  - Comprehensive (2-D) and reduced-order (1-D) spatio-temporal PSOFC model developed using Embedded MATLAB functions that seamlessly integrate with Simulink;
  - Comprehensive BOPS model developed in gPROMS; reduced-order model being developed in Simulink;
  - Comprehensive (switching) and reduced-order (state-space averaged) PES models developed in Simulink and SimPower Systems;
  - Modeling of ALs in SimPowerSystems;
  - Glueless integration of PSOFC and PES and AL models in Simulink; integration of BOPS model in gPROMS with rest of the PCS Simulink models via gO:Simulink software. Once the reduced-order BOPS model in Simulink is completed, an all-Simulink software model will be available that can potentially be used for real-time simulation (RTS).

- Conduct detailed parametric studies on the PSOFC PCS to investigate the effects of variations of the air and fuel flow rates, operating temperature, load power factor and magnitude of low-frequency ripple on the PSOFC stack and the PCS as a whole. This work leads to a detailed database.
- Analyze the effects of load transients (e.g., no-load to full-load) on the residual thermal stresses inside the fuel cell using finite element analysis and estimate the probability of failure on a test PSOFC.
- Identify ways to mitigate the effects of single and multiple load transients and low- and high-frequency current ripples via
  - A current-injection based active-power filter for battery based power-management control system;
  - Choice of PES topologies and how they shape the PSOFC ripple current;
  - Studying the effects of variations in the power factor of the AL and the impact of load-current distortions due to nonlinear ALs on the PSOFC output current.

Accomplishments

- Developed a low-cost, transient, and spatio-temporal PSOFC PCS modeling platform with varying degree of details (i.e., comprehensive and reduced-order).
- Established a comprehensive database that gathers the effects of various electrical feedbacks on the PSOFC.
- Using a unique multi-organizational (UIC, Ceramatec, and ORNL) approach, demonstrated that certain load transients may develop electrically induced thermal stresses in a PSOFC, which may lead to higher probability of failure of the electrolyte of the PSOFC.
- Developed a highly efficient PES which will be used for experimental validation of modeling data by integrating with an experimental PSOFC stack.

Future Directions

- Realization of all-Simulink reduced-order PSOFC PCS model.
- Scoped validation of the electrical-feedback effects using an experimental PES (fabricated at UIC) and an experimental PSOFC stack (fabricated at Ceramatec).
- Development of power-management control strategies for PES and BOPS to enhance the performance and life of the PSOFC.

Introduction

A comprehensive model of the PSOFC PCS is being developed to meet the following objectives: i) to resolve PSOFC power system interactions and dynamics and develop design insights towards the achievement of reliable system configurations; ii) to enable interaction analysis, control, and optimization on a low-cost modeling platform; and iii) to potentially enable faster and real-time simulation for long-term reliability analysis.

A hierarchical modeling framework is being designed, based on the MATLAB/Simulink platform, which enables seamless integration of the subsystems to obtain a full-scale system model. The huge order (due to the bulky BOPS model) and very fast switching discontinuity (due to switching PES) of the system model are eliminated by creating accurate reduced-order models for each of the subsystems. The effects of various electrical feedbacks (such as different load transients, load power factor, current ripple), PES topology, and the battery size on the performance of the PSOFC are analyzed. A detailed thermal stress analysis is carried out to investigate the effect of load transients on the reliability of the PSOFC. A parametric database of feedback effects (using the PCS model) is created, which will provide design guidelines and help with system identification and optimal controller design for the PCS.

Approach

For accurate prediction of the effects of system interactions on the PSOFC, one needs to analyze the PSOFC internal parametric variations [1-6]. Because a purely temporal model of the SOFC (e.g., [7]) cannot predict the spatial dynamics, a spatio-temporal electro-thermo-chemical model of the PSOFC (in Simulink), which includes spatial discretizations of the cell, has been developed. This model is designed to accept required system inputs (reactant stream flow rates, compositions, temperatures, cell geometric parameters, and cell current) and to compute the corresponding spatially varying properties of a cell. As shown in Figure 1, a single 10 x 10 cm cross-flow SOFC was discretized using a 30 x 30 control volume grid, with each control volume approximated as having homogenous properties throughout. The outer 1 cm perimeter is treated as electrochemically inactive seal area, leaving a 64 cm^2 active cell area. Radiation boundaries will be applied to each exit stream boundary, while both reactant inlet faces are treated as adiabatic (insulated) but open (mass inflow) boundaries. Temperature is the primary transient variable, which will be integrated through time using the Euler explicit method.

We designed a comprehensive modeling framework. The system model comprises PSOFC, BOPS, PES, ALs, and the battery bank. The flow of various parameters among the subsystems is ensured to ascertain proper system interaction. The comprehensive model requires two low-cost software packages for implementation (MATLAB/Simulink including SimPowerSystem and gPROMS including gO:Simulink).

The bulky BOPS model with hundreds of components and subcomponents is much slower than the high-frequency switching model of the PES; hence, the BOPS model slows down the overall speed of simulation of the integrated PCS model. Therefore, to reduce the simulation time and to potentially enable fast RTS, we needed to develop a reduced-order PCS model devoid of switching discontinuity. This is obtained by averaging the switching states of the PES switching model, leading to a continuous model of the power electronics. The lower-order 1-D PSOFC model is derived by

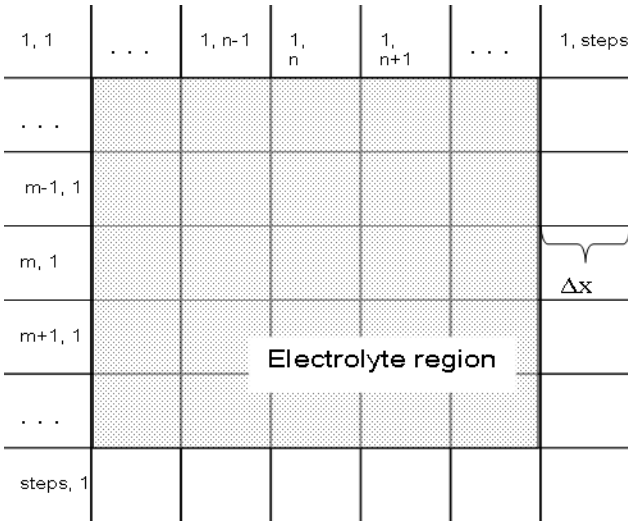

Figure 1. Spatial Homogenous Model for the PSOFC Providing Two-Dimensional Discretizations

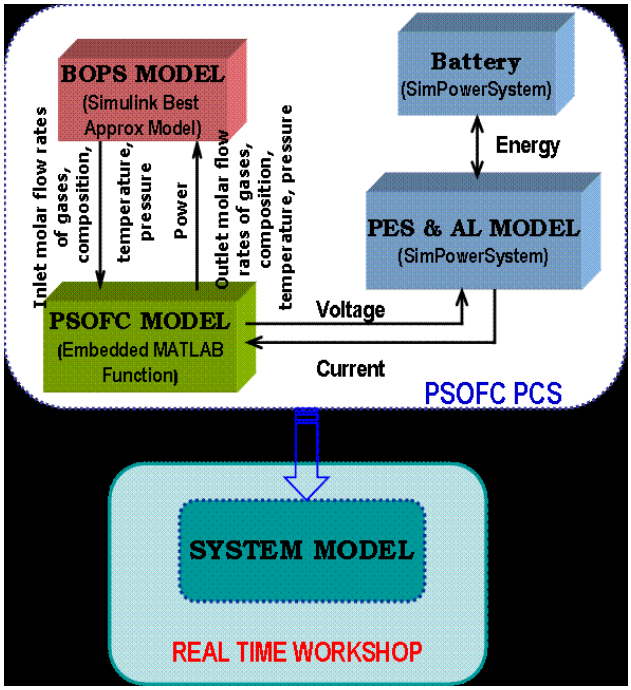

Figure 2. Reduced-Order Modeling Framework for PSOFC Based PCS, Developed in MATLAB/ Simulink Platform

reducing in one of the dimensions of the comprehensive 2-D model. Finally, the BOPS model is approximated using a multi-order polynomial approximation. The reduced-order PCS modeling framework, as shown in Figure 2, improves the simulation speed without compromising accuracy.

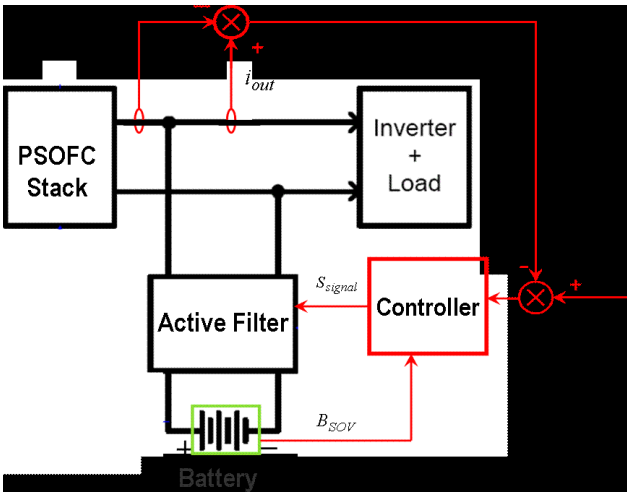

Figure 3. The Proposed Battery Management Controller

Figure 3 shows a battery based power-management control system to mitigate the effects of load transient on the PSOFC. The battery bank is connected at the stack output through an active filter. The components of the active filter are designed based on the high-frequency ripple limitations on the input and output currents and the output voltage. During a load transient, because the BOPS cannot provide the additional air and fuel instantaneously, the active filter, which is a boost-derived converter, supplies the excess load current. This required amount of current (i_{ref}^{*}) is computed based on the flow adjustment of the BOPS and the severity of the load transient. The difference between i_{ref}^{*} and the actual battery current i_{bat} is fed to the controller, which produces the switching signals for the active filter based on the state of the voltage of the battery, B_{SOV}. The controller gains for the active filter are designed and tuned using the AC equivalent model [9] of the filter.

A control scheme is proposed for the BOPS, which is integrated to the PES and the PSOFC stack [10]. A multilevel control approach is used in order to help improve the time response of the BOPS. The first level is determined by the air- and fuel-tank pressures. The objective of the fuel processing subsystem (FPS) and work recovery and air supply system (WRAS) is to keep the tank pressures at fixed values. Control strategies should guarantee that the fuel in the tank is never depleted and should ensure that no shut-down process is complete before proper levels of fuel in the tank are reached. Two additional control actions are implemented for the steam-methane reformer to regulate the exit composition and temperature of the reformate gases. The reformate temperature and composition of the steam-methane reformer are controlled using the inlet temperature and mass flow of the hot gases. The system-level optimization problem is that of minimizing the total cost of the system through its entire life cycle. It is formulated in terms of the capital cost of each subsystem and the total operation/control cost.

Results

We analyzed the effects of load transients on the performance and durability of the PSOFC. The drop in the output voltage of the stack due to the load transient [7, 8] is attributed to the enhanced polarization losses owing to a surge in the current density. Because the response of the BOPS is significantly slower than that of the PES/PSOFC stack, the input fuel flow rates of the stack will not change soon after the load transient. This leads to a sudden increase in fuel utilization inside the PSOFC stack to attain a new electrochemical steady-state condition.

Higher fuel utilization leads to increased rate of the exothermic reactions, which in turn increases the heat rate. This, added to the large response time of the BOPS (i.e., its inability to adjust the air and fuel flow rates instantaneously after the load transient), leads to a gradual increase in the fuel-cell temperature due to the higher thermal time constant of the PSOFC. This is demonstrated in Figure 4. Immediately after the load transient, the net change in the PSOFC mean temperature is minimal; however, at about 600 seconds after the transient, the PSOFC mean temperature reaches its peak. Figure 5 shows the temperature gradient inside the PSOFC corresponding to three separate time instants A, B, and C (shown in Figure 4). Owing to the temperature gradient, a tensile stress is developed at the interface of the electrolyte with the anode of the cell. (These data were calculated initially by ORNL without taking into account the residual stress. Work is in progress to recalculate these tensile stresses and the probability of failure.)

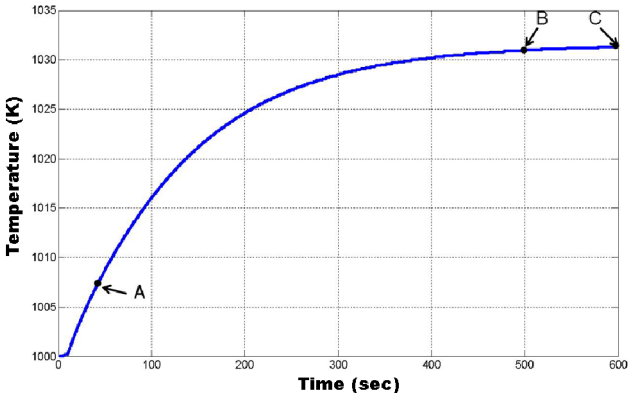

Figure 4. Variation of Mean PSOFC Temperature with Time. Three points, A (t = 50 s), B (t = 500 s) and C (t = 600 s) are chosen for analysis of stress inside the cell.

To investigate the effects of multiple load transients, we subject the PSOFC PCS to multiple short-duration loads in a fixed duration of 600 seconds. The duration of the load is kept fixed at 100 seconds. This type of load variation is attributed to a typical usage of microwave oven load. Temperature of the PSOFC increases with the number of load repetitions. This is because the frequency of the load transients is larger than the inverse of the PSOFC thermal time constant. Thus, multiple load transients can potentially affect the durability of the PSOFC.

The effect of load power factor on the hydrogen utilization and the cell voltage at a constant active output power to the utility is investigated. The fuel utilization increases at lower power factor. The variation in the hydrogen utilization increases as power factor is reduced. Thus, one needs to set the operating fuel utilization at a lower value to avoid the low-reactant condition in the cell; this reduces the efficiency of the cell.

With an increase in the ripple magnitude, the fuel utilization of the PSOFC increases; however, the cell efficiency decreases. In the PES, the loss in the circuit increases with increasing ripple magnitude due to an increased value of the current, thereby decreasing the efficiency of the system further. Therefore, the natural suggestion would be that the magnitude of the ripple should be reduced to achieve higher efficiency of the PSOFC and to reduce any unwanted increase in the fuel utilization. However, decreasing the current ripple requires higher values

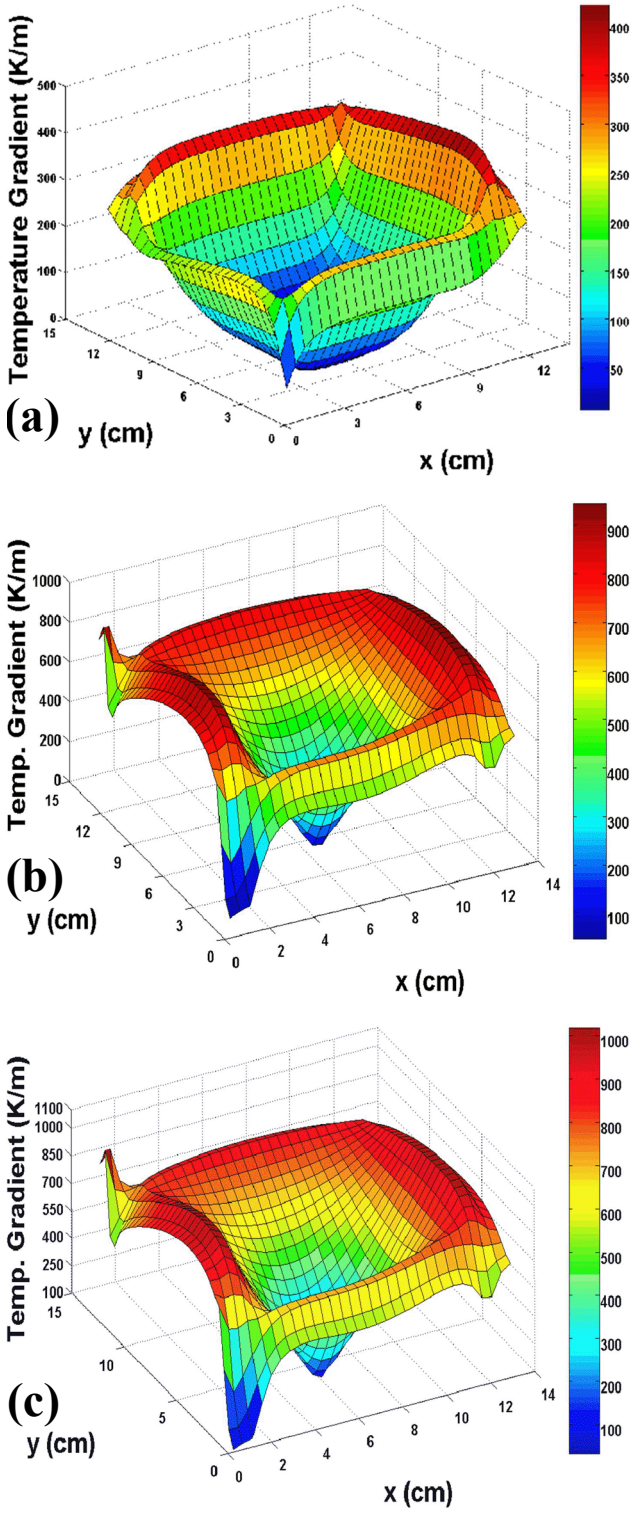

Figure 5. Temperature Gradient Inside the Cell at Instants A, B and C after the Load Transients (refer to Figure 4)

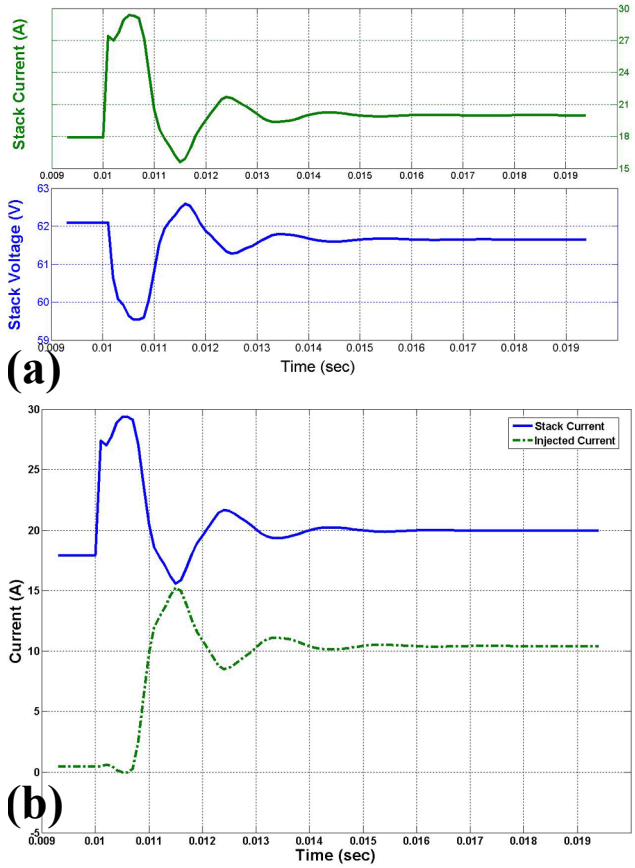

Figure 6. (a) Stack Current and Stack Voltage before and after the Load Transients; (b) Stack Current and Output Current of the Active Filter before and after the Load Transients

of the output electrolytic capacitor, or active-ripple-cancellation circuit, which increases the cost of the PES.

The dynamic optimum trajectories of the actual reformate tank pressure closely follow the optimum-pressure trajectory. The optimum tank pressure (i.e., in effect the system pressure) is a function of system demand [10, 11]. At high loads, the optimum pressure is higher because at low loads, both the stack and FPS efficiencies are higher and the increase in the pressure has a minor effect on the stack efficiency increment. On the other hand, the WRAS is less efficient at low loads and, therefore, the parasitic power due to the electrical motor at low loads increases as the system pressure increases. The dynamic trajectory of the methane flow rate into the reformer is the control variable for the reformate tank pressure. This mass flow is in fact regulated by a flow control valve. The rapid increase in the mass flow at 86,400 sec is due to the sudden change in the reference pressure, which produces an instantaneous error signal, which the controller tries to correct.

Finally, we investigate the effect of the battery buffering. As shown in Figure 6a, we subject the PCS to a load transient at time t=0.01 second. As a result, the stack output current increases to meet the new load demand. This increase in the stack current leads to a drop in the stack output voltage. Now, the required battery current i_{ref}^{*} is fed as a reference to the active filter controller shown in Figure 3. As illustrated in Figure 6b, the current output of the active filter, fed from the battery, increases to supply the excess load current, which in turn stabilizes the stack voltage close to its nominal value. Hydrogen utilization of the stack is maintained between 0.55 and 0.7.

Conclusions

The study conducted in the previous year gives detailed insight into the impacts on the PSOFC stack and the PSOFC power conditioning system of various electrical-feedback effects due to the power electronics and the application loads. This allows the determination of the required response time of the BOPS and power-buffering mechanism and control to avoid any degrading effect on the PSOFC. Our interaction analyses yield the following conclusions:

- A severe no-load to full-load transient increases the current density of the PSOFC immediately, which leads to a higher temperature inside the cell due to rapid exothermic reactions. The increase in the temperature increases the temperature gradient inside the cell, which in turn dictates the tensile stress on the PSOFC stack.
- Multiple load transients, with frequency of repetition higher than the inverse of the PSOFC thermal time constant, will be even more detrimental to the PSOFC durability, as compared to a single load transient.
- Apparently, the low-frequency ripple (e.g., 120 Hz ripple) current does not increase the PSOFC temperature even at high ripple magnitude. This is because the time period of the ripple is negligible as compared to the thermal time constant of the PSOFC. However, the higher the magnitude of the ripple current, the lower is the efficiency of the stack. Further, the impact of the

ripple current on the chemical stability of the electrodes and electrolytes needs to be investigated. This is a different mechanism of instability than that due to electrically induced temperature rise, as observed after load transients.

- Lower power factor of the load increases the fuel utilization of the stack due to higher circulating AC current in the circuit.

The optimization study leads to a system configuration which is able to meet all of the load requirements and system constraints. In particular, using reformate and air tanks as buffers between the BOPS and the PSOFC stack is shown to be an operational and cost-effective method which minimizes the transient effects on the SOFC stack due to changes in load.

Special Recognitions & Awards/Patents Issued

1. Dr. Mazumder presented the Keynote Lecture on fuel cell power electronics at the ASME Third International Conference on Fuel Cell Science, Engineering and Technology, held at Yipsilanti, Michigan, May 23 – 25, 2005.
2. A non-provisional patent (entitled "A novel efficient and reliable dc/ac converter for fuel cell power conditioning") was filed by the University of Illinois at Chicago (UIC).
3. Since the summer of 2004, a UIC student team comprising 10 undergraduate and graduate students has been working under the leadership of Prof. Mazumder on a prestigious International Fuel Cell Energy Challenge project sponsored by IEEE. This project has leveraged the fuel-cell knowledge gained as a part of the DOE Solid State Energy Conversion Alliance (SECA) work, leading to the design and the development of a 1-kW fuel-cell grid-connected inverter for residential power system. The UIC team has been selected as one of the 6 finalists. The final competition will be held in Colorado at the National Renewable Energy Laboratory test site in August.
4. Dr. Diego Rancruel, who was one of the Virginia Tech graduate students working on the DOE SECA project, has joined General Electric Energy and Power Generation Technology as a Lead Engineer for their New Product Introduction Division.

FY 2005 Publications/Presentations

1. S. Pradhan, S.K. Mazumder, J. Hartvigsen, M. von Spakovsky, "Effects of electrical feedbacks on the reliability of the planar solid-oxide fuel cell (PSOFC) power conditioning system", accepted for publication, Fuel Cell Seminar, 2005.
2. S.K. Mazumder, S. Pradhan, J. Hartvigsen, M. von Spakovsky, and D. Rancruel, "Effects of battery buffering and inverter modulation on the post load-transient performance of planar solid-oxide fuel cell", *IEEE Transactions on Energy Conversion*, in press for publication, 2005.
3. S.K. Mazumder, *Fuel Cell Power-Conditioning System*, Editor S.K. Basu, Kluwer Academic Publishers, expected year of publication: December 2005.
4. S.K. Mazumder, S. Pradhan, K. Acharya, J. Hartvigsen, M. von Spakovsky, and C. Haynes, "Load-transient mitigation techniques for solid-oxide fuel cell (SOFC) power-conditioning system", *Proceedings of the IEEE Telecommunications Energy Conference*, pp. 174-181, 2004.
5. S.K. Mazumder, K. Acharya, S. Pradhan, J. Hartvigsen, M. von Spakovsky, and C. Haynes, "Energy buffering techniques for load transient mitigation of solid-oxide fuel cell (SOFC) power conditioning system (PCS)", *Proceedings of the IEEE Power Electronics Specialists Conference*, vol. 6, pp. 4749-4754, 2004.
6. D.F. Rancruel, M.R. von Spakovsky, "Development and application of a dynamic decomposition strategy for the optimal synthesis/design and operational/ control of a SOFC based APU under transient conditions", *International Mechanical Engineering Congress and Exposition – IMECE'2005*, submitted for publication, ASME Paper No. IMECE2005-82986, 2005.
7. D.F. Rancruel, M.R. von Spakovsky, "A decomposition strategy based on thermoeconomic isolation applied to the optimal synthesis/design and operation of an advanced tactical aircraft system," *Energy: The International Journal*, Elsevier, 2004, accepted for publication.

References

1. J.R. Ferguson, J.M. Fiard, and R. Herbin, "A mathematical model of solid oxide fuel cells", *Journal of Power Sources*, vol. 58, pp. 109-122, 1996.

2. J. Hartvigsen, S. Elangovan, and A. Khandkar, *Science and Technology of Zirconia V*, Edited by Badwal, S., Bannister, M., and Hannink, R., Technomic Publishing Company, Inc., Lancaster, Pennsylvania, 1993.
3. I.V. Yentekakis, S. Neophytides, S. Seimanides, and C.G. Vayenas, "Mathematical modeling of cross-flow, counter-flow and co current-flow solid oxide fuel cells: theory and some preliminary experiments", *Proceedings of 2nd International Symposium on Solid Oxide Fuel Cells*, Athens, Greece, Official Publication of the EEC, Luxembourg, pp. 281-288, 1993.
4. E. Erdle, J. Gross, H.G. Muller, W.J.C. Müller, H.-J. Reusch, and R. Sonnenschein, *Proceedings of Second International Symposium on SOFCs*, Edited by Singhal et al., pp. 265, 1991.
5. J.R. Ferguson, *Proceedings of Second International Symposium on SOFCs*, Edited by Singhal et al., pp. 305, 1991.
6. P.V. Hendrikson, *Second Nordic Symposium on High Temperature Fuel Cells*, Edited by T. Nordby and F.W. Poulsen, 1994.
7. S.K. Mazumder, K. Acharya, C.L. Haynes, R. Williams, M.R. von Spakovsky, D.J. Nelson, D.F. Rancruel, J. Hartvigsen, and R.S. Gemmen, "Solid-oxide-fuel-cell performance and durability: resolution of the effects of power-conditioning systems and application loads", *Special Issue on Distributed Generation*, *IEEE Transactions of Power Electronics*, vol. 19, pp. 1263 - 1278, 2004.
8. S.K. Mazumder, S. Pradhan, J. Hartvigsen, M. von Spakovsky, and D. Rancruel, "Effects of battery buffering and inverter modulation on the post load-transient performance of planar solid-oxide fuel cell", *IEEE Transactions on Energy Conversion*, in press for publication, 2005.
9. R.W. Erickson and D. Maksimovic, *Fundamentals of Power Electronics*, Springer, 2nd edition, 2001.
10. D.F. Rancruel, *Dynamic synthesis/design and operation/control optimization approach applied to a solid-oxide fuel cell based auxiliary power unit under transient conditions*, Ph.D. dissertation, adviser: M.R. von Spakovsky, Virginia Polytechnic Institute and State University, February 2005.
11. D.F. Rancruel, M.R. von Spakovsky, "Development and application of a dynamic decomposition strategy for the optimal synthesis/design and operational/ control of a SOFC based APU under transient conditions", *International Mechanical Engineering Congress and Exposition, IMECE'2005*, submitted for publication, ASME Paper No. IMECE2005-82986.

III.D.4 Advanced Measurement and Modeling Techniques for Improved SOFC Cathodes

Stuart B. Adler (Primary Contact), Y. Lu, L. Dunyushkina, J. Wilson, S. Huff
University of Washington
Box 351750
Seattle, WA 98195-1750
Phone: (206) 543-2131; Fax: (206) 685-3451; E-mail: stuadler@u.washington.edu

DOE Project Manager: Lane Wilson
Phone: (304) 285-1336; E-mail: Lane.Wilson@netl.doe.gov

Objectives

- Develop nonlinear harmonic measurements for diagnosis of solid oxide fuel cell (SOFC) cathode limitations.
- Identify linkages between processing conditions and performance °V, in particular the role of the interface in determining electrode overpotential.
- Test the usefulness of nonlinear harmonic measurements for electrode development through a test-bed application involving participants in the vertical Solid State Energy Conversion Alliance (SECA) teams.

Approach

- Develop an improved mask layer that can better separate as-processed cathodes from contacting the electrolyte except along well-defined locations. By patterning this layer, it will be possible to make half-cell measurements with improved accuracy and throughput.
- Develop quantitative modeling tools that can be used to link nonlinear harmonic characteristics to specific mechanisms and reaction steps limiting performance.
- Build a second, improved, nonlinear electrochemical impedance spectrometer, which will be used to evaluate cathodes produced by the industrial teams.

Accomplishments

- Successfully demonstrated the use of microelectrode half-cells for isolating the characteristics of SOFC cathodes.
- Conducted first nonlinear electrochemical impedance spectroscopy (NLEIS) measurements of porous $La_{0.8}Sr_{0.2}CoO_{3-\delta}$ (LSC-82) electrodes on samaria-doped ceria (SDC).
- Quantified the relative roles of interfacial vs. chemical steps for LSC-82 on SDC as a function of firing temperature.
- Proved that the critical transport step for oxygen intermediates on LSC-82 involves both surface and bulk species.
- Conducted measurements of NLEIS on thin film cells.

Future Directions

- Complete NLEIS half-cell measurements on porous mixed-conducting electrodes with resolution in the high-frequency interfacial regime, identifying nonlinearities of the interface.
- Apply a combination of materials characterization, impedance, and NLEIS to identify the kinetics governing the interface, and how the kinetics depend on processing conditions and composition/ morphology of the interface.

Introduction

The high operating temperature of current state-of-the-art SOFC cathode materials (>800°C) limits performance and cost reduction efforts. Many of the most exciting new electrode systems incorporate mixed conducting ceramics (materials which carry both oxygen ions and electrons) in order to substantially improve the activity and selectivity of the electrode reaction at reduced temperature. While these electrodes have proven promising as electrodes in solid oxide fuel cells, they are only empirically understood, far from optimized, and they react unfavorably with the electrolyte to form insulating phases. Our overall goal is to provide improved diagnostic tools to developers, which can be used both to better understand what limits these electrodes and to accelerate materials selection and entry into the commercial realm.

Approach

Electrochemical impedance spectroscopy (EIS) is used extensively to probe the electrochemical characteristics of solid oxide fuel cell electrodes. While EIS has proven to be a powerful technique for isolating and characterizing electrode response, detailed analysis of EIS data provides only limited insight regarding the specific rate-determining steps governing electrode reaction mechanisms. A major factor limiting the usefulness of EIS data is overlap or dispersion in the frequency domain among physical processes governing electrode reactions, making them difficult to resolve entirely by timescale. Another factor is that different mechanistic models for a given reaction often predict very similar impedance response after the governing equations have been linearized.

In order to gain further insight into the mechanisms governing SOFC cathodes, we have extended EIS to probe both linear and nonlinear responses. This technique, which has been called nonlinear EIS (NLEIS), involves the measurement of nonlinear 2nd and higher order voltage harmonics resulting from moderate amplitude current perturbations. By the excitation of nonlinear responses and interactions, NLEIS potentially offers improved identification of physical steps via nonlinearity and extent of coupling, as well as time scale.

Results

Figure 1 compares our measurements of the linear first harmonic response (impedance) of porous LSC-82 electrodes on SDC electrolyte at 750°C in air. The data have been nondimensionalized [1] so as to compare to a reaction/transport model described in reference [2], where it is assumed that oxygen reduction is co-limited by a) absorption into LSC-82 and b) bulk transport through LSC-82 to the electrolyte. Although the agreement between model and data is reasonable, this result merely confirms that the model can be made to fit impedance data with appropriate values of the Gerischer parameters t_{chem} and R_{chem}[2]. This agreement holds true regardless of the values of several important parameters governing the nonlinear thermodynamics and kinetics of oxygen reduction. In particular, this fit tells us nothing about the rate-limiting catalytic step governing O_2 reduction.

Extending this comparison to the higher harmonics, Figures 2-4 show the magnitude and phase of the first and third harmonics of porous LSC-82 electrodes on SDC electrolyte at 750°C in air. $\hat{U}_{1,1}(\sigma)$, $\hat{U}_{1,3}(\sigma)$, $\hat{U}_{3,3}(\sigma)$ and (nondimensionalized voltages) refer to the linear first harmonic (impedance), cubic nonlinear component of the first harmonic, and cubic nonlinear component of the third harmonic, respectively [1]. The data in

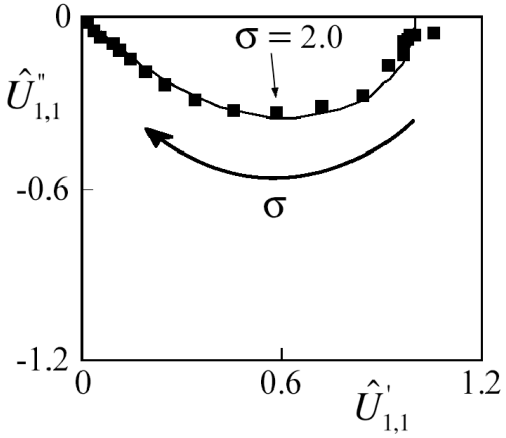

Figure 1. Nyquist plot of the measured (symbols) and calculated (line) linear first harmonic response (impedance) of porous LSC-82 on SDC at 750°C in air. As described in reference [1], this behavior is predicted regardless of the thermodynamics or kinetics governing oxygen absorption.

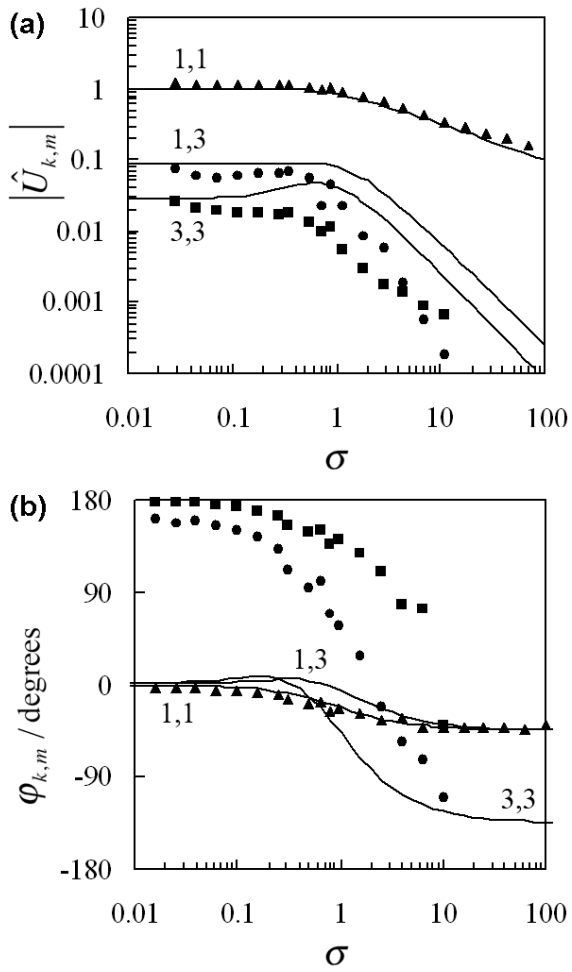

Figure 2. Bode plots of the measured (symbols) and calculated (line) Fourier coefficients of the nondimensionalized overpotential. a) Magnitude and b) Phase of $\hat{U}_{1,1}(\sigma)$ (triangles), $\hat{U}_{1,3}(\sigma)$ (squares), $\hat{U}_{3,3}(\sigma)$ (circles). The model assumes that the thermodynamic properties of the mixed conductor are those of bulk LSC-82, and that the oxygen absorption kinetics are limited by O_2 dissociation.

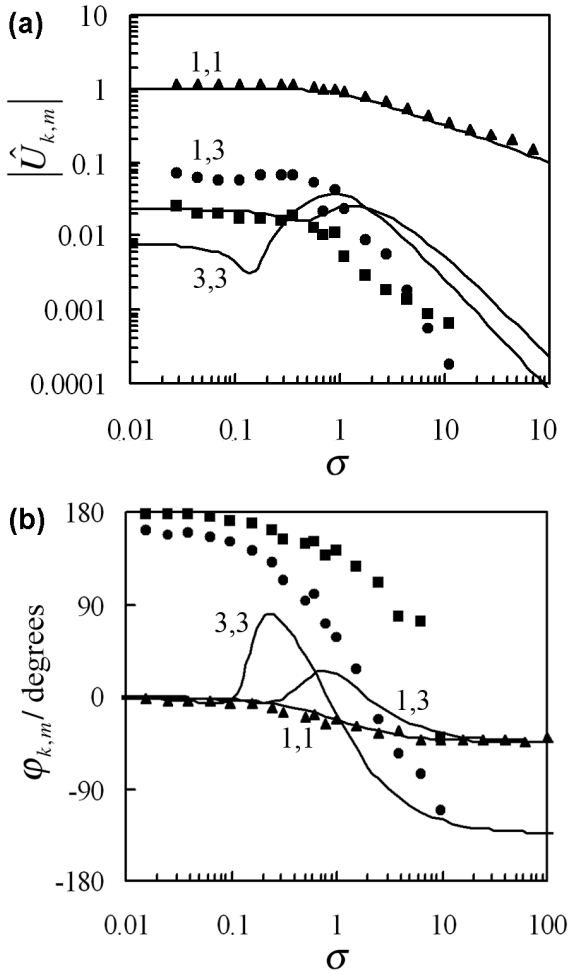

Figure 3. Bode plots of the measured (symbols) and calculated (line) Fourier coefficients of the nondimensionalized overpotential. a) Magnitude and b) Phase of $\hat{U}_{1,1}(\sigma)$ (triangles), $\hat{U}_{1,3}(\sigma)$ (squares), $\hat{U}_{3,3}(\sigma)$ (circles). The model assumes that the thermodynamic properties of the mixed conductor are those of bulk LSC-82, and that the oxygen absorption kinetics are limited by oxygen incorporation into LSC-82.

Figures 2-4 are the same, but the models shown in comparison to the data are different, as described below. The data for $\hat{U}_{1,1}(\sigma)$ are the same as those shown in the Nyquist plot (Figure 1).

In Figure 2, the data are compared to the model in reference [2], where we assume oxygen absorption is dissociative-adsorption-limited. As noted previously, experimental results for component $\hat{U}_{1,1}(\sigma)$ (Figure 1) show good agreement with theory. However, the sign of $\hat{U}_{1,3}(\sigma)$ and the sign of $\hat{U}_{3,3}(\sigma)$ are negative at low frequency (phase of 180°), while the model predicts positive values (phase of 0°). The magnitudes of $S\hat{U}_{1,3}(\sigma)$ and $\hat{U}_{3,3}(\sigma)$ are also in poor agreement with the model throughout the frequency spectrum, exhibiting a characteristic transition frequency much lower than predicted by the model based on the first harmonic. Finally, the divergent phase behavior of $\hat{U}_{1,3}(\sigma)$ and $\hat{U}_{3,3}(\sigma)$ predicted by the model at high frequency is absent in the data.

Under the assumption that the disparity in Figure 2 results from an incorrect assumption about the adsorption mechanism, a variety of other absorption rate expressions were considered. For example, Figure 3 compares the experimental data and model assuming oxygen absorption is limited by incorporation into the solid (vacancy-supply-limited). Since this model is degenerate in the first harmonic with that in Figure 2, the measured value of $\hat{U}_{1,1}(\sigma)$ shows equally good (identical) agreement with theory. However, the higher harmonic spectra $\hat{U}_{1,3}(\sigma)$ and $\hat{U}_{1,3}(\sigma)$ predicted by the model again show poor agreement, including incorrect phase (sign) and the presence of harmonic "nullifications", caused by sudden sign changes associated with destructive interactions among oscillating harmonics, not observed in the experimental data.

A variety of other rate expressions were considered; however, none of these rate expressions were found to be consistent with the higher harmonic data. Abandoning any particular exchange mechanism, and instead varying kinetic parameters empirically, we found moderate agreement for a situation in which oxygen *de*sorption depends on $(P_{O_2}^{gas})^{+1.4}$, which is difficult to rationalize based on any realistic exchange mechanism. Thus, the results shown in Figures 2 and 3 suggest that for LSC-82 on SDC at 750°C in air, the measured higher harmonics cannot be explained in terms of an entirely bulk transport path, assuming the thermodynamic properties of bulk LSC-82.

In order to gain some insight about what other mechanisms might be governing the electrode, we considered other sources of nonlinearity in the system. Figure 4 compares the experimental and theoretical values of $\hat{U}_{k,m}$ assuming O_2-dissociation-limited kinetics (as in Figure 2), but where the thermodynamic properties of LSC-82 are taken to be those of bulk $La_{0.43}Sr_{0.57}CoO_{3-\delta}$, a material with a much higher vacancy concentration than LSC-82 under the same conditions. As evidenced by the agreement between measured and calculated harmonic spectra $\hat{U}_{1,3}$ and $\hat{U}_{3,3}$, the nonlinear characteristics of the LSC-82 electrode would appear to be more consistent with the bulk thermodynamic properties of $La_{0.43}Sr_{0.57}CoO_{3-\delta}$ than those of LSC-82.

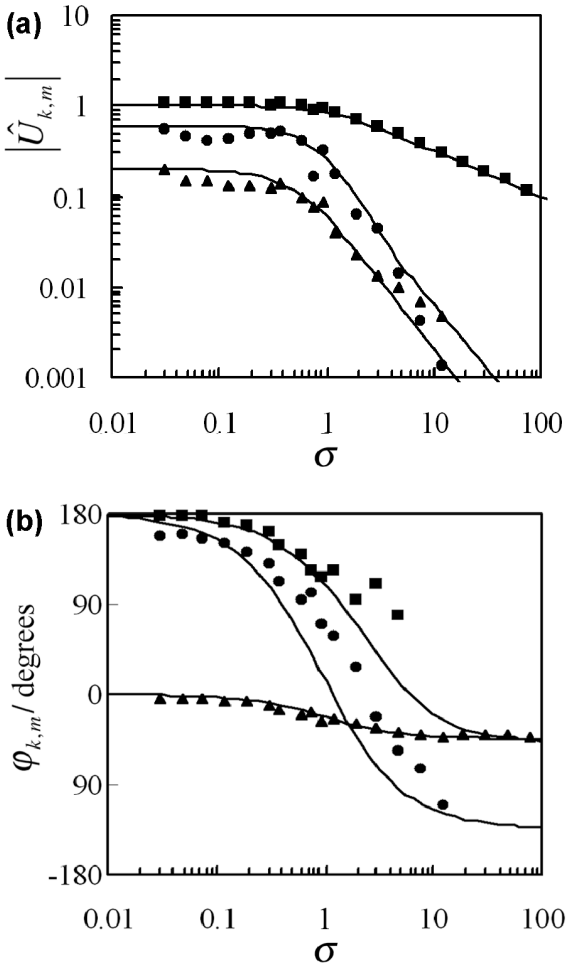

Figure 4. Bode plots of the measured (symbols) and calculated (line) Fourier coefficients of the nondimensionalized overpotential. a) Magnitude and b) Phase of $\hat{U}_{1,1}(\sigma)$ (triangles), $\hat{U}_{1,3}(\sigma)$ (squares), $\hat{U}_{3,3}(\sigma)$ (circles). The model assumes that the thermodynamic properties of the mixed conductor are those of bulk $La_{0.43}Sr_{0.57}CoO_{3-\delta}$ and that the oxygen absorption kinetics are described by equation 9 in reference [2].

One interpretation of Figure 4 is that the electrode operates *via* a mixed bulk and surface path, where the apparent "thermodynamic properties of the surface" (while similar to the bulk qualitatively) involve a much higher "surface vacancy concentration" than in the bulk. This hypothesis is consistent with some atomistic simulations, which suggest that defect energies at the surface are lower than in the bulk, leading toward segregation of strontium ions to the surface of the perovskite [3].

Possible experimental evidence for this effect includes X-ray photo-electron spectroscopy measurements of $La_{1-x}Sr_xMO_{3-\delta}$, which suggest that the strontium content of the surface is enriched relative to the bulk [4]. We are currently developing a model which incorporates such surface-transport effects and will be using it in the future to try to deconvolve surface and bulk contributions to the overall polarization.

Conclusions

For the case of porous LSC-82 electrodes on SDC at 750°C in air, the third-order harmonic spectra were found to exhibit distinctive features that could be used to distinguish various possible mechanisms which are degenerate in the first harmonic (impedance). Assuming oxygen reduction is co-limited by oxygen absorption and transport in the bulk of the mixed conductor, the measured harmonics were compared to those predicted for various scenarios for the oxygen absorption kinetics. This comparison shows that the measured harmonics are inconsistent with any realistic model for the absorption kinetics that assumes an entirely bulk-transport pathway. The data were found to be more consistent with a variation of this model that assumes oxygen absorption is governed by dissociative adsorption, but the thermodynamic properties of the electrode material are that of bulk $La_{0.43}Sr_{0.57}CoO_{3-\delta}$. One possible interpretation of this result is that the electrode operates by parallel surface and bulk paths, where the apparent concentration of mobile vacancies on the surface is much higher than in the bulk.

FY 2005 Publications/Presentations

1. L. A. Dunyushkina and S. B. Adler, "Influence of Electrolyte Surface Planarization on the Performance of the Porous SOFC Cathodes," *J. Electrochem. Soc.*, (*in press*) (2005).
2. L. A. Dunyushkina, Y. Lu, and S. B. Adler, "Microelectrode Array for Isolation of Electrode Polarization on Planar Solid Electrolytes," *J. Electrochem. Soc.*, (*in press*) (2005).
3. J. R. Wilson, D. T. Schwartz, and S. B. Adler, "Nonlinear Electrochemical Impedance Spectroscopy for Mixed-Conducting SOFC Cathodes," *Electrochemica Acta*, (*in press*) (2005).

References

1. J.R. Wilson, D.T. Schwartz, and S.B. Adler, "Nonlinear Electrochemical Impedance Spectroscopy for Mixed-Conducting SOFC Cathodes," *Electrochemica Acta*, (*in press*) (2005).
2. S.B. Adler, *Solid State Ionics* 111 (1998) 125.
3. M.S. Read, M.S. Islam, G.W. Watson, F. King, and F.E. Hancock, *J. Mater. Chem.* 10 (2000) 2298.
4. P. Decorse, G. Caboche, and L. Dufour, *Solid State Ionics* 117 (1999) 161.

IV Hybrids

IV Hybrids

IV.1 Direct Fuel Cell/Turbine Power Plant

Hossein Ghezel-Ayagh
FuelCell Energy, Inc.
3 Great Pasture Road
Danbury, CT 06813
Phone: (203) 825-6048; Fax: (203) 825-6273; E-mail: hghezel@fce.com

DOE Project Manager: Travis Shultz
Phone: (304) 285-1370; E-mail: Travis.Shultz@netl.doe.gov

Subcontractors:
Capstone Turbine Corporation, Chatsworth, CA
Montana State University, Bozeman, Montana
CTA Architects Engineers, Billings, Montana

Objectives

The overall project goal is to develop ultra-high-efficiency power plants based on Direct FuelCell/Turbine® (DFC/T®) technology. The specific objectives are as follows:

- Develop the conceptual design of multi-MW hybrid DFC/T systems with efficiencies approaching 75% (natural gas fuel), and with sulfur and nitrogen oxide emissions <0.01 lb/million BTU.
- Verify commercial viability of the DFC/T systems for near-term deployment.
- Design a packaged sub-MW DFC/T system for distributed power generation.
- Verify the potential benefits of hybrid technology and show its readiness for commercialization by a grid-connected field demonstration at a customer site.

Approach

- Conduct proof-of-concept tests of the DFC/T system in a sub-MW class power plant configuration.
- Evaluate the design of the key system components, including gas turbine, heat recuperators, and high-temperature catalytic oxidizer.
- Develop the preliminary design of a 40-MW DFC/T power plant representative of the multi-MW hybrid systems. Estimate the cost of the power plant to verify its commercial competitiveness with alternate technologies.
- Conduct experimental investigations to evaluate alternative designs for anode gas delivery to fuel cells to further increase fuel cell efficiency.
- Design, fabricate, and test two sub-MW class DFC/T units to assess the efficiency potential of the power plants and to demonstrate the technology.

Accomplishments

- Completed the construction of a sub-MW DFC/T power plant facility by integration of a full-size 250-kW DFC stack with a Capstone C60 microturbine.
- Completed the proof-of-concept demonstration tests by successful operation of the world's first grid-connected hybrid system (pre-alpha DFC/T).

- Completed the preliminary design of a 40-MW DFC/T hybrid system, including site plan and fuel cell module layouts. Estimated plant capital cost and performance characteristics of the 40-MW power plant.
- Completed experimental investigation to evaluate alternative designs for anode gas delivery to fuel cells to further increase fuel cell efficiency.
- Completed the detailed design of the sub-MW class DFC/T (Alpha) unit, including equipment layout, piping layout (isometric drawings), structural support, process instrumentation, DC-to-AC power conditioning, electrical panel layout, and power distribution drawings.
- Developed the process control system design and software, including details of microturbine operation, power plant start-up/shutdown strategies, safety alarms, Human Machine Interface (HMI) display screens, Programmable Logic Controller (PLC) program codes, and the control philosophy for operation of the Alpha DFC/T unit.
- Completed fabrication of the Alpha DFC/T unit, including the integration of a Capstone C60 microturbine, heat recuperators, and fuel preparation subsystems.
- Completed the conditioning and checkout tests of the fuel cell stack module and the acceptance tests of the key balance-of-plant equipment in the Alpha packaged unit.

Future Directions

- Conduct tests of the first sub-MW (Alpha) unit at FuelCell Energy (FCE) facilities in Danbury, Connecticut. Obtain operational data from grid-connected tests of the Alpha unit.
- Continue collaborative research with Montana State University to develop guidelines for heat exchangers and load monitoring equipment.
- Implement design improvements based on the Alpha unit (grid-connected) operational data and performance in a second sub-MW DFC/T (Beta) unit.
- Fabricate the Beta DFC/T unit and conduct field demonstration tests of the unit in Montana.

Introduction

FCE's DFC/T hybrid system concept is based on integration of the company's Direct FuelCell® with a gas turbine. The power plant design utilizes a heat recovery approach for extraction of heat from the balance-of-plant. The fuel cell plays the key role by producing the larger share of the power (>80%). The gas turbine is utilized for generation of additional power by recovering the fuel cell byproduct heat in a Brayton cycle, as well as for providing the air for the fuel cell operation.

Features of the DFC/T system include electrical efficiencies approaching 75% on natural gas (60% on coal gas), direct reforming internal to the fuel cell, minimal emissions, reduced carbon dioxide release to the environment, simple design, and cost competitiveness with existing combined cycle power plants.

Approach

The DFC/T system concept was implemented in a power plant test facility (pre-alpha power plant) by integration of a 250-kW DFC stack and a Capstone microturbine. Figure 1 shows a picture of the DFC/T power plant facility. The focus of the pre-alpha testing was the verification of the DFC/T concept, development of critical system components, and acquisition of design information for development of power plant products.

Test results from the proof-of-concept tests established the foundation for the design of the packaged sub-MW units. The hybrid technology development plan includes the design, construction, and testing of two sub-MW DFC/T units. The tests will demonstrate grid-connected operations and help assess the efficiency potential of the sub-MW plants, while providing valuable data on integration and operation of DFC/T power plants under laboratory and field conditions. The first unit, "Alpha", will be

Figure 1. Sub-MW DFC/T Hybrid Power Plant Showing Full-Size DFC Stack Integrated with a Capstone Microturbine

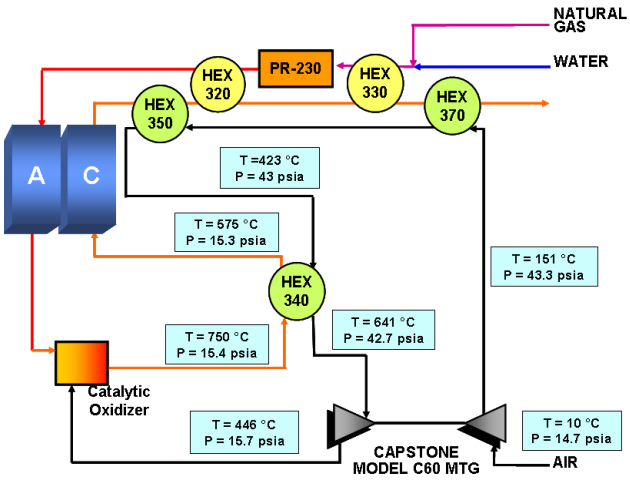

Figure 2. Sub-MW DFC/T Power Plant Facility Process Flow Diagram Along with a Typical Set of Operational Data

factory tested at FCE headquarters in Danbury, Connecticut. The test results and experience from the Alpha unit will be used to refine the design for the "Beta" unit, which will undergo one year of demonstration testing in Montana.

The design of a large-scale hybrid power plant focused on scalable products. FCE has developed the fuel cell cluster concept in order to scale up product capacities in a short design cycle. FCE has completed preliminary design of a 40-MW hybrid power plant.

Results

Proof-of-Concept Tests

The "pre-alpha" proof-of-concept tests verified the DFC/T concept by demonstrating that a substantial gain in efficiency is feasible in small-size power plants by integrating a microturbine with the fuel cell. A net grid-connected power of 247 kWac with efficiency of 52.4% LHV (including parasitic and inverter losses) was achieved. Figure 2 shows a simplified process flow diagram for the sub-MW DFC/T power plant, including a typical set of plant operating conditions. Three heat recuperators for indirect heating of air from the compressor side of the microturbine were included. The anode exhaust oxidizer included a high-temperature catalytic section.

The pre-alpha DFC/T operation in the power plant facility was terminated after 6,620 hours of operation. The tests established the stable and well-controlled operation of the DFC/T power plant. Thermal management of the system was confirmed by increasing microturbine expander inlet temperature while controlling the fuel cell operating temperature. The tests successfully demonstrated the ability of the control system to follow prescribed load ramps and to respond to abrupt utility grid outages. NOx emission levels of less than 0.25 ppm were achieved.

Multi-MW Power Plant Design

The preliminary design of a 40-MW power plant hybrid system concept was completed. An overall layout/plot plan of the 40-MW plant is shown in Figure 3. The site is approximately 273' x 325' in size. The design is based on a scalable approach using FCE's existing M-10 (MW-scale) fuel cell modules in a cluster arrangement. The fuel cell cluster design has five M-10 modules in a cluster with common distribution piping for the fuel and oxidant gases. Based on the scalable overall plant design concept, the plant is arranged in three sections (power blocks) in addition to the centralized equipment. Each power block consists of two

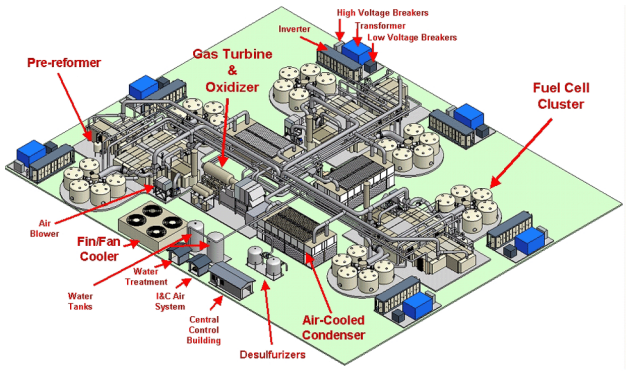

Figure 3. 40-MW Hybrid DFC/T Power Plant Layout and Site Plan for Near-Term Very Efficient Power Generation

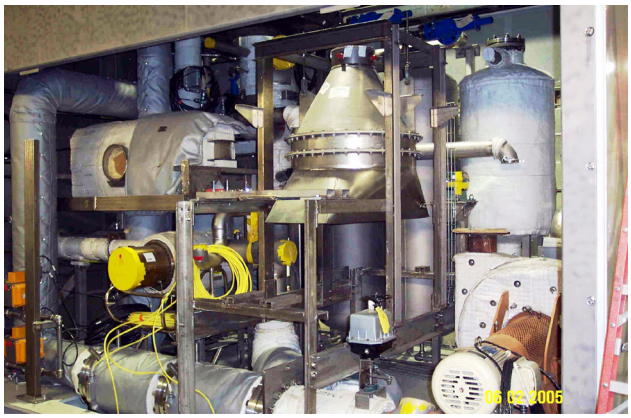

Figure 4. Fabrication of Alpha Unit in a Packaged Sub-MW Class Hybrid Power Plant Configuration

clusters of fuel cell modules together with supporting equipment. The centralized equipment, which supports all three sections, includes a gas turbine, an anode gas oxidizer and other common site equipment such as a fuel clean-up subsystem and a water treatment subsystem. The gas turbine incorporated in the 40-MW plant design is Man Turbo Model 1304-11 (MAN Turbomachinery Inc). Key characteristics of the gas turbine include pressure ratio of 8 and turbine inlet temperature of about 1800ºF.

Sub-MW Power Plant Design and Demonstrations

The detailed design of the packaged sub-MW hybrid unit was completed for civil, mechanical, and piping disciplines. Steady-state mass and energy balances for the power plant were completed for various modes of operation, including start-up, standby, and full-load operation. A process flow diagram and a detailed set of piping and instrumentation diagrams were prepared. Power and control system wiring diagrams, and design layouts for instrument and breaker panels, were completed.

Fabrication of the Alpha sub-MW DFC/T hybrid power plant was completed. The Alpha unit consists of three main sections—mechanical balance-of-plant, DFC stack module, and electrical balance-of-plant—which are transportable as separate units. The modular designs of the power plant sections allow for ease of installation and connection to the utility grid. Figure 4 shows a picture of the Alpha unit during fabrication of the balance-of-plant. The development of control software, including control philosophy documents, was completed. The control strategies for air, water, and fuel flows were also developed. Process control software for the Alpha unit's PLC was prepared. The power-conditioning module of the Alpha unit includes a DC-to-AC inverter and a tie-in connection for the microturbine.

Fabrication of a 250-kW stack module for integration in the Alpha DFC/T was completed at the Torrington (Connecticut) manufacturing plant. The conditioning and checkout tests of the fuel cell stack module were initiated at the full-scale test facility in Danbury, Connecticut. The test plan for the Alpha unit includes grid-connected operation for acquisition of real-time performance data.

Conclusions

The DFC/T concept was verified in the world's first grid-connected hybrid fuel cell/gas turbine sub-MW class power station. Power plant operation, using a microturbine as the only source of fresh air supply to the system, was demonstrated. The test results showed that DFC/T concept has potential for achieving very high efficiencies.

A scalable approach for the multi-MW plant design based on fuel cell clusters of the existing 1-MW (M-10) modules has been developed. Preliminary design of a 40-MW hybrid system for near-term deployment was completed.

Lessons learned during the proof-of-concept tests were incorporated in the detailed design of the Alpha DFC/T unit. The packaging of the key components for the Alpha hybrid power plant was

completed. The grid-connected performance results from operation of the Alpha unit will provide the basis for refinements in the mechanical design of the field demonstration (Beta) unit. The fabrication and operation of the Alpha and Beta units will demonstrate the feasibility of implementing the hybrid DFC/T system concept in a sub-MW packaged power plant design.

Special Recognitions & Awards/Patents Issued

1. Z.-H. Wang, and H. Ghezel-Ayagh, "Enhanced high efficiency fuel cell/turbine power plant", U.S. Patent No. 6,896,988, May 24, 2005.

FY 2005 Publications/Presentations

1. H. Ghezel-Ayagh, J. Walzak, D. Patel, J. Daly, H. Maru, R. Sanderson, and W. Livingood, "Status of Direct Fuel Cell/Turbine Systems Development", Fuel Cell Seminar 2004, San Antonio, Texas, November 1-5, 2005.
2. Direct Fuel Cell/Turbine Power Plant, Semi-Annual Technical Progress Report (November 1, 2004 through April 30, 2005), submitted to DOE by FCE, Contract No. DE-FC26-00NT40798.

IV.2 Solid Oxide Fuel Cell Hybrid System for Distributed Power Generation

Nguyen Minh (Primary Contact), Tom Logan
GE Hybrid Power Generation Systems
19310 Pacific Gateway Drive
Torrance, CA 90502-1031
Phone: (310) 538-7250; Fax: (310) 538-7250; E-mail: nguyen.minh@ge.com

DOE Project Manager: Don Collins
Phone: (304) 285-4156; E-mail: Donald.Collins@netl.doe.gov

Objectives

- Develop and demonstrate the feasibility of highly efficient hybrid systems integrating a planar solid oxide fuel cell (SOFC) and a gas turbine (GT).
- Identify and assess highly efficient coal power plant system configurations integrating a coal gasifier and gas clean-up train with a planar SOFC and bottoming cycle.
- Develop scale-up strategies for large SOFC-GT systems, and identify system architectures that minimize SOFC stack scale-up and technology development risks.

Approach

- Develop conceptual design for high-efficiency SOFC-GT hybrid systems based on the results of preliminary analysis and trade studies on a variety of system concepts. These trade studies are done for a variety of plant applications, sizes, and fuels, including 500-kW distributed power generation fueled with natural gas and 25-MW and 300-MW centralized power generation fueled with natural gas and coal. Evaluate the expected performance for these systems and establish the requirements of the SOFC subsystem.
- Fabricate and test laboratory-scale SOFCs to investigate their operating characteristics under hybrid conditions and identify key technical barriers.
- Assess SOFC stack technology, especially that currently under development in the SECA program, with a focus on critical near-term issues that must be resolved to demonstrate the feasibility to support the development of large hybrid systems and coal-based systems. Namely, demonstrate the potential of SOFC cell scalability for tape-calendered cells, operate SOFC stacks of increasing size under hybrid conditions, and assess the scalability of stack designs.
- Identify key technology gaps for SOFC-GT hybrid systems.

Accomplishments

Accomplishments in FY 2005 are summarized below.

- An scale-up effort for hybrid systems was completed. This study analyzed the performance and economics of power generation systems for centralized plants based on SOFC technology and fueled by natural gas. The main objective of this task was to develop credible scale-up strategies for large SOFC-GT systems. System concepts that integrate a SOFC with a gas turbine were developed and analyzed for plant sizes in excess of 20 MW. A 25-MW plant configuration was selected with projected system efficiency of over 65% and a factory cost of under $400/kW. The plant design is modular and can be scaled to both higher and lower plant power ratings. Technology gaps and required engineering development efforts were identified and evaluated.

- An integrated gasified fuel cell (IGFC) system efficiency improvement study indicated that the insertion of additional technologies such as ion transport membrane (ITM) and mid-temperature clean-up improved baseline system efficiency about 1%. The cost impact of using an ITM was about 5.4% reduction; the cost impact for using the mid-temperature clean-up was negligible. Reaching a feasible 60% system efficiency with CO_2 isolation will require significant improvements to the SOFC.
- Fabrication of large-area cells (up to 12.75" dia.) by tape calendering was demonstrated. Average fabrication yield of 70% was achieved. Literature review on theories indicates that though there are no obvious theoretical limitations, practical limitations may dictate the upper limit on cell sizes that can be made.
- Multi-cell stacks were built, tested, and evaluated under hybrid operating conditions. Stacks having 142 cm^2 active area per cell were tested at pressures up to 4 atmospheres to obtain performance maps. Large-area (12" dia.) cells and stacks were also assembled and operated. At 60 psia operation pressure, a 3-cell large-area stack achieved power density of 0.157 W/cm^2 at 75% fuel utilization (0.635 V at 0.245 A/cm^2) with simulated steam reformate.

Future Directions

- Stacks of increasing size (footprint and height) will be tested to demonstrate scalability.

Introduction

The overall objective of this project is to develop and demonstrate the feasibility of highly efficient SOFC-GT hybrid systems. The hybrid system concept has several attractive features: (i) efficiencies can be over 65% depending on system size, design, and operating conditions; (ii) the combination of planar SOFC and commercial gas turbine leads to low-cost solutions; (iii) the high efficiency will result in low greenhouse gas emissions; and (iv) the hybrid is a low-noise system that gives siting flexibility for distributed power generation. Many of these benefits stem from the integration of the SOFC stack with the gas turbine. The hybrid environment is distinguished from the simple cycle system by the pressurized operation of the SOFC, the general requirement for larger stacks and systems, and the fuel compositions entering the stack.

The work in this project focuses on defining and optimizing suitable system concepts for various size plants operating on different fuels, conducting experiments to resolve identified technical barriers, and demonstrating the scalability and operation of the SOFC in a hybrid environment.

Approach

System concepts and configurations are developed via a series of trade studies and performance and cost analyses. The feasibility of selected SOFC-GT hybrid systems is demonstrated through a comparison of the top-down requirements with the bottom-up estimates and technology demonstrations. This comparison results in identification of the technology gaps that must be addressed for commercialization. The top-down requirements are established through the conceptual design of the different plants, and the necessary operating requirements of the various subsystems, especially the SOFC stack subsystem, are defined to meet the performance needs of the plant. The bottom-up estimates represent the current technology capability. Several technology gaps identified through this process are then evaluated through laboratory testing and demonstrations.

Laboratory testing of the SOFC mainly concentrates on evaluating the effects of pressure on the performance and operating characteristics of the fuel cell. Due to the current development status of the SOFC stack technology, many of the SOFC tests are performed on test vehicles that are not optimized for hybrid systems. Such tests identify the design considerations that would be necessary to accomplish high-efficiency hybrid systems and, in many cases,

identify the approach by which to optimize the design.

Results

SOFC-GT System Scale-up

The study identified the requirements for a 20-MW central generation power plant based on the standards of competing GE products. The system is required to meet or exceed the factory cost goal of $400/kW and to target system efficiencies in the 55-75% (LHV) range. A large number of system and stack concepts for SOFC-GT hybrid systems were generated in the project. Four concepts were selected for conceptual analysis and analyzed for system efficiency, factory cost, and reliability. The analysis results were compared to the product specification, and a baseline concept was selected because it was projected to have the best chance of meeting the product requirements. A 25-MW plant design based on the downselected concept was completed, and its performance, factory cost and projected reliability were estimated. The design first focused on the SOFC stack subsystem architecture. The study determined that a 19.9-MW SOFC stack subsystem operating at 5 atm would be required for the 25-MW plant. The subsystem architecture included multiple stacks placed in pressurized modules.

An individual stack size was determined through cost and reliability studies while factoring in power electronics constraints. The study identified that the size of individual cells in a stack and the number of cells can be determined independently of each other. The cell size is found through a stack cost and reliability optimization. Given projections of the planar cell manufacturing technology capabilities, the stack cost was minimized in a wide range of cell diameters, 30-60 cm (12-24 inches) (Figure 1). Cost considerations favor large cell diameters and a smaller cell count; however, the cell reliability may decline rapidly with the cell diameter, thus placing a constraint on the cell size. The optimal stack voltage was determined through the optimization of the SOFC power conversion subsystem. Given the cell size and the number of cells per stack, the optimal stack building block for the 25-MW plant was estimated to have a nominal power rating of about 320 kW.

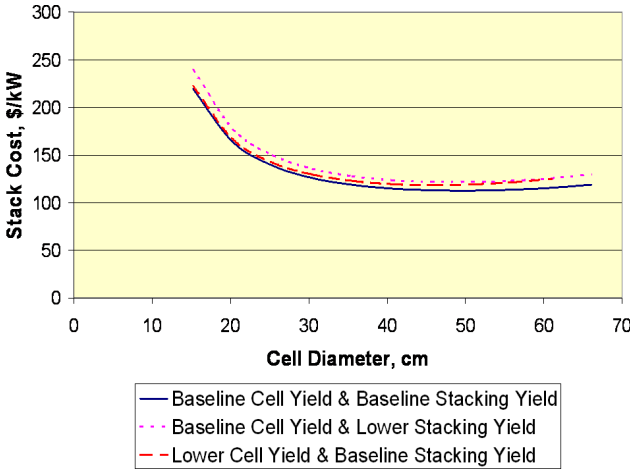

Figure 1. SOFC Stack Cost as a Function of Cell Diameter

Plant-level reliability analyses were performed on the 25-MW hybrid plant, including the selected plant architecture and the stack building block. The 25-MW plant factory cost and performance analyses were conducted next. The factory cost was determined to be about $317/kW, compared to the target of $400/kW. The calculated plant efficiency of 66% on natural gas also exceeds the product specification target of 65%. The 25-MW hybrid plant design developed in this study can be scaled to both higher and lower power levels using the same stack building block. Power plants of larger size can be built from the same pressurized modules used in the 25-MW plant design. A 250-MW hybrid plant was projected to have 67.6% plant efficiency and $260/kW plant factory cost. Both parameters exceed the 25-MW plant capabilities due to plant economies of scale. A 5-MW hybrid plant can use the same 320-kW stack building blocks as the 25-MW hybrid plant; however, the stacks would have to be arranged in smaller pressurized modules. The 5-MW hybrid plant efficiency and cost were projected to be 65.1% and $512/kW, respectively.

IGFC System Efficiency Improvement Study

The IGFC system design as created in the early IGFC study was used as a baseline to evaluate potential areas for system efficiency improvements, with the objective of achieving a feasible system with 60% system efficiency (AC power/coal HHV) including carbon dioxide isolation. The impact of ion transport membrane (ITM) technology on the

system efficiency and cost was evaluated. Four system configurations incorporating the ITM technology were reviewed. The concept chosen utilized the cathode exhaust air to create oxygen for the anode gas combustor and the gasifier. The amount of air required for the ITM to generate the anode O_2 is still in excess; hence, air is by-passed around the ITM. The system efficiency estimate for the baseline with the ITM inserted is 53.5%, which represents a 0.7% efficiency improvement compared with the baseline IGFC system. The insertion of ITM reduces the system cost by circa 5% compared to the baseline system cost.

Performance and cost estimates of mid-range gas clean-up of sulfur compounds from the syngas were evaluated. Mid-range refers to the operating temperature of the clean-up process, approximately 500 to 800°F; for this technology, an operating temperature of 600°F could be considered mid-range, or warm gas clean-up compared to low-temperature (~100°F) and high-temperature (~1000°F) clean-up technologies. The analysis indicated an improvement of only 0.2%, which is considered insignificant. Processing all the trace compounds, including the tars formed from the gasifier, could result in a negative performance impact. Costs were estimated to be in the order of $60-$75 per kW of net system power produced. This is comparable with other typical gas clean-up processes. It is judged that the cost impact, assuming the performance estimated above, is within the fidelity of the rough order of magnitude-type estimate and has a negligible effect for this study.

The baseline IGFC system configuration was selected to further analyze what would be required to achieve 60% system efficiency and yet be technically feasible. By changing the following operational parameters, the system efficiency could be improved further:

- SOFC extreme operating conditions: pressure, temperature, temperature rise, cell voltage and fuel utilization
- Gasifier methane yield
- Inverter efficiency

Since the SOFC is the largest generator, a significant improvement to its performance is a likely candidate to increase efficiency. Reaching a feasible 60% system efficiency with CO_2 isolation will require significant improvements to the SOFC; even with 'extreme SOFC' operating conditions, other constraints could limit the performance estimate to mid to high 50% efficiency.

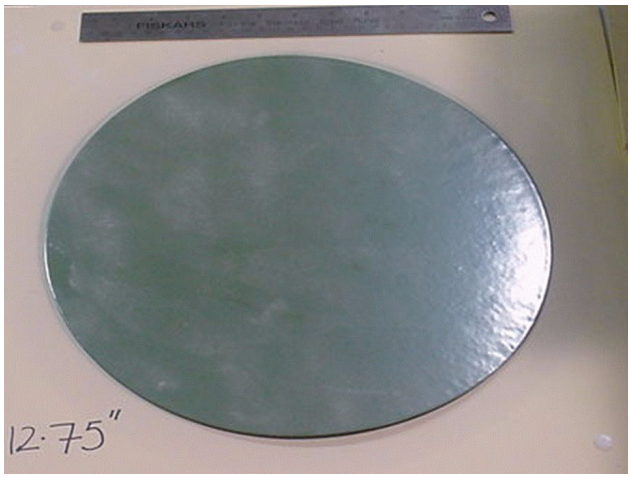

Figure 2. Large-Area Cell (12.74" Diameter)

Cell Scalability

The objective of this effort was to demonstrate cell area scale-up based on the tape calendering method. Both theoretical analysis and experimental work were conducted. The theoretical analysis involved a literature search to determine fundamental limitations, if any, on the size that can be sintered. Experimental work as well as theoretical studies was performed to identify the key process parameters that affect cell scalability. These key factors were optimized to demonstrate process scale-up to large-area cells (>10" diameter). In this effort, fabrication of bilayers >12" by tape calendering was demonstrated (Figure 2). More than 50 large bilayer tapes were produced and fired. The average firing yield on the critical bilayer firing step was 70%. Several steps in the fabrication process were modified to reduce/minimize defects. This resulted in an improvement in post-firing yields during bilayer cleaning and cathode application to about 80%.

A literature review on theoretical models to understand fundamental limitations on the maximum sizes that can be made using the tape calendering

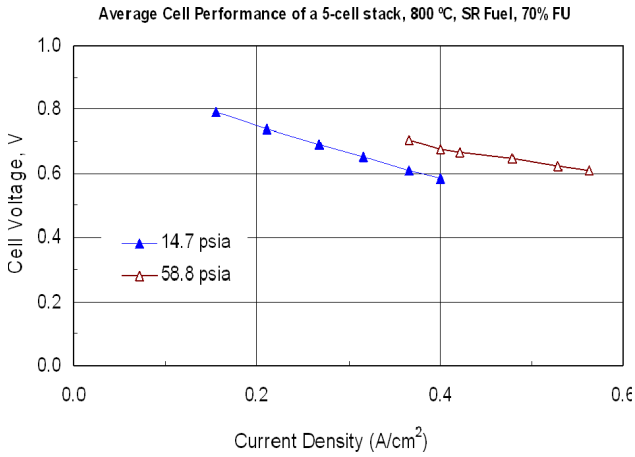

Figure 3. Performance of 5-Cell Stack (6.3" Diameter) as a Function of Operating Pressure at 800°C with Simulated Steam Reforming (SR) Fuel, 70% Fuel Utilization (FU)

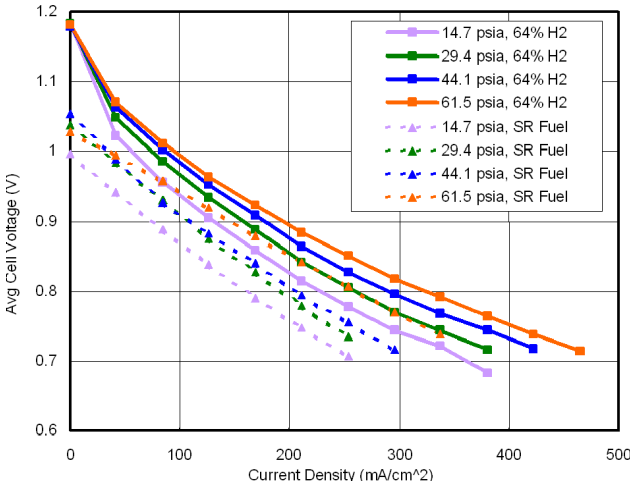

Figure 4. Performance of 3-Cell Stack (12" Diameter) as a Function of Operation Pressure with 37% H_2-Balance N_2 at 800°C

process was completed. During the course of review, it became clear that theoretical limitations on cell size couldn't be predicted using available binder burnout and sintering models. Current models need to be modified to take into account the effects of external forces (thermal, gravity, frictional, etc.). Though there are no obvious theoretical limitations, practical limitations—e.g., thermal gradients, uniform binder removal, friction between tape and setter plates, and warpage of setter plates—may dictate the upper limit on cells sizes that can be made.

Stack Hybridization

A number of single-cell modules and multi-cell stacks of various sizes were fabricated and tested to demonstrate operation under hybrid conditions. Figure 3 shows as an example the performance of a 5-cell stack having 142 cm^2 active area per cell tested at pressures up to 4 atmospheres on simulated steam reformate. The stack achieved a power density of 0.271 W/cm^2 (average cell voltage 0.677 V at 0.4 A/cm^2) with simulated steam reforming fuel and 70% fuel utilization at 4 atm. This stack showed about 16% performance improvement when the operating pressure increased from ambient to 4 atm. Performance maps of SOFC stacks as a function of pressure, temperature, and fuel composition were also obtained.

Cells and stacks of large footprint area (12" diameter) were also tested. The power density of a 12.5" single-cell module running on fixed flow with 64% H_2 fuel at 61.5 psia, for example, was about 250 mW/cm^2 at 800°C. Performance of a 12" 3-cell stack running on fixed flow with 37% H_2 fuel stream is shown in Figure 4 at different pressurization levels. The peak power density at ambient pressure (14.7 psia) was measured to be 213 mW/cm^2, and it reached 290 mW/cm^2 at 61.5 psia. From ambient pressure condition, the power density at similar operation conditions (36.4% fuel utilization and 0.342 A/cm^2) is calculated to increase about 4% at 30 psia, 10% at 45 psia and 19% at 60 psia. At 60 psia, the stack achieved total power of 532 W (0.592 V at 0.489 A/cm^2, power density of 0.290 W/cm^2) at 52% fuel utilization with 37% H_2 fuel stream. At 60 psia operation pressure and 75% fuel utilization, the stack achieved power density of 0.157 W/cm^2 (0.635 V at 0.245 A/cm^2) with simulated steam reformate.

Two smaller cells (4-3/8" diameter) were laser cut from different areas on a 12.75" bilayer. The cells were tested on diluted hydrogen fuel stream, and the performance of both tested cells was measured to be similar to the performance of standard baseline cells under similar testing conditions and test fixture.

Conclusions

- A 25-MW plant configuration based on the SOFC-GT concept operating on natural gas was projected to have a system efficiency of over 65% and a factory cost of under $400/kW. The plant design is modular and can be scaled to both higher and lower plant power ratings.
- An IGFC system efficiency improvement study indicates that the insertion of additional technologies such as ITM and mid-temperature clean-up improves baseline system efficiency about 1%. Reaching a feasible 60% system efficiency with CO_2 isolation will require significant improvements to the SOFC.
- Fabrication of large-area cells up to 12.75'' diameter by tape calendering was demonstrated. Literature review on theories indicates that though there are no obvious theoretical limitations, practical limitations may dictate the upper limit on cells sizes that can be made.
- Operation under hybrid conditions was demonstrated for cells and stacks of various sizes.

FY 2005 Publications/Presentations

1. N. Minh, "Solid Oxide Fuel Cell Technology Development Status", 2004 Fuel Cell Seminar Extended Abstracts, Courtesy Associates, Washington, DC, 2004.
2. N. Q. Minh, "Solid Oxide Fuel Cell Systems for Stationary Power Generation Applications", in SOFC IX, Electrochemical Society, Pennington, NJ, 2005, p. 76.

IV.3 The Hybrid Performance Project (Hyper)

David Tucker, Ph.D.
U.S. Department of Energy
National Energy Technology Laboratory
Office of Science, Technology and Analysis
Energy System Dynamics Division
3610 Collins Ferry Rd.
Morgantown, WV 26507-0880
Phone: (304) 285-1331; E-mail: dtucker@netl.doe.gov

Objectives

- Identify issues associated with the integration of high-temperature fuel cells and gas turbine cycles, and improve overall understanding of system limits and dynamic operability.
- Establish a viable control strategy for start-up of a fuel cell gas turbine hybrid power system.
- Propose control strategies for fuel cell gas turbine hybrids that minimize system impact and maximize system efficiency, and characterize the limits of operation for these strategies.
- Embed a fuel cell model that operates in real time into the control platform of the Hyper facility for hardware-in-the-loop simulation.

Approach

- Test the use of compressor bleed as a means to increase surge margin and decrease cathode air flow during startup.
- Test the use of cold air by-pass during startup and compare to the compressor bleed case for efficacy.
- Evaluate the impact of ramp rate of system startup on compressor surge margin.
- Evaluate the limits of operation for both bleed air and cold air by-pass as methods for managing air flow and energy during transient operation.
- Reduce a higher-order solid oxide fuel cell model to lumped parameter for operation in real time on the Atlas controller.
- Make use of expertise from Woodward Industrial Controls to accomplish the integration of the fuel cell numerical simulation with the Hyper facility hardware.

Accomplishments

- The use of compressor bleed was found to be an effective means of mitigating compressor surge and stall during startup. The maximum air flow diverted from the fuel cell cathode was equal to 18.5% of the compressor inlet flow.
- The results of the experiments using compressor bleed as a means of controlling system startup were presented at the ASME Turbo Expo in June of this year and were published in the proceedings.
- The use of cold air by-pass was also found to be an effective means of increasing surge margin during system startup. The maximum air flow diverted from the fuel cell cathode was equal to 50.2% of the compressor inlet flow.
- The use of cold air by-pass during startup resulted in significantly reduced fuel requirements and turbine inlet temperatures. Maximum fuel flows during startup using cold air by-pass were 22.8 g/s, while an equivalent compressor bleed required 32.4 g/s. A similar improvement was seen in maximum turbine inlet temperatures, 753ºC for cold air by-pass and 1045ºC for the use of compressor bleed. The results indicate

that cold air by-pass in a hybrid system is superior to compressor bleed in minimizing impact to both the fuel cell and turbine in the hybrid system.

- Experiments to parametrically vary the turbine acceleration ramp rate during startup are currently underway. Preliminary results indicate that the turbine acceleration ramp rate in a hybrid system is far more critical than in a simple cycle turbine.
- The steady-state limits of operation were evaluated for both compressor bleed and cold air by-pass. Cold air by-pass was found to have a greater range of operability, since the valve could be opened to 100%. Compressor bleed was limited by turbine exhaust gas temperature limits to 22.9% of compressor inlet flow, while 61.7% of the compressor inlet flow could be by-passed using cold air by-pass. Similarly, while no appreciable change in system pressure drop was observed for any use of compressor bleed, the total system pressure drop was reduced from 13.6% to 4.2% using cold air by-pass. The two control methods were shown to be complimentary. The results of these experiments were presented at the ASME Power conference in April of this year and published in the proceedings.
- A real-time fuel cell model has been developed and tested. It was successfully integrated into the Hyper facility control platform. The facility now has the capability of simulating fuel cell transients and evaluating fuel cell impact during transient operation of the system using a hardware-in-the-loop approach.
- System testing revealed considerable issues with regard to the manifolding of parallel heat exchangers. These issues are expected to translate to the manifolding of parallel fuel cell stacks.

Future Directions

- Fuel cell transients will be evaluated for both open and closed loop scenarios.
- The use of hot air by-pass as a control strategy will be evaluated and compared to compressor bleed and cold air by-pass.
- The application of the control strategies developed in previous studies to load transients will be evaluated.
- Numerical and hardware simulations will be conducted to quantify the magnitude of flow imbalance in the heat exchangers in the Hyper facility. The work will lead to the development of control strategies for balancing flow in parallel fuel cell systems in a pressurized environment.

Introduction

Hybrid fuel cell turbine power systems have been identified by the U.S. Department of Energy's National Energy Technology Laboratory (NETL) as a key technology in reaching high efficiencies and low emissions in future power generation [1]. The Hybrid Performance Project (Hyper) facility has been commissioned by the Office of Science, Technology, and Analysis at NETL to examine fundamental issues related to the dynamic operability of fuel cell gas turbine hybrid systems. The facility is made available for public research collaboration with universities, industry and other research institutions. The Hyper project research objectives have been described in some detail previously, but begin with the simulation of a direct-fired solid oxide fuel cell (SOFC) gas turbine (GT) hybrid system using a hardware-in-the-loop approach [2]. The experimental facility at NETL makes use of a natural gas burner controlled by a real-time fuel cell model to simulate the thermal output of a solid oxide fuel cell. Pressure vessels, used for simulating the cathode and post combustion volumes, and exhaust gas recuperators are integrated into the system with a modified turbine and compressor on a single shaft.

The potential of SOFC/GT hybrids has led to the evaluation of a project utilizing a recuperated cycle developed under the U.S. DOE Advanced Turbine Program in an SOFC hybrid [3]. Experimental efforts in pressurized, direct-fired SOFC/GT hybrids have provided insight to steady-state operation and efficiency [4]. However, dynamic performance evaluation of fuel cell turbine hybrids has been limited to numerical computer simulation [5-8]. While these studies have provided considerable insight into the dynamic nature of fuel cell turbine

hybrids, the addition of hardware into the simulation presents an opportunity to both validate model predictions and discover anomalies in dynamic system behavior that can not be adequately predicted by a computer model alone.

Approach

A compressor surge or stall could be catastrophic to the fuel cell in a hybrid system. The approach taken to study system startup was to parametrically vary the amount of bleed air or cold air by-pass used during a cold start, and compare the ramp data to the stall line of the compressor map. The results can be graphically compared to evaluate the impact of compressor bleed air flow on total surge margin during startup. A simplified process flow diagram is shown in Figure 1, and a picture of the facility is shown in Figure 2.

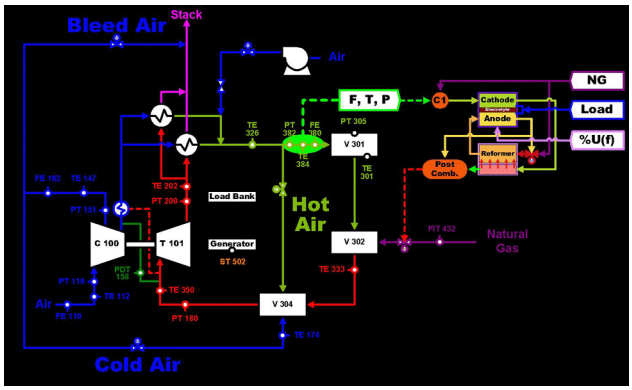

Figure 1. Simplified Flow Diagram for the Hybrid Simulation Facility at NETL

Figure 2. The Hybrid Performance Project Facility at NETL

The objective of the steady-state study was to identify potential methods for use in control strategies to regulate cathode air flow, absorb thermal transients, and mitigate risk of compressor stall and surge during operational transients. The change in system performance due to a change in by-pass flow was characterized in terms of the change in system air pressure drop and flow (air flow work) and change in input fuel flow rate. In order to separate various coupled phenomena, the work assumed a fixed fuel cell operation in spite of any change in cathode flow, and employed a fixed gas turbine generator output of no electrical load.

Results

A comparison is made in Figure 3 for the use of cold air by-pass and compressor bleed as strategies for managing air flow in a hybrid system. The data presented is the fuel required to divert air flow from the cathode, expressed in terms of percent of the fuel required for the case without any by-passed flow. Compressor bleed air is shown to have a much greater specific energy requirement, while cold air by-pass is shown to have an insignificant specific energy requirement over the same operable range of by-passed flow.

The huge increase in energy requirement shown for the case of compressor bleed indicates that it would be an effective means of absorbing a thermal transient impacting the turbine in the system. The data for the cold air by-pass shows that it would be

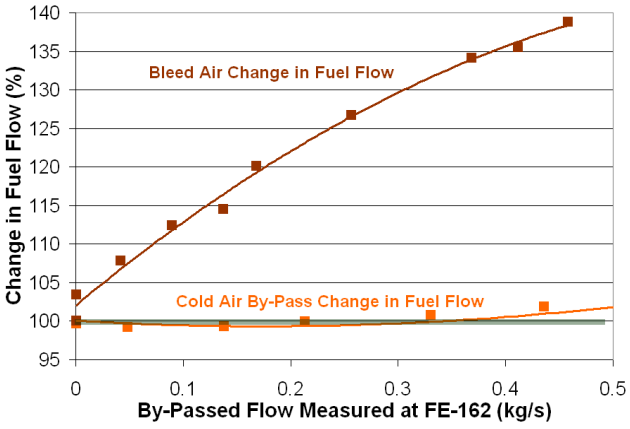

Figure 3. A Comparison of Percent Change in Fuel Required for Constant Turbine Speed as a Function of Air Flow Bled or By-Passed

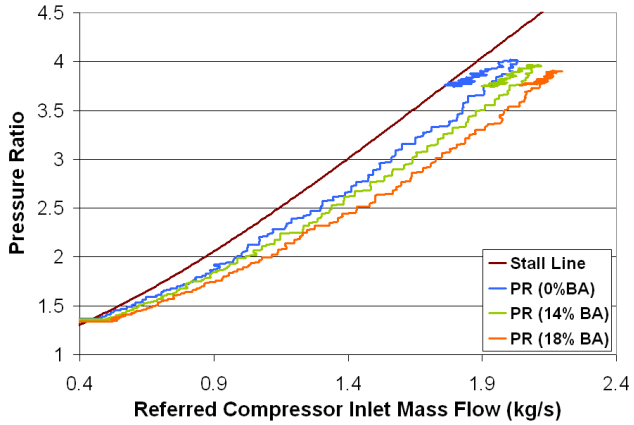

Figure 4. A Comparison of Startup Profiles for Three Bleed Air Cases to the Compressor Map Stall Line

an effective means of controlling cathode air flow without a significant penalty in system efficiency.

The studies performed using bleed air to increase compressor surge margin during startup are summarized for three different bleed air flow cases in Figure 4. The data are plotted with the stall line from the manufacturer's compressor map. The three cases plotted in the figure are 1) a valve setting of 0%, representing a case without compressor bleed; 2) a valve setting of 14%, representing a case with compressor bleed equivalent to 10.5% of the compressor inlet flow; and 3) a valve setting of 18%, representing a case with compressor bleed equivalent to 18.5% of the compressor inlet flow. The results can be used to illustrate how increasing compressor bleed air flow provides an increase in the operating surge margin during the startup.

Similar results were shown for the case of cold air by-pass, but with far less impact to the system. Turbine inlet temperatures were lower. System pressure drops were significantly decreased, and fuel requirements were substantially lower.

Conclusions

- Tests were conducted using the Hyper experimental facility at NETL to characterize the implementation of compressor bleed air and cold air by-pass as methods for manipulating hybrid system process variables through air flow management.
- For by-passed flows representing less than 25% of compressor inlet flow, cold air by-pass operation did not require any significant increase in energy.
- The cold air by-pass was also shown to be an effective method to increase the operating surge margin and avoid compressor stall.
- The use of compressor bleed air was found to be an effective method for increasing shaft load and absorbing thermal transients with reduced by-pass flow. This indicates potential for system control during fuel cell load loss or reduction.
- Compressor bleed air was also shown to be an effective means to increase the compressor surge margin. The method was limited because by-passed flows beyond 22% of compressor inlet air could not be sustained without exceeding the exhaust gas temperature (EGT) constraint.
- The data presented provide the first qualitative steps in characterizing possible control methods for hybrid fuel cell gas turbine power systems using compressed air flow management with valves only in cold-service side streams.
- The use of compressor bleed air and cold air by-pass simultaneously offer the potential for system control through a variety of transient scenarios.
- The methods studies show promise for effective control of a hybrid system without the direct intervention of isolation valves or check valves in the main pressure loop of the system, which introduce substantial pressure losses. The elimination of such measures for protection and control during transient operation would allow for the full potential efficiency of the hybrid system to be realized.
- Tests were conducted using the Hyper experimental facility at NETL to evaluate the use of compressor bleed air as a control strategy to avoid stall and surge during the initial startup of a solid oxide fuel cell turbine hybrid power system.
- The use of bleed air during startup was shown to be effective in increasing compressor mass flow and avoiding stall and surge during startup, and a base condition was established for future tests of other control strategies.

- The use of cold air by-pass during startup was shown to be effective in increasing compressor mass flow and avoiding stall and surge during startup with a significant reduction in system impact over compressor bleed.
- A real-time fuel cell model was successfully integrated into the control platform of the Hyper facility.

FY 2005 Publications/Presentations

1. Tucker, D.; Lawson, L. O.; Gemmen, R. S., "Evaluation of Hybrid Fuel Cell Turbine System Startup with Compressor Bleed," 2005 ASME Turbo Expo, GT2005-68784.
2. Tucker, D.; Lawson, L. O.; Gemmen, R. S., "Characterization of Air Flow Management and Control in a Fuel Cell Turbine Hybrid," Proceedings of the ASME Power Conference, April 2005, PWR2005-50127.

References

1 Dennis, R. A.; Samuelsen, G. S.; Williams, M. C.; Holcombe, N. T.; Layne, A. W., "The National Energy Technology Laboratory's Hybrid Power Systems Program," 2002 ASME Turbo Expo, Amsterdam, The Netherlands (GT-2002-30668).

2 Tucker, D.; Liese, E.; VanOsdol, J. G.; Lawson, L. O.; Gemmen, R. S., "Fuel Cell Gas Turbine Hybrid Simulation Facility Design," 2003 ASME International Mechanical Engineering Congress and Exposition, New Orleans, LA.

3 Kundberg, W. L.; Veyo, S. E.; Moeckel, M. D., "A High-Efficiency Solid Oxide Fuel Cell Hybrid Power System Using the Mercury 50 Advanced Turbine Systems Gas Turbine," *Journal of Engineering for Gas Turbines and Power, Transactions of the ASME,* Vol. 125, January 2003, pp. 51-66.

4 Veyo, S. E.; Lundburg, W. L.; Vora, S. D.; Litzinger, K. P., "Tubular SOFC Hybrid Power System Status," Proceedings of the ASME Turbo Expo 2003, June 2003, GT2003-38943.

5 Costamagna, P.; Magistri, L.; Massardo, A. F., "Design and Part-Load Performance of a Hybrid System Based on a Solid Oxide Fuel Cell Reactor and a Micro Gas Turbine," *Journal of Power Sources,* Vol. 96, (2001), pp. 352-368.

6 Campanari, S., "Full Load and Part-Load Performance Prediction for Integrated SOFC and Microturbine Systems," *Journal of Engineering for Gas Turbines and Power, Transactions of the ASME,* Vol. 122, April 2000, pp. 239-246.

7 Palsson, J.; Selimovic, A., "Design and Off-Design Predictions of a Combined SOFC and Gas Turbine System," Proceedings of the ASME Turbo Expo 2001, June 2001, 2001-GT-0379.

8 Crosa, G.; Fantini, L.; Farrari, G.; Pizzimenti, L.; Trucco, A., "Steady-State and Dynamic Performance Prediction of an Indirect Fired Gas Turbine Plant," Proceedings of the International Gas Turbine & Aeroengine Congress and Exhibition, June 1998, 98-GT-167.

V Advanced Research

V Advanced Research

V.1 Enhanced Power Stability for Proton-Conducting Solid Oxide Fuel Cells

Boris Merinov, Adri van Duin, Sossina Haile, and William Goddard III (Primary Contact)
California Institute of Technology
1200 East California Blvd.
Pasadena, CA 91125
Phone: (626) 395-2731; Fax: (626) 585-0918; E-mail: wag@wag.caltech.edu

DOE Project Manager: Lane Wilson
Phone: (304) 285-1336; E-mail: Lane.Wilson@netl.doe.gov

Objectives

- Develop modified electrolytes that exhibit both high proton conductivity and excellent chemical and mechanical stability. Doped $BaZrO_3$ has been selected as a basic material for further modifications.
- Develop a fundamental understanding of the mechanisms and barriers of proton transport in a proton ceramic fuel cell (PCFC).
- Develop highly efficient electrocatalysts for the anodes and cathodes of PCFCs based on the above-mentioned relatively new electrolytes.
- Develop rapid synthesis methodologies for both candidate electrolytes and candidate electrodes (or electrocatalysts).

Approach

- Perform quantum mechanical (QM) cluster and periodic calculations on relevant metals, metal oxides, and pure and Y-doped $BaZrO_3$ (BYZ).
- Determine equilibrium positions for hydrogen atoms in BYZ.
- Calculate transition barriers for hydrogen migration in doped BYZ.
- Develop ReaxFF Reactive Force Fields based on QM calculations for relevant materials.
- Perform ReaxFF molecular dynamics (MD) simulations on large systems to investigate physico-chemical processes in the electrolyte and electrode/electrolyte interfaces.
- Synthesize and characterize dense BYZ ceramics with desired grain size.
- Screen potential electrode materials (transition metal perovskites) and anode electrocatalysts (metals) for reactivity with BYZ.
- Fabricate complete membrane/electrode assembly (MEA) and establish baseline fuel cell performance.

Accomplishments

- *Calculated Energy Barriers for the Hydrogen Diffusion in BYZ*
  A series of QM calculations on clusters and BYZ periodic structures have been performed, and energy barriers for the hydrogen diffusion have been calculated. The activation energy for the intra-octahedron hydrogen transfer is found to be equal to 0.48 eV, while that for the inter-octahedra hydrogen transfer is 0.41 eV, which are in very good agreement with the experimental value, 0.44 eV. According to our calculations, both the inter-octahedra and intra-octahedron hydrogen transfers are possibly observed in the BYZ electrolyte.

- *Studied $BaZrO_3$ Surfaces*
  Electronic and atomic structures of different terminations of the (001) non-polar orientation of $BaZrO_3$ surfaces have been studied using first-principles calculations to determine surface structures, properties, and reactions. We found that surface energies at both possible (BaO and ZrO_2) surface terminations are very close. The (001)-BaO and (001)-ZrO_2 terminated surfaces have bandgap values smaller than the bulk crystal.
- *Developed ReaxFF for Modeling of Hydrogen Diffusion and Surface Reactions*
  Reactive force fields have been developed and successfully applied for MD simulation of the bulk hydrogen diffusion in the BYZ electrolyte. Initial ReaxFF potentials have been developed for further modeling of surface reactions and grain boundaries. This modeling might help us to find a way to modify the grain boundaries and improve overall conduction properties of the BYZ electrolyte.
- *Developed ReaxFF for Ni*
  Ni is commonly used as the anode material in solid oxide fuel cells. A series of QM calculations has been performed on Ni surfaces, Ni clusters, Ni bulk metal and oxides. The results of these calculations were used for developing ReaxFF potentials for Ni. The ReaxFF can describe H- and O-binding to both Ni surfaces and Ni clusters and reproduce the QM data.
- *Identified $BaZr_{0.40}Pr_{0.40}Gd_{0.20}O_3$ and $BaZr_{0.60}Y_{0.20}Co_{0.20}O_3$ as Most Promising Cathode Materials*
  Several potential cathode materials for the BYZ system have been synthesized and characterized. Of the five potential cathode materials examined, $BaZr_{0.40}Pr_{0.40}Gd_{0.20}O_3$ and $BaZr_{0.60}Y_{0.20}Co_{0.20}O_3$ appear to be the most promising for further applications in proton ceramic fuel cells.
- *Screened Anode Electrocatalysts*
  Potential anode electrocatalysts (metals) have been screened for reactivity with BYZ, fabrication compatibility, and chemical stability in fuel cell environment. It was found that NiO easily diffused into the BYZ layer during sintering. Bi-layer and tri-layer BYZ systems with varying porosity were developed.
- *BaO in the Atmosphere is Essential for High Proton Conductivity*
  Reproducibility and ease of barium zirconate fabrication have been improved. It was established that barium oxide loss during processing can result in dramatic reduction in conductivity; thus, excess BaO in the atmosphere is essential for obtaining high proton conductivity samples.
- *Demonstrated Pt | BYZ | Pt Fuel Cell*
  A Pt | BYZ | Pt fuel cell with a 100 μm thick BYZ electrolyte layer has been demonstrated. The peak power density and short circuit current density were 28 mW/cm^2 and 130 mA/cm^2, respectively. These are the highest values for this type of fuel cell in the literature.
- *Majority of Overpotential is at the Anode*
  Preliminary results indicated that the majority of overpotential is at the *anode* rather than the cathode. That is, Pt | electrolyte | Pt symmetric cells showed ~0.5 ohm resistance at the electrodes when operated under oxygen, whereas they showed ~6.7 ohm resistance under hydrogen.

Future Directions

- *Complete the ReaxFF development for PCFC*
  We will complete development of the ReaxFF for modeling of the complex physico-chemical processes in the BYZ electrolyte, electrodes, and electrode/electrolyte interface regions that are critical to device performance. This includes using the ReaxFF to describe more complex processes involved with experimental measurements and testing key structures and reaction steps found from ReaxFF by additional QM calculations.
- *Continue characterization of complete MEAs*
  The baseline performance data of fuel cells are based on using Pt as the electrocatalyst at both electrodes. We will fabricate complete cells using Ni as the anode electrocatalyst and selected mixed conducting

oxides as the cathode. We emphasize that, because of the reactivity of NiO with BYZ, it is not possible to utilize conventional anode fabrication procedures in which a composite of nickel oxide and the electrolyte serves as a precursor to the anode cermet. Instead, we will fabricate structures in which a thin electrolyte is supported onto a thick porous electrolyte structure and subsequently introduce the Ni via solution impregnation methods.

Introduction

At present, only electrolytes based on BYZ combine high bulk proton conductivity with almost perfect chemical and mechanical stability. This material is the best ionic conductor among solid oxide electrolytes. BYZ belongs to the family of cubic perovskite-type oxides. The cubic symmetry is essential for the high solubility limit of protonic defects and for the high isotropic proton mobility. Unfortunately, the conductivity of BYZ ceramic samples, which is usually used in solid oxide fuel cells, is significantly lower than the bulk conductivity. BYZ ceramics contain extended grain boundary regions, which separate highly conducting grains and which have high resistance for proton transport.

This problem might be solved either by increasing the proton conductivity of the grain boundaries or by decreasing the volume of the grain boundary regions and improving contacts between high-conducting grains. We believe that focused experimental synthesis and characterizations tightly connected with the theoretical efforts are a promising approach to make progress in this area.

Approach

A series of QM calculations based on density functional theory (DFT) has been performed on clusters and BYZ periodic structures, Ni surfaces, Ni clusters, Ni bulk metal and oxides. All *ab initio* cluster calculations were carried out using the Jaguar programs [1]. We used the nonlocal B3LYP generalized gradient approximation (GGA)-functional for the exchange-correlation term.

Periodic QM calculations were performed using the SeqQuest code [2], a Gaussian-based linear combination of atomic orbitals method being developed jointly between Sandia National Laboratories (Dr. Peter Schultz) and Caltech. Pseudopotentials were employed to replace the core electrons. The basis sets were high-quality, optimized "double zeta plus polarization" contracted Gaussian functions.

The obtained QM data were then used to develop ReaxFF potentials for BYZ and Ni for further ReaxFF MD simulations of physico-chemical processes in the BYZ electrolyte and at electrode/ electrolyte interfaces.

Several potential cathode (transition metal perovskites) and anode (metals) materials for the BYZ system have been synthesized and characterized (x-ray diffraction, scanning electron microscopy, impedance spectroscopy). The most promising candidates for further applications in PCFCs were found.

Two cathode deposition techniques based on colloidal methods were pursued for the fabrication of electrolyte-supported fuel cells. The method in which the colloidal solution is deposited by spraying provides better contact between the cathode and the BYZ electrolyte.

A robust method for fabricating crack-free thin membranes, as well as methods for sealing anode and cathode chambers, have successfully been developed.

Results

Theory

It is expected that the energy barrier for proton transfer significantly contributes to the activation energy. In previous work [3], the value of 0.83 eV was calculated for the activation energy for the proton diffusion in BYZ, while the experimental value is 0.44 eV [4]. The noticeable difference in the values for the calculated and experimental activation energies required further computational work to better describe the proton diffusion energetics in BYZ. We have carried out a series of QM

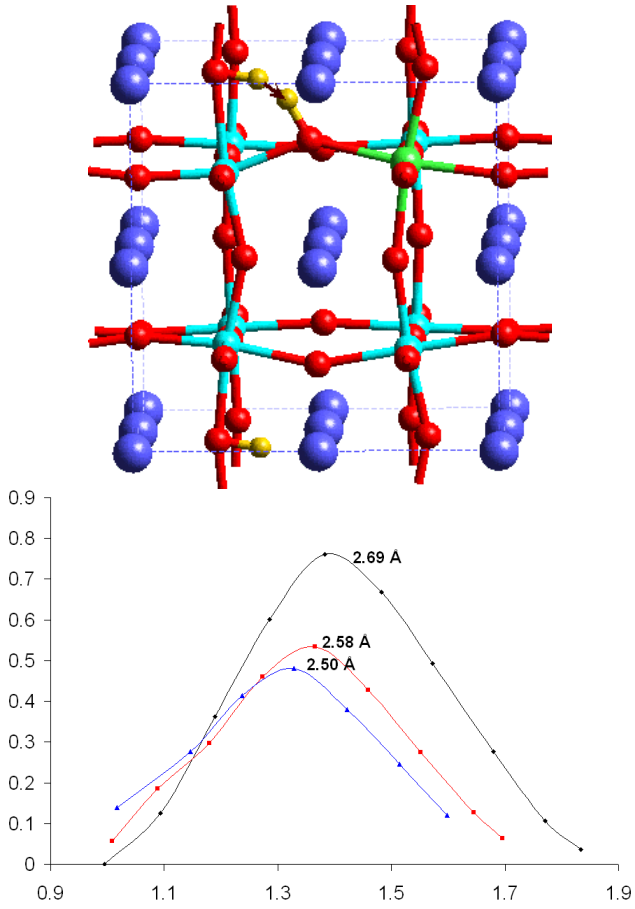

Figure 1. Intra-Octahedron Hydrogen Transfer in BYZ; (top) BYZ Structure (Ba – dark blue, Zr- blue, Y- green, O – red , and H – yellow balls, respectively); (bottom) Energy Barrier for Intra-Octahedron Hydrogen Transfer

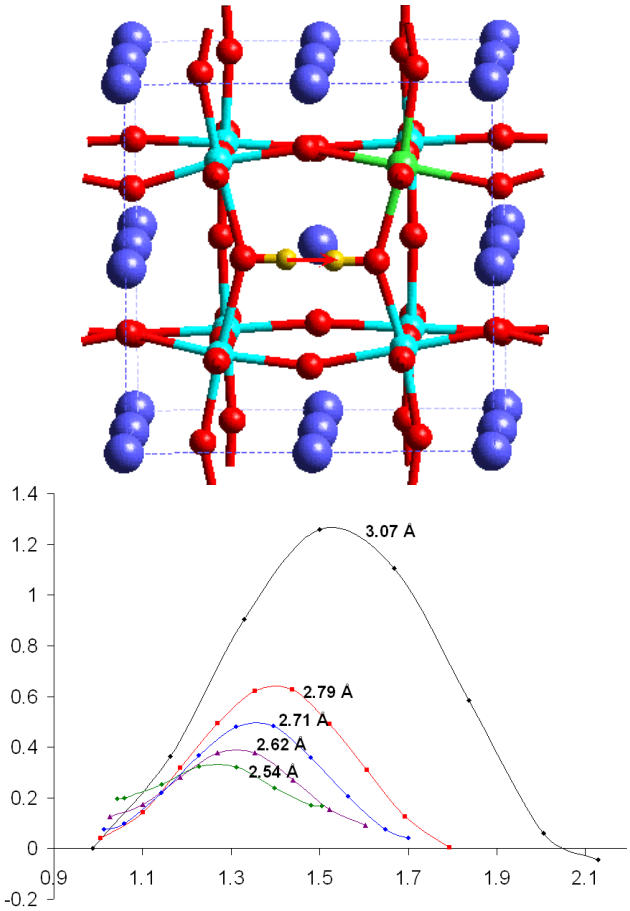

Figure 2. Inter-Octahedra Hydrogen Transfer in BYZ; (top) BYZ Structure (same notations as in Figure1); (bottom) Energy Barrier for Inter-Octahedra Hydrogen Transfer

calculations on BYZ periodic structures to find pathways and energy barriers for the proton diffusion. We started off by investigating the energy barrier for the intra-octahedron proton transfer on the edge of the distorted ZrO_6-octahedron. It turned out that the barrier significantly depends on the length of the O – O edge (Figure 1), and at 2.50 Å the activation energy for the intra-octahedron hydrogen transfer is approximately 0.48 eV.

Another possible proton pathway lies outside of the BO_6 octahedra, and hydrogen bonding occurs between oxygen atoms of the neighboring BO_6 octahedra. In this case, the proton transfer is inter-octahedra. We optimized the BYZ structure with hydrogen between two neighboring ZrO_6 octahedra and found the OH – O separation distance to be equal to 3.07 Å. For this distance, the calculated energy barrier for the inter-octahedra hydrogen transfer is 1.33 eV, which is significantly higher than the barrier for the intra-octahedron proton transfer. However, when we decreased the OH – O distance to 2.79 Å, the energy barrier dropped to 0.62 eV, while the energy of the overall BYZ structure increased only by 0.04 eV. Further shortening the OH – O distance (2.54 Å) leads to the value of 0.41 eV for the calculated activation energy (Figure 2). Therefore, most probably both the intra-octahedron and inter-octahedra proton transfers occur in the BYZ electrolyte.

In fuel cells, electrolytes are in contact with catalysts and electrodes, forming MEAs. The electrolyte-electrode interfaces are the primary source for power loss at small currents. Therefore, it

is very important to develop computational tools for modeling interfaces. We started this work from the anode side. The primary function of the anode in a PCFC is to facilitate the half cell reaction, ½ $H_2 \rightarrow H^+$ and e- [assuming H_2 as the fuel]. Ni has been particularly successful as the anode material for conventional solid oxide fuel cells. We carried out a series of QM calculations on Ni and used the obtained results for developing ReaxFF potentials. At present, the ReaxFF can describe H- and O-binding to both Ni surfaces and Ni clusters and reproduce the QM data. To complete the ReaxFF parameterization, we need more Ni cases, including QM calculations on various periodic structures. This work is in progress.

Experimental

Several potential cathode materials – $BaZr_{0.40}Pr_{0.40}Gd_{0.20}O_3$, $BaZr_{0.70}Pr_{0.10}Gd_{0.20}O_3$, $BaZr_{0.80}Co_{0.20}O_3$, $BaZr_{0.60}Y_{0.20}Co_{0.20}O_3$, $BaPr_{0.85}Y_{0.15}O_3$, $BaZr_{0.50}Pr_{0.30}Y_{0.20}O_3$, $BaZr_{0.60}Pr_{0.20}Y_{0.20}O_3$, $BaZr_{0.70}Pr_{0.10}Y_{0.20}O_3$ – for the BYZ system were synthesized via the glycine nitrate combustion method. All formed single-phase perovskites, as determined by X-ray power diffraction. The Pr-rich compound, $BaPr_{0.85}Y_{0.15}O_3$, however, proved to be unstable with time and at high temperature and was not considered further.

Potential cathodes were mixed with BYZ and calcined at 700°C (maximum fuel cell operating temperature) for 24 hours to observe the possibility of a reaction/interdiffusion. Under these conditions, $BaZr_{0.70}Pr_{0.10}Gd_{0.20}O_3$ and $BaZr_{0.80}Co_{0.20}O_3$ completely reacted with BYZ to yield a single, solid-solution perovskite phase and were not considered further. In contrast, mixtures of $BaZr_{0.40}Pr_{0.40}Gd_{0.20}O_3$ with BYZ and of $BaZr_{0.60}Y_{0.20}Co_{0.20}O_3$ with BYZ retained two perovskite phases, although the possibility of slight interdiffusion cannot be entirely ruled out.

The bulk conductivities of $BaZr_{0.40}Pr_{0.40}Gd_{0.20}O_3$, $BaZr_{0.60}Y_{0.20}Co_{0.20}O_3$, $BaZr_{0.50}Pr_{0.30}Y_{0.20}O_3$, $BaZr_{0.60}Pr_{0.20}Y_{0.20}O_3$, and $BaZr_{0.70}Pr_{0.10}Y_{0.20}O_3$ were measured by AC impedance methods in a wet air atmosphere and are shown in Figure 3. $BaZr_{0.40}Pr_{0.40}Gd_{0.20}O_3$ and $BaZr_{0.60}Y_{0.20}Co_{0.20}O_3$ are promising materials

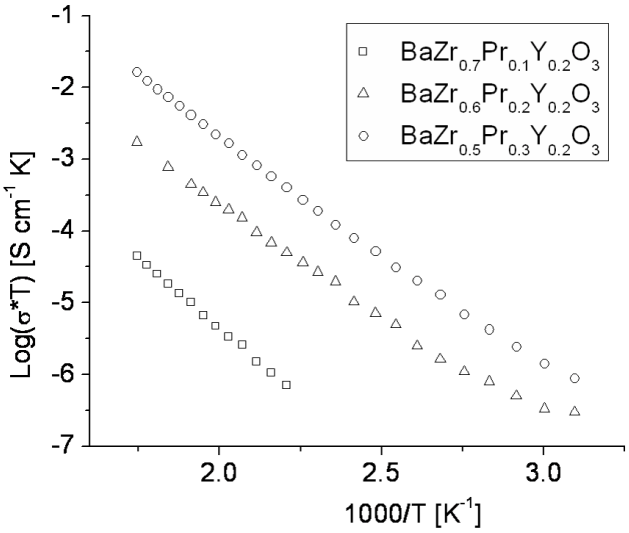

Figure 3. Bulk Conductivity of Three Potential Cathode Materials as Measured in Wet Air Atmosphere

because they have conductivities comparable to that of BYZ. Surprisingly, the activation energy for $BaZr_{0.40}Pr_{0.40}Gd_{0.20}O_3$ was measured as 0.40 eV and for $BaZr_{0.60}Y_{0.20}Co_{0.20}O_3$ as 0.42 eV, which are close to the value of 0.44 eV found for the BYZ bulk conductivity [4]. It was expected that the addition of transition metals would lead to an increase in electronic conductivity that should result in lower activation energies.

The $BaZr_{0.8-x}Pr_xY_{0.20}O_3$ systems with x = 0.1, 0.2, 0.3 show much lower conductivities than expected. Most probably, the high resistivity is caused by barium deficiency. The materials were sintered at 1600°C to prepare full dense samples for impedance measurements. Such high sintering temperature is due to the high zirconium content in the samples. To suppress the barium loss during the sintering, processing of the samples needs to be optimized (similar to the BYZ optimization). Further screening of cathode materials continues.

Ni has been established as a good catalyst for the anode reaction in yttria-stabilized zirconia (YSZ). For this reason, our initial intention was to use a NiO-BYZ porous support for a thin BYZ electrolyte membrane. However, according to our preliminary experiment, NiO easily diffuses into the BYZ layer during sintering. Attempts were made to prevent this diffusion by lowering sintering temperature. However, to obtain a high-density layer, sintering at

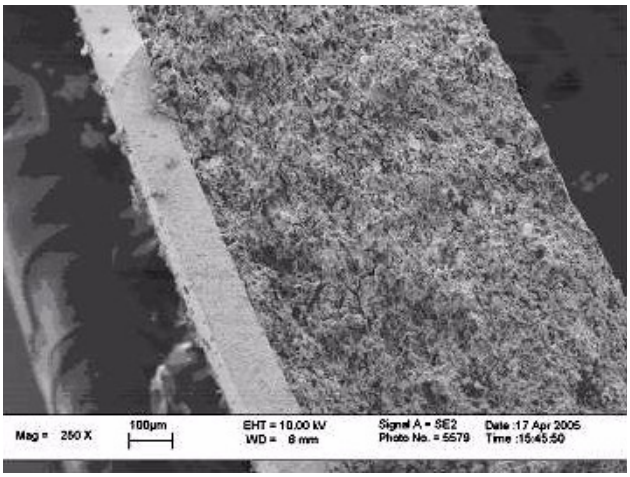

Figure 4. Cross-Section of 100 m Electrolyte BYZ Membrane on BYZ Porous Support

1600°C is needed. Therefore, we concluded that it is very difficult to use NiO as support material. To find an alternative support that has catalytic ability for the electrode reaction, FeOx, Ni, Fe and NiAl were examined, but all had fatal problems. Thus, we developed bi-layer and tri-layer BYZ systems with varying porosity. The support is a porous BYZ layer, while the electrolyte is a fully densified layer. Figure 4 shows scanning electron microscopy (SEM) micrographs of such a system. Future plans include using impregnation techniques to incorporate a metal catalyst into the porous layer.

Conclusions

To date, we have mostly finished developing the ReaxFF Reactive Force Field for a PCFC based on BYZ. This allows us to start modeling corresponding materials and complex physico-chemical processes observed in PCFCs, including the electrode/electrolyte interface both with Ni and Pt as anode material. The latter is important in light of recent experimental results, which showed that the majority of overpotential occurred at the anode rather than the cathode. Follow-up experiments will be used to validate the computational predictions of how to enhance power performance of a PCFC.

FY 2005 Publications/Presentations

1. "Reactive Force Field for Atomistic Modeling of Solid Oxide Fuel Cell Systems", B.V. Merinov, A.C.T. van Duin, S.S. Jang, W.A. Goddard III, Presented at the 15th International Conference on Solid State Ionics, Baden-Baden, Germany, July 17, 2005. Abstracts.
2. "Application of Quantum Methods to High Temperature Fuel Cell Materials: Use of first principles based modeling and simulation to characterize, design, and optimize new strategies for fuel cell technologies: applications to solid oxide, solid acid, and PEM fuel cells, cathode catalysts, anode catalysts, 3-phase interface", U.S. Department of Energy's National Energy Technology Laboratory (NETL) 6th SECA Annual Workshop, April 18-21, 2005 at the Asilomar Conference Grounds, Pacific Grove, CA. http://www.netl.doe.gov/events/05conferences/SECA-workshop/index.html

References

1. Jaguar 5.0, Schrodinger Inc., Portland, OR, 2000.
2. P.A. Schultz, unpublished [a description of the method is in P.J. Feibelman, Phys. Rev. B 35, 2626 (1987)].
3. W. Munch, K.-D. Kreuer, G. Seifert, J. Maier, Solid State Ionics 136-137, 183 (2000).
4. H.G. Bohn, T. Schober, J. Am. Ceram. Soc. 83, 768 (2000).

V.2 High Temperature Electrochemistry Center

LR Pederson (Primary Contact), GW Coffey, OA Marina, GL McVay, CD Nguyen, PC Rieke, SC Singhal, and EC Thomsen
Pacific Northwest National Laboratory
Richland, Washington 99352
Phone: (509) 375-2731; Fax: (509) 375-2167; E-mail: larry.pederson@pnl.gov

LH Spangler, M Deibert, H Gao, VI Gorokhovsky, YU Idzerda, MH Nehrir, VH Schmidt, SR Shaw, and RJ Smith
Montana State University
Bozeman, Montana 59717

ED Wachsman, KL Duncan, F Ebrahimi, X Guo, KS Jones, JC Nino, SR Phillpot, H-J Seifert, WM Sigmund, and SB Sinnott
University of Florida
Gainesville, Florida 32611

AV Virkar
University of Utah
Salt Lake City, Utah 84112

DOE Program Manager: Lane Wilson
Phone: (304) 285-1336; E-mail: Lane.Wilson@netl.doe.gov

Objectives

- Objectives of the High Temperature Electrochemistry Center are to advance solid oxide technology, such as solid oxide fuel cells (SOFCs), high temperature electrolyzers, reversible fuel cells, energy storage devices, gas separation membranes, and electrochemical sensors, for use in distributed generation and FutureGen applications, as well as to conduct fundamental research that aids the general development of all solid oxide technology.

Approach

- Develop reversible solid oxide fuel cell technology capable of efficiently producing hydrogen in an electrolyzer mode as well as producing electrical power from stored hydrogen in the fuel cell mode.
- Develop high temperature ceramic membranes for separating hydrogen from gasified coal and other complex mixtures.
- Advance the fundamental understanding of reactions and processes that occur at the electrode-electrolyte-gas interface, critical to the operation of a wide range of electrochemical technologies including fuel cells, electrolyzers, sensors, and gas separation membranes.
- Develop model corrosion-resistant, multilayer thin films aimed at extending the lifetime of metallic fuel cell interconnects.
- Develop tools necessary to monitor and model the response of fuel cells to transient electrical loads, and design power electronics modules to improve the performance and efficiency of fuel cells integrated with multiple power sources.
- Develop simulation methods to provide insight on ion and electron transport mechanisms, the structure and thermodynamic properties of vacancy clusters, and oxygen reactions at surfaces and interfaces.

Accomplishments

- A ceramic fuel electrode consisting of doped strontium titanate and doped ceria shows high activity for steam electrolysis and is electrically conductive. Doping of cerate phase with Group Va metals significantly enhances the catalytic activity for both steam electrolysis and hydrogen oxidation. Lower polarization losses associated with the ceramic composite electrode can lead to more efficient hydrogen production by steam electrolysis.
- Thin composite barium zirconium cerate/nickel membranes with submicron grain structures have been prepared on a porous support, intended to passively separate hydrogen from an impure mixture such as coal gas. The thin, supported structure provides enhanced transport while maintaining good mechanical properties.
- Copper-substituted lanthanum ferrite air electrodes have been developed that are exceptionally active at low temperature, but approximately equal to lanthanum ferrites at higher temperatures. Investigations of electronic and ionic conductivity, carrier density, oxygen content, electrode polarization and other properties have shown that copper is susceptible to reduction, leading to diminished activity.
- University of Utah and Pacific Northwest National Laboratory (PNNL) researchers have used cells with patterned electrodes to develop insights into the mechanism of the air electrode reaction. For platinum and lanthanum manganite electrodes, the charge transfer resistance was found to vary inversely with the length of the triple phase boundary for purely electron-conducting electrodes, thus confirming the validity of this novel experimental approach. Such information is critical in enabling cathode compositions to be optimized.
- Synchrotron radiation has been used by researchers at Montana State University (MSU) to examine reactions occurring at a buried electrode-electrolyte interface. By using polarization-dependent X-ray absorption spectroscopy (XAS), the chemical state of different elements of $La_XCa_{1-x}MnO_3$ (LCM) was shown to change as a function of the stress within the LCM film. These studies are expected to provide unique insight into reactions and processes that control the activity of fuel cell electrodes.
- In collaboration with the University of Missouri-Rolla, anomalous shrinkage behavior of porous Sr-doped lanthanum manganite has been found, occurring at temperatures hundreds of degrees lower than the sintering temperature. The mechanism for shrinkage is attributed to be enhanced metal ion diffusion in a vacancy gradient imposed by thermal and oxygen partial pressure cycles.
- Large area filtered arc deposition (LAFAD) has been utilized at MSU to fabricate multilayer coatings on steel coupons as a means of improving high temperature corrosion resistance through surface engineering. An order of magnitude improvement in oxidation resistance of 440 stainless steel was achieved by applying nanolayered coatings of CrAlON. The coating technology offers promise for extending the life of steel SOFC interconnects.
- Scale-up of the LAFAD process to apply corrosion-resistant coatings to interconnect plates of a size compatible with Solid State Energy Conversion Alliance (SECA) stack designs has been demonstrated at MSU. Uniform, nearly defect-free multilayer coatings were prepared on steel plates that were 10 cm by 10 cm in size.
- An electrical circuit based model for a fuel cell system has been developed and used in modeling and control of stand-alone and grid-connected distributed power generation systems. The control strategies developed could result in improved performance of grid-connected and stand-alone hybrid fuel cell power plants.
- A low-cost, high-efficiency DC-DC converter for residential fuel cell power generation systems has been designed and simulated. A scale-down prototype has been built. Preliminary experimental results show the validity of this unique approach to the current DC-DC converter design.
- A non-intrusive load monitor has been developed at MSU that can disaggregate currents measured at a central location and is capable of associating disaggregated current transients with individual loads. This

technology provides a useful tool for studying fuel cell models under real-world use conditions, for surveying the load served by the fuel cell, and for characterizing fuel-cell load interactions.

- A transient recognition control (TRC) predictive model that can recognize and respond to electrical load transients has been developed at MSU. The predictive modeling approach has been validated and appears to be useful for hybrid fuel cell systems.

Future Directions

- Develop an efficient reversible fuel cell with air and fuel electrode compositions and forms to minimize overpotential losses. Establish operating conditions leading to most efficient operation.
- Develop composite hydrogen separation membranes aimed at meeting the DOE Office of Fossil Energy's (FE's) targets for permeation and strength.
- Employ filtered arc plasma methods to deposit high-quality Mn-Co-O spinel films intended to enhance the corrosion resistance of metallic interconnects. Establish oxygen and chromium migration rates through these dense coatings. Investigate the applicability of filtered arc methods to prepare thin film fuel cell structures for intermediate temperature operation.
- Apply advanced X-ray techniques to study the oxygen reduction and oxygen ion oxidation mechanisms at the electrode/electrolyte interface at high temperature.
- Demonstrate the efficacy of cluster training methods in enhancing the transient load following of a solid oxide fuel cell system.
- Conduct fundamental research on the mechanisms of ionic transport in solids, combining experimental measurements with molecular dynamics and electronic structure simulation. Investigate the relation between external environment and mechanical properties through defect equilibria modeling.
- Use controlled microstructure processing methods to tailor the microstructure and composition of the solid electrolyte/electrode interface.

Introduction

The High Temperature Electrochemistry Center (HiTEC) was created in 2002 to provide crosscutting, multidisciplinary research that supports the Office of Fossil Energy's FutureGen Initiative. The National Energy Technology Laboratory (NETL), Montana State University (MSU), the University of Florida, the University of Utah and the Pacific Northwest National Laboratory (PNNL) currently are contributors to HiTEC. Objectives of the High Temperature Electrochemistry Center are to advance solid oxide technology, such as solid oxide fuel cells, high temperature electrolyzers, reversible fuel cells, energy storage devices, gas separation membranes, and electrochemical sensors, for use in distributed generation and FutureGen applications, as well as to conduct fundamental research that aids the general development of all solid oxide technology.

A broad range of research topics are currently being addressed. Current research activities being conducted at PNNL include the development of low-loss electrodes for reversible solid oxide fuel cells, the development of high temperature membranes for hydrogen separation, fundamental electrode reaction mechanism studies, and development of computational tools relevant to high temperature electrochemical systems. Research activities at MSU include the development of dynamic models of fuel cell systems for distributed generation applications, development of adaptive power controllers for fuel cells, development of multilayer thin film coatings to improve the corrosion resistance of interconnect materials, research on transport in hydrogen separation membranes, and advanced x-ray studies of buried interfaces. Research activities at the University of Florida include fundamental ion transport mechanisms investigation, development of electronic structure and molecular dynamics tools to study ion transport, microstructural characterization of model interfaces, studies of the relation of environment to thermo-mechanical properties, advanced synthetic research to provide tailored microstructures, and computational and experimental

investigations of the thermodynamic properties of high temperature fuel cell materials.

Results

Improved efficiency through lowered electrode polarization losses of a reversible solid oxide fuel cell is among the goals of this project. A composite consisting of doped strontium titanate and doped ceria is being developed for use as the fuel electrode. Good electronic conductivity is provided by lanthanum-doped $SrTiO_3$, an *n*-type semiconductor under reducing conditions, while the cerate phase doped with Group Va metals significantly enhances the catalytic activity for both steam electrolysis and hydrogen oxidation. Because this electrode is composed of metal oxides, it is less susceptible than nickel/zirconia to degradation by intermittent exposure to air. Lower polarization losses associated with the ceramic composite electrode can lead to more efficient hydrogen production by steam electrolysis.

Titanate/ceria composite electrodes exhibited promising polarization losses under both cathodic and anodic conditions, but operated most efficiently in the electrolysis mode. Polarization curves for a $La_{0.35}Sr_{0.65}TiO_{3-}$ -$Ce_{0.99}Nb_{0.01}O_{2-}$ in a 1:1 mole ratio electrode at different partial pressures of steam at 850°C are shown in Figure 1. Cell current densities increased with increased steam partial pressures at a constant initial hydrogen partial pressure in the electrolysis mode. In the fuel cell mode, cell current densities were insensitive to the steam partial pressure. The ceramic composite anode requires a minimum hydrogen partial pressure to operate efficiently, as shown in Figure 2. With insufficient hydrogen present, slow oxidation of the ceria led to higher polarization losses. Current densities were stable when sufficiently reducing conditions were maintained.

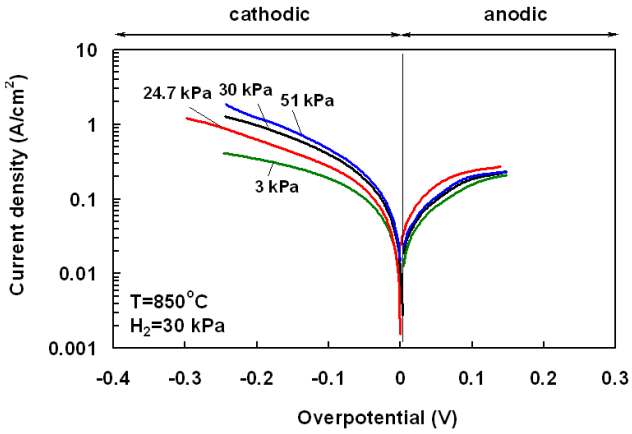

Figure 1. Polarization curves for a $La_{0.35}Sr_{0.65}TiO_{3-}$ -$Ce_{0.99}Nb_{0.01}O_{2-}$ in a 1:1 mole ratio electrode at different partial pressures of steam at 850°C. Polarization losses decreased with increased steam concentration in the electrolysis mode.

Copper-substituted lanthanum strontium ferrites have been shown to be exceptionally active as the air electrode in a reversible solid oxide fuel cell, though they perform similarly to lanthanum strontium ferrite at temperatures greater than ~800°C. The tendency for copper to be reduced in the perovskite at high temperatures and in low oxygen concentrations is at least partially responsible for such behavior. In Figure 3, the four-point electrical conductivity of LSCF-7337 versus temperature in varied oxygen concentrations shows a maximum at ~550°C and diminishes considerably as the oxygen concentrations are lowered. In contrast, LSF-30 shows only a small dependence on the oxygen concentration from 1 to 100% oxygen. Copper-substituted lanthanum strontium ferrites show high mixed electronic and ionic conductivity, which enhances electrocatalytic activity through extension of the dimensions of the triple phase boundary. Transference numbers for oxygen ions for a series of copper-substituted lanthanum strontium ferrites are given in Figure 4 versus temperature, where oxygen ion conductivities were determined by permeation.

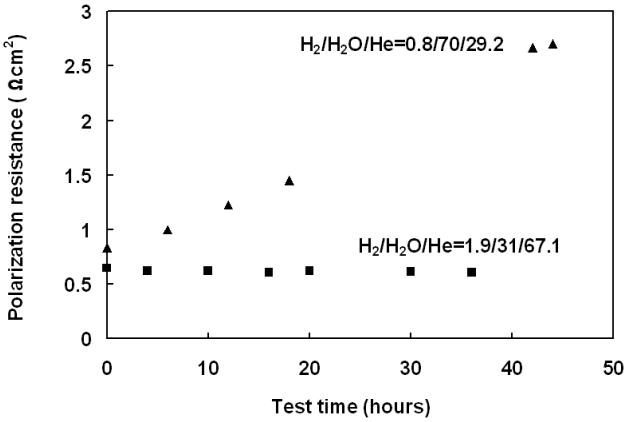

Figure 2. Durability test on $La_{0.35}Sr_{0.65}TiO_{3-}$ -$Ce_{0.99}Nb_{0.01}O_{2-}$ anode, 1:1 mole ratio, at different partial pressures of hydrogen at 900°C. The more oxidizing conditions led to a loss of electrical conductivity and electrode activity with time.

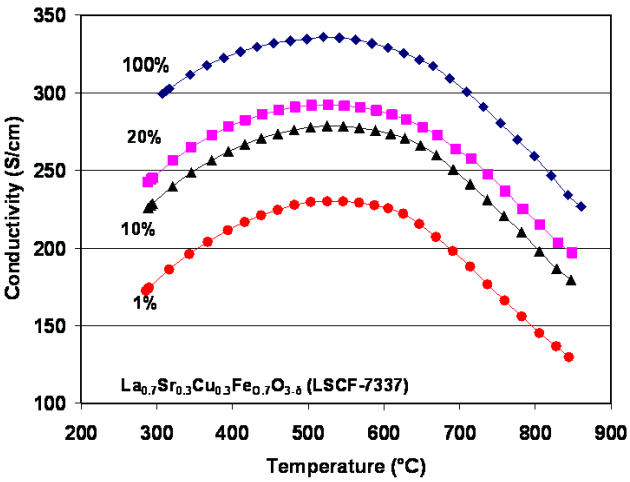

Figure 3. Electrical conductivity of LSCF-7337 versus temperature in varied oxygen concentrations. Copper reduction at high temperatures and low oxygen concentrations leads to a loss of electrical conductivity.

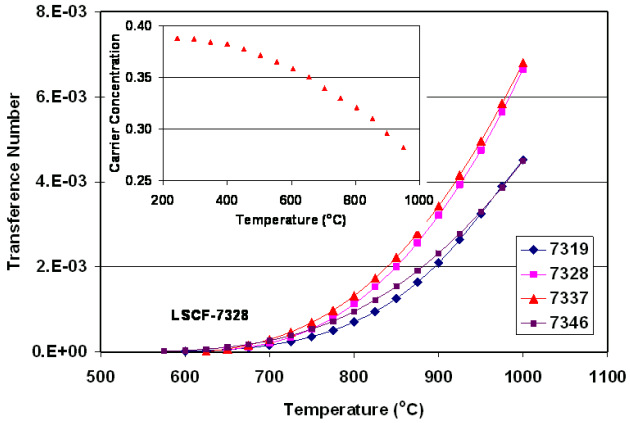

Figure 4. Transference numbers for oxygen ion conductivity for a series of copper-substituted lanthanum strontium ferrites. Oxygen ion conductivities were determined by permeation. The inset shows electronic carrier concentration as a function of temperature in air calculated from the Seebeck coefficient.

Oxygen ion conductivity contributes approximately 0.1% to the overall conductivity at 800°C, with the fraction rising with increased temperature. The inset in Figure 4 shows that the electronic carrier concentration, determined from the Seebeck coefficient, decreases significantly with increased temperature. Thus, while the copper-substituted ferrites are found to be very active electrocatalysts, they are most suited for intermediate or low temperature operation.

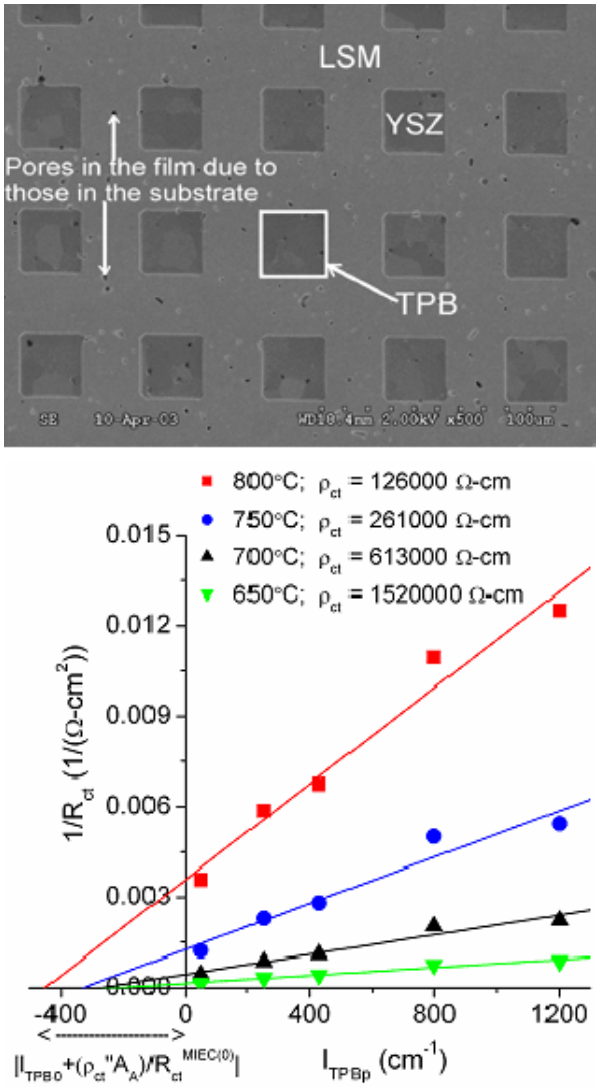

Figure 5. Estimation of the charge transfer resistivity of $La_{0.8}Sr_{0.2}MnO_3$ cathodes on 8YSZ electrolyte using patterned electrodes. By varying the geometric length of the triple phase boundary while maintaining the electrode area constant, University of Utah and PNNL researchers showed a linear dependence of 1/charge transfer resistivity on triple phase boundary length. Similar results were found for platinum.

To better understand the mechanisms of cathodic reactions, University of Utah and PNNL researchers have prepared novel, patterned electrode-electrolyte structures using lithographic techniques. These structures provide a well-defined triple phase boundary length, thus allowing intrinsic electrocatalytic activity to be determined without ambiguity. Figure 5 shows typical electrode design and includes charge transfer resistivity results as a

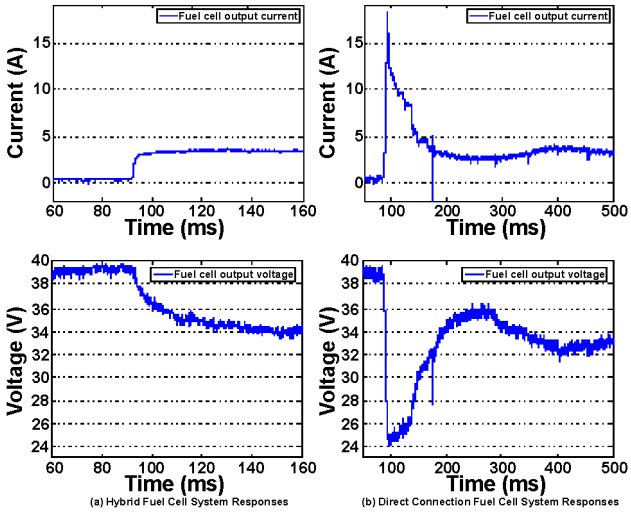

Figure 6. TRC technology has been developed at MSU, aimed at enabling a fuel cell system to recognize and respond to characteristic transients introduced by various appliances. Concepts were demonstrated using off-the-shelf electronics and a 500 We fuel cell. Figure 6a shows current and voltage response of the fuel cell to an incandescent light bulb being switched on. Figure 6b shows the instability of that same system to the same transient load without TRC.

function of geometric triple phase boundary length. Yttria-zirconia discs with patterned platinum, lanthanum strontium manganite, and lanthanum strontium cobaltite electrodes having three different triple phase boundary lengths but having the same macroscopic electrode-electrolyte interface areas were prepared and studied by electrochemical impedance spectroscopy. The charge transfer resistance was found to vary inversely with the length of the triple phase boundary for purely electron-conducting electrodes such as platinum and lanthanum strontium manganite, thus confirming the validity of this novel experimental approach. This relation did not hold for mixed conductors such as lanthanum strontium cobaltite. Such information is critical in enabling cathode compositions to be optimized.

A transient recognition control (TRC) predictive model has been developed at MSU that can recognize and respond to electrical load transients. A cluster-weighted modeling algorithm was utilized to build the electrical load transient recognition model.

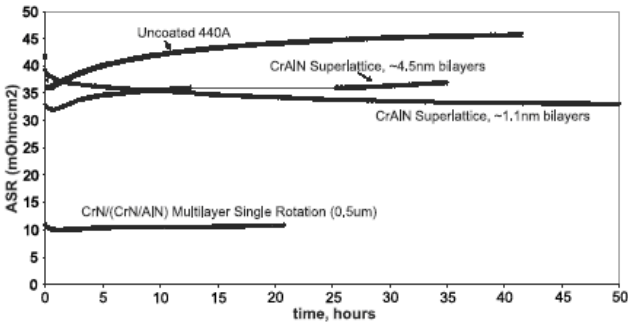

Figure 7. Area-specific resistances of coated and uncoated 440A stainless steel exposed to air at 800°C. Multilayer coatings consisting of alternating layers of chromium nitride and aluminum nitride deposited by filtered arc plasma methods resulted in improved ASR values for various steels. The technology may lead to improved performance of metal interconnects in solid oxide fuel cells.

Transient recognition control concepts have been simulated using MATLAB and demonstrated using off-the shelf power electronics and a 500 We fuel cell, as shown in Figure 6 for a transient electrode presented by turning on an incandescent light bulb. Figure 6a shows current and voltage response of the fuel cell to an incandescent light bulb being switched on. In this case, stack output currents and potentials became stable typically in less than 10 milliseconds. Figure 6b shows the instability of that same system to the same transient load without TRC control, where oscillations persisted for hundreds of milliseconds. The predictive modeling approach has been validated and appears to be useful for hybrid fuel cell systems.

Multilayer coatings consisting of alternating layers of chromium nitride and aluminum nitride were deposited onto 304 and 440 stainless steels and onto Crofer grade APU 22. After exposure to air at 800°C for varying periods, the corrosion layer was analyzed by Rutherford backscatter, nuclear reaction analysis, x-ray photoelectron spectroscopy, analytical electron microscopy, and atomic force microscopy. Changes in area specific resistance (ASR) due to exposure to air at high temperatures were also assessed. Both the short-term oxidation resistance and the ASR growth rate were improved significantly for some of the coated coupons. Results for a 440A martensitic stainless steel are given in Figure 7 for exposure of coated and uncoated coupons to air at

800°C. Best ASR values obtained for these coatings were approximately 10 m-ohm cm^2, which is significantly lower than that of the uncoated specimen. This technology holds significant promise for enabling the use of metallic interconnects in solid oxide fuel cells.

Conclusions

- Composite ceramic electrode compositions have been developed that show high activity for steam electrolysis.
- Copper-substituted lanthanum strontium ferrites were shown to be highly active fuel cell cathodes. The tendency for copper reduction limits application to intermediate temperature fuel cells.
- Charge transfer resistance for purely or nearly purely electronic conductors has been shown to be related to the geometric triple phase boundary length in studies utilizing patterned electrodes. The studies provide insight into the mechanism of oxygen reduction in fuel cells.
- Transient recognition control methodology has been developed that allows fuel cell systems to respond to transient electrical loads. The validity of the approach was demonstrated with a 500-watt fuel cell and off-the-shelf electronics.
- Filtered arc plasma has been applied to deposit multilayer metal nitride coatings. The coatings have resulted in substantial improvements in both the initial ASR as well as the growth in that value with long-term exposure to air at high temperatures.

FY 2005 Publications

1. Coffey GW, Hardy JS, Marina OA, Pederson LR, Rieke PC and Thomsen EC. "Copper doped lanthanum strontium ferrite for reduced temperature solid oxide fuel cells." Solid State Ionics 175 (1-4), 73-78, 2004.
2. Williams MC, Marina OA, Coffey GW, Pederson LR, Rieke PC, and Thomsen EC. "Electrode development for reversible solid oxide fuel cells." J. Electrochem. Soc. 2004 (accepted).
3. Marina OA and Pederson LR. "High temperature electrolysis of water in a 'reversible' solid oxide fuel cell." 6th European SOFC Forum, Lucerne, Switzerland, M. Mogensen, Ed. 1, 388, 2004.
4. Marina OA, Coffey GW, Pederson LR, Rieke PC, Thomsen EC, and Williams MC. Proc. Int. Electrochem. Soc. 2004 (in press).
5. Radhakrishnan R, Virkar AV, and Singhal SC. "Estimation of charge-transfer resistivity of Pt cathode on YSZ electrolyte using patterned electrodes." J. Electrochem. Soc. 152 (5): A927-A936, 2005.
6. Radhakrishnan R, Virkar AV, and Singhal SC. "Estimation of charge-transfer resistivity of $La_{0.8}Sr_{0.2}MnO_3$ cathode on $Y_{0.16}Zr_{0.84}O_2$ electrolyte using patterned electrodes." J. Electrochem. Soc. 152 (1): A210-A218, 2005.
7. Simner SP, Anderson MD, Xia GG, Yang Z, Pederson LR, and Stevenson JW. J. Electrochem Soc. 152 (4): A740-A745, 2005. (partial support).
8. Wang CS, Nehrir MH, and Shaw SR. "Dynamic models and model validation for PEM fuel cells using electrical circuits." IEEE Transactions on Energy Conversion 20 (2): 442-451, 2005.
9. Zhu T, Shaw SR, and Leeb SB. "Transient recognition control for hybrid fuel cell systems." IEEE Transactions on Energy Conversion (in press).
10. Gannon PE, Tripp CT, Knospe AK, Ramana CV, Deibert M, Smith RJ, Gorokhovsky V, Shutthanandan V, and Gelles D. "High-temperature oxidation resistance and surface electrical conductivity of stainless steels with filtered arc Cr-Al-N multilayer and/or superlattice coatings." Surface & Coatings Technology 188: 55-61, 2004.
11. Nelson DB, Nehrir MH, and Gerez V. "Economic evaluation of grid-connected fuel-cell systems." IEEE Transactions on Energy Conversion 20 (2): 452-458, 2005.
12. Wang CS and Nehrir MH. "Analytical approaches for optimal placement of distributed generation sources in power systems." IEEE Transactions on Energy Conversion 19 (4): 2068-2076, 2004.
13. Wang CS and Nehrir NH. "Pspice circuit model for PEM fuel cells." *Proceedings,* 2004 North American Power Symposium, Moscow, ID, August 9-10, 2004.
14. Lussier A, Dvorak J, Idzerda YU, Ogale SB, Shinde SR, Choudary RJ, and Venkatesan T. "Comparative X-ray absorption spectroscopy study of Co-doped SnO_2 and TiO_2." J. Appl. Phys. 95, 7190, 2004.
15. Idzerda YU, Stadler S, Chen Z, Wu T, Ogale SB, Venkatesan T, Godfrey R, Ramesh R. "Measuring interfacial disruption at a complex solid-state interface." Submitted to Phys. Rev. B 2004.

16. Dvorak J, Idzerda YU, Wu T, Ogale SB, and Venkatesan T. "Are strain-induced effects truly strain induced? A comprehensive study of strained LCMO thin films." Submitted to J. Appl. Phys 2004.
17. Lussier A, Dvorak J, Idzerda YU, Ogale SR, Ogale SB, and Venkatesan T. "Cobalt site symmetry and oxygen vacancies in ferromagnetic cobalt-doped oxides." Submitted to J. Appl. Phys. 2004.
18. Sharma R and Gao H. "Low cost high efficiency DC-DC converter for fuel cell residential power generation systems." Submitted to IEEE Applied Power Electronics Conference and Exposition, Austin, Texas, March 2005, and to be submitted to IEEE Transaction on Power Electronics.
19. Smith RJ, Zhang Y, Shutthanandan V, Bissell LJ, Thevuthasan S, Jiang W, and Weber WJ. "NRA and ERDA investigation of helium retention in SiC as a function of irradiation and annealing." Nuclear Instruments and Methods in Research B, 119-220, 631-635, 2004.
20. Muljadi E, Wang C, and Nehrir MH. "Parallel operation of wind turbine, fuel cell, and diesel generation sources." Proceedings IEEE PES General Meeting, Denver, CO, June 6-10, 2004.

V.3 Electrocatalytically Active High-Surface-Area Cathodes for Low-Temperature SOFCs

Eric D. Wachsman
Department of Materials Science and Engineering, University of Florida
Gainesville, Florida 32611
Phone: (352) 846-2991; Fax: (352) 846-0326; E-mail: ewach@mse.ufl.edu

DOE Project Manager: Lane Wilson
Phone: (304) 285-1336; E-mail: Lane.Wilson@netl.doe.gov

Objectives

- Develop a fundamental understanding of heterogeneous electrocatalytic phenomena at the surface of ion-conducting ceramics.
- Fabricate high-surface-area solid oxide fuel cell (SOFC) cathodes with controlled microstructure and porosity.
- Develop low-ASR (low area-specific resistance) cathodes for low- to intermediate-temperature SOFCs.

Approach

- Synthesize high-surface-area metal oxide powders and metal oxide powders decorated with nanoclusters of catalytically active metals (Co, Fe, Ni, Ru, and Pt).
- Elucidate the kinetics of surface reactions on these powders via heterogeneous catalysis experiments, such as temperature-programmed desorption (TPD), temperature-programmed reaction (TPR) and isotope exchange.
- Determine the ionic and electronic conductivity of the materials by AC impedance and blocking electrode techniques.
- Determine isothermal stability of the materials.
- Fabricate anode-supported cells using novel processing techniques and evaluate the cathode polarization of the cells.
- Distinguish the individual contributions to electrode polarization by combining the electrochemical characterization with heterogeneous catalysis techniques.

Accomplishments

- Demonstrated stability issues of Ag-ESB (silver – erbia-stabilized bismuth oxide) composite cathodes and improved stability by addition of 10-15 vol% nano-scale yttria-stabilized zirconia (YSZ) powder.
- Synthesized nano-sized $Bi_2Ru_2O_7$, $Pb_2Ru_2O_7$ and doped $Y_2Ru_2O_7$ powders via co-precipitation and a novel wet chemical route.
- Developed higher-conductivity Pr- and Eu-doped $Y_2Ru_2O_7$.
- Developed stable, low-ASR $Bi_2Ru_2O_7$-ESB composite cathodes.

Future Directions

- Improve yield of nano-sized $Bi_2Ru_2O_7$ powders.
- Optimize the microstructure of $Bi_2Ru_2O_7$-ESB composite cathodes.
- Analyze the role of lanthanide dopants and optimize their concentration in the $Bi_2Ru_2O_7$, $Pb_2Ru_2O_7$ and $Y_2Ru_2O_7$ system.

- Characterize catalytic activity by TPD/TPR of ruthenate and Ru-ruthenate system.
- Characterize electrochemical performance by AC impedance and polarization experiments with blocking electrodes.
- Deposit pyrochlore ruthenate cathodes on intermediate-temperature SOFCs and determine their performance.
- Compare catalytic and electrochemical results to elucidate mechanism.

Introduction

For extensive deployment of SOFCs into industrial and consumer markets to become a reality, further performance optimization is necessary. Currently, cathode overpotential is the most significant drag on total SOFC *electrochemical* performance. A significant increase in cathode performance would enable higher power densities at lower temperature and would mean lower cost and therefore greater commercial viability. Towards that end, we are in the process of developing high-performance cathodes for use on conventional (with YSZ electrolyte) and intermediate- to low-temperature (with, e.g., ceria or ceria/bismuth oxide electrolytes) SOFCs.

Approach

The proposed research follows a logical progression: (1) the low-temperature synthesis of high-surface-area metal oxide powders and metal oxide powders decorated with nanoclusters of catalytically active metals (Co, Fe, Ni, Ru, and Pt); (2) the use of heterogeneous catalysis techniques, such as TPD and TPR, and isotope exchange to elucidate the kinetics of surface reactions on these powders; (3) determination of the ionic and electronic conductivity of the materials by AC impedance and blocking electrode analysis; (4) fabrication of anode-supported cells using novel processing techniques; (5) evaluation of the electrode polarization of these cells, combining the electrochemical characterization with heterogeneous catalysis techniques to separate out the individual contributions to the electrode polarization.

Results

Metallic conducting pyrochlores possess a wider conduction band than the semiconducting phases, so the metal-versus-semiconductor dichotomy of the ruthenium pyrochlores is consistent with the Mott–Hubbard mechanism of electron localization. Based on the environment of each O atom shown in Figure 1a, it is expected that the larger the *A* cations, the farther the oxygen atoms will be pushed away from the *A* cations, thereby increasing the Ru–O–Ru angle and shortening the Ru–O bond length. This reasoning predicts a linear relationship between the ionic radii of the *A* cations and the Ru–O–Ru bond angles. This is indeed the case, as shown in Figure 1b, where eight-coordinate ionic radii [1] of the *A* cations (i.e., Bi^{3+}, Pb^{2+}) were used.

Therefore, these ruthenates have the necessary electronic conductivity (~10^3 S/cm), and since the

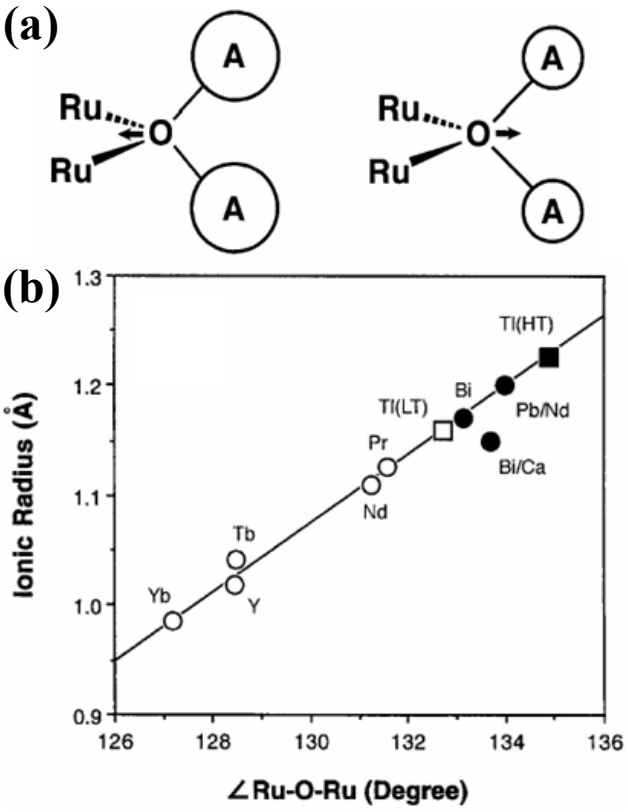

Figure 1. (a) Effect of A Site Cation on Ru-O-Ru Angle; (b) Dependence of Ionic Radius on Ru-O-Ru Angle (adapted from K. S. Lee, *J. Solid State Chem.* 131 (1997), 405)

conduction mechanism is metallic (rather than hopping as in most perovskite materials, e.g., lanthanum strontium manganite), their conductivity increases with decreasing temperature, making them suitable for low- to intermediate-temperature SOFCs. In addition, RuO_2 is known to be catalytically active for oxygen reduction. So a cathode consisting of an ionic phase (e.g., ESB) and an electronic phase (e.g., $Bi_2Ru_2O_7$) and surface decorated with nano particles of RuO_2 should make an ideal cathode. Toward this end, we are investigating $Bi_2Ru_2O_7$, $Pb_2Ru_2O_{6.5}$ and $Y_2Ru_2O_7$.

Bismuth Ruthenate. We obtained phase-pure $Bi_2Ru_2O_7$ after calcination and leaching with HNO_3 to remove the impurity sillenite type-phase. This was annealed with gadolinia-doped ceria (GDC) powder at 850ºC for 10 hours, and x-ray diffraction (XRD) showed there was no reaction between the powders, indicating stability.

An Arrhenius plot of the electrode ASR (cm^2) is shown in Figure 2a with an activation energy of ~1.26 eV. To understand the mechanism of oxygen reduction at the electrodes, impedance measurements were taken as a function of oxygen partial pressure. ASR of the electrode varies with the oxygen partial pressure according to the following equation:

$$[ASR] = [ASR]_o \, (p_{O2})^{-m}$$

The magnitude of the exponent *m* provides insight into the rate-limiting step in the oxygen reduction reaction at the electrodes. Figure 2b is a plot of ln [ASR] vs. ln P_{O2}. The values of *m* range between 0.5 and 0.6, suggesting that the rate-limiting step is surface diffusion of the dissociatively adsorbed oxygen at the electrode surface to the triple phase boundaries (TPBs). Therefore, mixing $Bi_2Ru_2O_7$ with an oxygen ion conducting phase such as ESB should significantly reduce the ASR.

To improve upon the performance of the $Bi_2Ru_2O_7$ cathodes, composite cathodes of $Bi_2Ru_2O_7$ and erbia-stabilized bismuth oxide (BRO-ESB) were fabricated, by solid-state synthesis, and characterized. Figure 3a shows a significant reduction in electrode impedance was achieved by using composite BRO-ESB electrodes, with the lowest impedance (>50% reduction) obtained for a 62.5:37.5 ratio of BRO to ESB. Moreover, switching from single-phase BRO to dual-phase BRO-ESB

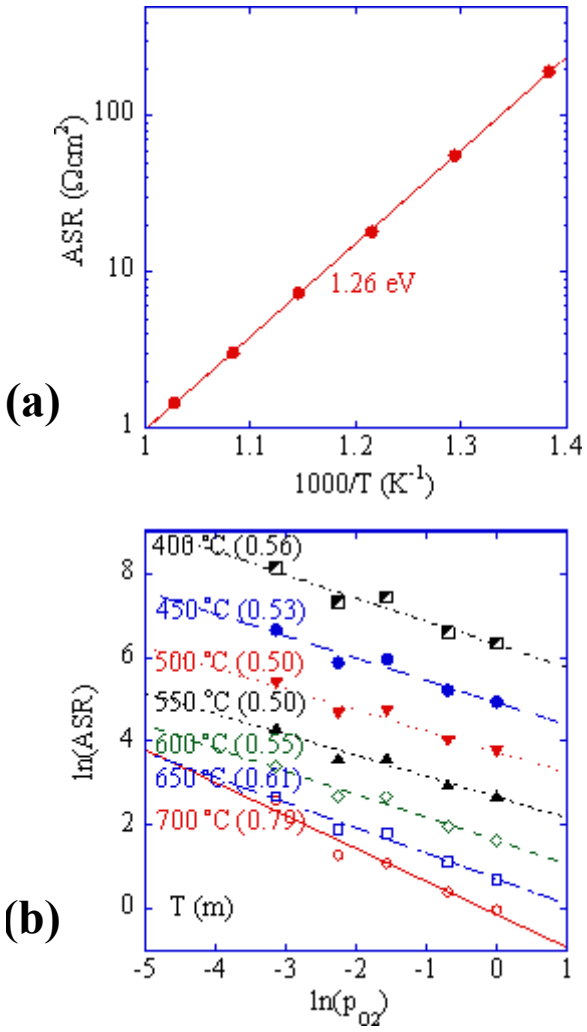

Figure 2. (a) Arrhenius Plot of the $Bi_2Ru_2O_7$ Electrode ASR (cm^2); (b) ln ASR vs. ln P_{O2} at Different Temperatures with *m* in Parenthesis T(*m*)

shifts the rate-limiting step to a much lower frequency (Figure 3b). This may suggest that the rate-limiting step is gas diffusion in the un-optimized BRO-ESB electrode microstructure; hence, even lower electrode impedances may be attainable through tailoring of the electrode microstructure. This will be verified in future experiments. Nevertheless, our initial BRO-ESB electrodes possess among the lowest impedances reported in the literature (Figure 4), with only Ag-ESB composite (which is unstable with time due to Ag migration, described below) and $Ba_xSr_{1-x}Co_yFe_{1-y}O_3$ (one report [2]) reported as better.

Lead Ruthenate. Our studies of $Pb_2Ru_2O_{6.5}$ (PRO) focused on making nano-sized powders for use in composite electrodes. Through novel

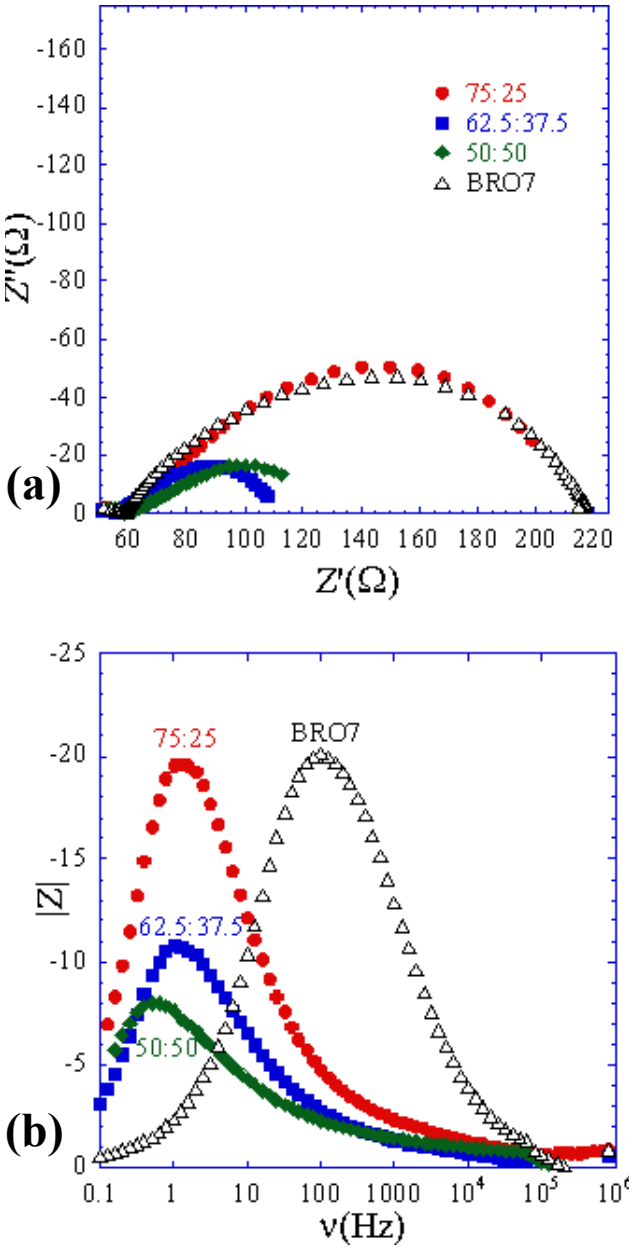

Figure 3. (a) Nyquist and (b) Bode Plots Comparing the Impedance of a $Bi_2Ru_2O_7$ Cathode with Composite $Bi_2Ru_2O_7$-ESB Cathodes in the Ratios 75 (BRO):25 (ESB), 62.5:37.5, 50:50 vol%

processing, we produced PRO crystallites surrounded by even smaller catalytically active RuO_2 particles, thereby obtaining our desired cathode microstructure.

Rare-Earth Doped Yttrium Ruthenate. $Y_2Ru_2O_7$ (YRO) was evaluated as a candidate for an intermediate-temperature SOFC cathode because of its stability in a wide range of temperatures and its lack of reactivity in contact with YSZ and GDC [3]. We prepared nanocrystalline powders of $Y_2Ru_2O_7$ by a co-precipitation method. Phase and morphology were studied by XRD and finite element scanning electron microscopy, showing a particle size of about 100 nm. The nanocrystalline particle size makes the powder amenable for the triple phase boundary tailoring in order to reduce power loss.

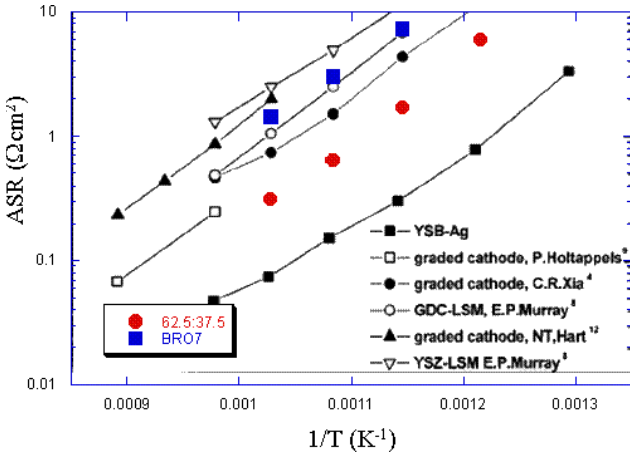

Figure 4. Comparison of ASR of $Bi_2Ru_2O_7$ and $Bi_2Ru_2O_7$-ESB Composite with Recent Literature Results (adapted from C. Xia *et al*, *Appl. Phys. Lett.*, 82 (2003) 10)

In order to obtain a metallic behavior and increase the electrical conductivity of the $Y_2Ru_2O_7$, Eu and Pr were chosen as A-site dopants. XRD confirmed that the doped powders were single-phase, and scanning electron microscopy (SEM)/energy-dispersive x-ray spectroscopy confirmed the presence of the dopant in the pyrochlore structure. The electrical conductivity was measured between 473-1073 K by DC 4-probe method for a dopant range of 5-25 mol%, and our results show that doping increased the conductivity of YRO by 20%.

Ag-ESB Composites. Ag-ESB composites have been described in the literature as possessing one of the lowest ASRs [4]; hence, their long-term stability was examined in order to evaluate the potential of such systems for use as cathodes in intermediate-temperature SOFCs. Cathode ASR was first minimized by optimizing the volume fraction of Ag phase at approximately 50%. The performance of this optimized composition at 600°C is among the

best reported to date. However, the polarization resistance isothermally increases by more than 200% over a seven-day testing period. SEM analysis revealed that the microstructure of the Ag phase undergoes dramatic growth during this timeframe. This microstructural growth and consequent reduction in porosity is believed to diminish cathodic reaction zone size and inhibit gas transport. Nano-scale YSZ ceramic powders were shown to markedly lower the rate of isothermal degradation of these composite cathodes, when added in proper proportion. SEM analysis reveals that the introduction of this third phase helps restrict the mobility of Ag at this temperature, allowing the porosity and reaction zone size to remain relatively high. The optimum YSZ composition appears to be between 10-15 vol%. XRD revealed no evidence of a reaction between the different cathode phases. In SEM micrographs of the microstructure, it was observed that the edges of the Ag particles in the as-fired sample are smooth, while in the tested sample, the edges are rough due to envelopment of YSZ into the Ag particles. It is possible that this effect reduces the triple phase boundaries between the Ag, ESB, and gas phases, contributing to the observed increase in ASR with time for these electrodes.

Conclusions

- Nano-sized $Bi_2Ru_2O_7$, $Pb_2Ru_2O_7$ and doped $Y_2Ru_2O_7$ powders can be synthesized via co-precipitation and a novel wet chemical route.
- $Bi_2Ru_2O_7$-ESB composite cathodes are stable and possess low ASR and impedance.
- $Y_2Ru_2O_7$ conductivity can be increased by 20% by doping with 15 mol% Pr.
- Stability of Ag-ESB composite cathodes can be improved by adding 10-15 vol% nano-scale YSZ powder.

FY 2005 Publications/Presentations

1. "RuO_2 and Pt Based Electrodes for ESB IT-SOFC," V. Esposito, E. Traversa, and E.D. Wachsman, *Solid Oxide Fuel Cells IX*, Electrochem. Soc., S.C. Singhal and J. Mizusaki, Ed.
2. "Bismuth-Ruthenate-Based Cathodes for IT-SOFCs," A. Jaiswal and E.D. Wachsman, *Journal of the Electrochemical Society*, 152, A787-790 (2005).
3. "Preparation and Characterization of Lead Ruthenate Based Composite Cathodes for SOFC Applications," V. Esposito, E. Traversa, and E.D. Wachsman, *Solid State Ionics-2004*, Materials Research Society, P. Knauth, C. Masqulier, E. Traversa, and E.D. Wachsman, Ed., 835, 217-222 (2005).
4. "The Search for a Low Temperature SOFC; How Low Can We Go?" MIT Department of Materials Science Seminar, February 18, 2005, Boston, MA.
5. "Isothermal Stability of Composite Ag-$Er_{0.4}Bi_{1.6}O_3$ Cathodes for Intermediate Temperature Solid Oxide Fuel Cells," American Ceramic Society, 29th International Conference on Advanced Ceramics and Composites, January 24-28, 2005, Cocoa Beach, FL.

References

1. K. S. Lee, *J. Solid state Chem*. 131 (1997), 405.
2. Z. Shao. and S. M. Haile, *Nature* 431 (2004) 170.
3. A. Bencan, M. Hrovat, J. Holc, and M. Kosec, *Materials Research Bulletin* 35 (2000) 2415.
4. C. Xia, Y. Zhang, and M. Liu, *Appl. Phys. Lett*. 82 (2003) 10.

V.4 Active Cathodes for Super-High Power Density Solid Oxide Fuel Cells through Space Charge Effects

Anil V. Virkar
University of Utah
Department of Materials Science & Engineering
122 S. Central Campus Drive
Salt Lake City, UT 84112
Phone: (801) 581-5396; Fax: (801) 581-4816; E-mail: anil.virkar@m.cc.utah.edu

DOE Project Manager: Lane Wilson
Phone: (304) 285-1336; E-mail: Lane.Wilson@netl.doe.gov

Objectives

- To fabricate and characterize mixed ionic electronic conducting (MIEC) materials as cathodes for solid oxide fuel cells (SOFCs).
- To investigate the effect of morphology and space charge on transport properties and on cathode polarization.
- To investigate use of patterned electrodes for measurement of fundamental charge transfer characteristics at a three-phase boundary (TPB).
- To develop a theoretical analysis of the effect of interfaces on transport through oxygen ion and electron (or electron hole) conducting materials, and implications concerning measurement of electrode polarization using the three-electrode system.
- To fabricate anode-supported cells with MIEC cathodes, evaluate performance, and relate it to electrode morphology and space charge effects.

Approach

- Synthesize powders of MIEC and oxygen ion conductors using (a) conventional method comprising mixing oxides or carbonates, milling, and calcining at an elevated temperature; and (b) combustion synthesis method comprising dissolving nitrates in water, adding a water-soluble hydrocarbon fuel, and combusting on a hot plate.
- Fabricate dense and porous bodies of MIEC and oxygen ion conductors.
- Measure total conductivity of porous bodies as a function of temperature and oxygen partial pressure.
- Deposit patterned electrodes using photo micro lithography and measure charge transfer resistivity as a function of oxygen partial pressure and temperature.
- Fabricate anode-supported cells and evaluate cell performance with MIEC cathodes.
- Conduct theoretical analysis of transport through membranes by including electronic conduction and the role of interfaces.
- Experimentally assess applicability of the three-electrode system for study of electrode polarization in solid state electrochemistry.

Accomplishments

- *Developed an Analytical Model for Dependence of Conductivity of Porous Bodies on Morphology and Space Charge*
  The model was verified by measuring conductivity on porous samples of Sm_2O_3-doped CeO_2 (SDC). The results demonstrated that particle-to-particle neck radius in porous electrodes must be as large as possible to ensure low polarization.

- *Developed a Methodology for Deposition of Patterned Electrodes by Photo Micro Lithography*
  Using this methodology, platinum electrodes were deposited on yttria-stabilized zirconia (YSZ) discs, and charge transfer resistivity was measured as a function of temperature and oxygen partial pressure.
- *Developed a Method for the Measurement of Surface Exchange Coefficient of MIEC Materials Using Conductivity Relaxation on Porous Bodies*
  Published work on measurement of the chemical surface exchange coefficient, k_{chem}, is on dense samples. Our work showed that there are significant errors associated with measurements on dense samples. Using a novel approach, k_{chem} was measured as function of oxygen partial pressure and temperature on porous samples of $La_{0.5}Sr_{0.5}CoO_{(3-\delta)}$ (LSC50). This parameter is critical for design of cathodes using MIEC materials.
- *Developed Theoretical Analysis of Transport through Predominantly Oxygen Ion Conducting and MIEC Membranes by Explicitly Taking into Account Interfaces*
  It was demonstrated that charge transfer across interfaces requires two parameters – one for ions and the other for electrons (or electron holes). This analysis has major implications concerning solid state electrochemistry and its applications to devices such as SOFCs and electrolyzers.
- *Constructed and Tested Amperometric Sensors for the Assessment of Three-Electrode System*
  It was demonstrated that the three-electrode system under applied DC bias, a technique commonly used, leads to erroneous measurements of electrode kinetics. Specifically, this technique grossly overestimates electrode activity.

Future Directions

- *Investigate the Effect of Space Charge and Porous Body Morphology on Cathodic Polarization*
  This will be done by incorporating the effective conductivity of porous ionic conductors into the cathode model, which gives polarization resistance as a function of electrode morphology.
- *Fabricate and Test Anode-Supported Cells with Cathodes Annealed at Various Temperatures*
  This will allow an experimental study of the effect of space charge on cathode polarization.
- *Investigate Ionic Conductivity of Dense Rare Earth Oxide Doped Ceria as a Function of Grain Size*
  The objective is to examine the effect of grain size on conductivity – which also provides a measure of the effect of space charge. Samples will be examined by transmission electron microscopy.

Introduction

In order to attain high efficiency and low overall cost of a power generating system based on SOFCs, it is necessary that the system operate at as low a temperature as possible – preferably below 700°C, while still delivering adequate power. However, at low temperatures, the internal resistance of state-of-the-art SOFCs is large, and it is currently not possible to achieve high enough performance. It is now recognized that one of the voltage losses is associated with cathode polarization, which increases with decreasing temperature.

Work done by our group has shown that cathode polarization resistance depends on materials, microstructures, and atmosphere. One objective of this work is to investigate factors related to materials, microstructure and atmosphere, which influence polarization. The material parameter of interest is the effect of grain boundaries and associated effects (such as space charge) on ionic conductivity. Another materials-related parameter is the charge transfer resistivity at electrode/electrolyte interfaces. The microstructure-related parameter relates to inter-particle neck size in porous bodies. The atmosphere-related studies involved measurement of parameters in various atmospheres and at several temperatures. The other objective is to ensure accurate measurement of cathodic polarization. The usual approach is to use the three-electrode system, and measure polarization under applied DC bias. The present work examined the validity of this approach.

Approach

The approach selected was twofold: theoretical and experimental. In the theoretical part, three problems were addressed. They included (1) effect of morphology and space charge on conductivity of porous bodies, (2) effect of oxygen partial pressure and temperature on space charge effects in rare earth oxide doped ceria, and (3) the role of interfaces in transport through oxygen ion and electron conducting membranes. On the experimental side, the approach was as follows. (1) Synthesis of powders by conventional and combustion methods. (2) Fabrication of dense and porous samples of varied microstructures. (3) Measurement of conductivity using four-probe DC method on porous and dense samples. (4) Measurement of surface exchange coefficient by conductivity relaxation. (5) Fabrication of samples with patterned electrodes and investigation of electrode polarization. (6) Fabrication of anode-supported cells and subsequent electrochemical testing. (7) Use of amperometric sensors for investigation of validity of the three-electrode system.

Results

- Demonstrated that electrode morphology (inter-particle neck size) has a large effect on polarization and cell performance. Figure 1 shows calculated polarization resistance as a function of morphology. Developed a method for fabrication of cells with high performance.

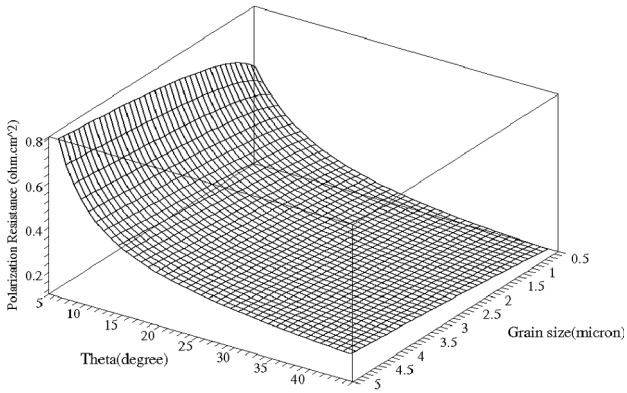

Figure 1. Calculated electrode polarization resistance, using YSZ as the ionic conductor in a composite cathode, as a function of angle (relative neck size) and grain size at 800°C. Note that the polarization resistance rises sharply at small angles (narrow necks).

- Demonstrated that patterned electrodes can be used to compare two different electrodes, free of microstructural effects. Based on this work, it was shown that platinum (Pt) is about 20 times superior to Sr-doped $LaMnO_3$ (LSM). Thus, infiltration of a small amount of Pt should improve performance. This was experimentally verified. Figure 2 shows the experimentally measured charge transfer resistivity as a function of oxygen partial pressure and temperature.
- Demonstrated that conductivity relaxation is an accurate method for measurement of surface exchange coefficient, k_{chem}, of MIEC cathodes. More importantly, work showed that over the temperature range 800 to 450°C, k_{chem} increases with decreasing temperature. Significance? It may be possible to develop cathodes that are highly active at low temperatures. Figure 3 shows the measured k_{chem} on LSC as a function of temperature.
- Fabricated cells with porous SDC cathode interlayer having wide necks. The cells were annealed at various temperatures. The electrocatalyst was introduced by infiltration, and cell performance was measured. Figure 4 shows the results of cell tests at 800°C.
- Developed theoretical analysis of transport through oxygen ion and electron conducting membranes, taking into account interfaces. Fundamental differences between fuel cells and electrolyzers were demonstrated.

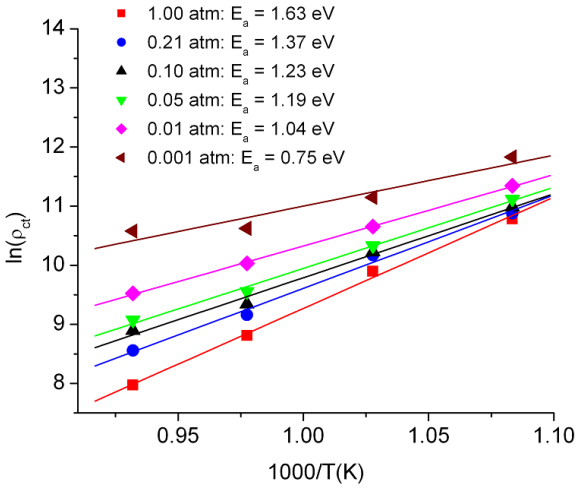

Figure 2. Arrhenius plots of charge transfer resistivity, ρ_{ct}, of platinum over YSZ at various oxygen partial pressures.

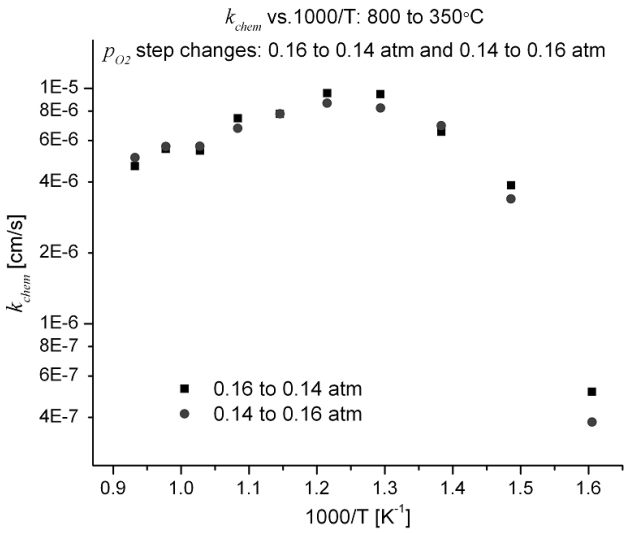

Figure 3. Surface exchange coefficient, k_{chem} vs. 1000/T: 350 to 800°C for the porous LSC50 sample sintered at 1000°C; P_{O_2} step changes from 0.16 to 0.14 atm (increasing and decreasing).

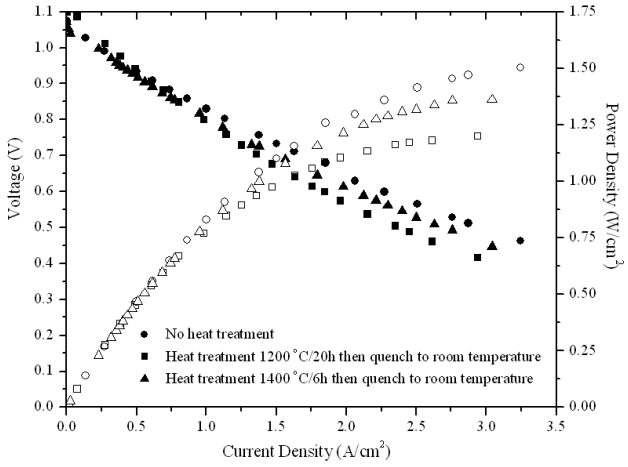

Figure 4. Voltage and power density vs. current density plots at 800°C for cells with cathode fabricated using the infiltration method, wherein the cell with the ionic conductor skeleton in the composite cathode was annealed and then quenched to room temperature prior to cathode infiltration.

Conclusions

- It is possible to lower cathode voltage losses by incorporating improved electrode morphology and addressing space charge effects. This should facilitate development of high-performance SOFCs.
- Measurements showed that k_{chem} increases with decreasing temperature. Thus, it should be possible to develop active cathodes at low temperatures. This should facilitate development of high-performance fuel cells operating at low temperatures – down to 600°C.
- Cells tested with cathodes annealed over a range of temperatures exhibited different performance levels. This observation is in accord with space charge effects.
- Theoretical analysis and experimental work on amperometric sensors showed that the three-electrode system overestimates cathode electrocatalytic activity. Thus, this technique should only be used under zero applied DC bias.

FY 2005 Publications/Presentations

1. "Theoretical Analysis of the Role of Interfaces in Transport through Oxygen Ion and Electron Conducting Membranes", A. V. Virkar, *J. Power Sources*, in press (2005).
2. "Estimation of Charge Transfer Resistivity of Platinum (Pt) Cathode on $Y_{0.16}Zr_{0.84}O_2$ (YSZ) Electrolyte Using Patterned Electrodes", R. Radhakrishnan, A. V. Virkar and S. C. Singhal, *J. Electrochem. Soc.*, 152 (5) A927-A936 (2005).
3. "Investigation of Electrolyte Stability Using Amperometric Sensors: Implications Concerning Electrode Polarization Measurements", A. V. Virkar and Y. Jiang, p. 1057-1067, Solid Oxide Fuel Cells-IX (SOFC-IX), Vol. 2, edited by S. C. Singhal and J. Mizusaki, Electrochemical Society, Proceedings Volume PV 2005-07, Pennington, NJ (2005).
4. "Effect of Microstructure and Space Charge on Cathodic Polarization", F. Zhao and A. V. Virkar, p. 1521-1531, Solid Oxide Fuel Cells-IX (SOFC-IX), Vol. 2, edited by S. C. Singhal and J. Mizusaki, Electrochemical Society, Proceedings Volume PV 2005-07, Pennington, NJ (2005).
5. "Measurement of Transport Properties of Perovskite Cathodes", R. Ganeshanathanan and A. V. Virkar, p. 1487-1498, Solid Oxide Fuel Cells-IX (SOFC-IX), Vol. 2, edited by S. C. Singhal and J. Mizusaki, Electrochemical Society, Proceedings Volume PV 2005-07, Pennington, NJ (2005).

VI Small Business Innovation Research (SBIR), Historically Black College and University (HBCU), & University Coal Research (UCR) Projects

VI SBIR, HBCU, & UCR Projects

VI.1 Materials System for Intermediate-Temperature SOFC

Uday B. Pal (Primary Contact), Srikanth Gopalan, Wenquan Gong
Department of Manufacturing Engineering, Boston University
15 St. Mary's Street
Brookline, MA 02446
Phone: (617) 353-7708; Fax: (617) 353-5548; E-mail: upal@bu.edu

DOE Project Manager: Lane Wilson
Phone: (304) 285-1336; E-mail: Lane.Wilson@netl.doe.gov

Objectives

- Synthesize and evaluate materials system for intermediate-temperature (600-800°C) solid oxide fuel cell (SOFC).
- Electrically test the SOFC fabricated with the intermediate-temperature materials system with the objective of achieving a power density of 0.2-1 W/cm^2.
- Identify industrial partners for manufacturing anode-supported SOFCs with the selected intermediate-temperature materials system.

Approach

- Selected the electrolyte, anode, and cathode materials for the intermediate-temperature SOFC system: lanthanum gallate ($La_{0.9}Sr_{0.1}Ga_{0.8}Mg_{0.2}O_3$ or LSGM) as electrolyte, nickel-gadolinium doped ceria ($Ce_{0.85}Gd_{0.15}O_{2-x}$ or GDC) cermet or nickel-lanthanum doped ceria ($Ce_{0.6}La_{0.4}O_3$) as anode, and LSGM-lanthanum cobaltite ($La_{0.6}Sr_{0.4}Co_{0.8}Fe_{0.2}O_3$ or LSCF) composite as cathode.
- Synthesized and confirmed the suitability of the LSGM electrolyte for intermediate-temperature operation.
- Measured the interfacial polarizations of the candidate electrodes for the LSGM electrolyte utilizing impedance spectroscopy.
- Evaluated lanthanum doped ceria ($Ce_{0.6}La_{0.4}O_3$ or LDC) as an effective barrier layer between LSGM electrolyte and Ni-cermet anode to prevent reaction between Ni in the anode and La in the electrolyte.
- After determining optimum electrode compositions, structures and thicknesses of the cathode and the anode, complete electrolyte-supported planar cells were fabricated and evaluated in terms of their I-V characteristics and stability.
- Based on the electrical performance results of the electrolyte-supported SOFC, the expected performance of an anode-supported SOFC consisting of the intermediate-temperature materials system was modeled.

Accomplishments

- LSGM electrolyte was synthesized. It was found to be stable under fuel cell operating conditions and had the required conductivity to function as an electrolyte for the intermediate-temperature SOFC.
- The optimum cathode, having the least polarization resistance and good thermal expansion match with the LSGM electrolyte, was determined to be a 50-50 volume % LSCF-LSGM composite having a thickness of 30-40 micrometers.
- The optimum anode was found to be a Ni-GDC or Ni-LDC cermet having a thin barrier layer of $Ce_{0.6}La_{0.4}O_{2-x}$ (LDC) between the anode and the LSGM electrolyte.
- Electrical performance of the electrolyte-supported intermediate-temperature SOFC was measured.

- Electrical performance of the anode-supported intermediate-temperature SOFC was modeled and found to provide the desired power density (0.2-1 W/cm^2).

Future Directions

- Explore low-cost manufacturing techniques for fabricating anode-supported intermediate-temperature SOFCs.

Introduction

Solid oxide fuel cells (SOFCs) are comprised of a layered structure of a dense electrolyte sandwiched between porous and permeable electrodes (anode and cathode). They provide a very attractive and versatile means of efficiently converting chemical energy from a wide variety of fossil fuels to electrical energy with much lower environmental impact than conventional power generation systems such as those based on gas turbines. In particular, electrical power generation systems based on SOFCs have the following advantages: high power generation efficiency; cogeneration capability; capability of operating on a wide variety of hydrocarbon fuels and generating much lower levels NOx and SOx; ability to internally reform hydrocarbon fuels; high power-to-weight ratio; noise-less operation; lower manufacturing time; solid-state structures that can be easily transported; and wide range of applications that include stationary, transportation and military uses. More details are available in [1].

It is clear that SOFCs are a very attractive and promising energy conversion technology. However, high processing costs and high operating temperatures are limiting the use of this technology. For commercial viability, there is a need to reduce the fuel cell stack processing cost to not exceed $400/kWe [2]. It is also necessary to identify new electrode-electrolyte materials in order to be able to decrease the operating temperature of the SOFC so that inexpensive manifolding materials can be used and the cost of the initial thermal energy required to heat the cells can be lowered. This work is directed towards the development of a new materials system for the SOFC that can enable lower operating temperatures (600-800°C).

Approach

The material selected to function as the electrolyte for the intermediate-temperature SOFC is strontium and magnesium doped lanthanum gallate, $La_{0.9}Sr_{0.1}Ga_{0.8}Mg_{0.2}O_3$, i.e., LSGM. The primary advantage of selecting LSGM as the electrolyte material in this work is its significantly higher oxygen-ion conductivity at lower temperatures compared to the conventional yttria-stabilized zirconia (YSZ) electrolyte. This work reports the performance in terms of the polarization resistance of several prospective anode and cathode materials for application in the intermediate-temperature (600-800°C) SOFCs employing LSGM electrolyte. However, the performance of a complete cell is described with the best-performing cathode and anode materials systems. For the purpose of demonstration and ease of fabrication, LSGM electrolyte-supported SOFCs with the most optimum cathode and anode materials system, including the barrier layer between the electrolyte and the anode, were electrochemically evaluated between 600-800°C. The results of the electrolyte-supported SOFC were used to simulate the electrical performance of the anode-supported SOFC with the selected materials system.

Results

Based on the results of the electrode polarization studies, complete LSGM electrolyte-supported SOFCs were fabricated for electrochemical evaluation. The cell components had the following dimensions and compositions:

- 1 mm thick dense LSGM electrolyte.
- Dense adherent barrier layer (15 μm) of lanthanum doped ceria (LDC) between the LSGM electrolyte and the anode.
- 50% by volume of Ni-LDC composite anode having a thickness of 30-40 μm and porosity of 25-35%.
- 50% by volume of LSCF-LSGM composite cathode having a fine microstructure (1-2 μm grains), with a porosity of 25-35% and thickness of 30-40 μm.

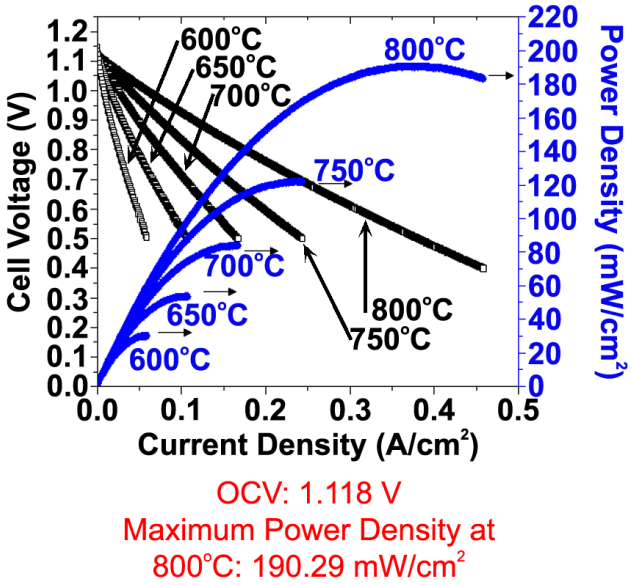

Figure 1. Electrical Performance of LSGM Electrolyte-Supported (1 mm thick electrolyte) SOFC with a LDC Barrier Layer on the Anodic Side

The tested cell had porous electrodes, dense electrolyte and well-bonded cell components. The open circuit voltages (OCVs) at a given temperature in the tested cell are very close to the Nernst potential. The calculated theoretical OCV for the cell at 800°C is 1.126 V when hydrogen is bubbled through water at 25°C (1.8% water vapor). The measured OCV at 800°C was 1.118 V, which was very close to the theoretical value. This result indicated good cell sealing. Shown in Figure 1 are the single-cell voltages and power densities of the LSGM electrolyte-supported cell as a function of the current densities tested at 600°C, 650°C, 700°C, 750°C and 800°C. The maximum power density ranged from 190 mW/cm^2 at 800°C to 30 mW/cm^2 at 600°C.

Since the single-cell testing was conducted on electrolyte-supported SOFCs, the current densities were not very high (below 500 mA/cm^2). Both electrodes (cathode and anode) had high porosity, and their thicknesses were small (around 30-50 µm), so the concentration polarization was negligible. At higher current densities, the relationship between the cell voltage and current density can be fitted as per the following equation:

$$E_{cell} = OCV - i \times R_{ohm} - (a + b \times \ln i) \qquad (8)$$

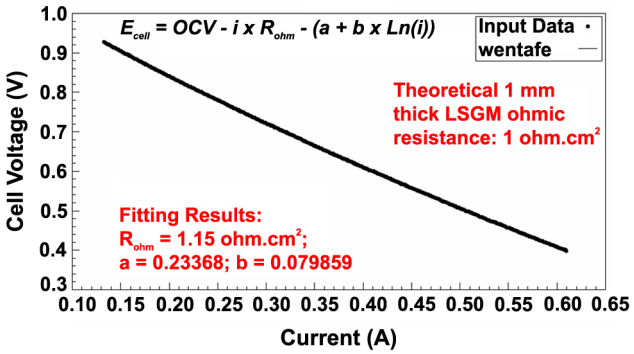

Figure 2. Modeling Electrode Polarization from Electrical Performance Data at 800°C of LSGM Electrolyte-Supported (1 mm thick electrolyte) SOFC with a LDC Barrier Layer on the Anodic Side

The experimental data was fitted to the above equation with three parameters, namely, R_{ohm}, a, and b. As seen in Figure 2, equation 8 fitted the experimental data well at 800°C. Similar fittings were obtained at other temperatures. R_{ohm} primarily consists of the ohmic resistances of the electrolyte, anode, cathode, current collectors, and the interfacial resistances between the electrodes and the electrolyte. The electrolyte resistance, R_{el}, can be calculated according to the thickness (1 mm) and the ionic conductivity measured earlier by the four-probe method. It was observed that R_{el} is a major portion (>95%) of R_{ohm}.

The performance stability of the LSGM electrolyte-supported SOFC was evaluated by operating the cell at 800°C starting with 0.72 V and a current density of 350 mA/cm^2. There was an initial 5% decay in the performance, but the cell stabilized after 3,500 minutes.

Higher power densities can be achieved with anode- or cathode-supported SOFCs rather than the electrolyte-supported SOFC. Such a cell may have the following component dimensions:

- 50% by volume of Ni-LDC composite anode having a fine microstructure near the LDC barrier layer and coarser microstructure away from the barrier layer; porosity 25-35%. Since the design is based on an anode-supported cell, the anode can be 1-2 mm thick and the fine microstructure region at least 30-40 µm thick.

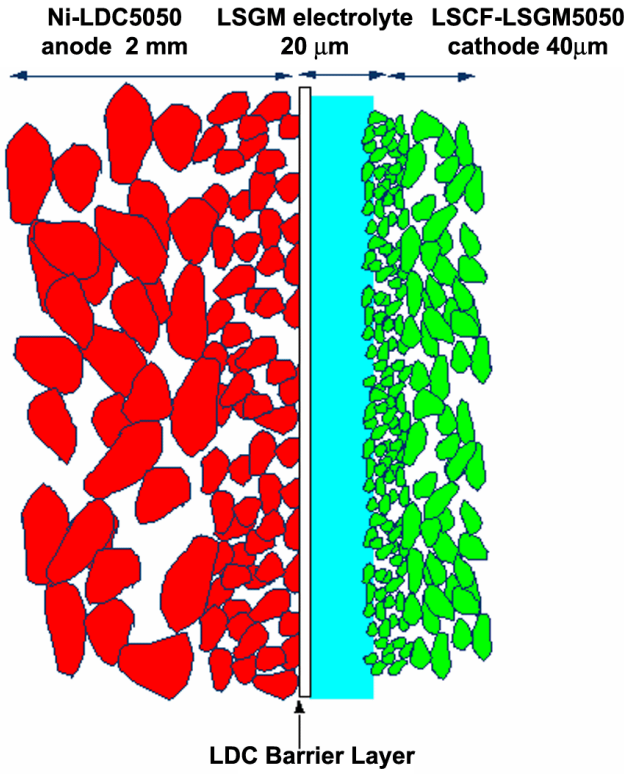

Figure 3. Schematic of the Desired Structure of the Anode-Supported Intermediate-Temperature SOFC Based on the LSGM Electrolyte

- A dense adherent barrier layer (5 μm) of lanthanum doped ceria (LDC) between the LSGM electrolyte and the anode.
- 10-20 μm thick dense LSGM electrolyte.
- 50% by volume of LSCF-LSGM composite cathode having a fine microstructure (1-2 μm grains), porosity of 25-35% and thickness of at least 30-40 μm.

The cell structure is schematically shown in Figure 3. The cell performance of this anode-supported SOFC based on the LSGM electrolyte can be simulated using the experimental results from the tested LSGM electrolyte-supported SOFC, since both cells consist of the same electrolyte and electrode materials. The only difference is the thickness of electrolyte and anode. The thickness of the electrolyte is 1 mm for the electrolyte-supported cell, but it is 20 μm for the anode-supported cell, while the thickness of the anode is around 30 μm for the electrolyte-supported cell, but is 1-2 mm for the anode-supported cell. The change in thickness of the

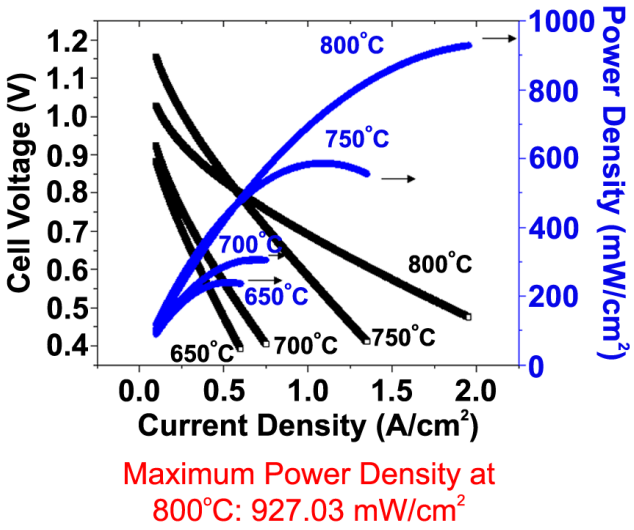

Figure 4. Simulated Electrical Performance of an Anode-Supported SOFC Based on the LSGM Electrolyte (20 m thick) with a LDC Barrier Layer on the Anodic Side

electrolyte will only influence the ohmic resistance of the electrolyte, R_{el}, and the changing thickness of the anode will only influence the concentration polarization of the cell. The desired anode-supported cell will use a graded electrode structure, i.e., coarser connected porosity away from the electrolyte-electrode interface to facilitate gas transport and finer connected porosity close to the electrolyte-electrode interface to aid in the charge-transfer reactions. The ideal anode-supported SOFC is thus expected to have negligible concentration polarization, and the electrode polarization behavior should be similar to that of the electrolyte-supported SOFC. Therefore, the difference in the performance of the tested electrolyte-supported cell and the ideal anode-supported cell will be due to the difference in the respective ohmic resistances of the electrolyte. Using the parameters obtained by modeling the electrode polarization behavior of the electrolyte-supported SOFC in equation 8, the cell performance of the ideal anode-supported SOFC based on LSGM electrolyte is simulated in Figure 4. Shown in Figure 4 are the simulated cell voltages and power densities of the ideal anode-supported LSGM cell as a function of current densities at 650°C, 700°C, 750°C and 800°C. The maximum power density ranges from 927 mW/cm^2 at 800°C to 239 mW/cm^2 at 650°C.

Conclusions

The objective of this work was to obtain a stable materials system for intermediate-temperature solid oxide fuel cells (SOFCs) capable of operating between 600-800°C with a power density greater than 0.2 W/cm^2. The solid electrolyte chosen for this system was $La_{0.9}Sr_{0.1}Ga_{0.8}Mg_{0.2}O_3$ (LSGM). To select the right electrode materials from a group of candidate materials, AC complex impedance spectroscopy studies were conducted between 600-800°C on symmetrical cells that employed the LSGM electrolyte. Based on the results of the investigation, LSGM electrolyte-supported SOFCs were fabricated with $La_{0.6}Sr_{0.4}Co_{0.8}Fe_{0.2}O_3$-$La_{0.9}Sr_{0.1}Ga_{0.8}Mg_{0.2}O_3$ (LSCF-LSGM) composite cathode and nickel-$Ce_{0.6}La_{0.4}O_3$ (Ni-LDC) composite anode having a barrier layer of $Ce_{0.6}La_{0.4}O_3$ (LDC) between the LSGM electrolyte and the Ni-LDC anode. Electrical performance and stability of these cells were determined, and the electrode polarization behavior as a function of cell current was modeled between 600-800°C. The electrical performance of the anode-supported SOFC was simulated assuming an electrode polarization behavior identical to the LSGM electrolyte-supported SOFC. The simulated electrical performance indicated that the selected material system would provide a stable cell capable of operating between 600-800°C with a power density between 0.2 to 1 W/cm^2.

FY 2005 Publications/Presentations

1. Wenquan Gong, Srikanth Gopalan and Uday B. Pal, "Cathodic Polarization Study on Doped Lanthanum Gallate Electrolyte Using Impedance Spectroscopy", Journal of Electroceramics, vol. 13, 2004, p. 653.
2. Wenquan Gong, Srikanth Gopalan and Uday B. Pal, "Materials System for Intermediate Temperature (600-800°C) Solid Oxide Fuel Cells (SOFCs) Based on Doped Lanthanum-Gallate Electrolyte", Accepted for Publication in the Journal of The Electrochem. Society, April 2005.
3. Wenquan Gong, "Materials System For Intermediate Temperature Solid Oxide Fuel Cells Based on Doped Lanthanum–Gallate Electrolyte", Ph.D. Thesis, 2005, Boston University, Boston, MA.
4. June 2005, "Materials System for Intermediate Temperature Solid Oxide Fuel Cell", DOE-UCR Meeting, Pittsburgh, PA.

References

1. S. Srinivasan, R. Mosdale, P. Stevens, and C. Yang, "Fuel Cells, Reaching the Era of Clean and Efficient Power Generation in the Twenty-First Century," *Annual Review of the Energy and the Environment, 24*, Edited by R. H. Socolow, Annual Reviews, Pao Alto, CA, 281 (1999).
2. Internet Bulletin of the Solid State Energy Conversion Alliance, NETL, Pittsburgh, PA, *http://www.seca.doe.gov/Publications/seca_related_documents.htm*

VI.2 Lanthanum Gallate Electrolyte Based Intermediate-Temperature Solid Oxide Fuel Cell Development

S. (Elango) Elangovan
Ceramatec, Inc.
2425 South 900 West
Salt Lake City, UT 84119-1517
Phone: (801) 978-2162; Fax: (801) 972-1925; E-mail: Elango@ceramatec.com

DOE Project Manager: Lane Wilson
Phone: (304) 285-1336; E-mail: Lane.Wilson@netl.doe.gov

Subcontractors:
Sandia National Laboratory, Albuquerque, New Mexico, contact: Dr. Ron Loehman
New Mexico Tech, Socorro, New Mexico, contact: Prof. Deidre Hirschfeld

Objectives

- Evaluate alternative anode materials in order to reduce anode-electrolyte reactivity
- Develop tape cast process to fabricate thin electrolyte cells
- Fabricate single cells using a supported structure
- Demonstrate intermediate-temperature fuel cell operation
- Test short stacks using 10x10 cm cells
- Evaluate mechanical properties of gallate material

Approach

- Modify the anode composition and verify reduction in reactivity using x-ray diffraction of reacted anode-electrolyte powder mixture
- Perform tape sintering studies to fabricate supported single cells
- Test single cells at 700 – 800°C for short-term and long-term performance
- Measure strength of gallate bars

Accomplishments

- Determined that the modification introduced into the nickel-based anode reduced the reactivity between nickel and lanthanum gallate
- Fabricated single cells using thin supported electrolyte with electrolyte thickness ranging from 30 to 75 microns
- Demonstrated single-cell performance with an area-specific resistance of 0.5 ohm-cm^2 at 700°C
- Demonstrated stable 2,500-hour performance at an operating temperature of 700°C
- Characterized mechanical strength of gallate at room temperature and at 800°C

Future Directions

- Fabricate full-size (10x10 cm) thin electrolyte cells
- Perform stack tests to verify performance and stability benefits demonstrated in single cells
- Evaluate alternative cathode materials for intermediate-temperature operation

Introduction

Reducing the operating temperature of solid oxide fuel cells (SOFCs) offers several benefits: improvement in long-term stability by slowing physical and chemical changes in the cell materials; lower-cost systems by the use of less expensive balance of plant components; compatibility with hydrocarbon reformation process, allowing partial internal reformation, which in turn reduces the heat exchanger duty; and, finally, the potential to improve thermal cycle capability. In addition, the use of stainless steel interconnects is facilitated by the lower operating temperature. A temperature range of 650 to 700°C is ideally suited to derive the performance stability, system integration and cost benefits.

In order to derive the advantages of the lower operating temperature, two factors that limit the cell performance, namely the electrolyte resistance and electrode polarization, must be addressed. Lanthanum gallate compositions have shown high oxygen ion conductivity when doped with Sr and Mg. Unlike other oxygen ion conductors such as ceria and bismuth oxide that are potential candidates for lowering cell operating temperature, the Sr- and Mg-doped lanthanum gallate (LSGM) compositions are stable over the oxygen partial pressure range of interest. The combination of stability in fuel gas environment and the high oxygen ion conductivity makes the LSGM material a potential choice for intermediate-temperature SOFCs. However, challenges in the development of electrode materials and cell fabrication processes need to be overcome to make use of the potential of the LSGM electrolyte.

Approach

The nickel-based anode has been successfully demonstrated to be catalytic for fuel oxidation in zirconia electrolyte based SOFC systems. A modified nickel anode composition was evaluated using powder mixtures of the anode and LSGM electrolyte. The reacted powder mixture was analyzed using x-ray diffraction technique. Additionally, an 8-cell stack was tested for over 1,000 hours, and the anode-electrolyte interface was analyzed using scanning electron microscopy for evidence of nickel diffusion into the electrolyte.

Tape cast process development was performed to cast LSGM tape of various thicknesses to provide sintered electrolyte thicknesses ranging from 75 to 300 microns. The process variables included powder surface area, organic content in the tape slip, and sintering temperature. The primary objectives of the activity were to achieve sintered electrolyte density and flatness required for stacking. Single cells with 1 to 2.5 cm^2 active area were tested for performance characteristics and long-term stability.

Mechanical property evaluation was done at the Sandia National Laboratories to measure electrolyte strength after subjecting bar samples to various exposure and thermal cycle operations.

Results

The modification to the nickel anode was found to significantly reduce the reactivity with the LSGM electrolyte. X-ray diffraction pattern for the powder mixture of the anode-electrolyte calcined at 1,300°C is shown in Figure 1. Diffraction pattern for the baseline LSGM, NiO, and a mixture of the two are also shown in the figure. It can be seen that the reaction phase peaks prominent in the baseline mixture are significantly reduced in their intensities for the modified anode.

In order to verify the long-term stability of the anode-electrolyte interface, a stack was built and tested for 1,200 hours. Although performance degradation was observed, attributable to chromium evaporation from the interconnect, scanning electron

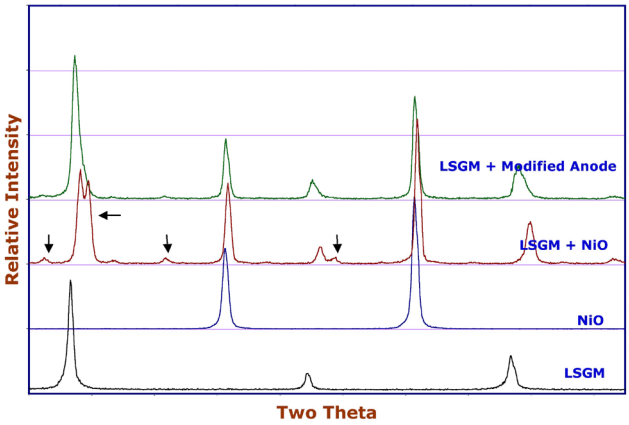

Figure 1. Powder X-ray of Baseline and Reacted Electrolyte, Anode Powders

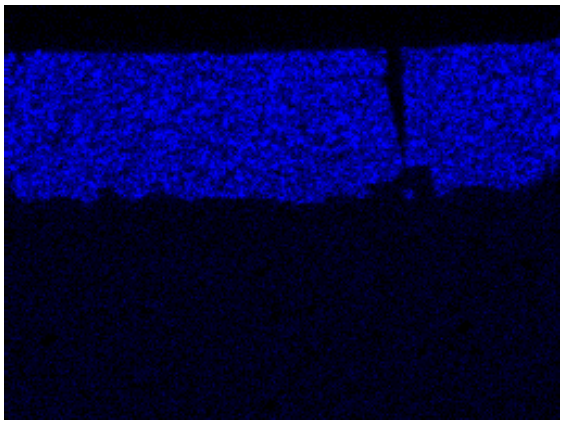

Figure 2. Nickel Map of Anode-Electrolyte Interface after 1,200-hr Stack Test

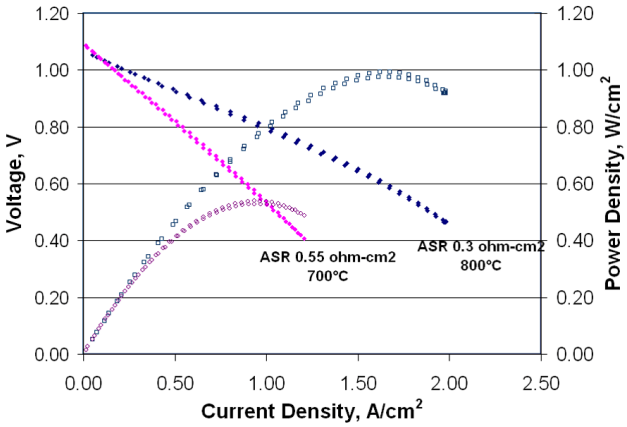

Figure 3. Performance of a Cathode-Supported LSGM Cell; Electrolyte Thickness of 75 Microns Was Used

microscopy of the anode-electrolyte interface showed no detectable diffusion of nickel into the electrolyte or an interfacial reaction product. The nickel x-ray map is shown in Figure 2.

Thin electrolyte single cells were fabricated using tape lamination technique. Both anode and cathode structures were evaluated as the support for the electrolyte. The performance of a cathode-supported cell is shown in Figure 3. The thin, 75-micron LSGM electrolyte cells showed an area-specific resistance (ASR) of 0.5 ohm-cm^2 at an operating temperature of 700°C. The long-term performance of selected cells is shown in Figure 4. Similar performance and stability results were also obtained using cells with the anode-support configurations. Thus, the performance benefits of using high-conductivity LSGM electrolyte and the

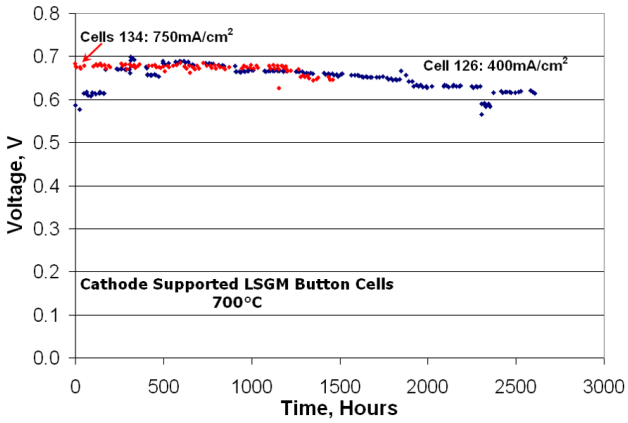

Figure 4. Long-Term Stability of Cathode-Supported Cells at an Operating Temperature of 700°C

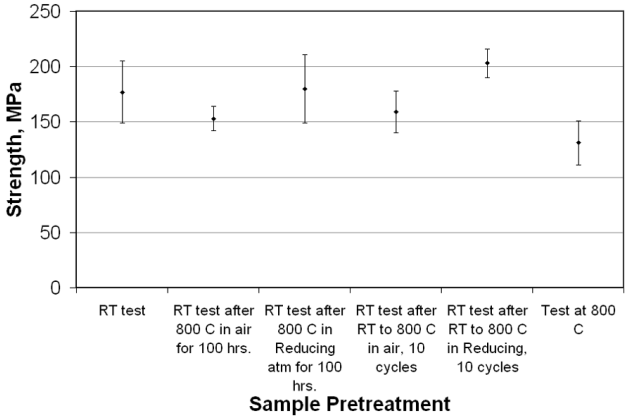

Figure 5. Strength Measurement of Gallate Bars at Room Temperature (RT)

stability improvement by using the modified anode were established in single-cell tests.

Mechanical characterization of gallate material was performed using ASTM bar samples. Both room-temperature and high-temperature strengths were evaluated. The results are summarized in Figure 5.

Conclusions

- Sr- and Mg-doped lanthanum gallate compositions show exceptionally high oxygen ion conductivity and stability in SOFC operating conditions for use at the intermediate temperatures of 650 – 700°C.
- The anode reactivity that is known to cause long-term instability has been addressed by introducing a modification to the nickel-based anode composition.

- A 1,000-hr stack test provided additional confirmation on the effectiveness of the anode modification.
- Thin, supported cells meet the performance target of 0.5 ohm-cm^2 resistance at 700°C.
- Long-term tests of single cells show stable performance.
- Mechanical tests show that the gallate material has adequate strength. Further improvement can be made by fabrication process improvements.

FY 2005 Presentations

1. Intermediate Temperature SOFC Operation Using Lanthanum Gallate Electrolyte, S. Elangovan, S. Balagopal, J. Hartvigsen, M. Timper, and D. Larsen, 29th International Conference on Advanced Ceramics and Composites, Second International Symposium on Solid Oxide Fuel Cells: Materials And Technology, January 2005.
2. Intermediate Temperature SOFC Operation Using Lanthanum Gallate Electrolyte, SECA Core Technology Program Review, Tampa, FL, January 27, 2005.

VI.3 Advanced Net-Shape Insulation for Solid Oxide Fuel Cells

Balakrishnan Nair (Primary Contact), Akash, Q. Zhao, and J. Persson
Ceramatec, Inc.
2425 S. 900 W.
Salt Lake City, UT 84115
Phone: (801) 956-1000; Fax: (801) 972-1925; E-mail: BNair@ceramatec.com

DOE Project Manager: Travis Shultz
Phone: (304) 285-1370; E-mail: Travis.Shultz@netl.doe.gov

Objectives

- Develop a new product line of low-cost, alumina-based, net-shape insulation materials for solid oxide fuel cell (SOFC) systems.
- Optimize materials processing to achieve the lowest possible thermal conductivity in CERCANAM (Ceramatec castable nano material) materials.
- Develop thick tape casting technology for CERCANAM insulation materials for low-cost bulk production.
- Demonstrate long-term stability (>2000 hours) of yttria-stabilized zirconia (YSZ) and lanthanum strontium magnesium gallate (LSGM) button cells with selected CERCANAM compositions in the fuel and air sides.

Approach

- Evaluate specific processing routes for their applicability to make insulation parts with low density and low thermal conductivity.
- Test the effect of different types of pore formers on the density and thermal conductivity of CERCANAM samples.
- Study the effect of specific binders and plasticizers on the aqueous-based tape casting technique to obtain various thicknesses, and laminate the tape to form 6”×6” slabs with 0.25” thickness.
- Use finite element modeling to simulate the insulating performance of CERCANAM materials.
- Test the long-term performance of YSZ- and LSGM-based button cells with the CERCANAM materials in the air/fuel streams.

Accomplishments

- *The density and thermal conductivity of CERCANAM materials have been successfully decreased from 0.8 g/cc to 0.57 g/cc and from 0.35 W/m-K to 0.16 W/m-K, respectively.*
  Using different pore formers at different volume contents and by using various processing techniques, the density of CERCANAM materials can be adjusted down to 0.57 g/cc and the thermal conductivity (at 600°C) can be lowered to 0.16 W/m-K.
- *Detailed 3-D thermal modeling of the insulation system was carried out.*
  Preliminary results show that about 4”-thick CERCANAM insulation would be sufficient to insulate a 1-kW SOFC stack, with sufficiently high thermal efficiency.
- *A thick tape casting technique was developed to produce 200-275 µm thick CERCANAM tape, which can be laminated to form slabs at high-volume production rate.*
  By using appropriate amount of binder and controlling the viscosity of the aqueous slurry, thick CERCANAM tape can be produced from CERCANAM slurry with various thicknesses. Those tapes can easily be laminated into slabs with built-in features. With Ceramatec’s existing tape casting capabilities, this technique forms the basis of a cost-effective, pilot-scale production process for CERCANAM insulation materials.

- *6"×6"×1/2" CERCANAM panels and other complex shape products were made by pressing technique.* By pressing CERCANAM powders, large size and complex shape products, such as square, circular, or tubular structures, can be made with good surface finishing.

Future Directions

- *Fabricate a test set-up using CERCANAM insulation for simulated stack testing.* A test set-up will be fabricated which will help to verify the thermal efficiency of SOFC stacks insulated with CERCANAM insulation, as determined by the thermal model. The test set-up will consist of an Inconel combustion chamber where air and fuel (H_2 or methane) can be brought in and combusted. The inside of the combustion chamber will be insulated with CERCANAM insulation. The post-combustion gas temperature, the inside wall temperature of the CERCANAM and the surface temperature of the Inconel reactor will be measured.
- *Further reduce the cost of CERCANAM insulation.* By using low-cost alumina powders and fibers (Saffil), the cost of CERCANAM materials can be decreased to make it economical for use in fuel cells. The cost target is \$350/ft^3 for large-volume production. Five kinds of powders from a potential vendor and two kinds of fibers are under evaluation. The mechanical properties, density, thermal conductivity, and the fuel cell compatibility will be carefully examined to qualify those low-cost materials.
- *Qualify CERCANAM for SOFCs by performing long-term testing (>2000 h) with CERCANAM in the air/fuel streams of SOFCs.* Once optimum CERCANAM compositions are identified, tests will be carried out to demonstrate the stability of YSZ- and LSGM-based button cells when CERCANAM is present in the air and fuel flow streams. Long-term SOFC stability will be evaluated for up to 2000 h.
- *Estimate the installed cost savings.* Cost savings will be estimated through a very high-level comparison of the cost of CERCANAM insulation and that of a "conventional" insulation approach. For maximum effectiveness, the conceptual partial oxidation (POX) SOFC system design developed by Arthur D. Little for DOE in 2000 will be used as a baseline.
- *Fabricate sub-scale tubular structures by tape casting, tape winding and sintering and qualify them for tubular fuel cell insulation.* Sub-scale tubular structures will be fabricated by winding dense and porous alumina tape around collapsible mandrels. The final goal will be to fabricate at least full-scale layered parts which can be supplied to Siemens-Westinghouse Power Corporation for evaluation.

Introduction

The goal of this project is to develop a low-cost insulation material for SOFCs. Cost considerations are becoming the primary barriers to commercialization of SOFCs, and the cost of insulation as a percentage of the total cost is becoming higher as the costs of other components of the system are lowered. The current options from insulation material manufacturers are not viable either due to high cost or low reliability/lifetime. We are developing a new product line of low-cost, alumina-based insulation materials that can provide efficient thermal shielding for SOFC systems. In addition, this product can be made by near net-shape or net-size techniques, which will further decrease the installed cost of SOFC insulation.

Approach

In order to fabricate net-shape insulation material cost-effectively, it is necessary to eliminate post-machining operations. CERCANAM is a reaction-bonded alumina material developed at Ceramatec which uses standard ceramic oxide powders and can be formed by traditional mass production methods for ceramics, such as casting, pressing, and tape casting followed by a low-temperature (~800°C) firing.

In order to make CERCANAM material suitable for SOFC insulation applications, fugitive pore formers are used in CERCANAM compositions, and advanced casting techniques have been investigated to decrease the thermal conductivity and density. Long-term button cell tests with CERCANAM samples at anode and cathode sides will demonstrate their compatibility with fuel cell systems. Prototype insulation systems will be built using CERCANAM materials based on thermal modeling results and qualified for SOFC applications.

Results

In order to achieve low thermal conductivity and density for CERCANAM materials, two different variables were studied – slip formulation and processing methods. The effect of pore former content on the density of cast CERCANAM samples is shown in Figure 1. The increase of pore former content results in lower density and higher open porosity. The effect of different types of pore formers on CERCANAM samples was also evaluated. The samples with pore formers from different vendors gave different densities, but results on thermal conductivity did not show any apparent difference between the samples made with different pore formers. Therefore, the selection of pore former can be based on bulk raw materials cost and the density requirement of the final product.

Various processing options are available to manufacture large, complex shapes: slip casting, tape casting, and/or dry powder pressing. Each of these processes results in CERCANAM materials with different microstructures and properties. Further, certain processes might allow a higher degree of complexity in fabricated parts. Such flexibility could become an important factor in our commercialization efforts, depending upon the final product requirements.

An alternate processing method has been developed that gives substantially lower densities than slip casting. The results are shown in Figure 2 and compared with samples made via the conventional slip casting method. Clearly, the samples made according to this new process have lower density and thermal conductivity compared to slip cast samples. In another run using this new process, a 39 vol% pore former containing sample showed thermal conductivity at 600°C as low as 0.16 W/m-K with a density of 0.57 g/cc and open porosity of 81%.

Figure 3 shows CERCANAM parts of various shapes and sizes that have been fabricated through this project. For cost-effective pilot-scale production and bulk manufacturing of CERCANAM, the most attractive processing technique is thick tape casting. By conducting a series of tape casting experiments with slips containing different binder contents and binder-to-plasticizer ratios, the optimum tape was obtained. The tapes were 200-275 μm thick and were dried at room temperature in order to minimize cracking or curling during drying. Two to four layers of tapes, in 1”-2” disc form, have also been successfully laminated together via heat lamination under pressure.

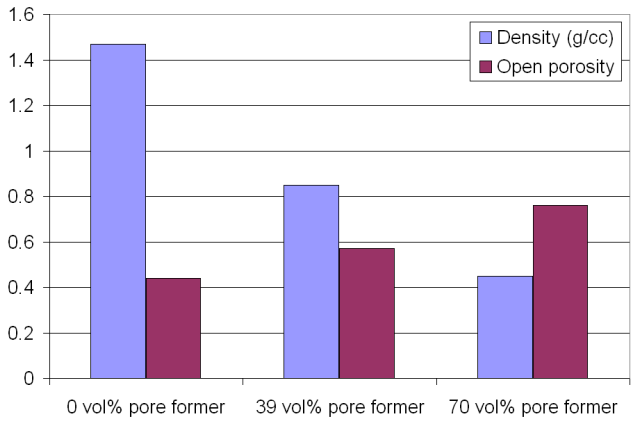

Figure 1. Effect of Pore Former Addition on Sample Density

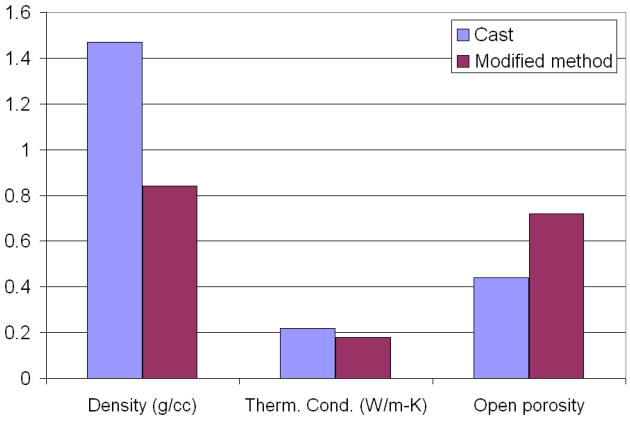

Figure 2. Comparison of Results from Two Different Forming Methods for CERCANAM Samples (without pore formers)

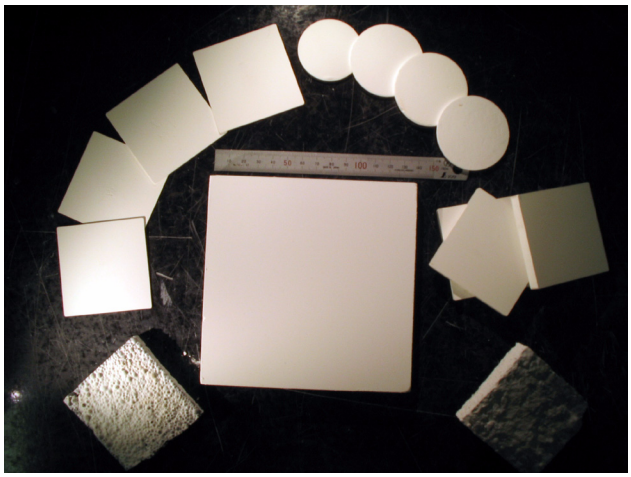

Figure 3. CERCANAM Insulation Materials Fabricated in Various Shapes and Sizes

A dry powder pressing study was carried out to map the effect of pressure on density and strength of formed parts. Results show that low-pressure forming can provide the same low-density samples as the tape casting technique, but with better surface finished parts. The dry pressing approach offers the advantage of significantly faster processing times and better-quality parts. Further, near **net-size** parts of varying complexity can be easily fabricated using this approach.

In order to obtain some insights on the volume of CERCANAM material required to insulate a 1-kW stack, a 3-D steady-state heat transfer model was built based on a two-layer insulation system using CERCANAM materials as the front layer and commercial microporous silica insulation material as the back layer. The model assumes an inside wall temperature of 850°C, typical of a SOFC, and a cavity large enough to house a 1-kW stack. The temperature profile through the insulation layers is shown in Figure 4. The insulation requirements are also affected by the heat loss due to the forced convection from the outside. In the case of no forced convection and using a standard CERCANAM insulation material with thermal conductivity 0.2 W/m-K, an insulation layer with total thickness of 7.7" can make the outer wall surface temperature decrease to 60°C. However, as shown in Figure 4, with a 20 W/m^2-K forced convection, the total thickness of the insulation layer can be further decreased to less than 4". This is quite typical of SOFC systems and corresponds to a thermal energy loss of less than 20% of the stack power output. A

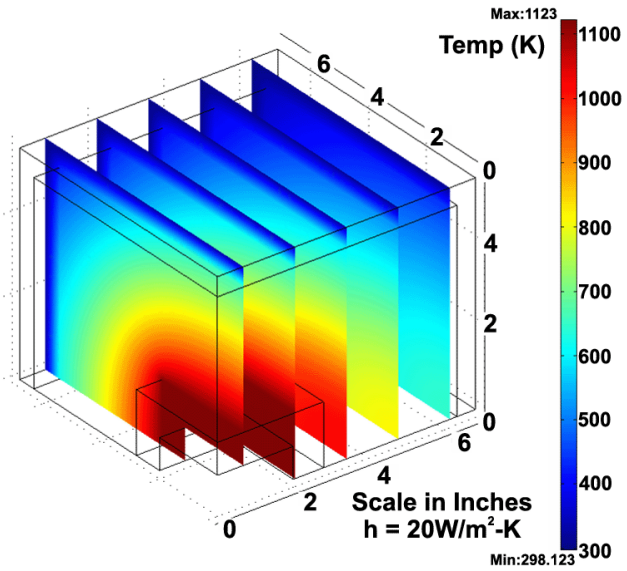

Figure 4. Thermal Modeling Results on the Temperature Profile of Two-Layer Insulation System with Inside Wall Temperature of 850°C, and a Cavity Large Enough to House a 1-kW Stack

prototype thermal insulation box will be built based on the above information to further qualify CERCANAM materials under SOFC operation conditions. Work is currently directed at cost-based optimization of the insulation system (amount of CERCANAM and microporous silica to be used), and the refinement of the model by coupling with a model that can predict the heat output and temperature profile of an actual 1-kW stack in operation.

Conclusions

- By adjusting the pore former content and using a new processing technique, CERCANAM samples with low density (0.57 g/cc) and low thermal conductivity (0.16 W/m-K) have been made.
- Larger area (in the order of ft^2) CERCANAM tape has been successfully made by tape casting, and samples with various shapes have been made via a new dry powder pressing (near net-size and near net-shape forming) technique.
- Stack thermal modeling has been developed to obtain a global thermal model to estimate the amount of CERCANAM insulation and other secondary insulation materials needed to ensure a tolerable thermal efficiency for the whole SOFC system.

Special Recognitions & Awards/Patents Issued

1. CERCANAM was selected as the winner of the 2004 Annual Stoel Rives Utah Innovation Award under the Mechanical Devices and Advanced Materials Category.

FY 2005 Publications/Presentations

1. A. Akash et al., "Advanced Net-Shape & Net-Size Insulation for Solid Oxide Fuel Cells," the annual ACERS conference at Cocoa Beach, FL, January 23-28, 2005.
2. B. Nair et al., "Advanced Net-Shape Insulation for Solid Oxide Fuel Cells," DOE SBIR Phase II Semi-Annual Report, February 18, 2004.
3. A. Akash, B. Nair, M. Wilson, Q. Zhao, and J. Persson, "Net-Shaped Nanoceramics," Amer. Ceram. Soc. Bull., Vol. 84 [6], 16-18, 2005.
4. A. Akash, B. Nair, J. Hartvigsen, M. Wilson, Q. Zhao, and J. Persson, "Net Shape Ceramic Components for Fuel Cell Systems," to be published in Fuel Cell Review Magazine.

VI.4 Carbon Ionic Conductors for Use in Novel Carbon-Ion Fuel Cells

F.H. Cocks (Primary Contact), W. N. Simmons, P.A. Klenk
Duke University
Pratt School of Engineering
Box 90300
Durham, NC 27708
Phone: (919) 660-5301; E-mail: hadley01@duke.edu

DOE Project Manager: Travis Shultz
Phone: (304) 285-1370; E-mail: Travis.Shultz@netl.doe.gov

Objectives

- To evaluate the possibility that ionic carbides could act as superionic membrane materials for carbon ions, allowing the development of a radically new fuel cell based on the transport of carbon ions rather than hydrogen or oxygen ions.

Approach

- Stabilization of the fluorite crystal structure via combining at least two lanthanides having substantially different ionic radii.
- Preparation of pseudo-binary ionic carbide compounds using carbon-13 together with the diffusion of carbon-12 vapor-deposited layers.
- Analysis of the in-diffusion profiles of carbon-12 into pseudo-binary ionic carbide compounds using SIMS (secondary ion mass spectrometry) to determine carbon ion diffusivities in these materials.
- Use of the Nernst-Einstein equation to estimate ionic mobilities from the measured diffusion data.

Accomplishments

- Successfully developed a novel method of preparing lanthanide carbides by sintering lanthanum oxide/ carbon admixtures heated to very high (>2500°C) temperatures using electron beam heating.
- Successfully prepared Ce-Tm carbide produced with carbon-13.
- Successfully stabilized La-Er carbide, La-Ce carbide, and La-Y carbide produced with carbon-13 so that these compounds retain the cubic fluorite structure in the temperature range from 300 K to 2800 K.
- Successfully coated/heat-treated and measured ionic mobility in La-Er carbide and La-Ce carbide.

Future Directions

- Determine the in-diffused carbon-12 depth profile using secondary ion mass spectrometry for Ce-Tm carbide.
- Calculate the carbon ion mobility using the Nernst-Einstein equation for Ce-Tm carbide.

Introduction

Carbon-consuming fuel cells have many potential advantages, including increased efficiency and reduced pollution. A large amount of work has already been done on coal fuel cells which utilize yttria stabilized zirconium carbide as an oxygen-ion superionic membrane material. However, no superionic membrane material for carbon ions is yet known. Such a solid-state superionic membrane material would enable an entirely new class of carbon fuel cell to be developed that would use coal

directly as the fuel source, without any intervening combustion process. A carbon-ion superionic conductor would be an enormous step forward because it would allow the direct conversion of coal to electricity without the formation of any of the pollutants (SO_2, etc.) other than CO_2 that can accompany coal combustion. Fuel cells utilizing yttria stabilized zirconium can require combustion of coal to carbon monoxide before final oxidation to carbon dioxide utilizing the oxygen-ion membrane. The objective of this research is to investigate specific ionic lanthanide carbide and ionic lanthanide carbide pseudo-binary solid solutions as possible superionic carbide-ion conductors. The discovery of such a material would have the potential of ushering in a truly revolutionary new coal technology.

Rare earth carbides have the fluorite structure when they are above their transition temperatures, which vary from 350°C (EuC_2) to 1450°C (LuC_2). This structure is perhaps the crystal structure most widely found in superionic materials. These cubic lanthanide carbide compounds could potentially be good ionic conductors for carbon.

Approach

Rare earth carbides of the form LnC_2 (where Ln refers to any element of the lanthanide series) are being investigated as potential superionic membrane materials. These compounds have the fluorite structure when they are above their transition temperatures. The carbon atoms in these compounds reside as anions in tetragonal positions equivalent to the positions of the mobile ions, F_- and O_{2-}, in the known superionic conductors CaF_2 and $Zr_{0.8}Y_{0.2}O_2$. Rare earth carbides represent perhaps the most favorable class of superionic carbon membrane materials. However, it is necessary to stabilize the cubic fluorite structure which these compounds exhibit at elevated temperature so that this structure is stable down to room temperature. Such stabilization is being sought by alloying rare earth carbides with substantially different lattice parameters. Carbon ion diffusivity is being measured via the in-diffusion of carbon-12 into the base carbide compound produced with carbon-13.

Results

The lanthanide dicarbides have been synthesized by reacting mixtures of Ln_2O_3 and amorphous ^{13}C under vacuum at high temperatures (>1600°C), using a newly developed synthesis technique which we have termed the reactive oxide electron beam (REOB) synthesis technique. These dicarbides were subsequently densified at high temperatures (<2500°C) using electron beam heating. Direct production of these materials by means of direct melting of lanthanide-series metals and carbon using water-cooled copper hearth arc-melting was found to be ineffective due to the uncontrollable dispersion of the carbon as a result of the arc blow generated by the high arc current.

La-Er carbide, La-Ce carbide, La-Y carbide, and Ce-Tm carbide have been successfully produced using the REOB procedure. Powder x-ray diffraction was used to confirm that their crystal structures remained stable in the fluorite structure in the temperature range of 300-2800 K. These compounds have been produced with carbon-13 in order that vapor-deposited carbon-12 coatings could be used in the diffusion measurements, since carbon-13 arcing electrodes or sputtering targets do not appear to be available from any source world-wide. Either arc evaporation or sputtering is needed to produce an adherent film for the high-temperature in-diffusion treatment.

Semi-thick coatings (>10 m) of ^{12}C were deposited on these samples using the arc-evaporation of high-purity commercially available graphite electrodes. Natural graphite contains ~1.11% carbon-13 and 99% carbon-12. The small amount (1%) of carbon-13 contained in this graphite can be readily factored into and mathematically accounted for in the deconvolution of the measured carbon-12 in-diffusion profile. To produce these samples, coated samples are being heated at 850°C, 950°C, and 1150°C in a custom-built high-vacuum furnace. Prolonged SIMS sputtering is being used to determine the complete surface-to-baseline carbon-12 diffusion profiles. From these measurements, together with semi-infinite diffusion equations, the carbon-12 diffusion constant can be determined, which is then used in the Nernst-Einstein equation to calculate carbon ion mobilities.

Conclusions

- A novel method for preparing lanthanide carbides by sintering lanthanum oxide/carbon admixtures heated to very high (>2500°C) temperatures using electron beam heating has been developed.
- Stabilized La-Er carbide, La-Ce carbide, La-Y carbide, and Ce-Tm carbide have been produced with carbon-13 so that these compounds retain the cubic fluorite structure in the temperature range from 300 K to 2800 K.
- Diffusion measurements together with the Nernst-Einstein equation enable the determination of the carbon-ion mobility in these fluorite structure stabilized lanthanide carbides.

FY 2005 Publications/Presentations

1. *Carbon Ionic Conductors for Use in Novel Carbon-Ion Fuel Cells*, Presented at the University Coal Research Contractors Review Conference, June 7-8, 2005, Pittsburgh, PA

VI.5 Advanced Control Modules for Hybrid Fuel Cell/Gas Turbine Power Plants

Hossein Ghezel-Ayagh
FuelCell Energy, Inc.
3 Great Pasture Road
Danbury, CT 06813
Phone: (203) 825-6048; Fax: (203) 825-6273; E-mail: hghezel@fce.com

DOE Project Manager: Magda Rivera
Phone: (304) 285-1359; E-Mail: Magda.Rivera@netl.doe.gov

Subcontractors:
National Fuel Cell Research Center, Irvine, CA
Carnegie Mellon University, Pittsburgh, PA

Objectives

The overall project goal is to develop advanced and intelligent control algorithms for hybrid fuel cell/gas turbine (FC/T) power plants. The specific objectives are as follows:

- Establish a dynamic modeling environment to facilitate simulation studies, as well as development and testing of control algorithms.
- Increase reliability and availability of the hybrid power system by investigating the application of model-based control algorithms.
- Develop robust controllers that maintain stable operation and high performance of the hybrid power plant.
- Develop optimal control strategies to improve performance and to accommodate fast response during rapid transients.
- Accommodate measurement errors, as well as sensor and actuator faults, to reduce the number of unplanned shutdowns.
- Extend service life of the components in the hybrid FC/T power plant.
- Integrate robust and optimal controllers into an overall supervisory framework.

Approach

- Develop modular dynamic models of the key system components based on the laws of conservation of mass and energy.
- Develop constitutive equations describing performance characteristics of fuel cell, gas turbine, and other balance-of-plant equipment.
- Synthesize integrated dynamic system models by incorporating key process equipment and controllers in FC/T hybrid power plants.
- Develop robust controllers that maintain stable operation of FC/T systems in spite of environmental disturbances, measurement errors, model simplifications, and incorrect model parameters.
- Employ dynamic optimization routines to improve plant performance and power output while maintaining operating constraints.
- Implement data reconciliation and disturbance estimation techniques in the overall control strategy.
- Develop a feedforward neural network supervisor based on results of optimization studies.
- Develop fuzzy logic techniques to accommodate sensor and actuator faults.

Accomplishments

- Completed the development of modular dynamic models for internally reformed carbonate fuel cells (Direct FuelCell®, DFC®) and solid oxide fuel cells (SOFCs) as well as microturbines and balance-of-plant equipment using the MATLAB®/Simulink® programming environment.
- Completed integration of sub-MW hybrid DFC/T® and SOFC/T simulation programs based on a 60-kW commercial microturbine generator.
- Refined control strategies for fuel cell stack temperature, gas turbine operation, and fuel feed rate during start-up and power ramps.
- Developed a dynamic optimization modeling environment and initiated FC/T system optimization studies.

Future Directions

- Linearize dynamic models; use linear process models to analyze plant controllability, to determine optimal input/output pairings, and to develop robust controllers.
- Determine optimal ramping strategies for a diverse set of load profiles via dynamic optimization modeling.
- Develop techniques for disturbance estimation and data reconciliation through optimization studies.
- Develop a neural network framework suitable for online control supervision. Train the neural network with results from the control optimization studies.
- Develop fuzzy logic fault detection and fault accommodation techniques.
- Integrate overall control strategies into the simulation environment for extensive testing of the algorithms for their robustness and stability.

Introduction

The control system for fuel cell/turbine hybrid power plants plays an important role in achieving synergistic operation of subsystems, improving reliability of operation, and reducing frequency of maintenance and downtime. The control strategy plays a significant role in system stability and performance as well as ensuring the protection of equipment for maximum plant life. Figure 1 shows a simplified process diagram of an internally reforming SOFC/T system, which is being studied for development of advanced control algorithms. The system is based on an indirectly heated Brayton cycle. The anode exhaust, which contains the remainder of the fuel, is mixed with the cathode exhaust in a catalytic oxidizer, where oxidation of fuel is completed. The hot oxidizer exhaust passes through a heat recovery unit (HRU) in which it preheats the compressed air before entering the turbine. The hot compressed air is expanded through the turbine section, driving an electric generator.

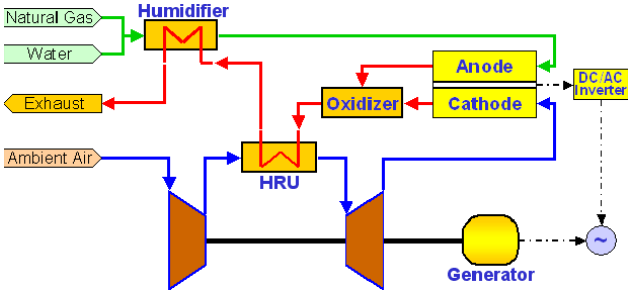

Figure 1. Conceptual Process Flow Diagram for SOFC/T System

Dynamic simulation has proven to be a powerful design tool to study the transient behavior of fuel cell/gas turbine hybrid systems. Development of an advanced control strategy is facilitated by using a dynamic model both as a simulation test bed and as part of the controller itself. Components of the advanced control module include a neural network supervisor, robust feedback controllers, and predictive system models. These advanced control components are used in the development and demonstration of an innovative algorithm that optimally controls hybrid power systems, and yet is easily adaptable to the type of fuel used, whether natural gas, coal gas, or digester gas.

Approach

The advanced control module shown in Figure 2 is based on a feedforward/feedback structure. It

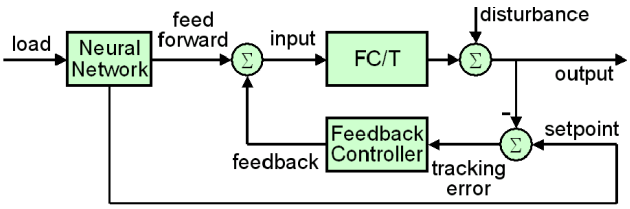

Figure 2. Advanced Control Module Comprising Neural Network Supervisor and Robust Feedback Controller

consists of a combined robust controller and a neural network supervisor that together manipulate the actuators to optimally control the hybrid system during load ramps. The feedforward controller will provide optimal dynamic scheduling based on the prescribed load profile and trends. Because the optimization routines are computationally too intensive for real-time application, they will be carried out offline. The resulting data will then be used to train a neural network supervisor. The feedforward controller performance depends strongly on the accuracy of the model employed to tune it. A feedback control strategy is utilized to compensate for setpoint deviations caused by imperfect feedforward control moves. The feedback controller will be designed using robust control techniques.

Robust Process Control

The approach is to develop low-level controllers suitable for implementation in a standard programmable logic controller (PLC). These controllers will be designed offline using information about the plant and will meet prescribed levels of robust stability and performance. The robust stability will be achieved for both the linear plant model as well as all sets of models corresponding to anticipated uncertainties. Robust performance will be achieved by virtue of exceeding a set of performance specifications (overshoot, rise time, etc.).

Nonlinear Dynamic Optimization

Feedforward control is typically based on steady-state mappings between the process variables and the controlled variables. To build feedforward action into the feedback-based robust design, the setpoints and supplementary feedforward control signals are found via dynamic optimization. The technique involves minimization of an objective function, subject to Multi-Input-Multi-Output (MIMO) nonlinear plant dynamics and specified constraints. The optimization model involves specification of hard input constraints (e.g., valve limits) and soft output constraints (e.g., functional within bounds). AMPL, a mathematical programming language, will be utilized for implementation of the derived large-scale constrained optimization equations. The nonlinear programming (NLP) solver, IPOPT, will be used for numerical solution of the dynamic optimization model. IPOPT is a state-of-the-art interior point NLP solver that will be used to handle constraints which arise in operation of the actuators in hybrid FC/T systems.

Results

Development of component models in MATLAB/Simulink has been completed. The models include software programs (modules) for internally reforming DFC and SOFC stacks, microturbine, and balance-of-plant equipment. Integrated system models were developed for both SOFC/T and DFC/T systems based on the component-level models. The modular nature of the computer models in Simulink allows for flexibility in development of integrated system models, as shown in the DFC/T example of Figure 3.

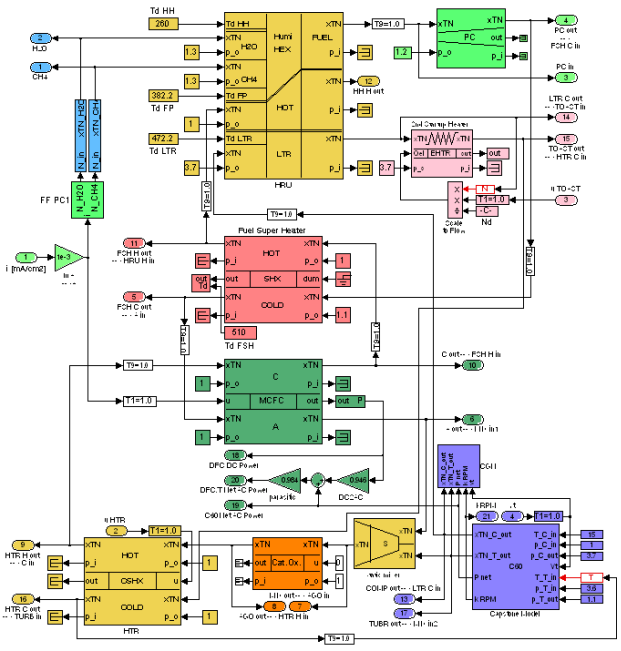

Figure 3. DFC/T Dynamic Simulation Model in MATLAB/Simulink

The integrated dynamic system models were utilized to refine the control strategies for start-up of the microturbine and fuel flow, as well as for control of the cathode inlet temperature throughout the operating range. The underlying principle for the developed control strategy is optimization of the waste heat recuperation to maximize the turbine inlet temperature and power generation. The strategy was implemented in the dynamic models to simulate and verify start-up and load operations of a sub-MW class hybrid power plant. The dynamic simulation studies have resulted in improvements of the control system design. As an example, thermal management of the fuel cell stack was improved by manipulating the microturbine speed.

The development of the optimization models based on the AMPL/IPOPT software platform has been completed. Using this framework, optimization is performed, and feedforward control moves and setpoints are scheduled based on the offline optimization results.

Conclusions

Dynamic simulation models for both DFC/T and SOFC/T systems were developed in MATLAB/ Simulink. The models included implementation of plug-and-play sub-models, which are easily connected to configure the entire systems. This modular approach decreased the time required for dynamic system model development and increased the flexibility for investigating system configurations. The developed dynamic simulation models have enabled testing of new system designs, verification of new control algorithms, and integration of system components early in the design phase. Activities are underway to develop a database of load change trajectories to facilitate the training of neural network based controllers.

FY 2005 Publications and Presentations

1. H. Ghezel-Ayagh, M. D. Lukas and S. T. Junker. "Dynamic Modeling and Simulation of a Hybrid Fuel Cell/Gas Turbine Power Plant for Control System Development", Proceedings of ASME/Fuel Cell Science, Engineering and Technology Conference 2004, ASME FuelCell 2004-2488.
1. H. C. Maru and H. Ghezel-Ayagh, "Direct Carbonate Fuel Cell – Gas Turbine Combined Cycle Power Plant", Presented in European Fuel Cell Forum, Lucerne, Switzerland, July 5-8, 2005.

VI.6 Highly Textured Glass Composite Seals for Intermediate-Temperature SOFCs

Amy Trujillo, Jeff Shunkwiler, Matt Seabaugh (Primary Contact)
NexTech Materials, Ltd.
404 Enterprise Dr.
Lewis Center, OH 43035
Phone: (614) 842-6606; Fax: (614) 842-6607; Website: www.nextechmaterials.com

DOE Project Manager: Travis Shultz
Phone: (304) 285-1370; E-mail: Travis.Shultz@netl.doe.gov

Consultant: Dr. Dick Brow
University of Missouri – Rolla, Rolla, MO

Subcontractor: Dr. John J. Lannutti
The Ohio State University, Columbus, OH

Objectives

- Fabricate a compliant seal that is hermetic at solid oxide fuel cell (SOFC) operating conditions.
- Achieve target leak rates with minimum compressive loading.
- Identify a glass composition that is chemically compatible with a metal interconnect and does not support chromium migration or silicon degradation.

Approach

- Design a textured composite seal consisting of a glass matrix and a crystalline particulate filler.
- Optimize composite seal composition by characterization and leak rate testing.
- Analyze each composition and tailor seal to meet Solid State Energy Conversion Alliance (SECA) SOFC requirements.

Accomplishments

- Fabricated pure glass seals that demonstrate a leak rate of $8.55E^{-4}$ sccm/cm from 650-850°C at 7.9 psi.
- Downselected composite design structure and two glass compositions.
- Demonstrated composite design seals that achieve a leak rate of $1.55E^{-1}$ sccm/cm from 650-850°C at 80 psi.

Future Directions

- Optimize composite seal composition.
- Conduct lifetime leak testing.
- Scale up to full SOFC seal testing at open circuit voltage (OCV).

Introduction

To achieve the high power densities promised by planar stacks in solid oxide fuel cells (SOFCs), reliable seal technology must be developed. Current seal technology has been successful in laboratory stack testing, but in practice is plagued by reliability and lifetime issues, particularly with respect to thermal cycling. Current seal materials are dependent upon glass and glass-ceramic technologies with significant alkali, borate, and phosphate contents, constituents that are known to be highly mobile at cell operating temperatures. The volatilization of these species can degrade cell performance and ultimately limit cell life. Many of the reported seal formulations have been designed to operate near 1000°C using ceramic interconnect materials, rather than the 600-800°C range, where the use of metallic interconnects is envisioned. A composite approach, in which a crystalline ceramic phase is oriented in a compliant glass matrix, achieves good thermal, mechanical, and chemical stability through the stress relief and self-healing character of the viscous seal material and the interlocking nature of the crystalline phase.

Approach

By adding a crystalline component to a glass matrix, the seal can adhere while staying thermally and mechanically compliant. The crystalline particulates restrict flow of the glass and maintain the coefficient of thermal expansion (CTE) of the seal in the same range as other common SOFC materials. Composite seals are adaptable to either compressive or non-compressive SOFC designs. These seals adhere to metallic interconnects and are designed to avoid barium chromate formation in contact with the seals and limit silica migration to the anode by limiting the glass content of the seals.

Results

Many different glass compositions were characterized and leak tested. A study was performed in parallel to optimize the design of the composite seal, which consisted of a glass matrix and a crystalline particulate filler. Textured alumina platelets and untextured zirconia particulates were investigated as the filler material. A single glass composition was selected to simplify processing and optimize the glass content of the composite seal. Increasing the surface area of the starting glass powder from 3.7 to 15 m^2/g was found to improve its wetting behavior. Slurry containing glass powder and filler material suspended in an organic solvent was tape cast, dried, laminated, and cut to the desired sample configuration. Painting the surfaces of the sample with glass ink or laminating a pure glass tape layer on the seal surface increased the adherence of the seal, and in turn resulted in lower leak rates.

The seal leak testing conditions also were optimized. The interconnect manifolds originally were fabricated from Inconel stock material (CTE $15.8E^{-6}$/°C), and the CTE mismatch with glass compositions (typically ~$6E^{-6}$/°C) was deemed too large for the glass-interconnect interface. The Inconel manifolds were replaced with Crofer 22 APU (CTE $12.6E^{-6}$/°C), which was an improvement, although still a significant difference in CTE. Therefore, the initial heating ramp rate of the test was decreased from 10 to 3°C/min to further ease the CTE mismatch between the sealing interfaces. A mechanical load of 80 psi was established, which is lower than those used by other seal research groups (1,2). At the start of the test, the temperature of the test rig was increased to 850°C and held for one hour to allow the glass to soften and adhere to the interfaces. After measuring the sample leak rate at 850°C with helium gas, the temperature was decreased 50°C and the sample was tested again after the temperature had equilibrated. This procedure was repeated until the leak rate was tested at 850°C, 800°C, 750°C, 700°C, and 650°C.

Figure 1 summarizes testing to date on the textured alumina platelet composite. Pure glass and pure alumina tested under the same conditions are shown for reference. Composite A has an average leak rate of $1.55E^{-1}$ sccm/cm from 650-850°C, which is near our target of $1.0E^{-1}$ sccm/cm. This contrasts with a pure alumina particulate leak rate of 4.19 sccm/cm and a pure glass seal leak rate of $7.57E^{-2}$ sccm/cm. In future testing, the optimized composite seal will be examined under typical SOFC operating conditions at OCV. The new test configuration monitors OCV and degradation of the cell. This test will determine the adherence of the seal to current NexTech Materials, Ltd. SOFC materials and

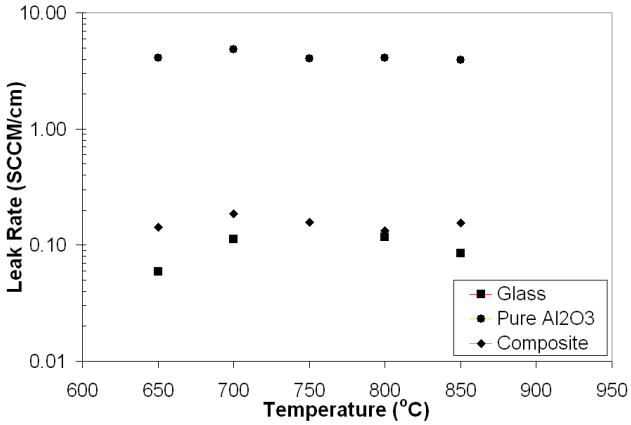

Figure 1. Alumina Composite Seal Leak Behavior at 80 psi Mechanical Loading

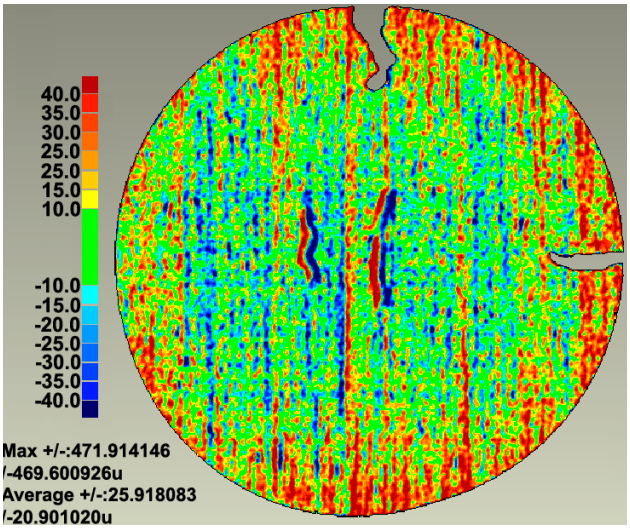

Figure 2. Observed Curvature Change at 556°C of E-Brite Joined to Glass

measure leak rates using a nitrogen/hydrogen gas mixture or air.

Ohio State University is currently characterizing the joining of glass to common SOFC components (YSZ, LSM, Inconel, E-Brite, Crofer, NiO) and scanning the samples by optical profilometry to detect curvature changes. Researchers are also using laser dilatometry on stacks integrated with glass seals to analyze CTE changes. In addition, they are analyzing the interfaces using scanning electron microscopy, energy-dispersive x-ray spectroscopy, and x-ray diffraction to detect phase changes due to chromate formation and mobilization. Figure 2 shows observed curvature changes (relative to room temperature) at 556°C in E-Brite joined to glass. Green indicates no change in curvature, red denotes an increase in curvature, and blue signifies a decrease in z-height. Areas in which no sample appears to be present constitute areas of dropout and can be ignored. Initial investigations gave no indication of a third phase, implying that no reaction has taken place between the materials. Also, curvature change of Crofer is minimal after joining to glass at 850°C.

Conclusions

- Fabricated pure glass seals that demonstrate a leak rate of $8.55E^{-4}$ sccm/cm from 650-850°C at 7.9 psi.
- Downselected composite design structure and two glass compositions.
- Converted manifolds to Crofer 22 APU to ease CTE mismatch.
- Demonstrated composite design seals that achieve a leak rate of $1.55E^{-1}$ sccm/cm from 650-850°C at 80 psi.

Special Recognitions & Awards/Patents Issued

1. Best Commercial Presentation, "Composite Seals for Intermediate Temperature SOFCs," ASM International Conference on Joining of Advanced and Specialty Materials VII, October 18-20, 2004, Columbus, OH.

FY 2005 Publications/Presentations

1. "Composite Seals for Intermediate Temperature SOFCs," ASM International Conference on Joining of Advanced and Specialty Materials VII, October 18-20, 2004, Columbus, OH.

References

1. "Novel infiltrated Phlogopite mica compressive seals for solid oxide fuel cells," Chou Y.S., Stevenson J.W. *Journal of Power Sources.* 135 (2004) 72-78.
2. "Deformation behavior and leakage tests of alternate sealing materials for SOFC stacks," Bram M., Reckers S., Drinovac P., Monch J., Buchkremer P., Stover D. *Journal of Power Sources*. 138 (2004) 111-119.

VI.7 Dense Membranes for Anode-Supported All-Perovskite IT-SOFC

Rambabu Bobba (Primary Contact), W. Zhao, S. Ghosh, Vinay S. Reddy, Kourtney L. Jacksom, Selissa Mitchell (Students)
Solid State Ionics Laboratory, Department of Physics
Southern University and A&M College
Baton Rouge, Louisiana 70813
Phone: (225) 771-2493; E-mail: rambabu@grant.phys.subr.edu

DOE Project Manager: Lane Wilson
Phone: (304) 285-1336; E-mail: Lane.Wilson@netl.doe.gov

Objectives

- Synthesize fine, homogeneous, phase-pure perovskites in the form of bulk (powders) and thin films to be used as components for developing zero-emission solid oxide fuel cells (SOFCs) capable of operating at reduced temperatures (800°C).
- Study the effect of composition on the microstructure (grain size, grain boundaries, surface texture), magnitude of oxygen permeation, O_2 exchange rates and long-term stability.
- Measure the AC impedance at higher temperatures and investigate the effect of electrical conductivity on the electronic structure using X-ray absorption near edge spectroscopy (XANES) and extended absorption fine structure spectroscopy (EXAFS).
- Assemble all-perovskite-based SOFC made from a dense ceramic electrolyte membrane ($La_{0.8}Sr_{0.2}Ga_{0.875}Mg_{0.125}O_{3-x}$) sandwiched between porous electrodes (based on Ni as anode and electronically conducting $LaNi_{0.6}Fe_{0.4}O_3$ and/or $La_{0.8}Sr_{0.23}CoO_3$ ceramic cathode).
- Evaluate the cost, performance, power generation capabilities, and emissions of the above SOFC while optimizing the reduced-dimensionality structures needed to demonstrate a zero-emission unit by the end of the three-year period.
- Create an interest among African American undergraduate and graduate students to develop theses related to the development of all-perovskite-based anode-supported intermediate-temperature SOFCs (IT-SOFCs).

Introduction

There are two major obstacles that have to be solved to operate SOFCs at intermediate temperatures, including the performance of electrolyte and electrodes. Lowering the operating temperature is possible with the use of alternative materials, appropriate cell design and manufacturing routes. In the search for dense electrolyte materials, the perovskite-based systems (ABO_3) have been considered as alternative options, particularly because ABO_3 can take on a number of different structures and can be doped with aliovalent cations on both the A and B sites. They can also accommodate very large concentrations of anion vacancies into their structures. $LaGaO_3$-based perovskite-type oxides—in particular, Sr- and Mg-doped $LaGaO_3$ (LSGM)—exhibit high oxide ion conductivity. The exceptional structural and chemical compatibility of LSGM with $La_{0.9}Sr_{0.1}Co_{0.9}M_{0.1}O_3$ (M= Fe, Ni, Mn) as perovskite-based cathode, and Ni-based perovskite cermet as anode, makes it a unique electrolyte for all-perovskite-based IT-SOFCs.

Approach

There is a critical need to optimize the processing conditions to obtain well-sintered LSGM electrolytes at low temperatures for developing miniaturized SOFC cells and stacks working at 600-800°C. The single-phase LSGM with high sintered density is not easy to obtain by conventional solid state technique. One of the requisites for application as SOFC electrolytes is high sinterability. The extent of sintering depends on the mode of synthesis. The

solid state route results in hard agglomerates and coarser grains, which inhibit sintering to obtain dense electrolyte materials. In view of increasing importance to produce dense LSGM ceramics on a large scale with better phase purity at lower temperatures in a cost-effective manner for use as electrolytes, an investigation was carried out to study the effect of conventional and microwave-assisted sintering of the recycled LSGM samples obtained from the regenerative sol gel (RSG) route, which is a combination of solid state reaction and Pechini-type method. The ability to recycle the same sample and use different processing conditions to tailor the properties of LSGM samples makes our regenerative sol-gel technique innovative and cost-effective.

RSG, microwave-assisted synthesis, and solid state conventional synthetic techniques have been employed to prepare 1) several compositions of $La_{1-x}Sr_xGa_{1-y}Mg_yO_{3-(x+y)/2}$ as an electrolyte, 2) porous $LaNi_{0.6}Fe_{0.4}O_3$ and deposited LSGM electrolyte on $LaNi_{0.6}Fe_{0.4}O_3$ as anode, 3) porous $LaSrCrMnO_3$ to be used as cathode, and 4) $LaCrO_3$ to be used as an interconnector. These components will be assembled in LSGM electrolyte-supported configuration, which is usually prepared by densifying the LSGM electrolyte first and then applying the anode and cathode layers afterwards.

Results and Discussion

For the first time, the Sr- and Mg-doped $LaGaO_3$ ($La_{1-x}Sr_xGa_{1-y}Mg_yO_{3-0.5(x+y)}$, LSGM) was regenerated to aqueous solution. LSGM with comparable quality to other solution routes was synthesized by sol-gel route from the regenerated solution. The LSGM solid was dissolved in hot doubly distilled water with pH adjusted in the range of 0.5 to 1.0. To 50 ml of the solution, 10 g of citric acid and 5 ml of glycerol were added and dissolved to form the regenerated solution for LSGM. $La_{0.8}Sr_{0.2}Ga_{0.85}Mg_{0.15}O_{2.825}$ (LSGM-2015) and $LaGaO_3$ were prepared through both the regenerative sol-gel (RSG) and conventional solid-state route at 1400°C. Figure 1 displays the complex-plane impedance spectroscopy measured at 325°C of the LSGM-2017 samples sintered at different temperatures for eight hours.

The LSGM pellets prepared by the two methods were compared in their X-ray diffraction (XRD),

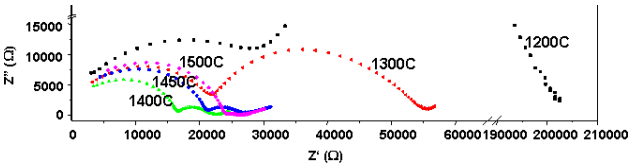

Figure 1. Complex Plane Plot of Impedance Spectroscopy Measured in Air at 325°C

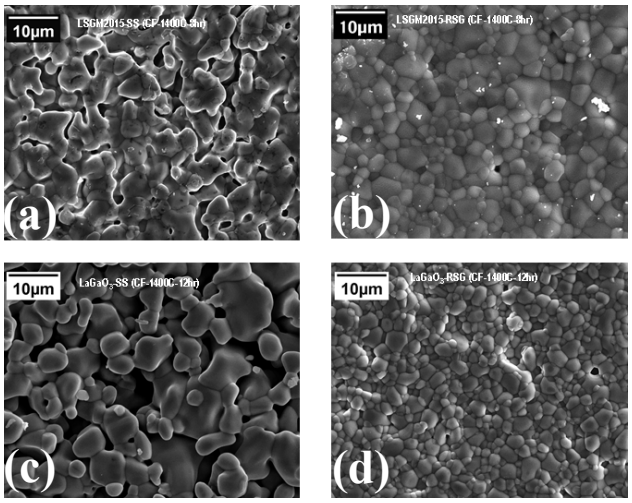

Figure 2. SEM Micrographs of $La_{0.8}Sr_{0.2}Ga_{0.85}Mg_{0.15}O_{2.825}$ (LSGM-2015) and $LaGaO_3$: (a) solid-state route precursor of LSGM-2015; (b) RSG route precursor of LSGM-2015; (c) solid-state route pellet of $LaGaO_3$; and (d) RSG pellet of $LaGaO_3$

scanning electron microscopy (SEM) (Figure 2), and electrochemical impedance spectroscopy (EIS) measurements. The LSGM-2015 synthesized via the RSG route exhibited conductivity $_t$ = 0.066 S/cm and 0.029 S/cm at 800°C and 700°C, respectively, and activation energy E_b= 0.97 eV, E_{gb}= 1.03 eV and E_t=1.01 eV for bulk, grain-boundary and whole material, respectively. Series of $La_{0.8}Sr_{0.2}Ga_{0.83}Mg_{0.17}O_{2.815}$ pellets were prepared by the RSG method at different sintering temperatures (1200-1500°C) and times. The sintering temperature severely affected the grain size (<0.1 m to 10 m) and the resistance (3 k to175 k) in all grain-boundary materials.

Ceria (CeO_2) and its substituted derivatives find immense potential as solid electrolytes in SOFCs, as oxygen sensor and as an automobile exhaust catalyst. Nano doped CeO_2 electrolyte shows promise with LSGM if they are used together either to block the

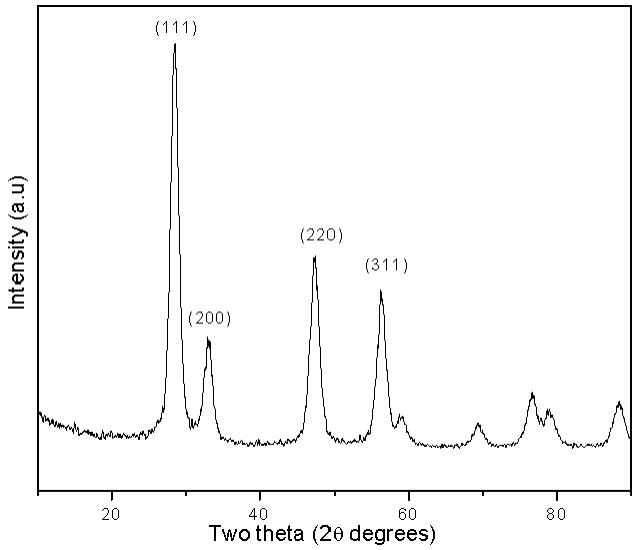

Figure 3. XRD of Nano CeO_2 Synthesized Using Hydrothermal Methods

electronic component in the doped ceria with the LSGM, or with the ceria, to block unwanted anode/electrolyte chemical reactions and/or to provide a catalytic surface for fuel oxidation at the anode. The surface layer on the anode side of these electrolytes can make these electrolytes viable for reduced temperature operations. In the past, fine CeO_2 powders have been prepared by using urea and hexamethylenetetramine-based precipitation. In these experiments, precipitation was carried out by conventional heating of the precursor solution at 80°C. We have prepared fine polycrystalline ceria powders at a temperature of 200°C by hydrothermal treatment of microwave-precipitated precursor from aqueous solution of $(NH_4)_2Ce(NO_3)_6$ and urea. Figure 3 shows the XRD pattern of nano CeO_2.

Simultaneously, we have also prepared nanocrystalline $Ce_{0.9}Gd_{0.1}O_{1.95}$ and lanthanide-doped ceria powders and multilayer thin films (using pulsed laser deposition) during this reporting period.

Future Plans

- We will attempt deposition of a thin layer of LSGM electrolyte on $LaNi_{0.6}Fe_{0.4}O_3$ cathode.
- We plan to carry out electrophoretic deposition of the dense LSGM samples on $LaNi_{1-x}Fe_xO_3$ porous cathodes presently being developed in our laboratory. To realize thin, dense O_2-semipermeable membranes on single crystalline substrates, we are preparing thin films using pulsed laser deposition (PLD). The technique of PLD seems very well suited to deposit prototype thin perovskite films with various compositions.
- Assembling and electrochemical measurements will be performed and will be reported in the future.

Summary

A promising perovskite cathode, electrolyte, and interconnect configuration was identified and synthesized. Three manuscripts were submitted for publication, and several presentations were made in national and international conferences.

One research associate and three (two graduate + one graduate) students were supported through this project at Southern University.

VI.8 Sorbents for Desulfurization of Natural Gas and LPG

Gökhan Alptekin
TDA Research, Inc.
12345 W. 52nd Avenue
Wheat Ridge, CO 80033
Phone: (303) 940-2349; Fax: (303) 422-7763; E-mail: galptekin@tda.com

DOE Project Manager: Magda Rivera
Phone: (304) 285-1359; E-mail: Magda.Rivera@netl.doe.gov

Subcontractor:
Jan Thijssen, Redmond, Washington

Objectives

- Develop a low-cost, high-capacity, expendable sorbent that can reduce the concentration of organic sulfur species in natural gas and liquefied petroleum gas (LPG) to less than ppb levels.
- Develop a regenerable version of the sorbent for large-scale stationary power generation applications.
- Scale up sorbent production using commercial manufacturing equipment.
- Demonstrate combined operation of the desulfurizer with a solid oxide fuel cell (SOFC).
- Carry out an independent engineering analysis to fully assess the potential of the new desulfurization sorbent.

Approach

- Carry out bench-scale screening tests to identify materials that adsorb organic sulfur species with high capacity.
- Perform parametric experiments with selected sorbents to optimize operating conditions.
- Demonstrate the regeneration potential and long-term durability of the best sorbent through many consecutive adsorption/regeneration cycles.
- Produce larger batches of the new material using high-throughput equipment (e.g., spray dryers, screw extruders) representative of commercial production.
- Establish partnerships with SOFC technology developers in the Solid State Energy Conversion Alliance (SECA) to demonstrate the potential of the new desulfurization sorbent in combination with SOFCs.
- Based on the performance results, assess the technical and economical impact of the new materials in SOFC-based distributed and stationary power generation systems.

Accomplishments

- *TDA's SulfaTrap™ sorbent achieves a sulfur capacity greater than 3.12% wt. (lb of sulfur removed per lb of sorbent).*
  In our accelerated bench-scale screening experiments, we identified a sorbent that can remove organic sulfur compounds from natural gas with high capacity. The sorbent reduces the sulfur content to less than 50 ppbv and tolerates the presence of water vapor and CO_2 impurities in the gas.
- *TDA's SulfaTrap™ sorbent maintained stable performance in a 10-cycle test.*
  We demonstrated that the sorbent can be regenerated by applying a mild temperature swing: heating up the bed to 350°C. Through 10 consecutive adsorption/regeneration cycles, the sorbent achieved a stable adsorption capacity and the pellets maintained their mechanical integrity.

- *Performance of TDA's SulfaTrap™ sorbent was demonstrated in combination with a 5-kW_e SOFC.*
  TDA supplied a 2.2 L batch of its sorbent to Siemens Westinghouse Power Corporation (SWPC). TDA's SulfaTrap™ sorbent successfully removed all the sulfur from the pipeline natural gas during the 2,700-hr alpha test at SWPC's Research Center in Pittsburg, Pennsylvania.
- *A modified version of the sorbent successfully desulfurizes LPG.*
  TDA's sorbent achieves a 2.65% wt. sulfur capacity to desulfurize commercial LPG. It has been shown that less than 20 cc sorbent can desulfurize a 20-lb commercial LPG tank.

Future Directions

- *Develop a 125-kW_e desulfurizer for SWPC.*
  This unit will be tested in the field at SWPC's customer site. The sorbent production will be scaled up to meet the requirement.
- *Demonstrate the long-term stability of the sorbent.*
  We will carry out a 100-cycle test to demonstrate sorbent life under representative conditions.
- *Assess the economic impact.*
  In collaboration with J. Thiessen, LLC, assess the techno-economic impact of the new technology.

Introduction

Advances in fuel cell technologies, together with the widespread restructuring of the power industry, have the potential to revolutionize the way power is produced and distributed. Distributed power generation is becoming a viable economic alternative to buying power from a central grid. In order to reach commercial potential in any of these markets, there must be an ample supply of high-quality fuel.

Pipeline natural gas is the fuel of choice for fuel-cell-based distributed power generation systems because of its abundant supply and well-developed infrastructure. However, effective utilization of natural gas in fuel cells requires that sulfur impurities (naturally occurring sulfur compounds and sulfur-bearing odorants) be removed to prevent them degrading the performance of the fuel cell stacks and poisoning the catalysts used in the fuel processor. Sulfur removal is important in all types of fuel cells. Even the more sulfur-tolerant SOFCs need the sulfur content of the natural gas to be reduced. TDA Research, Inc. (TDA) is developing a low-cost, high-capacity sorbent that can remove odorants from natural gas and LPG and enable effective utilization of natural gas in fuel cells.

Approach

While there are large-scale commercial technologies (e.g., hydrodesulfurization) that can remove organosulfur compounds to levels that fuel cells can tolerate, they are far too complex and expensive for small-scale systems. Most developers of the small-scale fuel cell systems prefer to remove sulfur from the feed gases using expendable (once-through) sorbents that operate at ambient temperature (a simple addition to the overall fuel cell system). For large-scale stationary systems, the use of regenerable sorbents that increase utilization is also considered a viable approach. In our work, we first prepared a large number of formulations and carried out bench-scale screening tests to identify materials that adsorb sulfur-bearing odorants with high capacity. We then performed parametric experiments with selected sorbents to optimize the conditions for their operation. We demonstrated the long-term durability and regeneration potential of the best sorbent formulation through many consecutive adsorption/regeneration cycles. In the future, we will produce larger batches of the new material using high-throughput equipment (e.g., spray dryers, screw extruders) representative of commercial production, and demonstrate the potential of the new desulfurization sorbents in combination with SOFCs. Based on the field performance results, we will assess the technical and economical impact of the new materials in distributed and stationary power generation systems.

Results

In extensive screening tests, we compared the performance of our sorbent with a number of

commercial and specially prepared physical adsorbents, including several samples supplied by SWPC. In 2000, SWPC initiated a test program to identify a strategic supplier for a natural gas desulfurization process and carried out extensive engineering tests to evaluate potential desulfurization sorbents [1]. The most promising sorbents identified in SWPC's study were further tested to compare their performance to that of the new materials developed at TDA. Some of these sorbents were cerium and copper exchanged zeolite-Y, respectively, prepared to be similar to those reported by University of Michigan [2], Pennsylvania State University [3] and Pacific Northwest National Laboratory [4]. For quick comparison, accelerated tests were carried out at a high gas hourly space velocity (GHSV) of 60,000 h^{-1} (corresponding to very short gas-solid contact times). The performance of each sorbent was evaluated at an identical baseline condition; the sulfur-laden natural gas stream contained 12.3 ppmv dimethyl sulfide (DMS), 8.9 ppmv tert-butyl mercaptan (TBM), and 8.9 ppmv tetrahydrothiophene (THT). These higher-than-pipeline-gas sulfur concentrations and short contact times allowed observation of the breakthrough profiles of these odorants in relatively short times. TDA's SulfaTrap^{TM} sorbent showed the best performance, achieving a pre-breakthrough sulfur capacity of 3.12% wt. while reducing the sulfur concentration of the natural gas to less than 50 ppbv (the pre-breakthrough sulfur adsorption capacity is defined as the lb of total sulfur adsorbed per lb of sorbent when the breakthrough of the first sulfur compound was observed). Figure 1 shows the breakthrough profile of DMS for various sorbents, and Table 1 lists their sulfur capacities.

We evaluated the effect of water on the performance of various sorbents. Typical U.S. pipeline natural gas may contain up to 155 ppmv of water vapor (~7 lbs of water per million cubic feet of natural gas). It is anticipated that competition by water vapor for adsorption sites reduces the sulfur capacity of activated carbon and zeolite based sorbents in real-world applications due to their affinity to water. Therefore, some of the samples were evaluated using a gas stream containing 45 ppmv water vapor with all other gas concentrations remaining identical (i.e., 12.3 ppmv DMS, 8.9 ppmv TBM and 8.9 ppmv THT at a GHSV of 60,000 h^{-1}).

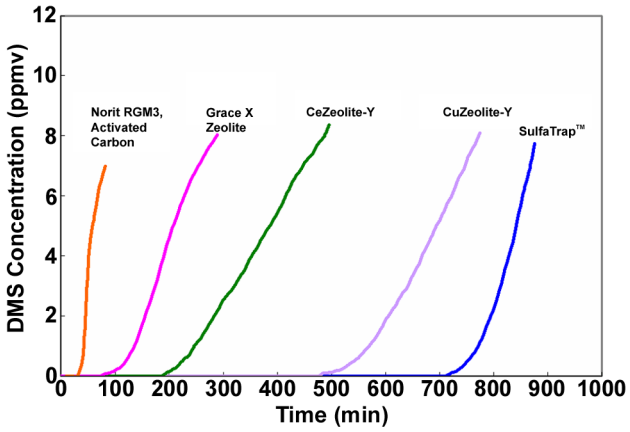

Figure 1. Comparison of Sulfur Removal Performance of TDA's SulfaTrap^{TM} Sorbent with Other Sorbents (All samples were tested at 60,000 h^{-1} in a natural gas mixture containing 12.3 ppmv DMS, 8.9 ppmv TBM and 8.9 ppmv THT at 5 psig)

Table 1. Sulfur Capacities of Sorbents

Sample	Pre-Breakthrough Capacity (% wt.)
TDA's SulfaTrap^{TM}	3.12%
Siemens Sample 5	1.96%
Siemens Sample 4	0.85%
Grace X Zeolite	0.36%
Norit RGM3 Activated Carbon	0.18%

Figure 2 shows the effect of 45 ppmv water vapor on the performance of Norit RGM3 Activated Carbon, unmodified zeolite-X (Grace) and TDA's SulfaTrap^{TM} sorbent. The presence of water reduced the sulfur adsorption capacity of the zeolite-X the most, approximately 83%, showing zeolite-X's high affinity for water vapor. The capacity of the SulfaTrap^{TM} sample remained unaffected from the presence of water vapor in the natural gas feed.

We also measured the sulfur adsorption capacity of the SulfaTrap^{TM} sorbent for 10 consecutive adsorption/regeneration cycles, increasing the bed temperature to 350°C during regeneration. We either

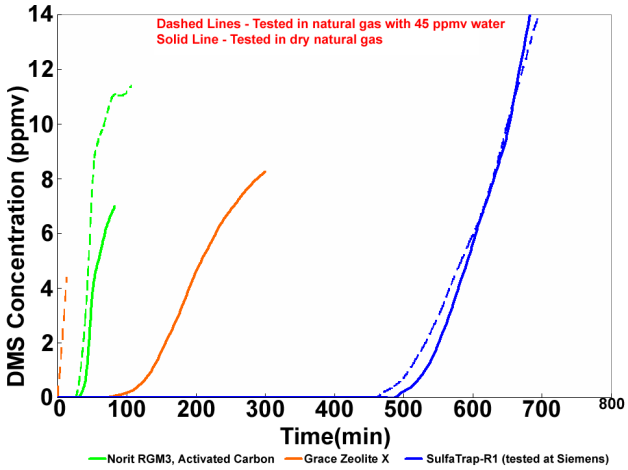

Figure 2. The Effect of Water Vapor on the Performance of TDA's SulfaTrap™ Sorbent and Other Common Sulfur Sorbents (T= 22°C, P= 5 psig, Natural gas with 12.3 ppmv DMS, 8.9 ppmv TBM and 8.9 ppmv THT at 60,000 h^{-1})

used a sulfur-free natural gas or a sulfur-free pre-reformed gas (simulated by hydrogen) to regenerate the sorbent. In both cases, the sorbent maintained a stable total sulfur capacity and DMS capacity through this 10-cycle test [5].

TDA supplied 2.2 L of SulfaTrap™ sorbent to SWPC to support alpha testing of their 5-kW_e SOFC (Figure 3). Test results show that during the 2,700-hr alpha test, TDA's desulfurizer successfully removed all the sulfur from pipeline natural gas (since the sorbent has more capacity, alpha testing of a new SOFC unit will be carried out using the same canister). Based on the successful demonstration results, SWPC requested two more desulfurization units for their 5- and 125-kWe SOFCs.

TDA also modified its sorbent to remove organic sulfur compounds present in the LPG. TDA's sorbent achieves a 2.65% wt. sulfur capacity when used to desulfurize commercial LPG. Less than 20 cc sorbent can desulfurize a 20-lb commercial LPG tank (Figure 4).

Conclusions

A low-cost, high-capacity, regenerable sorbent was developed for removing sulfur-bearing odorants from natural gas at ambient temperature. The sorbent does not interact with hydrocarbons or alter

Figure 3. TDA's Desulfurizer in Combination with SWPC's 5 kWe SOFC during Alpha Testing

Figure 4. TDA's LPG Desulfurization Sorbent

the composition of the natural gas. It does not alter the sulfur compounds that it removes by physical adsorption. It does not contain any toxic ingredients, and it is not pyrophoric. Therefore, it does not require any special handling for disposal if its regenerability is not exploited.

FY 2005 Publications/Presentations

1. "Sorbents for Desulfurization of Natural Gas and LPG," G. Alptekin, Presented at the Annual SECA conference, Pacific Grove, CA, 2005.
2. "Regenerable Sorbents for Desulfurization of Natural Gas and LPG," G. Alptekin, Presented at the Annual American Society of Material Engineers Meeting, Columbus OH, 2004.

References

1. G. Israelson, "Results of Testing Various Natural Gas Desulfurization Adsorbents," Journal of Materials Engineering and Performance, Vol. 13(3), June 2004.
2. A.J. Hernandez-Maldonado and R.T. Yang, "Desulfurization of Diesel Fuels via -Complexation with Nickel (II)-Exchanged X- and Y-Zeolites," Ind. Eng. Chem. Res. 43, 1081-1089, 2004.
3. S. Velu, X. Ma and C. Song, "Selective Adsorption for Removing Sulfur from Jet Fuel over Zeolite-Based Adsorbents," Ind. Eng. Chem. Res. 42, 5293-5304, 2003.
4. D.L. King, J.C. Birnbaum and P. Singh, "Sulfur Removal from Pipeline Natural Gas Fuel," Proceedings of Fuel Cell Seminar, p. 782, Palm Springs, CA, 2002.
5. G. Alptekin, M. Dubovik, S. DeVoss, B. Amalfitano, "Regenerable Sorbents for Natural Gas Desulfurization," Journal of Mat. Eng. and Performance, 2005 (in press).

VI.9 Feasibility of a SOFC Stack Integrated Optical Chemical Sensor

Michael A. Carpenter
College of Nanoscale Science and Engineering
University at Albany – SUNY
Albany, NY 12203
Phone: (518) 437-8667; Fax: (518) 437-8603; E-mail: mcarpenter@uamail.albany.edu

DOE Project Manager: Magda Rivera
Phone: (304) 285-1359; E-mail: Magda.Rivera@netl.doe.gov

Objectives

- Design thermally stable nano-cermets using radio frequency magnetron sputtering techniques.
- Synthesize nano-cermets with a narrow particle diameter distribution.
- Probe Au nanoparticle surface plasmon resonance (SPR) properties and Pd-YSZ optical properties as a function of temperature and chemical exposure.

Approach

- Synthesize Au, Pd and Au/Pd bimetallic alloy YSZ (yttria-stabilized zirconia) nano-cermets using physical vapor deposition techniques.
- Characterize Au, Pd and Au/Pd nanoparticles using optical and microstructural analytical techniques.
- Test thermal stability (500-1000°C) of nano-cermets and their corresponding optical properties.
- Determine the thermal and chemical stability (CO, SO_x, hydrogen) of nano-cermets and the corresponding optical properties.

Accomplishments

- Developed a Pd-YSZ nanocomposite film which has proven to be a reliable sensor for hydrogen at operating temperatures up to 650°C in the presence of an ambient air background. Film was tested through 80 cycles of hydrogen at concentrations ranging from 1.5 to 2.5% in an air carrier gas. The optical transmittance change observed for these films had a standard deviation of only ~10% over the 80 cycles.
- Upgraded the high-temperature all-optical sensor testing bench to include a charge coupled device (CCD) detection assembly. Initial testing of the bench will provide a time resolution on the seconds scale.
- Characterized the Au-YSZ nanocomposite film optical properties using both Uv-visible (Uv-vis) absorption spectroscopy and spectro-ellipsometric analysis. Determined through analysis of the SPR band as a function of nanoparticle diameter that the Au nanoparticles have a minimal interaction with the YSZ matrix. The spectro-ellipsometric analysis revealed a significant contribution of Au atoms on the dielectric function for nanocomposite films annealed only to 700°C. Films annealed between 800 and 1000°C had no noticeable atomic gold content.

Future Directions

- Evaluate the long-term stability (over several months) of the Pd-YSZ films towards both temperature and hydrogen exposures. Perform a materials and pretreatment optimization process using design-of-experiments techniques to improve the functionality of the Pd-YSZ films.
- Characterize the CO sensing capabilities of the Au-YSZ films as a function of oxygen background pressure, temperature and Au content.

- Implement the CCD optical detection system into the standard testing protocols for each of the nanocomposite material systems and optimize.
- Evaluate the sensing properties of the Au-YSZ tailored nanocomposite films for the detection of sulfur compounds, including H_2S, SO_2 and mercaptan.

Introduction

The DOE-NETL Innovative Concepts (IC) Phase II program is investigating the feasibility of harsh environment compatible chemical sensors based on monitoring the surface plasmon resonance (SPR) bands of metal and bimetallic nanoparticle doped YSZ nano-cermets as a function of fuel concentrations, impurities (CO and H_2S) and temperature (500-900°C). Since the SPRs of nano-cermets are directly correlated to the composition and shape of the metal particles [1], along with the composition of the surrounding matrix [2], the nano-cermets will be tested and designed to provide real-time sensory outputs for the chemicals of interest. The development of an integrated solid oxide fuel cell (SOFC) chemical sensor will provide the following benefits: 1) In situ monitoring of the fuel cell chemical composition, linked to a feedback loop, will allow smart control of the SOFC. 2) Monitoring the chemical composition of a low-temperature SOFC in real time will enable a more complete understanding of the catalytic and reaction mechanisms and thus lead to more efficient stack designs. 3) The development of sensors for operation within a simulated SOFC environment will at the same time be satisfying the need for chemical sensors for the Department of Energy Vision 21 Initiative. Our efforts during the IC Phase II program will be focused on performing significant upgrades to the optical bench so that we will be able to determine the dynamics of the nanocomposite interaction with changes in temperature and chemical environment. A series of experiments will be undertaken to continue the optimization, testing and analysis of Au-YSZ, Pd-YSZ and AuPd-YSZ nanocomposites so that the response time, sensitivity and reliability characteristics can be detailed.

Approach

The Au, Pd and AuPd YSZ nanocomposite films are deposited using dual target confocal physical vapor deposition, with the metal and metal oxide sputtering gun deposition rates tuned to achieve the desired metal to metal oxide composition. Thermal annealing in argon at temperatures above their respective operating temperatures is used both to thermally stabilize the films and also to grow nanoparticles of a given size. Materials characterization of the films using scanning electron microscopy, Auger spectroscopy, Rutherford backscattering spectroscopy and x-ray diffraction analyses is used to determine the microstructural and composition properties. Ex-situ optical characterization using Uv-vis absorption spectroscopy and spectro-ellipsometric analysis is used to correlate the material properties with the resulting optical properties. In-situ Uv-vis spectroscopy utilizing a CCD-based detection system as a function of both temperature and chemical exposure is used to determine the gas sensing properties with a time resolution on the seconds scale. Test gases will include H_2S, dimethyl sulfide, 1-dodecane and 1-octane thiol, SO_2, CO and hydrogen, which will provide a range of reducing and oxidizing environments whose absorption spectra effects combined with theoretical calculations will help deconvolute changes in both the dielectric and the chemical environment surrounding the bimetallic and metallic nanoparticles.

Results

During the first year of this program, we have performed a significant upgrade to the in situ optical detection system, including switching to a continuous wave (CW) Xe lamp source and integration of a Peltier cooled CCD camera-based detector. The testing bench is outlined schematically in Figure 1. Installation and implementation of this system is nearly complete and will allow for seconds-scale time resolution (a factor of 100 improvement over the previous design) and a sensitivity increase by a factor of 30 over the diode-based detection system. Final testing of the upgraded equipment is currently in progress.

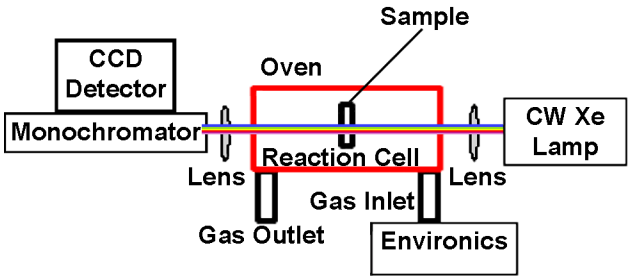

Figure 1. Schematic Diagram Displaying the Parallel Sensor Test Station

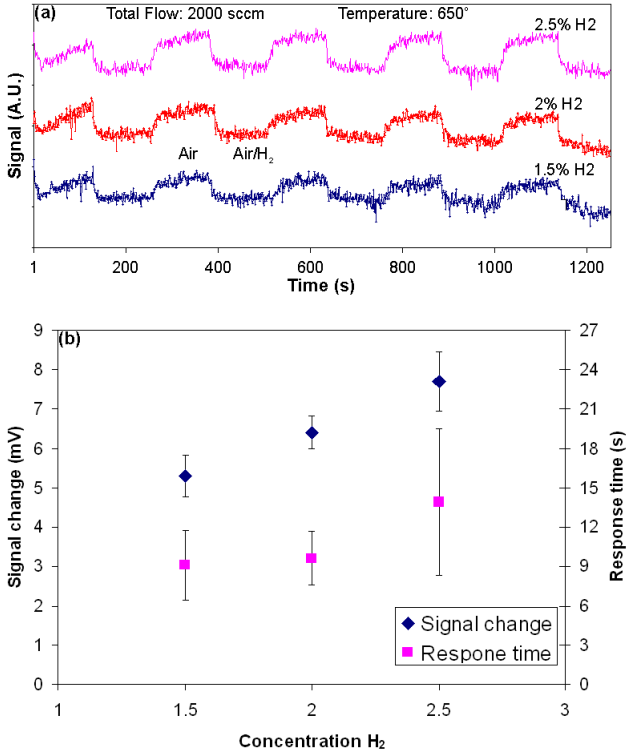

Figure 2. (a) Transmission Signal vs. Exposure Time and Hydrogen Concentration (b) Signal Change and Response Time vs. Hydrogen Concentration

The development of hydrogen-sensitive films designed using a Pd-YSZ nanocomposite film has improved significantly within the research program. Activation of the film requires the Pd to be oxidized, and the sensing principle is based on the change in transmission of PdO in comparison to the deactivated metallic Pd state. These nanocomposite materials show a reversible and reliable change in optical transmission upon exposure to hydrogen at 650°C. Figure 2A shows the transmission signal of a nanocomposite film exposed to 1.5, 2.0 and 2.5% hydrogen concentrations in an air carrier gas at

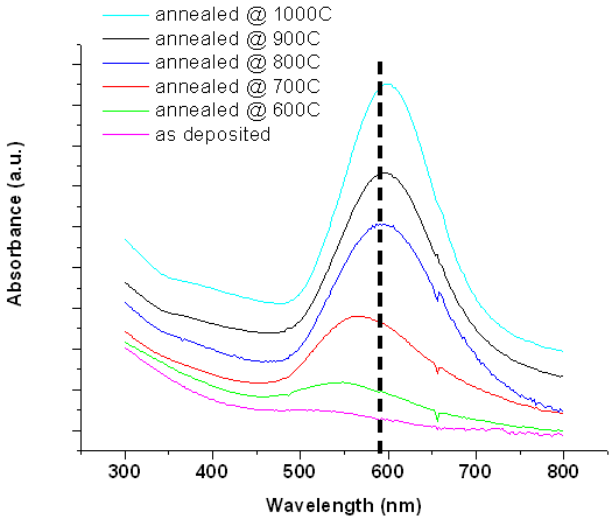

Figure 3. Absorption Spectra of YSZ-Au Nanocomposite Films as a Function of Annealing Temperature (The dashed vertical line indicates the position of the SPR band as predicted from the Mie theory using bulk dielectric functions for Au and for YSZ as measured by spectroscopic ellipsometry.)

650°C. When the gas flow is changed from air to a mixture of hydrogen in air, the signal drops due to interaction of some PdO with H_2, turning it into metallic Pd. When the gas flow is switched back to air, the signal returns to its initial level. Figure 2B plots the average transmission signal change and response time of this film as a function of hydrogen concentration resulting from 80 separate exposure cycles, and it is readily apparent that the signal change is a reliable sensing parameter to within a ~10% standard deviation.

An extensive characterization of the optical properties of the Au-YSZ nanocomposite system as a function of the annealing temperature was performed. In Figure 3, the absorption band attributed to the surface plasmon resonance of the Au nanoparticles was observed at ~600 nm. The peak of the SPR band red-shifted, and the full width half maximum (FWHM) decreased with increasing annealing temperatures. The red-shift of the SPR band was attributed to a structural phase transition from cluster to a bulk state for Au nanoparticles. The transition occurred at a nanocluster size of ~8 nm, in excellent agreement with prior work in the literature [3]. Furthermore, as seen in Figure 4, it was found that the YSZ-Au system follows the 1/R dependence

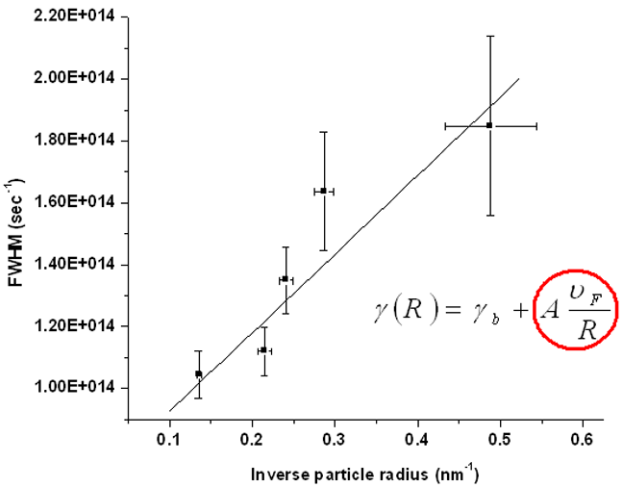

Figure 4. FWHM of the Surface Plasmon Resonance Absorption Band of YSZ-Au Nanocomposite Films versus Inverse Particle Radius

of the FWHM of the SPR band with a slope parameter *A*=0.18, indicating a weak interaction between the YSZ matrix and the Au nanoparticles. As such, the YSZ-Au nanocomposite system behaves in a similar manner as free Au nanoparticles. The optical constants of the resulting films were determined by spectroscopic ellipsometry and modeled within the context of Maxwell-Garnett effective medium theory. The extinction coefficient was found to exhibit a maximum at ~600 nm associated with the SPR band of Au nanoparticles. In the same wavelength region, the refractive index was found to follow an anomalous dispersion behavior. At longer wavelengths, an increase of ~20% was observed in the refractive index of Au-YSZ nanocomposites with respect to that of the YSZ matrix. This increase was attributed to the incorporation of Au within the YSZ. The model was successful at predicting the evolution of Au nanoparticle size with increasing annealing temperature above 800°C. For lower annealing temperatures, the average Au nanoparticle size was significantly underestimated by the model, as compared to standard interpretation of the SPR bands. This behavior was attributed to the relatively high concentration of atomic Au present in the YSZ matrix at the lower annealing temperatures.

Conclusions

The detection of hydrogen using all-optical techniques was demonstrated at an operating temperature of 650°C in the presence of an air carrier gas. An extensive materials and optical characterization of the Au-YSZ nanocomposite system was performed and will serve as our benchmark baseline study as we begin testing these films for their sensitivity towards CO and sulfur compound exposures. Further work on both the Pd-YSZ and Au-YSZ nanocomposite films will be performed to optimize and characterize their sensing capabilities.

FY 2005 Publications/Presentations

1. "Synthesis and Spectroellipsometric Characterization of Y_2O_3-stabilized ZrO_2-Au Nanocomposite Films for Smart Sensor Applications", George Sirinakis, Richard Sun, Rezina Siddique, Harry Efstathiadis, Michael A. Carpenter, and Alain E. Kaloyeros, *Materials Research Society Fall 2004 Meeting.*
2. "All-optical Chemical Gas Sensors for Harsh Environments Based on Au-YSZ Nanocomposite Films", George Sirinakis, Rezina Siddique, Zhouying Zhao, Michael A. Carpenter, *Materials Research Society Spring 2005 Meeting.*
3. "Microstructure and Optical Properties of Y_2O_3-stabilized ZrO_2-Au Nanocomposite Films", George Sirinakis, Rezina Siddique, Christos Monokroussos, Michael A. Carpenter, Alain E. Kaloyeros, *Accepted – Journal of Materials Research (2005).*
4. "Spectro-ellipsometric Characterization of Au-Y_2O_3-stabilized ZrO_2 Nanocomposite Films", George Sirinakis, Rezina Siddique, Kathleen A. Dunn, Harry Efstathiadis, Michael A. Carpenter, Alain E. Kaloyeros, Lianchao Sun, *Accepted – Journal of Materials Research (2005).*

References

1. R. Jin, Y. Cao, C. Mirkin, K. L. Kelly, G. C. Schatz, J. G. Zheng, "Photoinduced conversion of silver nanospheres to nanoprisms", *Science*, 294, 1901 (2001).
2. Y. Saito, Y. Imamura, A. Kitahara, "Absorption in the visible region of YSZ implanted with Ag ions", *Coll. Surf. B,* 19, 275 (2000).
3. D. Dalacu, L. Martinu, "Spectroellipsometric characterization of plasma-deposited Au/SiO_2 nanocomposite films", *J. Appl. Phys.* 87, 228 (2000).

VI.10 Carbon-based Fuel Cell

Steven S. C. Chuang
Department of Chemical Engineering
The University of Akron
Akron, OH 44325-3906
Phone: (330) 972-6993; Fax: (330) 972-5856; E-mail: schuang@uakron.edu

DOE Project Manager: Travis Shultz
Phone: (304) 285-1370; E-mail: Travis.Shultz@netl.doe.gov

Objectives

- Determine the technical feasibility of using coal as fuel for solid oxide fuel cells (SOFCs).

Approach

- Develop an anode catalyst to promote the electrochemical oxidation of coal.
- Use a cold-pressing technique to fabricate the electrolyte thin film.
- Use a screen-printing technique to attach the cathode on the electrolyte.
- Use mass spectroscopy and infrared spectroscopy to monitor the composition of the effluent from the fuel cell.

Accomplishments

- Design and construction of a SOFC capable of producing 100 mA/cm^2 at 0.6 V using Ohio #5 coal as the fuel.
- Successful test of the solid oxide fuel cell for the direct oxidation of methane.
- Test of the solid oxide fuel cell using activated carbon, petroleum coke, and Ohio #5 coal as fuels.
- Successful fabrication of an intermediate-temperature SOFC using SDC [i.e., samarium-doped ceria ($Sm_{0.2}Ce_{0.8}O_{1.9}$)] as the electrolyte and SSC [i.e., strontium-doped samarium cobaltite ($Sm_{0.5}Sr_{0.5}CoO_3$)] as the cathode.
- The fuel cell using Pt as the anode, SDC as the electrolyte, and SSC as the cathode produced 100 mA/cm^2 at 0.4 V using H_2 as the fuel at 700°C, and 125 mA/cm^2 at 0.4 V at 800°C.

Future Directions

- Further work is needed to improve the current density of coal-based fuel cells.

Introduction

The direct use of carbon from coal as a fuel for the solid oxide fuel cell to generate electricity is an innovative concept for power generation. This type of C-fuel cell (carbon-based fuel cell) could offer significant advantages in the following areas: (i) minimization of NO_x emissions due to the operating temperature range of 700-1000°C, (ii) high overall efficiency because of the direct conversion of carbon to CO_2, and (iii) low investment and maintenance cost due to simplicity of the process.

The objective of this study is to determine the technical feasibility of using coal as the fuel for solid oxide fuel cells. The performance of this C-fuel cell was determined by measuring the voltage output and current density as a function of temperature, time, anode catalyst compositions, concentration of CO_2, and composition of carbon black and coal. The results of this study will allow us to evaluate the

limitations and potential of the carbon-based fuel cell for practical applications.

Approach

To determine the technical feasibility of using coal as the fuel to the solid oxide fuel cell, the first step is to fabricate a SOFC with an anode which can resist sulfur poisoning during the electrochemical oxidation of coal. The second step is to determine the performance of the fuel cell using coke. Due to the long residence time of coal in the high-temperature SOFC, the majority of coal is devolatized and transformed into coke.

Results

Figure 1(a) shows the OCV (i.e., open circuit voltage) versus temperature for a solid oxide fuel cell with a modified Ni as the anode catalyst. The OCV increased with temperature for both H_2 and Ohio #5 coke. Ohio #5 coke was produced by heating Ohio #5 coal at 800°C for 20 minutes. The heating process resulted in devolatization of coal, producing coke. The major components in the coke are carbon and inorganic compounds such as silica, Fe oxides, and various oxides of transition metals which form the fly ash after carbon is electrochemically oxidized to CO_2.

The use of H_2 as a fuel produced H_2O as the only product, whereas the use of coke as the fuel produced CO, CO_2, O_2, H_2 and H_2O. At low temperature (30-200°C), a significant fraction of residual sulfur compounds is released in the form of SO_2, as illustrated in Figure 1 (b). Comparison of OCVs for H_2 and coke shows that the modified Ni anode performed significantly better for H_2 than for coke. The low performance of the fuel cell using Ohio #5 coke as the fuel could be a result of the sulfur compounds which were released in the form of SO_2.

Figure 2 compares the performance of a modified Ni anode SOFC with coke, H_2, and heptane (C_7H_{16}) as the fuels. All of the I-V (i.e., the fuel cell performance) curves show increases in current density (mA/cm^2) with decreases in voltage. This is a result of increases in internal resistance of the fuel cell due to increases in withdrawing the electrical current from the fuel cell.

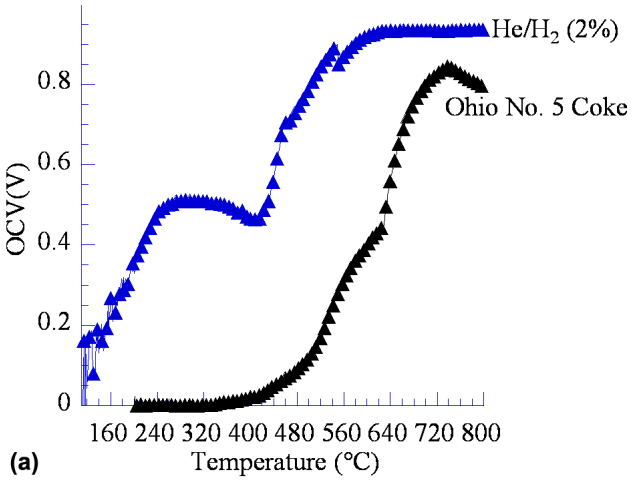

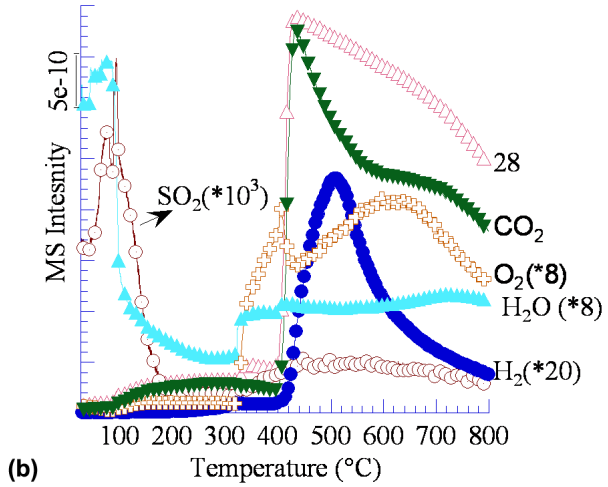

Figure 1. OCV (Voltage at zero current) and the Composition of the Effluent of the Anode Compartment

The fuel cell performance decreases in the following order: heptane > H_2 > coke. The low current density produced from coke appears to be due to the lack of catalyst activity for the electrochemical oxidation of coke. The modified Ni catalyst used in this study gave a higher current density for H_2 than for coke, reflecting its catalytic activity for H_2 oxidation.

The exposure of the anode to heptane caused a significant increase in the current density. This increase could be due to build-up of carbon filaments, which increase the electrical connection among Ni sites, facilitating the transport of electrons from the reaction sites to the external circuit, thus enhancing the current density.

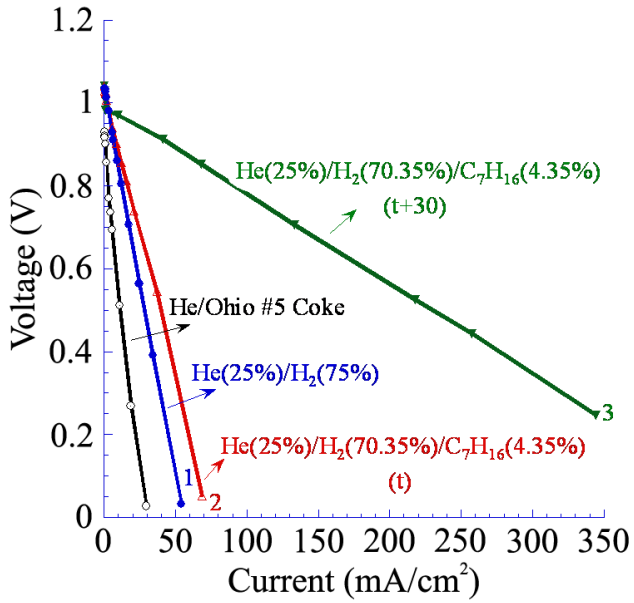

Figure 2. I-V Curves on a Modified Ni Anode Solid Oxide Fuel Cell at 800°C.

Replacement of the modified Ni catalyst with a transition metal catalyst and increasing the fuel cell temperature to 950°C resulted in an increase in the fuel cell performance to 100 mA/cm^2 at 0.6 V.

Conclusions

The performance of the carbon-based fuel cell developed in this study showed low current density. The performance of the fuel cell could be enhanced by improving the activity of the anode and the diffusion flux of the oxygen anion across the solid electrolyte. [1]

Special Recognitions & Awards/Patents Issued

1. "Carbon-based fuel cell," U.S. Provisional Application No. 60/558,856, filed April 2, 2004.

FY 2005 Publications/Presentations

1. Chuang, S. S. C., "Catalysis of Solid Oxide Fuel Cells," "Catalysis-a Specialist Periodical Report." Ed. J. J. Spivey, The Royal Society of Chemistry, Vol. 18, 2005. pp 186-198. Cambridge, U.K.

References

1. Chuang, S. S. C., "Catalysis of Solid Oxide Fuel Cells," "Catalysis-a Specialist Periodical Report." Ed. J. J. Spivey, The Royal Society of Chemistry, Vol. 18, 2005. pp 186-198. Cambridge, U.K.

VI.11 Modeling and Design for a Direct Carbon Fuel Cell with Entrained Fuel and Oxidizer

Alan A. Kornhauser (Primary Contact), *Ritesh Agarwal*
Virginia Tech, Mechanical Engineering
Mail Code 0238
Blacksburg, VA 24061-0238
Phone: (540) 231-7064; Fax: (540) 231-9100; E-mail: alkorn@vt.edu

DOE Project Manager: Travis Shultz
Phone: (304) 285-1370; E-mail: Travis.Shultz@netl.doe.gov

Objectives

- Develop a fuel cell concept in which the anode and cathode are electrically connected porous beds through which electrolyte flows with fuel and oxidizer entrained.
- Develop preliminary solutions to design problems such as electrode construction, gas-solid-electrolyte separation, and balance-of-plant design.
- Model overall plant mass and energy balances.
- Model processes within the electrodes.
- Develop to a stage where potential can be evaluated and research needs determined.

Approach

- Develop cell design.
- Develop balance-of-plant design.
- Model mass and energy balances for the plant.
- Model mass transfer, charge transfer, and chemical kinetics within the cell.
- Determine performance of cell and plant designs. Compare with alternate systems.

Accomplishments

- Selected correlations, from those available in the literature, for mass transfer, reaction rates, and electronic and ionic electrical resistances.
- Modeled performance of cell electrodes with a set of simultaneous differential equations.
- Developed Matlab computer code to solve differential equation set.
- Used electrode models to determine performance of cell design.
- Used electrode models for first-cut optimization of cell design.
- Compared performance with that of alternate direct carbon fuel cell designs.
- Developed design for prototype direct carbon fuel cell.

Future Directions

- Modify design to improve performance.
- Build and test prototype direct carbon fuel cell.

Introduction

Modern fuel cell development has concentrated on compact fuel cell designs in which immobile electrolyte is contained between porous membrane electrodes. Fuel and oxidizer are supplied to the electrodes on opposite sides of the electrolyte, and all reactions take place on the electrolyte-wetted surfaces of the electrode membrane. This design is effective for a compact cell using gaseous fuel, but it has serious limitations for utility-scale power generation using coal.

An alternate concept is proposed. In this concept, the anode and cathode are electrically connected porous beds. Molten salt electrolyte, with carbon fuel and oxidizer entrained, is pumped through the porous beds.

This fuel cell design can use impure solid fuel (coal or coke) and offers economies of scale for utility-size plants. It is particularly attractive since no microporous sintered membranes (both expensive and subject to fouling) are used.

Approach

The technology is more like a chemical refinery or an electrochemical plant than like a membrane electrode fuel cell. Accordingly, design techniques are those used for chemical reactors and electrochemical plants.

Initial designs for the cells and for the balance of plant have been developed. Techniques from the chemical engineering literature have been used to model these designs. The models have been used to predict the performance of the designs, to optimize them, and to design a laboratory prototype cell.

The reactions in the direct carbon molten carbonate fuel cell, the proposed cell design, and the proposed balance of plant design have been described previously [1][2].

One-dimensional models of the anode and cathode beds were developed, as shown schematically in Figure 1. For the anode, there were five dependent variables: CO_2 flux in the gas phase, CO_2 flux in the liquid phase, C flux as particles entrained in the liquid, ionic ($CO_3^{=}$) current in the liquid phase, and electric potential. For the cathode, there were six dependent variables: O_2 and CO_2 fluxes in the gas phase, O_2 and CO_2 fluxes in the liquid phase, ionic ($CO_3^{=}$) current in the liquid phase, and electric potential. Depth in the bed, *x*, was the independent variable for both electrodes. Differential equations (five for the anode and six for the cathode) were written for the changes in dependent variables, with terms in the equations based on liquid-gas and liquid-solid mass transfer, liquid ionic conductivity, solid electronic conductivity, and electrode surface reaction rates.

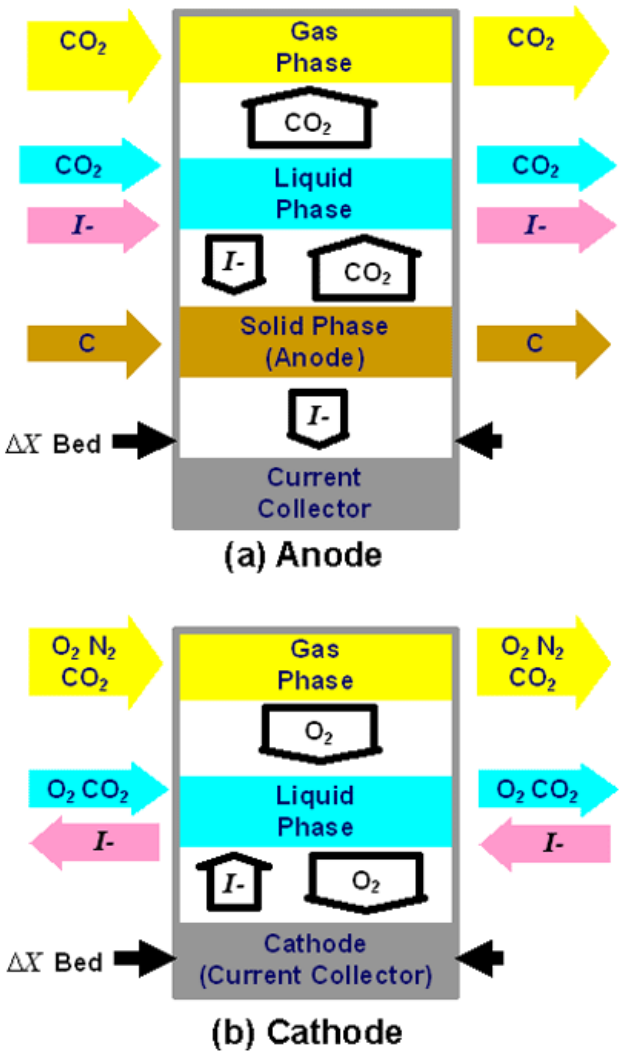

Figure 1. Schematic of Anode and Cathode Models Showing Independent and Dependent Variables

The simultaneous differential equations were written in *Matlab* [3] and solved using the *Matlab*

ordinary differential equation (ODE) solvers. Initial conditions were mole fluxes, current, and voltage at the electrode face. If satisfactory initial conditions were selected, the equations would be stepped forward until the ions representing the initial condition current had been created (cathode) or destroyed (anode). The electrode depth when the current flux went to zero was the minimum required depth for that operating condition. Unsatisfactory initial conditions – due to inadequate initial voltage or reactant flux – would result in overpotential decreasing to zero or reactants being exhausted before current flux went to zero.

Results

The model was used to predict the performance of the cell over a range of operating conditions.

Figure 2 shows voltage profiles for the anode and cathode at a typical operating condition: total potential losses of 0.326 volts, with 0.180 volts assigned to losses in the cathode and 0.146 volts assigned to losses in the anode. At the cathode inlet, losses are all from overcoming mass transfer and chemical overpotentials. At the anode inlet, electron contact resistance between the carbon particles and the current collector is added to these losses. For both electrodes, ionic resistance losses become dominant as distance into the electrode increases, until (at 0.0508 m for the cathode and 0.0092 m for the anode) there is no chemical or diffusion overpotential remaining to drive reactions.

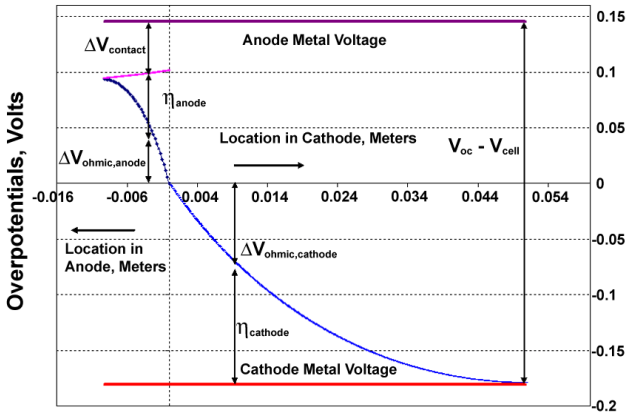

Figure 2. Variation in Overpotentials with Cathode and Anode Bed Depth

The model was run for various total voltage losses to determine both the maximum ionic current flux and the optimum division of losses between anode and cathode for each case. The results of this (for a single packing type, temperature, and reactant flux) are shown in Figure 3. The cell is seen to attain a maximum power density of 658 W/m^2 at a current density of 1315 A/m^2 and an output potential of 0.5 volts. Since the open circuit potential of the direct carbon molten carbonate cell is 1.026 volts, this corresponds to an efficiency of 49%. Higher efficiencies are obtained at lower power densities.

Design parameters were varied to determine their effect on cell performance. The most important parameter was cell temperature. Figure 4 shows the effect of cell temperature on output power density with other parameters held constant. Output increases dramatically with increasing temperature. This high output at high temperature requires that kinetics favor CO_2 instead of CO, as observed by Weaver et al [4] and Cherepy et al [5].

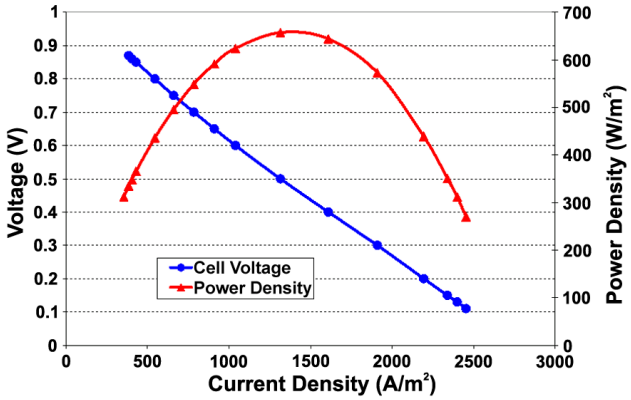

Figure 3. Variation in Output Voltage and Power Density with Bed Face Current Density

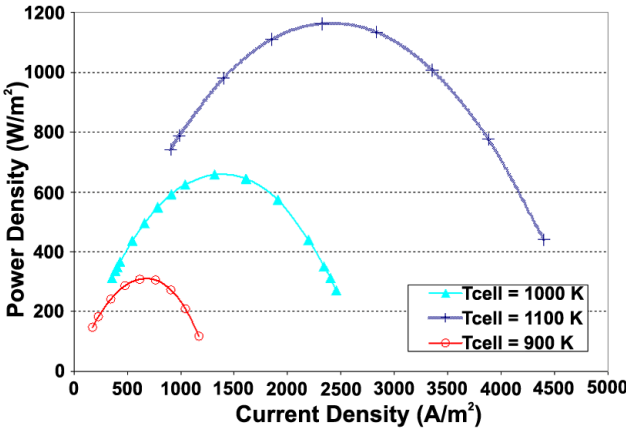

Figure 4. Variation in Output Power Density with Cell Temperature

Conclusions

The analysis performed has both encouraging and discouraging results.

The encouraging result is that the design appears to function basically as expected, allowing construction of a direct carbon fuel cell without microporous electrodes or separating membranes.

The discouraging result is that resistance losses limit the effective depth of the porous bed electrodes to a few centimeters. This, in turn, limits the current density. Predicted current densities are considerably smaller than those demonstrated at Lawrence Livermore National Laboratory on a direct carbon cell using a microporous membrane cathode [5].

The original design concept was based on considerable porous bed depth with relatively small bed face area. Lower bed depths and lower current densities require a modified design with shallow beds with larger face area. Various concepts for this modified design are being developed.

FY 2005 Publications/Presentations

1. Alan A. Kornhauser and Ritesh Agarwal, "Modeling and Design for a Direct Carbon Fuel Cell with Entrained Fuel and Oxidizer – Final Report," Virginia Tech / U.S. DOE, 2005.

References

1. R. Agarwal and A.A. Kornhauser, "Energy Balance for a Direct Carbon Molten Carbonate Fuel Cell," Proceedings of the 2004 ASME Heat Transfer / Fluids Engineering Summer Conference, Charlotte, NC, July 11-15, 2004, Paper HT-FED2004-56887.
2. A.A. Kornhauser and R. Agarwal, "Modeling and Design for a Direct Carbon Fuel Cell with Entrained Fuel and Oxidizer – FY 2004 Annual Progress Report," Virginia Tech / U.S. DOE, 2004.
3. *Matlab Release 14* software package, The Math Works, Woburn, MA, 2004.
4. R.D. Weaver, L. Tietz, and D. Cubicciotti. Direct Use of Coal in a Fuel Cell: Feasibility Investigation. Technical Report EPA-650/2-75-040, SRI International, Menlo Park, California, 1975.
5. N.J. Cherepy, R. Krueger, K.J. Fiet, A.F. Jankowski, and J.F. Cooper, "Direct Conversion of Carbon Fuels in a Molten Carbonate Electrolyte," *Journal of the Electrochemical Society*, 2004.

VII Novel Generation

VII Novel Generation

VII.1 Development and Testing of a Rotating Supersonic Shock Compressor

Aaron Koopman (Primary Contact), Peter Baldwin
Ramgen Power Systems, Inc.
11808 Northup Way Suite W-190
Bellevue, WA 98005
Phone: (425) 828-4919 ext. 235; Fax: (425) 828-7756; E-mail: hq@ramgen.com

DOE Project Manager: Tom George
Phone: (304) 285-4825; E-mail: Tom.George@netl.doe.gov

Objectives

- Demonstrate a high pressure ratio supersonic shock compression rotor (Rampressor™) to expand on the low pressure ratio success and show feasibility of high-efficiency shock compression technology for stationary devices

Approach

- Use analysis tools validated by the low pressure ratio testing to design a high pressure ratio aerodynamic flow path
- Design, manufacture and test a laboratory rig that will facilitate the understanding of the aerodynamic features of the high pressure ratio shock compression rotor
- Analyze the performance data from the compression rig test to anchor our analysis tools at high Mach number ~2.6
- Evaluate the technical potential of the novel compression technique

Accomplishments

- The lower pressure ratio supersonic shock compression rotor demonstrated several important milestones
- Shock structures were established in all of the supersonic shock inlets on the rotor (3 inlets per rotor)
- The rig operated near design pressure ratio (~2.2:1) and mass flow (~1.8 lbm/sec)
- The rig achieved ~75% rotor efficiency without the optimization of the geometry, bleeds, tip clearance, etc.
- The technical design and analysis tools have been validated for Mach 1.6 designs
- The design effort on the high pressure ratio compressor has yielded the following results:
- Improved computational fluid dynamics (CFD) analysis tools and techniques
- Enhanced performance modeling and prediction tool
- Designed superior tip clearance control system
- Identified and addressed the mechanical structure and system challenges of high compression ratios over a single-stage device, e.g., rotordynamics, bearing life, high rotational stresses, high secondary flow temperatures

Future Directions

- Design the second Rampressor test rig to run at higher pressure ratio and higher mass flow (1500 cfm)

- Achieve higher efficiency through optimization of the tip clearance and rotor geometry
- Investigate key technology challenges to successfully incorporate the superior compression technology into a commercially viable compressor product
  - Aerodynamic optimization
  - Tip leakage mitigation
  - Rotor mechanical design optimization
  - Diffusion pressure loss mitigation
  - Thrust load mitigation
- Apply the technical knowledge gained to compression of high volumes of CO_2 in support of Clean Coal, FutureGen and Carbon Capture & Storage programs

Introduction

Since the sound barrier was broken in the late 1940s, ramjet engines have been widely used as a means to propel aerospace vehicles at supersonic speeds. The underlying supersonic aerodynamic shock theory and technology is very well understood and fully characterized. Ramgen Power Systems' ("Ramgen") primary innovation has been to apply ramjet engine concepts in a stationary "shock" compressor. The principal advantage of shock compression is that it can achieve exceptionally high compression efficiency at very high compression ratios.

The importance of a breakthrough compression technology cannot be overstated. The air and gas compression industry is often referred to as the Fourth Utility. Compressed air is one of the most important utility requirements of industrial manufacturing. Air compression is also a critical element in determining the efficiency of all types of combustion engines, including gas turbines, internal combustion engines and hybrid fuel cells. Gas compression is the key to the efficient compression of CO_2, which is increasingly seen as pivotal to the clean generation of power from coal.

Approach

The technology development path for the Rampressor technology started with our rotor test rig at relatively low pressure ratio and performance. The next step is to design a higher pressure ratio and performance rotor test rig - the 2nd Rampressor Test Rig. This test will anchor our design and analysis tools at high pressure conditions. Successful rotor test results will allow us to design a compressor package at any commercially desirable pressure ratio and flow requirement. The bridge between successful rotor testing and a compressor package demonstration will be crossed by investigating the design requirements and options for an industrial drive, rotor manufacturing, controls, tip clearance system, self-contained supporting systems, etc. The next test rig (Alpha rig) will be a CO_2 compressor demonstrator including all the major components of a functional compressor package (drive, supporting systems, controls, etc.). Following the Alpha rig, there are four Beta pre-production test units planned to complete the development of the compressor.

Results

During FY 2004, Ramgen succeeded in completing testing of the first Rampressor compressor test rig; see Figure 1. Testing was run at the Boeing Nozzle Test Facility in Seattle, Washington. The test was successful in many ways.

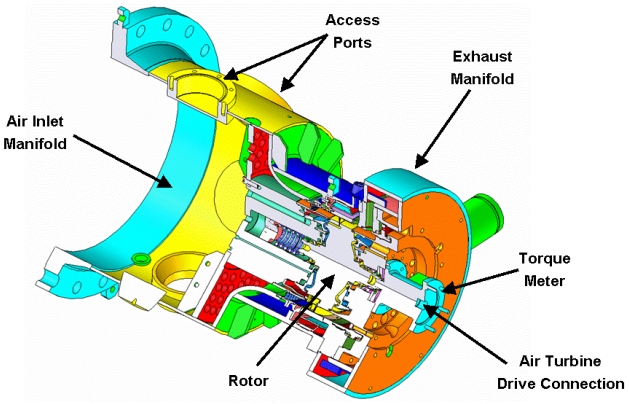

Figure 1. Test Rig

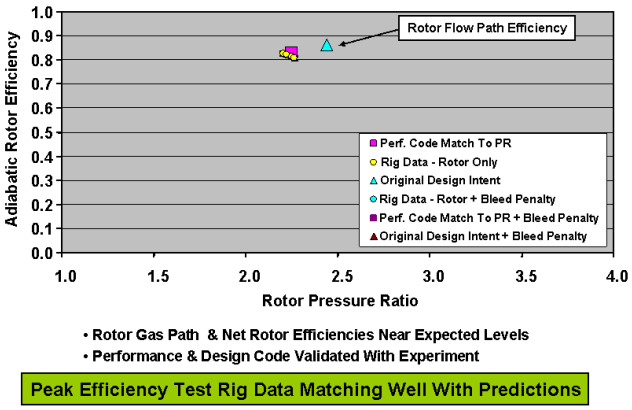

Figure 2. Rampressor Efficiency vs. Pressure Ratio

One of the testing accomplishments achieved by Ramgen was to successfully establish a shock structure within the inlet that permits compression of the air by supersonic compression waves – the inlet has been "started". Inlet "starting" is a significant milestone in any supersonic inlet test program, whether it is for supersonic air breathing missiles or aircraft (high-speed military jet fighters, SR-71, or the Concord). Inlet starting is defined as stable supersonic flow throughout the converging/ contracting portion of the inlet geometry. The minimum flow area of a fixed geometry inlet is sized for the design operating Mach number. As the inlet velocity (rotor tip speed) approaches Mach 1 (speed of sound), a fixed geometry inlet cannot swallow all of the air approaching the inlet. As a result, a normal shock wave is formed in front of and diverts flow away from the inlet. This normal shock wave results in subsonic flow into the inlet, an "unstarted" condition, which is not an efficient operating condition for an inlet designed for supersonic flow.

During the test, many different test conditions were run, from low pressure ratio/low mass flow to higher pressure ratios/mass flows. These collected data points form the basis for a preliminary compressor map. A key conclusion from our testing was that our performance prediction tools replicated the experimental results. The measured rotor efficiency, pressure ratio, rotor exhaust Mach number and flow angle all closely aligned with the predictions from the analysis tools; see Figure 2. In addition, our compressor mapping showed that the Rampressor rotor does not exhibit any violent surge (or failure to hold pressure ratio) characteristics. In

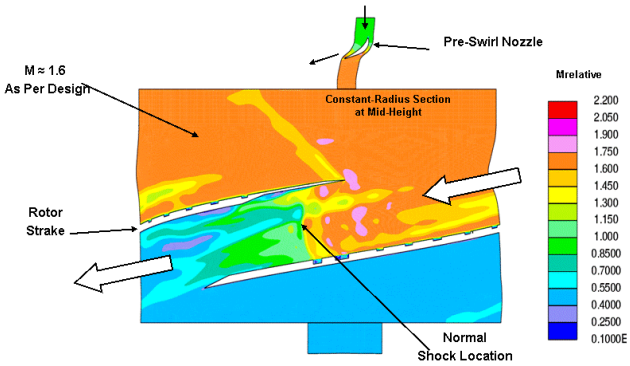

Figure 3. Sample CFD Run of Rampressor Flow Path

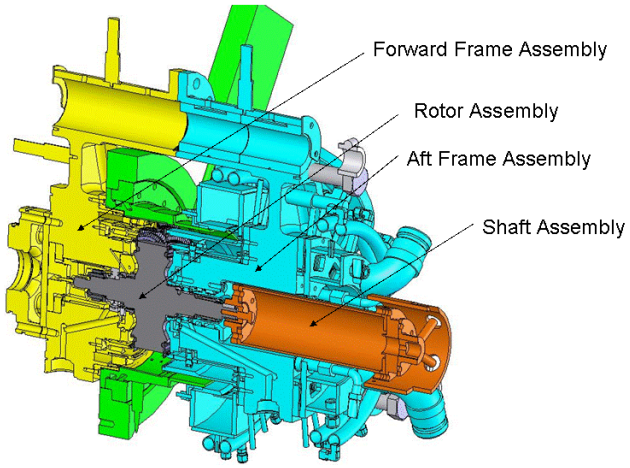

Figure 4. Next Generation Test Rig

fact, the surge characteristics were quite benign and reversible without having to go to great lengths to re-start the inlets.

After the testing was concluded, the test data was used to anchor or calibrate our CFD models. Full flow path 3-dimensional viscous modeling was used; see Figure 3. Once we established that CFD could duplicate the test conditions and results, we used the CFD tool to start designing the next generation test rig for high pressure ratio; see Figure 4.

Conclusions

Ramgen Power Systems Inc. has completed a series of tests that validates the technological base for a compressor product and for a small gas turbine (800 kW to 5 MW) to generate electricity. Past compressor tests have successfully demonstrated a number of the fundamental technical requirements that are critical to achieving high-efficiency

supersonic inlet compression as required for industrial gas compression and engine applications, like fuel cell hybrids. Ramgen will continue to validate the engineering design tools needed to move towards a successful product. These products will leapfrog current technology in terms of higher efficiency, lower cost and lower emissions.

Special Recognitions & Awards/Patents Issued

1. Provisional Patent application submitted for Fuel Fired Compressor and Method of Use in Oxygen; Ramgen Case Number RPS-3150; October 7, 2004

FY 2005 Publications/Presentations

1. Paper for IMECE 2004 on Supersonic Compression Stage Design & Test Results; dated November 14, 2004
2. Paper for ASME 2005 Conference on Conceptual Design of a Supersonic CO_2 Compressor; ASME 2005 Document GT2005-68349, dated June 6, 2005
3. Paper for ASME 2005 Turbo Expo on Insertion of Shock Wave Compression Technology into Micro Turbines for Increased Efficiency and Reduced Costs; dated June 6, 2005
4. Paper for ASNE 2005 Symposium on Critical Enabling Technologies for Long-Endurance Unmanned Surface Vehicles; dated July 19, 2005

VIII Acronyms & Abbreviations

°C	Degrees Celsius
°F	Degrees Fahrenheit
1-D	One-dimensional
2-D	Two-dimensional
3-D	Three-dimensional
A	Ampere
Å	Angstrom
A/cm^2	Amps per square centimeter
AC	Alternating current
AcerSoc	American Ceramic Society
AFM	Atomic force microscope
Ag	Silver
AIChE	American Institute of Chemical Engineers
Al	Aluminum
AL	Application load
Al_2O_3	Alumina, aluminum oxide
AMPL	A Mathematical Programming Language
ANL	Argonne National Laboratory
APS	Atmospheric plasma spray
APU	Auxiliary power unit
Ar	Argon
ASE	Arcomac Surface Engineering, LLC
ASM	ASM International, formerly American Society for Metals
ASME	American Society of Mechanical Engineers
ASNE	American Society of Naval Engineers
ASR	Area specific resistance
ASTM	American Society for Testing and Materials
atm	Atmosphere
ATR	Autothermal reforming
Au	Gold
AU	Air utilization
A.U.	Arbitrary units
AVS	American Vacuum Society
B	Boron
Ba	Barium
BaO	Barium oxide
$BaZrO_3$	Barium zirconate
BET	Bruner, Emmett and Teller surface area measurement method
Bi	Bismuth
BOP, BoP	Balance of plant
BOPS	Balance of plant subsystem
BRO	Bismuth ruthenate ($Bi_2Ru_2O_7$)
BTU	British thermal unit
BYZ	Barium zirconium yttrium oxide
C	Carbon
Ca	Calcium
CaF_2	Calcium fluoride
cal/g-mole	Calories per gram-mole
CARES	Ceramic analysis and reliability evaluation of structures
cc	Cubic centimeter
CCD	Charge coupled device
CCVD	Combusion chemical vapor deposition
Ce	Cerium
CeO_2	Ceric oxide
CERCANAM	Ceramatec Castable Nano Material
CFD	Computational fluid dynamics
cfm	Cubic feet per minute
CGO	Gadolinium-doped ceria
CH_4	Methane
CHEX	Cathode air heat exchanger
cm	Centimeter
cm/s	Centimeters per second
cm^2	Square centimeter
cm^3	Cubic centimeter
CMU	Carnegie Mellon University
CO	Carbon monoxide
Co	Cobalt
CO_2	Carbon dioxide
$CO_3^=$	Carbonate ion

CoO	Cobalt oxide
COx	Oxides of carbon (e.g., CO, CO_2)
CPG	Cummins Power Generation
CPOX	Catalytic partial oxidation
Cr	Chromium
Cr_2O_3	Chromic oxide
CrO_3	Chromium trioxide (chromic acid)
CTE	Coefficient of thermal expansion
CTP	Core Technology Program
Cu	Copper
CuO	Cupric oxide
CW	Continuous wave
DBT	Dibenzothiophene
DC	Direct current
DED	Defect equilibrium diagram
DFC	Department of Energy Fuel Cell Test Facility
DFC	Direct Fuel Cell
DFC/T®	Direct Fuel Cell/Turbine®
DFT	Density functional theory
DMS	Dimethyl sulfide
DOE	U.S. Department of Energy
DT	Double-torsion
DTA	Differential thermal analytical
e^-	Electron
EBPVD	Electron beam physical vapor deposition
ECR	Electrical conductivity relaxation
ECS	Electrochemical Society
EDS	Energy dispersive x-ray spectroscopy
EDX	Energy dispersive x-ray
EIS	Electrochemical impedance spectroscopy
EMI	Electromagnetic interference
EPA	U.S. Environmental Protection Agency
Er	Erbium
ESB	Erbia-stabilized bismuth oxide
Eu	Europium
EuC_2	Europium dicarbide
eV	Electron volts
EXAFS	Extended x-ray absorption fine structure
F	Farad (capacitance unit)
F	Fluorine
FAD	Filtered arc deposition
FAPSID	Filtered arc plasma source ion deposition
FCE	FuelCell Energy, Inc.
FC/T	Hybrid fuel cell/gas turbine
Fe	Iron
FE	DOE Office of Fossil Energy
FEA	Finite element analysis
Fe_2O_3	Ferric oxide
FMA	Fracture mechanical analysis
FPS	Fuel processing subsystem
FTIR	Fourier transform infrared
FU	Fuel utilization
FWHM	Full width half maximum
FY	Fiscal year
g	Gram
Ga	Gallium
g/cc, g/cm^3	Grams per cubic centimeter
Gd	Gadolinium
GDC	Gadolinia-doped ceria
GE	General Electric
GGA	Generalized gradient approximation
GHSV	Gas hourly space velocity
gm	Gram
GPa	Gigapascal
GPC	Gas phase combustor
g/s	Grams per second
GT	Gas turbine
GT	Georgia Institute of Technology
GTI	Gas Technology Institute
GTMO	$Gd_2Ti_{1.4}Mo_{0.6}O_7$
h	Hours
H	Enthalpy
H_2	Diatomic hydrogen
HBCU	Historically Black Colleges and Universities

HC	Hydrocarbon
He	Helium
HEX	Heat exchanger
HHV	Higher heating value
HiTEC	High Temperature Electrochemistry Center
HMI	Human Machine Interface
HNO_3	Nitric acid
H_2O	Water
H_2O/C	Ratio of steam to carbon
H_2S	Hydrogen sulfide
HPD	High power density
HPGS	Hybrid Power Generation Systems (General Electric)
hr	Hour
hrs	Hours
HRU	Heat recovery unit
Hyper	Hybrid Performance Project
Hz	Hertz
I	Current
IC	Innovative Concepts (DOE/NETL)
IC	Interconnection, interconnect
ICM	Integrated component manifold
ICP-MS	Inductively coupled plasma mass spectrometry
IEDP	Isotope exchange and depth profiling
IEEE	Institute of Electrical and Electronics Engineering
IGFC	Integrated gasified fuel cell
IMECE	International Mechanical Engineering Congress & Exposition
IPOPT	Interior Point OPTimization
IR-SOFC	Intermediate-temperature solid oxide fuel cell
ITM	Ion transport membrane
ITO	Indium tin oxide
i-V, I-V	Current-voltage
J	Joule
J	Current density
J/m^2	Joules per square meter
K	Kelvin
kg	Kilogram
kg/s	Kilogram per second
kHz	Kilohertz
kPa	Kilopascal
kW	1000 ohms
kV	Kilovolt
kW	Kilowatt
kWe	Kilowatt electric
kWh	Kilowatt-hour
L	Liter
La	Lanthanum
$LaAlO_3$	Lanthanum aluminite
$LaCrO_3$	Lanthanum chromite
LaDC	Lanthanum-doped ceria
LAFAD	Large area filtered arc deposition
$LaMnO_3$	Lanthanum manganite
LAO	Lanthanum aluminate
lb	Pound
lbm/sec	Pound mass per second
LCM	Lanthanum calcium manganese oxide ($La_xCa_{1-x}MnO_3$)
LDC	Lanthanum-doped ceria ($Ce_{0.6}La_{0.4}O_2$)
LHV	Lower heating value
Li	Lithium
Li_2O	Lithium oxide
LLC	Limited Liability Company
LnC_2	Lanthanide, where Ln is any element in the lanthanide series
LPG	Liquefied petroleum gas
Lpm	Liters per minute
LSC	Lanthanum strontium cobaltite (lanthanum strontium cobalt oxide)
LSC50	$La_{0.5}Sr_{0.5}CoO_{(3-\delta)}$
LSCF	Lanthanum strontium cobalt ferrite
LSCO	$LaSrCo_2O_{6-x}$
LSF	Lanthanum strontium ferrite
LSGM	Lanthanum strontium magnesium gallate (lanthanum strontium gallium magnesium oxide)

LSM	Lanthanum strontium manganite (lanthanum strontium manganese oxide)
LSV	$La_{0.7}Sr_{0.3}VO_3$ ($La_{1-x}Sr_xVO_3$)
LuC_2	Lutetium dicarbide
m	Meter
m^2	Square meter
m^2/g	Square meters per gram
mA/cm^2	Milliamperes per square centimeter
MCO	$MnCo_2O_4$
MD	Molecular dynamics
MEA	Membrane electrode assembly
mg	Milligram
Mg	Magnesium
M-G	Maxwell-Garnett
µg	Microgram
µg/mol	Microgram per mole
MgO	Magnesium oxide
MIEC	Mixed ionic and electronic conduction, mixed ionic and electronic conducting
MIM	Metal injection molding
MIMO	Multi-Input-Multi-Output
min	Minute
MIT	Massachussetts Institute of Technology
ml	Milliliter
ml/min	Milliliters per minute
mL min^{-1}	Milliliters per minute
µm	Micrometer, micron
mm	Millimeter
Mn	Manganese
Mn_2O_3	Manganese oxide
$mOhm.cm^2$	Milli-ohm square centimeter
mol%	Molar percent
MPa	Megapascal
MRS	Materials Research Society
MRSI	Materials and Systems Research, Inc.
m/s	Meters per second
ms	Millisecond
MSU	Montana State University
mV	Millivolt
MW	Megawatt
mW	Milliwatt
mW/cm^2	Milliwatts per square centimeter
N_2	Diatomic nitrogen
Nd	Neodymium
NETL	National Energy Technology Laboratory
Ni	Nickel
NiO	Nickel monoxide, nickel oxide
NLEIS	Nonlinear electrochemical impedance spectroscopy
NLP	Non-linear programming
nm	Nanometer
NO_x	Oxides of nitrogen
NRA	Nuclear reaction analysis
O_2	Diatomic oxygen
O_2/C, O/C	Oxygen to carbon ratio
OCV	Open circuit voltage
ODE	Ordinary differential equation
ORNL	Oak Ridge National Laboratory
P	Pressure
ΔP	Pressure drop
Pa	Pascal
P&IDs	Piping and instrumentation drawings
PAM	Process air module
Pb	Lead
PBCO	$PrBaCo_2O_{5.5+\delta}$
PCFC	Proton ceramic fuel cell
PCS	Power conditioning system
Pd	Palladium
PdO	Palladium oxide
PEN	Positive-electrolyte-negative (cathode-electrolyte-anode)
PES	Power electronics subsystem
PGM	Platinum group metal
PI	Proportional-integral
PLC	Programmable logic controller
PLD	Pulsed laser deposition

PNNL	Pacific Northwest National Laboratory
POM	Partial oxidation of methane
POX	Partial oxidation
ppb	Parts per billion
ppbv	Parts per billion by volume
pph	Pounds per hour
ppm	Parts per million
ppmv	Parts per million by volume
ppmw	Parts per million by weight
Pr	Praseodymium
PRO	Lead ruthenate ($Pb_2Ru_2O_{6.5}$)
psi	Pounds per square inch
psia	Pounds per square inch absolute
psid	Pounds per square inch differential
psig	Pounds per square inch gauge
PSOFC	Planar solid oxide fuel cell
Pt	Platinum
PtO_2	Platinum dioxide
QM	Quantum mechanical
RBS	Rutherford backscattering spectroscopy
ReaxFF	First Principles-Based Reactive Force Fields
Rh	Rhodium
ROEB	Reactive oxide electron beam
RSG	Regenerative sol gel
RT	Room temperature
RTS	Real-time simulation
Ru	Ruthenium
RuO_2	Ruthenium dioxide
s	Second
S	Sulfur
S	Entropy
S/C	Steam to carbon ratio
S/cm	Siemens per centimeter
ScSZ	Scandium-stabilized zirconia
ScSZ-10	Fully stabilized ScSZ: 90 mol% ZrO_2, 10 mol% Sc_2O_3
ScSZ-6	Partially stabilized ScSZ: 94 mol% ZrO_2, 6 mol% Sc_2O_3
SBIR	Small Business Innovation Research
sccm	Standard cubic centimeters per minute
sccm/cm	Standard cubic centimeters per minute per centimeter
SCG	Slow-crack growth
SDC	Samaria-doped ceria
sec	Second
SECA	Solid State Energy Conversion Alliance
SEM	Scanning electron microscopy
SERS	Surface-enhanced Raman spectroscopy
SIF	Stress intensity factor
SIMS	Secondary ion mass spectrometry
SiO_2	Silicon dioxide
Sm	Samarium
SO_2	Sulfur dioxide
SOFC	Solid oxide fuel cell
SOFCo	SOFCo-EFS Holdings LLC
SOFC/T	Solid oxide fuel cell/turbine
SOx	Oxides of sulfur (e.g., SO_2)
SPR	Surface plasmon resonance
SPU	Stationary power unit
SR	Steam reforming
Sr	Strontium
SrO	Strontium oxide (strontia)
$SrTiO_3$	Strontium titanate
SS	Stainless steel
SSC	Strontium samarium cobalt oxide
STO	Strontium titanate
SV	Space velocity
SWPC	Siemens Westinghouse Power Corporation
T	Temperature
Tb	Terbium
TBM	Tert-butyl mercaptan
T.C.	Temperature controller
TEM	Transmission electron microscopy or tunneling electron microscopy
TERS	Tip-enhanced Raman scattering

Tg	Glass transition temperature
THT	Tetrahydrothiophene
Ti	Titanium
TiO_2	Titanium dioxide
TIPS	Thermally integrated power system
Tm	Thulium
TMS	The Metallurgical Society
TPB	Triple-phase boundary, three-phase boundary
TPD	Temperature-programmed desorption
TPR	Temperature-programmed reduction or temperature-programmed reaction
TRC	Transient recognition control
TRS	Time-resolved spectroscopy
UCR	University Coal Research
UIC	University of Illinois at Chicago
UMR	University of Missouri - Rolla
U.S.	United States
UU	University of Utah
Uv	Ultraviolet
Uv-vis	Ultraviolet to visible
V	Volt
VASP	Vienna Ab initio Simulation Package
V-I	Voltage-current
vol	Volume
vol%	Volume percent
VPS	Versa Power Systems
W	Watt
W/cm^2	Watts per square centimeter
We	Watt electric
W/m-K	Watts per meter-Kelvin
WRAS	Work recovery and air supply system
wt	Weight
wt%, wt.%	Weight percent
WVU	West Virginia University
XANES	X-ray absorption near edge spectroscopy
XAS	X-ray absorption spectroscopy
Xe	Xenon
XRD	X-Ray diffraction
Y	Yttrium
Yb	Ytterbium
Y_2O_3	Yttrium oxide (yttria)
YRO	Yttrium ruthenate ($Y_2Ru_2O_7$)
YSZ	Yttria-stabilized zirconia
YSZ-8	Fully stabilized YSZ: 92 mol% ZrO_2, 8 mol% Y_2O_3
ZDC	Zirconia-doped ceria
Zr	Zirconium
ZrO_2	Zirconium dioxide (zirconia)
Ω	Ohm
Ωcm^2	Ohm centimeter squared

IX Primary Contact Index

A

Adler, Stuart B. 209
Alptekin, Gökhan 288

B

Berry, David A. 162
Bessette, Norman 13
Bobba, Rambabu 285
Borup, Rodney L. 156
Brow, Richard K. 125

C

Carpenter, Michael A. 293
Chou, Yeong-Shyung "Matt" 90
Chuang, Steven S. C. 297
Cocks, F.H. 275

D

Dieckmann, Gunther 146

E

Elangovan, S. (Elango) 51, 266

G

Gardner, Todd H. 167
Gemmen, Randall 72
Ghezel-Ayagh, Hossein 217, 278
Goddard, William 235
Gorokhovsky, Vladimir 47

H

Huang, Xinyu 121

K

Koopman, Aaron 307
Kornhauser, Alan A. 300
Krumpelt, Michael 43, 143

L

Lai, Jason 181
Lara-Curzio, Edgar 82
Liu, Meilin 55, 60
Loehman, Ronald E. 109

M

Mao, Chien-Pei 150
Marina, Olga 94
Mazumder, Sudip K. 201
Meier, Gerald H. 129
Minh, Nguyen 31, 222

N

Nair, Balakrishnan 270
Norrick, Daniel 18

O

Ozpineci, Burak 177

P

Pal, Uday B. 261
Patel, Pinakin 26
Pederson, LR 241

Q

Qu, Jianmin 187

S

Seabaugh, Matt 282
Shaffer, Steven 22
Shekhawat, Dushyant 171
Simner, Steve 97
Singh, Prabhakar 101
Singh, Raj N. 117
Swartz, Scott L. 77

T

Tucker, David 228

V

Virkar, Anil V. 138, 254
Visco, Steven J. 67
Vora, Shailesh D. 37

W

Wachsman, Eric D. 194, 249

Y

Yang, Zhenguo "Gary" 105

Z

Zhu, J.H. 113

National Energy Technology Laboratory

626 Cochrans Mill Road
P.O. Box 10940
Pittsburgh, PA 15236-0940

3610 Collins Ferry Road
P.O. Box 880
Morgantown, WV 26507-0880

One West Third Street, Suite 1400
Tulsa, OK 74103-3519

539 Duckering Bldg./UAF Campus
P.O. Box 750172
Fairbanks, AK 99775-0172

Mark C. Williams
Fuel Cell Technology Manager
304-285-4747
Mark C.Williams@netl.doe.gov

Visit the NETL website at:
www.netl.doe.gov

Visit the SECA website at:
www.seca.doe.gov

Customer Service:
1-800-553-7681

U.S. Department of Energy
Office of Fossil Energy

Printed in the United States on recycled paper

September 2005